MARTIN MARIETTA ENERGY SYSTEMS LIBRARIES
3 4456 0365281 1

5

ORNL-3417
UC-4 – Chemistry
TID-4500 (19th ed., Rev.)

# REACTOR CHEMISTRY DIVISION

# ANNUAL PROGRESS REPORT

# FOR PERIOD ENDING JANUARY 31, 1963

CENTRAL RESEARCH LIBRARY
DOCUMENT COLLECTION
LIBRARY LOAN COPY
DO NOT TRANSFER TO ANOTHER PERSON
If you wish someone else to see this document, send in name with document and the library will arrange a loan.

OAK RIDGE NATIONAL LABORATORY
operated by
UNION CARBIDE CORPORATION
for the
U.S. ATOMIC ENERGY COMMISSION

Printed in USA. Price: $4.00 Available from the
Office of Technical Services
U. S. Department of Commerce
Washington 25, D. C.

LEGAL NOTICE

This report was prepared as an account of Government sponsored work. Neither the United States, nor the Commission, nor any person acting on behalf of the Commission:

A. Makes any warranty or representation, expressed or implied, with respect to the accuracy, completeness, or usefulness of the information contained in this report, or that the use of any information, apparatus, method, or process disclosed in this report may not infringe privately owned rights; or

B. Assumes any liabilities with respect to the use of, or for damages resulting from the use of any information, apparatus, method, or process disclosed in this report.

As used in the above, "person acting on behalf of the Commission" includes any employee or contractor of the Commission, or employee of such contractor, to the extent that such employee or contractor of the Commission, or employee of such contractor prepares, disseminates, or provides access to, any information pursuant to his employment or contract with the Commission, or his employment with such contractor.

ORNL-3417
UC-4 – Chemistry
TID-4500 (19th ed., Rev.)

Contract No. W-7405-eng-26

# REACTOR CHEMISTRY DIVISION ANNUAL PROGRESS REPORT

For Period Ending January 31, 1963

**Director**

W. R. Grimes

**Associate Directors**

E. G. Bohlmann
H. F. McDuffie
G. M. Watson

**Senior Scientific Advisors**

F. F. Blankenship
C. H. Secoy

DATE ISSUED

APR 24 1963

OAK RIDGE NATIONAL LABORATORY
Oak Ridge, Tennessee
operated by
UNION CARBIDE CORPORATION
for the
U. S. ATOMIC ENERGY COMMISSION

SYSTEMS LIBRARIES
3 4456 0365281 1

# Summary

## PART I. MOLTEN-SALT REACTOR PROGRAM

### 1. High-Temperature Phase Equilibrium Studies

Investigations of high-temperature phase equilibria were continued for systems having potential use in molten-salt-reactor technology. Emphasis shifted from studies of phase behavior in the quinary fuel system $LiF-BeF_2-ZrF_4-ThF_4-UF_4$ to the crystallization reactions in the fuel solvent system $LiF-BeF_2-ZrF_4$, and to systems involving trivalent uranium phases, $UF_3-UF_4$, $LiF-UF_3-UF_4$, $LiF-BeF_2-UF_3$, and $LiF-BeF_2-ZrF_4-UF_3$. Studies of the system $LiF-ZrF_4-UF_4$ were initiated. Studies of the systems $NaF-YF_3$ and $CsF-ZrF_4$ were completed and detailed phase diagrams were constructed. Determinations were made of the crystal structures for the compounds $LiRbF_2$, $LiCsF_2$, and $Cr_2F_5$ from single-crystal x-ray diffraction data. An x-ray diffraction study was made of the structure of $Cs_3ZrF_7$. The crystal and molecular structure of $XeF_4$ was determined from x-ray and neutron diffraction data. Characteristic optical and x-ray diffraction properties were determined for 12 crystalline complex halide and oxyhalide phases.

### 2. Compatibility of MSRE Components

A series of three irradiations in the MTR was completed in which the interaction of fissioning MSRE fuel with INOR-8 and graphite was under study. Much of the postirradiation examination has now been performed. A general conclusion, which conforms to all the available evidence, is that no deleterious effects of the fuel, the graphite, or the INOR-8 will arise from irradiation behavior during the proposed operation of the MSRE with unclad graphite.

A potentially serious hazard had previously been recognized upon finding $CF_4$ in the vapor phase in capsules that were designed to study the effect of irradiation on the interfacial behavior of graphite. An even more alarming result was the subsequent discovery of high pressures of elemental fluorine in the gas spaces of other irradiated capsules. Moreover, tellurium caused a prominent radioactivity in the gas, and the amount of xenon was frequently far lower than expected on the basis of known fission yields.

Enlightening information was obtained from the results of MTR experiment 47-5, in which provisions had been made to sweep the vapor spaces of the capsules with helium and thus to collect for analysis any evolved gases. At no time when the capsules were exposed under operating conditions planned for the MSRE (fissioning molten fuel at 600 to 700°C) was there any evidence of a significant generation of fluorine, carbon tetrafluoride, or tellurium, and gaseous fission products were collected in the expected amounts. By contrast, when the fuel froze during scheduled and terminal reactor shutdowns, there was abundant evidence of the generation of fluorine and release of tellurium, and the xenon again disappeared. Such behavior was in accord with the literature concerning the release of fluorine from irradiation of solid lithium fluoride and with the recent reports of the reactivity of xenon toward elemental fluorine.

The experiments suggest strongly that fluorine is generated by the effects of fission product radiation on frozen fuel, below temperatures of about 100°C, and that all the other anomalous results could be attributed to this primary cause. Fluorine generated during the intermediate reactor shutdowns would, when the temperature was subsequently raised, have reacted more or less indiscriminately with the fluorine-depleted fuel, the graphite, the xenon, and the INOR-8 walls, but ultimately virtually all was restored as fluoride in the fuel. In the cold, reaction with the graphite under decay irradiation may have produced $CF_4$. The absence of reaction with the INOR-8 walls indicated that the fluorine reacted very rapidly

with the "reduced" fuel as the temperature was raised. Also, only in the cold, with fluorine present, was tellurium converted to a volatile fluoride that escaped from the solid state.

An experimental program was continued to confirm and extend the reassuring conclusions from the irradiation experiments thus far completed.

Evidence of a slow reaction of carbon tetrafluoride with "reduced" MSRE fuel salt mixtures at temperatures of 700 to 850°C was obtained by recirculating mixtures of $CF_4$ and helium through pots containing the molten salt but in the absence of graphite. When $CF_4$ was brought into contact with a similar molten salt at 600°C by introducing it through the porous walls of a submerged graphite cylinder, evidence of reaction was obtained; in blank experiments making use of an unreduced salt mixture at this temperature, no evidence of reaction was obtained. Attempts to measure the solubility of $CF_4$ in molten fluorides, by means of techniques which were suitable for use with the rare gases, failed to provide positive evidence of solubility; either the solubility is extremely low or the dissolved gas was somehow consumed by reaction with the system during the experimental process.

The discovery of the occurrence of fluorine in the gas space above irradiated and subsequently frozen capsules containing MSRE fuel called for the development of techniques for studying various aspects of the reactions of fluorine with MSRE materials. For such studies, apparatus was designed and constructed for the safe handling of fluorine in the laboratory. With this apparatus the preparation of xenon tetrafluoride was demonstrated, and the reaction of fluorine with frozen MSRE fuel which contained some of the uranium in the trivalent form was studied. Rapid reaction was indicated to begin as the temperature of the frozen salt approached the melting point of the material, suggesting that the irradiated containers found to contain fluorine when frozen were probably not exposed to high pressures of fluorine for appreciable periods at elevated temperatures following intermediate reactor shutdowns during the course of the irradiation experiment.

An experimental program was conducted to study the evolution of volatile impurities from graphite by helium purging while heating to 700°C at controlled rates. The apparatus and operational procedure were designed to simulate the initial preheat conditions of the MSRE. This method was found useful for studying the rates at which moisture was evolved from graphite blocks having the same cross-sectional configuration as an MSRE moderator element. Both physically adsorbed water and what appeared to be chemisorbed water were evolved during these experiments. The helium preheat and purging operation planned for the MSRE should be more than adequate to remove both types of water.

Studies of the precipitation of uranium and zirconium oxides from molten mixtures of LiF, $BeF_2$, and $ZrF_2$, with varying amounts of $ZrF_4$ and in the presence of small amounts of MSRE fuel as a contaminant, at 600°C, have yielded results which were correlated well by simple solubility product behavior implied by the two solubility products,

$$Q^s_{UO_2} = [U^{4+}]\,[O^{2-}]^2 = 1.2 \times 10^{-5}\ \text{mole}^3\ \text{kg}^{-3}\ ,$$

$$Q^s_{ZrO_2} = [Zr^{4+}]\,[O^{2-}]^2 = 3.2 \times 10^{-5}\ \text{mole}^3\ \text{kg}^{-3}\ .$$

The consequences of this model of behavior, with reference to operation of the MSRE, are that the presence of zirconium as a fuel or flush salt constituent *lowers* the tolerance of the salt for oxide contamination before precipitation occurs but protects against uranium precipitation by causing the preferential precipitation of $ZrO_2$. Moreover, such salts should even dissolve precipitates of $UO_2$, which might have been previously produced in some conceivable way, at the expense of the sacrificial precipitation of a corresponding amount of $ZrO_2$.

## 3. Physical Chemistry of Molten-Salt Systems

Studies of freezing-point depressions of sodium fluoride showed that 13 trifluoride solutes caused negative deviations from ideality. At a fixed solute concentration the excess partial molal free energy of mixing of NaF (calculated from the freezing-point depressions) was inversely proportional to the solute's interionic distance for 11 trifluorides (8 rare earths, scandium, yttrium, and lanthanum). The polarizing action of $In^{3+}$ ions was postulated to account for the difference in the effects of $InF_3$ and $ScF_3$ on NaF freezing points. The anomalous behavior of $AlF_3$ in NaF solution was explained in terms of steric considerations. The magnitudes of the freezing-point depressions

caused by $CdF_2$, which were larger than those of $CaF_2$, were also attributed to polarizing action.

Activity coefficients of $ZrF_4$ in the system $LiF-ZrF_4$ were evaluated over the entire concentration range. From 1.0 to 0.2 mole fraction of $ZrF_4$, activity coefficients were calculated from published vapor pressure information. From 0.2 to 0 mole fraction, the activity coefficients were calculated by means of the Gibbs-Duhem equation. To apply this equation the necessary activity coefficients of LiF were determined for this concentration range from measurements of liquidus temperatures. The activity coefficients of $ZrF_4$ for the concentration range of reactor interest (5 mole % and less) were calculated to be of the order of $10^{-5}$.

Apparatus has been constructed to measure manometric vapor pressures of fluoride melts by the Rodebush-Dixon method. Vapor pressures of two MSRE fuel mixtures (66.5-29.4-3.95-0.15 and 64.7-27.0-8.13-0.16 mole % $LiF-BeF_2-ZrF_4-UF_4$) were measured in the temperature range 1000 to 1200°C. Extrapolation of the data to the highest MSRE design temperature, 704°C, gave vapor pressures of 0.02 and 0.05 mm, respectively, for the mixtures containing 3.95 and 8.13 mole % $ZrF_4$. Measurements were begun on the $LiF-BeF_2$ system in order to obtain thermodynamic activities in this important binary system.

Density measurements in the $LiF-ThF_4$ system yielded molar volumes which were found to be additive, thus further supporting the hypothesis that molar volumes in all fluoride melts may, to a good approximation, be additive.

An oscillating cylinder viscometer, which permits observations to be made with the test fluid in a sealed vessel, has been constructed for use with molten-salt systems. Preliminary testing with water and with molten sodium chloride has yielded data in good agreement with accepted viscosity values.

### 4. Fluoride Salt Production

The fluoride production plant, previously operated as two separate batch-processing units, was modified by the addition of a premelting furnace which can deliver molten charges alternatively to both the processing units. A 64% increase in the rate of production may be achieved as a result of this modification. The facility for handling and charging the unmelted raw materials was relocated adjacent to the new premelting furnace and was modified to make use of a vibratory feeder to deliver dry materials into the furnace. All the tubing, valves, gages, and electrical controls for the batch-processing units were replaced to obtain better control of the temperature and of the rate of delivery of gaseous HF during the purification. This replacement will also avoid some possibility of inadvertent contamination of isotopically pure $Li^7$ compounds with natural lithium remaining from previous operations.

An enclosed wet sandblasting facility was installed for use in reclaiming salt storage pots and other containers used in molten-salt research. Containers contaminated with beryllium salts can be cleaned satisfactorily in this facility.

The requirements for fuel, coolant, and flush salts for the Molten-Salt Reactor Experiment have been anticipated. The necessary $Li^7F$ has been ordered from Y-12, hafnium-free zirconium has been purchased in the form of the tetrafluoride, and beryllium fluoride specifications have been established. As a result of cooperative discussions with suppliers of beryllium, it is believed that material which meets our specifications will soon be available in a competitive market.

Laboratory and production processes for removing oxides by treatment with a mixture of hydrogen and hydrogen fluoride were demonstrated in the purification of the oxide-contaminated salt charge of the Engineering Test Loop.

Some 2000 kg of various fluoride salt mixtures were prepared for use by the research and development groups associated with the MSRP and the fuel reprocessing studies of the Chemical Technology Division of ORNL.

## PART II. SUPPORT FOR AQUEOUS REACTOR PROGRAMS

### 5. Chemistry of Pressurized-Water Reactor Systems

In a continuing study of the chemical and radiochemical behavior of the water in the pressurized-water loop at the Oak Ridge Research Reactor, preliminary results confirmed the effectiveness of natural and synthetic magnetite as a high-temperature ion exchange material for decontaminating the loop water. From 95 to >99% of the iron, manganese, and cobalt activities was removed in a single pass through a filter bed of magnetite at 425°F.

Radiochemical analyses of the soluble and insoluble portions of the loop coolant have given results which are consistent with a simple hypothesis concerning the mechanism of the transport and deposition of radioactive materials in pressurized-water reactors.

### 6. Corrosion by Solutions

Studies of the effect of heat flux on the corrosion of aluminum have continued. Tests were conducted to simulate the decrease in heat flux across the aluminum fuel element cladding that will occur during an Advanced Test Reactor cycle. The results of these tests indicated that starting fuel element surface temperatures should be 340°F or less if final fuel element temperatures are not to exceed 400°F at the end of a cycle. Other tests showed that heat flux in the range of 1 to $2 \times 10^6$ Btu $hr^{-1}$ $ft^{-2}$ was not a significant variable in determining the rate of oxide formation on aluminum cooled by water at a pH of 5. However, at lower heat flux levels the results indicate that heat flux is an important variable. An attempt is presently being made to correlate all the data obtained at a pH of 5 so that the correlation can be used to predict oxide growth as a function of time and surface temperature in the range of 1 to $2 \times 10^6$ Btu $hr^{-1}$ $ft^{-2}$.

In tests conducted for the High Flux Isotope Reactor it was shown that the corrosion of beryllium by water adjusted to a pH of 5 and at 100°C is independent of velocity in the range of 12.5 to 81 fps. Constant corrosion rates of about 2 mils/yr were observed during tests that lasted as long as 4800 hr. Other tests showed that the electrical coupling of stainless steel to aluminum in the same environment results in the formation of random deep pits in aluminum in crevice areas.

### 7. Mechanism of Corrosion of Zircaloy-2

As part of the Aqueous Homogeneous Reactor Corrosion Program, experiments were made on the effects of reactor radiations on Zircaloy-2 corrosion in oxygenated solutions of $UO_2SO_4$ with uranium depleted of $U^{235}$, $D_2O$, and dilute acids in the temperature range 250 to 300°C. The results of of the experiments have been reexamined and reevaluated on the basis of presently available information. Significant corrosion effects occurred which could be ascribed to fast-neutron damage. Comparisons of the characteristics of this corrosion with those known for fission-recoil-induced corrosion in $UO_2SO_4$ solutions, and correlations between radiation damage rates and corrosion rates for neutrons and fission recoils, suggest that the mechanism by which corrosion is affected is the same for the two types of radiations and involves the production of displaced atoms as an initial step. The radiation corrosion in hydrogenated water, tested in one experiment, was significant but probably substantially less than that in the oxygenated solutions.

Improvements were made in the impedance-measuring instrumentation. A simple capacitance cell was developed which provides reliable film impedance values; this cell can measure the film impedance on a specimen without interfering with subsequent film impedance or film growth. Two specimens were irradiated in boron for two days in the LITR lattice and are presently undergoing postirradiation exposure to 300°C steam plus oxygen with periodic measurements of weight gain and film impedance. Others, irradiated in cadmium for four weeks in the ORR lattice, will be in storage until cool enough to handle.

Additional experiments on the corrosion of Zircaloy-2 in oxygenated, dilute $H_2SO_4$ near 300°C were made using the previously developed electrochemical apparatus. It was found that the corrosion during the period from 6 to 300 min after the initiation of exposure conformed to a logarithmic rate law and, in this respect, agreed with previous findings at 208 and 258°C. Considerations of the present results and of data of others for the initial corrosion in some other aqueous environments near 300°C lead to the conclusions that the mechanism of the initial corrosion is the same in each of these environments, and that at a given temperature near 300°C, the value of the most important rate-controlling parameter does not change with change in these aqueous environments.

A salt bridge was designed, constructed, and tested for the purpose of performing measurements of the potentials of the Zircaloy-2 electrode with respect to an external calomel reference electrode at 25°C and atmospheric pressure. Equipment has been designed, constructed, and tested for determining the capacitance of the corroding electrode.

### 8. Physical Chemistry of High-Temperature Aqueous Systems

The electrical conductivities of aqueous potassium sulfate solutions (0.00050, 0.0022, and 0.0050 *m*) were measured at pressures up to 4000 bars and in the temperature range 25 to 800°C. The maximum observed equivalent conductance of $K_2SO_4$ was 1080 $cm^2$ $ohm^{-1}$ $equiv^{-1}$, approximately seven times the value of the limiting equivalent conductance at 25°C. The precision of these measurements was estimated to be of the order of ± 1%.

Phase boundaries of liquid-liquid immiscibility and critical phenomena (where $L \equiv V$) were determined for the condensed systems $UO_3$-CuO-$SO_3$-$D_2O$, $UO_3$-NiO-$SO_3$-$D_2O$, and $UO_3$-CuO-NiO-$SO_3$-$D_2O$ at temperatures from 280 to 410°C; at $SO_3$ concentrations varying from 0.02 to 1.0 *m*; and at varying molal ratios, $UO_3$:CuO:NiO. With these results three-dimensional models were constructed which specified the saturating phases or critical phenomena, and the variation in phase boundaries as a function of temperature (260 to 430°C) and composition (0.02 to 1.0 *m* $SO_3$), for the four-component systems $UO_3$-CuO-$SO_3$-$D_2O$ and $UO_3$-NiO-$SO_3$-$D_2O$. Critical surfaces were defined over which maximum molal ratios, Σ(metallic oxide):$SO_3$, varying from 0.3 to 0.5 were observed.

A glass-to-metal connector was devised by the use of which the effects of pressure on liquid-liquid immiscibility at high temperatures were determined visually.

The effect of hydrostatic pressures up to 300 bars in raising the temperature of second-liquid-phase formation in the system $UO_2$-$SO_4$-$H_2O$ for solutions varying from 0.14 to 4.5 *m* in $UO_2SO_4$ was found to be +0.082°C per bar. This temperature of liquid-liquid immiscibility appeared to show a strong dependency on solvent density. The temperature of heavy-liquid-phase formation from the supercritical fluid $UO_3$-$SO_3$-$H_2O$ near 400°C appeared also to show a strong dependency on solvent density. The vapor pressures for the deliquescence of solid $UO_2SO_4$ hydrate were determined at temperatures from 345 to 425°C.

The solubilities of $Li_2SO_4$ in $H_2SO_4$-$H_2O$ and in $D_2SO_4$-$H_2O$ solutions in equilibrium with vapor were determined at temperatures between 200 and 350°C and at concentrations of free acid from 0 to 1.5 *m*. Temperatures of critical phenomena (where liquid ≡ vapor) varying between 374 and 470°C were determined visually for solutions of $Li_2SO_4$, $D_2SO_4$, and $D_2O$ at concentrations of $SO_3$ from 0.02 to 2.5 *m* and at molal ratios, $m_{Li_2O}:m_{SO_3}$, varying from 0 to ~0.5.

Isopiestic ratios with reference to NaCl solutions were determined at 140°C for the chlorides of lithium, potassium, and barium, and for sodium sulfate at concentrations below those previously reported. The data for these salts now extend down to approximately 0.2 *m*. Plots of isopiestic ratios at constant molality as a function of temperature are approximately linear and, for a given salt, extrapolate to a common value at about 160°C. This behavior suggests the existence of a "critical structural temperature" above which the salt no longer influences the structural character of water.

A study of Th(IV) hydrolysis at 94°C in 1 *m* $NaClO_4$ was completed. Although the equilibria involved appeared to be rapidly reached and reversible, separate $ThO_2$ solubility results indicated that most of the solutions involved were metastable with respect to the much slower hydrolytic precipitation of $ThO_2$. From the preliminary results of a study of Th(IV) hydrolysis behavior at 0°C, it appears that sufficient data may soon be available to deduce with confidence the rather complex hydrolysis equilibria involved and their temperature coefficients.

## PART III. HETEROGENEOUS SYSTEMS

### 9. Compatibility of Coated Particles and Matrix Graphites with Liquid Coolants

Matrices containing coated fuel particles might be attractive as unclad reactor fuel elements in liquid coolants if the systems are adequately compatible. The high thermal conductivity of graphite and the small size of fuel particles indicate that internal temperature gradients should not become excessive at high power densities. Limitations on the rates of heat generation in such fuel elements could, however, occur as a result of other phenomena, such as high rates of heat transfer at the liquid interface. Studies of graphite matrix–water coolant compatibility under high heat flux conditions have been inaugurated. Unfueled and fueled ¼-in.-diam graphite rods were heated internally by electrical resistance in a stream of flowing high-temperature pressurized water. The rod was observed visually by a sight glass arrangement at various levels of heat input.

Failures did not occur in fueled or unfueled extruded graphite rods due to thermal stresses at heat fluxes below 900,000 Btu $hr^{-1}$ $ft^{-2}$. The linear heat loads of the rods were about 5000 Btu $hr^{-1}$ $in.^{-1}$, far below estimated thermal stress limits. Transverse cracking was observed in some instances at heat fluxes above 1,000,000 Btu $hr^{-1}$ $ft^{-2}$. However, it was not necessarily due only to the high rates of heat transfer.

Rods machined from pyrolytic graphite showed evidence of attack at a linear heat load of 3400 Btu $hr^{-1}$ $in.^{-1}$ (600,000 Btu $hr^{-1}$ $ft^{-2}$) and splintered at a linear heat load of 4700 Btu $hr^{-1}$ $in.^{-1}$ (860,000 Btu $hr^{-1}$ $ft^{-2}$). This attack is attributed to thermal stresses between the layers of the weakly bonded laminar pyrolytic graphite.

When the heat flux exceeded calculated "burnout" limits on the extruded rods, film boiling occurred and attack of the graphite surface by the steam was observed. The burnout heat flux limits depend on the overpressure and flow velocity of the coolant. By increasing these it was possible to operate at a heat flux exceeding 1,000,000 Btu $hr^{-1}$ $ft^{-2}$ for 12 days without damage to the graphite. No differences in performance were noted between unfueled graphite rods and rods fueled with about 8 vol % of pyrolytic-carbon-coated uranium carbide particles. It is believed that the results of these studies may also be applicable to other liquid coolants.

One of the simplest radiation stability requirements for systems involving liquids, matrix materials, and coated particles is that the system should retain its integrity for a substantial period of time at temperature in the presence of strong gamma radiation.

Irradiations have been completed on two autoclave experiments using a 10,000-curie $Co^{60}$ source.

In one experiment, balls of four grades of graphite were exposed to liquid and vapor phases of $D_2O$ under helium atmosphere at 330°C for 2115 hr, developing a gamma radiation dose of 5.1 whr/g. Very slight swelling and pitting of the graphites were observed, along with very small weight losses. Carbon dioxide and a below-stoichiometric quantity of $D_2$ were found in the gas.

In a second experiment, balls of four grades of graphite were exposed to liquid and vapor phases of Santowax R (mixed terphenyls) under helium atmosphere at 400°C for 1770 hr, developing a gamma radiation dose of 4.1 whr/g. Little or no effect on the graphite spheres was noted. The Santowax R had become discolored. Analysis of the gas phase indicated production of methane in rough agreement with the literature, and a quantity of hydrogen substantially less than anticipated.

The compatibility of coated-particle materials with molten fluoride salts has been studied in accelerated tests at temperatures of 800–1000°C in static crucibles under vacuum, or with hydrogen or helium cover gas. Salt mixtures included LiF-NaF eutectic and LiF-NaF-KF eutectic.

Alumina coatings of $UO_2$ particles, and pure alumina spheres, either dissolved or were cracked in LiF-NaF eutectic at 800–1000°C. The attack was more severe under hydrogen.

Pyrolytic-carbon-coated $UC_2$ particles were not attacked in this salt at 900°C. Chromium appeared to have been transported from vessel walls to the carbonaceous particles at 900°C, possibly by fluoride vapors.

## 10. Rheology of Suspensions of Thoria from First In-Pile Slurry Loop Experiment

Rheological determinations were conducted on slurries prepared from irradiated thoria drained from the first in-pile slurry loop experiment during and after in-pile operation and recovered from the loop drain tank. Determinations of flow rate at a variety of pressures were made at room temperature in a capillary viscometer on several concentrations of suspensions of the irradiated material and on several concentrations of suspensions of unirradiated batch DT-22 thoria-urania used to load the loop. These measurements were used to calculate the yield stress and coefficient of rigidity according to the Bingham plastic model.

The yield stress results were consistent with the anticipated dependence on the cube of volume fraction solids. Although the ratio of yield stress to cube of volume fraction solids, which is an index of flocculation, was higher for the irradiated material, it changed less than in proportion to the inverse square of the particle diameters. This was interpreted as implying that the flocculation properties and yield stress of thoria slurries irradiated to full breeder blanket dose, although increasing with irradiation, might remain within tolerable limits.

## 11. In-Pile Loop Studies of Aqueous Thorium Oxide Slurries

The second in-pile slurry loop experiment was operated in beam hole HN-1 of the Oak Ridge Research Reactor from February 12 to May 15, 1962. It was desired to irradiate a circulating high-temperature aqueous suspension of pure thoria to produce substantial fissions from in-bred $U^{233}$ and to observe the effects of such exposure on the properties of the slurry. The loop was operated 2036 hr in-pile, in addition to 324 hr of preirradiation testing, receiving a mean neutron flux in the slurry of $1.0 \times 10^{13}$ *nv* for 79.4% of this time. Approximately 0.06% of the thorium atoms were transmuted and a total of $2 \times 10^{16}$ fissions per gram of solids was developed. The thoria concentration was ~900 g of Th per liter at 280°C.

The ability of the irradiated slurry to be resuspended after a substantial period of settling was demonstrated. No handling problems were encountered with the slurry during operation.

Slurry samples taken during the irradiation indicated that the mean particle size changed from 2.3 to 1.5 $\mu$, the x-ray crystallite size from ~2000 to 1000 A, and the surface area from ~1 to 24 $m^2/g$ as the irradiation continued.

The run was terminated when electrical leads to the circulating pump were shorted outside the loop containment bulkhead by water leakage.

Instead of carrying out a thorough postirradiation examination of the experiment, which did not reach the desired fission dose, a replacement experiment was constructed.

## 12. Construction and Out-of-Pile Testing of Third In-Pile Slurry Loop Experiment

A third in-pile slurry loop of enlarged core capacity was designed, constructed, and loaded with thoria slurry. It operated satisfactorily during out-of-pile tests and was ready for shipment for insertion into the reactor beam hole. It will not be operated in-pile as the program has been discontinued.

## 13. Surface Chemistry of Aqueous Systems

The adsorption of HCl on a fused sample of thoria is compared with previously reported data for the adsorption of $HNO_3$ on thoria of higher surface area. The results from the two cases are in surprisingly good agreement with each other in view of the fact that the fusion of the thoria was expected to reduce the internal surface markedly and thus significantly affect the adsorption capacity. Efforts are in progress to produce, by fusion in a plasma torch, spherical particles with no internal surface.

The heats of immersion of several thorium oxide samples in water at 25°C have been measured with a sensitive thermistor calorimeter. Specific surface areas of the thorium oxide samples ranged from approximately 1 to 15 $m^2/g$ as measured by nitrogen adsorption. Prior to the calorimetric measurements, the samples were outgassed at a pressure of $1 \times 10^{-5}$ mm Hg for 24 hr at temperatures ranging from 100 to 500°C. In general, the heat of immersion per unit area increased with increasing outgassing temperature. There was also a unique dependence of the heat of immersion per unit area on the thermal history of the sample prior to outgassing.

## 14. Phase-Equilibrium Studies in the System $UO_2$-$ThO_2$-$O_2$

Mixtures of uranium and thorium hydroxides containing from 10 to 90% thorium were prepared by coprecipitation. These were converted to solid solutions by heating to 1500°C and, in some cases, by subsequent reduction with hydrogen at 800°C. Samples of these materials were exposed to air at temperatures from 200 to 1500°C for periods of time ranging from 10 hr to 6 months. The results of weight changes, chemical analysis, x-ray diffraction, electron diffraction, and metallography were interpreted in terms of the composition-temperature relations of the system at a fixed oxygen partial pressure (that of air).

The desirability of testing mixtures of high surface area, which might attain equilibrium rapidly, led to the preparation of high-surface-area, low-bulk-density solid solutions of $ThO_2$-$UO_2$ by low-temperature thermal decomposition of the coprecipitated U(IV) and thorium oxalate solid solution. Traces of residual carbon could be removed only by alternate treatment with oxygen and hydrogen at about 1200°C. Such treatment reduced the surface area and increased the bulk density of the material.

Efforts to determine the equilibrium partial pressure of oxygen over an equimolar solid solution of $ThO_2$ and $UO_{2.13}$ gave pressures about 1 order of magnitude higher than those reported for pure $UO_{2.13}$ in the temperature range 900 to 1200°C. In all cases the gas contained high percentages of $CO_2$ and CO. Modifications in the apparatus have been completed to permit a study of the system at higher temperatures.

## PART IV. SUPPORT FOR HIGH-TEMPERATURE SOLID-FUELED REACTORS

### 15. Diffusion Processes

**Transport of Gases in Porous Media.** – The "dusty-gas" model, previously employed to describe gaseous transport through porous media under conditions of both uniform and nonuniform pressure, has been extended to include temperature gradients. In this model the porous medium is visualized as a collection of "dust" particles constrained to remain stationary in space. For binary systems (a single gas and "dust"), the phenomenon of thermal transpiration is accounted for by the model in a consistent way for all aspects which are diffusive in character but, as before, needs modification at high pressures by the addition of an expression to account for the viscous backflow. With this modification an equation is obtained which describes thermal transpiration over the entire pressure range. This equation discloses two new relations not previously noticed: a relation between the maximum in the thermal transpiration curve and the Knudsen minimum in the permeability curve and a relation between the height of the thermal transpiration maximum and the translational heat conductivity of the gas.

A remarkable feature of the results, as applied to capillary systems, is that one can calculate rotational relaxation times in gases from the height of the thermal transpiration maxima; this suggests much simpler experimental techniques than those previously employed for the measurement of this phenomenon.

Experimentally, results for the diffusion of the gas pair, helium and argon, through a uranium-impregnated graphite demonstrated that the model could be applied to fueled graphites, while tentative data on a coated graphite specimen showed no deviations from the theoretical expectations because of the different graphite strata constituting the diffusion medium. Insofar as diffusion in the presence of pressure gradients is concerned, the experimental work has come abreast of the theoretical advances, and the behavior of the adjustable parameter required in the theoretical extension to include pressure gradients has been studied.

Two additional programs of research have been initiated: (1) a set of experiments to test the predictions of the dusty-gas model for the case where a gradient in temperature provides the driving force for transport, and (2) an experimental and theoretical approach to the elucidation of the effect of intermolecular interactions on gas-transport mechanisms.

The model was useful in calculations comparing the release of fission gases in ventilated fuel-element configurations that are being considered for use in high-temperature gas-cooled reactors. For example, the calculations showed that fuel elements consisting of a cylindrical fueled matrix enclosed by a gas annulus and a porous sleeve with helium flowing through the sleeve to sweep fission gases out of the annulus is approximately 10,000 times more efficient in preventing fission-gas contamination of the coolant than a bare, porous, hollow cylinder with helium flowing through the matrix and sweeping fission gases into the central void space to be exhausted.

**Diffusion of Fuel in Ceramic Materials.** – Uranium and thorium migration through ceramic matrices is of considerable importance with respect to the design of gas-cooled fuel elements and to an evaluation of anticipated levels of gas-coolant contamination for a given fuel-element design. Advances in the technology of coating fuel particles and the ability to support coated particles within porous ceramic materials have defined two fuel-migration investigations. These investigations involve uranium, graphites, and carbon. One investigation covers uranium migration within pyrolytic carbon, which is representative of a fuel coating material; while the second covers uranium migration in porous graphite, which is representative of a fuel-particle-supporting matrix. In addition, some diffusion experiments have been performed on BeO with the ultimate goal of studying fuel-migration phenomena within this material, if it can be shown that BeO represents a stable fuel-element matrix.

Experimental work performed in the last year has resulted in the development of several satisfactory techniques applicable to the study of diffusion in ceramic materials at high temperature (1000 to 2000°C). The results reveal that solid-state processes control migration in the dense ceramic materials (such as pyrolytic carbon and BeO), whereas surface processes appear to control migration in porous materials. The uranium concentrations in pyrolytic-carbon specimens were found to be high in contrast to the observed migration rates, which were relatively slow. This situation was completely reversed in the porous graphite specimens. However, all the results reinforce uranium migration behavior observed in-pile.

At present the final set of experiments involving the uranium–pyrolytic-carbon systems and uranium–porous graphite systems are under way. Experiments involving thorium and pyrolytic carbon have been initiated, as well as auxiliary experiments on the self-diffusion of beryllium in various forms of beryllia.

## 16. Reactions of Graphite and Pyrolytic Carbon with Gases

The rate of reaction of Speer Moderator-2 graphite with a helium-$CO_2$ mixture having a $CO_2$ concentration of 550 vpm (volume parts per million) was measured at 875, 925, 975, and 1025°C. The rates ranged from $7 \times 10^{-4}$ to $1 \times 10^{-2}$ mg of C per gram-hr at 875 and 1025°C respectively. Satisfactory agreement between the reaction rates as determined by weight changes of the specimen and by analyses of the effluent gas for CO was found. Limited data for the reaction rate at a $CO_2$ concentration of 1100 vpm indicate that the apparent order of the reaction with respect to partial pressure of $CO_2$ is less than unity in this temperature range.

Five lots of pyrolytic-carbon-coated uranium carbide particles (all laminar-type coating) have been exposed to partial pressures of steam ranging from 20 to 635 mm Hg at temperatures of 700 to 1100°C. The rate of reaction of the pyrolytic-carbon coating and the integrity of the coatings have been established. Marked differences in the behavior of coatings present on the various lots of particles are attributable, at least in part, to two types of attack by steam, a localized or pitting type and a more general type. The coatings of some of the lots examined appear to be protective at 800°C and below, but rapid failure is indicated at and above 1100°C. The degree of protection afforded the cores by pyrolytic-carbon coatings at 900 to 1000°C would have to be established experimentally for any particular lot of particles.

## 17. Measurement of Temperature in Reactor Environments

Emf error profiles were determined for stainless-steel-sheathed Chromel-P/Alumel thermocouples exposed to $H_2$ and CO at 870°C. Emf drifts in thermocouples exposed to 7-psig $H_2$ were found to be due to changes in the thermal-gradient region of the Chromel leg. Thermocouples exposed to 7-psig CO did not develop appreciable emf error, but showed a region of severe attack of the Chromel wire deep in the furnace and rather widespread attack of the Alumel wire. The sheath showed heavy carbide precipitation.

Similar thermocouples exposed to graphite in a flowing stream of purified helium and helium containing 350 ppm CO at 700°C have operated satisfactorily for 5 and 8 months respectively. However, emf error profiles have shown that nonhomogeneous regions are developing in thermocouples exposed to both atmospheres.

Tests in 7-psig $H_2$ at 870°C have shown large variations in reliability of sheathed thermocouples obtained from different vendors.

Screening tests on a large number of thermocouple and sheath materials were carried out in graphite and in Si-SiC-coated graphite with an atmosphere of helium containing 500 ppm CO and 500 ppm $H_2$ at 760 and 982°C. These tests showed that several nickel alloys, molybdenum, and tungsten were stable (emf error <0.05%) for at least 54 days at 760°C. However, at 982°C, only the Ni–18% Mo and the tungsten were stable within this range. The Si-SiC coating did not affect the errors except for the noble-metal alloys. Tests are continuing.

Tungsten, tungsten–5% rhenium, tungsten–26% rhenium, and rhenium wires were tested extensively in pure helium and helium contaminated with CO and $O_2$. All wires decomposed rapidly at 1200°C in atmospheres containing as little as 10 ppm $O_2$. Emf output was usually erratic until thermocouple failure occurred. Pure rhenium appeared to be the most stable material in atmospheres containing carbon monoxide at temperatures in the range 1150

to 1750°C. Tungsten and its alloys developed rapid negative emf drifts at temperatures over 1150°C. The rates of drift were dependent upon temperature and wire size, but they were apparently independent of CO concentration in the range used. Tungsten and tungsten–5% rhenium appeared stable in helium containing CO at temperatures below 1150°C.

An experiment was designed in cooperation with members of the Reactor Division to determine thermocouple emf errors resulting from composition changes by transmutation in common thermocouple materials. A mockup of the in-pile experimental assembly is presently undergoing out-of-pile thermal cycling tests from room temperature to about 800°C without difficulty. The experiment is designed to allow irradiation of test wires in the F-9 facility of the ORR in a reasonably uniform neutron flux at about 200°C. The assembly will be removed periodically from the reactor and hung on the side of the pool for emf measurements at about 800°C.

### 18. Alternate Coolants for Gas-Cooled Reactors

The following compounds have been proposed as possible nuclear-reactor gas coolants solely on the basis of their physical properties: $B_2H_6$, $BF_3$, $CF_4$, $MoF_5$, $MoF_6$, $NbF_5$, $NF_3$, $SF_6$, $SiF_4$, and $SiH_4$. As the result of a detailed literature survey and thermodynamic calculations, only $CF_4$, $SF_6$, and $SiF_4$ are considered to be promising possibilities. Plans are being made to use $Co^{60}$ irradiation for the initial investigation of the radiolytic stability of these compounds. Decomposition reaction rates will be determined for pure and contaminated gases. The initial emphasis will be on measurement of fluorine generation. Absolute *G* values, based on chemical dosimetry, will be calculated.

The effects of various parameters on the heat transfer properties of dissociating gaseous mixtures at high temperatures were studied. Estimates were made for the thermal conductivity, specific heat, specific volume, and viscosity of helium–aluminum chloride and helium-fluorine mixtures as a function of temperature at various pressures and compositions. Although present technology is not sufficiently advanced to make the use of fluorine practical in a closed cycle at high temperatures, fluorine serves as an excellent example of the effects of dissociation on the thermal properties of a dissociating gas due to its high heat of dissociation and low molecular weight. Under certain conditions a helium-fluorine mixture has a thermal conductivity and a specific heat considerably greater than the corresponding values for pure helium, while the thermal properties and viscosity of a helium–aluminum chloride mixture are considerably less than those of helium.

### 19. Effect of Irradiation on Beryllium Oxide

Examination of two irradiated assemblies containing a total of 54 specimens has confirmed the severe damage of beryllium oxide on exposure to large dosages of fast neutrons.

One assembly, containing six large specimens of low-density fine-grain-size material showed serious fracturing of the specimens at neutron dosages from 0.2 to $1.0 \times 10^{21}$ *nvt*; the circumferential fracturing in these specimens and the relatively small fast-neutron damage revealed by changes in other properties suggest that thermal stresses contributed markedly to damage in this assembly.

In the second assembly, 35 of 48 specimens survived intact at fast-neutron dosages of 1.2 to $3.65 \times 10^{21}$ *nvt* and temperatures from 583 to 1100°C. Volume increases of 0.9 to 4.4% occurred in these specimens with hot-pressed specimens expanding more than cold-pressed and sintered specimens under similar conditions. Metallographic examination reveals grain boundary separations, which are more marked in the hot-pressed specimens, and which can account for most of the changes in physical properties observed.

Lattice parameter expansion and lattice defect agglomeration both contribute to preferential growth of BeO crystals in the *c* axis direction; lattice parameter expansion is much reduced in irradiations at higher temperatures but it still appears proportional to neutron dose to $3.6 \times 10^{21}$ *nvt*.

A suggestion of flux dependence on decrease of thermal conductivity under irradiation was obtained from specimens at the same temperature but at different neutron flux levels.

## PART V. IRRADIATION BEHAVIOR OF HIGH-TEMPERATURE REACTOR MATERIALS

### 20. Postirradiation Examination of Fuel Materials

Six stainless-steel-clad $UO_2$ capsules were irradiated at cladding temperatures of 1300 to

1600°F to burnups of 1000 to 3000 Mwd per metric ton of uranium in the ORR. These consisted of two instrumented EGCR prototype fuel elements and four tamped and swaged fuel elements. The EGCR prototype tests demonstrated that small strains could cause void formation in the cladding material. The swaged and tamp-packed $UO_2$ elements were stable under the irradiation test conditions.

Several 19-in.-long, ¾-in.-diam stainless-steel-clad $UO_2$ fuel elements were irradiated at temperatures to 1500°F under flowing helium at 300 psi. The results of these tests indicated that the cladding was attacked in the loading tube, probably by $HNO_3$ formed by the action of gamma radiation on $N_2$ and water.

Four capsules of the continuing ETR irradiation series have been examined. These fuel capsules simulate the EGCR fuel elements except for length. Pellets of bulk $UO_2$ are contained in type 304 stainless steel tubing, 0.75 in. in OD and 0.020 in. in wall thickness. Two of these capsules suffered severe cladding failures during irradiation. The reason for these failures was "overpowering" of the experiments combined with nitriding of the cladding. No other evidence of capsule failure has been observed, but examination of the two capsules that did not fail has not been completed.

Two French-made, thin-walled, stainless-steel-clad $UO_2$ fuel elements were irradiated at cladding temperatures of 1150°F to burnups of 7500 Mwd per metric ton of uranium. Postirradiation examination showed excellent fuel element integrity under the irradiation conditions even though two pinhole leaks were observed in one of the capsules. The reason for failure of the cladding is not known.

Four more Maritime Reactor fuel-irradiation experiments have been examined. Each experiment consisted of a three-rod bundle of rods (0.5 in. in diameter by 18 in. long) which contained low-enrichment $UO_2$ powder. The rods were fabricated by swaging or vibratory compaction. No changes were apparent in the exterior appearance of the rods except for the presence of a dark oxide film. Changes in diameter and in bowing of the rods were small. About 4% of the $Kr^{85}$ was released from the fuel in ten of the rods; the gas-release values for the other two rods were 10 and 23%. These higher release values were due to higher temperature and/or greater burnup. There was partial sintering of the fuel in several of the rods that were heated to the higher temperatures. One rod contained a central void and exhibited columnar grain growth.

Small irradiated fuel plates of $UO_2$ dispersed in stainless steel were examined. These plates simulate those planned for the core B fuel element of the Enrico Fermi sodium-cooled reactor. Examination of two plates irradiated to about 6 at. % uranium burnup (reported previously) showed very little change. Three other plates, which were irradiated to approximately 25 at. % burnup, were badly swollen, and a fourth was partially melted. Although there were no obvious flaws in the cladding of the swollen plates, significant quantities of fission products had escaped to the sodium coolant.

Test fuel rods containing vibratory-compacted $UO_2$-$ThO_2$ powder have been examined as a part of the ORNL Fuel Cycle Program. The type 304 stainless steel tubes are filled with $ThO_2$–4.5 wt % fully enriched $UO_2$ at densities of about 85% of theoretical. Both sol-gel oxides and oxides which were fused and then ground have been tested. Three rods have been examined, and 12 similar rods are being examined. No evidence of significant radiation effects on the rods has been found. The fuel burnup in these rods varied from about 3500 to about 20,000 Mwd per metric ton of U + Th. Approximately 2% of the $Kr^{85}$ was released from the fuel in most of the rods.

Three types of pyrolytic-carbon-coated uranium carbide particles supplied by three different manufacturers were irradiated in tantalum cans in a helium atmosphere. The particles were irradiated in four double capsules to about 6 at. % uranium burnup at temperatures of 1900 to 2500°F. Some of the capsules suffered air leaks, which caused loss of fission gas and oxidation of the particle coatings. The fission-gas release for good capsules was about 0.1% of that formed. The irradiated particles were leached in $HNO_3$, and the fraction of particles with cracked coatings was estimated from the uranium content of the solution. Metallographic examination was used to study the type and extent of particle fracturing, reactions at the core-coating interfaces, and changes in the microstructure of the fuel cores. The duplex coating was found to be the most reliable of the three types tested for protecting the fuel particles and for containing fission gases.

Three assemblies were examined in which fueled graphite specimens were irradiated in the MTR. In one of these, a low-permeability graphite can contained four fuel cylinders of uncoated $UC_2$ particles dispersed in graphite; in the other two experiments, single fuel cylinders of pyrolytic-carbon-coated fuel particles dispersed in graphite were irradiated in unsealed containers. Maximum fuel temperatures ranged from 2000 to 2800°F, and fuel burnups varied from 1 to 17 at. % $U^{235}$. The fuel cylinders exhibited good physical stability. Considerable migration of fuel and fission products from the fuel cylinders into the graphite containers was found in all cases. Fuel concentrations in the graphite reached 4% of those in the fuel cylinders. Metallographic examination indicated that fuel-particle structure was affected at uranium burnups of about 2 at. %. All the particle coatings were broken in one experiment, while about 10% were broken in the other.

Three graphite-matrix fuel elements containing pyrolytic-carbon-coated $UC_2$ particles were irradiated at temperatures to 2400°F and burnups to 9 at. % U in the ORR. Results of the postirradiation examination indicated that specimens containing particles with duplex coatings were most resistant to irradiation.

### 21. Fission-Gas Release

Study of fission-gas release from $UO_2$ during irradiation has been extended to include thin plates of coarse crystals of fused $UO_2$ and of single crystals of $UO_2$ as well as sintered compacts. In addition, electrical resistivity of the three types of $UO_2$ has been measured during radiation. Evidence was obtained to show that defects in the $UO_2$ structure retard the emission of fission gases. Release rates of xenon, krypton, and iodine have been obtained as functions of temperature, specimen structure, stoichiometry, and neutron flux; no combination of direct fission recoil and classical diffusion of fission products in solids accounts for the data.

Pyrolytic-carbon-coated uranium carbide particles are being irradiated to determine in-pile fission-gas release rates. Uranium carbide particles having three different types of coatings, as well as bare uranium carbide particles, have been irradiated at temperatures up to 1800°F, and burnups up to 30% uranium. Mechanisms of fission-gas release from each particle type have been considered on the basis of the relations of fission-gas release to particle temperature and the ratios of the isotopes released.

A postirradiation anneal experiment designed for $Kr^{85}$ release studies is now in operation with sintered $UO_2$ pellets which have been irradiated to high burnups. These studies have shown an accelerating release rate with time and the "burst" phenomenon during isothermal operation at 1500°C.

### 22. Radiation Stability of Ceramics

Apparatus has been developed for thermal analysis of small samples of poorly conducting materials. Calibration by means of Peltier power makes the method quantitative below about 900°C.

Irradiation in a reactor causes zircon ceramic to resemble metamict zircon in that subsequent heating to successively higher temperatures may produce some or all of the following: partial annealing of damage, decomposition to zirconia and silica, and re-formation of zircon.

## PART VI. NUCLEAR SAFETY PROGRAM

Large quantities of dangerous fission products are generated in the fuel during the operation of nuclear reactors. Because of this, reactors are housed in containment vessels and located in remote areas in order to assure the public of adequate protection. Both of these precautions are costly, and it is generally conceded that the economics of nuclear power could be improved if the public safety could be reasonably assured by other means. However, relaxation of present siting criteria and/or containment philosophy requires much more knowledge of the mechanism and phenomenology of reactor accidents than now exists. Investigations are under way in the Reactor Chemistry Division, as part of the ORNL Nuclear Safety Program, to provide information which will be useful in assessing the consequences of reactor accidents.

### 23. Release of Fission Products on Out-of-Pile Melting of Reactor Fuels

Fission product release data have been obtained by use of two new techniques which permit melting

of larger amounts of irradiated $UO_2$ than was previously possible. The two scaled-up procedures gave results that are essentially in agreement and confirm most of the data obtained earlier with milligram amounts of $UO_2$ irradiated at tracer level. When 30-g quantities of tracer-irradiated $UO_2$, contained in a tungsten crucible surrounded by a helium atmosphere, were melted by use of rf heating, essentially quantitative release of rare gases and iodine, but somewhat lower releases of tellurium and cesium, were observed. Essentially no ruthenium or strontium was released. The most apparent explanation of the lower release values observed, as compared with those obtained in earlier, small-scale, experiments, is that the greatly increased volume-to-surface ratio prevailing in the new experiments resulted in a longer diffusion path for the fission products. The lack of oxygen in the helium atmosphere also contributed to the reduced ruthenium volatility.

Experiments on a similar scale, in which clad, cored $UO_2$ pellets surrounding a tungsten resistor were melted, permitted a comparison of the effect of two different metal cladding materials on fission product release. It was found that stainless steel cladding simply segregated and had little effect on release as compared with that observed from unclad $UO_2$. Molten Zircaloy, however, apparently wet the $UO_2$ and spread over its surface, producing a 100-fold smaller tellurium release and a nearly 10-fold increase in strontium release. The molten zirconium seems to serve as a getter for excess oxygen, causing increased strontium volatility, and as an alloying material with tellurium.

Hot-cell construction is under way to permit the melting of both larger quantities of irradiated $UO_2$ in tungsten crucibles and the clad $UO_2$ specimens currently being irradiated. A new ultra-high-frequency generator has been tested for use in both programs.

## 24. Release of Fission Products on In-Pile Melting of Reactor Fuels Under Transient Reactor Conditions

A series of experiments on the release of fission products from $UO_2$ melted under reactor transient conditions will be conducted in the TREAT facility at the NRTS. A program proposal that was reviewed with TREAT management resulted in an agreement on the design of the experimental assembly.

The proposed experiments will permit the study of fission product release on melting fully clad, 10%-enriched $UO_2$ in an argon-filled autoclave by means of fast transients of varying magnitude. Provision will be made for preheating the samples to 1200°C and for sampling the released gases and smoke promptly by admission through a filter into an evacuated autoclave. The fuel specimens in the first experiments in this facility will not be irradiated prior to melting, but specimens with a high degree of burnup will be melted later. Heat-transfer determinations and leakage testing of the autoclaves have been satisfactorily completed. A hazards analysis is presently being prepared and the first experiment is expected to be inserted in the reactor during the early part of 1963.

## 25. Release of Fission Products on the In-Pile Melting or Burning of Reactor Fuels

Experiments were conducted in the Oak Ridge Research Reactor to study the amounts and forms of fission products released during melting of miniature stainless-steel-clad $UO_2$ fuel elements in a helium atmosphere and burning of $UC_2$-graphite fuel specimens in air. Fission and gamma heat raised the temperature of both types of fuel element high enough to cause their destruction.

In the $UO_2$-melting experiments, nearly all the iodine, tellurium, and cesium were released from the fuel. Although more than half the strontium, zirconium, ruthenium, barium, and cerium were released from the fuel, less than 3% of these fission products and of the uranium were released from the high-temperature zone. The retention of fission products within the high-temperature zone is considered to be significant since, during an actual reactor accident, temperatures corresponding to those of the high-temperature zone in these experiments would probably occur only in the region immediately surrounding the fuel.

Release values obtained in the experiment with $UC_2$-graphite fuel were lower than those obtained in $UO_2$-melting experiments for all fission products except ruthenium, which probably formed a volatile ruthenium oxide.

Analysis of the distribution of fission products on the wall of the tube connecting the $UO_2$-melting furnace to the filter compartment showed that they

were associated with two groups of particle sizes in the millimicron range. The distribution of fission products and of uranium is being analyzed and interpreted in terms of the fractionation processes which govern the behavior of these materials.

### 26. Characterization and Control of Accident-Released Fission Products

Two methods of determining the form of radioactivity in gases were investigated. Diffusion coefficients of small particles and of radioactive vapors such as iodine are determined by measuring the distribution of radioactivity on the walls of a channel previously exposed to gas carrying radioactive materials and flowing under laminar conditions. This technique was employed to demonstrate that high-efficiency, low-pressure-drop filters removed about 10 to 75% of the activity from air streams carrying $I^{131}$ adsorbed on 0.004-$\mu$-diam $Al_2O_3$ particles. Beds containing a 0.75-in. depth of $-6$ +16 mesh activated carbon removed essentially all the iodine vapor but only 75 to 90% of the 0.003- to 0.006-$\mu$ $Al_2O_3$ particles, the higher efficiency being associated with the finer particles. Fog-condensation and foam-encapsulation methods removed 85 to 99% of these very small particles.

The second method of measuring the size of radioactive aerosols makes use of a filter having a uniform fiber diameter to permit theoretical analysis and having a layered structure to facilitate separation of the fiber bed into discrete layers for radioassay after exposure to the aerosol. Preliminary results obtained with a radioactive aerosol of 0.004- to 0.03-$\mu$ particles labeled with $Zn^{65}$ indicate that the techniques used are satisfactory.

### 27. Fission Product Transport Evaluations

Two methods of determining the heat of vaporization of radioactive species were tested with $I^{131}$-labeled iodine in the search for a technique that can be employed to identify the chemical form of fission products released in simulated reactor accident experiments. One method, which depended on the rate of transfer of iodine by helium flowing at a constant rate, gave values for the heat of vaporization of iodine ranging from 13 to 15 kcal/mole. The average value, 14.2, agrees reasonably well with the literature value of 14.9 for solid iodine. A completely sealed glass system, consisting of two small bulbs connected by a long capillary tube, comprised the sample container employed in the second method. The change in concentration of iodine vapor in one bulb which was in equilibrium with solid or liquid iodine in the other bulb was measured over a range of temperatures by means of a crystal detector. Early results obtained by this method varied over a wider range than those obtained by the transport method, but recent data indicate that this may be a useful technique and experiments are in progress to obtain a better understanding of iodine behavior in this apparatus. Evidences of adsorption of iodine on glass or quartz walls were observed in both types of experiments.

## PART VII. SUPPORT FOR OTHER ORNL PROGRAMS

### 28. Molten Fluoride Mixtures as Possible Fuel Reprocessing Solvents

A preliminary study of the ternary system LiF-$BeF_2$-$AlF_3$ was made as part of an investigation seeking high-capacity solvents for use in the Fluoride Volatility Process for recovering uranium from aluminum-based reactor fuels. The maximum capacity of this solvent at 600°C was ~31 wt % $AlF_3$.

### 29. Radioiodine-Adsorption Systems for the NS "Savannah"

Studies of the removal of radioiodine from steam-air mixtures continued in support of the NS "Savannah" program. Over 60 small-scale tests and 14 large-scale tests have been completed. Activated-charcoal units, prepared in the same manner and using materials similar to those employed in the units installed on the NS "Savannah," were utilized in the large-scale laboratory tests. These tests, conducted with continuous iodine injection at 96 to 100°C and with 80 to 90% saturated steam in air, have shown the efficiency of the charcoal unit to be (99.86 ± 0.07)% at the 95% confidence level. In-place tests of the full-scale filter-adsorber units in the reactor compartment ventilation systems of the NS

"Savannah" have been conducted with radioactive $I^{131}$ and nonradioactive $I^{127}$. The emergency ventilation system, containing activated charcoal, exhibits an efficiency generally greater than 99.9%, whereas the main ventilation system, containing no charcoal, has shown iodine-retention efficiencies ranging from 90 to 98% in several series of tests.

## 30. Effects of Radiation and Heat on Organic Materials

The acid concentration produced by irradiation of solutions of $C_2H_2Cl_4$ in $C_8F_{16}$ and in $C_{10}H_{22}$ has been measured to determine the suitability of these systems as dosimeters. The $C_8F_{16}$ solutions, to which 0.3 wt % $C_{10}H_{22}$ had been added to provide an adequate source of hydrogen, showed inconsistent acid yields unless water in excess of saturation (0.2 wt %) was present. The $C_{10}H_{22}$ solution showed a dependence on both the temperature and the dose rate during irradiation.

The investigation of differences in the effects on polystyrene of gamma radiation and mixed reactor radiation was extended to infrared and gas-chromatographic analyses. Infrared spectrum measurements showed more rapid growth of certain bands in reactor-irradiated specimens than in specimens exposed to gamma radiation alone. The volatile products of gamma irradiation of polystyrene indicated by gas chromatography were hydrogen, $G(H_2) \approx 1.5 \times 10^{-2}$ molecule per 100 ev, and benzene, $G(C_6H_6) \approx 5 \times 10^{-4}$ molecule per 100 ev.

A versatile gamma source comprising a $Co^{60}$ assembly in a 7 × 10 ft shielded compartment has been designed for the irradiation of plastics and rubbers during mechanical testing.

Pure biphenyl was pyrolyzed at 425°C under such conditions that less than 1% decomposition occurred. The initial primary products were separated in a vacuum system into three fractions having different boiling ranges and analyzed by gas chromatography. A silica-gel column in series with a molecular sieve (Linde 5A) column showed the presence of hydrogen, methane, ethane, propylene, ethylene, and propane in the gaseous products, with hydrogen as the major component. Benzene was identified as the lone intermediate-boiling component, using a column of 30 wt % Apiezon L on Chromosorb P. Terphenyl and quaterphenyl isomers comprised the high-boiling or polymeric fraction. They were identified by means of an inorganic salt column, 20 wt % LiCl on Chromosorb P. Quantitative determination of these products suggests that the pyrolytic decomposition of biphenyl proceeds essentially by symmetrical splitting of the biphenyl molecule to form phenyl radicals which either (1) add hydrogen to form benzene or (2) react with other biphenyl molecules to produce terphenyls, quaterphenyls, and hydrogen.

## 31. Chemical Support for Saline Water Program

The solubility of $CaSO_4$, a major constituent of scale formed in seawater desalination processes, has been determined in $H_2SO_4$-$H_2O$ solutions at temperatures from 125 to 350°C and at concentrations of $H_2SO_4$ from 0.1 to 1.0 *m*.

The results of preliminary corrosion tests, made with seawater at 100°C in 100-gpm dynamic loops constructed of titanium alloys, indicate the potential usefulness of aluminum alloys for service in seawater at elevated temperatures. In the absence of impingement, bulk solution velocities of up to 75 fps did not cause accelerated corrosion.

## 32. Corrosion Studies for Chemical Reprocessing Plants

The materials evaluation program for the Transuranium Processing Facility has continued. Tests with Hastelloy C have shown it to be generally unacceptable in hydrochloric acid solutions containing oxidizing agents even at temperatures as low as 35°C. Tantalum has excellent corrosion resistance in all process solutions, although the problem of hydrogen embrittlement has not been fully evaluated. Zircaloy-2 was shown to have excellent corrosion resistance in hydrochloric acid solutions, and, under certain conditions, small amounts of nitric acid in the hydrochloric acid did not result in prohibitively high rates. In addition to the tests with metals and alloys, a number of different plastics were shown to be satisfactory in the organic solutions used in various stages of the chemical process.

The corrosion program supporting the Chemical Technology Division's development of power-reactor fuel-element reprocessing schemes has involved testing many metals and alloys in numerous environments. The greatest number of

tests, however, was concerned with the selection of materials for the processing of graphite-bearing fuels and for use in the Chloride Volatility Process. In the associated waste problem, tests have been carried out in liquids, and in systems for evaporating liquid wastes to dryness followed by subsequent calcination. In addition, a number of standard acceptance tests were performed on various materials to be used in ORNL and Y-12 projects.

### 33. Chemical Support for Thermonuclear Program

Improvements in the techniques for obtaining high vacuum in large metal systems included studies on composite pumping systems, in which vapor deposition of titanium vapor is supplemented by diffusion pumps, and studies on system design for component testing. Studies of the factors affecting the operation of ionization gages for reading low pressures demonstrated the importance of considering the pumping action by the gage for high-molecular-weight (organic) species.

### 34. Research and Development on Pure Materials

Techniques of growing large (~300-g) single crystals of LiF containing no more than 10 ppm of cation contaminants were developed and employed for the production of several crystals varying in their $Li^6/Li^7$ isotopic ratio. Four such crystals were produced which were strain-free and in which hydroxyl ions were not detected.

Pure crystals of MgO were grown as the primary phase from molten fluoride mixtures at temperatures of ~800°C in thermal convection loops containing molten-salt solvents.

The investigation, development, and application of an acetylacetone solvent extraction process, which employs EDTA as a masking agent, for the preparation of high-purity BeO has continued. The distribution of the neutral beryllium acetylacetonate, its aqueous phase formation equilibria, and its aqueous solubility all were found to have a large dependence on aqueous ionic strength. These effects all are in the direction of salting out but are several times larger than is usually encountered. Data now available were used to predict beryllium extraction behavior as a function of pH, acetylacetone concentration, aqueous pH, and aqueous ionic strength. With adequate agitation, extraction rates were surprisingly rapid in view of the dehydration of the small $Be^+$ ion which is involved. The losses associated with each step in the purification process were examined; modification of the process and improvements in the equipment were made in order to achieve significantly increased process yields.

# Contents

SUMMARY ..... iii

PART I. MOLTEN-SALT REACTOR PROGRAM

1. HIGH-TEMPERATURE PHASE EQUILIBRIUM STUDIES ..... 3

Phase Equilibria Among the Fluorides ..... 3
- $LiF-UF_4$ Eutectic as a Concentrated Solution of $UF_4$ for Fuel Makeup ..... 3
- Fractionation of $LiF-BeF_2-ZrF_4-ThF_4-UF_4$ on Freezing ..... 5
- The System $LiF-ZrF_4-UF_4$ ..... 6
- Solubility of $UF_3$ in Molten Fluoride Mixtures ..... 6
- Core and Blanket Fluids for a Molten-Salt Fast Breeder Reactor ..... 7
- Liquid-Solid Equilibria Among $NaF-YF_3$ Phases ..... 7
- The System $CsF-ZrF_4$ ..... 10

Crystal Structure Investigations ..... 11
- Crystallographic Data for Some Pure Crystalline Salts ..... 11
- The Crystal Structures of $LiRbF_2$ and $LiCsF_2$ ..... 11
- X-Ray Diffraction Study of $Cs_3ZrF_7$ ..... 14
- The Crystal Structure of $Cr_2F_5$ ..... 15
- The Crystal and Molecular Structure of Xenon Tetrafluoride by Neutron Diffraction ..... 16
- A Second Crystalline Phase of $XeF_4$ ..... 16

2. COMPATIBILITY OF MSRE COMPONENTS ..... 17

Radiation Chemistry of MSR System ..... 17
- Experiment ORNL-MTR-47-4 ..... 18
- Experiment ORNL-MTR-47-5 ..... 24
- Conclusions ..... 30

Behavior of Carbon Tetrafluoride in Molten Fluorides ..... 30
- Preparation of "Reduced" Fuel Mixtures ..... 31
- $CF_4$ Reactions in the Absence of Graphite ..... 31
- $CF_4$ Reactions at a Graphite-Salt Interface ..... 32
- Attempted Solubility Measurements of $CF_4$ ..... 33

Fluorine Chemistry Studies ..... 34
- Fluorine Gas Control Unit ..... 34
- Preparation of Xenon Tetrafluoride ..... 35
- Reaction of Fluorine with Reduced Salt ..... 35

Evolution of Water Vapor from Graphite ..... 36
- Experimental ..... 36
- Discussion of Results ..... 36

Oxide Behavior in Flush Salt–Fuel Salt Mixtures ..... 38

3. PHYSICAL CHEMISTRY OF MOLTEN-SALT SYSTEMS ..... 41
Freezing-Point Depressions in Sodium Fluoride ..... 41
Effect of Trivalent Fluorides ..... 41
Effect of $CdF_2$ ..... 43
Activity Coefficients of $ZrF_4$ in the $LiF-ZrF_4$ System ..... 44
Vapor Pressure of Molten Fluoride Mixtures ..... 46
Technique and Apparatus ..... 46
MSRE Fuel System ..... 46
System $LiF-BeF_2$ ..... 46
Densities in the $LiF-ThF_4$ System ..... 47
Viscosities of Molten Salts ..... 48

4. FLUORIDE SALT PRODUCTION ..... 51
Fluoride Production Operations ..... 51
Plant Modifications ..... 51
Anticipated MSRE Production ..... 53
Raw Material Procurement ..... 53
Lithium Fluoride ..... 53
Zirconium Fluoride ..... 57
Beryllium Fluoride ..... 57
General Chemical Specifications ..... 57
Removal of Oxides from the Engineering Test Loop Salt Mixture ..... 58

## PART II. SUPPORT FOR AQUEOUS REACTOR PROGRAMS

5. CHEMISTRY OF PRESSURIZED-WATER REACTOR SYSTEM ..... 61

6. CORROSION BY SOLUTIONS ..... 64
Effect of Heat Flux on the Corrosion of Aluminum by Water ..... 64
Introduction ..... 64
Results ..... 64
Discussion ..... 66
Corrosion Studies for the High Flux Isotope Reactor ..... 66
Acceptance Tests ..... 68

7. MECHANISM OF CORROSION OF ZIRCALOY-2 ..... 69
Effect of Reactor Radiations on Zircaloy-2 Corrosion in High-Temperature Aqueous Environments ..... 69
Oxide Growth and Capacitance on Preirradiated Zircaloy-2 ..... 70
Electrochemistry of High-Temperature Aqueous Zircaloy-2 Corrosion ..... 72
Kinetics of the Initial Corrosion ..... 72
Experiments at Long Exposure Times ..... 75
Apparatus ..... 75

8. PHYSICAL CHEMISTRY OF HIGH-TEMPERATURE AQUEOUS SYSTEMS ..... 77
The Electrical Conductivity of Aqueous Solutions from 25 to 800°C and at Pressures up to 4000 Bars ..... 77

Introduction ..... 77
Experimental Procedures ..... 77
Results and Discussion ..... 78

Phase Studies of Liquid-Liquid Immiscibility and Critical Phenomena in the Systems $UO_3$-CuO-$SO_3$-$D_2O$, $UO_3$-NiO-$SO_3$-$D_2O$, and $UO_3$-CuO-NiO-$SO_3$-$D_2O$ from 260 to 410°C ..... 83
Introduction ..... 83
Experimental ..... 83
Results and Discussion ..... 83

Glass-to-Metal Connector for Visual Observation of the Effect of Pressure on Phase Equilibria ..... 87

Effect of Pressure on Liquid-Liquid Immiscibility in the System $UO_2SO_4$-$H_2O$ and Liquid–Supercritical Fluid Equilibria in the System $UO_2SO_4$-$H_2SO_4$-$H_2O$, 290 to 430°C, 75 to 300 Bars ..... 88
Introduction ..... 88
Experimental ..... 88
Results and Discussion ..... 89

The System $Li_2SO_4$-$H_2SO_4$-$H_2O$ and Its $D_2O$ Analog, 200 to 470°C: Solubilities and Critical Phenomena ..... 92
Introduction ..... 92
Experimental Procedures ..... 92
Results ..... 92

Osmotic Coefficients of Aqueous Electrolytes at Elevated Temperatures ..... 94
Experimental Results ..... 94
Discussion ..... 95

Hydrolysis of Thorium(IV) at 95 and 0°C ..... 96

## PART III. HETEROGENEOUS SYSTEMS

9. COMPATIBILITY OF COATED FUEL PARTICLES AND MATRIX GRAPHITES WITH LIQUID COOLANTS ..... 101

Factors Limiting High Rates of Heat Transfer from Fueled and Unfueled Graphite Rods to Flowing Pressurized Water ..... 101

Gamma Irradiation of Coated-Particle and Matrix Materials in High-Temperature Liquids Including MSRE Fuel Salt ..... 107
Materials Used in Gamma Irradiation Studies ..... 107
Pressurized-Water Autoclave Irradiation ..... 108
Santowax Autoclave Irradiation ..... 108

Compatibility of Coated-Particle Fuel Element Materials with Molten Fluoride Salts ..... 109

10. RHEOLOGY OF SUSPENSIONS OF THORIA FROM FIRST IN-PILE SLURRY LOOP EXPERIMENT ..... 111

11. IN-PILE LOOP STUDIES OF AQUEOUS THORIUM OXIDE SLURRIES ..... 114
Introduction ..... 114
In-Pile Operation ..... 114
Slurry Circulation ..... 115
Measurements of Recombination of Hydrogen-Oxygen Mixtures in In-Pile Loop ..... 116

Corrosion ..... 116
Effects on Slurry Particles ..... 116
Determination of Average Slurry Flux and Total Fissions ..... 117

12. CONSTRUCTION AND OUT-OF-PILE TESTING OF THIRD IN-PILE SLURRY LOOP EXPERIMENT ..... 120

13. SURFACE CHEMISTRY OF AQUEOUS SYSTEMS ..... 121

Ionic Adsorption Equilibria ..... 121
Adsorption by Fused $ThO_2$ ..... 121
Blank Adsorption Run ..... 123
Fusing of $ThO_2$ in a Plasma Torch ..... 124

The Heat of Immersion of Thorium Oxide in Water ..... 124
Experimental ..... 124
Results and Discussion ..... 126

14. PHASE-EQUILIBRIUM STUDIES IN THE SYSTEM $UO_2$-$ThO_2$-$O_2$ ..... 130

Optical and X-Ray Analysis of Air-Equilibrated Mixtures ..... 130
Equilibration and Examination of Urania-Thoria Mixtures ..... 130
Composition-Temperature Relations ..... 130
Identification of $U_3O_8$ ..... 132
Unidentified Phases ..... 134

Oxygen Dissociation Pressure Studies ..... 134
Introduction ..... 134
Preparation of Urania-Thoria Solid Solutions ..... 134
Dissociation Pressure Measurements ..... 138

## PART IV. SUPPORT FOR HIGH-TEMPERATURE SOLID-FUELED REACTORS

15. DIFFUSION PROCESSES ..... 143

Transport of Gases in Porous Media ..... 143
Discussion of the "Dusty-Gas" Model ..... 143
Experimental ..... 145
Additional Programs ..... 145
Applications ..... 146

Diffusion of Fuel in Ceramic Materials ..... 146
Uranium Diffusion in Pyrolytic Carbon ..... 149
Uranium Migration in Porous Graphites ..... 151
Diffusion in Beryllium Oxide Matrices ..... 153

16. REACTIONS OF GRAPHITE AND PYROLYTIC CARBON WITH GASES ..... 157

Reaction of Graphite with Carbon Dioxide ..... 157

Reaction of Pyrolytic-Carbon-Coated Particles with Water Vapor ..... 158

17. MEASUREMENT OF TEMPERATURE IN REACTOR ENVIRONMENTS ..... 163

Stability of Chromel-P/Alumel Thermocouples Sheathed in Stainless Steel ..... 163

Thermocouple Stability Under PBRE Conditions ..... 166

Refractory Metal Thermocouples ..... 167

Thermocouple Transmutation Studies ..... 168

18. ALTERNATE COOLANTS FOR GAS-COOLED REACTORS ..... 170
Thermal and Radiation Stability of Proposed Nuclear Reactor Gas Coolants ..... 170
Heat Transfer Properties of Dissociating Gaseous Mixtures ..... 171

19. EFFECT OF IRRADIATION ON BERYLLIUM OXIDE ..... 176
Observations from Experiment 41-6 ..... 176
Observations from Experiment 41-7 ..... 178
Visual Observation of Specimens ..... 178
Crushing Strength ..... 178
Thermal Conductivity ..... 178
Dimensional Changes ..... 179
Metallographic Examinations ..... 179
Discussion ..... 184

## PART V. IRRADIATION BEHAVIOR OF HIGH-TEMPERATURE REACTOR MATERIALS

20. POSTIRRADIATION EXAMINATION OF FUEL MATERIALS ..... 189
Fuel Materials with Metal Claddings ..... 189
Postirradiation Examination of $UO_2$ Fuel Capsules – EGCR Program ..... 189
Maritime Reactor Fuel – Postirradiation Examination ..... 196
Fast-Breeder Reactor Fuel – Postirradiation Examination ..... 197
Fuel Cycle Program – Postirradiation Examination of Fuel ..... 200
Systems Without Metal Cladding ..... 200
Postirradiation Examination of Coated Particles ..... 200
Postirradiation Examination of Graphite-Matrix Fuel ..... 201

21. FISSION-GAS RELEASE ..... 207
Continuous Release of Fission Gas During Irradiation of $UO_2$ ..... 207
Continuous Release of Fission Gas During Irradiation of $UC_2$ Coated Particles ..... 210
Fission-Gas Release from High-Burnup Fuel ..... 214

22. RADIATION STABILITY OF CERAMICS ..... 217
Apparatus for Thermal Analysis ..... 217
Radiation Stability of a Zircon Ceramic ..... 217

## PART VI. NUCLEAR SAFETY PROGRAM

23. RELEASE OF FISSION PRODUCTS ON OUT-OF-PILE MELTING OF REACTOR FUELS ..... 221
Fission-Product Release from $UO_2$ Melted by the Tungsten-Crucible Method ..... 221
Release as a Function of Length of Time in the Molten State ..... 221
Size of Uranium Oxide Particles Plated Out from Molten $UO_2$ ..... 222
Fission-Product Release from $UO_2$ Melted by a Centered Tungsten Resistor ..... 226
Comparison with Previous Melting Experiments ..... 226
Effect of Cladding Material on Fission-Product Release ..... 228
Scaleup of the Tungsten-Resistor Melting Method to a Multiple-Pin Assembly ..... 230
Hot-Cell Construction for Melting MTR-Irradiated Capsules ..... 232

24. RELEASE OF FISSION PRODUCTS ON IN-PILE MELTING OF REACTOR FUELS UNDER TRANSIENT REACTOR CONDITIONS ..... 233
Hazards Analysis ..... 233
Gas Transfer ..... 233
Melting Schedule ..... 235
25. RELEASE OF FISSION PRODUCTS ON THE IN-PILE MELTING OR BURNING OF REACTOR FUELS ..... 236
Release of Fission Products by In-Pile Melting of $UO_2$ ..... 236
Release of Fission Products by In-Pile Burning of $UC_2$-Graphite Fuel ..... 240
Determination of Particle Size and Fission Product Distribution by Diffusion Coefficient Measurement ..... 240
Fractionation Studies ..... 242
Summary ..... 243
26. CHARACTERIZATION AND CONTROL OF ACCIDENT-RELEASED FISSION PRODUCTS ..... 244
Diffusional Characterization of Millimicron-Size Radioactive Aerosols and Their Removal from Reactor Gases ..... 244
Behavior of Millimicron-Size Particles in Conventional Gas-Cleaning Systems ..... 245
Removal of Millimicron Particles by Less-Conventional Methods ..... 246
Measurement of Radioactive Aerosols by Use of Fibrous Filters ..... 248
27. FISSION PRODUCT TRANSPORT EVALUATIONS ..... 251
Particle-Size Studies ..... 251
Identification of Chemical Species ..... 251

## PART VII. SUPPORT FOR OTHER ORNL PROGRAMS

28. MOLTEN FLUORIDE MIXTURES AS POSSIBLE FUEL REPROCESSING SOLVENTS ..... 257
29. RADIOIODINE-ADSORPTION SYSTEMS FOR THE NS "SAVANNAH" ..... 260
Laboratory Iodine Studies ..... 260
Radioiodine Tests on Board NS "Savannah" ..... 262
Development of In-Place Test Using Stable Iodine ..... 264
Development of Environmental Monitoring Cartridge ..... 265
30. EFFECTS OF RADIATION AND HEAT ON ORGANIC MATERIALS ..... 267
Radiation Dosimetry ..... 267
Effects of Radiation on Polymers ..... 269
Differences in the Effects of Gamma and Reactor Radiation on Polystyrene ..... 269
Infrared Analysis ..... 269
Gas-Chromatographic Analysis ..... 270
Infrared Studies of Elastomers ..... 271
A Versatile Gamma Irradiation Facility ..... 272
Pyrolysis and Radiolysis of Biphenyl ..... 272

31. CHEMICAL SUPPORT FOR SALINE WATER PROGRAM ..... 277
Determination of the Solubility of $CaSO_4$ in $H_2SO_4$-$H_2O$ Solutions at High Temperature ..... 277
The Solubility of $CaSO_4$ in $H_2SO_4$-$H_2O$ Solutions, 125 to 350°C ..... 277
Corrosion of Aluminum Alloys in Salt Solutions ..... 279

32. CORROSION STUDIES FOR CHEMICAL REPROCESSING PLANTS ..... 280
Corrosion Studies for the Transuranium Processing Facility ..... 280
Corrosion Testing Program in Support of Power-Reactor Fuel-Element Reprocessing ..... 282

33. CHEMICAL SUPPORT FOR THERMONUCLEAR PROGRAM ..... 283
Vacuum Studies ..... 283
Ionization Gage Studies ..... 283

34. RESEARCH AND DEVELOPMENT ON PURE MATERIALS ..... 285
Preparation of Single-Crystal LiF ..... 285
Crystals Produced ..... 285
Preparation of Charge ..... 285
Crystal Growth from the Melt ..... 291
Discussion ..... 294
Preparation of Single-Crystal MgO ..... 294
Purification of Beryllium by Acetylacetone-EDTA Solvent Extraction ..... 297
Chemistry of Extraction ..... 297
Increased Processing Efficiency ..... 299

PUBLICATIONS ..... 301

PAPERS PRESENTED AT SCIENTIFIC AND TECHNICAL MEETINGS ..... 307

# Part I

# Molten-Salt Reactor Program

# 1. High-Temperature Phase Equilibrium Studies

Experimental studies of many fluoride systems which have potential use in molten-salt-reactor technology have been continued. The data from which phase diagrams have been derived were obtained from thermal-gradient-quenching experiments, thermal analyses of melts (using both heating and cooling cycles), and visual observations of phase changes produced by heating and cooling.[1] In samples from all experiments, the solid phases were identified by use of the polarizing light microscope and the x-ray diffractometer. The crystal structures of new compounds isolated in the course of these studies have been determined with single-crystal x-ray diffraction techniques.

## PHASE EQUILIBRIA AMONG THE FLUORIDES

R. E. Thoma

H. A. Friedman
G. M. Hebert
B. J. Sturm
H. Insley[2]
T. N. McVay[3]
G. D. Robbins[4]
H. Steinfink[5]
C. F. Weaver
R. L. Boles[6]
W. H. Zahler[7]

A simplification was made in the MSRE fuel by omitting $ThF_4$ as a component. The required concentration of $UF_4$ in the thorium-free fuel was consequently reduced to 0.15 mole %. Investigations which sought to describe fuel phase behavior then necessarily changed emphasis from the quinary system $LiF-BeF_2-ZrF_4-ThF_4-UF_4$ to the ternary solvent system $LiF-BeF_2-ZrF_4$ in order to prescribe the most suitable solvents for $UF_4$ in the lower concentration now needed for criticality. Studies pertaining to fuel makeup and segregation in the quinary system that includes $ThF_4$ in MSRE fuels were nearing completion at approximately the same time that it was proposed that the inconvenience of carrying token amounts of $ThF_4$ could be avoided. The conclusions from these investigations are applicable, in a representative fashion at least, to fuels from the quaternary system that do not contain $ThF_4$. These results are presented as examples of the type of behavior that can be expected.

### $LiF-UF_4$ Eutectic as a Concentrated Solution of $UF_4$ for Fuel Makeup

One of the means considered for fueling the MSRE included an initial nonnuclear operation with a solvent mixture followed by conversion to the fuel composition $LiF-BeF_2-ZrF_4-ThF_4-UF_4$ (70-23-5-1-1 mole %) by titrating to criticality with the liquid $LiF-UF_4$ eutectic mixture (73-27 mole %; melting point, 527°C). It has also been proposed[8] that the fuel makeup salt be added as the frozen $LiF-UF_4$ eutectic mixture. A study of the phase behavior and characteristics of that composition section which gives all possible combinations of solvent and concentrate shows (Fig. 1.1 and Table 1.1) that the melting temperature of the $LiF-UF_4$ mixture is higher than that of any intermediate

[1] H. A. Friedman, G. M. Hebert, and R. E. Thoma, *Thermal Analysis and Gradient Quenching Apparatus and Techniques for the Investigation of Fused Salt Phase Equilibria*, ORNL-3373 (Dec. 18, 1962).

[2] Consultant, National Bureau of Standards (retired).

[3] Consultant, University of Alabama (retired).

[4] Summer employee from the University of North Carolina.

[5] Summer research participant from the University of Texas.

[6] Summer employee from the University of Tennessee.

[7] Summer employee from Alfred University.

[8] P. N. Haubenreich and J. R. Engel, *Safety Calculations for MSRE*, ORNL TM-251, p 22 (May 15, 1962).

**Table 1.1. Phase Transition Temperatures in the System $LiF-BeF_2-ZrF_4-ThF_4-UF_4$ and Intermediate Compositions Between $LiF-UF_4$ (73-27 mole %) and $LiF-BeF_2-ZrF_4-ThF_4-UF_4$ (70-23-5-1-1 mole %)**

| Composition (mole %) | | | | | Transition Temperature (°C) | Phases Observed Above Transition Temperature | Phases Observed Below Transition Temperature |
|---|---|---|---|---|---|---|---|
| LiF | $BeF_2$ | $ZrF_4$ | $ThF_4$ | $UF_4$ | | | |
| 72.4 | 4.6 | 1.0 | 21.8 | 0.2 | 476 ± 2[a] | *L*[b] | *L* + $4LiF{\cdot}UF_4$ *ss*[c] + $7LiF{\cdot}6(U,Th)F_4$ *ss* |
| | | | | | 465 ± 2 | *L* + $4LiF{\cdot}UF_4$ *ss* + $7LiF{\cdot}6(U,Th)F_4$ *ss* | *L* + LiF + $7LiF{\cdot}6(U,Th)F_4$ *ss* |
| | | | | | 426 ± 2 | *L* + LiF + $7LiF{\cdot}6(U,Th)F_4$ *ss* | *L* + LiF + $7LiF{\cdot}6(U,Th)F_4$ *ss* + $6LiF{\cdot}BeF_2{\cdot}ZrF_4$ |
| | | | | | 421 ± 2 | *L* + LiF + $7LiF{\cdot}6(U,Th)F_4$ *ss* + $6LiF{\cdot}BeF_2{\cdot}ZrF_4$ | *L* + LiF + $7LiF{\cdot}6(U,Th)F_4$ + $6LiF{\cdot}BeF_2{\cdot}ZrF_4$ + $2LiF{\cdot}BeF_2$ |
| | | | | | 417 ± 2 | *L* + LiF + $7LiF{\cdot}6(U,Th)F_4$ + $6LiF{\cdot}BeF_2{\cdot}ZrF_4$ + $2LiF{\cdot}BeF_2$ | LiF + $7LiF{\cdot}6(U,Th)F_4$ *ss* + $6LiF{\cdot}BeF_2{\cdot}ZrF_4$ + $2LiF{\cdot}BeF_2$ |
| 71.8 | 9.2 | 2.0 | 16.6 | 0.4 | 457 ± 3 | *L* | *L* + LiF + $7LiF{\cdot}6(U,Th)F_4$ *ss* |
| | | | | | 426 ± 2 | *L* + LiF + $7LiF{\cdot}6(U,Th)F_4$ *ss* | *L* + LiF + $7LiF{\cdot}6(U,Th)F_4$ + $6LiF{\cdot}BeF_2{\cdot}ZrF_4$ |
| | | | | | 422 ± 2 | *L* + LiF + $7LiF{\cdot}6(U,Th)F_4$ + $6LiF{\cdot}BeF_2{\cdot}ZrF_4$ | LiF + $2LiF{\cdot}BeF_2$ + $7LiF{\cdot}6(U,Th)F_4$ *ss* + $6LiF{\cdot}BeF_2{\cdot}ZrF_4$ |
| 71.2 | 13.8 | 3.0 | 11.4 | 0.6 | 458 ± 2 | *L* | *L* + LiF |
| | | | | | 439 ± 2 | *L* + LiF | *L* + LiF + $7LiF{\cdot}6(U,Th)F_4$ *ss* |
| | | | | | 432 ± 2 | *L* + LiF + $7LiF{\cdot}6(U,Th)F_4$ *ss* | *L* + LiF + $7LiF{\cdot}6(U,Th)F_4$ *ss* + $6LiF{\cdot}BeF_2{\cdot}ZrF_4$ |
| | | | | | 424 ± 2 | *L* + LiF + $7LiF{\cdot}6(U,Th)F_4$ *ss* + $6LiF{\cdot}BeF_2{\cdot}ZrF_4$ | LiF + $2LiF{\cdot}BeF_2$ + $7LiF{\cdot}6(U,Th)F_4$ *ss* + $6LiF{\cdot}BeF_2{\cdot}ZrF_4$ |
| 70.6 | 18.4 | 4.0 | 6.2 | 0.8 | 436 ± 2 | *L* | *L* + $6LiF{\cdot}BeF_2ZrF_4$ |
| | | | | | 428 ± 2 | *L* + $6LiF{\cdot}BeF_2{\cdot}ZrF_4$ | *L* + $2LiF{\cdot}BeF_2$ + $6LiF{\cdot}BeF_2{\cdot}ZrF_4$ + $7LiF{\cdot}6(U,Th)F_4$ *ss* |
| | | | | | 424 ± 2 | *L* + $2LiF{\cdot}BeF_2$ + $6LiF{\cdot}BeF_2{\cdot}ZrF_4$ + $7LiF{\cdot}6(U,Th)F_4$ *ss* | $2LiF{\cdot}BeF_2$ + $6LiF{\cdot}BeF_2{\cdot}ZrF_4$ + $7LiF{\cdot}6(U,Th)F_4$ *ss* |
| 70.0 | 23.0 | 5.0 | 1.0 | 1.0 | 440 ± 2 | *L* | *L* + $6LiF{\cdot}BeF_2{\cdot}ZrF_4$ |
| | | | | | 431 ± 2 | *L* + $6LiF{\cdot}BeF_2{\cdot}ZrF_4$ | *L* + $2LiF{\cdot}BeF_2$ + $6LiF{\cdot}BeF_2{\cdot}ZrF_4$ |
| | | | | | 429 ± 2 | *L* + $2LiF{\cdot}BeF_2{\cdot}6LiF{\cdot}BeF_2{\cdot}ZrF_4$ | $2LiF{\cdot}BeF_2$ + $6LiF{\cdot}BeF_2{\cdot}ZrF_4$ + $7LiF{\cdot}6(U,Th)F_4$ *ss* |

[a]The uncertainty in temperature shown in this column indicates the temperature differences between the quenched samples from which the values were obtained.

[b]The symbol *L* refers to liquid (observed as glass or quench growth).

[c]The term *ss* means solid solution.

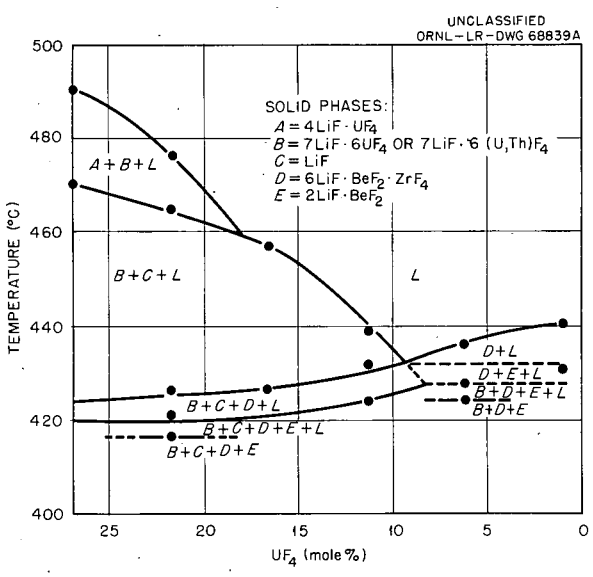


**Fig. 1.1. The Section $LiF\text{-}UF_4$ (73-27 mole %) – $LiF\text{-}BeF_2\text{-}ZrF_4\text{-}ThF_4\text{-}UF_4$ (70-23-5-1-1 mole %).**

composition formed during fueling, that at least four crystalline compounds appear as primary phases at various intermediate compositions, and that uranium and thorium crystallize together in a single solid-solution phase. From the phase relations observed in this composition section it appears that the $LiF\text{-}UF_4$ eutectic mixture should serve as a suitable fueling mixture for the MSRE. At decreasing concentrations of $UF_4$, uranium-containing phases precipitate later in the crystallizing sequence. In the fuel itself, the uranium compound $7LiF\cdot6(U,Th)F_4$ precipitates as the tertiary phase, and solids that do not contain $UF_4$ are formed during crystallization of the primary and secondary phases.

## Fractionation of $LiF\text{-}BeF_2\text{-}ZrF_4\text{-}ThF_4\text{-}UF_4$ on Freezing

An assumed sequence of equilibrium fractionations in the freezing of the five-component MSRE fuel mixture $LiF\text{-}BeF_2\text{-}ZrF_4\text{-}ThF_4\text{-}UF_4$ (70-23-5-1-1 mole %) was studied by quenching tests to provide information regarding (1) the fraction of $ZrF_4$ remaining in the liquid state at the onset of crystallization of phases containing $UF_4$ and whether this $ZrF_4$ concentration was adequate for protection against precipitation of $UO_2$, (2) the concentration of uranium in the crystalline equilibrium phases within which it is contained during freezing and the relative position of these phases in the sequence of crystallization reactions, and (3) the approximate concentration of $BeF_2$ in the liquid remaining at temperatures just above the solidus.

Although only an exploratory study of the freezing reactions was made, some qualitative statements regarding the crystallization are warranted. During freezing, the $ZrF_4$ concentration in the liquid fraction of the mixture is reduced as the primary and secondary phases ($6LiF\cdot BeF_2\cdot ZrF_4$ and $2LiF\cdot BeF_2$) are formed, while the $UF_4$ concentration within the liquid is increased and the zirconium-to-uranium concentration ratio is decreased. As noted previously,[9] the limit of protection can be exceeded.

The apparent solidus temperature for the five-component mixture is 429°C. Comparison with solidus values in the limiting $LiF\text{-}BeF_2\text{-}MF_4$ systems implies that the composition of the five-component liquid at the solidus consists of no more than 40 mole % $BeF_2$. The relatively short temperature interval required for complete freezing is not conducive to extensive segregation or to a large difference in the average composition of the initial and final residual liquids. Hence the products of crystallization do not contain so much free $BeF_2$ that the cooled fuel mixture should be expected to be very hygroscopic. The last solid phase observed on freezing the fuel mixture is $7LiF\cdot6(U,Th)F_4$, which contains 13.3 mole % $UF_4$. The proportion of $UF_4$ was determined by two independent methods: (1) by calculation of the material balance and (2) from measurements of the refractive indices of solid solution. Three nonhygroscopic solid phases were found in melts cooled under equilibrium conditions: $6LiF\cdot BeF_2\cdot ZrF_4$, $2LiF\cdot BeF_2$, and $7LiF\cdot6(U,Th)F_4$. It is noted that specimens obtained from a variety of experiments and experimental engineering tests, in which equilibrium cooling did not occur, often contain the compounds $3LiF\cdot ZrF_4$, $2LiF\cdot ZrF_4$, $2LiF\cdot BeF_2$, and $7LiF\cdot6(U,Th)F_4$, rather than the equilibrium

[9] *MSRP Progr. Rept. Aug. 31, 1961*, ORNL-3215, p 124.

solids. Since crystallization reactions in large volumes of molten $LiF-BeF_2-ZrF_4-ThF_4-UF_4$ mixtures sometimes do not proceed under equilibrium conditions, additional studies of nonequilibrium fractionation may be required in the future.

### The System $LiF-ZrF_4-UF_4$

Previous experience with MSRE fuel mixtures consisting of $LiF-BeF_2-ZrF_4-UF_4-ThF_4$ has not suggested that $U^{4+}$ ions substitute in $Zr^{4+}$ sites in the $LiF-ZrF_4$ compounds, $3LiF \cdot ZrF_4$, $2LiF \cdot ZrF_4$, or $3LiF \cdot 4ZrF_4$. The fact that $ZrF_4$ and $UF_4$ form a continuous series of solid solutions suggested that conclusions regarding the low solubility of $UF_4$ in $LiF-ZrF_4$ mixtures be tested. For this reason, an investigation of the system $LiF-ZrF_4-UF_4$ was initiated. The results of preliminary experiments have established some of the temperature-composition relations along boundary paths separating the primary phase fields of $LiF \cdot 4UF_4$, $7LiF \cdot 6UF_4$, $2LiF \cdot ZrF_4$, and $3LiF \cdot 4ZrF_4$. Data from these experiments show the occurrence of two invariant points, namely, the peritectic involving the solid phases $LiF \cdot 4UF_4$, $7LiF \cdot 6UF_4$, and $2LiF \cdot ZrF_4$ at $LiF-ZrF_4-UF_4$ (60-14-26 mole %) and at 541°C, and the eutectic involving the solid phases $3LiF \cdot ZrF_4$, $2LiF \cdot ZrF_4$, and $7LiF \cdot 6UF_4$ at $LiF-ZrF_4-UF_4$ (62-24-14 mole %) and at 539°C. Optical properties and x-ray diffraction data obtained from each of the solid phases crystallizing from these and other $LiF-ZrF_4-UF_4$ mixtures were identical with those derived for the pure $LiF-ZrF_4$ and $LiF-UF_4$ phases, and therefore indicate that no appreciable exchange of $Zr^{4+}$ and $U^{4+}$ ions occurs in the above compounds.

### Solubility of $UF_3$ in Molten Fluoride Mixtures

Results of radiation interaction with MSRE fuel materials (Chap. 2) indicate that the fuel mixture may experience a reducing environment as a part of MSRE operating conditions. For this reason, experiments were initiated within the last few months whose purpose was to examine the solubility and phase behavior of $UF_3$ in $LiF-BeF_2-ZrF_4-UF_4$ and related mixtures. Measurements of the $PuF_3$ solubility in molten $LiF-BeF_2$ mixtures were reported by Barton,[10] who showed that in $LiF-BeF_2$ the solubility ranges from 0.16 to 1.0 mole % at 550°C and from 0.4 to 2.5 mole % at 650°C. The solubility of $UF_3$ under the same conditions is expected to be approximately equal to that of $PuF_3$. Preliminary examinations were made of the following systems: $UF_3-UF_4$, $LiF-UF_3-UF_4$, $LiF-BeF_2-UF_3$, and $LiF-BeF_2-ZrF_4-UF_3$. A short summary of the results obtained is given below.

**System $UF_3-UF_4$.** – No intermediate compounds are formed in this system. Results of thermal-gradient-quenching experiments indicate that the freezing-point depressions are rather large, resulting in the occurrence of a eutectic in the system at 25 mole % $UF_3$ and at 860°C. Though no appreciable solubility of $U^{3+}$ in $UF_4$ was observed, $UF_3$ appears to be capable of containing approximately 35 mole % $UF_4$ at the solidus. Optical properties of the saturated $UF_3$ solid solution differ from those of pure $UF_3$ only in their slightly increased double refraction and slightly reduced refractive index (~1.72).

**System $LiF-UF_3-UF_4$.** – The liquidus surface of the $LiF-UF_3-UF_4$ system is dominated by the primary phase of $UF_3-UF_4$ solid solution, which extends to within 5 mole % of the $LiF-UF_4$ limiting system. A somewhat surprising observation is that a significant number of $U^{4+}$ sites in the crystalline compounds $7Li \cdot 6UF_4$ and $LiF \cdot 4UF_4$ can be occupied by $U^{3+}$. Uranium trifluoride is only slightly soluble in molten fluoride mixtures at ~500°C because of its high melting point (~1400°C); however, mixtures having compositions near that of the $LiF-UF_4$ eutectic (27 mole % $UF_4$) can accommodate approximately 5 mole % of the $UF_3$ in the liquid state in the temperature range 500 to 550°C. In this composition region the crystallizing solids are $4LiF \cdot UF_4$, LiF, and $UF_3$.

**System $LiF-BeF_2-UF_3$.** – The major fraction of the liquidus surface in the system $LiF-BeF_2-UF_3$ consists of the primary phase fields of LiF and $UF_3$. The boundary curve separating the LiF and $UF_3$ primary phase fields lies principally between 70 and 75 mole % LiF, though it terminates in a eutectic tentatively established as $LiF-BeF_2-UF_3$ (68-30-2 mole %) and at 450°C. The investigation has been confined to compositions containing more than 60 mole % LiF. Within this composition region no ternary compounds have been observed. Though no solubility has been noted of $UF_3$ in $LiF-BeF_2$ solid phases, the thermal-gradient-quenching data

[10] C. J. Barton, *J. Phys. Chem.* **64**, 306 (1960).

indicate that disproportionation of $UF_3$ proceeds more rapidly in this system as temperatures are increased from about 450 to 700°C.

**System $LiF-BeF_2-ZrF_4-UF_3$.** —Thermal-gradient-quenching experiments were conducted with the purpose of determining the solubility of $UF_3$ in the MSRE solvent mixture $LiF-BeF_2-ZrF_4$ (67-29-4 mole %). Mixtures containing 0.5 to 2.0 mole % $UF_3$ were equilibrated in the temperature range 425 to 550°C and quenched. Uranium trifluoride was observed as the primary phase at 471°C for the composition containing 1.5 mole % $UF_3$, though as the secondary phase at lower concentrations. The solid phases crystallizing from these mixtures consisted of $2LiF \cdot BeF_2$, $6LiF \cdot BeF_2 \cdot ZrF_4$, and $UF_3$. The results of these experiments suggest the capability of the MSRE fuel to retain $UF_3$ in a dissolved state during approximately the same operating conditions as would be employed for MSRE.

The identity and relative quantity of coexisting phases in $UF_3$-containing species quenched from temperatures in the range 400 to 600°C indicate that the disproportionation of $UF_3$ proceeds more rapidly above the liquidus temperature, though only very slowly below the liquidus. It was suggested[11] that at temperatures below the liquidus a layer of the crystalline primary phase coated the interior surfaces of the nickel quench tubes used in these experiments and minimized the loss of $U^0$ through alloy formation with the nickel. Future experiments in which liquid-solid mixtures of $UF_3$ are annealed for comparably long periods (2 to 4 weeks) will necessarily utilize more nearly inert containers.

## Core and Blanket Fluids for a Molten-Salt Fast Breeder Reactor

A conceptual model of a molten-salt fast breeder reactor utilizes a core fluid of $NaF-KF-UF_4$ and a blanket fluid consisting of $NaF-KF-ThF_4$. A previous investigation[12] of the fuel system $NaF-KF-UF_4$ showed that the lowest-melting composition in the system has the composition $NaF-KF-UF_4$ (50-22-28 mole %; melting point, ~450°C). The melting temperature of this mixture is sufficiently low to make it useful as the core fluid for the reactor. A preliminary investigation of similar compositions in the corresponding $ThF_4$ system indicated the presence of a eutectic melting at ~570°C. Optical and x-ray examination of the crystallized $NaF-KF-ThF_4$ mixtures indicated the occurrence of the subsystem $NaF-2NaF \cdot ThF_4-NaF \cdot KF \cdot ThF_4$. The compound $NaF \cdot KF \cdot ThF_4$ discovered in this investigation is isomorphous with its uranium analog and is uniaxial (–) with $N_\omega$ = 1.454 and $N_\epsilon$ = 1.448.

## Liquid-Solid Equilibria Among $NaF-YF_3$ Phases

An investigation of phase equilibria in the system $NaF-YF_3$ was completed. The phase diagram for this system, shown in Fig. 1.2, because of the isomorphism of $YF_3$ with the trifluorides of the rare-earth elements samarium through lutetium, is expected to serve as an approximate model for the phase behavior in each of the binary systems $SmF_3$ through $LuF_3$ with NaF. The phase equilibrium diagram of the system $NaF-YF_3$ contains several features which have seldom if ever been observed in phase behavior among salt mixtures. Of particular interest is the behavior near the middle of the diagram, where the two intermediate compounds $NaF \cdot YF_3$ and $5NaF \cdot 9YF_3$ crystallize from the melt as fluorite-like cubic crystals, form a continuous series of solid solutions with the maximum melting temperature at the latter composition, and invert to other forms at lower temperatures.

Temperatures and compositions of invariant and singular points are given in Table 1.2.

Though previous investigators have observed the marked composition variability of the fluorite cubic $NaF-YF_3$ phase, no consensus was reached as to its composition limits. Dergunov[13] regarded the entire system as comprised of a continuous solid solution of the components. Hund[14] concluded that fluorite $NaYF_4$ phase extends to 50–75% $YF_3$. In an attempt to prepare a cubic modification of $YF_3$ in an aqueous solution of NaF and

[11] F. F. Blankenship, private communication.

[12] C. J. Barton, L. M. Bratcher, and W. R. Grimes, *Phase Diagrams of Nuclear Reactor Materials*, ORNL-2548, p 103 (Nov. 6, 1959).

[13] E. P. Dergunov, *Dokl. Akad. Nauk SSSR* **60**, 1185 (1948).

[14] F. Hund, *Z. Anorg. Allgem. Chem.* **261**, 106 (1950).

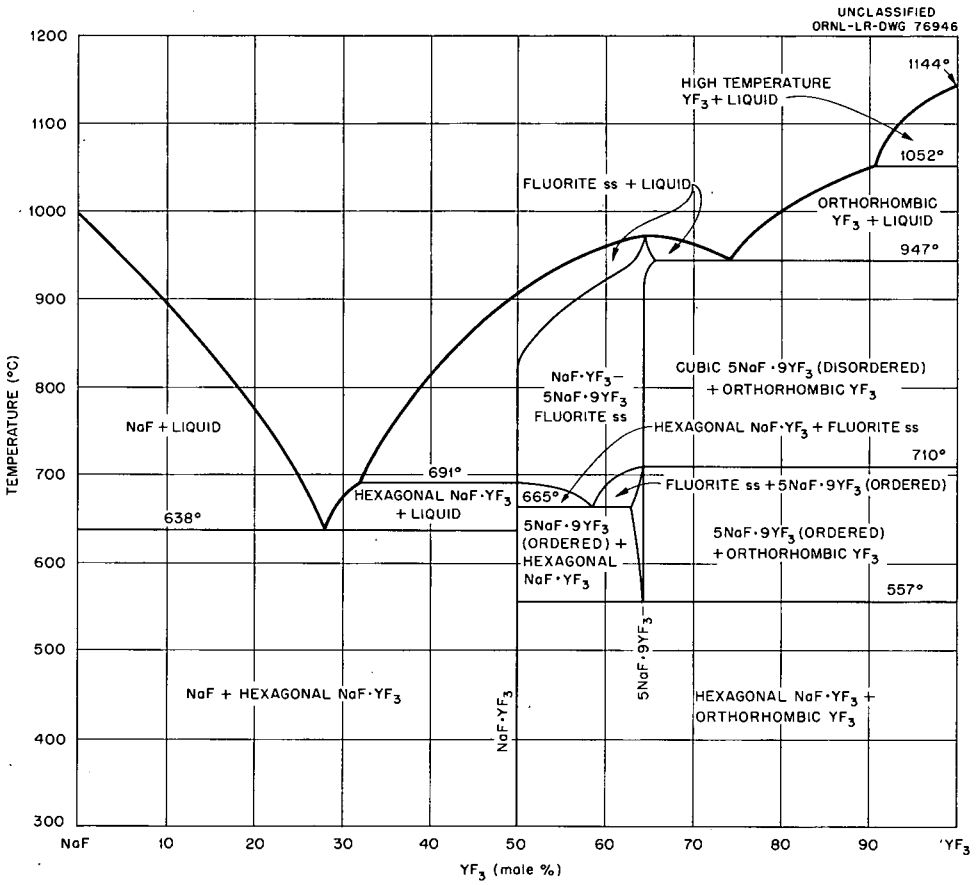


**Fig. 1.2. The System NaF-$YF_3$.**

**Table 1.2. Invariant and Singular Points in the System NaF-$YF_3$**

| Composition (mole % $YF_3$) | Temperature (°C) | Type of Equation at Invariant Temperature | Equilibrium Reaction |
|---|---|---|---|
| 29 | 638 | Eutectic | $L^a \rightleftharpoons$ NaF + hexagonal NaF·YF |
| 32 | 691 | Peritectic | Cubic NaF·$YF_3$ + $L \rightleftharpoons$ hexagonal NaF·$YF_3$ + $L$ |
| 58.5 | 665 | Eutectoid | Fluorite $ss^b \rightleftharpoons$ hexagonal NaF·$YF_3$ + orthorhombix $YF_3$ |
| 64.28 | 975 | Congruent melting point for 5NaF·9$YF_3$ | $L \rightleftharpoons$ cubic 5NaF·9$YF_3$ |
| 75 | 947 | Eutectic | $L \rightleftharpoons$ cubic 5NaF·$YF_3$ $ss$ + orthorhombic $YF_3$ |
| 91 | 1052 | Peritectic | $L$ + high temp $YF_3 \rightleftharpoons L$ + orthorhombic $YF_3$ |

[a]The symbol $L$ refers to liquid (observed as glass or quench growth).
[b]The term $ss$ mean solid solution.

$YF_3$, Nowacki[15] concluded that he had in a single instance obtained a primitive cubic modification. Zalkin and Templeton[16] inferred that a compound, $NaF \cdot 3YF_3$, was obtained instead. The phase diagram of the system $NaF\text{-}YF_3$, reported here, is based on a very much greater quantity of experimental data than was obtained in any previous investigation. It became evident from the purity assays employing the complementing analytical techniques, chemical, petrographic, and x-ray, that rigorous methods of excluding small amounts of contaminant oxide were necessary if definitive phase data were to be obtained. It was evident that contaminant oxide in concentrations of 1000 to 1500 ppm would significantly alter the apparent composition and temperatures of $NaF\text{-}YF_3$ phase transitions. It seems probable that previous investigators were unable to obtain equilibrium phase data because of the difficulty of obtaining oxygen-free $YF_3$ and $NaF\text{-}YF_3$ crystal phases and verifying their purity. The principal impurity usually found in $YF_3$ is cubic YOF, which is quite soluble in $NaF\text{-}YF_3$ fluorite solid solutions. Minor concentrations of contaminant YOF affect markedly the phase transition, optical, and x-ray data involving the $NaF\text{-}YF_3$ fluorite solid solution. The refractive indices and lattice parameters of the $NaF \cdot YF_3\text{-}5NaF \cdot 9YF_3$ solid solutions shown in Fig. 1.3 are reproducible only if oxygen analyses by the $KBrF_4$ method run below 1000 ppm. Hydrolysis of $NaF\text{-}YF_3$ samples at high temperatures is prevented by (1) purifying specimens for the phase studies by melting the components with $NH_4F \cdot HF$, (2) exposure of cooled melts only in an environment of predried argon or helium, and (3) maintenance of the water vapor concentration of the dry-box atmosphere at less than 100 ppm.

Calibration data for the fluorite solid solution were established statistically over a period of years for very pure solids, so that composition variation and concentration of contaminant phases dissolved could be estimated. The concentration of contaminant oxides was evidenced by anomalously high refractive indices.

The definition of the upper $YF_3$ limit of the fluorite solid-solution phase boundary as the compound is of considerable interest. The lack of composition variation with temperature, the stoichiometric ratio, the maximum on the melting curve, and the shape of the solidus lines near the compound all indicate its compound character. Yet, the phase boundary is similar to that limiting the single phase $UO_{2+x}$ as it occurs in high-temperature oxidation. If the analogy can be extended, it must be inferred that the $UO_{2+x}$ phase limit at high temperatures also must be interpreted as the high-temperature form of $U_4O_9$. Structure

[15] W. Nowacki, *Z. Krist.* **100**, 242 (1938).

[16] A. Zalkin and D. H. Templeton, *J. Am. Chem. Soc.* **75**, 2453 (1953).

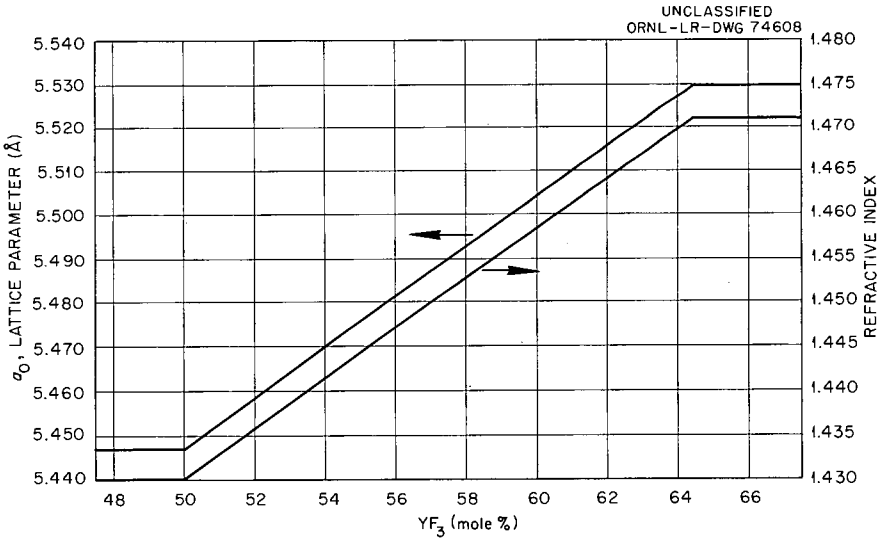


**Fig. 1.3. Lattice Parameters and Refractive Indices of $NaF\text{-}YF_3$ Fluorite Solid Solutions.**

data, indicating the mechanism of ordering which occurs between the high- and low-temperature forms of $5NaF \cdot 9YF_3$, must be obtained from single crystals. A study of the ordering phenomena has been initiated.

## The System $CsF\text{-}ZrF_4$

A tentative phase diagram for the system $CsF\text{-}ZrF_4$ published from this Laboratory by Barton and co-workers[17] was based entirely on information from cooling curves of appropriate mixtures. Since the phase relation of other alkali fluoride–sodium fluoride systems are considerably more complex than those disclosed by that study, a reexamination of the $CsF\text{-}ZrF_4$ system has been performed. The thermal-analysis and thermal-gradient-quenching techniques,[18] with examination of the resultant solids by x-ray diffraction and optical microscopy, yielded the information shown as Table 1.3 and Fig. 1.4. This study has shown the liquidus as defined by the previous study to be generally correct but provides much additional information concerning the crystalline materials. Of the three $CsF \cdot ZrF_4$ compounds, 3:1, 2:1, and 1:1, polymorphism is exhibited only by $CsF \cdot ZrF_4$, for which the inversion on cooling below 326°C is markedly exothermic. Accordingly, well-formed crystals of the high-temperature form of this compound are impossible to retain on quenching, and crystallographic verification of liquid-solid transitions are unobtainable over this region of the diagram.

The 3:1 compound is variable in composition and can occur as a single phase with as much as 20% of additional CsF in the lattice at the solidus. Stoichiometric crystals of $3CsF \cdot ZrF_4$, such as have been used for determination of the crystal structure,[19] can be produced only from melts with at least 25 mole % of $ZrF_4$. This solubility phenomenon is unlike that of any 3:1 compound previously observed in alkali fluoride–metal tetrafluoride systems. All other such compounds form no solid solutions or accommodate in their lattices small quantities of $MF_4$.

[17] C. J. Barton, L. M. Bratcher, and W. R. Grimes, *Phase Diagrams of Nuclear Reactor Materials*, ORNL-2548, p 58 (Nov. 6, 1959).

[18] H. A. Friedman, G. M. Hebert, and R. E. Thoma, *Thermal Analysis and Gradient Quenching Apparatus and Techniques for the Investigation of Fused Salt Phase Equilibria*, ORNL-3373 (Dec. 18, 1962).

[19] J. H. Burns and G. D. Robbins, section "X-Ray Diffraction Study of $Cs_3ZrF_7$" (this chapter).

**Table 1.3. Invariant Equilibria in the System $CsF\text{-}ZrF_4$**

| Mole % $ZrF_4$ in Liquid | Invariant Temperature (°C) | Type of Equilibrium | Phase Reaction at Invariant Temperature |
|---|---|---|---|
| 8 | 622 | Eutectic | $L^a \rightleftharpoons CsF + 3CsF \cdot ZrF_4 ss^b$ |
| 25 | 782 | Congruent melting point | $L \rightleftharpoons 3CsF \cdot ZrF_4$ |
| 35 | 527 | Peritectic | $L + 3CsF \cdot ZrF_4 ss \rightleftharpoons 2CsF \cdot ZrF_4$ |
| 42 | 416 | Eutectic | $L \rightleftharpoons 3CsF \cdot ZrF_4 ss + 2CsF \cdot ZrF_4$ |
| 50 | 511 | Congruent melting point | $L \rightleftharpoons \alpha\text{–}CsF \cdot ZrF_4$ |
| | 329 | Inversion of $CsF \cdot ZrF_4$ | $\alpha\text{–}CsF \cdot ZrF_4 \rightleftharpoons \beta\text{–}CsF \cdot ZrF_4$ |
| 54 | 471 | | $L \rightleftharpoons CsF \cdot ZrF_4 + ZrF_4$ |

[a] The symbol *L* refers to liquid (observed as glass or quench growth).

[b] The term *ss* means solid solution.

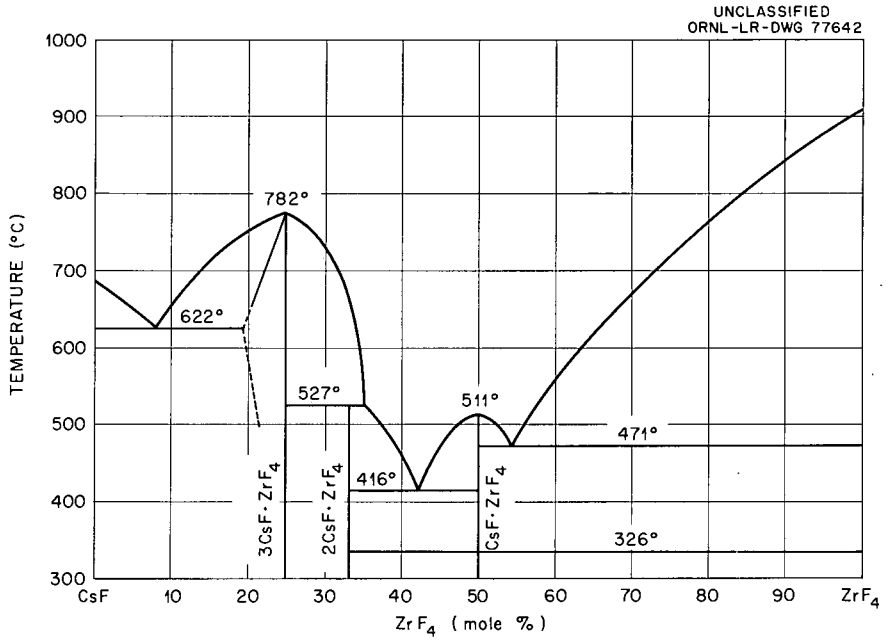


**Fig. 1.4. The System $CsF\text{-}ZrF_4$.**

## CRYSTAL STRUCTURE INVESTIGATIONS

### Crystallographic Data for Some Pure Crystalline Salts

Crystallographic data were obtained for a number of new phases isolated in the phase studies in addition to newly obtained data on crystal phases whose identity is well established. These measurements were made using standard petrographic, x-ray powder, and single-crystal techniques. Only the three principal peaks in the x-ray powder diffraction patterns are listed for crystal phases whose symmetry has not yet been established (see Table 1.4).

### The Crystal Structures of $LiRbF_2$ and $LiCsF_2$

J. H. Burns

Preliminary studies[20] of the binary alkali fluorides $LiRbF_2$ and $LiCsF_2$ had shown them to be monoclinic, unlike any of the components; therefore, a determination of the detailed structure was made.

The crystals of both compounds are very hygroscopic, so they were manipulated under oil and sealed in glass capillaries for x-ray study. Handling of the specimens was also complicated by their tendency to undergo polysynthetic twinning when pressed. This effect is illustrated in Fig. 1.5, a photomicrograph of multiply twinned $LiCsF_2$ viewed through crossed Nicols. The ease of twinning is attributed to the pseudo-orthorhombic symmetry of the crystals.

An approximate structure for these two isomorphous crystals was obtained with a computer program devised by W. R. Busing.[21] With this program all structures consistent with the unit cell, space group, and ionic radii were computed, and the one providing closest agreement with a few visually estimated photographic intensities was selected as a starting point for structure refinement. Counter-measured intensities of 138 reflections from $LiRbF_2$ and 147 reflections from $LiCsF_2$ provided the observations for least-squares refinements of each of the two crystal structures which are described as follows:

[20] J. H. Burns, *Reactor Chem. Div. Ann. Progr. Rept. Jan. 31, 1962*, ORNL-3262, p 17.

[21] W. R. Busing, paper presented at American Crystallographic Association, Villanova, Pa., June 18–22, 1962.

**Table 1.4. Crystallographic Data for Some Pure Crystalline Salts**

| Compound | Optical Properties | X-Ray Data |
|---|---|---|
| $CsBrO_3$ | Uniaxial (–), $N_\omega = 1.542$, $N_\epsilon = 1.682$ | Trigonal, $a = 6.507$, $c = 8.232$ A, S.G.: $C_{3v}^5 - R3m$[a] |
| $2CsF \cdot 3UF_4$ | Biaxial (+), $2V \cong 70°$, $N_\alpha = 1.560$, $N_\gamma = 1.570$ | 3.56, 3.65, 6.06 A |
| $CsF \cdot 6UF_4$ | Uniaxial (–), $N_\omega = 1.598$, $N_\epsilon = 1.590$ | 4.16, 3.48, 2.05 A |
| $3CsF \cdot ZrF_4$ | Isotropic, $N = 1.471$ | FCC, $a = 9.70$ A[b] |
| $InF_3$ | Uniaxial (+), $N_\omega = 1.442$, $N_\epsilon = 1.452$, $B \cong 0.010$ | Rhombohedral, $a = 5.73$ A, $\alpha = 56°40'$[c] |
| $3LiF \cdot AlF_3$ | Biaxial (–), $2V$ large, $N_\alpha = 1.368$, $N_\gamma = 1.3675$ | 4.13, 2.17, 2.14 A |
| $LiF \cdot NaF \cdot 4ZrF_4$ | Biaxial (+), $2V \cong 75°$, $N_\alpha = 1.486$, $N_\gamma = 1.500$ | 7.05, 4.00, 3.37 A |
| $5NaF \cdot 9YF_3$ (disordered form) | Isotropic, $N = 1.473$ | FCC, $a = 5.530$ A |
| $5NaF \cdot 9YF_3$ (ordered form) | Uniaxial (–), $N_\omega = 1.478$, $N_\epsilon = 1.465$, polysynthetic twinning | |
| $NaF \cdot KF \cdot ThF_4$ | Uniaxial (–), $N_\omega = 1.454$, $N_\epsilon = 1.448$ | 7.94, 3.14, 2.24 A |
| $XeO_3$ | Biaxial (+), $N_\alpha \cong 1.79$, $N_\gamma \gg 1.80$, $2V = 5–10°$, max birefringence $\cong 0.16$ | |
| $ZrF_4$ (cubic form) | Isotropic, $N = 1.560$ | FCC, $a = 7.88$ A, $Z = 8$ |
| $ZrOF_2$ | Biaxial (–), large $2V$, high birefringence, parallel extinction, $N_\alpha = 1.730$, $N_\gamma = 1.840$ | Orthorhombic (pseudo-hexagonal), $a = 13.10$, $b = 8.10$, $c = 11.48$ A. |

[a] *Natl. Bur. Std. (U.S.), Circ.* No. 539, 8 (1958).
[b] See section "X-Ray Diffraction Study of $Cs_3ZrF_7$" (this chapter).
[c] J. H. Burns, unpublished work.

For both substances, the atoms are located in these sites of space group $C2/c$:

$(0, 0, 0; \frac{1}{2}, \frac{1}{2}, 0) +$
$8Li^+$ in $8(f)$: $\pm(x, y, z; x, \bar{y}, \frac{1}{2} + Z)$,
$8Rb^+$ (or $Cs^+$) in $8(f)$,
$8F^-$ in $8(f)$,
$4F^-$ in $4(e)$: $\pm(0, y, \frac{1}{4})$,
$4F^-$ in $4(e)$.

Individual isotropic temperature factors were applied to each atom and allowed to vary, except for lithium. Table 1.5 shows, for each compound, the least-squares adjusted parameters and their standard deviations. The agreement factor, $\Sigma|F^2_{obs} - F^2_{calc}| / \Sigma F^2_{obs}$, was 0.099 for $LiRbF_2$ and 0.134 for $LiCsF_2$.

A schematic drawing of the $LiCsF_2$ structure is given in Fig. 1.6 (the $LiRbF_2$ structure appears approximately the same). The fluoride ions are grouped together into tetrahedra around each $Li^+$ ion (not shown), and these tetrahedra share edges and corners in such a way as to form a continuous sheet. The larger cations occupy holes between the sheets and bind them together. An ion such as $K^+$ would not be able to make a sufficient number of close contacts with the $F^-$ ions of two sheets to satisfy its coordination shell, so this type of structure cannot occur in the system KF-LiF.

Fig. 1.5. Photomicrograph of Multiply Twinned $LiCsF_2$.

**Table 1.5. The Least-Squares Adjusted Parameters and Their Standard Deviations of $LiRbF_2$ and $LiCsF_2$**

| | $x$ | $y$ | $z$ | $B$ |
|---|---|---|---|---|
| $LiRbF_2$ | | | | |
| Li | 0.219 ± 0.007 | 0.194 ± 0.004 | 0.363 ± 0.006 | 2.5 |
| Rb | 0.2650 ± 0.0004 | 0.4106 ± 0.0002 | 0.0709 ± 0.0004 | 1.60 ± 0.05 |
| F(1) | 0.219 ± 0.002 | 0.362 ± 0.001 | 0.417 ± 0.002 | 1.7 ± 0.3 |
| F(2) | 0 | 0.115 ± 0.002 | ¼ | 1.4 ± 0.3 |
| F(3) | 0 | 0.683 ± 0.002 | ¼ | 2.1 ± 0.4 |
| $LiCsF_2$ | | | | |
| Li | 0.254 ± 0.012 | 0.207 ± 0.006 | 0.359 ± 0.009 | 2.5 |
| Cs | 0.2536 ± 0.0003 | 0.4088 ± 0.0002 | 0.0723 ± 0.0003 | 2.03 ± 0.07 |
| F(1) | 0.242 ± 0.003 | 0.355 ± 0.002 | 0.423 ± 0.002 | 1.7 ± 0.4 |
| F(2) | 0 | 0.150 ± 0.003 | ¼ | 2.5 ± 0.6 |
| F(3) | 0 | 0.664 ± 0.003 | ¼ | 3.2 ± 0.7 |

An interesting feature of the two difluoride structures presented here is the tetrahedral coordination of the $Li^+$ ions. X-ray diffraction studies[22] of molten LiF have shown an average coordination of 3.7 for $F^-$ about $Li^+$ (and *vice versa*), while in solid LiF these ions are mutually six-coordinated. The existence of tetrahedral coordination in the difluorides raises the possibility that such a configuration may contribute appreciably to the structure of liquid LiF.

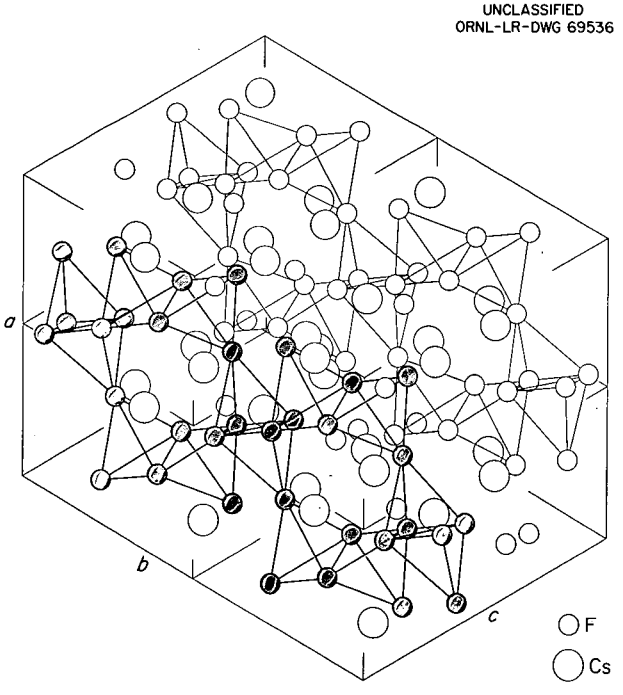


**Fig. 1.6. Structure of $LiCsF_2$.**

## X-Ray Diffraction Study of $Cs_3ZrF_7$

J. H. Burns G. D. Robbins

Single crystals of $Cs_3ZrF_7$, prepared during a determination of the phase diagram[23] of $CsF\text{-}ZrF_4$, were studied by x-ray diffraction because of their similarity to several other compounds having the stoichiometry of 3 alkali fluoride : 1 tetravalent metal fluoride.

The face-centered cubic crystals have $a_0 = 9.70 \pm 0.02$ A and contain four formula weights per cell. The x-ray density is 4.53 g/cm$^3$. Precision photographs of $0kl$, $1kl$, $2kl$, and $hhl$ zones established the diffraction symmetry as $m3mF$---; the probable space group is therefore either $F\bar{4}3m$,

[22] J. Zarzyki, "Structure of Molten Fluorides and Chlorides," p 131 in *Non-Crystalline Solids* (ed. by V. D. Frechette), Wiley, New York, 1960.

[23] G. D. Robbins and R. E. Thoma, "The System $CsF\text{-}ZrF_4$" (this chapter).

$F432$, or $Fm3m$. The cations are located at the following positions:

$4Zr^{4+}$ at (0, 0, 0) + face centering,

$4Cs^{+}$ at ($\frac{1}{2}$, $\frac{1}{2}$, $\frac{1}{2}$) + face centering,

$8Cs^{+}$ at ($\frac{1}{4}$, $\frac{1}{4}$, $\frac{1}{4}$; $\frac{3}{4}$, $\frac{3}{4}$, $\frac{3}{4}$) + face centering.

However, once these atoms are placed, there is no combination of sites left in either of the space groups which will provide for the 28 fluoride ions. Thus it is concluded, as was done previously by Hampson and Pauling[24] for $(NH_4)_3ZrF_7$ and $K_3ZrF_7$ and by Zachariasen[25] for $\alpha$-$K_3UF_7$, that there is some randomness in the structure of $Cs_3ZrF_7$. If, then, the fluoride ions are statistically distributed over sites of high multiplicity so that, on the average, only a fraction of an atom occupies a given site, it is not likely that the exact configuration of fluoride ions about a given zirconium can be determined by x-ray diffraction methods due to the great discrepancy in scattering power of the atoms.

The powder diagram of $Cs_3ZrF_7$ was made with a Debye-Scherrer camera and Cu $K_\alpha$ radiation. The indexed pattern is presented in Table 1.6 for use in identification of the compound.

**Table 1.6. X-Ray Powder Pattern of $Cs_3ZrF_7$**

| *hkl* | $d_{obs}$ (A) | $d_{calc}$ (A) | $I_{obs}$ |
|---|---|---|---|
| 220 | 3.43 | 3.43 | *vS* |
| 311 | 2.92 | 2.92 | *vw* |
| 222 | 2.803 | 2.799 | *vw* |
| 400 | 2.424 | 2.424 | *S* |
| 422 | 1.980 | 1.989 | *S* |
| 440 | 1.715 | 1.714 | *m* |
| 620 | 1.535 | 1.533 | *ms* |
| 642 | 1.297 | 1.296 | *ms* |

## The Crystal Structure of $Cr_2F_5$

H. Steinfink[26] J. H. Burns

In the structures of $CrF_2$ and $CrF_3$, the fluoride-ion coordination about the chromium cation is octahedral.[27] The octahedron is regular in $CrF_3$ and the Cr-F distance is 1.90 A, but in $CrF_2$ two of the Cr-F distances are 2.43 A while the other four are about equal at 1.98 to 2.01 A. This effect is explained by crystal-field theory.[28] The presence of an electron in the $d_y$ orbital of the divalent chromium exerts a repulsive force on the fluoride ions along the $z$ axis, thereby lengthening the Cr-F distance. In $CrF_3$ the $d_y$ orbital is unoccupied and all six Cr-F distances are equal.

A study of the phase diagram of the $CrF_2$-$CrF_3$ system revealed the existence of a single-phase region of composition $CrF_{2.40}$ to $CrF_{2.45}$.[29] Preliminary x-ray diffraction measurements[30] on crystals within this composition range indicated the likelihood of a structure based on the nominal stoichiometry $Cr_2F_5$, with a small deficiency of fluoride ions. This presented the intriguing possibility that if, in the crystal, divalent and trivalent chromium ions are distributed in an ordered arrangement, they might be distinguishable by their fluoride-ion environments, and that the effect of crystal field on the two types of ions might be demonstrated in one crystal.

The crystal structure of $Cr_2F_5$ has been determined from electron-density projections calculated from visually estimated $h0l$ and $hk0$ x-ray diffraction intensities. Refinement is now in progress using three-dimensional counter data. The structure is described in terms of a new choice of monoclinic unit cell related to the previously reported[30] one by the transformation: $\mathbf{a}' = \mathbf{c} - \mathbf{a}$, $\mathbf{b}' = \mathbf{b}$, $\mathbf{c}' = \mathbf{c}$. The atoms are distributed over the following equipoints of space group $C2/c$:

Cr(1) in 4($a$): 0, 0, 0; 0, 0, $\frac{1}{2}$,

Cr(2) in 4($b$): 0, $\frac{1}{2}$, 0; 0, $\frac{1}{2}$, $\frac{1}{2}$,

[24] G. C. Hampson and L. Pauling, *J. Am. Chem. Soc.* **60**, 2702 (1938).

[25] W. H. Zachariasen, *Acta Cryst.* **7**, 792 (1954).

[26] Consultant, University of Texas.

[27] K. H. Jack and R. Maitland, *Proc. Chem. Soc.* **1957**, 232 (1957).

[28] A. G. Sharpe, "Transition Metal Fluorides and Their Complexes," p 46 in *Advances in Fluorine Chemistry* (ed. by M. Stacey *et al.*), Butterworths, London, 1960.

[29] B. J. Sturm, *Inorg. Chem.* **1**, 665 (1962).

[30] J. H. Burns, *Reactor Chem. Div. Ann. Progr. Rept. Jan. 31, 1962*, ORNL-3262, p 16.

F(1) in 4(*e*): $\pm (0, y, \frac{1}{4})$,

F(2) in 8(*f*): $\pm (x, y, z; x, \bar{y}, \frac{1}{2} + z)$,

F(3) in 8(*f*),

+ *C*-centering.

After four cycles of least-squares refinement, using partial three-dimensional data, the positional parameters are as follows:

F(1): $y = 0.0444$;

F(2): $x = 0.2957$, $y = -0.0185$, $z = 0.1772$;

F(3): $x = 0.0238$, $y = 0.2475$, $z = -0.0333$.

The structure consists of an array of chromium ions, each coordinated by an octahedron of fluoride ions; and, in accordance with prediction, the two oxidation states of chromium can be distinguished. The chromium at 4(*a*) appears to be trivalent since it has fluoride-ion neighbors at 1.89, 1.90, and 1.91 A (plus three others related by inversion), and the chromium at 4(*b*) has fluoride ligands at 1.95, 2.00, and 2.58 A (and the inversion-related set) and is therefore the divalent ion. Such an arrangement of ions gives rise to the possibility of either a ferromagnetic or antiferromagnetic ordering at low temperature. A neutron-diffraction investigation of the magnetic behavior is being planned.

### The Crystal and Molecular Structure of Xenon Tetrafluoride by Neutron Diffraction

J. H. Burns P. A. Agron[31] H. A. Levy[31]

Xenon tetrafluoride was prepared by reaction of the elements at about 400°C and its purity verified by infrared analysis.[32] The compound was sublimed into evacuated, thin-walled quartz tubes and sealed off; then a single crystal weighing about 20 mg was grown for neutron-diffraction study. All of the independent reflections out to $\sin \theta/\lambda = 0.76$ were then measured with the Oak Ridge automatic neutron diffractometer.[33]

Previous x-ray diffraction work[34,35] had determined the unit cell and space group of $XeF_4$ as well as the general features of the molecule, so this information was used as a starting point for least-squares refinement of the structure, employing the approximately 630 neutron-diffraction intensities. The procedure involved the determination of anisotropic thermal parameters for all atoms in addition to the adjustment of positional parameters of the fluorine atoms. Convergence was completed after three cycles, and the reliability factor, $R = \Sigma F^2_{obs} - F^2_{calc}/\Sigma F^2_{obs}$, was 0.067.

The $XeF_4$ molecules are planar by crystal symmetry and are shown by this determination to be square to a high degree of precision. The Xe-F bond length, corrected for thermal motion, is 1.952 ± 0.002 A, and the F-Xe-F angle is 90.0 ± 0.1°.

### A Second Crystalline Phase of $XeF_4$

J. H. Burns

Crystals of a second phase of $XeF_4$, in addition to that described above, were grown in the same quartz tubes. This phase appeared to be more volatile and is probably the less stable at room temperature. This hypothesis is in agreement with the greater density of this modification. The crystal habit is pyramidal, while the low-density form grows as platelets.

This second polymorph is also monoclinic, with probable space group $P2_1/c$. The unit-cell dimensions are $a = 6.64 \pm 0.01$, $b = 7.33 \pm 0.01$, $c = 6.40 \pm 0.01$ A, and $\beta = 92° 40' \pm 5'$. Four molecules of $XeF_4$ are contained in the unit cell; the calculated density is 4.42 g/cm$^3$, considerably higher than the value of 4.07 g/cm$^3$ of the other phase.

General *hkl* reflections are strong only when *h*, *k*, and *l* are all odd or all even, implying a face-centered arrangement of the heavy atoms. Therefore, the xenon atoms may occupy either the two sets of special positions, 2(*a*): 0, 0, 0; 0, $\frac{1}{2}$, $\frac{1}{2}$ and 2(*d*): $\frac{1}{2}$, 0, $\frac{1}{2}$; $\frac{1}{2}$, $\frac{1}{2}$, 0, or the general positions 4(*e*): $\pm (x, y, z; x, \frac{1}{2} - y, \frac{1}{2} + z)$, with $x = \frac{1}{4}$, $y = 0$, and $z = \frac{1}{4}$. The fluorine atoms must occupy 4(*e*) and be of four crystallographically independent kinds. If the xenon atoms are at 2(*a*) and 2(*d*), they will be at inversion centers; and the $XeF_4$ molecules will be centrosymmetric and planar as they are in the other phase. This restriction would not apply if they are in 4(*e*).

Further x-ray diffraction work on this phase is in progress.

---

[31] ORNL Chemistry Division.

[32] D. F. Smith, Oak Ridge Gaseous Diffusion Plant.

[33] W. R. Busing and H. A. Levy, paper presented at American Crystallographic Association, Boulder, Colo., July 31–Aug. 1, 1961.

[34] J. A. Ibers and W. H. Hamilton, *Science* **139**, 106 (1963).

[35] D. H. Templeton *et al.*, *Journal of American Chemical Society* (in press).

# 2. Compatibility of MSRE Components

## RADIATION CHEMISTRY OF MSR SYSTEM[1]

F. F. Blankenship J. E. Savolainen
S. S. Kirslis W. R. Grimes

Compatibility of molten fluoride mixtures, near in composition to those proposed for the MSRE, with graphite and with INOR-8 has been demonstrated convincingly in many out-of-pile tests over a period of several years. A few in-pile capsule studies of graphite-fluoride-INOR systems with fluoride melts of a rather different composition have been performed in past years; examination of those capsules showed no deleterious effects of radiation on the system. However, in-pile testing of this combination of materials under conditions similar to those expected in the MSRE has been attempted only recently. Accordingly, no completely realistic experiments have been reported.

An ORNL-MTR-3 assembly containing four capsules was irradiated in the MTR during the summer of 1961 to provide assurance as to the nonwettability of graphite by molten $LiF\text{-}BeF_2\text{-}ZrF_4\text{-}UF_4\text{-}ThF_4$; though such assurance was obtained, this experiment yielded the following surprising results:[2-4]

1. The cover gas within the sealed capsules contained appreciable quantities of $CF_4$.
2. The cover gas contained the expected quantity of krypton from all capsules; xenon was present at the expected level in two capsules, but its concentration was less by 100-fold in the other two.
3. No evidence of wetting of the graphite by the salt was observed. However, the irradiated salt was deep black in color; it contained loose, roughly spherical beads of condensed salt of various colors from clear through blue to black.

The difference in behavior of krypton and xenon seemed quite inexplicable. The black color of the salt was removed by annealing at temperatures below the liquidus and was shown to be due largely, if not entirely, to radiation-induced discoloration of crystalline LiF and $2LiF\cdot BeF_2$. This color, and the occurrence of the salt beads (which were clearly due to condensation of distillate from the salt pool on the capsule walls), were judged to be trivial. The appearance of $CF_4$ in the cover gas, however, remained a most disturbing observation. Thermodynamic data for reactions of fluorides with carbon such as

$$4UF_4 + C \rightleftharpoons CF_4 + 4UF_3$$

suggest that the equilibrium pressure of $CF_4$ over such a system should not exceed $10^{-8}$ atm. Moreover, out-of-pile controls with identical material, geometry, and thermal histories (insofar as possible to obtain same with external heat sources) showed no evidence of $CF_4$. (The limit of detection was 1 ppm.) This gas, accordingly, clearly arose from some previously unknown radiation-induced reaction; its generation might, of course, have serious consequences. If $CF_4$

[1] Work reported under this heading represents a cooperative effort involving several divisions of the Laboratory. The authors are indebted to many people whose efforts have been essential to these experiments. Reactor Division personnel, under D. B. Trauger, are responsible for design and operation of the assemblies; Metals and Ceramics Division and Operations Division personnel, under A. R. Olsen and E. M. King, have conducted the hot-cell disassembly operations; and Metals and Ceramics personnel under A. Taboada are responsible for evaluation of attack on metal and graphite.

[2] *Reactor Chem. Div. Ann. Progr. Rept. Jan. 31, 1962*, ORNL-3262, pp 19 ff.

[3] *MSRP Semiann. Progr. Rept. Feb. 28, 1962*, ORNL-3282, pp 97 ff.

[4] *MSRP Semiann. Progr. Rept. Aug. 31, 1962*, ORNL-3369, pp 105 ff.

were generated at an appreciable rate in the MSRE core it might be removed in the gas stripping section of the MSRE pump; an appreciable loss of fluoride ion from the melt, with the resultant appearance of $U^{3+}$ or other reduced species in the fuel, would, at the least, cause frequent shutdowns to reoxidize the fuel. Two additional in-pile experiments were, therefore, conducted in an attempt to establish the quantity of $CF_4$ to be expected under power levels, temperatures, and graphite-fuel geometries more representative of the MSRE. The following is a brief statement of progress to date in this experimental program and a review of the conclusions which can presently be drawn from the information.

### Experiment ORNL-MTR-47-4[3,4]

**Irradiation of Specimens.** – The irradiation assembly, designated as 47-4 in the following, contained six INOR-8 capsules. These were immersed in a common pool of molten sodium which served to transfer the heat generated during fission through a helium-filled annular gap to water circulating in an external jacket. The four large capsules, as shown in Fig. 2.1, were 1 in. in diameter by 2.25 in. long and contained a core of CGB graphite (½-in. diameter × 1-in. length) submerged about 0.3 in. (at temperature) in about 25 g of fuel. The two smaller capsules, see Fig. 2.2, contained 0.5-in.-diam cylindrical crucibles of CGB graphite containing about 10 g of fluoride melt. Each large capsule included a thermowell which permitted measurement of temperature within the submerged graphite specimen; detailed analysis suggests that this measured temperature should approximate closely the temperature at the salt-graphite interface. No such provision for temperature measurement could be incorporated into the smaller capsules.

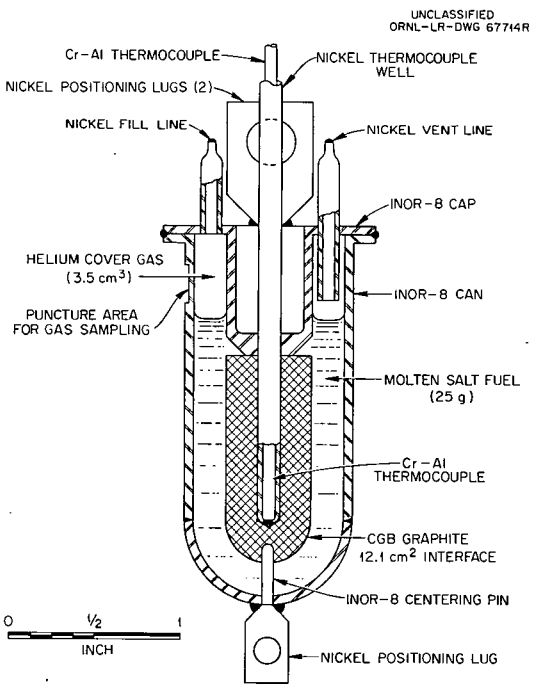


**Fig. 2.1. Submerged Graphite – Molten-Salt Capsule.**

The CGB graphite used in all capsules of 47-4 had a surface area of 0.71 $m^2/g$ as determined by the BET method. Other properties of this material follow:

| | |
|---|---|
| Permeability of a 1.5-in.-OD, 0.5-in.-ID, 1.5-in.-long specimen | $6.56 \times 10^{-4}$ $cm^2$ of He (STP) per second |
| Density (Beckman air pycnometer) | 2.00 $g/cm^3$ |
| Bulk density | 1.838 $g/cm^3$ |
| Bulk volume accessible to air | 8.7% |
| Total void volume as percentage of bulk volume | 19.5% |

Spectrographic analysis of the graphite revealed only the usual low levels of trace elements.

The $UF_4$ used in preparing the salt mixtures was fully enriched in all cases. The four large (submerged graphite) capsules and one of the small capsules each contained fluoride mixtures of $LiF$-$BeF_2$-$ZrF_4$-$ThF_4$-$UF_4$ for which analyzed samples indicated the composition 71.0-22.6-4.7-1.0-0.7 mole %. The other small capsule was loaded with a very similar mixture but with the uranium content raised to 1.4 mole %. The fused salt mixtures were prepared by mixing the proper quantities of pure fluorides, and then, at 750 to 800°C, sparging for 2 hr with $H_2$, 8 hr with a 5:1 mixture of $H_2$ and HF, and 48 hr with $H_2$.

The large capsules were filled by transferring the molten fluoride mixture under an atmosphere of helium; the level to which they were filled was controlled by blowing excess liquid back through a dip line adjusted to the proper level. Final closure was made in a helium-filled glove box where the ends of the fill tubes were crimped and then welded shut. The smaller capsules were filled, in the glove box, with ingots of solid fuel

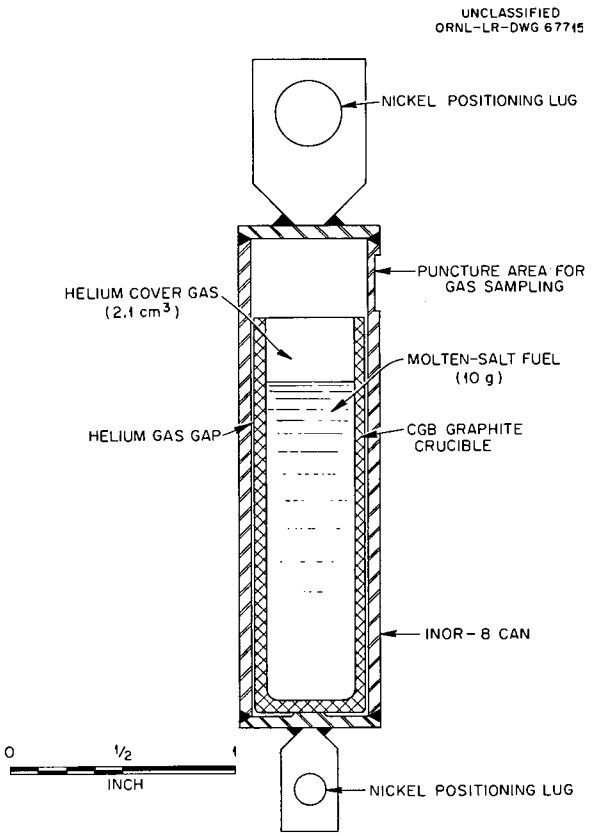


**Fig. 2.2. Crucible – Molten-Salt Capsule.**

**Table 2.1. Temperature History of Fuel Salt in Capsules from 47-4**

| Temperature Interval (°C) | Time at Temperature (hr): Submerged Graphite Core (24, 36, 45, 12, 6[a])[b] | Time at Temperature (hr): Graphite Crucible[c] (4)[b] |
|---|---|---|
| Steady-state operation | | |
| 0–100 | 390.6 | 390.6 |
| 100–700 | 44.0 | 12.1 |
| 700–750 | 1203.7 | 3.8 |
| 750–800 | 254.0 | 17.6 |
| 800–850 | | 11.4 |
| 850–900 | | 1456.9 |
| Total | 1892.3 | 1892.3 |
| Nonsteady-state operation | 51.7 | 51.7 |
| Total irradiation | 1553.4 | 1553.4 |

[a]Graphite crucible capsule containing fuel with 0.7 mole % $UF_4$.

[b]Capsule identification number.

[c]Calculated temperature history based on temperatures measured in submerged graphite capsules.

mixture. They were closed by inert-gas arc welding of the end cap. The amount of fuel chosen for each capsule should have yielded a vapor volume of 3.5 $cm^3$ in the large capsule and 2 $cm^3$ in the small capsule at temperature.

Assembly 47-4 was irradiated through three MTR cycles in the period March 15 to June 4, 1962. The temperature history of the six capsules (as read from the Chromel-Alumel thermocouples in the four large capsules and as calculated for the two small capsules) is shown in Table 2.1. The maximum measured temperature among the four instrumented capsules was 1400 ± 50°F. The mean measured temperatures of the other three instrumented capsules were approximately 1380, 1370, and 1310°F respectively. The corresponding calculated INOR-8 capsule wall-to-salt interface temperatures were 1130, 1125, 1115, and 1110°F.

The accumulated time during transient operation includes only times for temperature changes of more than about 30°C. Of the 121 such temperature changes recorded, 60 included decreases to or below the solidus temperature of the fuel salt. It is estimated that the fuel freezes within 5 min after shutdown of the MTR, and cooling to below 200°F should occur within half an hour.

Exposure data for the capsules in 47-4, and those for out-of-pile controls which were given as similar a thermal history as was practicable, are summarized in Tables 2.2 and 2.3.

The temperatures were controlled from capsule 24, and the changes in the retractor position required to hold a constant temperature were not unusual. The thermocouple reading for capsule 45 appeared to drift downward by about 35°C during the 12-week exposure, but this was the only symptom of deviant temperature recordings.

**Postirradiation Examination.** – The assembly was removed from the MTR and partially disassembled at that location for shipment to ORNL. The assembly was completely dismantled in ORNL

Table 2.2. Exposure Data for Large Capsules in Assembly 47-4

| Capsule | Weight of Fuel (g) | Uranium Content | | Thermal-Neutron Flux[a] Based on $Co^{60}$ Activation (neutrons $cm^{-2}$ $sec^{-1}$) | Fast-Neutron (> 3 Mev) Flux Based on $Co^{58}$ Activation (neutrons $cm^{-2}$ $sec^{-1}$) | Temperature (°C) | | Power Density ($w/cm^3$) | Calculated Burnup (% $U^{235}$) |
|---|---|---|---|---|---|---|---|---|---|
| | | Mole % | g | | | Graphite-to-Salt Interface | INOR-8-to-Salt Interface[b] | | |
| | | | | $\times 10^{13}$ | $\times 10^{12}$ | | | | |
| 3[c] | 25.532 | 0.7 | 0.993 | | | 750 | | | |
| 8[c] | 26.303 | 0.7 | 1.023 | | | 750 | | | |
| 12 | 25.174 | 0.7 | 0.979 | 2.10 | 2.1 | 680[d] | 610 | 67 | 5.5 |
| 24 | 25.374 | 0.7 | 0.987 | 2.70 | 3.2 | 760[d] | 605 | 83 | 7.0 |
| 36 | 24.886 | 0.7 | 0.968 | 2.71 | 3.3 | 710[d] | 595 | 85 | 7.0 |
| 45 | 25.598 | 0.7 | 0.996 | 3.85 | 3.8 | 710[d] | 600 | 117 | 9.7 |

[a]Average external neutron flux.
[b]Estimated temperatures.
[c]Unirradiated controls.
[d]Thermocouple readings prior to termination of final irradiation cycle.

Table 2.3. Exposure Data for Small Capsules in Assembly 47-4

| Capsule | Weight of Fuel (g) | Uranium Content | | Thermal-Neutron Flux[a] Based on $Co^{60}$ Activation (neutrons $cm^{-2}$ $sec^{-1}$) | Fast-Neutron (> 3 Mev) Flux Based on $Co^{58}$ Activation (neutrons $cm^{-2}$ $sec^{-1}$) | Temperature of Central Region (°C) | Power Density ($w/cm^3$) | Calculated Burnup (% $U^{235}$) |
|---|---|---|---|---|---|---|---|---|
| | | Mole % | g | | | | | |
| | | | | $\times 10^{13}$ | $\times 10^{12}$ | | | |
| 1[b] | 9.381 | 0.7 | 0.365 | | | 750 | | |
| 3[b] | 6.805 | 0.7 | 0.265 | | | 750 | | |
| 5[b] | 9.829 | 1.47 | 0.737 | | | 895 | | |
| 4 | 10.101 | 1.47 | 0.758 | 4.79 | 5.2 | 895[c] | 260 | 11.4 |
| 6 | 9.915 | 0.7 | 0.386 | 1.31 | 1.3 | 715[c] | 43 | 1.3 |

[a]Average external neutron flux.
[b]Unirradiated controls.
[c]Thermocouple readings prior to termination of final irradiation cycle.

hot cells and the capsules were recovered for complete examination. All dismantling operations went smoothly, and no evidence of failure of any capsule was observed.

*Analysis of Cover Gas.* – The six irradiated and two unirradiated control capsules were punctured, and the cover gas was recovered for analysis in the interval August 8 to October 23, 1962. These operations, conducted in the hot cells of Building 4501, used a screw-driven puncturing tool sealed with a bellows and by a neoprene O-ring which butted on a flat previously machined into each capsule (see Figs. 2.1 and 2.2). Gas escaped into a collection system whose volume was calibrated and which had, in each case, been evacuated and checked for leaks. The initial collections were performed with a mercury-in-glass Toepler pump and glass sample bulbs in a glass and metal system; when this system proved inadequate, as described below, it was replaced by an all-metal gas-collection system without a pump. The metal system was conditioned with elemental fluorine according to well established procedures before use.

Capsule 6, which suffered the least burnup of uranium, and its out-of-pile control (capsule 5) were handled without difficulty with the glass-metal system. Data obtained, including analyses of the gases by the mass spectrometer, are shown in Table 2.4. The puncturing device leaked slightly, presumably at the O-ring seal, during opening of irradiated capsule 6. After correction of the analyses for the quantity of air (47%), the total volume of He + Ar agreed very well with that from the out-of-pile control. The xenon and krypton were recovered at very nearly the expected ratio, and the absolute volume of these gases agreed reasonably well with the quantity (0.35 $cm^3$ total) calculated from the burnup shown in Table 2.3. The only radioactive materials recovered on Toepler pumping from capsule 6 were krypton and xenon.

Cover-gas recovery and analysis from all other capsules revealed very different behavior.

Capsule No. 24, the first of the large capsules to be opened, showed the cover gas to be quite reactive; the product of reaction with mercury in the Toepler pump was shown to be $Hg_2F_2$ alone. Truly quantitative analysis of the gas was precluded by the inadequacy of the gas handling system. In spite of the considerable but unknown loss of gas by reaction, a large quantity (84 $cm^3$ at STP) of gas was collected. The gas was quite radioactive; tellurium activity (presumably as volatile $TeF_6$) was primarily responsible. Since the measured free volume in capsule 24 at ambient temperature was shown to be 4.6 $cm^3$, a pressure of at least 18 atm existed within the capsule at the time of puncturing. Based on mass spectrometry of two 0.1-$cm^3$ samples, the gas from capsule 24 was 5% He, 0.1% Xe, 0.4% Kr, 4% ($CO + N_2$), 6% $CO_2$, and 17% $CF_4$. The remainder was $O_2$ and $SiF_4$ in roughly equal amounts, matching the products of the reaction of $F_2$ with the glass:

$$SiO_2 + 2F_2 \longrightarrow SiF_4 \uparrow + O_2 \uparrow .$$

The krypton yield listed above is in fair agreement with the calculated value, but the xenon yield is far too low. Some xenon was recovered, with very little additional krypton, in subsequent samples obtained by connecting the capsule to an evacuated 3-liter container.

All other capsules in this series were opened into an essentially all-metal, preconditioned gas system, which permitted much more representative samples of the gas to be obtained. Table 2.5,

**Table 2.4. Cover-Gas Analysis for Capsules 5 and 6 of Assembly 47-4**

| | Capsule 5 | Capsule 6 |
|---|---|---|
| Gas collected, $cm^3$ | 1.3 | 3.2 |
| Corrected value,[a] $cm^3$ | | 1.7 |
| Gas volume in capsule, $cm^3$ | 2.7 | 2.5 |

| Gas | Gas in Capsule 5 | | | Gas in Capsule 6 | | |
|---|---|---|---|---|---|---|
| | Percent | Volume ($cm^3$) | | Percent[a] | Volume ($cm^3$) | |
| He | 15 | 0.2 | 1.2 | 23 | 0.38 | 1.2 |
| Ar | 79 | 1.0 | | 51 | 0.86 | |
| O | 0.7 | 0.01 | | | | |
| $CO + N_2$ | 5.3 | 0.07 | | | | |
| Kr | 0 | 0 | | 4.2 | 0.07 | 0.4 |
| Xe | 0 | 0 | | 19.0 | 0.32 | |
| $CF_4$ | 0 | 0 | | 4.2 | 0.07 | |

[a]Corrected for leakage of air (as indicated by mass spectrometric analysis) at time of sampling.

for example, shows data obtained from capsule 36, the near duplicate in irradiation conditions of capsule 24.

**Table 2.5. Analyses of Cover Gas from Irradiated Capsule 36**

Volume of gas space in capsule at room temp: 4.6 $cm^3$
Volume of gas space at operating temp: 2.6 $cm^3$
Volume of gas removed from capsule: 188 $cm^3$

| Gas | Quantity (vol %) | Volume ($cm^3$) |
|---|---|---|
| $F_2$ | 84.1 | 156 |
| $CF_4$ | 10.0 | 19 |
| $O_2$ | 2.5 | 4.7 |
| Xe | 0 | 0 |
| Kr | 0.4 | 0.56 |
| He | 2.8 | 5.3 |
| CO + Ne | 0.1 | 0.19 |
| $CO_2$ | 0.7 | 1.3 |
| Ar | 0 | |

By contrast, capsule 3A, which was an unirradiated control for capsules 24 and 36 and which had been thermally cycled in a manner similar to their in-pile history, yielded 4.5 $cm^3$ (STP) of 99.7% He, 0.05% CO + $N_2$, and 0.2% $CO_2$. The lack of argon and the total pressure of almost precisely 1 atm was expected because of the speed and simplicity of the final closure of capsules of this type.

The pertinent data for all irradiated capsules in 47-4 are shown in Table 2.6. Inspection of this information shows that all irradiated capsules except No. 6 (previously described) yielded large quantities of $F_2$ and considerable quantities of $CF_4$. The total gas yield from capsule 45 indicated a pressure of 60 atm at room temperature before opening; had this gas been present at the operating pressure and in the considerably smaller volume then available it must have exceeded 300 atm. It is almost certain that the capsule could not have withstood such a pressure even had the gas been inert.

It appears that most, if not all, of the krypton was recovered from all samples, while the xenon is recovered poorly, if at all, from all capsules

**Table 2.6. Quantity and Composition of Gases from 47-4 Capsules**

| | Small Capsules | | Large Capsules | | | |
|---|---|---|---|---|---|---|
| | No. 6 | No. 4 | No. 24 | No. 36 | No. 45 | No. 12 |
| Fuel content (g) | 9.915 | 10.101 | 24.374 | 24.886 | 24.598 | 25.174 |
| Uranium content (g) | 0.386 | 0.758 | 0.987 | 0.968 | 0.957 | 0.979 |
| Burnup (%) | 1.3 | 11.4 | 7.0 | 7.0 | 9.7 | 5.5 |
| Sampling date | 8/6 | 10/19 | 8/14 | 9/7 | 10/16 | 10/23 |
| Gas collected ($cm^3$ STP) | 1.6 | 98 | 84[a] | 188 | 270 | 153 |
| Gas composition (%) | | | | | | |
| $F_2$ | 0 | 90.5 | 65.3[b] | 84.1 | 88.7 | 48.1[b] |
| $CF_4$ | 4.3 | 4.2 | 17.1 | 10.0 | 8.1 | 41.1 |
| Xe | 19.0 | 0 | 0.1 | 0 | 0 | 0 |
| Kr | 4.1 | 0.26 | 0.4 | 0.4 | 0.8 | 0.2 |
| He + Ar | 72.6 | 3.6 | 5.7 | 2.7 | 2.95 | 4.0 |
| Other | | 1.44 | 11.3 | 3.5 | 0.17 | 6.6 |

[a]Minimum value; some gas lost in reaction with container.
[b]Corrected from original analysis which showed $SiF_4 + O_2$.

except No. 6. Though no positive proof is available, it seems highly probable that xenon recovery fails because of formation of $XeF_4$ (or perhaps of other fluorides or oxyfluorides) which may be strongly adsorbed on the fuel or graphite within the system.

While it is possible to see that the production of $F_2$ (or $F_2 + CF_4$) generally increases with quantity of uranium burned, no quantitative correlation of yields of either (or of both together) with any of the experimental parameters can be shown. It is worthy of note that the $F_2 + CF_4$ produced in the most extreme case (capsule 45) represents 3% of the fluorine contained in the salt or 1.6 times the quantity of fluorine in the $UF_4$ in that sample.

*Gross Examination of Capsules.* – Visual examination of the capsules after removal from the 47-4 assembly showed them to be sound and in good condition. No dimensional changes were apparent.

All capsules have been sectioned to permit direct observation of the metal, graphite, and salt.

Fig. 2.3. Capsule 24, Assembly 47-4, After Exposure.

Figure 2.3 shows a view of capsule 24 obtained after rough polishing of the sawed specimens. The fuel salt is black in color, but seems to show no unusual tendency to crack or shatter during the sawing process. No evidence of wetting of the graphite by the salt is apparent. Nonwetting of the metal by the salt is occasionally observed; this behavior, which is unusual, seems to be due to a layer of "scum" on the salt surface near the capsule wall.

One bit of curious behavior, not matched by the out-of-pile controls, is the occurrence of smooth-surfaced voids, which have apparently been gas bubbles during high-temperature operation, in the bottom hemispherical section of all the large capsules.

*Examination of the Metal.* – Fluorine at elevated temperatures is an extremely corrosive material, and examination of the capsule metal should permit definitive statements as to whether $F_2$ was produced and was present during the high-temperature operation. Accordingly, a very careful metallographic examination has been made of sections from capsule 24, and selected specimens from other capsules are under study. Especial attention has been paid to metal surfaces exposed in the gas phase as well as at the gas-salt interface and within the molten salt. Typical photomicrographs from capsule 24 are shown in Figs. 2.4 and 2.5.

There is no evidence of attack on the INOR-8 at any portion of capsule 24, and no evidence of reduction in metal thickness can be observed. The appearance of all other capsules makes it highly unlikely that evidence of attack will be observed. It can be stated with certainty that none of these capsule walls was exposed to fluorine at high temperature for appreciable periods of time.

*Examination of Salt.* – Small samples of salt from the irradiated capsules have been examined carefully with the optical microscope to determine the nature of the crystalline material. As is frequently the case for rapidly cooled specimens, these specimens are generally too fine grained to permit positive identification. However, a sample from near the graphite at the center of capsule 24 has been shown to contain the normally expected phases, though some are discolored and blackened; these phases included $7LiF \cdot 6ThF_4$, which was shown to contain $UF_4$ (green in color) in solid solution. It seems certain, therefore, that the

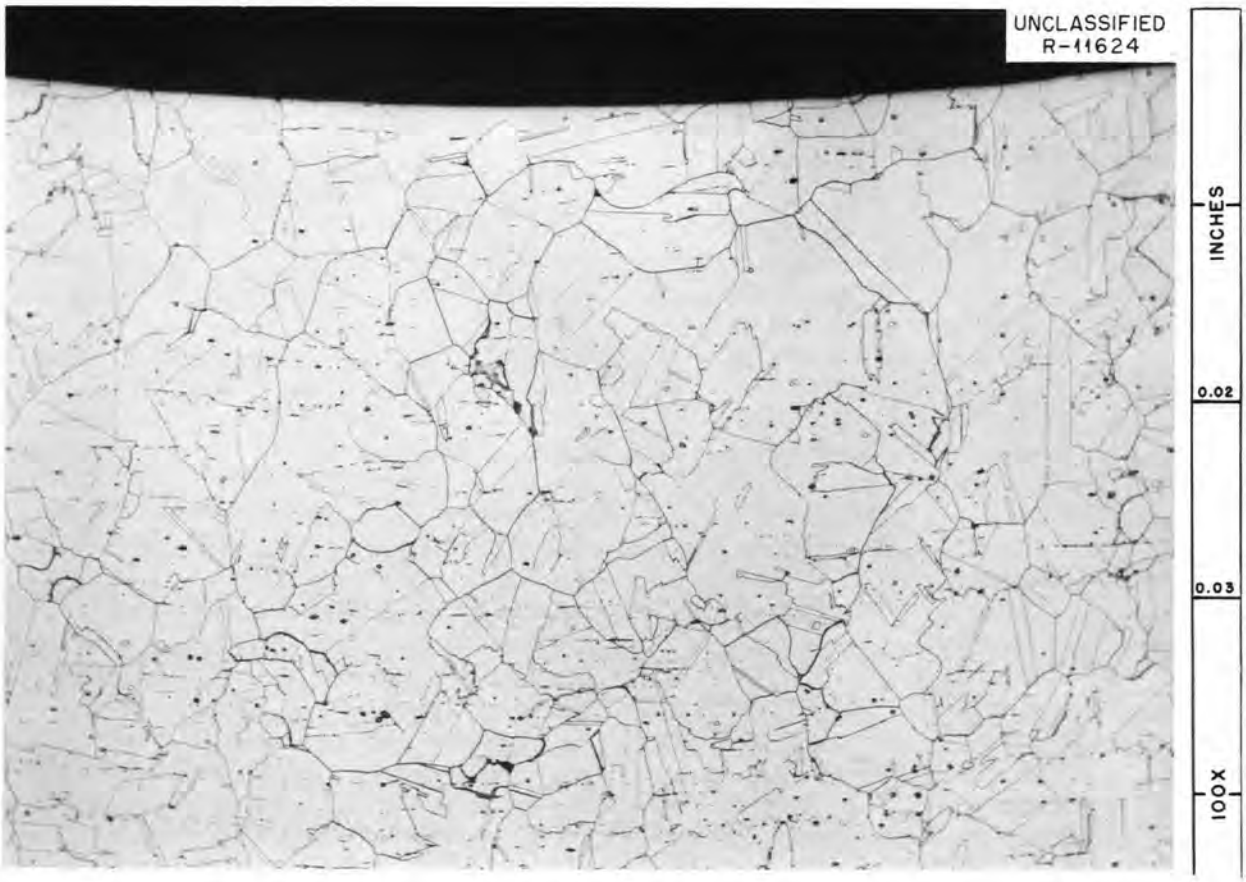


Fig. 2.4. Longitudinal Section of INOR-8 from Hemispherical Portion of Capsule 24.

uranium was not markedly reduced at the time the fuel was frozen.

Salt specimens have been examined by gamma-ray spectrometry to evaluate gross behavior of fission product elements. In general, the ruthenium activity appears to be concentrated near the bottom of the capsules; this may indicate its existence largely in the metallic state so that a gravity separation could occur. Cerium as well as zirconium-niobium activity appears, as expected, to be fairly evenly distributed in the fuel. Some cesium, with some zirconium-niobium, activity is found on metal surfaces exposed to the gas phase.

*Condition of the Graphite.* – Graphite specimens from all the capsules have been removed and have been examined visually with low-power microscopes. No evidence of damage can be observed. The surface of the graphite appears identical to unirradiated specimens, the specimen in all cases appears structurally sound, and the saw cuts (see Fig. 2.3) appear normal. No quantitative measurements of physical and structural properties have been completed.

### Experiment ORNL-MTR-47-5[3,4]

Assembly ORNL-MTR-47-5, designated 47-5 in the following, contained six capsules of INOR-8. The overall design, including sodium tank, cooling apparatus, containment system, etc., was very similar to that employed in 47-4 described above. Of the six capsules, four contained graphite specimens such that large variation in salt-graphite interface area was obtained; these capsules, for which no data are yet available, will not be described further. The other two capsules, whose behavior is described below, were provided with inlet and outlet gas lines to permit sampling of the cover gas during reactor operation.

The two purged capsules, referred to as A and B in the following and illustrated in Fig. 2.6,

UNCLASSIFIED
PHOTO 60623

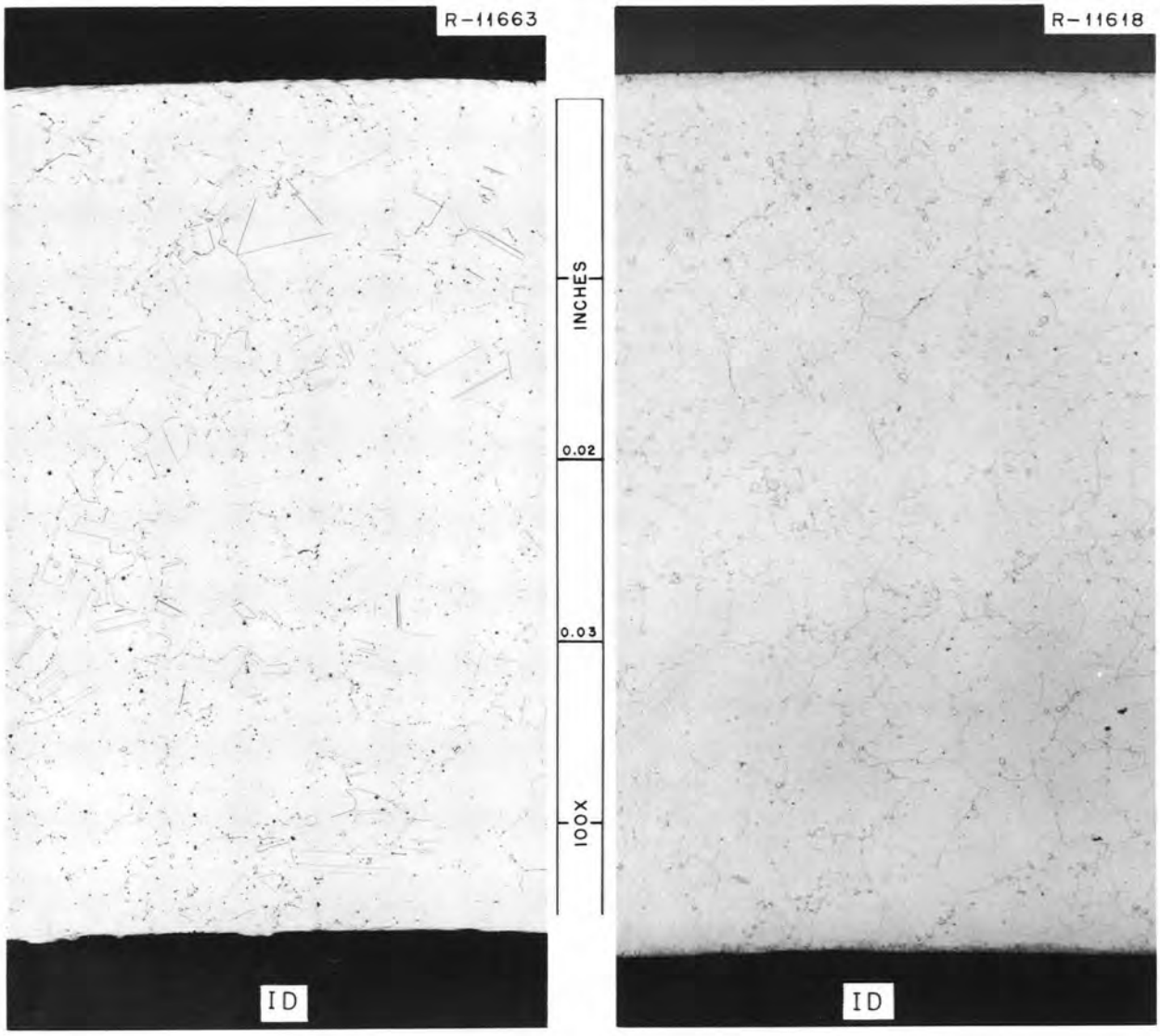


ETCHED CONTROL

ETCHED IRRADIATED

**Fig. 2.5. Transverse Section of INOR-8 Control Material and Specimen from Hemispherical Portion of Capsule 24.**

are 0.050-in.-thick INOR-8 vertical cylinders, 1-in. OD by 2.25 in. long with hemispherical end caps. Each capsule contains a core of CBG graphite $\frac{1}{2}$ in. in diameter by 1 in. long submerged approximately 0.3 in. in about 25 g of salt. The top cap contains two $\frac{1}{4}$-in.-diam purge lines, a $\frac{1}{8}$-in.-diam thermocouple well, and a projection to keep the graphite submerged. The two capsules differ only in the composition (primarily in the uranium concentration) of the fuel salt. Table 2.7 shows the nominal composition of the salt mixtures in each capsule.

Preparation of the salt and handling and filling operations were very similar to those described for assembly 47-4 above.

The twin manifolds which comprise the pressure monitoring and gas collection systems were carefully calibrated to ensure that the samples drawn

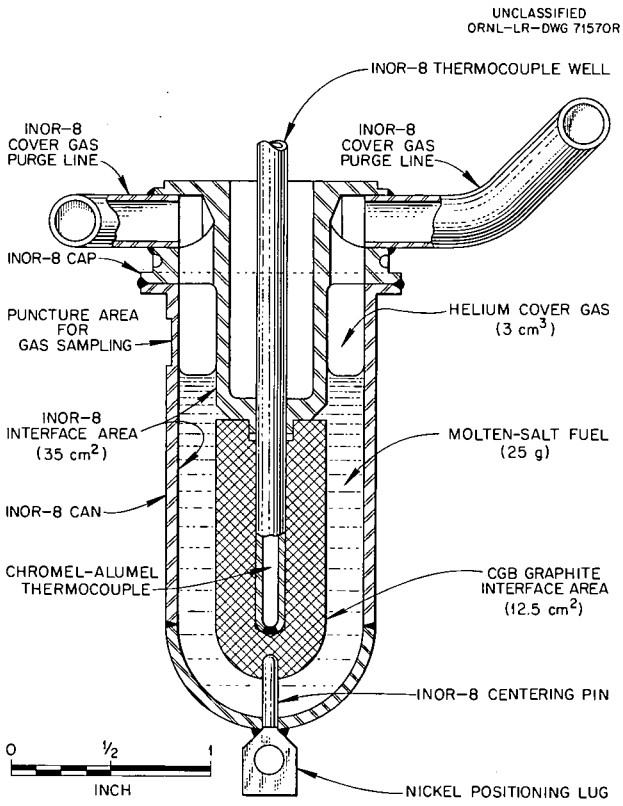


**Fig. 2.6. Purged Graphite–Molten-Salt Capsule.**

as desired into 200-cc metal sampling bulbs included a large and known fraction of the gas contained in the capsule.

Unfortunately, this experimental assembly was designed and constructed before the capsules of assembly 47-4 were opened, and the entire complex was designed to handle $CF_4$ but not $F_2$. In the short time between recogniton of $F_2$ in the previous capsules and the insertion of 47-5 into the MTR, several changes were made to improve the ability to handle fluorine. For example, valves seated with fluorocarbon plastic were substituted for less desirable types in the assembly, and sample bulbs of preconditioned nickel were substituted for the original ones of stainless steel. However, some stainless steel tubing, which could not have been replaced without a complete dismantling and reconstruction operation requiring several months, was retained in the assembly. Stainless steel contains $CF_4$ quite well, but it is not at all resistant to fluorine at elevated temperatures. Accordingly, evolution of $F_2$ with the salt molten under reactor power and with the sodium bath at near 600°C might well

**Table 2.7. Fuel Composition**

| | |
|---|---|
| Specific gravity at 1200°F | 2.13 |
| Liquidus | 842°F |
| Thermal conductivity at 1200°F | 3.21 Btu $hr^{-1}$ $ft^{-1}$ $(°F)^{-1}$ |
| Specific heat at 1200°F | 0.455 Btu $lb^{-1}$ $(°F)^{-1}$ |

| Fuel | Composition (mole %) | |
|---|---|---|
| | Capsule A | Capsule B |
| LiF | 67.36 | 67.19 |
| $BeF_2$ | 27.73 | 27.96 |
| $ZrF_4$ | 4.26 | 4.51 |
| $UF_4$ | 0.66 | 0.34 |

have been obscured by reaction of $F_2$ with the stainless steel.

**Behavior Under Irradiation.** – Assembly 47-5 was carried through five MTR cycles during the 4½ months ending January 23, 1963. Operating conditions for this assembly were varied as desired throughout the test to simulate conditions anticipated in different regions of the MSRE. Temperature and power level in capsules A and B were varied independently over a considerable interval but were, insofar as possible, held constant during periods represented by accumulation of the gas samples. Fuel temperatures during reactor operation ranged from 190 to 1500°F; power levels were varied between 3 and 80 w/cc within the fuel.

Gas samples were taken by isolating the capsule for a known and predetermined interval (6 to 96 hr) and then purging the accumulated gases into the sample bulb. Pressure was carefully monitored (to the nearest 0.1 psi) while the capsule was isolated. A total of 59 gas samples were taken from the two capsules during the first four MTR cycles under five distinct sets of conditions within the capsules. These sets of conditions (and numbers of samples) are:

1. reactor at full power (40 Mw) with fuel molten (34),
2. reactor at intermediate power (5 to 20 Mw) with fuel frozen (8),
3. reactor shut down with the fuel at about 90°F (9),

4. periods spanning fuel melting at reactor startup (4),
5. periods spanning freezing of fuel following reactor shutdown (4).

In addition, after termination of the experiment on January 23, the assembly was removed from the MTR, the purge lines were capped with valves, and the assembly was quickly shipped to ORNL. Pressure monitoring of capsules A and B at ambient temperature in the hot cell is under way, and samples of the evolving gas have been analyzed.

*Behavior with Reactor at Full Power.* – Pressure monitoring of the capsules with the reactor at 40 Mw and with the fuel molten showed no case of perceptible pressure rise. Moreover, none of the 32 gas samples taken during such conditions (over power level ranges of 3 to 80 w/cc) have shown any $F_2$ or more than faint traces of $CF_4$. (The presence of heated stainless steel in the lines might, as stated earlier, conceivably be responsible for nonobservance of $F_2$.) Analyses of gas samples collected during the first MTR cycle are shown in Tables 2.8 and 2.9. These analyses, which are typical of all that have been collected under these conditions, show considerably more xenon than krypton (the proper ratio is about 6:1) and very little if any $CF_4$.

Qualitative spectral analysis of gamma rays penetrating the nickel sample bottles have shown $Xe^{133}$ to contribute the only detectable peak under these collection conditions.

*Behavior During Reactor Shutdowns.* – During the $4\frac{1}{2}$-month exposure of 47-5, the MTR was shut down for refueling on four separate occasions; each such shutdown required approximately 100 hr. Since fission of the uranium is responsible for nearly all the energy available to the capsules, the capsules cooled to the fuel solidus in a few minutes and to below 150°F within an hour after each shutdown.

Six and one-half hours after the final shutdown a perceptible pressure increase was observed in capsule A; some 36 hr elapsed after shutdown before capsule B showed a pressure increase. Rate of pressure increase decreased with time for both capsules but showed no evidence of reaching equilibrium during the 4-day shutdown. A plot of observed pressure vs time for these capsules during the final shutdown is shown in Fig. 2.7.

**Table 2.8. Analysis of Gas Samples from Capsule A, MTR-47-5, During First MTR Cycle**

Fuel composition (mole %): LiF, 68.0; $BeF_2$, 27.0; $ZrF_4$, 4.3; $UF_4$, 0.7
Fuel weight: 24.822 g
Graphite weight: 5.696 g

| Accumulation Time (hr) | Temp (°F) | Power Level (w/cc) | Gas Analysis | | | | | | | | | |
|---|---|---|---|---|---|---|---|---|---|---|---|---|
| | | | Percent (by volume) | | | | | | | Parts per Million | | |
| | | | He | $N_2$ + CO | $O_2$ | $H_2O$ | Ar | $CO_2$ | $H_2$ | Kr | Xe | $CF_4$ |
| 29 | 1050 | 13 | 99.2 | 0.45 | 0.00 | 0.04 | 0.01 | 0.11 | 0.15 | 24 | 95 | <1 |
| 0[a] | 1050 | 13 | 99.5 | 0.31 | 0.00 | 0.10 | 0.00 | 0.06 | 0.03 | 3 | 18 | <1 |
| 50 | 1248 | 33 | 96.7 | 2.54 | 0.03 | 0.20 | 0.04 | 0.40 | 0.00 | 77 | 439 | <1 |
| 24 | 1250 | 33 | 98.0 | 1.34 | 0.00 | 0.22 | 0.02 | 0.29 | 0.05 | 39 | 248 | <1 |
| 24 | 1380 | 65 | 98.9 | 0.40 | 0.00 | 0.10 | | 0.18 | 0.34 | 71 | 405 | 0 |
| 96 | 1400 | 57 | 98.5 | 0.60 | 0.00 | 0.05 | 0.01 | 0.20 | 0.44 | 222 | 1762 | <2 |
| 16.3[b] | 90 | | 99.1 | 0.63 | 0.00 | 0.07 | 0.01 | 0.09 | 0.11 | 14 | 22 | 7 |

[a]Second sweep to find residual gases not collected during usual sampling.
[b]Unscheduled scram: 4 hr 17 min at 33 w/cc, 12.5 hr at zero power.

**Table 2.9. Analysis of Gas Samples from Capsule B, MTR-47-5, During First MTR Cycle**

Fuel composition (mole %): LiF, 68.0; $BeF_2$, 27.0; $ZrF_4$, 4.65; $UF_4$, 0.35
Fuel weight: 25.240 g
Graphite weight: 5.587 g

| Accumulation Time (hr) | Temp (°F) | Power Level (w/cc) | Gas Analysis | | | | | | | | | |
|---|---|---|---|---|---|---|---|---|---|---|---|---|
| | | | Percent (by volume) | | | | | | | Parts per Million | | |
| | | | He | $N_2$ + CO | $O_2$ | $H_2O$ | Ar | $CO_2$ | $H_2$ | Kr | Xe | $CF_4$ |
| 29 | 900 | 7 | 96.9 | 2.18 | 0.31 | 0.08 | 0.03 | 0.40 | 0.08 | 6 | 28 | <1 |
| 0[a] | 900 | 7 | 97.8 | 1.70 | 0.37 | 0.09 | 0.02 | 0.04 | 0.02 | | | |
| 50 | 1100 | 17 | 94.1 | 4.65 | 0.70 | 0.20 | 0.06 | 0.26 | 0.00 | 16 | 96 | 0 |
| 24 | 1090 | 17 | 95.0 | 3.91 | 0.61 | 0.19 | 0.05 | 0.25 | 0.00 | 6 | 56 | 0 |
| 24 | 1200 | 34.6 | 62.5 | 29.26 | 5.95 | 0.27 | 0.35 | 0.28 | 0.14 | 10 | 140 | 0 |
| 96 | 1230 | 30 | 96.7 | 2.54 | 0.03 | 0.20 | 0.04 | 0.40 | 0.00 | 77 | 439 | <1 |
| 16.3[b] | 90 | | 97.1 | 2.26 | 0.27 | 0.09 | 0.03 | 0.19 | 0.00 | 4 | 36 | 0 |

[a]Second sweep to find residual gases not collected during usual sampling.
[b]Unscheduled scram: 4 hr 17 min at 17 w/cc, 12.5 hr at zero power.

Capsule A had, at the time of the first MTR shutdown, been irradiated under conditions corresponding to 35 w/cm$^3$ fission density for 15.5 days; capsule B had received slightly more than half this dosage. Evolution of $F_2$ at low temperature through radiolysis of the solid fuel by radiation from fission product decay is suggested by the data from both 47-4 and 47-5.

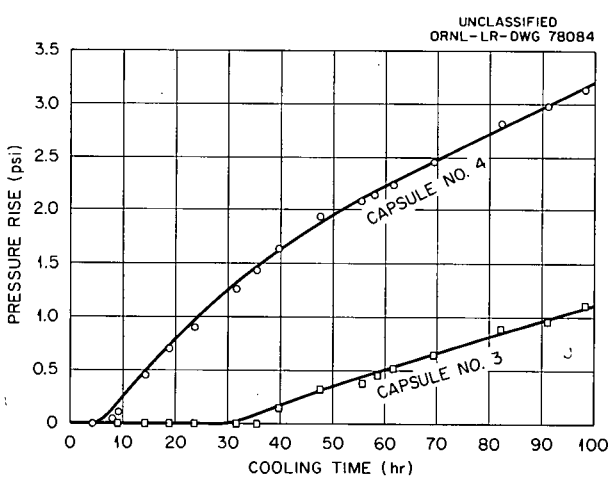


**Fig. 2.7. Pressure Rise in Capsules A and B, Assembly 47-5, During First Fueling Shutdown of MTR.**

*Behavior at Intermediate Reactor Power Levels.* The design of assembly 47-5 allowed considerable variation of capsule temperature and neutron flux (fission power). However, the adjustment range would not permit maintenance of the fuel below the melting point with the MTR at 40 Mw. Since no evidence of $F_2$ generation over molten fuel had been obtained, it was of interest to observe whether intermediate MTR power levels (5 to 20 Mw) with frozen fuel would produce the material. Accordingly, such experiments were performed for short time intervals and with the assembly set at the fully retracted position with minimum gas gap. Capsule pressure was observed and gas samples were taken for analysis. Data obtained from these experiments are shown in Table 2.10.

Examination of these data indicates that $F_2$ generation may have occurred in capsule A with the MTR at 5 Mw and the salt temperature at about 200°F and, perhaps, in capsule B with the MTR at 20 Mw and the salt at 410°F. The fact that the solid salt can withstand such energy releases at these relatively low temperatures seems quite reassuring. Since $F_2$ generation at 95°F (see section above) occurs with much less energy

**Table 2.10. Data from 47-5 with MTR at Intermediate Power Levels**

| Capsule No. | MTR Power (Mw) | Estimated Capsule Power Density (w/cc) | Capsule Temp (°F) | Sodium Bath Temp[a] (°F) | Results[b] |
|---|---|---|---|---|---|
| A | 20 | 10 | 610 | 378 | No pressure rise |
| B | 20 | 6 | 510 | 378 | No pressure rise |
| A | 10 | 5 | 312 | 200 | $\Delta P = 0$, 0% $F_2$ |
| B | 10 | 3 | 285 | 200 | $\Delta P = 0$, 0% $F_2$ |
| A | 15 | 7.5 | 380 | 260 | $\Delta P = 0$, 0% $F_2$ |
| B | 15 | 4.5 | 350 | 260 | $\Delta P = 0$, 0% $F_2$ |
| A | 5 | 2.5 | 199 | 122 | $\Delta P = +0.43$ psia[c] |
| B | 5 | 1.5 | 180 | 122 | $\Delta P = 0$ |
| A | 20 | 9 | 480 | 303 | $\Delta P = -0.1$ psia |
| B | 20 | 5 | 410 | 303 | $\Delta P = +0.2$ psia |

[a]The sodium bath temperature is the highest temperature occurring in the stainless steel tubing leading out from the capsules. Tests indicate negligible attack of stainless steel by 1% $F_2$ at temperatures below 400°F.

[b]Pressure readings, probably accurate to 0.1 psi, were taken during 2 to 3 hr of constant-temperature operation.

[c]The pressure rise occurred over a period of 65 min; for the subsequent 2 hr of the 5-Mw operation there was no further pressure rise.

available, it would appear that the "recombination" phenomenon is most sensitive to temperature.

*Behavior Through Startup and Shutdown.* – The last entries in Tables 2.8 and 2.9 show data for samples taken near the end of the first MTR cycle for a 16.4-hr period which included an unscheduled MTR scram, so that the sample collected represents 4 hr 17 min at power and 12.5 hr at zero power. While the gas in capsule B shows no unusual behavior, that from capsule A does show the only case so far observed in which a real concentration (7 ppm) of $CF_4$ has been observed; it may be observed as well that the Xe:Kr ratio appears to be low. The radioactivity of the gas sample (through the nickel bottle) was low and its activity peaks were not unusual.

*Behavior of Capsules After Termination of MTR Exposure.* – Assembly 47-5 was removed from the MTR and detached from the manifold system; the purge lines from capsules A and B were closed off by valves. After transfer to ORNL and removal of the assembly to a hot cell, the capsule lines were attached to manifolds. Capsule pressures were measured, samples were taken, and the very radioactive gas was pumped from the capsules into chemical traps. The evacuated samples were isolated in sections of the manifold containing pressure gages and were allowed to stand at ambient temperature (70°F). Generation of gas was immediately apparent in both capsules with pressure increases from capsule A larger than those from capsule B. Rate of generation decreased appreciably during the first 72 hr but seemed nearly linear thereafter. Sampling of the gas shows it to contain high concentrations of $F_2$ with considerable concentrations of $O_2$ (but little $N_2$), suggesting that air in-leakage is small but reaction of $F_2$ with oxide films on the apparatus is still appreciable. Small quantities of $CO_2$, $COF_2$, and $OF_2$ are also observed, but virtually no $CF_4$ is found. The capsules are still under observation, and a series of experiments to ascertain the effect of temperature on the rate of $F_2$ generation is beginning.

The quantity of $F_2$ generated from capsule A since the start of experiments at ORNL is estimated (February 12) to exceed 160 $cm^3$ (STP). This quantity plus that previously removed in samples, purges, etc., during reactor shutdowns

now approaches the quantities observed in the most highly irradiated capsules from MTR-4.

### Conclusions

Of the six capsules in assembly 47-4, five were found on examination to contain large quantities of $F_2$ and $CF_4$, while the sixth, which had received a considerably smaller radiation dose, showed no $F_2$ but a small quantity of $CF_4$. This latter capsule alone yielded the expected quantity of xenon, while all others retained this element nearly quantitatively. The quantity of $F^-$ released from the fuel generally increases with increase in uranium fissioned (or any of the consequences of this), but no quantitative correlation is found. Neither the quantity of $CF_4$ nor the ratio $CF_4$:$F_2$ shows an obvious correlation with fission rate, burnup, or time of cooling before examination. The appearance of the opened capsules, and all completed examination of components from these, seem to preclude the possibility that the $F_2$ was present for any appreciable period during the high-temperature operation of this assembly. Accordingly, the generation of $F_2$ from the salt at low temperatures during the long cooling period must have occurred.

All data from assembly 47-5 indicate that neither fluorine nor appreciable quantities of $CF_4$ are generated when the fission process is occurring in the molten salt. Fluorine is certainly released from the irradiated salt when it is held at temperatures below 100°F, but little, if any, $CF_4$ is generated under these conditions. Generation of $F_2$ when the salt is at low temperature occurs only after an appreciable time delay; the delay does not depend entirely on extent of prior irradiation. No auxiliary evidence, pressure rise, unusual Kr:Xe ratio, or unusual radioactivity of the sampled gas suggests difficulty during operation when the salt is molten. All of these phenomena, however, occur when the irradiated salt is maintained at low temperature.

Behavior of the system when fission occurs in the frozen salt at intermediate temperatures is here well defined. No gas generation has been observed under these conditions with the salt at temperatures above 400°F. Out-of-pile studies indicate that $F_2$ deliberately added to specimens of reduced (fluorine deficient) fuel reacts rapidly at temperatures well below the melting point of the salt. It seems very likely that "recombination" processes are sufficiently rapid at temperatures below 350°C to prevent any loss of $F_2$ from the salt.

The virtual nonappearance of $CF_4$ at any of the conditions experienced in MTR-5 is most encouraging. It may suggest that the $CF_4$ found in previous capsules from MTR-3 and MTR-4 arose in the following manner: $F_2$ was generated in those capsules during some or all of the MTR shutdown periods; this $F_2$ was not removed from the sealed capsules, and on subsequent heatup by reactor power it reacted indiscriminately with the fuel, the metal, and the graphite. The $CF_4$ formed was partially retained and was observed at termination of the test.

The process by which the $F_2$ is generated during low-temperature self-irradiation of the salt is, as yet, unknown. Considerable energy is available from fission product decay to produce radiolytic reactions in the fuel salt. Gamma rays originating in capsules such as were used in this study would be absorbed to a very slight extent; perhaps as much as one-half of the beta energy would be absorbed. A yield (*G* value) of less than 0.05 fluorine atom per 100 ev absorbed would suffice to explain the fluorine produced in any of the capsules. Production of $F_2$ with such a low *G* value seems a reasonable hypothesis, though no observations of fluorine production from salts on bombardment by beta irradiation have been published. Attempts to demonstrate $F_2$ generation by electron bombardment of fuel salt mixtures at ambient temperatures are under way.

The evidence to date does not permit a decision as to whether the graphite influences the generation of $F_2$. It is, however, apparent that the generation of $F_2$ is a low-temperature process occurring only under circumstances of relatively little importance to the MSRE and that generation of $CF_4$ occurs to a negligible extent, if at all, at MSRE temperatures and power levels.

## BEHAVIOR OF CARBON TETRAFLUORIDE IN MOLTEN FLUORIDES

J. H. Shaffer F. A. Doss
W. Jennings W. P. Teichert

As part of an investigation to evaluate the implied effects of elemental fluorine generation and carbon tetrafluoride synthesis in the MSRE,

an experimental study of the behavior of $CF_4$ in molten fluorides simulating the reactor fuel mixture was initiated. Since the formation of either $F_2$ or $CF_4$ in the MSRE would deplete the fuel mixture of fluoride ion, the primary objective of this program was a study of the back-reaction of $CF_4$ with a "reduced" fuel mixture both in the presence and absence of graphite. In addition, attempts were made to measure the solubility of $CF_4$ in the molten fluoride mixture.

### Preparation of "Reduced" Fuel Mixtures

For studies related to this program, "reduced" fuel mixtures were obtained by adding zirconium metal turnings to molten mixtures of $LiF$-$BeF_2$-$ZrF_4$-$ThF_4$-$UF_4$ (70-23-5-1-1 mole % respectively). In these preparations, reductions corresponding to about a 70% conversion of $UF_4$ to $UF_3$ in the molten mixture have been maintained for long time periods at 600 to 850°C in nickel containers. Evidence of these reductions was based on analyses of salt samples by a hydrogen evolution technique. While this analytical method for trivalent uranium is indirect, the presence of $UF_3$ in these melts was confirmed by petrographic observations and by interpretation of x-ray diffraction data in salt samples withdrawn from the reaction vessels.

### $CF_4$ Reactions in the Absence of Graphite

During one series of experiments, the reaction of $CF_4$ with $UF_3$ was studied by recirculating a known mixture of $CF_4$ in helium (initially about 20% $CF_4$) through a "reduced" mixture of $LiF$-$BeF_2$-$ZrF_4$-$ThF_4$-$UF_4$ (70-23-5-1-1 mole % respectively) contained in nickel at temperatures of 700 to 850°C. The recirculated gas was bubbled through the melt [at flow rates of about 1.7 liters (STP)/min] by means of a nickel dip line extending nearly to the bottom of the reaction vessel. [A total gas charge of about 3 liters (STP) was used in each experiment.] Evidence of chemical reaction, noted by mass spectrographic analyses of gas samples periodically withdrawn from the reaction system, is shown in Fig. 2.8.

While the precision of the analytical method used in these studies was not sufficient to obtain an accurate analysis of the data, an attempt was made to determine the rate of reaction of $CF_4$.

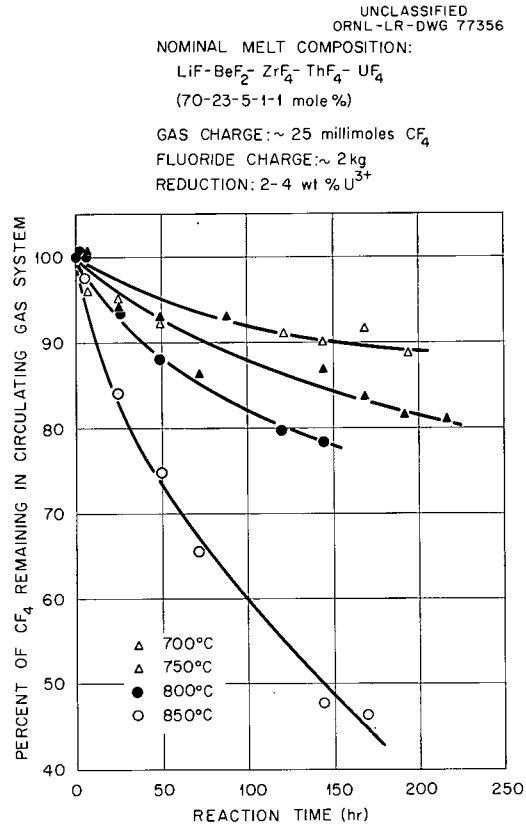


**Fig. 2.8. Reaction of $CF_4$ with "Reduced" MSRE Fuel Mixture in the Absence of Graphite.**

Since the concentrations of $UF_3$ in the fluoride mixture were maintained at relatively high values, the reaction rate was assumed to be dependent upon the $CF_4$ concentrations alone. A fair correlation of the data with the first-order rate equation,

$$\ln \frac{N_0}{N_t} = k_c t ,$$

was obtained. Calculated values of the relative reaction velocity constants are as follows:

| Temperature (°C) | $k_c$ ($hr^{-1}$) $\times 10^{-4}$ |
|---|---|
| 700 | 6.4 |
| 750 | 11.4 |
| 800 | 31.4 |
| 850 | 47.1 |

From a temperature-dependence plot of these velocity constants (Fig. 2.9), an activation energy of about 32 kcal/mole for this assumed first-order reaction rate was obtained.

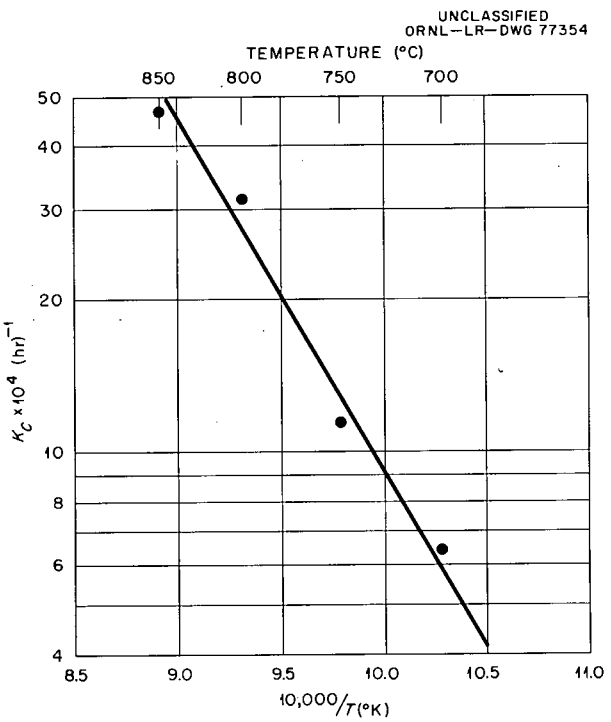


**Fig. 2.9. Temperature Dependence of the Reaction of $CF_4$ with $UF_3$ in a "Reduced" Fuel Mixture in the Absence of Graphite.**

## $CF_4$ Reactions at a Graphite-Salt Interface

Since the reactor core of the MSRE will consist essentially of an unclad graphite moderator submerged in the fissioning fluoride fuel mixture, the synthesis of $CF_4$ and possibly any significant back-reaction of $CF_4$ with the "reduced" fuel mixture would presumably occur at a graphite-salt interface. Accordingly, an experimental method for determining the rate at which $CF_4$ reacted with a "reduced" fuel-salt mixture under these simulated conditions was developed. In these experiments, $CF_4$ was admitted to the reaction system at very low flow rates through a hollow graphite cylinder which was brazed to the end of a nickel dip tube. The graphite was machined so that $CF_4$ would effuse through the thin vertical wall of the cylinder.

Since the anticipated reaction

$$CF_4 + 4UF_3 \longrightarrow 4UF_4 + C \qquad (1)$$

would not introduce a new constituent into the gas phase, the experimental procedure was essentially limited to techniques for ascertaining the consumption of $CF_4$ by the reaction system. The procedure chosen to detect and measure the reaction rate of $CF_4$ was based on measurements of its rate of appearance in the gas phase above the salt.

By introducing helium at a known rate as a sweep gas into the gas space above the melt, while introducing $CF_4$ at a known rate through the graphite effusion cylinder, the effective concentration of $CF_4$ entering the gas phase in a nonreacting system could be calculated. If the total gas flow rate leaving the system equals the combined inlet flow rates of $CF_4$ and helium, then the concentration of $CF_4$ in the gas phase (initially pure helium) above the melt at any time can be expressed by the equation

$$\frac{dN_{CF_4}}{dt} = \frac{f}{n_t}(A - N_{CF_4}) , \qquad (2)$$

where $N_{CF_4}$ is the mole fraction of $CF_4$ in helium at any time $t$, $A$ is the effective mole fraction of $CF_4$ entering the system, $n_t$ is the total moles of gas in the system, and $f$ is the total gas flow rate in moles per unit time. From a plot of $\Delta N_{CF_4}/\Delta t$ vs $N_{CF_4}$, the value of $A$ may be determined from values of the slope and intercept of a line drawn through the data points. In control experiments with a nonreduced fuel-salt system in which concentrations of $CF_4$ in helium were analyzed by thermal conductivity measurements, values of $A$ calculated from the rate data shown in Fig. 2.10 were found to be the same as those calculated from the actual inlet He and $CF_4$ flow rates within a flow-rate variation of less than ±1 cc of $CF_4$ per hour. In addition to demonstrating the accuracy of the experimental system, these "blank" determinations at 600°C demonstrated that $CF_4$ did not react with the nonreduced fuel mixture at a detectable rate.

If $UF_3$ were present in relatively large concentrations in a "reduced" salt system, the reaction rate of $CF_4$ should not be affected by small changes in the $UF_3$ concentration. Further, under

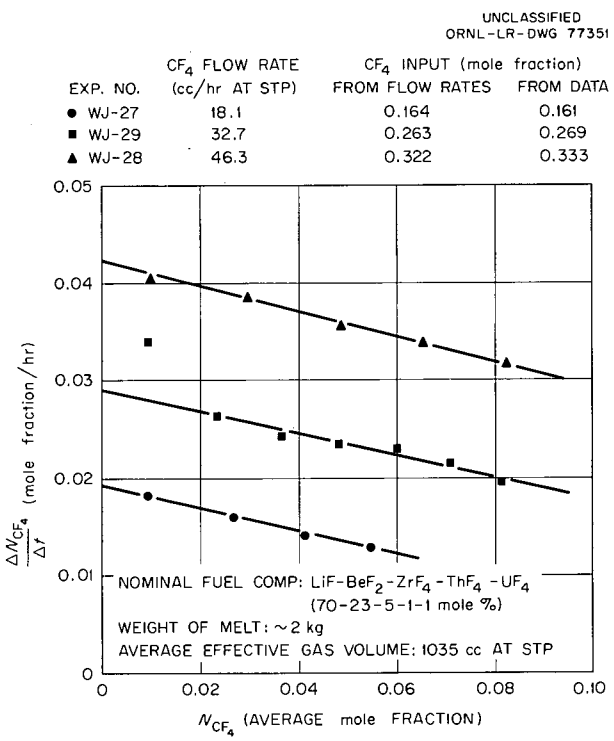


**Fig. 2.10. Rate of Appearance of $CF_4$ in the Gas Phase Above "Nonreduced" Fuel Mixture at 600°C.**

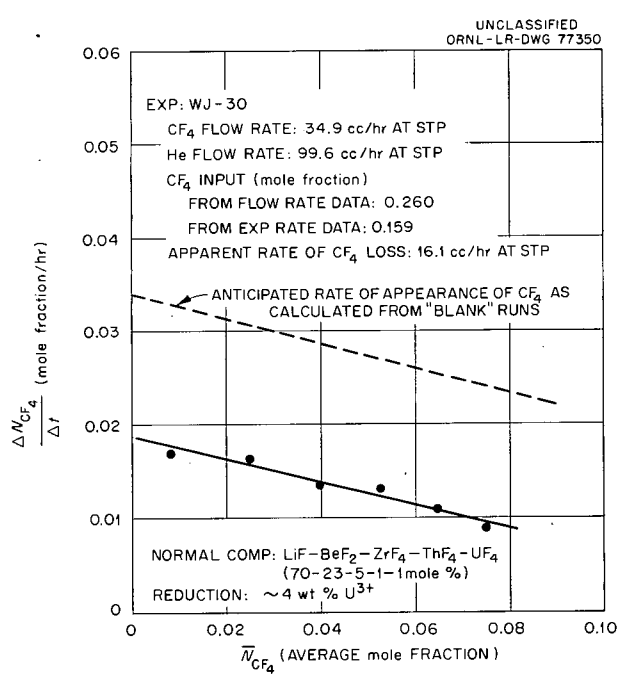


**Fig. 2.11. Rate of Appearance of $CF_4$ in the Gas Phase Above "Reduced" Fuel Mixture at 600°C.**

the flow conditions of the reaction system, the concentration of $CF_4$, with respect to the fluoride melt, should remain constant. Therefore, a zero-order reaction with respect to $CF_4$ would be anticipated and should be evident in the reaction system as a consumption of $CF_4$ at a constant rate. Thus, the evidence of chemical reaction noted as Eq. (1) could be detected by comparing the experimentally determined $A$ value of Eq. (2) with a value based on the input He and $CF_4$ flow rates. Such values, calculated from the rate data obtained in one experiment conducted thus far (Fig. 2.11), indicated that $CF_4$ had reacted with the "reduced" fuel mixture at a rate of about 16 cc (STP) of $CF_4$ per hour. In this experiment $CF_4$ was admitted at a flow rate of 35 cc (STP) per hour into approximately 2 kg of a fuel mixture which contained about 4.8 wt % $U^{3+}$. Additional experiments are in progress to confirm this finding and to examine the effects of temperature and $UF_3$ concentrations on the rate process.

## Attempted Solubility Measurements of $CF_4$

The apparatus and experimental techniques used in this investigation were essentially unchanged from those used previously to determine the solubility of noble gases in molten fluorides.[5] The molten fluoride mixture was contained in a nickel saturating vessel which was connected to a stripping vessel by a small-diameter transfer tube welded to the bottom of each container. After saturation with $CF_4$ at a constant temperature and pressure, a portion of the melt was transferred to the stripping section by melting the frozen-salt seal in the transfer tube. Measurements of the solubility of $CF_4$ in the fluoride melt were to be based on its recovery with a known quantity of recirculating helium which was used as the stripping gas.

While the results of tests of the experimental procedure with argon compared favorably with previous determinations,[6] attempts to measure the solubility of $CF_4$ in the molten fluoride fuel mixture have not thus far been successful. In several experiments at 600 and 800°C, the concentrations of $CF_4$ in samples taken from the gas

[5] W. R. Grimes, N. V. Smith, and G. M. Watson, *J. Phys. Chem.* **62**, 862 (1958).

[6] G. M. Watson *et al.*, *J. Chem. Eng. Data* **7**, 285 (1962).

stripping section of the apparatus were below detectable limits of the mass spectrographic analytical method. The application of thermal conductivity measurements to this system is currently being attempted.

## FLUORINE CHEMISTRY STUDIES

J. E. Eorgan

### Fluorine Gas Control Unit

A unit to regulate and control fluorine gas was built. In addition to the following experiments, its principal uses have been the prefluorination of gas sampling capsules and other equipment needed in connection with the MSRE radiation effects tests, as well as the preparation of standard gases for various program needs.

The unit consists of an arrangement of valves and gages in a semienclosed panel located in a hood. The flow diagram of the system is shown in Fig. 2.12. The first requirement of the system was that it withstand pure fluorine at a pressure of 3 atm. This limited the structural material to Monel, nickel, and bronze. To assure leak-tightness, all valve-to-tubing connections were silver-soldered and the connectors used were of special Holse ultrahigh-vacuum type.

The unit was prefluorinated by admitting fluorine gas slowly into the evacuated system.[7] At 5 psia the fluorine flow was stopped, and after a 10-min period the system was evacuated through the soda lime trap. This procedure was continued, increasing the fluorine pressure in 5-psia steps until 45 psia was reached.

Strict procedures[7] for the safe handling of fluorine in this apparatus have been followed, thus making available the means conveniently to supply, monitor, sample, or remove a fluorine-containing gas, as well as to prefluorinate experimental equipment.

[7] "Handling Elemental Fluorine Gas in the Laboratory," General Chemical Division (Allied Chemical and Dye Corp.) Manual PD-TA-35413, revised Aug. 15, 1958, Lib. of Congress Number QD 181.FL G 315.

UNCLASSIFIED
ORNL-LR-DWG 78090

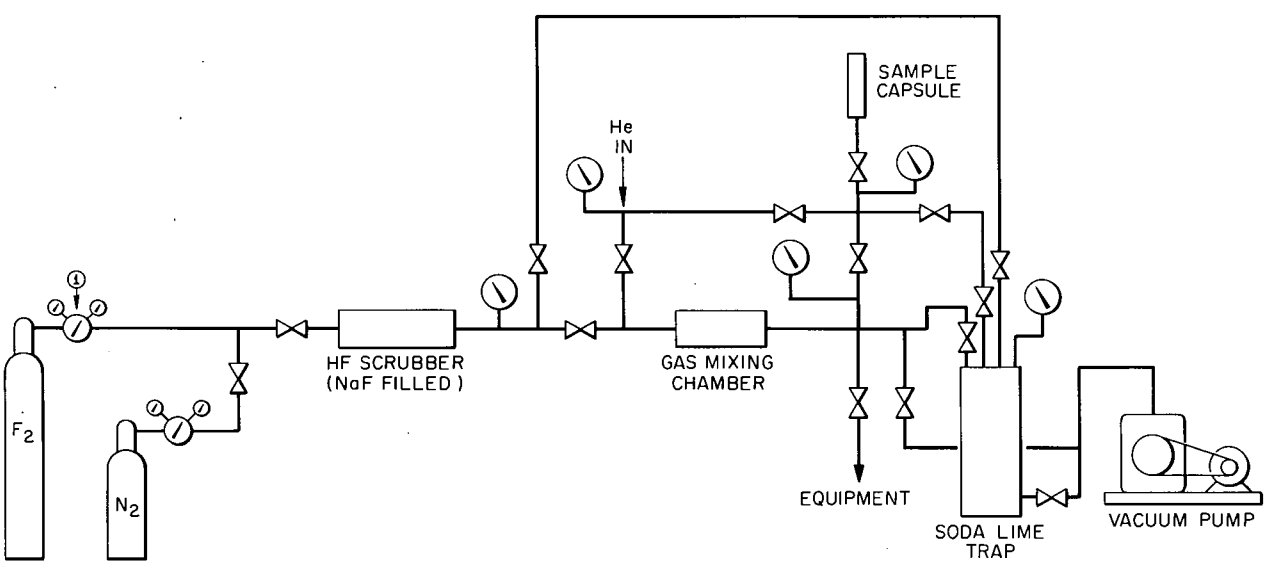


—— 1/4-in. NICKEL TUBING x 0.065-in. WALL PROCESS PIPING
HOKE DIAPHRAGM VALVE NO. 413 MONEL
ASHCROFT "DURAGAUGE", 30-in. Hg VACUUM TO 30 psig
① MATHESON FLUORINE REGULATOR, MODEL 15F-670

**Fig. 2.12. Fluorine Gas Control Unit.**

### Preparation of Xenon Tetrafluoride

Xenon tetrafluoride suitable for x-ray diffraction and microscopic studies was prepared by the following procedure, based on the work of Claassen *et al.*[8] The reactor capsule was connected to the fluorine gas control unit and prefluorinated by using fluorine at 45 psia and a temperature of 600°C. Xenon (0.42 g) and fluorine (0.24 g), giving a volume ratio of 1:3, were charged into the reaction capsule to a pressure of 24 psia. The mixture was heated to a maximum temperature of 480°C, which was reached after 1 hr (Fig. 2.13).

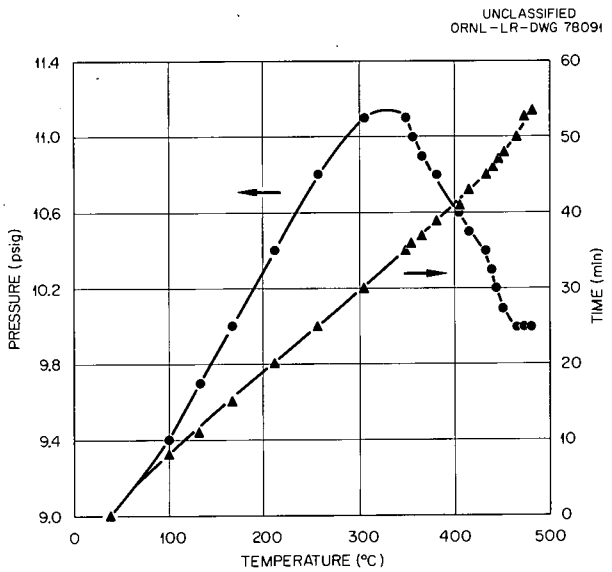


**Fig. 2.13. Reaction of Xenon and Fluorine.**

The reaction of xenon and fluorine appears to have started at 307°C and apparently was complete at 480°C, as shown in Fig. 2.13. The reaction capsule was then cooled to −78°C and the unreacted gases pumped off. The reaction products were then sublimed to a Pyrex U-tube. The yield, estimated to be approximately the theoretical 600 mg, was a colorless, crystalline material which was stable at room temperature. It was observed that the crystals, sealed in the Pyrex U-tube, grew to a few millimeters in width in a few hours. These observations are in agreement with those of Claassen *et al.*[8]

[8]H. H. Claassen, H. Selig, and J. G. Malm, *J. Am. Chem. Soc.* **84**, 3593 (1962).

### Reaction of Fluorine with Reduced Salt

The presence of fluorine in MSRE radiation-effects capsules is now believed to result from the effects of radiation on the frozen salt. The escape of fluorine required that some reduced material be left in the cold salt ("Radiation Chemistry of MSR System," this chapter). An experiment was performed to determine at what temperature fluorine would begin to react rapidly with a reduced salt of the type used in the MTR experiments: $LiF\text{-}BeF_2\text{-}ZrF_4\text{-}ThF_4\text{-}UF_4$ (70-23-5-1-1 mole %).

The reaction capsule was connected to the fluorine gas control unit and prefluorinated by using fluorine at 45 psia and 600°C. The salt was added, 360 g, to a depth of 3.63 in. and again prefluorinated by using 1 atm of fluorine at 600°C. No adsorption of fluorine was noted during this treatment. Zirconium metal, 0.0988 g, was added to the salt and heated to 600°C under a helium atmosphere to accomplish partial reduction of the $U^{4+}$. Then the salt was allowed to cool to room temperature, the system was evacuated to 5 $\mu$, and 0.002 mole of fluorine was added to the capsule (diluted to 1 atm with helium).

The frozen reduced salt, in the presence of the helium-fluorine gas mixture, was heated to 100°C. It was then cooled and the gas pressure was noted. This procedure was repeated four times, the temperature being increased by 100°C each time. The results, listed in Table 2.11, show

**Table 2.11. Fluorination of Reduced Salt**

| Time at Temperature (hr) | Temperature (°C) | Reference Pressure (in. Hg below atmospheric pressure) | |
|---|---|---|---|
| | | Before Heating | After Heating |
| 118 | 27 | 0 | 1.5 |
| 1.4 | 100 | 1.5 | 1.5 |
| 4.2 | 200 | 1.5 | 2.0 |
| 2.6 | 300 | 2.0 | 1.9 |
| 3.1 | 400 | 1.9 | 4.0[a] |
| 5.7 | 500 | 4.0 | 4.0 |

[a]Corresponds to completed reaction of the fluorine.

that the reaction was complete at 400°C. This temperature is ~42°C below the melting point of the salt.

The exposure of capsules in the MTR involves numerous ups and downs in radiation and temperature. While graphite and the containment material (INOR-8) are not compatible with the fluorine pressure at elevated temperatures for long periods of time, it seems probable from the present test that fluorine produced at intended shutdowns recombined quickly with the reduced salt when the temperature was subsequently raised – so quickly that very little $CF_4$ production or corrosion of the container occurred.

## EVOLUTION OF WATER VAPOR FROM GRAPHITE[9]

W. K. R. Finnell F. A. Doss
J. H. Shaffer

Since the unclad graphite moderator of the MSRE will comprise about 80% of the reactor core volume, the presence of impurities normally found in commercial-grade graphite[10] might provide a source of contamination to the molten-fluoride fuel mixture. Of the various volatile impurities, water vapor would probably represent the greatest nuisance for reactor operations. The release of water vapor into molten-fluoride systems similar to the MSRE fuel mixture has been found to cause the precipitation of beryllium, thorium, and uranium from solution as oxides.[11] In the MSRE the introduction of water vapor into the fuel system would probably result in the deposition of zirconium dioxide.

As part of the MSRE startup operations (prior to salt loading), it is planned that the reactor core will be heated to about 650°C while circulating helium through the fuel system. This operation should promote the release of volatile impurities from the graphite into the helium stream, from which they may be removed by the purification system.[12] In order to simulate this operation on a small scale, an experimental program was devised and performed during the past year.

### Experimental

In the experiments, pieces of graphite having the same machined cross section as that designed for an MSRE moderator element (but only 6 to 12 in. long) were each canned in a close-fitting nickel container and mounted vertically in a tube furnace connected to a helium recirculation system. Provision was made for the continuous analysis of a small portion of the gas stream emerging from the container for its water vapor content. A MEECO model W electrolytic water analyzer was found to have convenient sensitivity to changes in water vapor content over the range from 0 to 1000 ppm. The main body of the recirculating gas stream was passed through a magnesium perchlorate drying column, followed by a dry-ice trap, to reduce the moisture content to below 4 ppm before reexposing the gas to the heated graphite.

The gas recirculation rate through the system, 3000 cc/min (STP), was chosen so that when the graphite was at 600°C the linear velocity of the gas past the graphite surface would be 25 cm/sec, about the same as that calculated from the estimated gas recirculation rate in the MSRE (when the fuel pump would be used to recirculate the helium gas). The rate at which the temperature of the graphite was increased was controlled so as to provide a range of values covering the anticipated rate for the reactor startup operation. Heating rates from 5 to 65°C/hr were employed.

### Discussion of Results

The predominant characteristics of water vapor removal from graphite, as illustrated by the results for ETL graphite[13] shown in Fig. 2.14, were found

[9] To be published.

[10] L. G. Overholser and J. P. Blakely, *Proceedings of the 5th Conference on Carbon*, vol 1, p 194, Pergamon Press, New York, 1962.

[11] *Reactor Chem. Div. Ann. Progr. Rept. Jan. 31, 1961*, ORNL-3127, p 158.

[12] *MSRP Progr. Rept. Aug. 1, 1960, to Feb. 28, 1961*, ORNL-3122, pp 15–16.

[13] ETL denotes a specific grade of graphite purchased for experimentation in the Engineering Test Loop (Reactor Division, ORNL). The specifications for this graphite are similar to those applied for the purchase of the MSRE moderator elements.

to be the removal of physically adsorbed water at temperatures up to 150°C and the removal of what appeared to be chemisorbed water within the temperature interval of 200 to 400°C. The release of water to circulating helium at temperatures above 400°C appeared to be inconsequential.

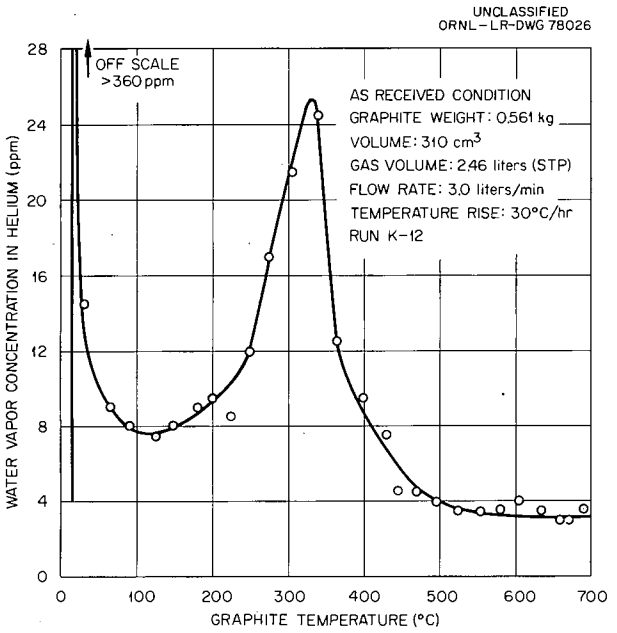


**Fig. 2.14. Removal of Moisture from ETL Graphite by Helium Purge.**

In several experiments, prior to the water-removal treatment, graphite specimens were exposed to moist helium at room temperature for 2-hr periods. It was not established that this exposure was sufficient to saturate the graphite completely, but the quantity of water so introduced was about the same as that present in samples of as-received graphite of the same quality. During subsequent experimental studies of water evolution from these samples, it was found that they behaved quite like the samples of as-received material. The pattern of reproducibility in repeated tests with the same piece of graphite is illustrated in Fig. 2.15.

The experimentally observed rate of water evolution from graphite must certainly be dependent upon diffusion within the pores of the graphite as well as the adsorption characteristics of the graphite. Both of these parameters must be quite

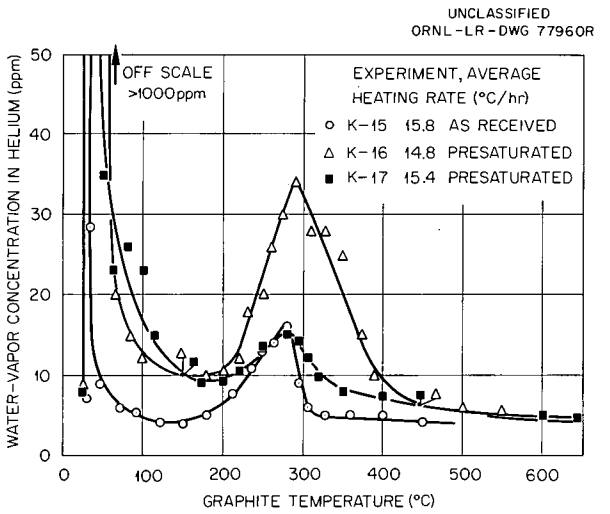


**Fig. 2.15. Reproducibility of Water Vapor Evolution from a Graphite Block "Presaturated" by Exposure to Moist Helium.**

temperature-dependent. To demonstrate the overall dependence of the water evolution on temperature, a series of experiments was performed on a single piece of ETL graphite at different heating rates. Before each experiment the graphite was exposed to moist helium for a 2-hr period. As shown in Fig. 2.16 the temperature at which the chemisorbed water evolution reached its maximum value was found to increase from 270°C to 400°C as the heating rate was increased from 5°C/hr to 65°C/hr.

Since there are no provisions for an initial evacuation of gases from the MSRE reactor core prior to heatup, and since the graphite will almost certainly contain some entrapped air in its pores or cracks, it is expected that some volatile products arising from the interaction of air with graphite will be released during the heatup operation. In an experiment with ETL graphite the accumulation of air and carbonaceous gases in the circulating stream was found to be negligible in amount.

Because the upper concentration limit (1000 ppm) of the moisture analyzer was exceeded for short periods of time while the physically adsorbed moisture was being removed, it was not possible to obtain a quantitative measure of its amount. Nevertheless, it was clear that such water was easily released during the test (and presumably should be easily released from the

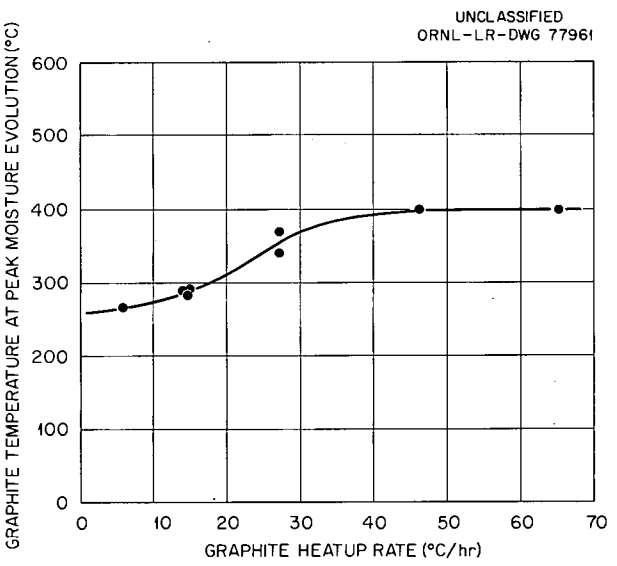


**Fig. 2.16. Effect of Heating Rates on the Evolution of Apparent Chemisorbed Water from Graphite.**

MSRE). With respect to the chemisorbed water, quantities of about 9 cc (STP) of water vapor per 100 cc of graphite were found in both as-received and presaturated graphite. This amount of chemisorbed water would correspond to about 30% of the maximum oxygen content permitted by the specifications.

Because the removal of water was accomplished so readily in the experimental apparatus, it seems highly probable that the planned heatup treatment of the MSRE will be very effective in removing whatever water may be present, either as physically adsorbed or as chemisorbed material. Moreover, the reactor engineers appear to have considerable latitude in the rates of heating which may be employed without sacrificing the effectiveness of the treatment.

## OXIDE BEHAVIOR IN FLUSH SALT–FUEL SALT MIXTURES

J. E. Eorgan B. F. Hitch
J. H. Shaffer R. G. Ross
C. F. Baes

The composition of the flush salt to be used in the MSRE should be chosen such that in use its contamination with fuel salt and with oxide will not cause $UO_2$ precipitation. Previous studies have indicated that the presence of excess $Zr^{4+}$ will prevent $UO_2$ precipitation for one or both of the following reasons: (1) a mass-action effect will cause $ZrO_2$ to precipitate preferentially,[14] and (2) $Zr^{4+}$ may complex oxide ion, thus producing an appreciable oxide capacity in the melt.[15] There remains, however, a need for more quantitative information on the solubilities of $UO_2$, $ZrO_2$, and BeO as well as their mass action or equilibrium behavior in flush salt–fuel salt mixtures. Accordingly, additional oxide precipitation studies, similar to those reported previously,[14] are in progress.

Such studies continue to be handicapped by the inaccuracy of direct oxide analyses of such melts in the concentration range of interest here (<1000 ppm).[16] To circumvent this problem, in the present experiments, wherein known amounts of BeO were added to known weights of melt, careful material balances have been made between the oxide added and the oxide removed by precipitation or sampling as a means of estimating the oxide remaining in solution. In general, it was found that these calculated values were more reliable than the oxide analyses.

Figure 2.17 presents a log-log plot of equilibrium $U^{4+}$ and $Zr^{4+}$ concentrations vs the oxide ion concentration so calculated for a precipitation experiment in which BeO was added to $Li_2BeF_4$ containing 5 wt % fuel salt[17] at 600°C. The straight lines of slope −2 drawn through the data points represent the expected mass-action behavior for the reactions

$$UO_2(s) \rightleftharpoons U^{4+} + 2O^{2-} ,$$

$$ZrO_2(s) \rightleftharpoons Zr^{4+} + 2O^{2-} ,$$

wherein the solubility products are

$$Q^s_{UO_2} = [U^{4+}][O^{2-}]^2 = 1.2 \times 10^{-5} \text{ mole}^3 \text{ kg}^{-3} ,$$

$$Q^s_{ZrO_2} = [Zr^{4+}][O^{2-}]^2 = 3.2 \times 10^{-5} \text{ mole}^3 \text{ kg}^{-3} .$$

[14] *MSRP Progr. Rept. Aug. 1, 1960, to Feb. 28, 1961,* ORNL-3122, p 120.

[15] *MSRP Progr. Rept. Mar. 1 to Aug. 31, 1961,* ORNL-3215, p 124.

[16] *MSRP Semiann. Progr. Rept. Aug. 31, 1962,* ORNL-3369, p 130.

[17] The fuel composition was $LiF$-$BeF_2$-$ZrF_4$-$ThF_4$-$UF_4$, 70-23-5-1-1 mole %.

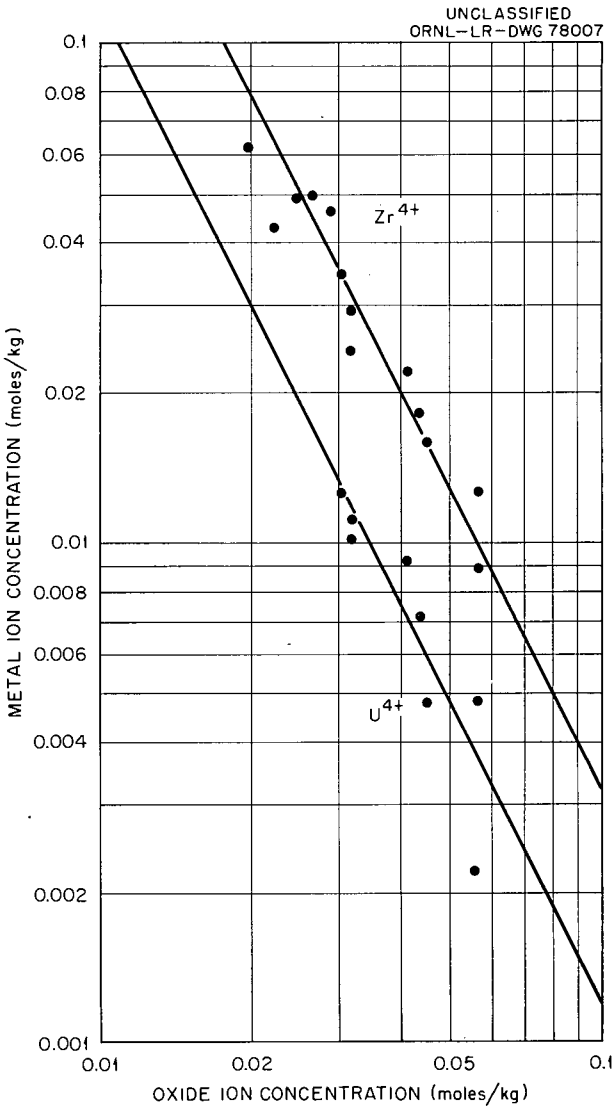


**Fig. 2.17. Apparent Relation Between $U^{4+}$ and $Zr^{4+}$ Concentration and $O^{2-}$ Concentration in $Li_2BeF_4$ Melt at 600°C.**

The correlation of the data with this simple solubility behavior indicates that complexing of $M^{4+}$ with $O^{2-}$ in this medium is not an important effect in the range studied. The above solubility products indicate the following solubilities in $Li_2BeF_4$ initially free of $Zr^{4+}$, $U^{4+}$, and $O^{2-}$ at 600°C:

$$UO_2,\ 0.014 \text{ mole/kg};$$

$$ZrO_2,\ 0.020 \text{ mole/kg}.$$

The precipitation behavior observed for 5 wt % fuel salt in $Li_2BeF_4$ is compared with that calculated from these simple mass-action relationships (indicated by the curves) in Fig. 2.18. Precipitation of $ZrO_2$ occurs when $\sim$0.0023 mole of oxide per kg has been added (370 ppm). Uranium dioxide precipitation occurs when the ratio $[Zr^{4+}]/[U^{4+}]$ falls to $\sim$2.7 (which is the ratio of their estimated solubility products). The concentrations of uranium and zirconium in the melt continue to fall until BeO saturation has been reached (estimated here to occur at $\sim$0.07 mole per kg of oxide in the melt, $\sim$1100 ppm).

It was found in similar tests that when 5 mole % $ZrF_4$ ($\sim$1.3 moles of Zr per kg) initially was present in the $Li_2BeF_4$, immediate precipitation of $ZrO_2$ occurred upon the addition of BeO. This too is in agreement with the above mass-action relations, from which it may be calculated that an oxide concentration >0.005 mole per kg (80 ppm) would produce precipitation in this melt. The result suggests that even at this higher $Zr^{4+}$ concentration there was no oxide ion complexing.

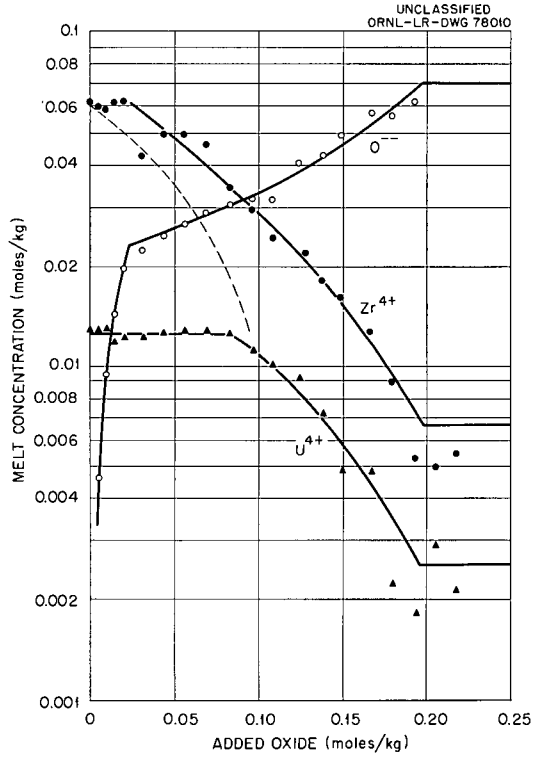


**Fig. 2.18. $ZrO_2$ and $UO_2$ Precipitation from $Li_2BeF_4$–5 wt % Fuel Salt by BeO at 600°C.**

The present results thus indicate that oxide behavior in flush salt–fuel salt mixtures may be predicted reasonably well from the simple solubility product relationships (Fig. 2.17). This means that a flush salt such as $Li_2BeF_4$ can accumulate oxide ion, which may be present in the drained reactor system, up to a limit determined by the amount of fuel salt which the flush salt may accumulate as it is circulated in the system. If this oxide limit is exceeded, $ZrO_2$ will precipitate before $UO_2$ is precipitated. The addition of $Zr^{4+}$ to the flush salt will provide added protection against $UO_2$ precipitation and is expected to dissolve any $UO_2$ which may be produced when the reactor is drained of fuel. At the same time, however, such a flush salt can tolerate less oxide contamination without precipitation of $ZrO_2$.

These considerations suggest that this investigation of oxide behavior be extended to a range of temperatures. Possible adsorption of $U^{4+}$ by $ZrO_2$ and/or uranium(IV)-zirconium(IV) oxide solid solution formation could be investigated at the same time.

# 3. Physical Chemistry of Molten-Salt Systems

The researches described under this heading seek to establish the basic principles which determine the chemical behavior of molten-salt mixtures. Although this program is broad in scope, it primarily aims to provide support, at the fundamental research level, for the development of molten-salt reactors. Hence, most of the investigations involve molten-fluoride compounds and mixtures. However, investigations which use other molten-salt media frequently provide valuable results which are analogous to those in fluoride media and, at the same time, broaden the general knowledge of molten-salt interactions.

## FREEZING-POINT DEPRESSIONS IN SODIUM FLUORIDE

S. Cantor W. T. Ward

This study is part of a comprehensive investigation which seeks to relate the effects of structural parameters of the components, such as radius, charge, and polarizability, to the thermodynamic properties of fused fluoride solutions. The approach used in this study has been to investigate a conveniently determined thermodynamic property of a solvent, in which type and concentration of solute can be systematically altered, and then to relate variations in this property to structural parameters of the solutes. The object of the researches described here was to measure the depressions of freezing points in the solvent, NaF, and correlate the excess partial molal free energies of mixing of NaF, $(\overline{F} - F^0)^E_{NaF}$, with the structure of the solutes. These free energies are calculated from the equation

$$(\overline{F} - F^0)^E_{NaF} = RT \ln \gamma_{NaF} , \qquad (1)$$

where $T$ is the liquidus temperature and $\gamma_{NaF}$ is the activity coefficient of NaF. The values of $\ln \gamma_{NaF}$ are calculated from the liquidus temperatures by integration of the equation

$$R d \ln \gamma_{NaF} N_{NaF} = \frac{\Delta H_F}{T^2} dT , \qquad (2)$$

where $N_{NaF}$ is the mole fraction of NaF and $\Delta H_F$ is the heat of fusion of NaF at temperature $T$ [simple methods for integrating Eq. (2) are given in any chemical thermodynamics text]. For accurate values of $\ln \gamma_{NaF}$, heat capacity corrections for $\Delta H_F$ (ref 1) were used in integrating Eq. (2).

Studies dealing with the effects of univalent,[2] divalent,[3,4] and tetravalent[5] fluoride solutes on NaF have been previously reported.

### Effect of Trivalent Fluorides

The rare-earth trifluorides, in concentrations up to 15 mole %, caused negative excess partial molal free energies of mixing. The $(\overline{F} - F^0)^E_{NaF}$ vs concentration curves for eight rare-earth trifluorides are given in Fig. 3.1. At concentrations lower than 8 mole %, the free energy curves converge. The trend in $(\overline{F} - F^0)^E_{NaF}$ is similar to that observed for the alkaline-earth fluorides;[3] at fixed concentration, the smaller the cation radius the more negative the value of $(\overline{F} - F^0)^E_{NaF}$

[1] C. J. O'Brien and K. K. Kelley, *J. Am. Chem. Soc.* **79**, 5616 (1957).

[2] S. Cantor, W. T. Ward, and G. D. Robbins, *Reactor Chem. Div. Ann. Progr. Rept. Jan. 31, 1962*, ORNL-3262, p 35.

[3] S. Cantor, *J. Phys. Chem.* **65**, 2208 (1961).

[4] S. Cantor, *Reactor Chem. Div. Ann. Progr. Rept. Jan. 31, 1961*, ORNL-3127, p 22.

[5] S. Cantor and T. S. Carlton, *J. Phys. Chem.* **66**, 2711 (1962).

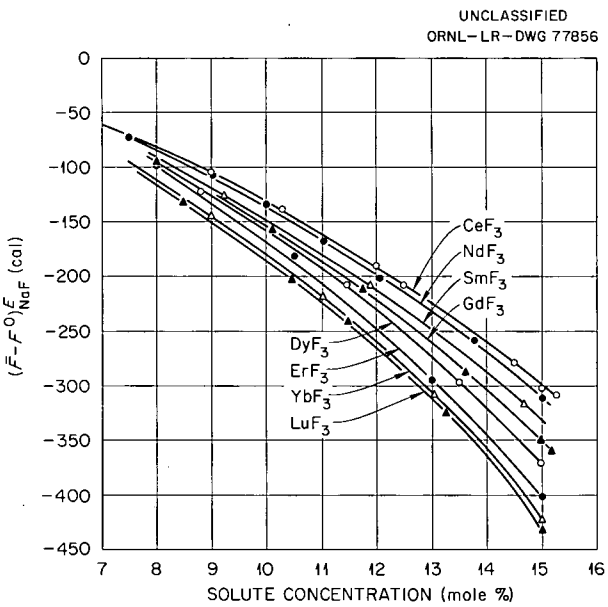


**Fig. 3.1. Excess Partial Molal Free Energy of Solution of NaF vs Solute Concentration of Rare-Earth Fluorides.**

(i.e., the lower the liquidus temperature). Also, the smaller the solute cation radius, the greater the attraction for fluoride ions, and consequently the greater the difficulty for NaF to crystallize out of solution.

The effects of some other trifluoride solutes on NaF are shown in Fig. 3.2. The $(\bar{F} - F^0)^E_{NaF}$ vs concentration curves for $ScF_3$, $YF_3$, and $LaF_3$ follow the trend of the rare-earth fluorides, that is, the smaller the solute cation radius the more negative is $(\bar{F} - F^0)^E_{NaF}$.

The nature of the dependence of $(\bar{F} - F^0)^E_{NaF}$ on the molecular geometry of eleven trifluoride solutes is indicated by Fig. 3.3. Within the probable limits of error of both coordinates [±5 cal for $(\bar{F} - F^0)^E_{NaF}$ and ±0.004 $A^{-1}$ for the reciprocal of distance] the plots are linear. Therefore, these plots have the analytical form

$$(\bar{F} - F^0)^E_{NaF} = \frac{f(N)}{d_{M-F}} + g(N) , \qquad (3)$$

where $f(N)$ and $g(N)$ are functions of concentration only and $d_{M-F}$ is the interionic distance of the trivalent fluoride solute. The first term on the right-hand side of Eq. (3) is analogous to the Madelung term for lattice energies and suggests that the energy of interaction is Coulombic in character. The $g(N)$ term can be interpreted to mean that, at fixed concentration, the entropy of mixing is constant for all eleven solutes. This constancy is not surprising in that all the solute cations probably have the same coordination number in solution.

If interionic distance were the only consideration in determining $(\bar{F} - F^0)^E_{NaF}$ curves with trivalent fluoride solutes, the effects of $InF_3$ and $ScF_3$ would be about the same because $In^{3+}$ and $Sc^{3+}$ ions are, approximately, equal in size. But if two cations have the same charge and size, the cation with the greater polarizing power would be expected to have the greater fluoride ion affinity, thereby causing a more negative $(\bar{F} - F^0)^E_{NaF}$. For $InF_3$ and $ScF_3$ the significant difference is the greater polarizing power of the $4d^{10}$ electronic configuration ($In^{3+}$) over that of the inert-gas

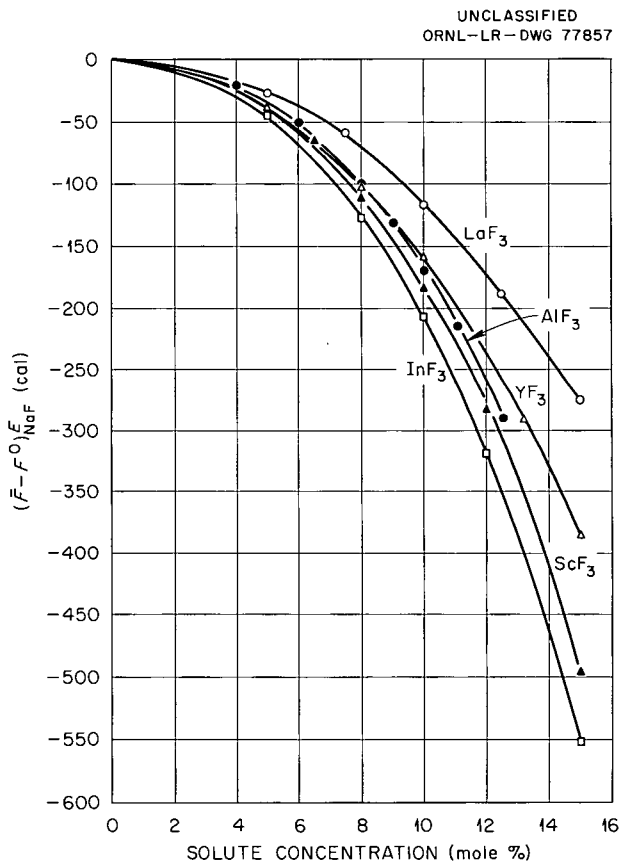


**Fig. 3.2. Excess Partial Molal Free Energy of Solution of NaF vs Solute Concentration of Some Trifluorides.**

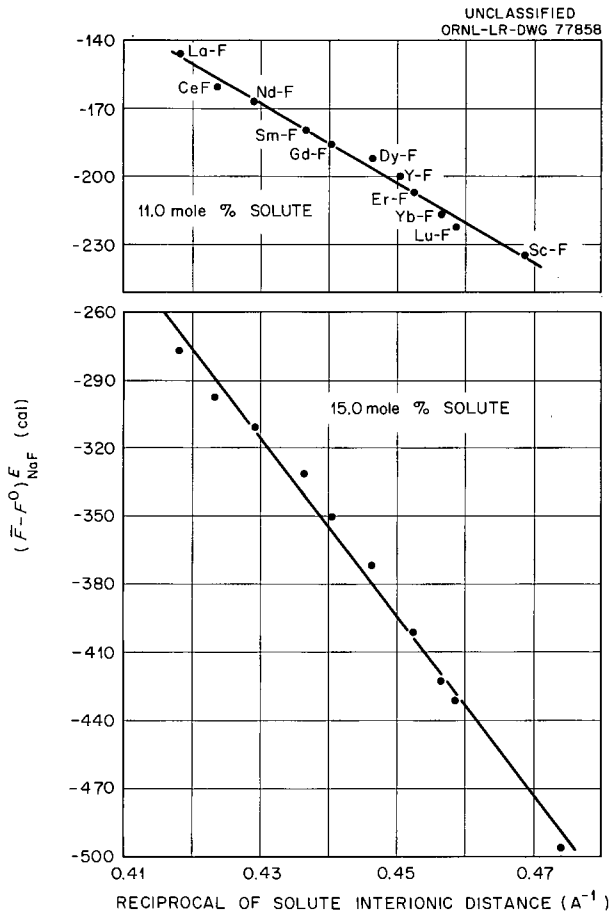


**Fig. 3.3. Excess Partial Molal Free Energy of Solution of NaF in NaF-$MF_3$ Systems as a Function of Solute Interionic Distance.**

configuration ($Sc^{3+}$). The difference is the reason why, at the same concentration, $InF_3$ causes a more negative $(\bar{F} - F^0)^E_{NaF}$ than $ScF_3$. Exactly the same effect was held to be responsible for differences in $(\bar{F} - F^0)^E_{NaF}$ caused by $MgF_2$ and $ZnF_2$.[4]

If Eq. (3) held for $AlF_3$, the $(\bar{F} - F^0)^E_{NaF}$ values would be the most negative since the aluminum-fluoride interionic distance is the shortest of any trivalent fluoride solute investigated. However, as seen in Fig. 3.2, $AlF_3$ gives higher values of $(\bar{F} - F^0)^E_{NaF}$ than $ScF_3$. This reversal in trend of interionic distance on $(\bar{F} - F^0)^E_{NaF}$ may be better understood if the high electric field strength of the $Al^{3+}$ ion is taken into account. If this high field caused six or more fluorides to be coordinated to each $Al^{3+}$ ion in NaF solution, then the relative sizes of $Al^{3+}$ and $F^-$ ions do not permit simultaneous contact of all six $F^-$ ions with the $Al^{3+}$ ion (all the other 12 trivalent cations are large enough to permit contact with 6 fluoride nearest neighbors). Those $F^-$ ions out of contact are more "available" to the sodium ion for crystallization. In short, a steric effect operates in a direction opposite to the expected Coulombic effect. The coordination number of six is considered probable because $Al^{3+}$ in crystalline $AlF_3$ has such a coordination number.[6] A similar reversal in trend of interionic distance on $(\bar{F} - F^0)^E_{NaF}$ was exhibited by the tetravalent fluorides in NaF,[5] where the order of $(\bar{F} - F^0)^E_{NaF}$ at fixed concentration was $ZrF_4 > UF_4 > ThF_4$. For that series of solutes each tetravalent cation was assumed to have at least eight fluoride nearest neighbors (as $Zr^{4+}$, $U^{4+}$, and $Th^{4+}$ have in crystalline $ZrF_4$,[7] $UF_4$,[8] and $ThF_4$), with the result that $Zr^{4+}$ and $U^{4+}$ were too small to have eight fluorides contact each cation simultaneously.

## Effect of $CdF_2$

When $CdF_2$ was dissolved in NaF in concentrations up to 20 mole %, the resulting $(\bar{F} - F^0)^E_{NaF}$ vs concentration curve lies below the corresponding curve with $CaF_2$ solutes (see Fig. 3.4). The

[6] A. F. Wells, *Structural Inorganic Chemistry*, 3d ed., p. 341, Oxford University Press, Oxford, England, 1962.

[7] R. D. Burbank and F. N. Bensey, Jr., *The Crystal Structure of $ZrF_4$*, K-1280 (1956).

[8] R. D. Burbank, *The Crystal Structure of $UF_4$*, K-769 (1951).

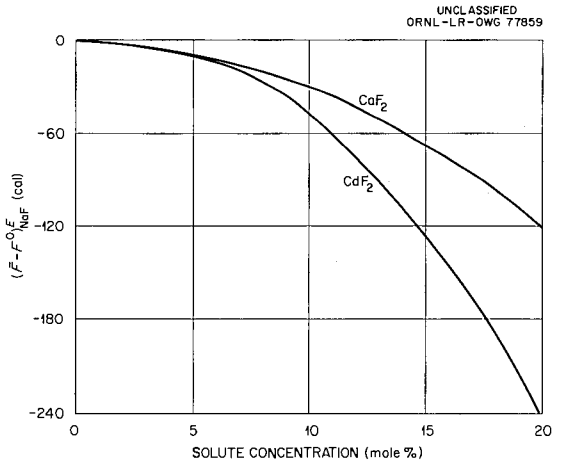


**Fig. 3.4. Excess Partial Molal Free Energy of Solution of NaF vs Solute Concentration of $CdF_2$ and $CaF_2$.**

comparison between these two solutes is made because $Cd^{2+}$ and $Ca^{2+}$ ionic radii are approximately the same. The hypothesis which explains the differences between $CaF_2$ and $CdF_2$ in their effects is precisely the same as that discussed above for $InF_3$ and $ScF_3$. In this case, the $Cd^{2+}$ ion has the $4d^{10}$ electronic configuration (and therefore the enhanced fluoride affinity) while $Ca^{2+}$ has the inert-gas electronic core.

## ACTIVITY COEFFICIENTS OF $ZrF_4$ IN THE $LiF$-$ZrF_4$ SYSTEM

S. Cantor W. T. Ward

The purpose of this investigation was to obtain activity coefficients of $ZrF_4$ at low concentration (10 mole % and less) in a fluoride melt not too different in character from MSRE fuel. These activity coefficients might also be useful in estimating, in the same melts, coefficients for $UF_4$ and $ThF_4$, which are chemically similar to $ZrF_4$.

The $LiF$-$ZrF_4$ system was chosen for this investigation because (*a*) reliable vapor pressure measurements[9] were available for calculating activity coefficients of $ZrF_4$ for the composition range 1.0 to 0.2 mole fraction $ZrF_4$, and (*b*) liquidus temperatures from 0.2 to 0.0 mole fraction $ZrF_4$ could yield the activity coefficients of LiF which, in turn, could give the activity coefficients of $ZrF_4$ over the same composition range by means of the Gibbs-Duhem equation.

From 1.0 to 0.273 mole fraction $ZrF_4$ the activity coefficients of $ZrF_4$ were calculated from the equation

$$\gamma_Z = \frac{p}{N_z p^0}, \tag{4}$$

where $\gamma_Z$ is the activity coefficient of $ZrF_4$ at mole fraction $N_Z$ of $ZrF_4$; $p$ and $p^0$ are the partial pressures of $ZrF_4$, at the same temperature, over the solution and pure liquid $ZrF_4$ respectively. The vapor pressure of pure liquid $ZrF_4$, as yet unmeasured, was calculated from the vapor pressure of solid $ZrF_4$ as reported by Cantor *et al.*[10] using the heat of fusion of $ZrF_4$ recently measured by Stull and associates.[11] The $\gamma_Z$'s at 1000°K calculated from vapor pressure are shown in Fig. 3.5. These values of $\gamma_Z$ were then put in a function suitable for linear extrapolation to $N_Z \sim 0.20$. This function had the form

$$\frac{\ln \gamma_Z}{(1 - N_Z)^2} = a + b(1 - N_Z), \tag{5}$$

where $a$ and $b$ are constants.

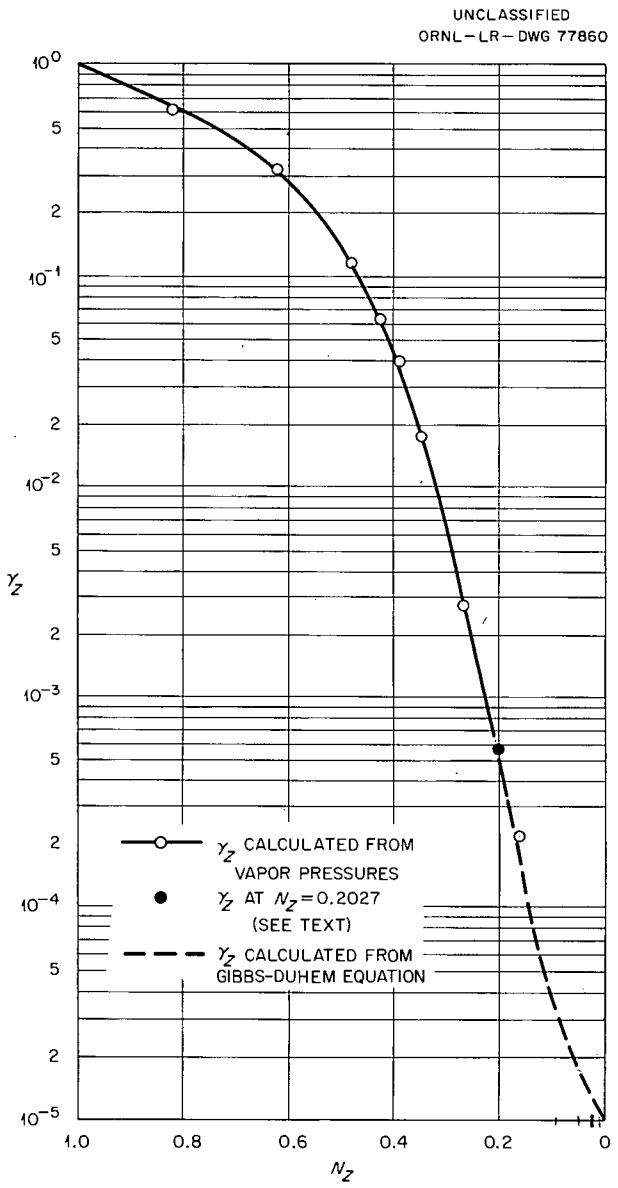


**Fig. 3.5. Activity Coefficient of $ZrF_4$ vs Mole Fraction of $ZrF_4$ in the $LiF$-$ZrF_4$ System at 1000°K.**

[9] K. A. Sense and R. W. Stone, *J. Phys. Chem.* **62**, 1411 (1958).

[10] S. Cantor *et al.*, *J. Phys. Chem.* **62**, 96 (1958).

[11] R. A. McDonald, G. C. Sinke, and D. R. Stull, *J. Chem. Eng. Data* **7**, 83 (1962).

The activity coefficients of LiF were obtained from the liquidus temperatures by the equation

$$-R \ln \gamma_L N_L = \left[ \Delta H_M - (a' - a) T_M + \frac{b}{2} T_M^2 + \frac{c}{T_M} \right] \left( \frac{1}{T} - \frac{1}{T_M} \right) + (a' - a) \ln \frac{T_M}{T} - \frac{b}{2}(T_M - T) + \frac{c}{2} \left( \frac{1}{T_M^2} - \frac{1}{T^2} \right) , \quad (6)$$

where $\gamma_L$ is the activity coefficient of LiF at mole fraction $N_L$; $\Delta H_M$ is the heat of fusion at the melting point $T_M$; $T$ is the liquidus temperature; $a'$ is the molar heat capacity of liquid LiF; and $a$, $b$, and $c$ are constants in the heat capacity–temperature equation ($C_p = a + bT - c \times T^{-2}$) for solid LiF. For Eq. (6) the values of the constants in Kelley's compilation[12] were used ($\Delta H_M = 6470$, $a' = 15.50$, $a = 10.41$, $b = 3.90 \times 10^{-3}$, $c = 1.38 \times 10^5$) and $T_M$ was found to be 1119.7°K. The measured liquidus temperatures are shown in Fig. 3.6. These temperature determinations were extended beyond the composition where pure LiF crystallizes out in order to locate the eutectic composition, $N_Z = 0.2027$, with greater precision. If it is assumed that the partial molal heat of solution of LiF is negligible in the composition range $N_Z = 0$ to 0.2027, then $\gamma_L$ evaluated from Eq. (3) is temperature-independent. Accordingly, the measured $\gamma_L$'s may be used in the Gibbs-Duhem equation in the form

$$d \ln \gamma_Z = -\frac{N_L}{N_Z} d \ln \gamma_L . \quad (7)$$

To facilitate integration of Eq. (7), $\gamma_L$ was cast in the form of a polynomial:

$$\frac{\ln \gamma_L}{N_Z^2} = A_2 + A_3 N_Z + A_4 N_Z^2 + A_5 N_Z^3 \ldots , \quad (8)$$

where the $A$'s are constants. Three terms of the polynomial were sufficient to fit the data with $A_2 = -4.35$, $A_3 = -26.5$, and $A_4 = -101$. The limits of integration for Eq. (7) are $N_Z = 0.2027$ and $N_Z$ equal to any $N_Z$ from 0 to 0.2027. Therefore, the left-hand side of Eq. (7) was integrated to give $\ln \gamma_Z$ at $N_Z = 0.2027$ minus $\ln \gamma_Z$ for any $N_Z$ up to 0.2027. The desired $\gamma_Z$'s were then evaluated once $\gamma_Z$ at $N_Z = 0.2027$ had been obtained from Eq. (4). The activity coefficients of $ZrF_4$ calculated from the Gibbs-Duhem equation are shown in Fig. 3.5.

The accuracy of $\gamma_Z$ for $N_Z < 0.2$ is somewhat uncertain (probably to within a factor of 5) because of the previously discussed assumption that $\gamma_L$ is not a function of temperature. However, it should be noted that at $N_Z = 0.163$, $\gamma_Z$ calculated from the published vapor pressure[9] agrees quite well with $\gamma_Z$ calculated from the Gibbs-Duhem equation. While the validity of inferred partial pressure measurements of $ZrF_4$ at the

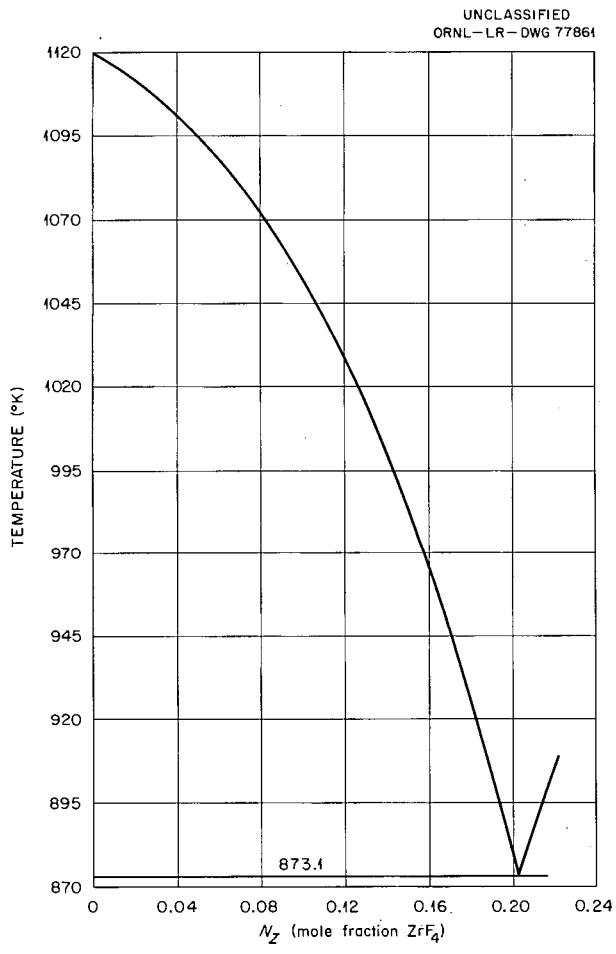


**Fig. 3.6. Partial Phase Diagram of the System LiF-$ZrF_4$.**

[12]K. K. Kelley, *Bur. Mines Bull.* **584**, 108 (1960).

composition is questionable, this agreement for $\gamma_Z$ is nevertheless reassuring. The very low values for the activity coefficients of $ZrF_4$ in the low concentration range are, of course, a measure of the very high degree of chemical interaction of $ZrF_4$ and LiF.

## VAPOR PRESSURE OF MOLTEN FLUORIDE MIXTURES

D. R. Cuneo S. Cantor

Vapor pressure measurements were undertaken to provide information (1) for molten-salt reactor development, and (2) for calculation of thermodynamic parameters of molten fluoride solutions.

### Technique and Apparatus

The technique (previously used at this Laboratory[13–15]) employed for the vapor pressure measurements was devised by Rodebush and Dixon.[16] In this quasi-static method, the melt is contained in a cell provided with two vertical tubes. Vapor is allowed to reflux in the lower end of the tubes. One tube leads to a valve which can be opened to vacuum; the other is attached to either a gage or a manometer which measures inert-gas pressure. A mechanical differential manometer indicates the difference in pressure in the two tubes. Initially the apparatus is filled with an inert gas at a pressure greater than the vapor pressure. The inert-gas pressure is changed in small decrements by manipulation of the valve leading to the vacuum, allowing enough time after each withdrawal from the differential manometer to give a steady reading. As long as the inert-gas pressure is greater than the vapor pressure in the cell, no permanent difference in pressure is established between the tubes; but when the vapor pressure is very slightly greater than the inert-gas pressure, a permanent difference is shown on the differential manometer and the inert-gas pressure, now virtually equal to the vapor pressure, can be read on the absolute manometer.

Temperatures of the samples were measured with calibrated Pt vs Pt–10% Rh thermocouples in a thermowell extending approximately 2 cm into the melt. The emf's were read with a precision potentiometer.

The vapor pressure cell, welded from either INOR-8 or nickel, provided a melt reservoir of 95 cc. When the cell was loaded, loose graphite plugs of the geometry discussed by Fiock and Rodebush[17] were inserted to diminish the area for diffusion at the vapor-gas interface.

The reliability of the apparatus was tested by measuring the vapor pressure of water at 14.25°C. The observed pressure was 12.07 mm, in good agreement with an accepted value of 12.18 mm.[18]

### MSRE Fuel System

Two compositions (given in Table 3.1) were measured. The mixture containing about 4 mole % $ZrF_4$ approximates the composition of MSRE fuel. A second mixture was measured to observe the effect of doubling the concentration of $ZrF_4$. Pressures, extrapolated to MSRE operating temperatures, indicate that the second mixture would exert a vapor pressure about twice that of the MSRE fuel.

### System $LiF-BeF_2$

Measurements of vapor pressures in the system $LiF-BeF_2$ have been started. Table 3.2 gives the constants $A$ and $B$ for the equation $\log P_{mm} = A - B/T(°K)$ for two compositions and LiF. Sufficient variance exists between values of pure LiF obtained in this study and those from previous work[19] to indicate need of further work with this compound. To aid in determining partial pressures in this system, use of the transpiration technique is contemplated to supplement the manometric pressures obtained by the Rodebush-Dixon method.

---

[13] R. E. Moore, *ANP Quart. Progr. Rept. Sept. 10, 1952*, ORNL-1375, p 147.

[14] S. Cantor *et al.*, *J. Phys. Chem.* **62**, 96 (1958).

[15] C. C. Beusman, *Activities in the $KCl-FeCl_2$ and $LiCl-FeCl_2$ Systems*, ORNL-2323 (May 15, 1957).

[16] W. H. Rodebush and A. L. Dixon, *Phys. Rev.* **26**, 851 (1925).

[17] E. F. Fiock and W. H. Rodebush, *J. Am. Chem. Soc.* **48**, 2522 (1926).

[18] N. A. Lange (ed.), *Handbook of Chemistry*, 9th ed., Handbook Publishers, Sandusky, Ohio, 1956.

[19] S. Cantor, *ANP Quart. Progr. Rept. Mar. 31, 1957*, ORNL-2274, p 128.

Table 3.1. Vapor Pressures in the System $LiF-BeF_2-ZrF_4-UF_4$

| Composition (mole %) | | | | Constants[a] | | Temperature Range of Measurement (°C) | Extrapolated Vapor Pressure at 704°C[b] (mm) |
|---|---|---|---|---|---|---|---|
| LiF | $BeF_2$ | $ZrF_4$ | $UF_4$ | *A* | *B* | | |
| 66.52 | 29.38 | 3.95 | 0.14 | 9.015 | 10,438 | 1003–1178 | 0.02 |
| 64.67 | 27.01 | 8.13 | 0.16 | 8.562 | 9,661 | 1001–1217 | 0.05 |

[a]$\text{Log } P_{mm} = A - B/T(°K)$.
[b]Highest design temperature of MSRE.

Table 3.2. Vapor Pressures in the System $LiF-BeF_2$

| Composition (mole %) | | Constants[a] | | Temperature Range of Measurement (°C) |
|---|---|---|---|---|
| LiF | $BeF_2$ | *A* | *B* | |
| 100 | 0 | 7.509 | 9,615 | 1002–1288 |
| 90 | 10 | 7.428 | 9,106 | 1007–1305 |
| 80 | 20 | 8.718 | 10,787 | 1027–1317 |

[a]$\text{Log } P_{mm} = A - B/T(°K)$.

## DENSITIES IN THE $LiF-ThF_4$ SYSTEM

D. G. Hill[20] S. Cantor

A previously conducted examination[21] of all the published density data of ionic fluoride melts had shown that molar volumes of molten fluoride mixtures were additive functions (by mole fractions) of the molar volumes of the components. The binary $LiF-ThF_4$ system exhibits very marked negative deviations from ideality for many thermodynamic solution properties. Accordingly, densities of selected compositions in this system were measured to determine the molar volume of $ThF_4$ in solution and to establish whether departures from additivity of molar volumes would be observed.

Densities were determined by the Archimedes immersion method using a platinum plummet hung from one arm of an analytical balance. The melts were contained in nickel apparatus. Corrosion of the apparatus was minimized by flowing argon gas in and around the containing vessel.

The data obtained are shown in Fig. 3.7. These experimental data, as functions of temperature, are given by the equations in Table 3.3. Molar volumes at 600, 800, and 1000°C, deduced from the equations, are plotted in Fig. 3.8. These molar volumes are all for the liquid state; except for LiF at 1000°C, the molar volumes of the pure components are those for supercooled liquids and were obtained by substituting in the appropriate equation in Table 3.3. The good agreement between molar volumes based on additivity (represented by lines in Fig. 3.8) and molar volumes based on (or extrapolated from) experimental data lends further support to the hypothesis that molar volumes in all ionic fluoride melts are, to a good approximation, additive.

Table 3.3. Density-Temperature Equations for the $LiF-ThF_4$ System

| Composition (mole %) | | Equation (*t* is in °C) |
|---|---|---|
| LiF | $ThF_4$ | |
| 100 | 0 | $\text{Density} = 1.729 + 5 \times 10^{-4}(1000 - t)$ |
| 80 | 20 | $3.695 + 8.5 \times 10^{-4}(1000 - t)$ |
| 60 | 40 | $4.832 + 10.2 \times 10^{-4}(1000 - t)$ |
| 40 | 60 | $5.594 + 12 \times 10^{-4}(1000 - t)$ |
| 20 | 80 | $5.998 + 9.5 \times 10^{-4}(1000 - t)$ |
| 0 | 100 | $6.312 + 9 \times 10^{-4}(1000 - t)$ |

[20]Consultant to Reactor Chemistry Division.

[21]S. Cantor, *Reactor Chem. Div. Ann. Progr. Rept. Jan. 31, 1962*, ORNL-3262, p 38.

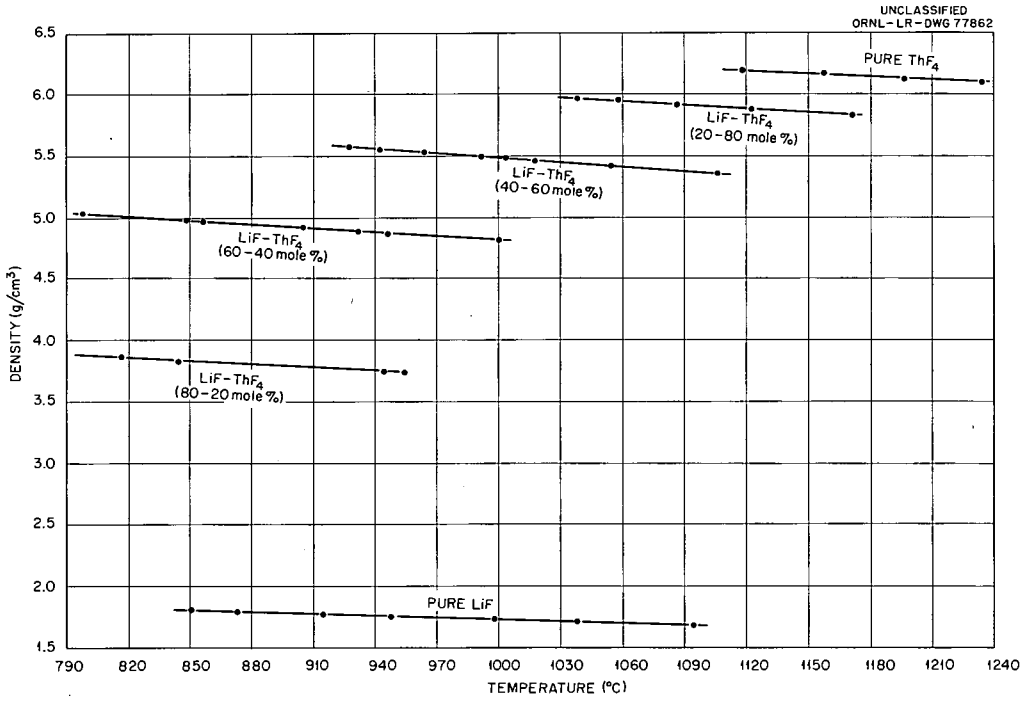


**Fig. 3.7. Densities in the LiF-ThF$_4$ System.**

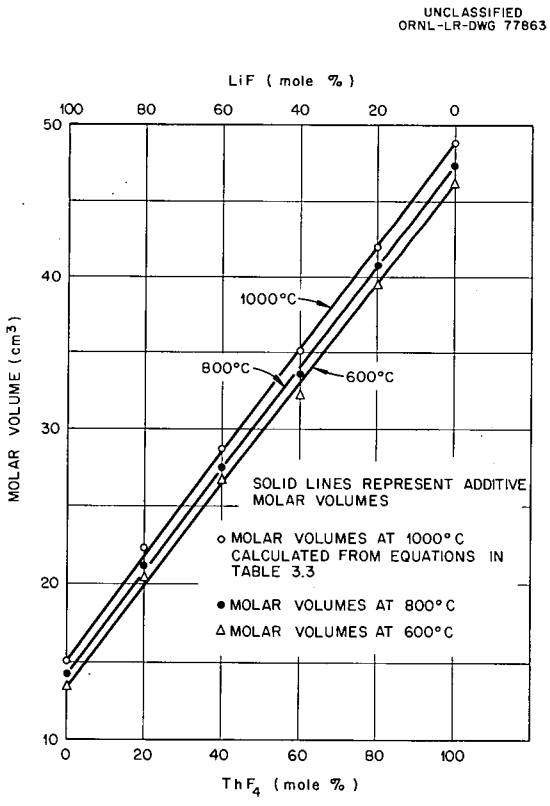


**Fig. 3.8. Molar Volumes in the LiF-ThF$_4$ System.**

## VISCOSITIES OF MOLTEN SALTS

P. B. Bien S. Cantor

An oscillating cylinder viscometer has been constructed to measure viscosities of molten salts in the fluid region (0.1 to 10 centipoises). The viscometer consists of a containing vessel held by a torsional suspension. When the viscometer is made to oscillate about a vertical axis, the viscous drag of the liquid on the walls damps the motion of the vessel. The viscosity of the liquid is obtained from measurements of the frequency and decrement of the damped oscillations. The hydrodynamic equations which describe the operation of this type of viscometer have been developed by Hopkins and Toye[22] and by Roscoe.[23]

Such a viscometer, which uses a small sample of liquid in a sealed vessel, prevents sample contamination by reaction with the atmosphere and permits simple control of sample temperature.

[22] M. R. Hopkins and T. C. Toye, *Proc. Phys. Soc.* **63**, 773 (1950).

[23] R. Roscoe, *Proc. Phys. Soc.* **72**, 576 (1958).

For these reasons, viscometers of this type have been used extensively in studies of molten metals.[22,24]

The apparatus is shown in Fig. 3.9. The viscometer is set in motion by the action of a solenoid on soft iron pins embedded in the inertial bar. The motion of the vessel is followed by reflecting a ribbon of light from the mirror glued to the vertical shaft which is coupled to the vessel. The mirror reflects the light onto a rotating drum which is covered by a metal cover with a horizontal slit 0.5 mm wide and 30 cm long (see Fig. 3.10). The portion of the light ribbon which enters the slit traces the oscillational motion (a damped sine curve) onto a piece of photosensitive paper mounted on the drum. When about 50 oscillations have been recorded, the paper is removed and processed. The amplitudes of the oscillations are then measured with the aid of a cathetometer. The ratio of successive amplitudes is the decrement of the oscillation. The ribbon of light also actuates a photoelectric cell, mounted on the drum cover at the midpoint of the oscillation. The signal from the photocell triggers an electronic counter, which registers the number of passes made by the light beam, and a scaler which records the accumulated time of the passes. The time divided by twice the number of passes gives the frequency of oscillation.

The moment of inertia of the oscillating system is determined from changes in position of threaded weights screwed onto the inertial bar. Viscosity is obtained from the measurements by an equation modified from Roscoe's equation (19):[22]

$$A\left(\frac{T\eta}{\rho}\right)^{1/2} - BT\frac{\eta}{\rho} + C\left(T\frac{\eta}{\rho}\right)^{3/2} - D\left(\frac{T\eta}{\rho}\right)^{5/2} = \frac{2\pi^{1/2}\, I(\delta - \delta_0)}{\rho},$$

[24] L. J. Wittenberg, L. V. Jones, and D. Ofte, Memoire No. 28, *Conference Internationale sur la Metallurgie du Plutonium*, Grenoble, France, April 1960.

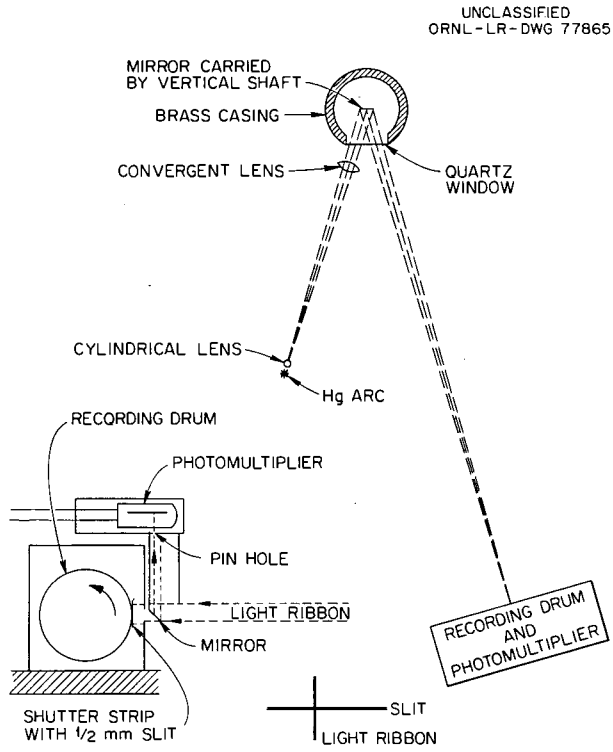


**Fig. 3.10. Optics and Recording System for Oscillating Cylinder Viscometer.**

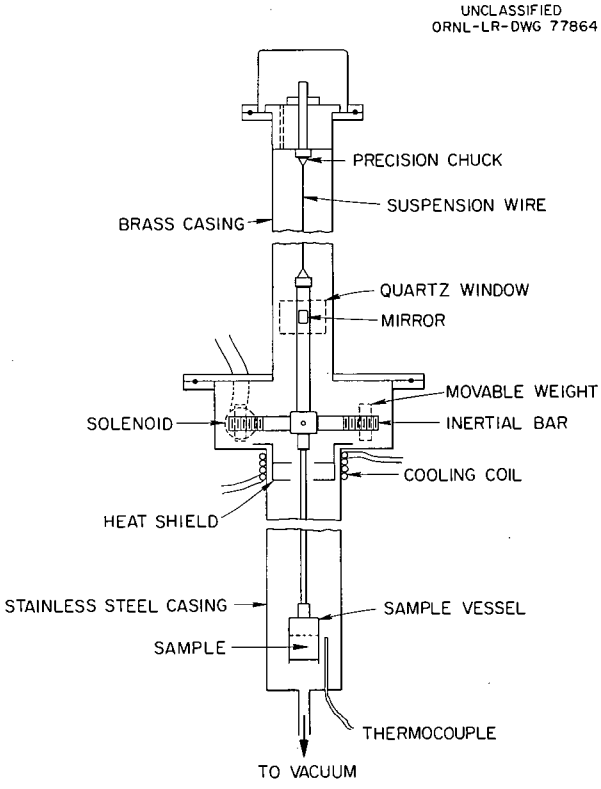


**Fig. 3.9. Oscillating Cylinder Viscometer.**

where

$A$, $B$, $C$, and $D$ are quantities, characteristic of the apparatus, dependent only on the radius of the vessel and the volume of liquid,

$T$ is the period of oscillation,

$\eta$ and $\rho$ are the viscosity and density of the liquid respectively,

$I$ is the moment of inertia of the oscillating system,

$\delta$ is the natural logarithm of decrement for the vessel and sample,

$\delta_0$ is the natural logarithm of decrement of the vessel alone.

The equation is, of course, solved for $\eta$ by successive approximation.

To test the reliability of the apparatus, the viscosity of water was measured at 25°C. The value obtained was 0.885 centipoise, which compares well with the generally accepted value of 0.8937.[25]

Measurements of molten-salt viscosities, starting with pure NaCl, have just begun. At 885°C the viscosity of NaCl was measured as 1.10 centipoises, in good agreement with Dantuma's value of 1.09.[26]

---

[25] E. C. Bingham and R. F. Jackson, *Bull. Bur. Stds.* **14**, 75 (1918).

[26] R. S. Dantuma, *Z. Anorg. Chem.* **175**, 1 (1928).

# 4. Fluoride Salt Production

J. H. Shaffer F. A. Doss
W. K. R. Finnel Wiley Jennings W. P. Teichert

As an integral part of the Molten-Salt Reactor Program, the Reactor Chemistry Division operates a facility for the preparation of fused fluoride mixtures and provides technical service operations for the various related experimental programs of the Laboratory. Whereas these activities are maintained primarily for support of intermediate-scale engineering tests on reactor components, the diversified production capability is adaptable to the small-batch preparation of fused fluoride mixtures for bench-scale experimentation and to the large multibatch operations for preparing the flush, coolant, and fuel mixtures for the MSRE.

The fluoride production process consists of batch unit operations in which fluoride salt mixtures that melt below 800°C can be prepared. Although the raw charge materials for these operations are purchased on a "best commercially available" basis, the molten fluoride mixtures are further purified during the production process to meet product specifications for reactor-grade materials. As described previously the purification treatment has been specifically developed to remove impurity compounds of sulfur and oxygen and to reduce structural metal impurities to very low concentrations.[1] A method for treating molten fluorides with mixtures of anhydrous hydrogen fluoride and hydrogen is used as the purification process.

## FLUORIDE PRODUCTION OPERATIONS

During 1962 the large-batch production facility was operated intermittently to prepare some 670 kg of fluoride mixtures containing LiF, $BeF_2$, $ZrF_4$, $ThF_4$, and $UF_4$ for MSRP experimental engineering tests. An additional 1200 kg of the mixture NaF-LiF-$ZrF_4$ (37.5-37.5-25.0 mole %) was prepared for use in the development and demonstration of reactor fuel reprocessing schemes by the Chemical Technology Division. Small-batch operations were conducted to prepare some 90 kg of various fused fluoride mixtures for other groups of the Reactor Chemistry Division, the Analytical Chemistry Division, the Chemical Technology Division, the Reactor Division, and the Battelle Memorial Institute.

## PLANT MODIFICATIONS

To accelerate the rate of fluoride production, the plant facility has been modified so that the two batch-processing units can be operated as a semi-continuous process. An examination of the batch production schedule showed that 60 hr of the 154-hr production cycle has been used for cooling the treatment vessel after salt transfer and for melting the starting materials of the next batch. In the large multibatch preparation of fluorides for the MSRE, a premelting furnace assembly, adjoining both batch facilities, will be used to charge each treatment vessel with molten starting materials. By proper scheduling this arrangement will effectively increase the rate of fluoride production by approximately 64%. This furnace assembly is shown in Fig. 4.1.

As a further modification to the production plant, the facility for handling and charging the unmelted raw materials was relocated adjacent to the new furnace assembly. Although techniques for handling raw materials were improved, the

[1] *Reactor Chem. Div. Ann. Progr. Rept. Jan. 31, 1962*, ORNL-3262, p 27.

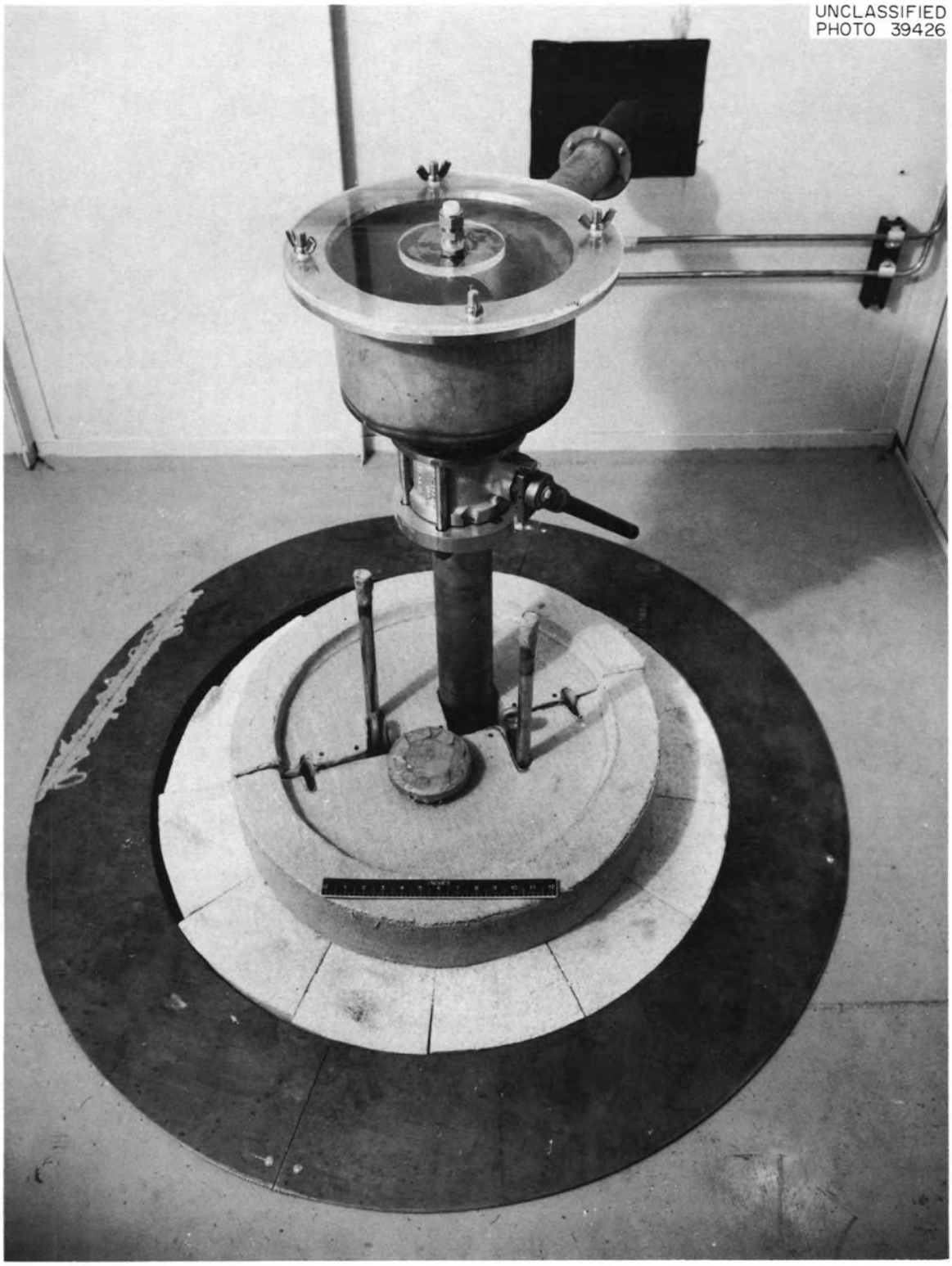


Fig. 4.1. Fluoride Production Facility, Premelting Furnace Assembly.

primary purpose of this construction was to facilitate the loading of the new charge furnace assembly. As shown in Fig. 4.2, batches of raw materials can be prepared in a well-ventilated hood enclosure and transferred into the furnace assembly by means of a vibratory conveyor.

In preparation for the production of fluorides for the MSRE, the batch-processing units have been renovated by replacing the tubing, valves, and gages in the gas manifold system. This action was taken primarily to avoid the inadvertent isotopic contamination of $Li^7F$, which will be used in the MSRE salt preparations. Additional improvements in the furnace temperature control equipment and the apparatus for metering HF into the reaction vessel were also included in this program. One of the batch-processing units is shown in Fig. 4.3.

As an economic improvement to the fluoride production plant, a facility for reclaiming equipment contaminated with beryllium compounds has been installed at a capital investment cost of less than $10,000. As shown in Fig. 4.4, this facility consists of two wet sandblast cabinet units in a tandem arrangement. These units were obtained commercially and required only minor modifications to the ventilation and waste disposal systems to comply with regulatory standards for handling beryllium contamination. As installed, one unit is used to remove salt deposits and scale from used equipment by wet sandblasting; the second cabinet is used for rinsing contaminants from the cleaned equipment. In preparation for the production of MSRE fluoride mixtures, this facility will be used to reclaim some 20 existing salt storage containers (valued at $40,000) that have been used previously for beryllium salts.

## ANTICIPATED MSRE PRODUCTION

Beginning in July 1963 the primary function of the fluoride production facility will be the preparation of flush, coolant, and fuel mixtures required for operation of the MSRE. The total inventory of materials planned for the initial reactor loading will be approximately 11,500 kg of fluoride mixtures. To conform to the scheduled reactor operations, the initial production of about 2500 kg of $LiF\text{-}BeF_2$ (66-34 mole %) will be prepared and loaded into the reactor coolant drain tank. An additional 3900 kg of this mixture, having a very slightly higher isotopic abundance of $Li^7$, will be prepared and introduced into the reactor fuel system for use in prenuclear test operations and as a flush salt for the reactor core.

The production of the fuel salt mixture, $LiF\text{-}BeF_2\text{-}ZrF_4\text{-}UF_4$ (66.85-29-4-0.15 mole %), will be a dual operation. Because of nuclear safety considerations, the enriched uranium component of the fuel mixture will be prepared in small-batch operations, probably as the eutectic mixture $LiF\text{-}UF_4$ (73-27 mole %). The bulk of the 5100 kg of fuel salt will be prepared as a "barren" fuel salt in the large-batch facility. During reactor fuel loading operations a portion of the enriched fuel concentrate will be cast into solid rods and loaded through the sampler-enricher port on the primary fuel pump. This prepared material will also be used to maintain the uranium concentration in the fuel system during reactor operations.

## RAW MATERIAL PROCUREMENT

Because of the unique requirements of materials used in nuclear reactors, an evaluation of chemicals that would be available for preparing the MSRE fluoride salt mixtures was made. The results of this study, as they apply to materials procurement, are as follows.

### Lithium Fluoride

For neutron-absorption cross-section consideration, the lithium fluoride which will be used in the MSRE salt mixtures will contain almost isotopically pure $Li^7$. Since this material is available as the hydroxide in batches of varying $Li^7$ abundance, provisions were made with the Y-12 Plant to convert this hydroxide to fluoride and to group these batches so that the order of isotopic purity, fuel > flush > coolant, could be controlled. These operations are currently in progress.

An examination of the lithium fluoride from this source indicated that the precipitated fluoride formed very small particles of relatively low density. Since this physical form would create severe handling problems, methods which could be employed to increase the particle size and density of the LiF were studied. Although this

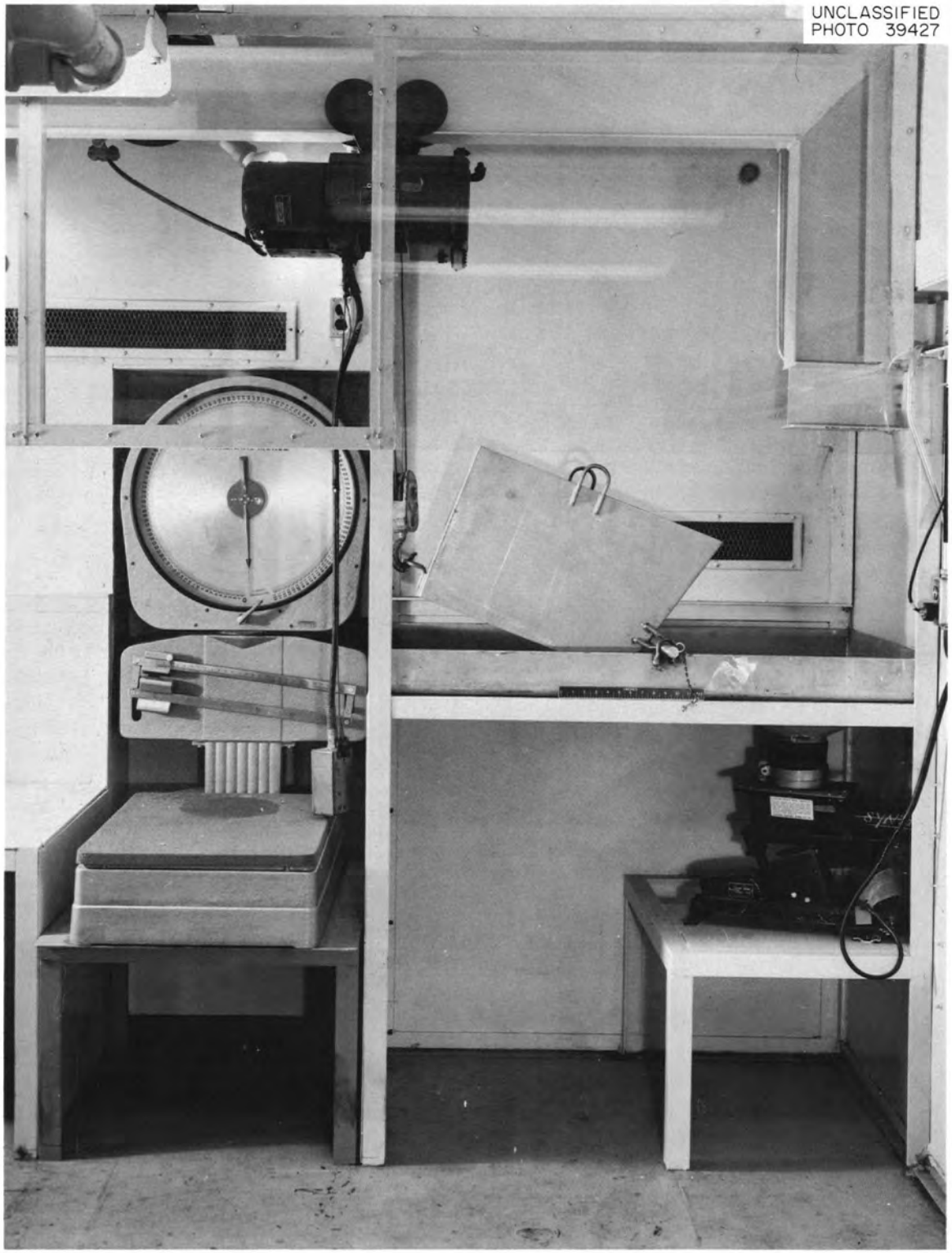


Fig. 4.2. Fluoride Production Facility, Raw Materials Handling Area.

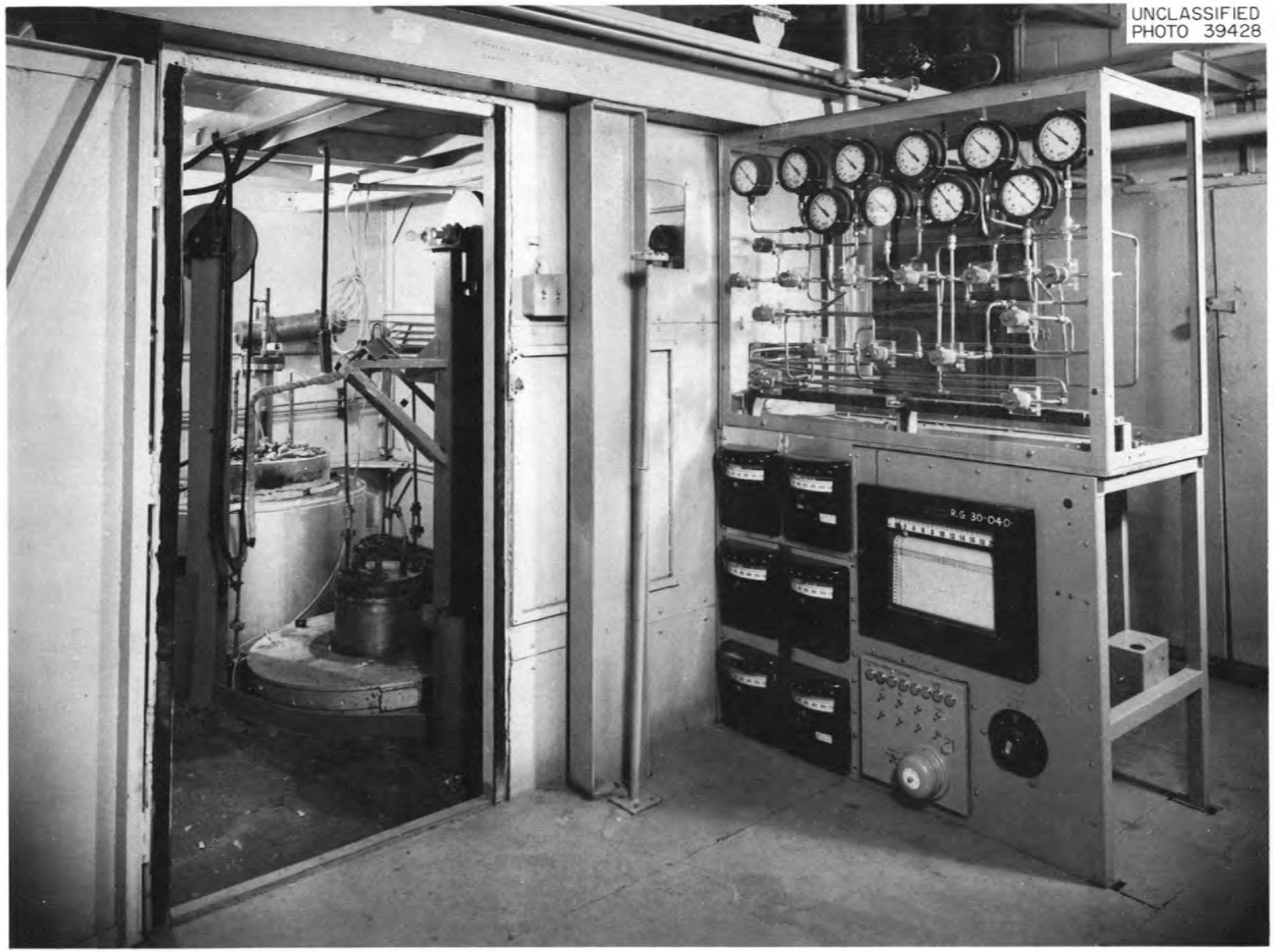


Fig. 4.3. Fluoride Production Facility, Batch-Processing Unit.

Fig. 4.4. Fluoride Production Facility, Equipment Reclamation Area.

material was found economically unsuitable for pelletizing, the results of a study of its sintering characteristics[2] shown in Fig. 4.5 indicated that a suitable material could be obtained by a relatively inexpensive operation. Larger-scale tests are currently in progress at ORGDP on some normal lithium fluoride having approximately the same physical characteristics.

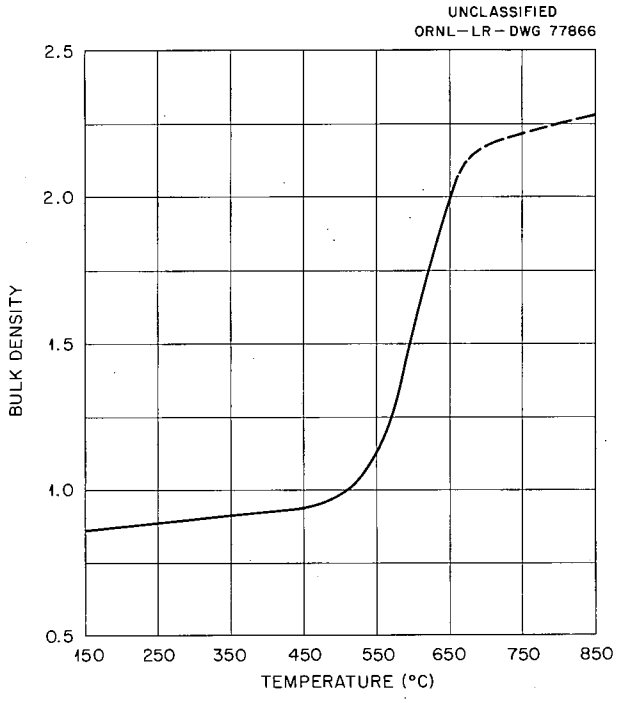


**Fig. 4.5. Densification of Precipitated LiF by Annealing at Various Temperatures.**

### Zirconium Fluoride

Hafnium-free zirconium tetrafluoride which meets specifications for MSRE application was found to be commercially available. Sufficient $ZrF_4$ for one reactor fuel loading has been procured.

### Beryllium Fluoride

Since beryllium fluoride is normally available from commercial sources as a manufacturer's intermediate product, its chemical purity has not been regulated according to "reactor-grade" standards. However, two major producers have planned improvements in their production process so that $BeF_2$ which is sufficiently free of impurities for MSRE application should be commercially available soon. The procurement of this material for delivery in July 1963 has been scheduled.

### General Chemical Specifications

After reviewing the results of chemical and spectrographic analyses of the various fluorides which will be used in preparing MSRE salt mixtures, chemical specifications which would generally apply to all fluorides purchased for the MSRE program were established (see Table 4.1). Since beryllium fluoride is a major component of the MSRE salt mixtures, these allowable impurities were determined on a "best commercially available $BeF_2$" basis. Although exceptions to specific impurities have been made for some materials, the chemical purity of the prepared MSRE fluoride mixtures should be more than adequate for use in reactor operations.

**Table 4.1. General Chemical Specifications for MSRE Fluoride Mixtures**

| Impurity | Allowable Concentration (wt %) (1 ppm = 0.0001 wt %) |
|---|---|
| Water | 0.1 |
| Cu | 0.005 |
| Fe | 0.01 |
| Ni | 0.0025 |
| S | 0.05 |
| Cr | 0.0025 |
| Al | 0.015 |
| Si | 0.01 |
| B | 0.0005 |
| Na | 0.05 |
| Ca | 0.01 |
| Mg | 0.01 |
| K | 0.01 |
| Li (natural) | 0.005 |
| Zr (natural) | 0.025 |
| Cd | 0.001 |
| Rare earths (total) | 0.001 |

[2]B. J. Sturm, *A Method for Densifying Lithium Fluoride Powder*, MSR-62-94 (Nov. 20, 1962).

## REMOVAL OF OXIDES FROM THE ENGINEERING TEST LOOP SALT MIXTURE

As a joint project with the Reactor Division,[3] the removal of oxides from molten fluoride salt systems similar to those planned for the MSRE has been studied using the technique of HF-$H_2$ treatment. Since a capability for chemically reprocessing fluoride mixtures in the MSRE plant facility is planned, this experimental program has been directed toward the chemical development of this process. The specific objectives of this program are (1) to determine the effectiveness of HF-$H_2$ treatment for removing oxides from large volumes of molten fluoride mixtures; (2) to study methods for analyzing the gas effluent from the reaction system; and (3) to evaluate the corrosion damage during the purification treatment to molten-salt containers fabricated of nickel-base alloys. The results of these studies are also of particular interest for application of the fluoride production process.

As currently developed, the method used for analyzing the effluent gas stream consists in low-temperature condensation of HF and $H_2O$. By this procedure the liquid contents of a small trap in the effluent gas stream are periodically drained and submitted for analysis. The water content of this mixture is determined by titration with Karl Fischer reagent. The condensation chamber is maintained at about −10°C by refrigerating a surrounding ethylene glycol–water bath. A second cold trap in the effluent gas system is chilled with dry ice; analyses of the contents of this trap after the hydrofluorination treatment indicate the accumulation of only small quantities of water. Typical results obtained thus far in this program are shown in Fig. 4.6. Tests currently in progress are directed toward the recovery of water resulting from HF-$H_2$ treatment of the molten-salt mixture to which a known amount of BeO has been added.

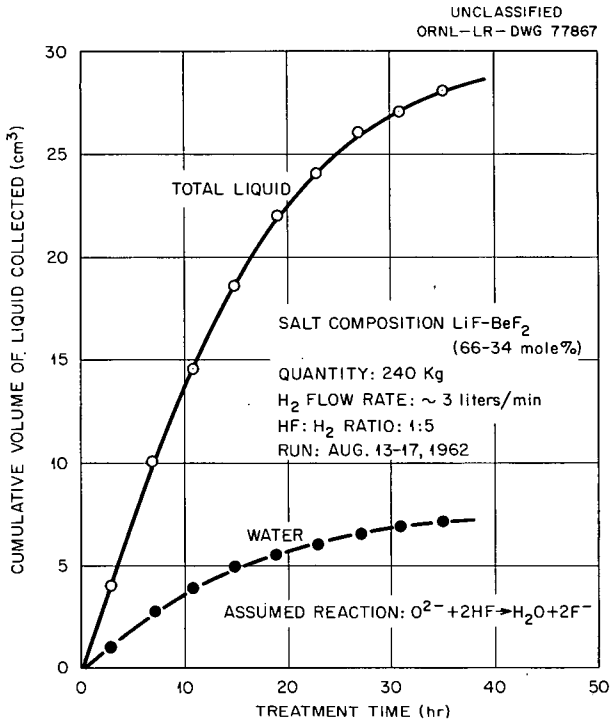


**Fig. 4.6. Recovery of Water from Gas-Effluent Line During HF-$H_2$ Treatment of Fluoride Salt at ~550°C in the Engineering Test Loop.**

[3] J. L. Crowley, Reactor Division.

# Part II

# Support for Aqueous Reactor Programs

# 5. Chemistry of Pressurized-Water Reactor Systems[1]

C. F. Baes T. H. Handley[2]

This program was initiated early in 1961 in connection with the Oak Ridge Research Reactor pressurized-water in-pile loop operation. Its principal objective, aside from providing chemical and radiochemical data on water conditions pertinent to loop operations, was to increase the basic understanding of PWR water chemistry as an approach to more economical PWR operation. In particular, there is a strong incentive to learn more of the mechanism of the transport and deposition of corrosion product crud and its associated radioactivity.

Results reported previously[3] have indicated that the relatively low levels of water-borne corrosion products and radioactivity in the ORR loop were composed of two distinct fractions: (1) a particulate or "crud" fraction which (from filtration tests, electron-microscopic, and x-ray diffraction examination) had a sharp lower limit in particle size of $\sim 0.5\ \mu$ and was well crystallized with the magnetite structure; and (2) a dissolved fraction which was not removed by the lowest-porosity filters ($0.01\ \mu$) and (from electromigration experiments and conductivity) appeared to be present as simple ions (probably the bivalent metal hydroxides of manganese, iron, cobalt, and nickel) at very low concentration. The specific activities of these two fractions were comparable. This, and the well-crystallized appearance of the insoluble fraction, suggested that appreciable radiochemical exchange between the two fractions occurs and that this may be an important mechanism of activity transport in neutral pH PWR systems. The possibility that nonradioactive magnetite would be an effective, high-temperature filter–ion exchange medium for accumulating activity in neutral pH PWR systems was explored in preliminary tests.

During the past year, the radiochemical examination of loop water has continued. Typically, the nonfilterable, dissolved activity level has been roughly constant during normal loop operation (260°C at neutral pH and with dissolved hydrogen present), the sum of $Fe^{59}$, $Co^{58}$, $Co^{60}$, and $Mn^{54}$ activities being $\sim 2 \times 10^3$ dis $sec^{-1}$ $liter^{-1}$. The filterable crud activity, while more variable, has been lower than this. The distribution of each nuclide between the two water fractions has been roughly the same for both the longer-lived ($Fe^{55}$ and $Co^{60}$) and the shorter-lived ($Fe^{59}$ and $Co^{58}$) activities in a given sample. This is reflected in the comparable $Fe^{55}/Fe^{59}$ and $Co^{60}/Co^{58}$ ratios shown for the two water fractions in Fig. 5.1 and is consistent with complete radiochemical exchange between the two water fractions. Assuming this to be the case, the specific activity of the dissolved fraction (in disintegrations per second per gram of dissolved solids) should in turn equal the specific activity of the water-borne crud. From this the concentration of dissolved solids may be estimated at $\sim 1 \times 10^{-5}$ g/liter (Table 5.1), which is equivalent to $1.3 \times 10^{-7}\ M$ as $Fe(OH)_2$. This dissolved activity, even at such low concentrations, is evidently a principal cause of activity transport in the ORR loop and presumably in other PWR primary systems operating under similar conditions. With the present ion exchange purification rate at the ORR loop, it can be calculated that corrosion product magnetite is being removed from the system in the form of this dissolved material at the rate of $\sim 1$ g/month. With a primary system area of $1.4 \times 10^5\ cm^2$, if there is assumed to be a steady-state corrosion

[1]Summary of contributions to be published in the *Maritime Reactor Program Ann. Progr. Rept. Nov. 30, 1962*, ORNL-3416; and the *Army Reactors Program Ann. Progr. Rept. Oct. 31, 1962*, ORNL-3386. This work was also described in a paper before *The Third Conference on Nuclear Reactor Chemistry, Gatlinburg, Tenn., Oct. 9–11, 1962*. Proceedings published in TID-7641.

[2]Analytical Chemistry Division.

[3]*Reactor Chem. Div. Ann. Progr. Rept. Jan. 31, 1962*, ORNL-3262, p 55.

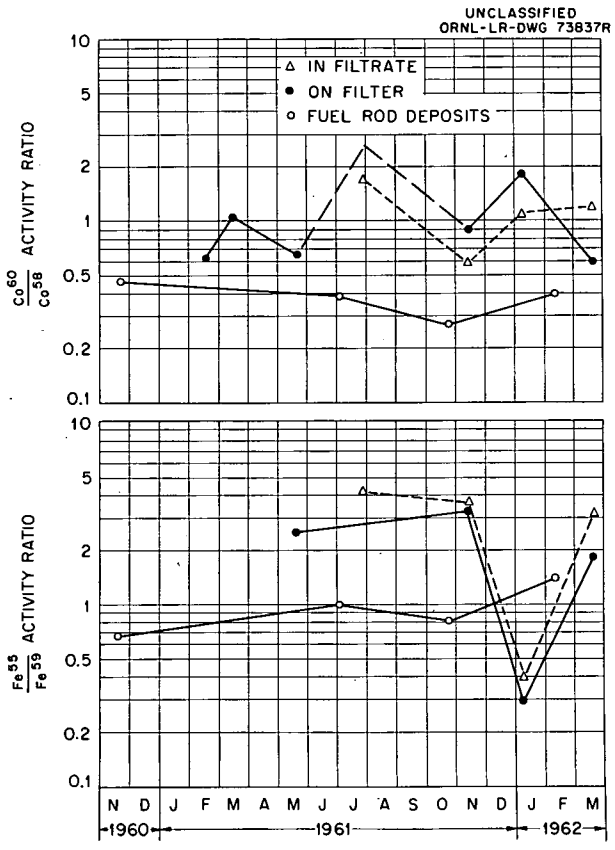


**Fig. 5.1. Nuclide Ratios Found in Filterable and Nonfilterable ORR Loop Water Fractions and in Fuel-Rod Crud Deposits.**

rate of 1 mg $dm^{-2}$ $month^{-1}$, then crud should be produced at a rate of 1.4 g/month, that is, at about the same rate at which it is removed.

The dissolution rate and the equilibrium solubility of magnetite, which under loop operating conditions is assumed to dissolve by the following reaction,

$$Fe_3O_4 + 6H^+ + H_2 \rightarrow 3Fe^{2+} + 4H_2O ,$$

thus may be important parameters in determining the effectiveness of side-stream purification by ion exchange and, along with the dissolution of other active elements in crud, important parameters in the activity transport process. Attempts are now being made to determine these dissolution rates and equilibria more accurately under controlled laboratory conditions.

Samples of crud deposited on fuel-rod test assemblies which have been irradiated in the loop test section, while having specific activities which were generally comparable to the fractions of water-borne activity, were found to have a greater abundance of the shorter-lived ($Fe^{59}$ and $Co^{58}$) compared with the longer-lived ($Fe^{55}$ and $Co^{60}$) activities (Fig. 5.1). This clearly indicates that radiochemical exchange between in-flux crud deposits and the coolant is not rapid compared with the rates of decay of $Fe^{59}$ and $Co^{58}$ ($T_{1/2}$ = 45 and 72 days respectively). In order to determine whether incomplete exchange was consistent with the hypothesis

**Table 5.1. Estimation of Dissolved Solids Concentration in ORR Loop Water**

| Nuclide | Specific Activity in Water-Borne Crud (dis/sec per g of crud) | Activity in Dissolved Solids (dis/sec per liter of coolant) | Dissolved Solids Concentration (g/liter)[a] |
|---|---|---|---|
| | | | $\times 10^{-6}$ |
| $Fe^{59}$ | $7 \times 10^7$ | $4.3 \times 10^2$ | 6 |
| $Fe^{55}$ | $1.8 \times 10^8$ | $1.4 \times 10^3$ | 8 |
| $Co^{58}$ | $5 \times 10^7$ | $4.6 \times 10^2$ | 9 |
| $Co^{60}$ | $3 \times 10^7$ | $4.4 \times 10^2$ | 15 |
| | | Av | $1.0 \times 10^{-5}$ [b] |

[a]These values are obtained by dividing the numbers in column 3 by those in column 2, based on the assumption that the specific activity of the two water fractions is equal.

[b]This is equivalent to $1.3 \times 10^{-7}$ $M$ $Fe(OH)_2$.

of reasonably complete exchange between the two water fractions, a simple, steady-state, kinetic analysis of activity transport in the loop was carried out. It was assumed that crud present on the influx and out-of-flux loop surfaces released a given nuclide to the coolant at a rate which was proportional to the nuclide concentration in the crud and to the interfacial area. Correspondingly, it was assumed that this nuclide was deposited from the coolant at a rate which was proportional to its concentration in the coolant and to the interfacial area. It has been found that this simple model is indeed consistent with the observed nuclide ratios and specific activities in fuel-rod deposits and in the two fractions of water-borne activity, provided the average thickness of deposited crud is $>0.4\ \mu$, a limit which is quite consistent with crud particle size. This kinetic analysis of the system has also supported the view that natural magnetite would be an effective high-temperature decontaminating medium for use in PWR systems at neutral pH.

In order to examine this potential application of magnetite, experiments were performed in which a high-temperature loop-water bleed stream was passed through a cartridge containing $\sim 100$ g of magnetite. Results for two kinds of magnetite (Table 5.2), a natural and a synthetic material, showed quite favorable decontamination factors for loop water activity, most of which was nonfilterable. Because of its higher purity the synthetic material (manufactured in large quantities as a black pigment) is being examined further. Owing to its fine particle size (0.2 to 0.8 $\mu$), it was sintered before use to obtain desired flow rates in the tests. The effects of changes in such variables as sintering temperature, particle size, flow rate, and temperature are currently being examined both at the loop test assembly and in the laboratory.

**Table 5.2. Decontamination of Loop Water by Magnetite in High-Temperature (425°F) Filter Unit**

| Date | Medium | Flow Rate (ml/min) | Activity Removed (%) | | |
|---|---|---|---|---|---|
| | | | $Mn^{56}$ | $Co^{58} + Mn^{54}$ | $Co^{60} + Fe^{59}$ |
| 7-5-62 | Prince Mfg. Co. +80 mesh | 60 | >99 | >99 | 95 |
| 9-11-62 | Mapico Black, sintered | 80 | >99 | 97 | 98 |

# 6. Corrosion by Solutions

J. C. Griess H. C. Savage
J. L. English J. G. Rainwater
L. L. Fairchild J. F. Winesette

## EFFECT OF HEAT FLUX ON THE CORROSION OF ALUMINUM BY WATER

### Introduction

For the past three years the effect of very high heat fluxes on the corrosion of aluminum by water has been under investigation. The purpose of the program has been to demonstrate the adequacy of aluminum cladding for the fuel elements to be used in the High Flux Isotope Reactor (HFIR) and the Advanced Test Reactor (ATR). The fuel elements of both reactors will be subjected to very high heat fluxes.

A series of reports[1-4] has described the experimental procedures and many of the results. Briefly it has been shown that corrosion of aluminum by water results in the formation of an adherent layer of boehmite ($\alpha$-$Al_2O_3 \cdot H_2O$) which has low thermal conductivity. Under conditions of high heat flux, the boehmite layer presents a significant barrier to heat transfer. Thus at a given heat flux, the temperature of the aluminum increases as corrosion proceeds. It was further demonstrated that the rate of corrosion, and consequently the rate of corrosion-product accumulation on the surface, was much less when the pH of the coolant was adjusted to 5 with nitric acid than when deionized water was used. Regardless of pH, however, the results indicated that the temperature at the specimen-water interface was rate controlling, at least with regard to the buildup of the corrosion-product layer. With the coolant at a pH of 5, corrosion of the aluminum alloys tested (6061, X8001, and 1100) was such that under the most severe conditions expected in either reactor, penetration of the cladding would not exceed 2 mils during a reactor cycle. The testing program showed, however, that from the standpoint of reactor operation, corrosion-product film is a more serious problem than corrosion damage. Since aluminum alloys lose their strength rapidly as the temperature increases, the mechanical stability of fuel plates under the hydrodynamic forces to which they will be exposed places more of a limitation on the use of aluminum than does corrosion damage *per se*.

Most of the tests during the past year were conducted under conditions approximating those that will exist during operation of the ATR. For this reason all tests were conducted with coolant flow rate and pH of 45 fps and 5.0 respectively. Both 6061 and X8001 aluminum served as specimens. Heat fluxes varied from 0.5 to $2.0 \times 10^6$ Btu $hr^{-1}$ $ft^{-2}$, and surface temperatures (temperature at specimen-water interface) between 300 and 400°F were used.

### Results

**Tests with Decreasing Heat Flux.** – During the operation of the ATR, both the hot channel heat

[1] J. C. Griess, H. C. Savage, *et al.*, *Effect of Heat Flux on the Corrosion of Aluminum by Water. Part I. Experimental Equipment and Preliminary Test Results*, ORNL-2939 (Apr. 29, 1960).

[2] J. C. Griess, H. C. Savage, *et al.*, *Effect of Heat Flux on the Corrosion of Aluminum by Water. Part II. Influence of Water Temperature, Velocity and pH on Corrosion Product Formation*, ORNL-3056 (Feb. 10, 1961).

[3] J. C. Griess, H. C. Savage, *et al.*, *Effect of Heat Flux on the Corrosion of Aluminum by Water. Part III. Final Tests Relative to the High Flux Isotope Reactor*, ORNL-3220 (Dec. 5, 1961).

[4] J. C. Griess, H. C. Savage, *et al.*, *Proceedings of the Research Reactor Fuel Element Conference Held at Gatlinburg, Tennessee, September 17–19, 1962*, USAEC Report TID-7642 (to be published).

flux and coolant temperature will decrease during a reactor cycle. Therefore tests were conducted to simulate this condition at three different starting surface temperatures. In each case the heat flux was decreased in a stepwise fashion from an initial value of $1.44 \times 10^6$ Btu $hr^{-1}$ $ft^{-2}$ to a final value of $1.24 \times 10^6$ Btu $hr^{-1}$ $ft^{-2}$ over the 17-day test period. The cooling-water temperature at the start of each test was adjusted to give the desired surface temperature, and then during the run it was also decreased in a stepwise fashion by a total of 26°F. The change in temperature at the specimen oxide-metal interface during the test is illustrated in Fig. 6.1 for starting surface temperatures of 340, 360, and 387°F. Each curve represents the average of duplicate tests. Each point on the graph represents the temperature immediately preceding a decrease in either heat flux or coolant temperature or both. Obviously, a small temperature decrease occurred after decreasing either the heat flux or coolant temperature, but this decrease is not shown on the graph.

Since fuel element temperatures in excess of 400°F are undesirable because of structural weakening, these data show that starting fuel element surface temperatures should not exceed 340°F. Design calculations indicate that this temperature will be exceeded occasionally at hot spots, but the surface areas involved will be so small that fuel plate stability will not be affected.

**Effect of Heat Flux.** – Most of the results previously reported were obtained at heat fluxes near $1.5 \times 10^6$ Btu $hr^{-1}$ $ft^{-2}$ with only one test at $1 \times 10^6$ Btu $hr^{-1}$ $ft^{-2}$ and two at $2 \times 10^6$ Btu $hr^{-1}$ $ft^{-2}$. Within the range of 1 to $2 \times 10^6$ Btu $hr^{-1}$ $ft^{-2}$ the data indicated no significant effect of heat flux.[3] It also appeared that the rate of oxide accumulation was a function of the temperature at the specimen-water interface. To reexamine the above conclusion and to extend the heat flux range to lower values, a series of tests was conducted in which the heat flux was changed from run to run, but the surface temperature of the specimen was held constant at approximately 400°F by adjustment of the cooling-water temperature. All tests, with the exception of those indicated, lasted 142 hr. The oxide thicknesses on the specimens at the end of the tests were determined metallographically. The results are shown in Table 6.1.

Both runs at the $2 \times 10^6$ heat flux level were terminated prematurely. However, extrapolation of the time-temperature curves (as discussed later) indicates an oxide thickness of about 1.8 mils had the first run continued for 142 hr and 1.3 for the same time in the second. Comparing the data obtained in the 1 to $2 \times 10^6$ Btu $hr^{-1}$ $ft^{-2}$ range, it appears that heat flux does not affect oxide thickness. On the other hand, thinner oxide formed at

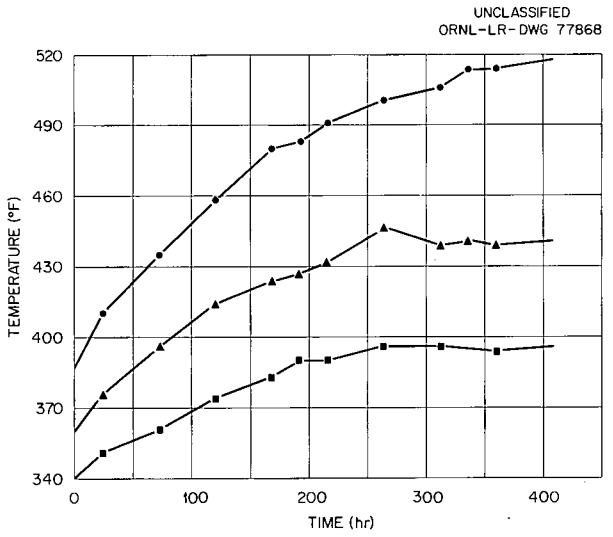


**Fig. 6.1. The Temperature at the Aluminum–Aluminum Oxide Interface During Tests in Which the Heat Flux and Coolant Temperature Were Decreased.**

**Table 6.1. The Effect of Heat Flux on the Formation of a Corrosion-Product Film at 400°F During 142-hr Tests**

| Heat Flux (Btu $hr^{-1}$ $ft^{-2}$) | Corrosion-Product Thickness (mils) |
|---|---|
| $\times 10^6$ | |
| 2.0 | 1.31[a] |
| 2.0 | 0.84[b] |
| 1.5 | 1.28 |
| 1.0 | 1.36 |
| 0.75 | 1.15 |
| 0.50 | 0.75 |
| 0.50 | 0.75 |

[a]Exposed only 93 hr.
[b]Exposed only 83 hr.

heat fluxes less than $1.0 \times 10^6$ Btu $hr^{-1}$ $ft^{-2}$. Thus, the data generally support the conclusion previously reported[5] that, in the range of heat fluxes between 1 and $2 \times 10^6$ Btu $hr^{-1}$ $ft^{-2}$, heat flux *per se* is not a particularly significant variable; however, at the lower levels, heat flux does appear to be an important variable. Before any useful correlation of the effect of heat flux on oxide buildup can be derived, additional testing must be completed.

### Discussion

It was reported previously that under constant conditions the corrosion-product thickness (as indicated by the temperature increase of the specimen) increased approximately linearly with exposure time, and the data were treated in that manner.[5] The above conclusion was based on tests of short duration, usually about ten days, at relatively low temperatures. Tests conducted during the past year generally lasted longer and were carried out for the most part at higher temperatures. The results of these tests clearly indicated that the oxide did not accumulate at a constant rate but that the rate decreased with exposure time. Reexamination of all the data indicates that the temperature-time curves are best described by the relationship $T = T_0 + m\theta^p$, where $T$ is the aluminum temperature at time $\theta$, $T_0$ is the starting temperature, and $m$ and $p$ are constants. The best value of $p$ appears to be between 0.7 and 0.8 and to be independent of temperature and pH. On the other hand, the value of $m$ depends on the water-oxide interfacial temperature and on the pH. The temperature dependence is of the Arrhenius type so that $m$ can be expressed in terms of temperature.

The above equation can be expressed as $\Delta T = m\theta^p$, and $\Delta T$ can be related to oxide thickness from the standard relation $Q = k\Delta T/X$, where $Q$ is the heat flux, which is known from the test conditions, $k$ is the thermal conductivity of the oxide film, estimated to be 1.3 Btu $hr^{-1}$ $ft^{-2}$ $(°F)^{-1}$ $ft^{-1}$ (ref 5), and $X$ is the oxide film thickness. Thus, at a fixed pH, it is possible to express the oxide thickness by a relation of the type $X = A\theta^p \exp(-B/T)$, where $A$, $p$, and $B$ are constants and $T$ is the temperature at the specimen-water interface expressed in degrees Kelvin.

Sufficient data to evaluate the constants in the above equation are only available at a pH of 5, but as mentioned before, the constant $p$ appears to be independent of pH. The test data obtained at a pH of 5 and in the heat flux range of 1 to $2 \times 10^6$ Btu $hr^{-1}$ $ft^{-2}$ are currently being evaluated to arrive at the best values of the constants.

One of the major aims of the program to date has been the establishment of an empirical relation such as the one above. Fuel element surface temperatures can be estimated from a knowledge of heat generation rates and fluid-film coefficients. Then by use of a relation such as given above and from a knowledge of the thermal conductivity of the oxide, it is possible to estimate the fuel element temperatures during a reactor cycle. A knowledge of such temperatures is essential to the design of structurally adequate fuel elements, particularly in high-performance reactors using thin aluminum fuel plates.

## CORROSION STUDIES FOR THE HIGH FLUX ISOTOPE REACTOR

During the past year two areas of interest have received attention in the corrosion program for the High Flux Isotope Reactor, namely, the behavior of dissimilar metal combinations and the effect of water velocity on the corrosion of reactor-grade QMV beryllium which serves as the reflector. The environment consisted of pH 5 water (adjusted with nitric acid) at 100°C containing between 4 and 5 ppm of dissolved oxygen. Coupled specimens were prepared by bolting together two or more flat specimens with a bolt of the same alloy as one in the couple. Thus, in addition to being electrically coupled, a large crevice existed between the dissimilar materials. Specimens were exposed in a stainless steel pump loop; the couple specimens were placed in the loop pressurizer where the solution flow was approximately 0.4 fpm. The beryllium specimens were positioned in lines where the velocity ranged from 12.5 to 81 fps. All specimens were electrically insulated from the stainless steel loop components.

A summary of the pertinent dissimilar-metal data is given in Table 6.2. The most serious problem was the behavior of 6061-T4 aluminum coupled with type 304 stainless steel. Considerable pitting took

[5] J. C. Griess, H. C. Savage, *et al.*, *Effect of Heat Flux on the Corrosion of Aluminum by Water. Part III, Final Tests Relative to the High Flux Isotope Reactor*, ORNL-3220 (Dec. 5, 1961).

place on the aluminum contact surface next to the stainless steel. Pit depths up to 35 mils were not uncommon after 6860 hr. The true pit depths were somewhat greater than the microscopically measured values because it was impossible to remove all of the corrosion products from the pits. Substantial pitting was experienced also by aluminum in contact with hardened 420 stainless steel. Pits up to 17 mils in depth were measured on the aluminum contact surface after an exposure of 6860 hr. Considerable film appeared on the stainless steel specimen. No particular problem was disclosed in the 6061-to-6061 aluminum couple although a few random pits up to 4 mils in depth were detected on contact surfaces after 5353 hr. Some pitting was observed on contact surfaces of a beryllium-to-beryllium couple but the attack was not specific to the contact surfaces. The pit depths did not exceed 6 mils, identical with the attack observed on uncoupled beryllium specimens. Specimens of type 304L stainless steel which were sensitized by heating for 1 hr at 677°C exhibited negligible attack after 2500 hr.

In the HFIR, the reactor core will be supported on 6061 aluminum which must be joined to the stainless-steel-clad pressure vessel. The aluminum members will be of substantial thickness, and it is possible that the random, and eventually deep, pitting may not produce serious consequences. However, means of minimizing the problem are

**Table 6.2. Galvanic Behavior of Selected Materials in pH 5 Water at 100°C**

| Material | Exposure Time (hr) | Corrosion Rate (mils/yr) | Observations |
|---|---|---|---|
| 6061-T4 Al (control) | 6860 | Gain | No pitting; medium dark-gray film |
| 6061-T4 Al to 304 SS | 6860 | 0.2 (Al)<br>Gain (SS) | Pits up to 35 mils on aluminum contact face; voluminous white deposits; negligible attack on stainless steel |
| 6061-T4 Al to QMV Be | 6860 | Gain (Al)<br>0.3 (Be) | Uniform attack on aluminum contact face; pits up to 7 mils distributed over all of beryllium surface |
| QMV Be (control) | 6860 | 0.6 | Metallic surface; pits up to 6 mils over all of beryllium surface |
| 6061-T4 Al to 17-4 PH SS in 1150°F condition RC-33 | 6860 | Gain (Al)<br>Gain (SS) | Pits up to 9 mils on aluminum contact surfaces; red-brown film on stainless steel with no pitting |
| 304 SS to 6061-T4 Al to 17-4 PH SS (H 1150) | 6860 | Gain (304 SS)<br>0.1 (Al)<br>Gain (17-4 PH) | Pits up to 7 mils on aluminum contact surfaces; only tarnish film on 304 SS; red-brown film on 17-4 PH SS with no pitting |
| 304 SS to 6061-T4 Al to hardened 420 SS | 6860 | Gain (304 SS)<br>Gain (Al)<br>0.2 (420 SS) | Pits up to 17 mils on aluminum contact surfaces; tarnish film on 304 SS; red-black deposit on 420 SS with pits to 2 mils |
| 304 SS to QMV Be | 6860 | Gain (SS)<br>0.2 (Be) | Pits up to 8 mils over all of beryllium surface; no pitting on 304 SS |
| QMV Be to QMV Be | 5355 | 0.3 | Metallic; pits up to 6 mils over all beryllium surfaces |
| 6061-T4 Al to 6061-T4 Al | 5355 | Gain | Few shallow pits, 4 mils and less, on contact surfaces |
| Sensitized 304L SS | 2500 | <0.1 | Uniform attack |

being investigated. These include tests to determine the practicability of eliminating the stainless-steel–to–aluminum crevice region by either coating the aluminum with a chromium deposit or by coating the stainless steel with aluminum. Preliminary tests with both types of specimens prepared by commercial vendors have shown promising results.

Four specimens of hot-pressed QMV beryllium were exposed to each of two velocities, 12.5 and 23 fps, in the pH 5 water at 100°C. As shown in Fig. 6.2, measured weight losses were linear with exposure time, and there was no effect of velocity on the rate of attack. Average corrosion rates after 4830 hr were 2.2 mils/yr in both tests. After 2500 hr, pitting was observed on all specimens and by the end of 4830 hr ranged in depth from 4 to 10 mils.

In the same environment the effect of velocity over a range from 22 to 81 fps on the corrosion of QMV beryllium was also examined by using a specimen holder that produced a velocity gradient over each specimen. The velocity ranges studied with duplicate specimens at each range were 22 to 33, 33 to 51, 51 to 72, and 72 to 81 fps. As in the previous flow tests, observed weight losses were linear with time and there was no significant effect of velocity on corrosion. After 4590 hr, the average rates were: 2.1 mils/yr at 22 to 33 fps; 1.9 mils/yr at 33 to 51 fps; 2.2 mils/yr at 51 to 72 fps; and 2.1 mils/yr at 72 to 81 fps. Pitting attack was initiated after 2300 hr of exposure and after 4590 hr ranged in depth from 3 to 5 mils.

The reflector in the HFIR will be cooled by water flowing through vertical holes drilled in the massive beryllium. The flow rate of the coolant will be approximately 20 fps and the surface temperature of the beryllium will be somewhat less than 100°C. The data presented above indicate that corrosion will not be a factor in limiting the life of the reflector.

## ACCEPTANCE TESTS

Approximately 200 boiling 65% $HNO_3$ and electrolytic oxalic acid etch tests (ASTM: A262-55T) were completed on austenitic stainless steels for use in various ORNL and Y-12 programs. Of this number, about 50 tests were concerned with materials for the High Flux Isotope Reactor (HFIR). The balance of the tests dealt with various Y-12 programs.

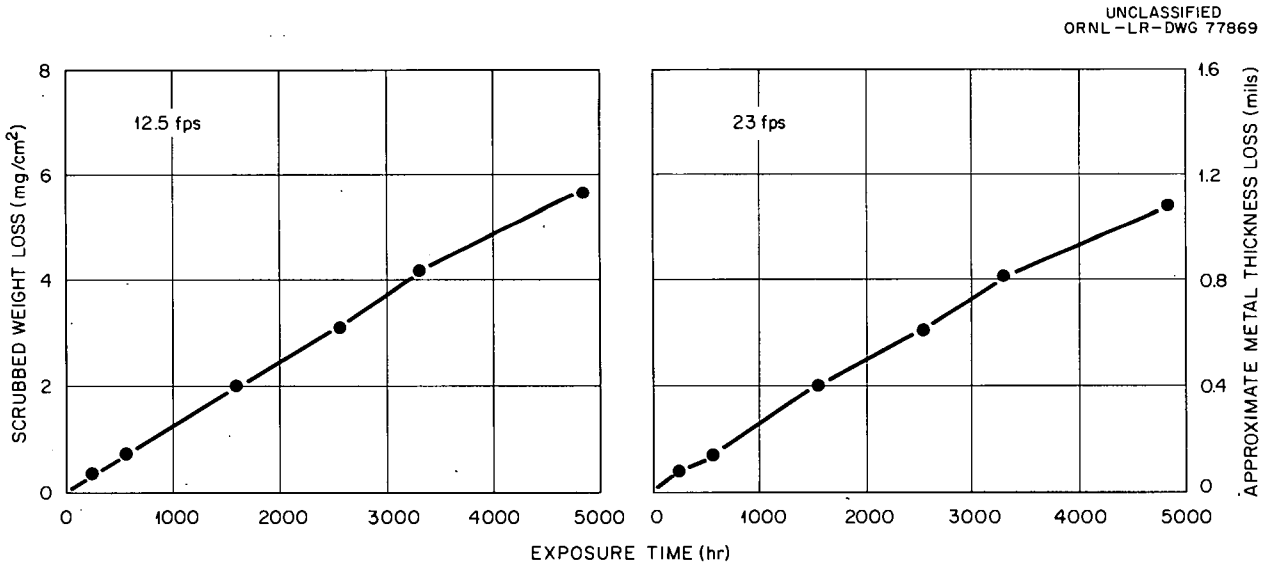


**Fig. 6.2. Effect of Velocity on Corrosion of QMV Beryllium in pH 5 Water at 100°C.**

# 7. Mechanism of Corrosion of Zircaloy-2

G. H. Jenks

## EFFECT OF REACTOR RADIATIONS ON ZIRCALOY-2 CORROSION IN HIGH-TEMPERATURE AQUEOUS ENVIRONMENTS[1]

R. J. Davis

Zircaloy-2 exposed in-pile to fissioning solutions of oxygenated $UO_2SO_4$ at high temperatures corrodes at a steady rate which depends upon the rate of fissioning near the surface and, at high rates of fissioning, upon the temperature. The detailed mechanism of this radiation corrosion is uncertain; but the corrosion is believed to result primarily from damage produced in the metal or oxide by the heavy fission fragment recoils, rather than from the ionizing effects of these and other types of radiations.

It has been recognized in the past that quantitative information on the effects of other types of heavy particles would be useful in evaluating the mechanism of the fission recoil induced corrosion as well as in reactor development where Zircaloy-2 is commonly used as fuel plate cladding. Accordingly, experiments to determine the effects on Zircaloy-2 corrosion of reactor radiations alone, including fast neutrons, and of reactor radiations together with small amounts of fission recoil irradiation were carried out as part of the program of Aqueous Homogeneous Reactor corrosion studies. These experiments were of the rocking-autoclave type. Oxygenated solutions of $UO_2SO_4$ with uranium depleted of $U^{235}$, $D_2O$, and dilute acid were tested in the temperature range 250 to 300°C. Hydrogenated water was also tested in one experiment. Radiation exposures were performed in the LITR and the MTR.

The results of these experiments were reexamined and reevaluated on the basis of presently available information regarding (1) neutron flux levels in the experiments, $1 \times 10^{12}$ to $7.5 \times 10^{12}$ (>1 Mev) $cm^{-2}$ $sec^{-1}$, (2) probable effects of fissioning of residual $U^{235}$ and of plutonium formed in the $UO_2SO_4$ experiments, and (3) the effects of nitrogen gas, initially present in some of the experiments, on the interpretation of gas-pressure-change measurements.

It was concluded that significant effects of reactor radiations alone occurred in all the experiments employing oxygenated solutions, with the amount of corrosion increasing approximately linearly with time. After allowance for the effects of the low-intensity fission recoil irradiations in the $UO_2SO_4$ experiments, it was found that the corrosion rates increased regularly with increasing fast neutron flux but were independent of temperature and solution composition. The rates ranged from about 0.5 to 3.0 mils/yr. Most of the characteristics of this corrosion were similar to those previously observed for corrosion in fissioning solutions. The rate data obtained in the experiments are shown in Fig. 7.1. The portions of the rates in the $UO_2SO_4$ experiments which were not accounted for by fission recoil irradiation are shown in Fig. 7.2.

Beta and gamma radiations are assumed to be ineffective on the basis of the results of previously reported studies with fast electrons at high intensities, so that the corrosive effects observed are ascribed to fast neutrons.

The results of comparisons of the characteristics of this corrosion with those known for fission recoil induced corrosion in $UO_2SO_4$ solutions, and of correlations between radiation damage rates

[1] G. H. Jenks and R. J. Davis, "Effect of Reactor Radiations on Zircaloy-2 Corrosion in High-Temperature Aqueous Environments," *Proceedings of the Third Conference on Nuclear Reactor Chemistry, Gatlinburg, Tenn., Oct. 9–11, 1962*, TID-7641.

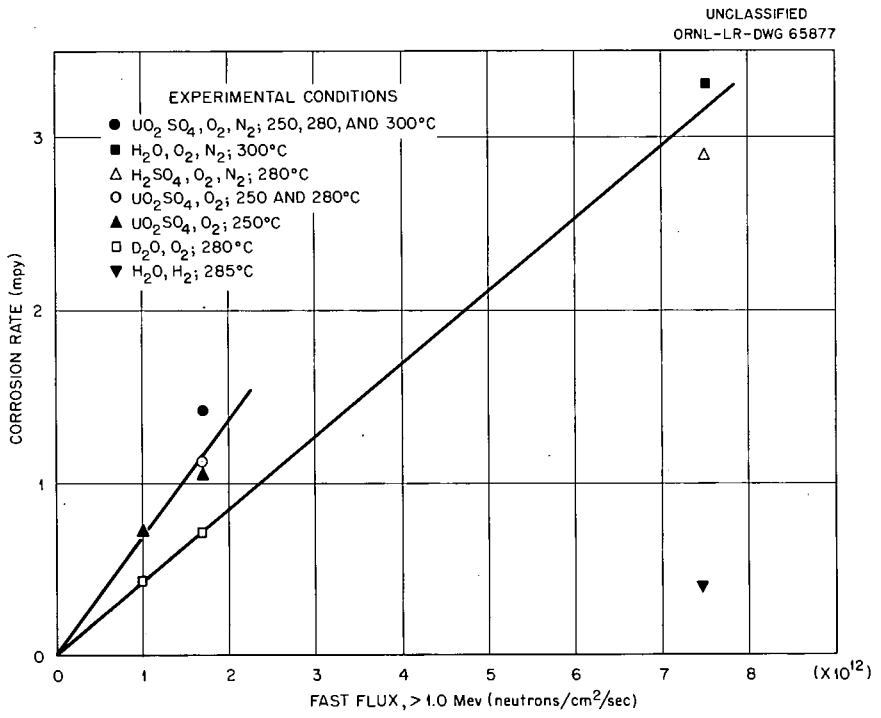


**Fig. 7.1. Corrosion Rate of Zircaloy-2 vs Fast-Neutron Flux.**

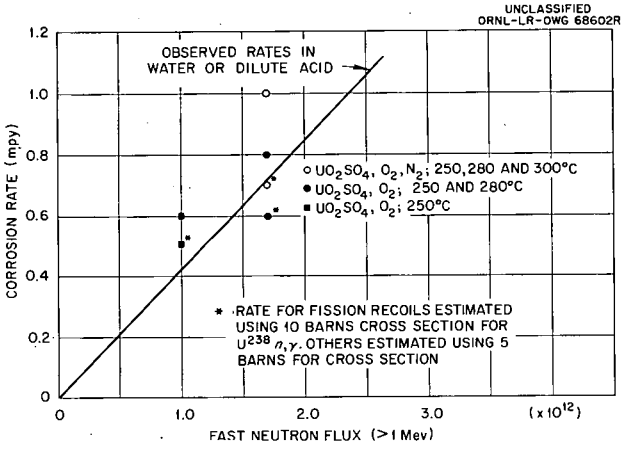


**Fig. 7.2. Corrosion Rate in $UO_2SO_4$ Experiments After Subtracting Rate Ascribed to Fission Recoils.**

and corrosion rates for neutrons and fission recoils, suggest that the mechanism by which corrosion is affected is the same for the two types of radiations and involves the production of displaced atoms as an initial step.

The radiation corrosion in the hydrogenated water was significant but probably less than that in the oxygenated solutions.

## OXIDE GROWTH AND CAPACITANCE ON PREIRRADIATED ZIRCALOY-2

R. J. Davis

Previous in-pile and Van de Graaff electron irradiation studies of corrosion of Zircaloy-2 in oxygenated, high-temperature solutions of either $UO_2SO_4$, dilute acids, or water have shown that fission fragments[2,3] and fast neutrons[4] accelerate corrosion in these oxygenated environments, but beta and gamma radiation[5] do not. Considerations of these data indicate that the initial step in the mechanism of the radiation effect is the displacement of atoms in the corroding surface material.[4] The specific mechanisms which have been proposed

[2]G. H. Jenks, *Review and Correlation of In-Pile Zircaloy-2 Corrosion Data and a Model for the Effect of Irradiation*, ORNL-3039 (July 6, 1961).

[3]B. Cox, K. Alcock, and F. W. Derrick, *J. Electrochem. Soc.* **108**, 129 (1961).

[4]R. J. Davis, this report, preceding section.

[5]B. O. Heston and M. D. Silverman, *Effects of Electron Irradiation on the Corrosion of Zircaloy-2 in a Thermal Loop*, ORNL CF-56-2-2 (Feb. 2, 1956).

or can be visualized to explain the radiation corrosion fall into two groups: (1) those in which the radiation produces damage in the oxide (easy diffusion paths, for example) which leads to corrosion acceleration and (2) those in which radiation damage in the metal leads to corrosion acceleration due to formation of a less protective film on the damaged metal or due to an increase in the reactivity of the metal. Experiments with the objective of determining whether the principal radiation effects are in the metal or oxide and, thus, aiding in establishing the corrosion mechanism have been undertaken[6] and are in the process of development.

In these experiments, specimens are irradiated with fast neutrons or fission fragments while in an inert environment, and subsequently exposed to a steam-oxygen mixture at 300°C. The amounts and protective qualities of the oxide formed in these subsequent exposures are compared with those for oxide formed on unirradiated control specimens. Amounts of oxide are determined from microbalance measurements which are reproducible to $<0.3$ $\mu g/cm^2$. The protective qualities of an oxide in place on a specimen is gaged from the measured capacitance of the specimen in an electrolytic solution. Such measurements have been shown by others[7,8] to be suitable for this purpose.

The capacitance measuring equipment was improved to readily enable measurements with only a few-millivolt ($<10$ mv RMS) potential across the capacitance cell. The input voltage from a Hewlett-Packard model 200 oscillator is fed through a G. R. type 546-C Audio-Frequency Microvolter to give a small measured voltage to the impedance bridge (G. R. type 1650-A). Sensitive null detection is provided by a G. R. type 1232-A Tuned Amplifier and Null Detector.

A simple capacitance cell has been developed. The cylindrical specimen is hung concentrically inside a platinum electrode. The approximately 1-mm annular space is filled with an electrolyte solution. The ends of the specimen are shielded from the solution by tightly fitting pieces of Teflon which can be rearranged to vary the exposed area of the specimen.

In order to demonstrate the significance of the measurements with this cell, impedance measurements on a 23-v anodized Zircaloy-2 film in 0.1 *M* $HNO_3$ were made at frequencies of $10^2$ to $10^5$ cps over a range of areas by the use of the Teflon shields mentioned above and also by the use of wax (Apiezon W) as used by other workers. The values of capacitance $C$, and of reciprocal resistances, $1/R$, for the entire cell increased linearly with specimen area exposed in both cases (wax or Teflon shields), and the slopes, $\Delta C/\Delta A$ and $\Delta(1/R)/\Delta A$, in both cases were similar. Also, the $\Delta C/\Delta A$ values were similar to those reported for film capacitance by others.[9] The values obtained using Teflon shields, however, did not extrapolate to zero $C$ or $1/R$ at zero area. The procedure for estimating film impedances is therefore to measure impedances at two areas and calculate the changes in $C$ and $1/R$ per unit area.

Further evidence of reliability of the system was obtained from a series of impedance measurements on a bare specimen at frequencies $10^2$ to $10^5$ cps in 1 *M* $NH_4NO_3$. Linearity of $C$ and $1/R$ with area was demonstrated, but again the values did not extrapolate to zero at zero area. The values of solution resistance were estimated by plotting $R$ vs $1/f$ (reciprocal frequency) and extrapolation to $1/f = 0$.[8] It was found that the values of $1/R_s$ (solution resistance) were linear with area and extrapolated to zero at zero area. Furthermore the solution resistance values were very near values calculated from the solution concentration and resistivity.

In order to show that film-impedance and weight-gain measurements could be made periodically on a specimen without affecting the film or its rate of growth, the following experiment was performed on unirradiated specimens. Two specimens were exposed to steam-oxygen mixture at 300°C for a total of four days but were removed from the furnace seven times for measurements. Weight gain of both specimens and the film impedance of one were measured. Two other specimens were exposed for four days in two periods, and, as before, weight gains were measured on both and the capacitance

[6] R. J. Davis and G. H. Jenks, *Reactor Chem. Div. Ann. Progr. Rept. Jan. 31, 1962*, ORNL-3262, p 84.

[7] J. N. Wanklyn and D. R. Silvester, *J. Electrochem. Soc.* **105**, 647 (1958).

[8] L. Young, *Anodic Oxide Films*, pp 150–52, Academic Press, New York, 1961.

[9] A. B. Riedinger, "*Corrosion Behavior of Zircaloy-2*," p 33, MS Thesis, Union College, Schenectady, N.Y., May 1958.

on one, after each period. The weight gain vs time behavior was not significantly changed either by periodic removal from the furnace or by periodic film-impedance measurement. The capacitance vs weight-gain relation was also unchanged by the periodic measurements.

Four specimens ($3\frac{1}{2}$ in. long, $\frac{3}{16}$ in. in diameter) have been exposed in the ORR lattice to a fast (>3.0 Mev) neutron flux of $1.1 \times 10^{14}$ neutrons $cm^{-2}$ $sec^{-1}$ for 587 hr. During irradiation the specimens were shielded in cadmium and were in a helium atmosphere. Also, cooling was provided so that the specimen temperature during irradiation was estimated to be about 65°C. Two specimens were irradiated with an oxide film represented by a weight gain of about 40 $\mu g/cm^2$, formed by a 96-hr preirradiation exposure to 300°C steam plus oxygen. The other two specimens were irradiated bare. These specimens will be in storage for about six more months until they are cool enough to handle with tongs. They will then be exposed to the 300°C steam-oxygen environment along with unirradiated control specimens, and periodic weight-gain and film-impedance measurements will be made in search of effects attributable to the fast neutron irradiation.

Two tubular specimens, $1\frac{3}{4}$ in. long, $\frac{3}{16}$ in. OD, $\frac{1}{18}$ in. ID, were irradiated in the LITR lattice, surrounded by 0.2 g of $B^{10}$ per $cm^2$, for 48 hr to an estimated fast flux of $2 \times 10^{13}$ neutrons $cm^{-2}$ $sec^{-1}$. One was irradiated with a film grown in 300°C oxygen plus steam (about 40-$\mu g/cm^2$ weight gain), and the second was irradiated bare. The irradiation was done in helium, and the temperature during irradiation was estimated to be less than 100°C. The specimens have been recovered, and the postirradiation exposure and measurements are under way. Some differences between the irradiated and control specimens have been noted but cannot, at this time, be unambiguously related to the irradiation.

Some planning has been made for experiments in which specimens would be irradiated at elevated temperature with fast neutrons in the ORR lattice and for other experiments in which specimens would be irradiated with fission fragments in the ORNL Graphite Reactor exposures.

## ELECTROCHEMISTRY OF HIGH-TEMPERATURE AQUEOUS ZIRCALOY-2 CORROSION

A. L. Bacarella

In previously reported work,[10-12] equipment and techniques were developed for investigations of the electrochemistry of corrosion in high-temperature aqueous environments, and these were utilized in studies of the electrochemistry of Zircaloy-2 corrosion in oxygenated, 0.05 *m* $H_2SO_4$ solutions in the temperature range 200 to 300°C. Additional experiments with this corrosion system near 300°C have been made to determine: (1) the kinetics of the initial corrosion and (2) various parameters, including the kinetics, of the corrosion during extended exposure periods. Also, facilities have been developed for determining the high-temperature electrode potentials with respect to the calomel reference electrode and for determining the capacitance of the corrosion specimen in place and at temperature in the cell. The interpretations of the current and potential measurements at the longer exposure times is not yet clear (for reasons mentioned in a subsequent paragraph) and these experiments will be only briefly summarized.

### Kinetics of the Initial Corrosion

Knowledge of the kinetic law to which a corrosion system conforms, particularly the initial corrosion, is generally of substantial aid in establishing the corrosion mechanism in that system.[13] No previous information on the kinetics of the initial corrosion of Zircaloy-2 in aqueous environments near 300°C has been found in the literature. However, the corrosion of zirconium in 33-mm steam during the initial 120 min of exposure has been reported by Mallett *et al.*[14] In their work, the specimens were at temperature in a

[10] A. L. Bacarella, *J. Electrochem. Soc.* **108**, 33 (1961).

[11] A. L. Bacarella, *HRP Quart. Progr. Rept. Oct. 1959*, ORNL-2879, p 149.

[12] A. L. Bacarella, *HRP Quart. Progr. Rept. July 1960*, ORNL-3004, p 75.

[13] E. A. Gulbransen and K. F. Andrew, *Trans. AIME* **209**, 397 (1957).

[14] M. W. Mallett, W. M. Albrecht, and R. E. Bennett, *J. Electrochem. Soc.* **104**, 349 (1957).

vacuum prior to the steam exposure. They interpreted their results in terms of conformity to the cubic rate law. However, it can be shown[15] that their results also obey a logarithmic rate law. Cox[16] studied the corrosion kinetics of zirconium and Zircaloy-2 in 15-psi steam starting at about 500 min exposure and employing interference color measurements to determine oxide film thickness. He reported[16] that the corrosion followed a logarithmic rate law during the six- to ten-day period in which the colors were visible. He also reported that the film thicknesses calculated from weight gains agreed with those determined from interference colors during the initial two- to three-day exposure, and that the initial growth rate of Zircaloy-2 in oxygenated sulfate solution was substantially the same as for zirconium in steam.[17] It has been previously shown[11,12] that logarithmic kinetics are obeyed initially at 208 and 258°C in the corrosion system used in the present work.

The specimen for this experiment was machined from stock of the highest available quality and was emery polished. The "stem" was preoxidized in air at 340 to 360°C. As with previously described experiments, the cell was of titanium, and the platinum reference electrode was in a side arm of the cell where the temperature was about 70 to 90°C and approximately constant. The temperature was raised to the exposure temperature during a period of 2 min. Small current polarizability measurements were started about 6 min after the exposure temperature was reached, and more complete current-potential measurements were made at 8000 min. Consideration of the Tafel slopes indicated that the best value for $\Sigma(\alpha\lambda)$ was 0.30; 0.05 for $\alpha\lambda$ anodic and 0.25 for $\alpha\lambda$ cathodic. Corrosion rates calculated using this value for $\Sigma(\alpha\lambda)$ together with measured values of small current polarizability are shown in Fig. 7.3 in a plot of reciprocal rate vs time. A straight line is formed by the data taken during the initial 300-min exposure, which shows that logarithmic kinetics were obeyed during this period. A log rate–log $t$ plot leads to the same conclusion regarding the kinetics.

For purposes of discussion and comparison of corrosion under different conditions, the following equations and definitions are listed:

$X_T$ = total amount of oxygen reacted at time $t$,

$X_1$ = amount of reacted oxygen in protective film,

$X_0$ = unknown amount of oxygen in protective oxide at zero time,

$X_T - X_0 = X$ = measured amount of oxygen reacted after zero time.

The kinetic equation which gives rise to the direct logarithmic relation is shown in Eq. (1).

$$dX_T/dt = Ae^{-BX_T}, \qquad (1)$$

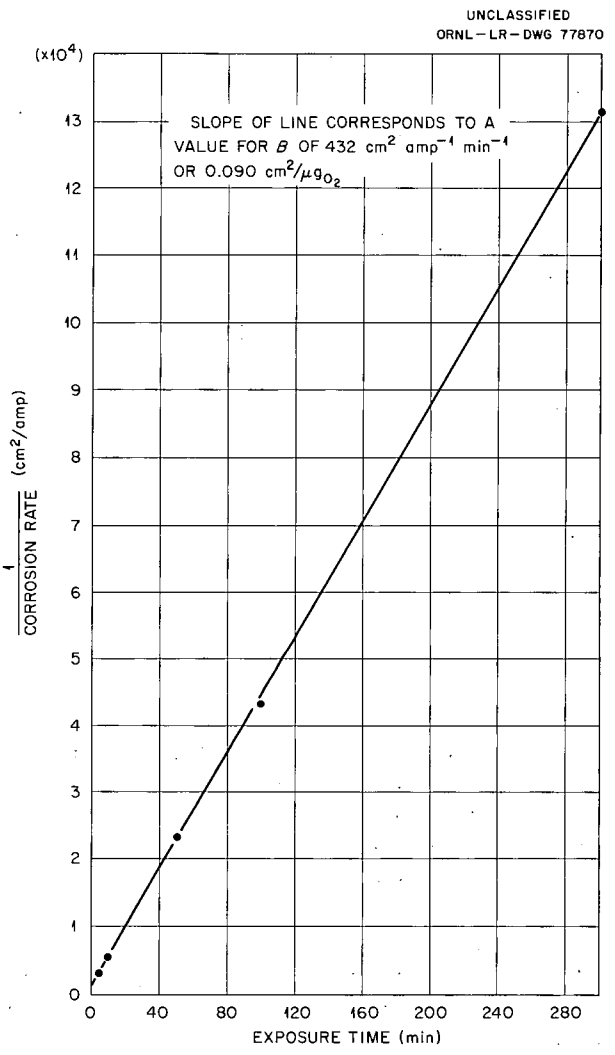


**Fig. 7.3. Reciprocal Corrosion Rate for Zircaloy-2 in Dilute $H_2SO_4$ vs Time.**

[15] G. H. Jenks, unpublished work.

[16] B. Cox, AERE-R 2874 (March 1959).

[17] B. Cox, *J. Electrochem. Soc.* **108**, 24 (1961).

where $A$ and $B$ are constants for a given set of experimental conditions. Assuming that the logarithmic law is followed after an initial period, $t_2$, during which the corrosion amounts to $X_2$, the integral of Eq. (1) is Eq. (2),

$$X_T - X_0 = X = 1/B \ln (ABte^{-BX_0} + a) , \qquad (2)$$

where $a = e^{-BX_0}(e^{BX_2} - ABt_2)$. If the logarithmic law is followed from $t = 0$, the value of $a$ is unity. Substitution of Eq. (2) in Eq. (1) and inverting yields

$$1/(dX_T/dt) = Bt + ae^{BX_0}/A , \qquad (3)$$

which is the basis for the statements regarding the kinetics shown by the plot in Fig. 7.3. The applicability of Eq. (2) to appropriate data can be determined, and the constant $B$ evaluated, with the aid of a plot of the type described by Mangelsdorf.[18] The values of $a$ and $Ae^{-BX_0}$ can then be evaluated by substitution of the value of $B$ together with experimental data in Eq. (2).

It may be noticed that the values of $B$ found for Eq. (2) are independent of the presence of film at zero time if the properties represented by $B$ for this initial film are essentially the same, at the times during which the data are fitted to the equations, as those for the subsequently grown film. The values of $Ae^{-BX_0}$ are dependent upon the presence of initial film, and the true $A$ values are greater than or equal to the calculated values of $Ae^{-BX_0}$. Also, for data for which Eq. (3) is appropriate, the true value of $A$ cannot be found unless values of $e^{-BX_0}$ and of $a$ are known. Comparisons and discussions of available data must then be confined to considerations of obedience to a logarithmic law and to values of $B$.

Values of $B$ obtained electrochemically at three different temperatures are compared in Fig. 7.4 with those evaluated from data reported by Cox[16] and by Mallett *et al.*[14] The 208 and 258°C electrochemical values were calculated using 0.30 for $\Sigma(\alpha\lambda)$ as evaluated from the present 292°C data. This is justified for the 208°C data by the fact that the Tafel slopes at the low temperature were comparable to those found at the higher temperature and a similar analysis leads to approximately the same $\Sigma(\alpha\lambda)$ value. The value for $\Sigma(\alpha\lambda)$ at 258°C was not established, but it is reasonable to assume that it was the same as that at the other temperatures. The values of $B$ for the Zircaloy-2 data of Cox and for the zirconium data of Mallett *et al.* were found by replotting the published data and employing the Mangelsdorf-type analysis. The value of $B$ for Cox's 300°C zirconium data was calculated from the slope of the line in a log $t$ vs weight gain plot presented by that investigator.[16]

The values for Zircaloy-2 in dilute $H_2SO_4$ at the three different temperatures fall near a straight line which is nearly parallel to that drawn through the values for zirconium in steam deduced from the data of Mallett *et al.* The several values deduced from data for corrosion at directly comparable temperatures near 300°C are in near agreement, although those for zirconium are slightly greater than those for Zircaloy-2.

From the foregoing, it is concluded that the mechanism of initial corrosion of zirconium and

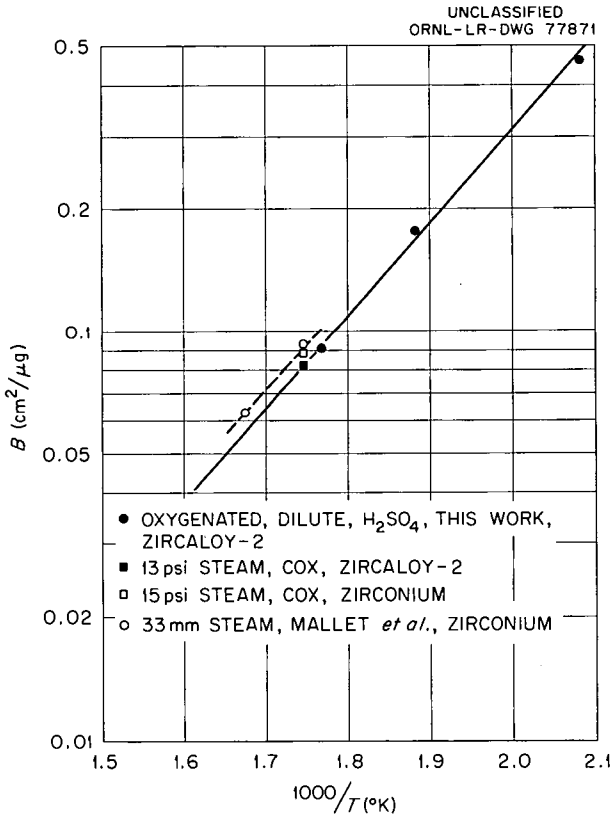


**Fig. 7.4. Values for Logarithm $B$ vs Reciprocal Temperature for Initial Corrosion of Zircaloy-2 and Zirconium.**

[18] P. C. Mangelsdorf, Jr., *J. Appl. Phys.* **30**, 442 (1959).

Zircaloy-2 near 300°C in the several different environments considered is the same and is one which gives rise to the logarithmic rate law. Further, the amounts of corrosion, as controlled by the important parameter $B$, are essentially the same in the different environments. It is very likely that these conclusions are also true for other aqueous environments, including the oxygenated sulfate solutions (investigated by Cox) and deaerated water. In oxygenated dilute $H_2SO_4$, the mechanism of initial corrosion remains the same at temperatures down to at least 208°C. The mechanism of the corrosion leading to the logarithmic law has not been established. The significance of the $B$ values as well as that of the apparent activation energy for the factor $1/B$ remains to be assessed.

### Experiments at Long Exposure Times

The one previous experiment[19] near 300°C employed a chemically polished specimen fabricated from stock which proved to be of poor quality. The 20-mil extension of the specimen, the stem, which comprised the electrical lead was anodized at 180 v prior to exposure. In polarization resistance measurements starting several hundred minutes after the initiation of exposure, it was found that the corrosion current decreased with increasing exposure time until after several days the current approached a steady-state value. The corrosion current at the steady state was independent of potentials anodic to the corrosion potential. The activation energy of the anodic partial process, from about 240 to 300°C, was 31 to 32 kcal/mole. Additional experiments of this general type were carried out to determine the effects of specimen quality, surface preparation, and of relative areas of stem and specimens on the occurrence and characteristics of the steady state and to help define its nature. In general, a steady-state current with characteristics similar to those previously observed was found with all specimens. However, some results indicated that a substantial part of this current arose in corrosion of the stem surfaces. Since part of the stem is at temperatures below the test temperature, the interpretation of the results is not yet clear and they are, therefore, not presented yet.

[19] A. L. Bacarella, *Reactor Chem. Div. Ann. Progr. Rept. Jan. 1962*, ORNL-3262, p 86.

### Apparatus

A salt bridge was designed and constructed for the purpose of performing measurements of the potentials of the Zircaloy-2 electrodes at operating temperature (292°C) and pressure (110 atm) with respect to an external calomel reference electrode at 25°C and atmospheric pressure. The bridge is shown in Fig. 7.5. The asbestos string is saturated

UNCLASSIFIED
ORNL-LR-DWG 77882

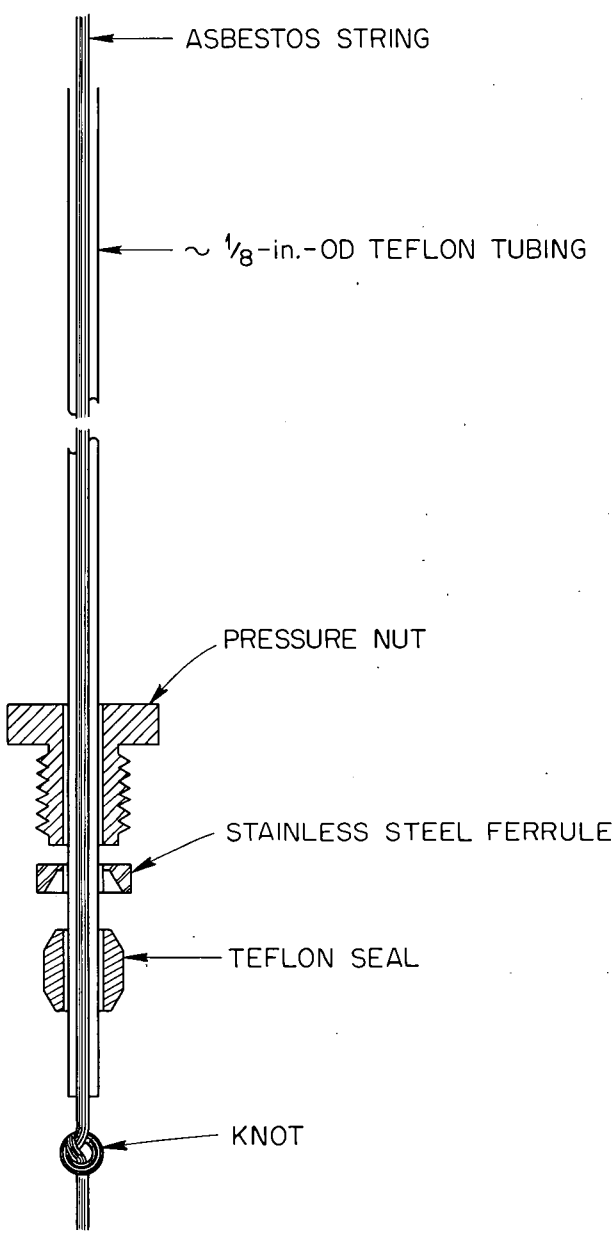


**Fig. 7.5. Salt Bridge for External Reference.**

with the test solution, pulled tightly through approximately 3 ft of Teflon capillary tubing, and knotted at the end to prevent its expulsion from the high-pressure autoclave. The high-pressure seal was accomplished with the same type Teflon cone fittings as used on the electrode seals.[20] A comparison of the Zircaloy-2 potentials vs both reference electrodes is shown in Table 7.1. These potentials are internally self-consistent within 50 mv, which is adequate for corrosion potential measurements.

Equipment has been developed for performing capacitance measurements at operating temperature using a d-c technique. A constant current is pulsed through the electrode for less than 1 msec and the linear voltage transient during the first 10 to 100 μsec is measured on a type 533A oscilloscope using a high gain differential d-c preamp input. The capacity is then calculated as

$$C = \frac{\Delta Q}{\Delta V} = \frac{i\Delta t}{\Delta V},$$

where $C$ is the capacity, $i\Delta t = \Delta Q$ is the charge passed through the system, and $\Delta V$ is the voltage change. Some preliminary measurements of the capacity of the corroding electrode as a function of time have been made using this apparatus.

[20] A. L. Bacarella, *J. Electrochem. Soc.* **108**, 33 (1961).

**Table 7.1. Comparison Between Platinum and Calomel Reference Electrodes**

| Solution | Temperature (°C) | Potential,[a] Zircaloy-2 vs $Pt/O_2$ (v) | Potential,[a] Zircaloy-2 vs S.C.E.[b] (v) | Potential, $Pt/O_2$ vs S.C.E.[b] (v) |
|---|---|---|---|---|
| 0.05 *m* $H_2SO_4$ | 25 | −0.450 | +0.250 | |
| | 292 | −0.950 | −0.200 | |
| 1.0 *m* $KHSO_4$ | 25 | | +0.280 | +0.760 |
| | 292 | | −0.175 | |

[a] These are average values; measured values differed by ±50 mv.
[b] The term S.C.E. means saturated calomel electrode.

# 8. Physical Chemistry of High-Temperature Aqueous Systems

## THE ELECTRICAL CONDUCTIVITY OF AQUEOUS SOLUTIONS FROM 25 TO 800°C AND AT PRESSURES UP TO 4000 BARS

A. S. Quist H. R. Jolley[1]
W. L. Marshall

### Introduction

The extent of electrolytic dissociation of a salt dissolved in a liquid or a gas can be determined by measuring the electrical conductance of the solution. By measurement of the conductances of many different salts under similar conditions of temperature, concentration, and pressure, not only can the extent of dissociation be determined but also the types of ions which are formed and the relative velocities with which they move in an electrical field. Using electrical conductance as a tool, the behavior of salts in water solution is being investigated at temperatures up to 800°C and at pressures up to 4000 bars. Above 374°C and 219 bars, water ceases to behave as a liquid and can only exist as a gas or fluid which fills its container. In a continuing study on the behavior of sulfate salts at extremes of high temperature and pressure, the electrical conductances of $K_2SO_4$ dissolved in $H_2O$ at three concentrations were measured at temperatures from 25 to 800°C and at pressures from 1 to 4000 bars. Sufficient data were collected to show that $K_2SO_4$ at high temperatures and at moderately high pressures behaves as a relatively strong electrolyte.

[1]Summer participant, 1961 and 1962, Loyola University, New Orleans, La.

### Experimental Procedures

The conductivity cell for use at high temperatures and high pressures has been described previously.[2-4] The experimental method for attaining the highest pressures, a maximum of 4000 bars ($\cong$ 4000 atm), was modified by the use of a high-pressure pump (Sprague air-driven diaphragm pump) and an intensifier (Harwood Engineering Co.) in the place of a direct, hand-turned pressure generator used previously. Pressure was determined by the use of a set of strain-gage pressure transducers (Baldwin-Lima-Hamilton Corp.) and their output was measured with a Leeds and Northrup K-3 potentiometer. The output of the transducers also was recorded for a permanent record. The strain gages were calibrated against a pressure balance (Hart Co.); these calibrated gages were then accurate to 0.1%. Bourdon gages (Heise Bourdon Tube Co.), also calibrated against the pressure balance, were used as a further means for determining pressure. In the modification of the pressure-generating system, oil was substituted for water used previously, and two separator units were used to isolate the electrolyte solution from the rest of the system. Each unit consisted of a high-pressure cylinder containing a close-fit, floating piston and a high-pressure connection at both ends. The first unit, in series with the

[2]E. U. Franck, J. E. Savolainen, and W. L. Marshall, *Reactor Chem. Div. Ann. Progr. Rept. Jan. 31, 1961*, ORNL-3127, pp 50–52.

[3]A. S. Quist *et al.*, *Reactor Chem. Div. Ann. Progr. Rept. Jan. 31, 1962*, ORNL-3262, pp 73–75.

[4]E. U. Franck, J. E. Savolainen, and W. L. Marshall, *Rev. Sci. Instr.* **33**, 115 (1962).

second, isolated the oil (used throughout the pressure-generating and measuring assembly) from pure water, and the second unit isolated the electrolyte solution from the water, thus providing two barriers between electrolyte solution and oil. Both units were maintained in vertical positions, with water in the bottom section of the first unit and electrolyte solution in the bottom of the second unit; thus, if either of the floating pistons very slowly fell, the electrolyte solution would not be contaminated. The solution was then pressed into or removed from the conductivity cell, maintained at constant temperature, in order to make the measurements.

Solutions of $K_2SO_4$ in $H_2O$ were prepared from reagent-grade[5] $K_2SO_4$ dried at 120°C and from conductivity water (laboratory distilled water which had been passed through a cation-anion exchange resin and then distilled from quartz). The conductivity water so prepared gave a specific conductance of $10^{-7}$ $ohm^{-1}$ $cm^{-1}$. All solutions were prepared gravimetrically, using calibrated weights. The cell constant was determined by the use of 0.01 demal KCl solutions (prepared from single-crystal KCl) at 1 atm pressure and at 25.00 ± 0.01°C. A special constant-temperature water bath was constructed and was placed around the high-pressure cell to make these measurements of the cell constant. For the three inner electrodes used in this series of measurements, the experimentally determined cell constants were 0.3050, 0.2902, and 0.2394.

The conductivity cell and the high-pressure tubing leading from the separator unit to the conductivity cell were rinsed thoroughly with the solution before each run. The system was then pressurized in order that, when the cell reached the desired temperature, the pressure on the solution would be in the range of 2000 to 3000 bars. The conductivity cell was then held at constant temperature while conductance measurements were made at a series of pressures, first by raising the pressure to 4000 bars, then by decreasing the pressure to the lowest values, and finally by increasing the pressure to near the original value. Measured conductances were the same, within experimental error, whether measured on increasing or on decreasing the pressure. After the conductivity cell cooled to room temperature and the pressure was adjusted to atmospheric pressure, the conductance of the solution remaining in the cell was determined to establish that it was not significantly different from that measured prior to the start of the run.

In the experimental procedures many measurements were made with conductivity water over the entire range of pressure and temperature. These measurements were used to make the corrections of the conductance data for the contribution of water and impurities to the measured conductances in order to calculate equivalent conductivities. These corrections varied from about 2 to 10% of the conductances for 0.001 equivalent of $K_2SO_4$ per kilogram of solvent to 0.5 to 2% for the solutions containing 0.01 equivalent of $K_2SO_4$. The measured conductances also were corrected for the effect of frequency. Many measurements were made over the entire range of temperature, pressure, and concentration at frequencies between 500 and 20,000 cps; these values were extrapolated to the values at infinite frequency. The correction between a frequency of 2000 cps and infinite frequency varied between 0.5 and 2%, depending on the conductivity of the solution.

## Results and Discussion

The experimental values for specific conductivities of $K_2SO_4$ as a function of pressure at various temperatures, before making the correction for the conductance of $H_2O$, are shown in Figs. 8.1–8.3 for the three concentrations under investigation. These data are believed to be the best available and represent a significant addition to those values presented previously.[3] Some indication of the reproducibility of these measurements at 300 and 600°C is shown in Fig. 8.4, where the results (uncorrected for the conductance of water) of two series of measurements at each temperature, using two different electrodes and electrode holder assemblies, are plotted. The maximum difference between smooth curves drawn through the two series of points at 600°C represents a difference of 2%, or a deviation of ±1% from the average value. Plotting specific conductance as a function of temperature at constant pressures yields a series of curves as shown in Fig. 8.5 for the intermediate concentration of $K_2SO_4$. The maximum in the curve is displaced toward higher temperatures with increasing pressure.

[5]Mallinckrodt analytical reagent.

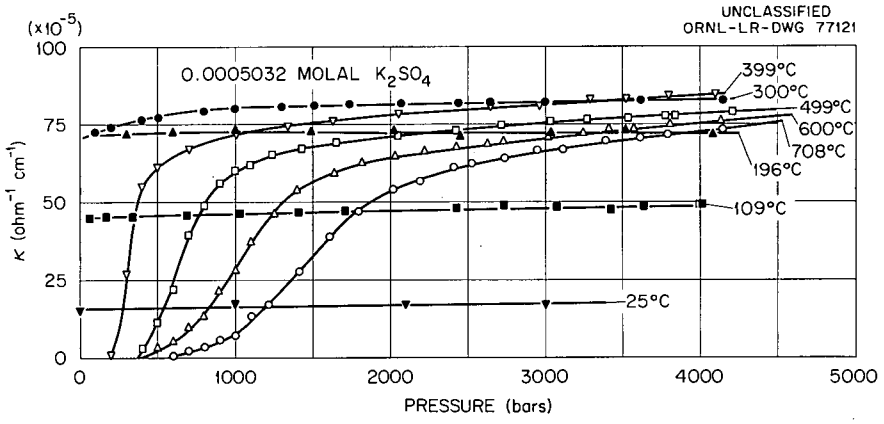


Fig. 8.1. Specific Conductances of 0.0005032 $m$ $K_2SO_4$ Solutions as a Function of Pressure at Several Temperatures.

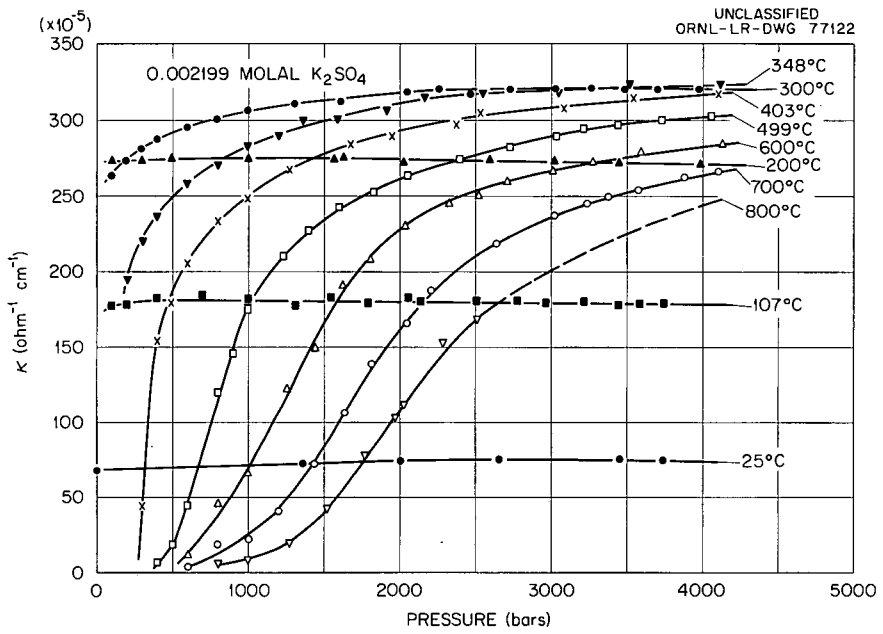


Fig. 8.2. Specific Conductances of 0.002199 $m$ $K_2SO_4$ Solutions as a Function of Pressure at Several Temperatures.

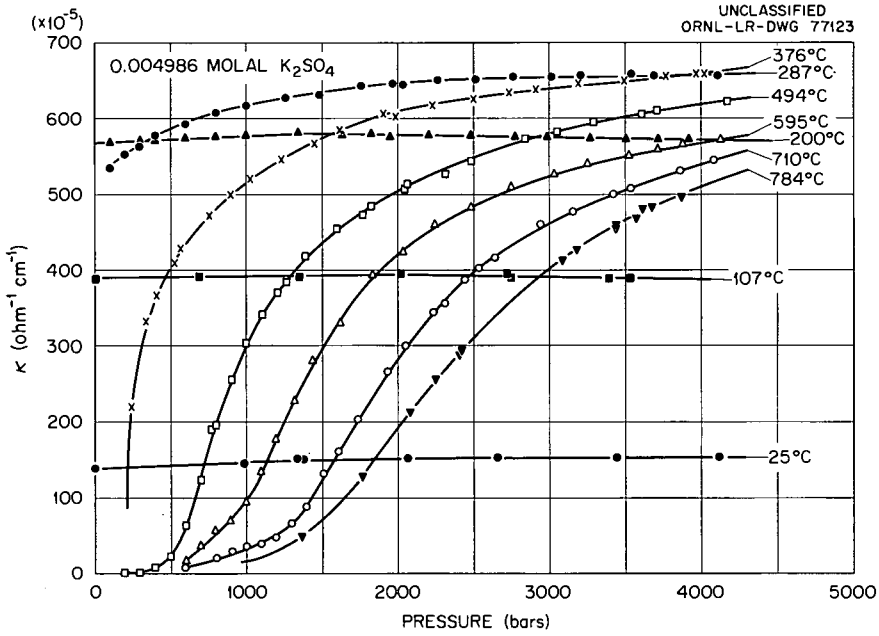


Fig. 8.3. Specific Conductances of 0.004986 *m* $K_2SO_4$ Solutions as a Function of Pressure at Several Temperatures.

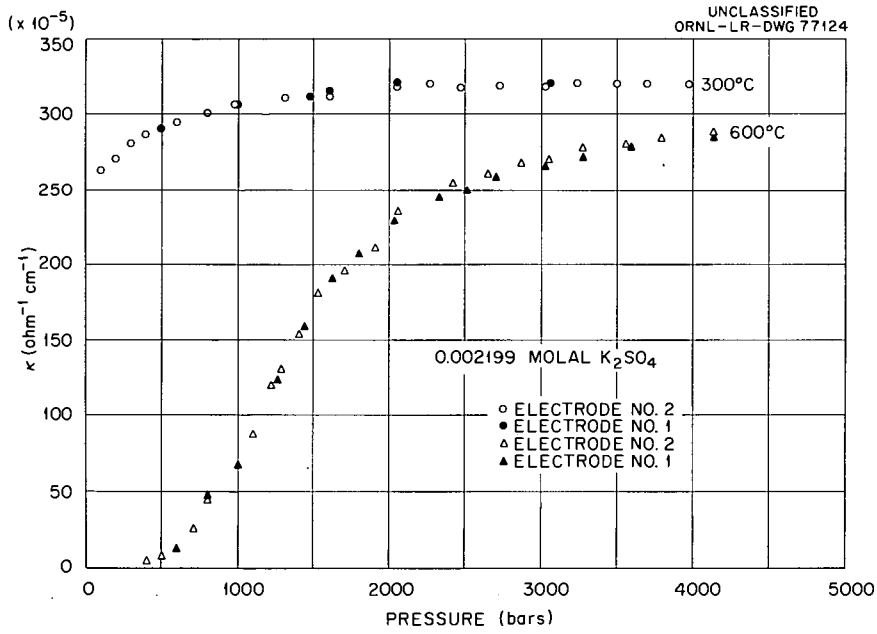


Fig. 8.4. Specific Conductances of 0.002199 *m* $K_2SO_4$ Solutions as a Function of Pressure at 300 and 600°C.

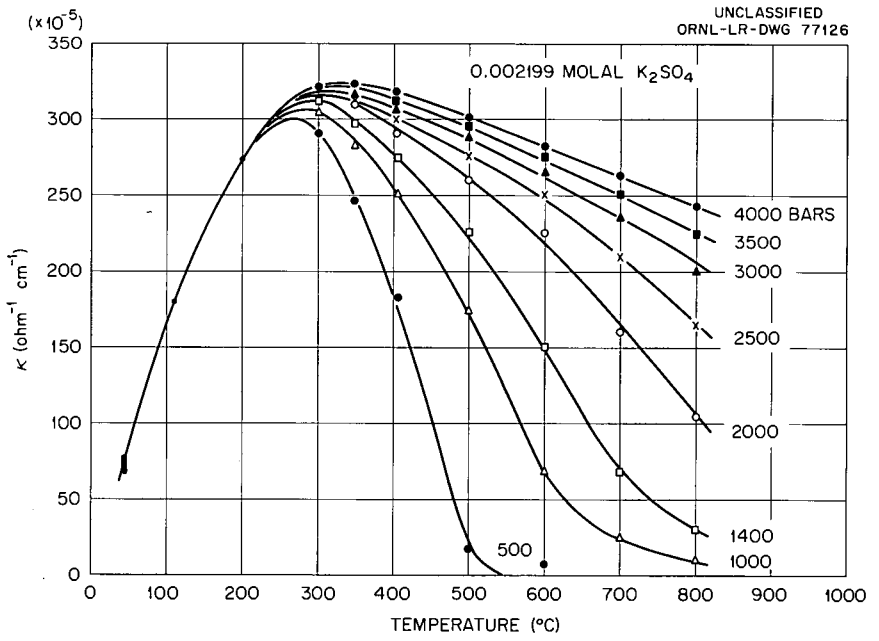


**Fig. 8.5. Specific Conductances of 0.002199 *m* $K_2SO_4$ Solutions as a Function of Temperature at Several Pressures.**

The specific conductances were converted to equivalent conductivities by first subtracting the background conductance of $H_2O$ and then using the densities of water as given by Kennedy[6–10] or extrapolated values (to 4000 bars). Figures 8.6 and 8.7 show values of the equivalent conductivity of 0.004986 *m* $K_2SO_4$ as functions of pressure and density at several temperatures.

Results for each of the three concentrations of $K_2SO_4$ indicate that $K_2SO_4$ dissociates into ions in supercritical water at densities greater than approximately 0.2 g/cm$^3$. Below this density the observed conductivity was negligible. The equivalent conductivity increased with increasing density, reaching a maximum value at approximately 0.5 to 0.7 g/cm$^3$. The highest observed value for the equivalent conductance, 1080 cm$^2$ ohm$^{-1}$ equiv$^{-1}$, which was observed at 499°C and at a density of 0.52 g/cm$^3$ (1000 bars) with a $K_2SO_4$ solution containing 0.0010065 equivalent per kilogram of water, is approximately seven times the value observed at 25°C and 1 atm pressure.

The equivalent conductivities of $K_2SO_4$ are about 25% lower than those measured by Franck[11] for KCl. Since, at temperatures up to 100°C, the limiting equivalent conductance of the chloride ion is less than that of the sulfate ion, the present data suggest that at elevated temperatures and pressures $K_2SO_4$ may be more associated than KCl.

---

[6] W. T. Holser and G. C. Kennedy, *Am. J. Sci.* **257**, 71 (1959).

[7] W. T. Holser and G. C. Kennedy, *Am. J. Sci.* **256**, 744 (1958).

[8] G. C. Kennedy, W. L. Knight, and W. T. Holser, *Am. J. Sci.* **256**, 590 (1958).

[9] G. C. Kennedy, *Am. J. Sci.* **255**, 724 (1957).

[10] G. C. Kennedy, *Am. J. Sci.* **248**, 540 (1950).

[11] E. U. Franck, *Z. Physik. Chem. Neue Folge* **8**, 92 (1956).

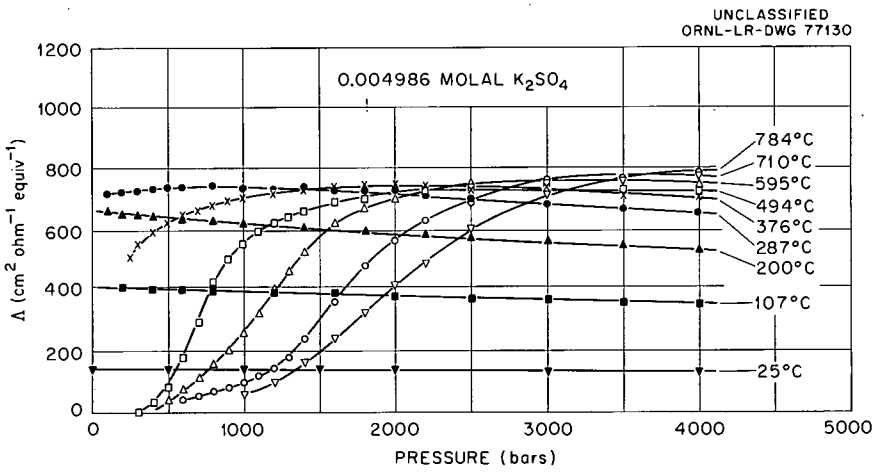


**Fig. 8.6. Equivalent Conductances of 0.004986 *m* $K_2SO_4$ Solutions as a Function of Pressure at Several Temperatures.**

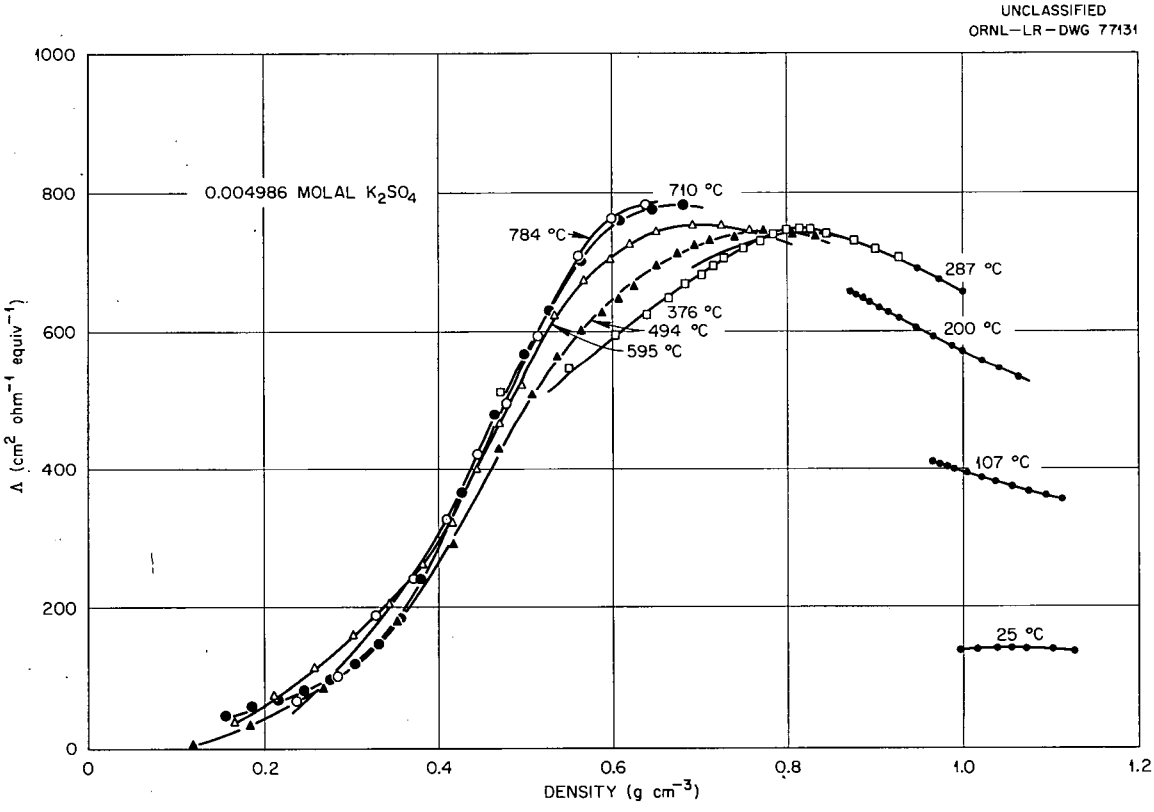


**Fig. 8.7. Equivalent Conductances of 0.004986 *m* $K_2SO_4$ Solutions as a Function of Density of the Solution at Several Temperatures.**

# PHASE STUDIES OF LIQUID-LIQUID IMMISCIBILITY AND CRITICAL PHENOMENA IN THE SYSTEMS $UO_3$-CuO-$SO_3$-$D_2O$, $UO_3$-NiO-$SO_3$-$D_2O$, AND $UO_3$-CuO-NiO-$SO_3$-$D_2O$ FROM 260 TO 410°C (ref 12)

W. L. Marshall E. V. Jones

## Introduction

Liquid-liquid immiscibility and high concentrations of metallic oxide component in the supercritical fluid have been found previously in the condensed systems $UO_3$-$SO_3$-$H_2O$, $UO_3$-$SO_3$-$D_2O$, and CuO-$SO_3$-$D_2O$ at temperatures[13] between 270 and 430°C. The results of these investigations were of use in the selection of fuel compositions for aqueous homogeneous reactors. Systematic information concerning the boundary regions of liquid-liquid and -solid equilibria and critical phenomena (where $L \equiv V$) of systems containing all the primary components of a reactor fuel should be of more general value. (For the aqueous homogeneous reactor, the system included $UO_3$ as the fuel component, CuO as a component utilized for the catalytic recombination of radiolytic $H_2$ and $O_2$, and NiO which dissolves into solution as a corrosion product of stainless steels.) Such a systematic study, initiated several years ago, has now been completed. For completeness and clarity of presentation, results presented previously[14,15] on the four- and five-component systems are incorporated herein. When part of this information was combined with previous data for the separate three-component systems ($UO_3$-$SO_3$-$D_2O$,[13] CuO-$SO_3$-$D_2O$,[13] and NiO-$SO_3$-$D_2O$)[16] and the four-component systems ($UO_3$-CuO-$SO_3$-$D_2O$ and $UO_3$-NiO-$SO_3$-$D_2O$ at 300°C)[17] and with some additional data presented in the detailed paper,[12] it became possible to construct three-dimensional models to describe portions of the four-component systems as a function of temperature.

## Experimental

Reagents and the general methods of preparation of the synthetic solutions have been discussed previously.[13,14] The synthetic method[18] was used to define boundaries of liquid-liquid immiscibility and critical phenomena.

True critical phenomena, where liquid ($L$) becomes identical with vapor ($V$), are observed only when the volumes of the two phases are identical. For a single experiment it is difficult to adjust the liquid-to-vapor volume ratio at 25°C to give a 50% filling at the observed critical temperature. Consequently, it was of interest to determine the error introduced in the estimation of the critical temperature as a function of liquid-volume filling. The results for two solutions, 1.0 and 0.6 $m$ in $SO_3$ and both containing $UO_3$ (plotted in Fig. 8.8), show a maximum difference of about −8° between a 50 and 70% filling. For pure $D_2O$ the difference[19] in apparent critical temperature between these two limits would be about −1°. Temperatures reported for critical phenomena were obtained for liquid fillings at temperature between these limits and, therefore, might be expected not to exceed an error of −1 to −2°C at low concentrations of $SO_3$ and −8°C at 1 $m$ $SO_3$.

## Results and Discussion

**The Four-Component Systems $UO_3$-CuO-$SO_3$-$D_2O$ and $UO_3$-NiO-$SO_3$-$D_2O$.** – When the additional component, CuO or NiO, is added to the system $UO_3$-$SO_3$-$D_2O$, a further restriction of composition must be made in order to retain simplicity in the presentation of the data. For any set of particular experiments, this additional restriction was that the molal ratio of metallic oxides to each other, $R$(MO), as specific examples,

$$m_{UO_3} : m_{CuO} = R(UO_3 : CuO) ,$$

[12] A detailed paper by W. L. Marshall and E. V. Jones is in press [*Journal of Inorganic and Nuclear Chemistry* (1963)]. An abstract of this paper is presented here.

[13] W. L. Marshall *et al.*, *J. Inorg. Nucl. Chem.* **24**, 995 (1962).

[14] W. L. Marshall and E. V. Jones, *Reactor Chem. Div. Ann. Progr. Rept. Jan. 31, 1961*, ORNL-3127, p 39.

[15] W. L. Marshall and E. V. Jones, *Reactor Chem. Div. Ann. Progr. Rept. Jan. 31, 1962*, ORNL-3262, p 57.

[16] W. L. Marshall, J. S. Gill, and Ruth Slusher, *J. Inorg. Nucl. Chem.* **24**, 889 (1962).

[17] W. L. Marshall and J. S. Gill, *J. Inorg. Nucl. Chem.* **22**, 115 (1961).

[18] C. J. Barton, G. M. Hebert, and W. L. Marshall, *J. Inorg. Nucl. Chem.* **21**, 141 (1961).

[19] G. M. Hebert, H. F. McDuffie, and C. H. Secoy, *J. Phys. Chem.* **62**, 431 (1958).

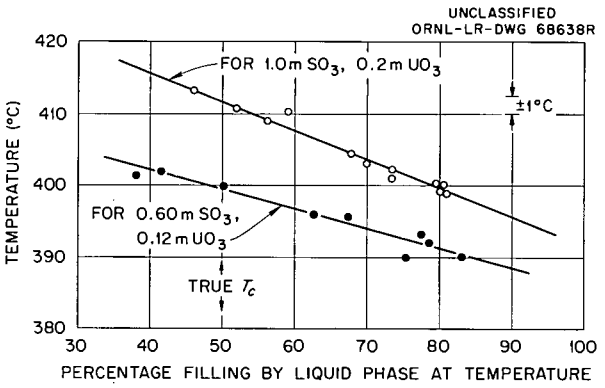


**Fig. 8.8. Effect of Tube Filling on the Apparent Critical Temperature for Solutions of $SO_3$, $UO_3$, and $D_2O$.**

or

$$m_{UO_3} : m_{\text{additional metallic oxides}} = R(UO_3 : MO) ,$$

was kept constant. Experiments on these restricted solution compositions provide a set of boundary curves of liquid-liquid immiscibility, critical phenomena, or precipitation of solid as a function of temperature, each *curve* representing conditions at a fixed concentration of $SO_3$ and value of $R$(MO) but at a variation of $R$, where

$$R = \Sigma m_{\text{metallic oxides}} : m_{SO_3} .$$

Figure 8.9 shows the two complete sets of curves for each of the two four-component systems and includes values[13] presented previously at $R = 0$.

From these curves, from some additional data given in the detailed paper,[12] and from the data presented previously,[13,16,17] five drawings were constructed to describe the CuO- and NiO-containing systems. Each drawing showed isotherms of the phase boundaries plotted on two-dimensional, orthogonal axes of $R_U$ against $R_{Cu}$ or $R_{Ni}$ (where $R_U = m_{UO_3} : m_{SO_3}$, etc.) at a fixed molality of $SO_3$.

From isotherms, selected from one drawing only, the dimensions were obtained from which a three-dimensional model could be constructed to show the variation of phase boundaries both as a function of $R$ for each of the metallic oxide components and as a function of temperature. Drawings made from photographs of sets of these models of the two systems $UO_3$-CuO-$SO_3$-$D_2O$ and $UO_3$-NiO-$SO_3$-$D_2O$ are shown in Fig. 8.10. Each model shows the region of solution unsaturation and its boundaries, where particular solid phases or second-liquid phases saturated the liquid phase or where critical phenomena were observed, for compositions containing a fixed concentration of $SO_3$.

In all models the linear distance for one unit of $R$ (at constant temperature) is the same; the temperature scales are also identical. Therefore, distances on the models are directly comparable by dimension on the basis of $R$ (and $T$) but *not* on the basis of molality of components. Otherwise, lengths along these scales on the model depicting phase boundaries for solutions 0.02 $m$ in $SO_3$ would be roughly one-fiftieth those of the model for compositions 1.0 $m$ in $SO_3$.

Inspection of the system, as revealed by the models, brings out several points of interest. First, the proportional area of liquid-liquid immiscibility is seen to increase as the concentration of $SO_3$ increases, both for the system containing CuO and the one containing NiO. Second, the lowest temperatures of liquid-liquid immiscibility decrease further with increasing $SO_3$ concentration. Third, for the system containing CuO, the surface area of liquid-liquid immiscibility extends from the system $UO_3$-$SO_3$-$D_2O$ to CuO-$SO_3$-$D_2O$ and, at higher concentrations of $SO_3$, covers proportionally the largest area. In contrast, the areas of liquid-liquid immiscibility in the system containing NiO never extend to the system NiO-$SO_3$-$D_2O$ and cover a proportionally smaller area; the predominant saturating phase is the solid $NiSO_4 \cdot D_2O$. These observations might be explained by speculating that $CuSO_4$ behaves in solution analogously to $UO_2SO_4$; considerable association to form nonionic species may occur and thus enhance the probability of forming two liquid phases. On the other hand, $NiSO_4$ may exist largely in the form of several ionic species, which would not be expected to favor the formation of immiscible liquids. A fourth point of interest is related to the supercritical surface, over which the liquid phase becomes identical with the vapor phase in all respects. (The vapor pressure of the system for any composition on this surface is also defined uniquely as the critical pressure.) In contrast to a one-component system, on increasing the temperature of the system above that at the critical point, while maintaining a constant pressure, a second liquid or solid phase may form from the supercritical fluid. Figure 8.9 and the

derived models give only the boundary limits at the critical temperature. Of considerable interest, however, is the extent over which metallic oxides in one form or another are soluble in supercritical $SO_3$-$D_2O$ (or in $SO_3$-$H_2O$).

Values of temperature and concentration at selected boundary points of saturation for each of the ten models have been documented and are presented in the detailed paper.[12]

**The Five-Component System $UO_3$-CuO-NiO-$SO_3$-$D_2O$.** – A simple description of the five-component system $UO_3$-CuO-NiO-$SO_3$-$D_2O$ is exceedingly difficult. Previously, part of the system was defined at a constant temperature of 300°C.[17] These experimental data, together with the present data and the previous values at $R = 0$,[13] plotted in Fig. 8.11, could be used to construct three-dimensional models depicting the phase boundaries in which

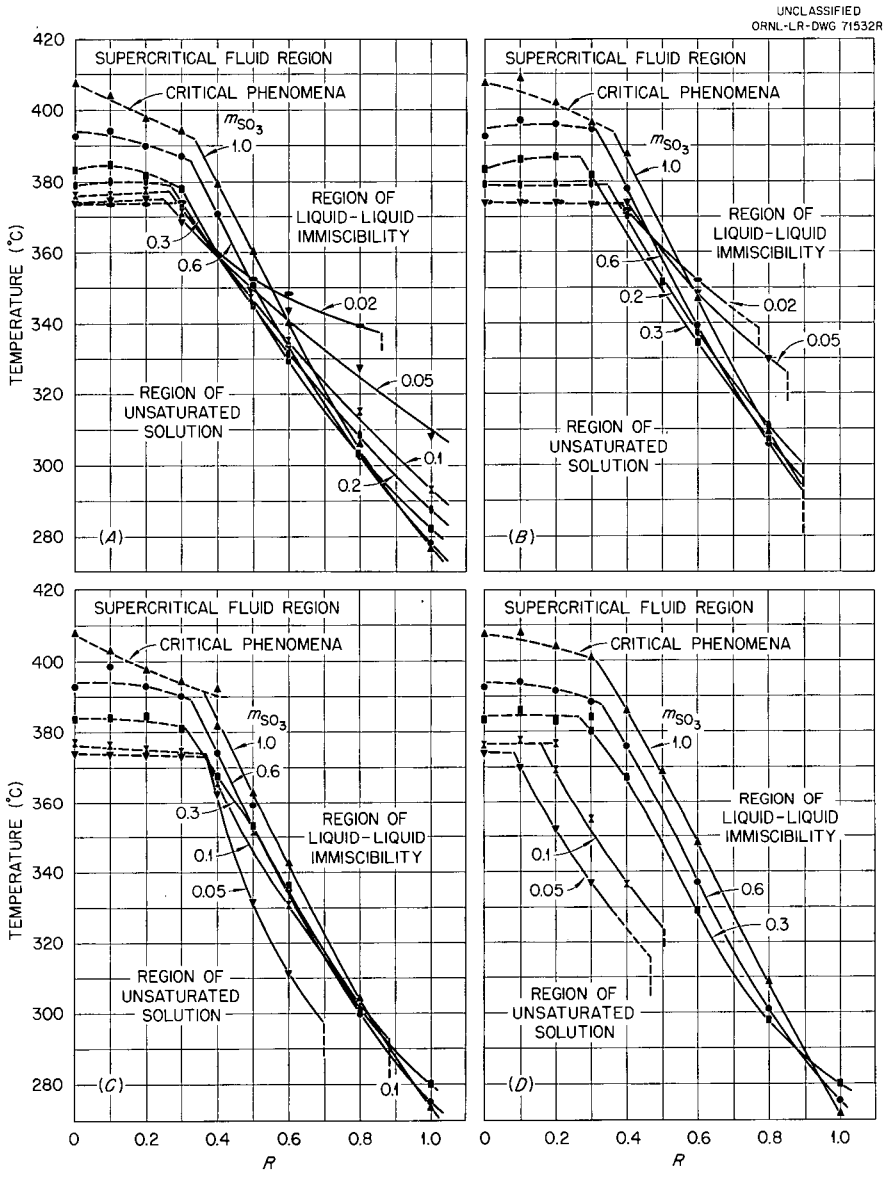


**Fig. 8.9. Liquid-Liquid Immiscibility and Critical Phenomena in the Systems $UO_3$-CuO-$SO_3$-$D_2O$ (Sets *A* and *B*) and $UO_3$-NiO-$SO_3$-$D_2O$ (Sets *C* and *D*), 260–410°C. (Key: $R = \Sigma m_{\text{metallic oxides}}/m_{SO_3}$; in sets: *A*, $m_{CuO}/m_{UO_3} = 0.333$; *B*, $m_{CuO}/m_{UO_3} = 1$; *C*, $m_{NiO}/m_{UO_3} = 0.333$; *D*, $m_{NiO}/m_{UO_3} = 1$).**

the CuO and NiO components are combined – $R$(CuO:NiO) is kept constant at 1:1 – in order to correspond to a pseudo, single component.

**Simplification of Phase Boundaries of Liquid-Liquid Immiscibility.** – If values of $R$ are plotted against temperatures of liquid-liquid immiscibility at constant molality of $SO_3$ but for variations of $R$(MO) (sets $A$–$H$, Figs. 8.9 and 8.11), then a series of curves are obtained which are not far removed from the boundary curve for the three-component system $UO_3$-$SO_3$-$D_2O$. Plots of temperature against the mole fraction of $UO_3$ = $(m_{UO_3}):(m_{UO_3} + m_{CuO} + m_{NiO})$ at constant $m_{SO_3}$ and $R$ have been made as well as plots of $R$ against mole fraction of $UO_3$ at constant $m_{SO_3}$ and temperature. As an approximation it appears that CuO, NiO, or both can be substituted for $UO_3$ until the mole fraction of $UO_3$ is lowered to about 0.7, with not more than a few degrees increase in temperature of liquid-liquid immiscibility at constant $R$ or with not more than about +6% change in $R$ at constant temperature.

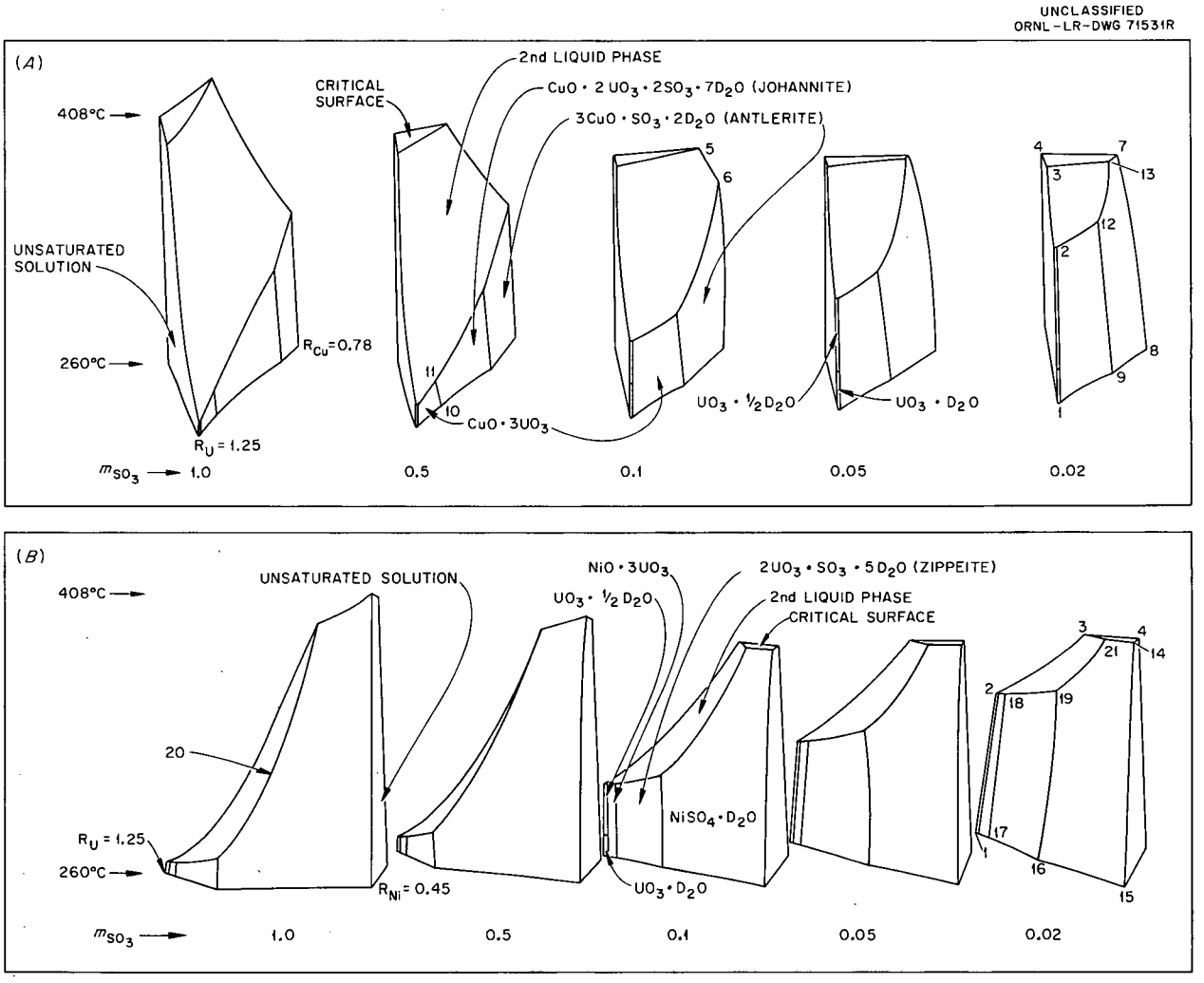


**Fig. 8.10. Drawings of Three-Dimensional Models, Showing the Surfaces of Saturation and Critical Phenomena for the Systems $UO_3$-CuO-$SO_3$-$D_2O$ ($A$) and $UO_3$-NiO-$SO_3$-$D_2O$ ($B$).**

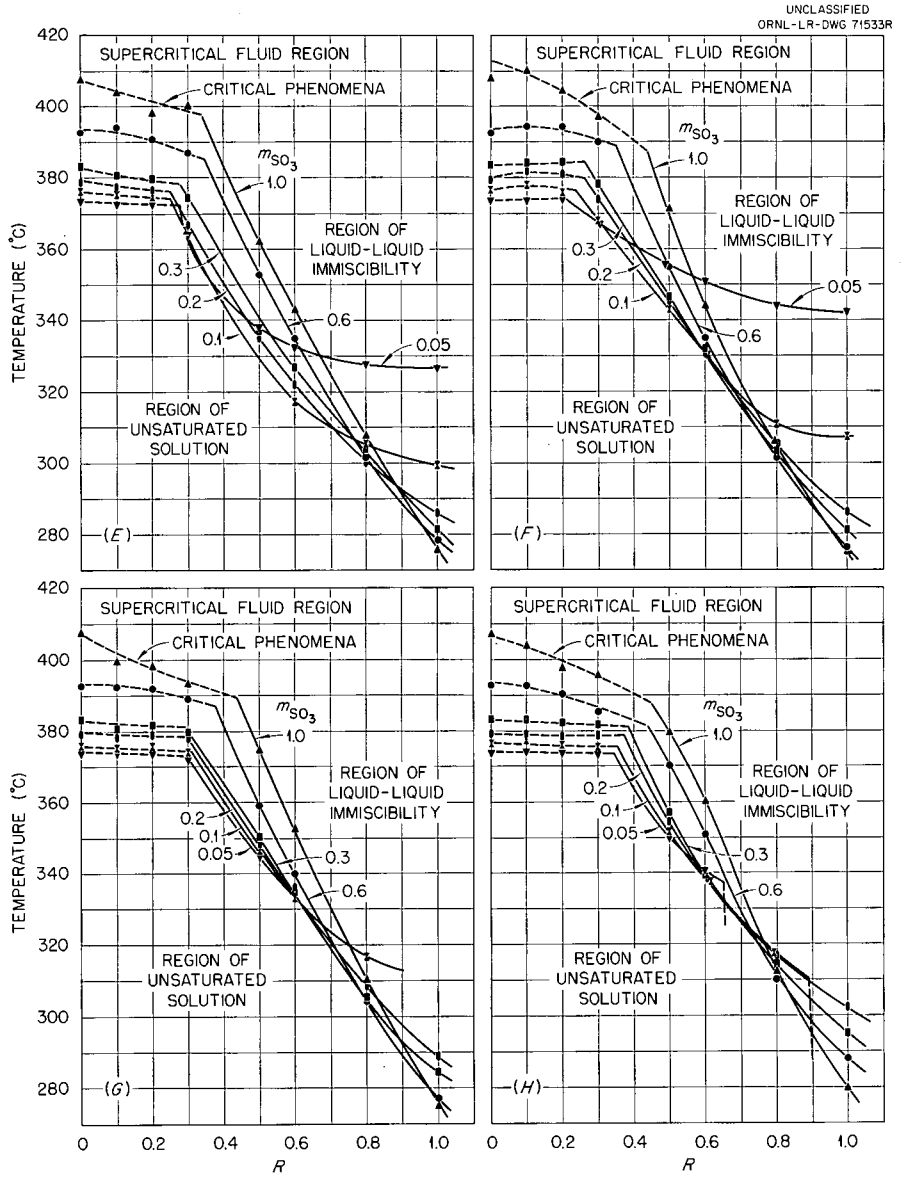


**Fig. 8.11. Liquid-Liquid Immiscibility and Critical Phenomena in the System $UO_3$-CuO-NiO-$SO_3$-$D_2O$ (Sets *E*, *F*, *G*, *H*), 260–410°C.** [Key: $R = \Sigma m_{\text{metallic oxides}}/m_{SO_3}$; molal ratio ($UO_3$:CuO:NiO) in sets: *E*, 8:1:1; *F*, 4:1:1; *G*, 2:1:1; *H*, 1:1:1].

## GLASS-TO-METAL CONNECTOR FOR VISUAL OBSERVATION OF THE EFFECT OF PRESSURE ON PHASE EQUILIBRIA[20]

J. S. Gill W. L. Marshall

In the usual application of the synthetic method for the determination of phase equilibria, a mixture of known composition is sealed in a glass tube, the tube is inserted into a zone of controllable temperature, and the temperature is recorded at which a phase in the condensed system appears or disappears.[21] The pressure is generally unknown. In order to know with certainty the pressure and its effect on the phase equilibria of

[20] A detailed note has been submitted for publication in the *Review of Scientific Instruments*.

[21] A. W. C. Menzies, *J. Am. Chem. Soc.* **58**, 934 (1936).

systems, and also in order to eliminate the vapor phase, a glass-to-tube metal tube connector was devised.

A drawing of the connector is shown in Fig. 8.12. Metal parts were constructed from a titanium alloy containing 4% vanadium in order to reduce corrosion of the inner surfaces which come in contact with the solution. In operation a Teflon gasket provided the seal between glass and metal.

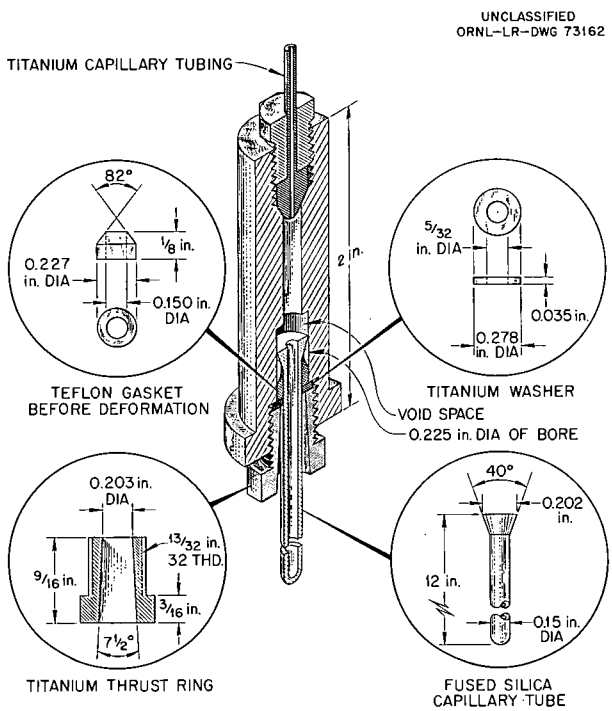


**Fig. 8.12. Glass-to-Metal Tube Connector for Use at Pressures Up to 300 Bars.**

As the internal pressure was increased, the Teflon, fitted snugly under a small amount of pressure, deformed sufficiently to support the glass tube and to maintain a seal with a minimum amount of stress on the glass. The present design, incorporating silica glass, has been used successfully, in a routine fashion, to pressures of about 300 to 350 bars. An example of research making use of this apparatus is given in the next section.

## EFFECT OF PRESSURE ON LIQUID-LIQUID IMMISCIBILITY IN THE SYSTEM $UO_2SO_4$-$H_2O$ AND LIQUID–SUPERCRITICAL FLUID EQUILIBRIA IN THE SYSTEM $UO_2SO_4$-$H_2SO_4$-$H_2O$, 290 TO 430°C, 75 TO 300 BARS[22]

W. L. Marshall J. S. Gill

### Introduction

For stoichiometric $UO_2SO_4$ solutions in the presence of vapor, as the concentration of $UO_2SO_4$ increases, the temperature of liquid-liquid immiscibility drops sharply from about 350°C to a flat minimum at about 288°C and then increases slowly. In this report, data are presented showing the effect of hydrostatic pressure on the temperatures of second-liquid-phase formation from stoichiometric $UO_2SO_4$-$H_2O$ solutions at concentrations from 0.14 to 4.53 *m* in $UO_2SO_4$, at temperatures from 290 to 330°C, and at pressures up to 300 bars. Some additional data are presented which show the effect of pressure on the temperature of formation of heavy-liquid phases from supercritical $UO_2SO_4$-$H_2O$ fluids containing excesses of $H_2SO_4$.

### Experimental

All experimental procedures are described or referenced in a detailed paper[22] and, with the following exceptions, will not be discussed here. By means of the glass-to-metal tube connector described in the preceding section, the solution within the tube was pressurized to a value at which a second-liquid phase would not form at the temperature of a constant-temperature liquid-salt bath. The tube was then inserted into the bath, and the external pressure was slowly lowered until immiscibility was observed as evidenced by opalescence throughout the solution. The pressure was then raised immediately, and immiscibility disappeared. For further determinations the temperature was changed to another constant value, and the lowering and subsequent raising of pressure were repeated to obtain another boundary limit of pressure and temperature.

[22] A detailed paper is in press (*Journal of Inorganic and Nuclear Chemistry*). An abstract of this paper appears here.

## Results and Discussion

**Effect of Pressure on Liquid-Liquid Immiscibility in the System $UO_2SO_4$-$H_2O$.** – Preliminary plots of the data as temperature vs pressure revealed that the slopes of the lines were nearly parallel. To test for the presence of a common factor in all the data, they were normalized and plotted, as shown in Fig. 8.13, as Δ temperature vs Δ pressure. This normalization involved measuring the increases in temperature of immiscibility from the three-phase invariant point ($L_1 + L_2 + V$) for each solution. The actual vapor pressures of the various solutions at that point were estimated roughly to be near that for $H_2O$ (72 bars at 288°C and 91 bars at 304°C); these pressures did not need to be known exactly since the lowering in vapor pressure due to the concentration of solute was very small compared with the relative amount of hydrostatic pressure applied to the solution phase in the tests.

The remarkable adherence of all the data to a single line suggested that there must be a factor of major importance which was independent of the concentration of the dissolved $UO_2SO_4$ over the wide range of 0.14 to 4.5 *m*. The density of the solvent water appears to be this factor. Values of $(\partial T/\partial P)_d$ for liquid water were evaluated from the data of Holser and Kennedy[23] and were found to vary from +0.087° per bar at 288°C to +0.096° per bar at 304°C at the lower limit of temperature and pressure (where vapor was present). Above these lower limits the value of $(\partial T/\partial P)_d$ of water remains constant to pressures much greater than

[23] W. T. Holser and G. C. Kennedy, *Am. J. Sci.* **256**, 744 (1958).

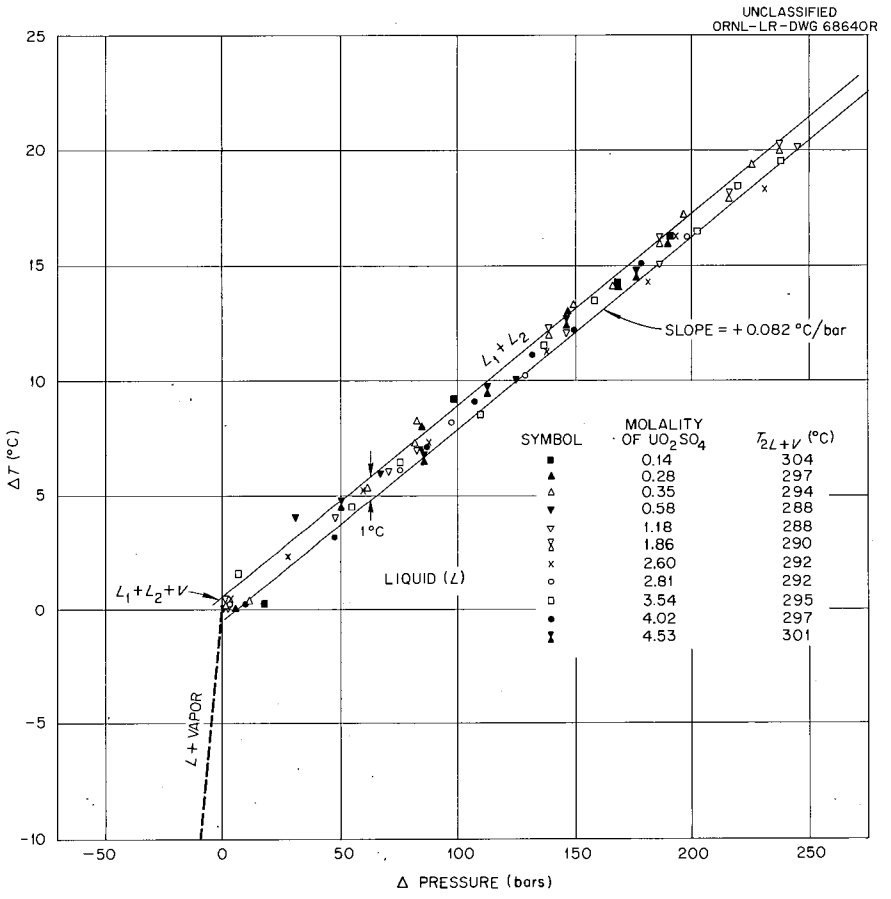


**Fig. 8.13. Effect of Hydrostatic Pressure on Liquid-Liquid Immiscibility for Stoichiometric $UO_2SO_4$ Solutions (in $H_2O$); 11 Separate Runs.**

300 bars. The average slope of the relation illustrated in Fig. 8.13 is +0.082° per bar, which is very close to the values of $(\partial T/\partial P)_d$ for the pure solvent, $H_2O$. Although immiscibility, and not density, was measured in the tests with uranyl sulfate solutions, the quantitative agreement between the immiscibility and density relations suggests that density is the factor of most importance in determining the effect of temperature and pressure on immiscibility.

One experimental run each, made with a 2.758 *m* stoichiometric $UO_2F_2$ solution and with a 1.306 *m* $CuSO_4$ solution containing 0.242 *m* $H_2SO_4$, both of which exhibit liquid-liquid immiscibility near 320°C, gave values of $(\partial T/\partial P)_x$ of ~+0.10 and ~+0.11, respectively, for the change in immiscibility temperature with pressure (Fig. 8.14). The corresponding values, $(\partial T/\partial P)_d$, for $H_2O$, at the temperature of appearance of $2L$ in the presence of $V$ for each system, were +0.105 and +0.112 respectively.

The data in Fig. 8.13 were used to make diagrams of pressure and composition showing two-liquid phase boundaries for stoichiometric $UO_2SO_4$ solutions at constant temperature. An example of these, showing the relations at 310°C, is given in Fig. 8.15.

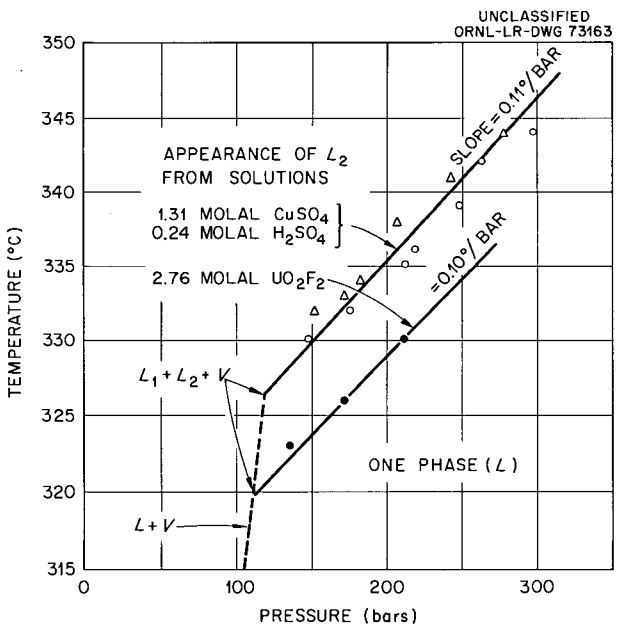


**Fig. 8.14. Effect of Pressure on the Temperature of Liquid-Liquid Immiscibility for One $H_2O$ Solution of $UO_2F_2$ and One of $CuSO_4$ and $H_2SO_4$.**

**Effect of Pressure on Liquid–Supercritical Fluid Equilibria in the System $UO_3$-$SO_3$-$H_2O$.** – If the system is designated in terms of the components $UO_3$, $SO_3$, and $H_2O$, and sufficient $H_2SO_4$ is added to lower the molal ratio ($R_U = m_{UO_3} : m_{SO_3}$) below about 0.35, then the critical temperature (where $L \equiv V$) of $L$ is reached before the appearance of a second-liquid phase. This liquid phase will separate from the supercritical fluid (Fl) at temperatures above the critical temperature.

The results of several runs on solutions containing $UO_3$, $SO_3$, and $H_2O$ which had values of $R_U$ of less than 0.35 are shown in Fig. 8.16. In some experiments, not only were the pressure-temperature relations of the equilibria $L_2$ + Fl established but also bubble points, where vapor is produced from liquid phase on lowering the pressure on the system. These bubble points thus correspond closely to the vapor-pressure curve which extends to the critical temperature and pressure for the particular composition of the condensed system. At higher temperatures the supercritical fluid exists from which, on lowering its pressure, $L_2$ appears.

The values of $(\partial T/\partial P)_d$ for pure $H_2O$ at the lowest pressure and temperature of observation of $L_2$ were used to draw the dashed lines in Fig. 8.16 and are approximately the same magnitude as those of $(\partial T/\partial P)_{x,R_U}$ for the *P-T* curve for $L_2$-Fl. Therefore at temperatures near 400°, as was observed for the formation of a second-liquid phase near 300°, the boundary limit of liquid-phase formation from supercritical fluid seems to show a first-order dependency on density of the solvent.

It appears that moderately low pressures (of the order of 300 to 1000 bars) would extend the *T-P* boundaries of liquid phase in contact with supercritical fluid to temperatures over 500°C for aqueous fluids at least 0.2 to 0.3 *m* in $UO_3$ and 1.0 *m* in $SO_3$.

**Vapor Pressures of Deliquescence of Solid $UO_2SO_4$ Hydrate.** – By making use of the visual method, some vapor pressures at which solid $UO_2SO_4$ hydrate deliquesced were determined. The data of several runs are shown in Fig. 8.17. This curve describes the pressure-temperature relations in accordance with which three phases (gas, liquid, and solid) are in equilibrium, originating from the system $UO_2SO_4$-$H_2O$.

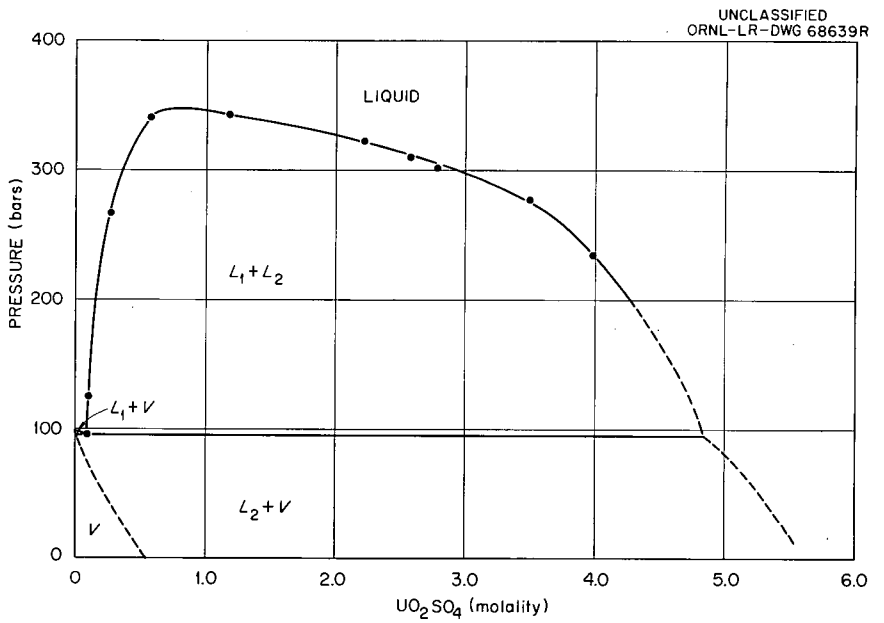


**Fig. 8.15. Two-Liquid-Phase Boundary for Stoichiometric $UO_2SO_4$ Solutions at 310°C.**

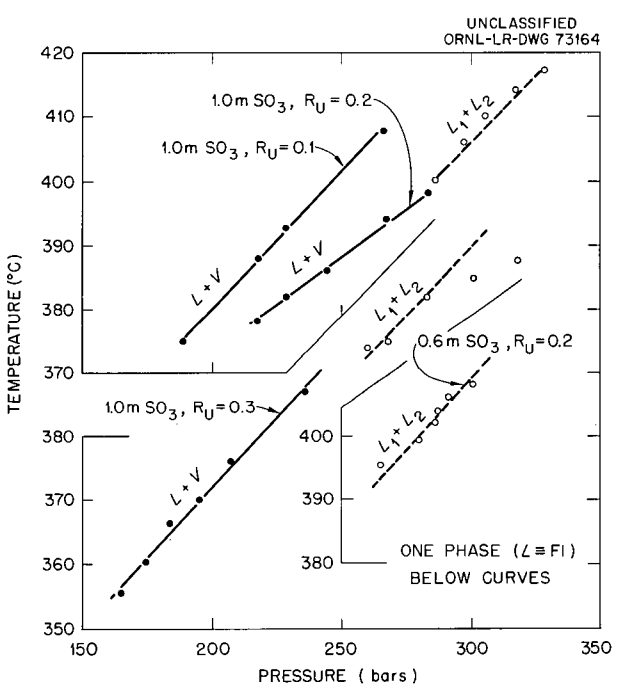


**Fig. 8.16. Effect of Pressure on the Temperature of Liquid-Liquid Immiscibility for Solutions of $UO_3$, $SO_3$, and $D_2O$. $R_U = m_{UO_3}:m_{SO_3}$.**

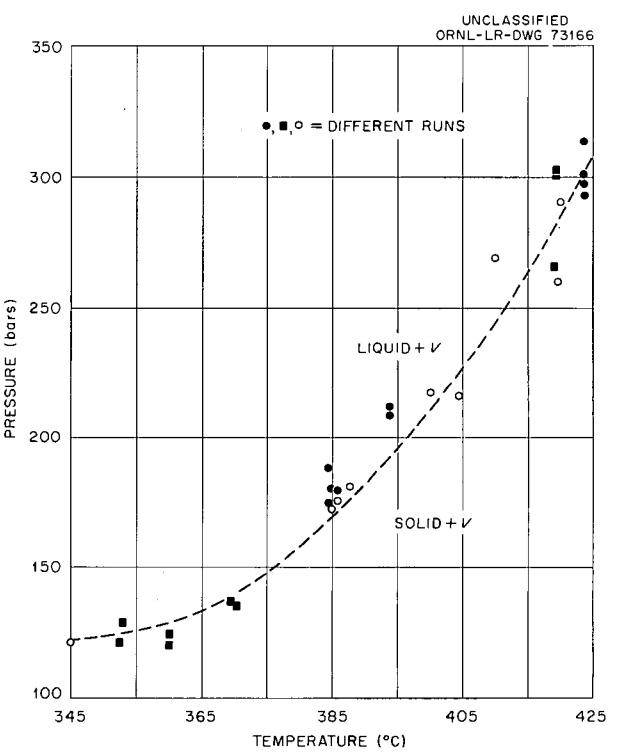


**Fig. 8.17. Vapor Pressures of the Deliquescence of $UO_2SO_4$ Hydrate Solid, 345–425°C.**

## THE SYSTEM $Li_2SO_4$-$H_2SO_4$-$H_2O$ AND ITS $D_2O$ ANALOG, 200 TO 470°C: SOLUBILITIES AND CRITICAL PHENOMENA[24]

W. L. Marshall Ruth Slusher
F. J. Smith[25]

### Introduction

Recently at this Laboratory, in an investigation of the condensed system NiO-$SO_3$-$H_2O$ and its $D_2O$ analog at temperatures up to 400°C,[26] nickel sulfate was found to hydrolyze to form oxysulfate solids from solutions containing low concentrations of $SO_3$ and even from those containing an excess of free $H_2SO_4$. Determinations of critical phenomena (where liquid ≡ vapor) showed stable concentrations of the NiO component as high as 0.1 *m* in a supercritical fluid 1.0 *m* in $SO_3$. Since $NiSO_4$ is a 2:2 electrolyte, it appeared desirable to compare its behavior with that of a 1:2 sulfate electrolyte. Lithium sulfate was chosen for such a study. It was believed that $Li_2SO_4$ would not hydrolyze to form oxy salts in acidic media or in water and that relatively high concentrations would be phase stable in supercritical fluids. Since there are practically no reports of investigations of solubilities in $D_2O$ media at temperatures above 200°C, comparative studies were made in both $H_2O$ and $D_2O$. Lithium sulfate was also of interest because of the anomalies in physical and chemical behavior exhibited by lithium salts, its potentialities as an additive to sulfate-based aqueous homogeneous reactor fuels for inhibiting corrosion,[27] and its ability to raise the temperature of appearance of liquid-liquid immiscibility.[28]

[24]A detailed paper by W. L. Marshall, Ruth Slusher, and F. J. Smith is in press [*Journal of Inorganic and Nuclear Chemistry (1963)*]. An abstract of the paper is presented here.

[25]Summer participant, 1960; present address: Department of Chemistry, Louisiana State University, Baton Rouge, La.

[26]W. L. Marshall, J. S. Gill, and Ruth Slusher, *J. Inorg. Nucl. Chem.* **24**, 889 (1962).

[27]J. C. Griess and E. G. Bohlmann, U.S. Patent 2,950,167 (to U.S. Atomic Energy Commission, Aug. 23, 1960); *Chem. Abstr.* **55**, 344c (1961).

[28]H. F. McDuffie, *Review in Fluid Fuel Reactors* (ed. by J. A. Lane, H. G. MacPherson, and F. Maslan), chap. 3, pp 91, 93, Addison-Wesley, Reading, Mass., 1958.

### Experimental Procedures

For the most part, experimental procedures were identical to those used previously.[17,18,29] Modifications of some of the procedures, a few additional procedures, and purity of reagents used are given and discussed in a detailed paper.[24]

### Results

**The Two-Component System $Li_2SO_4$-$H_2O$ and Its $D_2O$ Analog.** – Experimental values for the solubilities of $Li_2SO_4$ in $H_2O$ and in $D_2O$ solutions are shown in Fig. 8.18. The results in light water are in good agreement with those of Elenevskaya and Ravich,[30] published recently, which are also included in Fig. 8.18. The solubility of $Li_2SO_4$ is lower in $D_2O$ than in $H_2O$ solvent and, in both solvents, shows the retrograde solubility with increasing temperature which is characteristic of many other sulfate salts.[31,32]

[29]J. S. Gill and W. L. Marshall, *Rev. Sci. Instr.* **32**, 1060 (1961).

[30]V. M. Elenevskaya and M. I. Ravich, *Zhur. Neorgan. Khim.* **6**, 2380 (1961).

[31]See the numerous papers of A. Benrath and others, *Z. Anorg. Allgem. Chem.* (1924–1941); H. S. Booth and R. M. Bidwell, *J. Am. Chem. Soc.* **72**, 2567 (1950).

[32]W. C. Schroeder, A. Gabriel, and E. P. Partridge, *J. Am. Chem. Soc.* **57**, 1539 (1935).

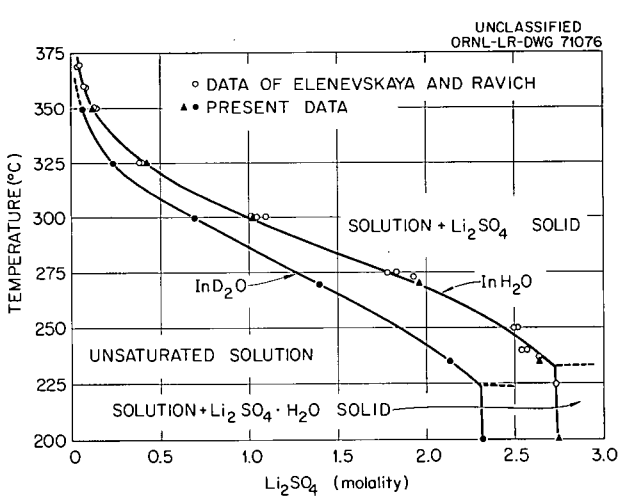


**Fig. 8.18. Solubilities in the System $Li_2SO_4$-$H_2O$ and Its $D_2O$ Analog, 200–370°C.**

**The Three-Component System $Li_2SO_4$-$H_2SO_4$-$H_2O$ and Its $D_2O$ Analog.** – The experimentally determined solubilities of $Li_2SO_4$ in various concentrations of $H_2SO_4$ at different temperatures are given in Fig. 8.19. In contrast to the behavior of the 2:2 electrolyte, $NiSO_4$, stoichiometric $Li_2SO_4$ is stable in water as well as in dilute solutions of $H_2SO_4$. The solubility curves show the same general characteristics as those for $NiSO_4$ over the region of $H_2SO_4$ concentration where $NiSO_4 \cdot H_2O$ is the saturating solid. The solubility increases as a function of increasing $H_2SO_4$ concentration and decreases with temperature.

Analogous solubilities in $D_2SO_4$-$D_2O$ solutions are shown in Fig. 8.20. At constant temperature, solubilities in $D_2O$ are lower than those in $H_2O$ and are considered to be caused by a first-order effect of solvent. There is an approach on a percentage basis of the solubility of $Li_2SO_4$ in $D_2SO_4$-$D_2O$ to that in $H_2SO_4$-$H_2O$ as the concentration of acid is increased. A crossover in the two solubilities (observed for the system $NiO$-$SO_3$-$H_2O$)[26] was not observed, probably because of the high solubility of $Li_2SO_4$ in the solvent alone.

**Dense, Supercritical Fluids Containing $Li_2SO_4$, $D_2SO_4$, and $D_2O$: Critical Phenomena.** – Observed temperatures of critical phenomena, that is, the temperature at which the composition of liquid becomes identical with that of vapor, are plotted in Fig. 8.21 and show that considerably higher concentrations of $Li_2SO_4$ are soluble in the supercritical fluid than those found for $NiSO_4$ in $H_2SO_4$-$H_2O$ fluids. At 0.02 $m$ $SO_3$, $Li_2SO_4$ is soluble in the supercritical fluid as a stoichiometric salt ($R_{Li} = 1$).

At temperatures between 375 and 425°C, the formation of $DSO_4^-$ ions can account for the high solubility of $Li_2SO_4$ in the supercritical $SO_3$-$D_2O$ and, with the exception of solutions 0.02 $m$ in $SO_3$, the approach of $R_{Li}$ to a limiting value of 0.5. In a study at lower temperature[33] the constant for the dissociation,

$$HSO_4^- \rightleftharpoons H^+ + SO_4^{2-} ,$$

has been shown to decrease considerably with temperature, reaching a value of about $1.24 \times 10^{-5}$ at 225°C.

Visual observations at saturation vapor pressures did not reveal a second-liquid phase as has been observed for sulfate-containing systems such as $UO_3$-$SO_3$-$H_2O$[34] and $CuSO_4$-$H_2SO_4$-$H_2O$.[35] At

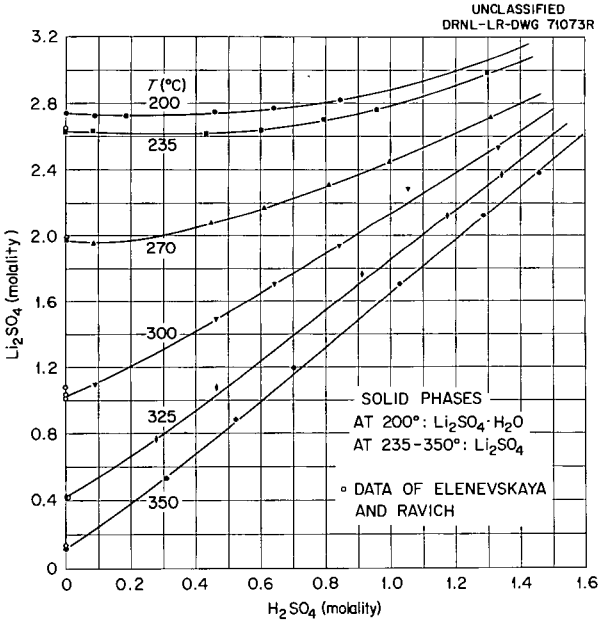


**Fig. 8.19. Solubilities in the System $Li_2SO_4$-$H_2SO_4$-$H_2O$, 200–350°C.**

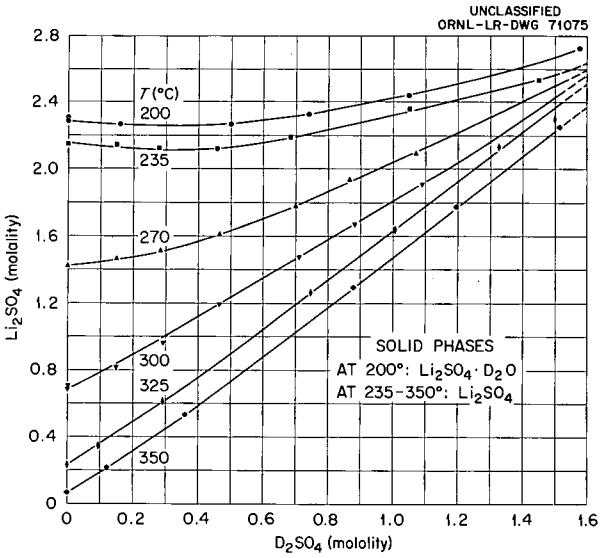


**Fig. 8.20. Solubilities in the System $Li_2SO_4$-$D_2SO_4$-$D_2O$, 200–350°C.**

[33] M. H. Lietzke, R. W. Stoughton, and T. F. Young, *J. Phys. Chem.* **65**, 2247 (1961).

[34] E. V. Jones and W. L. Marshall, *J. Inorg. Nucl. Chem.* **23**, 287 (1961); C. H. Secoy, *J. Am. Chem. Soc.* **72**, 3343 (1950).

[35] F. E. Clark *et al.*, *J. Chem. Eng. Data* **4**, 12 (1959).

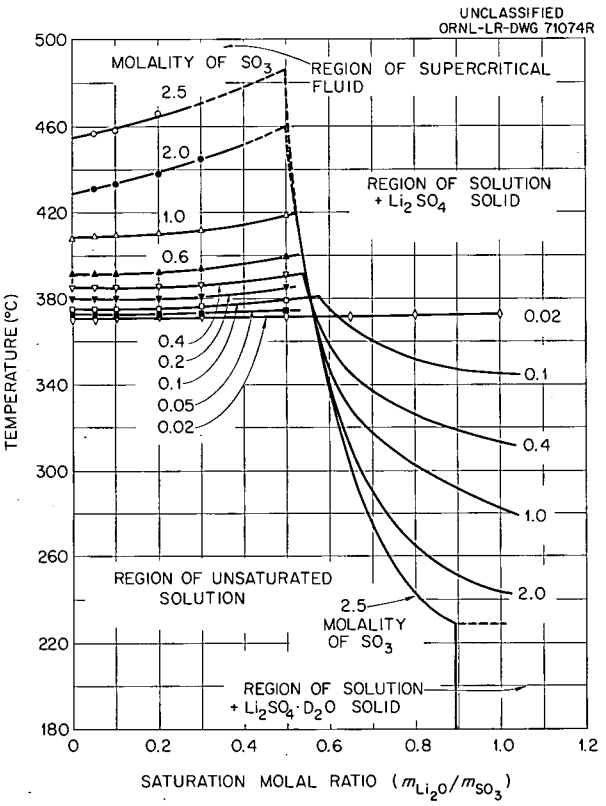


**Fig. 8.21. Critical Phenomena and Solid-Liquid Phase Boundaries in the System $Li_2O$-$SO_3$-$D_2O$.**

400°C and 422 bars and at 500°C and 653 bars, however, Morey and Chen[36] found that $Li_2SO_4$ solid can be dissolved in water solution in contact with supercritical fluid. An additional study on this system at high temperatures and pressures will be of considerable interest.

## OSMOTIC COEFFICIENTS OF AQUEOUS ELECTROLYTES AT ELEVATED TEMPERATURES

B. A. Soldano M. Meek[37]

Study was continued of the osmotic behavior of representative aqueous electrolytes at elevated temperatures. Previous reports have discussed the results of work at 100,[38] 121,[39] and 140°C.[40] The work at 140°C covered concentrations from 1 *m* to saturated solutions. These studies have now been extended to lower concentrations (0.2 *m*), involving a fivefold dilution from the previous lower concentration limit at this temperature. Details of the experiments and apparatus are reported elsewhere.[41]

### Experimental Results

Since the isopiestic technique ensures that the various solutions of electrolytes come to equilibrium at identical thermodynamic water activities (via a common vapor phase), the experimental results are presented, in Fig. 8.22, as isopiestic ratios relative to NaCl, the usual arbitrary standard solute. The isopiestic ratio, *R*, at a fixed water activity is defined as

$$R \equiv \frac{\nu m_{\text{std}}}{\nu m},$$

[36] G. W. Morey and W. T. Chen, *J. Am. Chem. Soc.* **78**, 4250 (1956).

[37] ORINS summer student trainee, 1962, Washburn University, Topeka, Kan.

[38] C. S. Patterson, L. O. Gilpatrick, and B. A. Soldano, *J. Chem. Soc.* **1960**, 2730.

[39] B. A. Soldano and C. S. Patterson, *J. Chem. Soc.* **1962**, 937.

[40] *Reactor Chem. Div. Ann. Progr. Rept. Jan. 31, 1962*, ORNL-3262, p 70.

[41] B. A. Soldano and M. Meek, *Journal of the Chemical Society*, in press.

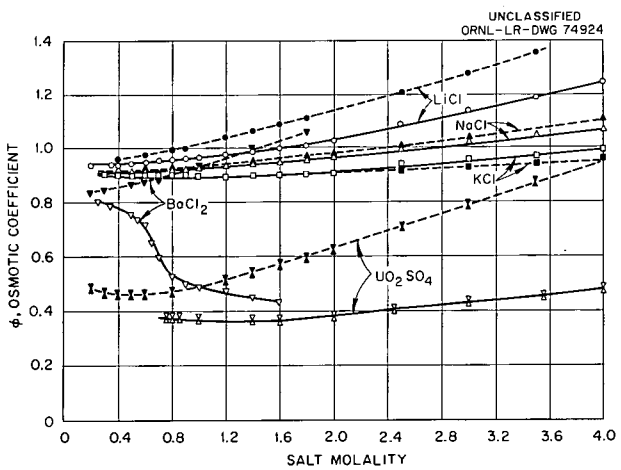


**Fig. 8.22. Comparative Osmotic Coefficients as a Function of Temperature.**

where $\nu$ is the idealized number of ions formed per mole of salt (e.g., three for $BaCl_2$), and $m$ is the molality of the test solute. The plotted values for the 1-1 electrolytes at 140.3°C were read at convenient concentrations from large-scale graphs of experimental values of $R$ vs molality.

## Discussion

There was some apprehension that the isopiestic technique could not, at high temperatures, be successfully extended to the dilute solution range (where extrapolated connection with the Debye-Hückel limiting law would become meaningful). At 25°C,[42] the lower useful concentration limit had been established as ~0.1 $M$. The present results have given no indication that such a limit has even been approached at 0.2 $m$, and an attempt to extend them to even lower concentrations at elevated temperatures is clearly warranted. The consistency of the present results with those previously reported for higher concentrations of the same salts at 140°C lends confidence to the use of both sets of measurements.

Since a main objective of the isopiestic program has been to study the effect of temperature on aqueous systems, it now appeared appropriate to examine the isopiestic ratios as functions of temperature. To this end the data from the work of others[42] at 25°C were combined with our own at 100, 121, and 140°C, arranged to group together the values for various concentrations of each salt, and displayed, as shown in Fig. 8.23, as plots of $R$ vs $T$ for each concentration of each salt.

It seems noteworthy that, for each salt, the values for $R$ for each concentration converge toward a single value at high temperatures. It seems even more remarkable that, for every salt, the temperature is so nearly the same, ~160°C.

Bernal and Fowler[43] originally proposed that dissolved electrolytes introduce order or disorder into the tetrahedral structure of water. Many investigators have suggested that increasing the temperature tends to break down this structure, removing those properties derived from the hydrogen bonding and ultimately converting water into a more nearly ideal liquid. From these two points of view the variation of salt concentration at constant temperature may be considered analogous to the variation of temperature at constant salt concentration. Alternatively, the addition of a salt to water may change the temperature at which the tetrahedral structure of the water can no longer be supported. Although this *critical structural temperature* concept was originally proposed for dilute solutions only, it is, nevertheless, interesting to consider its applicability to the osmotic data for, predominantly, concentrated

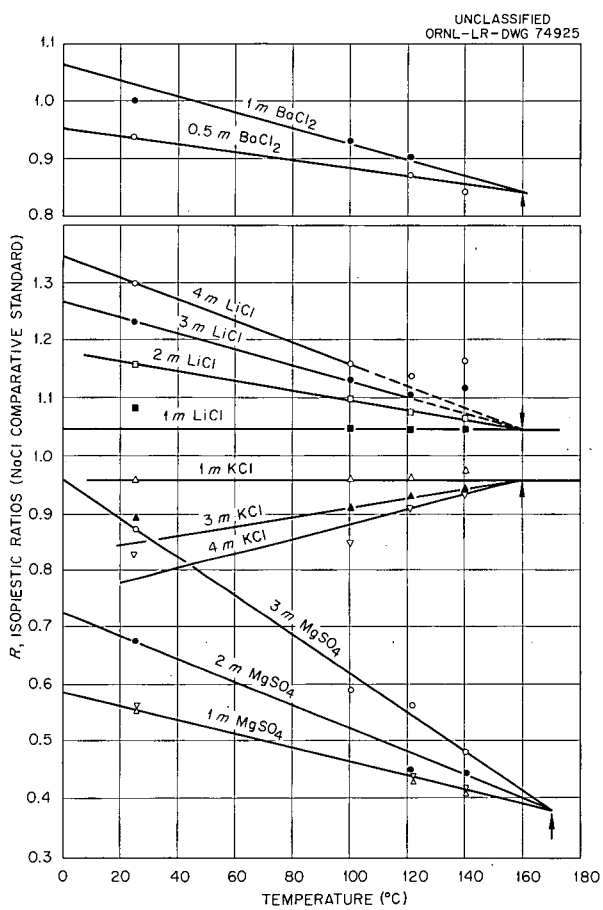


**Fig. 8.23. Temperature Dependence of Isopiestic Ratios, Normalized to NaCl, as a Function of Both Salt Concentration and Salt Type.**

[42] R. A. Robinson and R. H. Stokes, *Electrolyte Solutions*, Butterworth, London, 1935.

[43] J. D. Bernal and R. H. Fowler, *J. Chem. Phys.* 1, 515 (1933).

solutions. In recent years many investigators[44–46] have demonstrated that structural considerations, involving the characterization of changes in either the entropy or the free energy, could be employed profitably in the interpretation of the results of diverse experiments with concentrated aqueous salt solutions.

The obvious approach to linearity of the $R$ vs $T$ relation of Fig. 8.23 deserves comment. Since the 2-1 and the 2-2 as well as the 1-1 electrolytes show this linearity, it may well be that the temperature effect is based on factors which are common to all these solutions. Such factors may be the presence of water, as the solvent, and/or the use of NaCl, the reference standard.

The convergence to a common temperature of approximately 160°C may be especially significant. The pressure-volume-temperature studies of NaCl solutions by Gibson and Loeffler,[44] in which both temperature and concentration were varied, indicated that somewhere between 140 and 170°C the effectiveness of NaCl in ordering the tetrahedral structure of water is overcome by the disordering effect of temperature. At higher temperatures, therefore, aqueous NaCl solutions (and perhaps those of other electrolytes as well) should be expected to behave more like ideal solute-solvent mixtures.

The behavior of KCl solutions is interesting in that the effect of concentration on $R$ for this salt is opposite to that observed for the other salts tested. Potassium chloride is generally considered to be a "structure breaker" which introduces disorder into solutions, and, from this point of view, its isopiestic behavior is not surprising. Even with KCl the effect of temperature on $R$ is largest at the highest concentration and decreases at lower concentrations.

The isopiestic apparatus has been modified to permit tests at temperatures up to 170°C. Such studies should be valuable, not only in testing the behavior of salts in general above the 160°C convergence temperature, but also in revealing whether the properties of the various salts differ significantly above this temperature.

[44] R. E. Gibson and O. N. Loeffler, *Ann. N.Y. Acad. Sci.* **51**, 727 (1949).

[45] R. W. Gurney, *Ionic Processes in Solution*, McGraw-Hill, New York, 1953.

[46] F. A. Long and W. F. McDevit, *Chem. Rev.* **51**, 119 (1952).

## HYDROLYSIS OF THORIUM(IV) AT 95 AND 0°C

C. F. Baes, Jr. N. J. Meyer[47]
C. E. Roberts

The measurements of Th(IV) hydrolysis at 95°C, described previously,[48] were completed. They were made in 1 $m$ aqueous sodium perchlorate, and they include thorium concentrations in the range 0.002 to 0.02 $m$ and hydroxyl numbers, $\bar{n}$ (i.e., the average number of $OH^-$ ions bound per $Th^{4+}$ ion), in the range 0.08 to 1.8 (Fig. 8.24). The upper limit in $\bar{n}$ was imposed by hydrolytic precipitation; the lower limit in $\bar{n}$ was imposed by the high aqueous acidities encountered (approaching 0.1 $m$ in $H^+$).

As was previously indicated,[48] a hydrogen electrode concentration cell,

$$H_2 \,|Pt|\, \text{test soln} \,||\, \text{ref soln} \,|Pt|\, H_2 ,$$

was found to yield more reproducible results at the higher acidities (>0.01 $m$ in $H^+$) than the analogous glass electrode concentration cell,[49]

$$\text{glass electrode} \,|\, \text{test soln} \,||\, \text{ref soln} \,|\, \text{glass electrode} ,$$

used for most of these measurements.

During the course of Th(IV) hydrolysis measurements at 94°C at $\bar{n} < \sim 1.8$, the equilibria were evidently rapidly attained and reversible, concordant results being obtained by the addition of base to initially unhydrolyzed solutions or by the addition of acid to initially hydrolyzed solutions. In the region of $\bar{n} \sim 1.8$ and above, however, a drift in the cell potential toward higher acidities was encountered, evidently the result of hydrous $ThO_2$ precipitation or colloid formation. Analogous behavior has been found[50,51] at 25°C and $\bar{n}$ values of ~2.5 or greater. In several experiments at 95°C, the changing acidity with time was followed for several days without the system's

[47] ORINS summer participant, 1961. Professor of Chemistry, Bowling Green State University, Bowling Green, Ohio.

[48] *Reactor Chem. Div. Ann. Progr. Rept. Jan. 31, 1962*, ORNL-3262, p 67.

[49] *Reactor Chem. Div. Ann. Progr. Rept. Jan. 31, 1960*, ORNL-2931, p 130.

[50] K. A. Kraus and R. W. Holmberg, *J. Phys. Chem.* **58**, 325 (1954).

[51] S. Hietanen, *Acta Chem. Scand.* **8**, 1626 (1954).

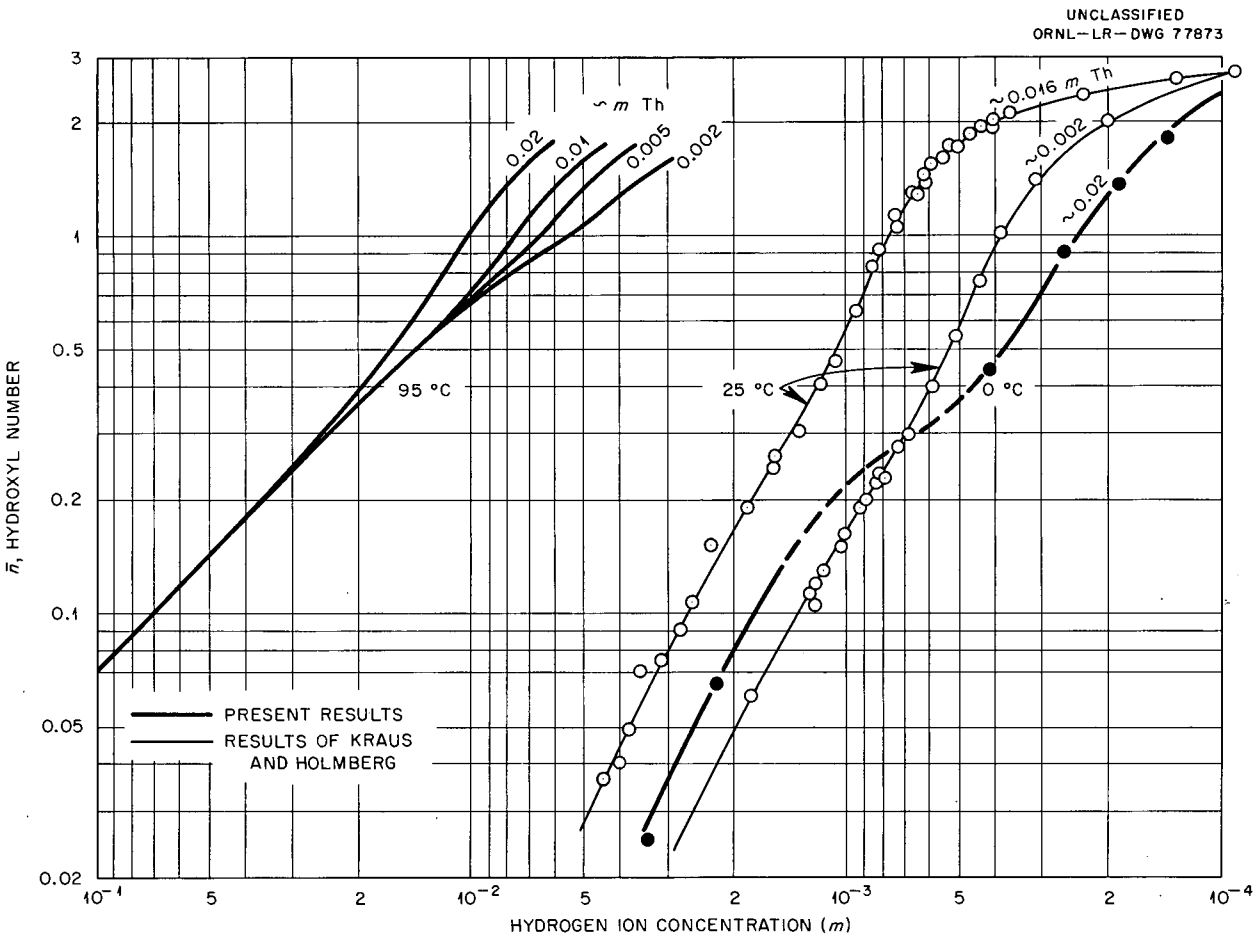


**Fig. 8.24. Hydrolysis of Th(IV) in 1 *m* $NaClO_4$ Solution, 0–95°C.**

reaching an equilibrium value, and it became clear that considerable supersaturation with respect to hydrous $ThO_2$ had occurred in the hydrolysis titrations.

Supersaturated $ThO_2$ solutions of known composition were seeded with $ThO_2$ and equilibrated at 94°C in sealed Pyrex tubes for periods of several weeks. The compositions of the resulting saturated, or nearly saturated, solutions (Fig. 8.25) showed that in the range of the present hydrolysis measurements (0.002 to 0.02 *m* thorium) at all acid concentrations below ~0.017 *m* (which included the majority of the measurements), the solutions were metastable with respect to $ThO_2$ precipitation. This condition does not, however, impair the usefulness of the hydrolysis data, since the equilibria which they describe are rapid and reversible, whereas the approach to an ultimately more stable state of $ThO_2$ saturation is relatively a much slower process.

One series of hydrolysis measurements thus far has been made at 0°C (Fig. 8.24), using a hydrogen electrode cell. This low temperature was employed for two reasons: (1) The much lower tendency of Th(IV) to hydrolyze permits much lower acidities to be reached in the presence of thorium without appreciable hydrolysis. This permitted a more accurate acid balance to be made for the purpose of determining the excess or deficiency of acid present in the thorium stock solutions used. (2) As has been noted,[48] the mechanism of Th(IV) hydrolysis is evidently complex, and additional data at other temperatures may prove of value in deducing it.

Analysis of the present data is now in progress in an effort to determine the hydrolysis mechanism

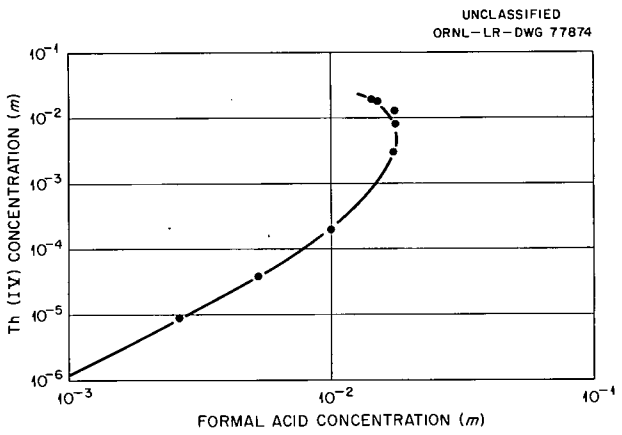


**Fig. 8.25. Solubility of $ThO_2$ in 1 *m* $NaClO_4$ Solution at 95°C.**

(i.e., the composition of the important hydrolysis products and their formation constants). It seems at once obvious from the data at the three temperatures (the results of Kraus and Holmberg[50] at 25°C are also indicated in Fig. 8.24) that the relative importance of various hydrolytic species changes significantly with temperature. The data at 94°C conform to a single curve below $\bar{n} = 0.3$, indicating that $\bar{n}$ is independent of the thorium concentration. This may be taken to mean that here only mononuclear products are formed. At higher hydroxyl numbers, the data at various thorium concentrations diverge, indicating the appearance of polynuclear products. Kraus and Holmberg[50] and Hietanen[51] found, at 25°C, that polynuclear products were important over the entire range of $\bar{n}$ values studied. From the one curve available thus far at 0°C, the presence of polynuclear products cannot be confirmed, although this is expected to be the case. It is apparent, however, that the shape of the curve is again different, showing an apparently much more pronounced break in the range $\bar{n} = 0.2$ to 0.4 than is seen in the curves at 25°C. Such varied behavior offers the prospect that, as a result of the temperature range of the data, one set of hydrolysis products can be established with greater certainty than would be possible otherwise. This prospect, as well as the knowledge of temperature coefficients of hydrolysis gained at the same time, has been a principal incentive in this program of high-temperature acidity measurements.

# Part III

# Heterogeneous Systems

# 9. Compatibility of Coated Fuel Particles and Matrix Graphites with Liquid Coolants

## FACTORS LIMITING HIGH RATES OF HEAT TRANSFER FROM FUELED AND UNFUELED GRAPHITE RODS TO FLOWING PRESSURIZED WATER

S. A. Reed T. H. Mauney
E. L. Compere

One phase of the program which is directed toward the study of the compatibility of coated fuel particles and graphite matrices with liquid coolants is concerned with the effect of high rates of heat transfer on the integrity of the materials during exposure to the flowing liquids of interest. The experimental approach has been to increase heat transfer rates until some type of failure occurred. The information gained from such failure was used to ascertain the factors which could be altered to permit higher rates to be developed.

Demonstration tests using rod-type samples of graphite and electrical resistance heating for studying the effects of high rates of heat transfer on the compatibility of graphite and flowing pressurized water were reported previously.[1] The technique was employed during the present report period in three series of tests that were made in which two grades of commercial graphite and special proprietary grades of unfueled and fueled matrix graphite were exposed in flowing pressurized water at generated heat fluxes of 300,000 to $\sim$1,600,000 Btu $hr^{-1}$ $ft^{-2}$.

The apparatus used for the tests and the manner in which the specimens were suspended axially in the flowing water are illustrated in Fig. 9.1. The device is essentially a high-pressure sight glass installed in a bypass line of a 100-gpm pressurized water loop. Insulated high-current electrodes permit a $\frac{1}{4}$-in.-diam graphite rod test specimen to be mounted in the center of the sight glass flow channel. The specimen is heated by electrical resistance using a 20-kva, 800-amp, ac power supply.

Materials tested included spectrographic electrode, extruded graphite rod, unfueled matrix graphite extruded rod, extruded graphite rod fueled with pyrolytic-carbon-coated uranium carbide particles, and rod machined from pyrolytic graphite plate. Determined properties of the graphite rods used in the tests are shown in Table 9.1, and estimated values of properties based on manufacturer's and other literature are shown in Table 9.2.

Pertinent operating data for the various tests are shown in Table 9.3.

Before discussing the results in the individual tests it is well to consider the possible mechanisms by which the damage to or failure of the specimens could have occurred. These include possible excessive thermal stresses in the rods, oxidation of the graphite by the water, and whether or not the critical (burnout) heat fluxes were reached or exceeded in the various tests.

The allowable heat generation per unit length of the rods (linear heat load), as limited by thermal stresses equal to the ultimate strength, was estimated by using a rearrangement of the equation for thermal stresses due to uniform heat generation in long isotropic solid cylinders,[2]

$$\frac{Q}{L} = \frac{8\pi k(1-\nu)S}{E\alpha},$$

[1] S. A. Reed and E. L. Compere, *Reactor Chem. Div. Ann. Progr. Rept. Jan. 31, 1962*, ORNL-3262, p 107.

[2] Robert Daane, "Thermal Stress and Distortion," sec 9-4 in *Nuclear Engineering Handbook*, ed. by Harold Etherington, McGraw-Hill, New York, 1958.

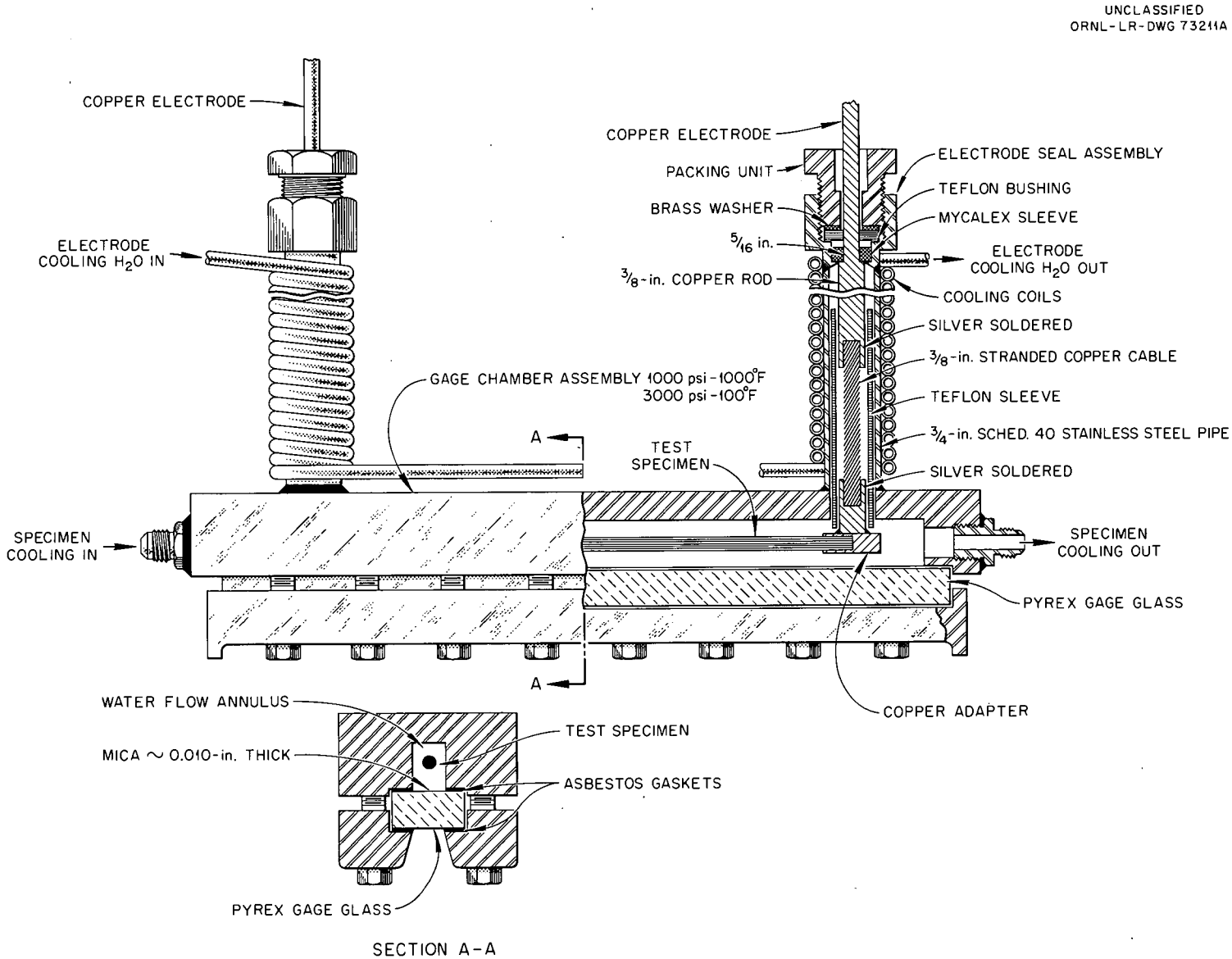


**Fig. 9.1. Test Apparatus for Electrically Heated and Liquid-Cooled Specimens.**

**Table 9.1. Property Determinations for Graphite Specimens Used in Heat Flux Tests**

| Specimen | Porosity (vol %)[a] | Surface Area ($m^2/g$)[b] | Density (g/cc) by Immersion in | | Specific Resistance (ohm-cm) |
|---|---|---|---|---|---|
| | | | Hg | $CCl_4$ | |
| Grade U-1 spectrographic electrode[c] | 19.9 | 0.138 | 2.15 | 2.11 | $1.04 \times 10^{-3}$ |
| Pyrolytic graphite[d] | | | | | |
| *a* direction | 0.5 | 0.008 | 2.26 | 2.22 | $4.7 \times 10^{-4}$ |
| *c* direction | | | | | 0.52 |
| NCC grade FE-4, 2800°C | 6.73 | 0.141 | 1.98 | 1.89 | $9.04 \times 10^{-4}$ |
| Speer unfueled No. 48 | 28.6 | 0.210 | 2.16 | 1.88 | $1.40 \times 10^{-3}$ |
| Speer unfueled No. 60 | 24.3 | 0.250 | 2.07 | 2.00 | $1.93 \times 10^{-3}$ |
| Speer No. 67 fueled with pyrolytic-carbon-coated uranium carbide | ND | ND | 1.90[e] | 1.85 | $1.73 \times 10^{-3}$ |

[a]By mercury porosimetry.
[b]BET, nitrogen.
[c]United Carbon Products Co., grade U-1, high density.
[d]High Temperature Materials, Inc., ⅜-in.-thick plate stock, unannealed.
[e]Density in helium.

**Table 9.2. Estimated Properties of Graphite Rods Used in Heat Flux Tests**

| Specimen | Thermal Conductivity [Btu $hr^{-1}$ $in.^{-1}$ $(°F)^{-1}$] | Poisson's Ratio | Ultimate Strength (psi) | Modulus of Elasticity (psi) | Coefficient of Linear Expansion [in. $in.^{-1}$ $(°F)^{-1}$] |
|---|---|---|---|---|---|
| Spectrographic electrode[a] | 8 | 0.25 | 1,450 | $0.9 \times 10^6$ | $0.6 \times 10^{-6}$ |
| Pyrolytic graphite[b] | | | | | |
| *a* direction | 17 | +0.9 | 7,000 to 14,000 | $3.7 \times 10^6$ | $0.1 \times 10^{-6}$ |
| *c* direction | 0.06 | −0.1 to −0.2 | 460 | | $7 \times 10^{-6}$ |
| NCC grade FE-4,[c] 2800°C | 9[d] | 0.25 | 5,200 | $0.9 \times 10^6$ | $0.6 \times 10^{-6}$ |
| Speer unfueled grade No. 48 | 6[d] | 0.25 | 4,100 | $0.9 \times 10^6$ | $0.6 \times 10^{-6}$ |
| Speer unfueled grade No. 60 | 4[d] | 0.25 | 4,100 | $0.9 \times 10^6$ | $0.6 \times 10^{-6}$ |
| Speer grade No. 67 fueled with 9.2 vol % fuel particles, uranium carbide in pyrolytic carbon | 5[d] | 0.25 | 4,100 | $0.9 \times 10^6$ | $0.6 \times 10^{-6}$ |

[a]United Carbon Products Co., grade U-1, high density.
[b]High Temperature Materials, Inc.
[c]National Carbon Company.
[d]Estimate based on specific conductivity.

**Table 9.3. Operating Conditions for Heat Flux Tests of Graphite Rods in Pressurized Water**

| Run No. | Hours | Watts | Loop Temperature (°C) | Saturation Temperature (°C) | Pounds per Square Inch Absolute | Flow Velocity (fps) | Remarks |
|---|---|---|---|---|---|---|---|
| **Spectrographic Electrode Graphite, United Carbon Co., Grade U-1, Extruded Rod, 1/4 in. in Diameter by 9 in. Long** | | | | | | | |
| D-125 | 0.8 | 4,400 | 300 | 308 | 1415 | 2.1 | No attack |
| D-126 A | 0.5 | 14,000 | 300 | 309 | 1425 | 2.1 | General attack, maximum loss in diameter of 19% |
| B | 0.3 | 13,200 | 300 | 309 | 1425 | 2.1 | |
| **Pyrolytic Graphite, High Temperature Materials, Inc., Machined from Plate, 1/4 in. in Diameter by 4 3/4 in. Long** | | | | | | | |
| D-127 A | 24.0 | 4,000 | 250 | 286 | 1015 | 2.1 | No attack |
| B | 0.8 | 6,600 | 250 | 286 | 1015 | 2.1 | Failed: splintered |
| D-128 A | 129.2 | 5,300 | 250 | 286 | 1015 | 2.1 | No attack |
| D-130 B | 120.8 | 4,700 | 250 | 286 | 1015 | 2.1 | Mild laminar edge attack |
| **Unfueled Matrix Graphite, National Carbon Co., FE-4/2800°C, Extruded Rod, 1/4 in. in Diameter by 4 15/16 in. Long** | | | | | | | |
| D-131 A | 0.5 | 5,500 | 243 | 300 | 1250 | 2.1 | No attack |
| B | 19.2 | 7,000 | 243 | 305 | 1335 | 2.1 | Failed: transverse crack |
| **Unfueled Matrix Graphite, Speer Carbon Co., No. 60, Extruded Rod, 1/4 in. in Diameter by 4 7/8 in. Long** | | | | | | | |
| D-132 A | 0.4 | 6,700 | 250 | 301 | 1265 | 2.1 | No attack |
| B | 243.7 | 6,800 | 250 | 301 | 1265 | 2.1 | No attack |
| **Unfueled Matrix Graphite, Speer Carbon Co., No. 48, Extruded Rod, 1/4 in. in Diameter by 5 in. Long** | | | | | | | |
| D-133 | 246.6 | 7,400 | 250 | 303 | 1305 | 2.1 | No attack |
| **Fueled Graphite, Speer Carbon Co., No. 67, Extruded Rod, 1/4 in. in Diameter by 4 5/16 to 5 in. Long Containing Pyrolyticolly Coated Uranium Carbide Particles, 120 mg of Uranium per cc of Specimen[a]** | | | | | | | |
| D-134 | 29.5 | 12,100 | 225 | 310 | 1435 | 3.2 | General attack with loss of diameter |
| D-135 | 0.1 | 10,500 | 226 | 312 | 1475 | 3.2 | No attack – arced at connection |
| D-136 A | 0.6 | 5,700 | 225 | 309 | 1415 | 6.4 | No attack |
| B | 1.8 | 7,700 | 225 | 309 | 1415 | 4.7 | Failed: transverse crack |

[a]Equivalent to 2.7 vol % as $UC_2$, or 9.2 vol % as coated particles.

where

$Q$ = Btu/hr,

$L$ = length, in.,

$k$ = thermal conductivity, Btu $hr^{-1}$ $in.^{-1}$ $(°F)^{-1}$,

$\nu$ = Poisson's ratio (dimensionless),

$S$ = ultimate strength, psi,

$E$ = modulus of elasticity, psi,

$\alpha$ = coefficient of linear expansion, in. $in.^{-1}$ $(°F)^{-1}$.

The critical or burnout heat fluxes for each test were computed by using the equation proposed by Zenkevich and Subbotin:[3,4]

[3]B. A. Zenkevich and B. I. Subbotin, "Critical Heat Fluxes in Sub-Cooled Water with Forced Circulation," *At. Energ.* **3**, 149 (1957); English translation in *J. Nucl. Energy, Pt. B: Reactor Technology* 1(2), 134–36 (1959).

[4]W. R. Gambill and R. D. Bundy, *HFIR Heat Transfer Studies of Turbulent Water Flow in Thin Rectangular Channels*, ORNL-3029 (June 5, 1961).

$$\phi_{bo} = 396 G_{bulk}^{0.5} (t_{satn} - t_{bulk})^{0.33} \left( \frac{\rho_l - \rho_v}{\rho_l} \right)_{satn}^{1.8},$$

where the liquid and vapor density terms are taken at the same saturation temperature corresponding to the overpressure. Heat flux, $\phi$, is in Btu $hr^{-1}$ $ft^{-2}$; mass velocity, $G$, is in lb $hr^{-1}$ $ft^{-2}$; temperature, $t$, is in °F; and density, $\rho$, is in lb/$ft^3$.

Comparisons of the linear heat load and critical heat flux criteria for the materials under the conditions of the various tests are shown in Table 9.4.

A comparison of the results of runs D-125 and D-126 employing electrode graphite specimens is of particular interest since both tests were of ¾-hr duration and operating conditions were essentially identical except for the generated heat fluxes. A burnout flux was not reached in run D-125 and the specimen was not detectably damaged. In run D-126 the generated heat flux attained was nearly twice the value estimated for the critical flux and the rod was extensively damaged in about 15 min. The fueled graphite specimen used in run D-134 was similarly attacked and probably failed as a result of exceeding the critical flux as indicated by the estimated burnout condition.

It appears reasonable to assert that under the film-boiling conditions above burnout which were observed in these tests, the rods became hot enough to permit the steam-carbon reaction to proceed at a substantial rate.

In none of the runs with extruded graphites was the limiting linear heat load approached. Thermal stresses due to internal heat generation do not appear to be a problem with these materials.

Experimental conditions were altered to inhibit burnout by increasing the difference between bulk temperature and saturation temperature and later also by increasing the flow velocity from 2 fps to ~6 fps.

Thus in run D-133 it was possible to sustain a heat flux of 1,000,000 Btu $hr^{-1}$ $ft^{-2}$ for 247 hr without any apparent attack on the graphite.

Failures of the pyrolytic graphite were of a different nature (due to the highly anisotropic, laminar characteristics of this material) as indicated by the differences between properties in the *a* direction and *c* direction as shown in Table 9.2. Estimated burnout heat fluxes were not exceeded. However, it appears that thermal stress limits may have been exceeded. In order to estimate this limit, the value of the thermal conductivity in the *a* direction was used, and values of the strength and thermal expansion in the *c* direction were used. These values lead to an estimated critical linear heat load of 8300 Btu $hr^{-1}$ $in.^{-1}$ in the *c* direction. A value in the *a* direction of 800,000 Btu $hr^{-1}$ $in.^{-1}$ was also estimated.

These estimates are regarded as quite naive because of the highly anisotropic character of pyrolytic graphite, since the equations were developed for an isotropic substance. However, pyrolytic graphite would appear susceptible to thermal stress effects in the *c* direction.

A linear heat load of 2800 Btu $hr^{-1}$ $in.^{-1}$ was sustained without attack of the pyrolytic graphite rod in run D-127A. At a linear heat load of 4700 Btu $hr^{-1}$ $in.^{-1}$, a splintering failure occurred.

In runs D-128A and D-130B, mild attack at laminar pyrolytic graphite plane edges was noted, at a linear heat load of 3400–3800 Btu $hr^{-1}$ $in.^{-1}$. Failures of pyrolytic graphite can reasonably be attributed to thermal stresses between the laminar layers of the material.

A third class of failures was observed in other tests. In these tests, D-131 and D-136, heat fluxes were 60–80% of the estimated burnout values, and the rods were broken transversely near the downstream end. It is not evident that axial or circumferential thermal stresses, or burnout heat fluxes, satisfactorily account for these failures. However, in each case failure occurred at relatively high heat flux values, ~1,000,000 Btu $hr^{-1}$ $ft^{-2}$.

In summary, it appears that failures may occur in pyrolytic graphite due to thermal stresses in the *c* direction, and in extruded graphites, unfueled or fueled, if the burnout heat flux is exceeded. Breakage failures of some extruded graphites can also occur, for unestablished causes at high heat fluxes, below the estimated burnout heat flux.

It may be noted that both fueled (run D-136A) and unfueled (run D-133) graphite rods appeared capable of sustaining a heat flux of over ~800,000 Btu $hr^{-1}$ $ft^{-2}$ without evident damage. Further runs to establish longer-term effects were not made as funds were not available to continue the program.

Table 9.4. Comparison of Critical Heat Flux and Linear Heat Generation Data for Graphite Specimens

| Run No. | Graphite Grade | Burnout Criterion: Calculated Burnout Heat Flux (Btu $hr^{-1}$ $ft^{-2}$) | Burnout Criterion: Heat Flux Generated During Test (Btu $hr^{-1}$ $ft^{-2}$) | Thermal Stress Criterion: Limiting $Q/L$ Calculated (Btu $hr^{-1}$ $in.^{-1}$) | Thermal Stress Criterion: $Q/L$ Generated During Test (Btu $hr^{-1}$ $in.^{-1}$) | Comments |
|---|---|---|---|---|---|---|
| D-125 | Electrode | 481,000 | 306,000 | 400,000 | 1670 | Not detectably damaged |
| D-126 A | Electrode | 502,000 | 973,000 | 400,000 | 5300 | Attacked, maximum loss in diameter of ~19% |
| B | Electrode | 502,000 | 918,000 | 400,000 | 5000 | |
| D-131 A | FE-4, 2800 | 1,015,000 | 752,000 | 1,600,000 | 3770 | OK |
| B | FE-4, 2800 | 1,032,000 | 964,000 | 1,600,000 | 4810 | Failed, cracked perpendicular to axis of extrusion |
| D-132 A | SCC No. 60 | 967,000 | 955,000 | 600,000 | 4720 | Not detectably damaged |
| B | SCC No. 60 | 967,000 | 960,000 | 600,000 | 4780 | Not detectably damaged |
| D-133 | SCC No. 48 | 972,000 | 1,009,000 | 800,000 | 5070 | Not detectably damaged |
| D-134 | SCC No. 67 (fueled) | 1,405,000 | 1,598,000 | 700,000 | 8470 | Failed, attack appeared similar to that in run D-126 |
| D-135 | SCC No. 67 (fueled) | ~1,400,000 | 1,673,000 | 700,000 | 8350 | Test terminated due to faulty copper plating on specimen |
| D-136 A | SCC No. 67 (fueled) | 1,987,000 | 794,000 | 700,000 | 3890 | OK |
| B | SCC No. 67 (fueled) | 1,709,000 | 1,077,000 | 700,000 | 5250 | Failed, cracked perpendicular to axis of extrusion |
| D-127 A | Pyrolytic, *a* direction | 881,000 | 518,000 | 800,000 | 2820 | OK |
| | Pyrolytic, *c* direction | 881,000 | 518,000 | 8,300 | | OK |
| B | Pyrolytic, *a* direction | 881,000 | 860,000 | 800,000 | 4690 | Failed, separated into two splinter-like sections |
| | Pyrolytic, *c* direction | 881,000 | 860,000 | 8,300 | | |
| D-128 A | Pyrolytic, *a* direction | 881,000 | 693,000 | 800,000 | 3780 | OK |
| | Pyrolytic, *c* direction | 881,000 | 693,000 | 8,300 | | OK |
| D-130 B | Pyrolytic, *a* direction | 881,000 | 622,000 | 800,000 | 3400 | Mild attack at edges of laminar graphite planes |
| | Pyrolytic, *c* direction | 881,000 | 622,000 | 8,300 | | |

## GAMMA IRRADIATION OF COATED-PARTICLE AND MATRIX MATERIALS IN HIGH-TEMPERATURE LIQUIDS INCLUDING MSRE FUEL SALT

L. F. Woo T. H. Mauney
E. L. Compere

One of the simplest radiation stability requirements for systems involving liquids, matrix materials, and coated particles is that the system should retain its integrity for a substantial period of time at temperature in the presence of intense gamma radiation. Certainly before more complex in-pile experiments are conducted, tests to check compatibility of the system under the combined action of gamma radiation and temperature should be carried out. In the case of molten-salt systems, it is also of interest to see whether radiation damage effects of interest to the Molten-Salt Reactor Project can be produced in fluoride salt–graphite systems by gamma irradiation at selected temperatures.

Irradiations have been completed on two autoclave experiments for the Coated-Particle Program using the nominal 10,000-curie $Co^{60}$ source of the Chemical Technology Division. The first experiment, designated GRA-1, employed $D_2O$ with 75 psia helium at 330°C and the second, designated GRA-2, utilized Santowax R with 35 psia helium at 400°C. A third autoclave experiment, designated GRA-3, employing fluoride salts of compositions considered for the Molten-Salt Reactor Experiment is being fabricated.

### Materials Used in Gamma Irradiation Studies

In each of the autoclaves prepared for irradiation studies, a set of 16 machined graphite spheres, ¼ in. in diameter with 1/32-in. holes, were strung on a U-shaped wire. Two spheres of each of four kinds of graphite were in the liquid phase and a similar array in the vapor phase of the autoclave. The graphites shown in Table 9.5 were used; they simulated possible types of matrix materials which might be used for coated-particle fuel elements.

In the second experiment, employing Santowax R as liquid, in addition to a set of the above graphite spheres, two sealed glass ampoules containing liquid and a given type of coated particles were also placed in the autoclave. Coated particles obtained from Nuclear Materials and Equipment Company[5] contained $UO_2$ particles of 150-$\mu$ average diameter with a spiny coating of $Al_2O_3$ of 40-$\mu$ thickness. Coated particles obtained from National Carbon Company[5] contained $UC_2$ particles of 150-$\mu$ average diameter, with a laminar pyrolytic carbon coating of 80-$\mu$ thickness.

Santowax R is a high-melting (mp, 145°C) low-vapor-pressure (bp, 364–418°C) mixture of terphenyls of interest as an organic reactor coolant liquid. It was obtained from the Monsanto Chemical Company.

[5]S. A. Reed and E. L. Compere, *Reactor Chem. Div. Ann. Progr. Rept. Jan. 31, 1962*, ORNL-3262, p 107.

**Table 9.5. Properties Determined on Graphites Used in Gamma Irradiation Studies**

| Type | AGOT (extruded) | TS-148/2000°C (extruded) | TS-160/2000°C (extruded) | Pyrolytic (deposited plate) |
|---|---|---|---|---|
| Source | NCC[a] | NCC[a] | NCC[a] | HTM[b] |
| Bulk density, g/cc | 1.67 | 1.64 | 1.70 | 2.21 |
| Void fraction, % | 18 | 14 | 12 | 0.5 |
| Pore volume,[c] ml/g | 0.099 | 0.076 | 0.065 | 0.0023 |
| Average pore radius,[c] $\mu$ | 1.6 | 1.0 | 0.9 | 0.6 |

[a]National Carbon Company.
[b]High Temperature Materials, Inc.
[c]Pore volume determined by Hg intrusion; includes volume in pores with radii between 0.05 and 5 $\mu$ (approx).

### Pressurized-Water Autoclave Irradiation

Experiment GRA-1 utilized a type 347 stainless steel autoclave containing the graphite sphere set indicated above, with 3.56 g $D_2O$ in a net gas-liquid volume of 9.7 ml. The autoclave had a partial pressure of helium of 75 psi at its operating temperature of 330°C. The autoclave was irradiated at this temperature for 2115 hr by $Co^{60}$ gamma rays at a dose rate of $2.4 \times 10^{-3}$ w/g (equivalent to an adjusted calibration of $0.9 \times 10^{18}$ ev/min per ml of $H_2O$).

Examination of the spheres after this irradiation indicated almost trivial changes, with no noteworthy dependence on liquid or vapor phase. In general the spheres lost about 0.5 mg in weight (original level ~0.2 g) and gained about 0.0002 in. in diameter. A profusion of tiny pits was found on the surface of the various spheres, which could have been artifacts of the machining. Pyrolytic graphite exhibited the widest variations in effects.

Pore size analysis by mercury intrusion indicated changes barely significant only in AGOT graphite. In specimens from both phases, average pore radius of AGOT spheres increased to 1.5 from 1.4 $\mu$, and pore volume to 0.09 from 0.07 ml/g.

Gas was removed from the autoclave and analyzed by mass spectrometry and gas chromatography. Based on a postirradiation autoclave pressure reading of 39 psia at 25°C, the following amounts of material were found (in addition to original helium and air inleakage during sampling):

| | Mass Spectrometry ($\mu$moles) | Gas Chromatography ($\mu$moles) |
|---|---|---|
| $D_2$ | 6 | 33 |
| $CO_2$ | 140 | 125 |
| CO | 0 | 0 |
| Hydrocarbons | 0 | |

The simple reaction of carbon with $D_2O$ should produce twice as much $D_2$ as $CO_2$. An alternative and thermodynamically feasible reaction would produce methane and $CO_2$. Since air was purged from the autoclave prior to irradiation by purging three times with helium at 1600 psi, it does not appear reasonable that the $CO_2$ was produced from this source. Although no direct evidence is available, the discrepancy could be a result of uptake of hydrogenous material by the graphite, or of diffusion of hydrogen[6] through vessel walls.

### Santowax Autoclave Irradiation

Experiment GRA-2 utilized a type 347 stainless steel autoclave containing the graphite sphere set indicated above and two ampoules containing Santowax R and the indicated coated particles. Liquid contents were 3.69 g of Santowax R in a net gas-liquid volume of 6.4 ml. The autoclave had a partial pressure of 35 psi of helium at its operating temperature of 400°C. The autoclave was irradiated at this temperature for 1770 hr (including 31 hr below 100°C) at a dose rate of $2.3 \times 10^{-3}$ w/g.

Postirradiation microscopic examination of the graphite spheres did not reveal any evidence of deposition of solids. A few small pits were observed. Weight changes were of the order of 0.3 mg with little difference between liquid and vapor phases. The AGOT graphite in the liquid phase showed weight gains of ~1 mg.

The color of the Santowax R in the autoclave had changed from an original clear yellow to brown after irradiation. Results of the analysis of the liquid phase, which smelled of benzene, are not complete.

Gas was removed from the autoclave after irradiation using a Toepler pump. Mass spectrographic analyses permitted calculation of the following yields (uncorrected for any gases dissolved in the liquid fraction):

| | $\mu$moles | Std ml per g of Santowax |
|---|---|---|
| $H_2$ | 13 | 0.08 |
| $CH_4$ | 15 | 0.09 |
| Ethane | 3 | 0.02 |
| Benzene | 0.4 | 0.002 |
| Other hydrocarbons | 0.9 | 0.008 |
| CO | 18 | 0.11 |
| $CO_2$ | 4 | 0.02 |

[6] M. C. Bloom and M. Krulfeld, "A Hydrogen Effusion Method for the Determination of Corrosion Rates in Aqueous Systems at Elevated Temperature and Pressure," *J. Electrochem. Soc.* **104**(5), 264–69 (1957).

The integrated dose in the above experiment was 4.1 whr per g of organic.

It has been stated that absorbed gamma radiation and fast electrons have essentially the same effects in the irradiation of organic liquids. From this point of view it is of interest to compare our data with the results of Burns, Wild, and Williams,[7] who reported the irradiation by fast electrons of *p*-terphenyl at 400°C to a dose of 3.8 whr/g as yielding the following quantities of gas: $H_2$, 0.91 ml/g; $CH_4$, 0.057 ml/g; and $C_2$ hydrocarbons, 0.082 ml/g.

Again the yield of hydrogen is lower in our irradiation experiment which included the graphite spheres. Hydrogen uptake by the graphite or diffusion through walls[6] could have been a factor. The yields of methane and other hydrocarbons are more nearly comparable.

## COMPATIBILITY OF COATED-PARTICLE FUEL ELEMENT MATERIALS WITH MOLTEN FLUORIDE SALTS

D. M. Richardson

The compatibility of coated-particle materials with molten fluorides has been studied in static crucible tests in vacuum and with helium and hydrogen as cover gases. Test temperatures in the range 800 to 1000°C were selected to produce accelerated effects as well as to investigate the region of hot-spot conditions of interest in nuclear reactors employing molten fluorides.

The fluoride salt mixture used in almost all tests was the LiF-NaF eutectic (mp, 652°C) and was prepared by mixing pure commercial materials. The advantages of using this mixture were that it is not very hygroscopic, there is no health hazard as would be the case with $BeF_2$, the vapor pressure is relatively low, and accelerated effects might be expected in such a "basic" melt. The high melting point was not a disadvantage in view of the elevated test temperatures chosen. Ultimately the eutectic mixtures with lower melting points should be tested. Examples are LiF-NaF-KF (mp, 454°C), LiF-$BeF_2$ (mp, 355°C), and LiF-NaF-$ZrF_4$ (mp, 425°C).

[7]W. G. Burns, W. Wild, and T. F. Williams, "The Effect of Fast Electrons and Fast Neutrons on Polyphenyls at High Temperatures," *Proc. Intern. Conf. Peaceful Uses At. Energy, Geneva, 2nd (1958)* **29**, 266, paper 51.

Alumina-coated $UO_2$ particles were found to be incompatible with the molten fluorides. The coatings were either dissolved or severely corroded, and cracking was frequently observed. Concurrent tests were made with 1-mm-diam $\alpha$-alumina spheres obtained from Linde Company. These spheres corroded more rapidly with increasing temperature and with increasing partial pressure of hydrogen as shown in Table 9.6.

**Table 9.6. Average Attack by LiF-NaF Eutectic on $\alpha$-Alumina Spheres**

| Partial Pressure of $H_2$ (atm)[a] | ($\mu$/100 hr) | | |
|---|---|---|---|
| | 800°C | 900°C | 1000°C |
| 1 | 21 | *b* | Spheres consumed |
| 1/20 | 0[c] | 29 | *b* |
| 0 | 0[c] | 13 | *b* |

[a]Total pressure 1 atm, helium plus hydrogen.
[b]Not determined.
[c]Surfaces lightly etched; some cracks visible.

The alumina spheres were also tested in LiF-NaF-KF eutectic ("flinak") at 600°C with helium cover gas. The average attack was 38 $\mu$ in 100 hr. Since the "flinak" used had been specially treated to remove water and oxide impurities, the aggressive attack might have been due to the KF component or to $FeF_2$ and $CrF_2$ impurities.

Early tests of pyrolytic-carbon-coated fuel particles were performed concurrently with those for alumina spheres. The particles were placed on top of the salt and remained there throughout the test. (This behavior was indicative of nonwetting since the average particle density was greater than the density of the molten salt.) Under these conditions there was never any evidence of damage to the coatings.

Subsequent tests of pyrolytic-carbon-coated fuel particles were conducted with the particles submerged in salt. A run was made with nickel crucibles at 900 to 1000°C for 200 hr under 3 atm of hydrogen. The coatings were damaged and in some batches a stain identified as $UO_2$ was found on the bottom of the crucibles. Many particles were flattened where they contacted metallic nickel. The coating damage in this run is believed to be the result of carbon diffusion into nickel as

well as the nickel-catalyzed reaction of carbon and hydrogen to form methane.

Submerged pyrolytic-carbon-coated particles were then exposed under helium for 100 hr at 900°C. There was no apparent damage. In order to recover all the particles free of salt, the crucibles were uncovered, returned to the furnace, and distilled for a day at 900°C under vacuum. After this operation it was found that extensive particle damage had occurred due to contact with the nickel crucibles. It was also observed that the particles had become coated with chromium and showed an x-ray pattern resembling $Cr_3C_2$. The chromium is believed to have originated in the walls of the type 347 stainless steel furnace tube.

The previous run was repeated without coated particles but with ATJ graphite crucibles inside the nickel crucibles. One assembly contained a specimen of INOR-8 tubing. After the final day of vacuum distillation at 900°C, the same results were found, but the graphite crucible that contained INOR-8 was more strongly discolored and had cracked. Since the chromized layer was very thin compared to the thick crucible wall it is likely that a secondary effect may have caused cracking to occur.

A possible mechanism for these phenomena occurring at 900°C under vacuum has been suggested.[8] Sodium fluoride vapor reacts with chromium to produce $CrF_3$ and sodium vapor. The sodium vapor reacts or intercalates with graphite and thus may cause cracking. Chromic fluoride vapor reacts with the sodium carbides to produce solid $Cr_3C_2$ and NaF. The total free energy change for these reactions is strongly negative.

[8]B. J. Sturm, private communication.

# 10. Rheology of Suspensions of Thoria from First In-Pile Slurry Loop Experiment

A. J. Shor E. L. Compere

Rheological determinations were carried out on light-water suspensions of irradiated thoria-urania solids drained from the first in-pile slurry loop experiment,[1] L-2-27S. The determination of the rheological parameters, particularly the yield stress, is important since they provide a quantitative measure of the thickening of the slurry. There is reason to believe that the degradation of slurry particles by irradiation and circulation would result in some degree of thickening, which could lead to problems of circulation, heat transfer, and loss from suspension in various ways. For example, with a yield stress of 0.3 $lb_f/ft^2$, a flow of about 5 fps is required[2] to develop turbulence and prevent dropout from suspension in pipes of 1- to 12-in. diam with suspensions at a density of 100 $lb/ft^3$. With a yield stress of 3 $lb_f/ft^2$, a flow of 16 fps would be required to develop turbulence. It is of course desirable to develop a basis for estimating the rheological properties of breeder blanket slurries and other suspensions which have been irradiated to the full extent anticipated for reactor extrapolations; reliable quantitative estimates have not yet been achieved.

The original batch DT-22 powder, which was used in experiment L-2-27S, was prepared by oxalate coprecipitation and air calcination at 1225°C. It contained 87 wt % thorium and 0.4 wt % uranium (91% $U^{235}$). A recombination catalyst consisting of a small amount of palladium supported on finely divided thoria was added prior to irradiation. The material subjected to irradiation contained 89% DT-22 powder and 11% catalyst mixture.

Approximately 80% of the recovered material was drained from the loop after irradiation was complete. The rest had been withdrawn into the loop drain tank as sample purges at various times during the irradiation. The fully irradiated material had received a neutron dose of $1.6 \times 10^{19}$ *nvt* in 2200 hr in-pile, and developed $7 \times 10^{16}$ fissions per gram of solids.

The average particle size of the original DT-22 thoria-urania was 1.7 $\mu$, and the surface area ~2 $m^2/g$. The average particle size of the L-2-27S drain tank material was 0.76 $\mu$, and the surface area was 33 $m^2/g$.

Suspensions of the irradiated solids in light water, and DT-22 thoria-urania powder in light and in heavy water were prepared at nominal concentrations of 5, 7½, and 10 vol % solids. The suspensions were prepared by blending for about 5 min in a Waring Blendor.

Shear diagrams were obtained at room temperature for the above suspensions by the use of a 0.046-in.-diam 12-in. capillary tube viscometer. Determinations on the irradiated material were made remotely in a hot cell. The same instrument was used also on the laboratory bench to determine the shear diagram of the unirradiated suspensions. The method[3] and techniques[4,5]

[1] H. C. Savage, E. L. Compere, and A. J. Shor, "Examination of In-Pile Slurry Loop," *Reactor Chem. Div. Ann. Progr. Rept. Jan. 31, 1962,* ORNL-3262, p 114.

[2] D. G. Thomas, personal communication; see also ref 6.

[3] K. H. McCorkle, *Measurement of Yield Stress and Modulus of Rigidity of $ThO_2$ Slurry* (unpublished).

[4] D. G. Thomas, "Transport Characteristics of Suspensions: III. Laminar Flow Properties of Flocculated Suspensions," *A.I.Ch.E. J.* **7**, 431–37 (1961).

[5] S. Oka, "The Principles of Rheometry," pp 17–80 in *Rheology, Theory and Applications* (ed. by F. R. Eirich), vol 3, Academic Press, New York, 1960.

have been well described in the literature. Absolute and relative calibrations of the viscometer and corrections for slurry head and for kinetic energy were made.

Additional determinations were made using a 0.050-in.-diam 50-in. capillary tube viscometer, with $D_2O$ and $H_2O$ slurries of unirradiated DT-22 powder.

Flow was varied by changing pressure. The resultant wall shear stress and rate of shear were calculated. Rate of shear was in the range 0 to 150 in $(8v/g_cD)$ units. For each suspension a corrected plot of wall shear stress vs rate of shear was used to obtain, according to the Bingham plastic model, the yield stress and modulus of rigidity. Results of the determinations of these rheological parameters are shown in Table 10.1. The coefficient of rigidity did not display any pronounced changes due to irradiation.

At each concentration the yield stress of the irradiated material was higher than that exhibited by the unirradiated material. It will be noted that the yield stress for each kind of sample varied sharply with the volume percent solids.

It has been shown by D. G. Thomas[6] that the yield stress, $\tau_y$, normally varies with the cube of the volume fraction solids, $\phi$, for suspensions of various concentrations of a given material. Thomas has also shown that the function $\tau_y/\phi^3$, which would be constant for a given series of suspension concentrations, is a good measure of the flocculation characteristics of the suspensions. In the development of a theoretical basis for the rheology of flocculated suspensions, Thomas argued that the ratio $\tau_y/\phi^3$ would be inversely related to the radius of curvature of the particle-particle contact regions. For many particles he found that $\tau_y/\phi^3$ was proportional to the inverse square of the particle diameter.

It may be argued, however, that some kinds of particles, such as the irradiated thoria particles, exhibit a high proportion of internal surface and a crystallite size much smaller than the particle size. With this class of particles, crystallite size or related surface area, rather than gross particle diameter, probably best characterizes the particle-particle interaction.

[6]D. G. Thomas, "Transport Characteristics of Non-Newtonian Suspensions," paper presented at the *Princeton University Summer Conference on Non-Ideal Behavior of Solids and Liquids*, August 17, 1962.

**Table 10.1. Rheological Properties of Irradiated and Unirradiated Thoria-Urania Suspensions**

| Slurry Density (g/ml) | Vol % Solids, 100 $\phi$ | Observed Coef. of Rigidity[a] (centipoises) | Observed Yield Stress,[b] $\tau_y$ ($lb_f/ft^2$) | Flocculation Index, $\tau_y/\phi^3$ | Remarks |
|---|---|---|---|---|---|
| | | **Irradiated Thoria-Urania from L-2-27S Drain Tank** | | | |
| 1.50 | 5.55 | 3.08 | 0.053 | 310 | |
| 1.71 | 7.96 | 2.49 | 0.128 | 254 | |
| 1.91 | 10.23 | 3.43 | 0.222 | 207 | |
| | | **Unirradiated DT-22 Thoria-Urania** | | | |
| 1.66 | 7.48 | 3.01 | 0.012 | 29 | |
| 2.00 | 11.24 | 3.66 | 0.129 | 91 | |
| 1.58[c] | 5.44 | 2.23 | 0.022 | 131 | Large viscometer |
| 1.90 | 10.04 | 2.56 | 0.120 | 119 | Large viscometer |

[a]Slope of linear portion of pseudo-shear diagram in region of 0 to 150 rate of shearing strain ($8v/g_cD$ units); viscosity of $H_2O$ taken as 0.936 centipoise at 23°C.

[b]Yield stress equals three-fourths of the wall stress extrapolated to zero shear rate.

[c]In heavy water.

In the experimental values noted above, it may be seen that the flocculation index, $\tau_y/\phi^3$, of the irradiated material is a factor of approximately 3 to 4 greater than that of the unirradiated material.

The square of the ratio of average particle diameters would give a factor of 5. The ratio of surface areas was 33/2 = ~16. Crystallite sizes are not presently available.

Thus it appears that the flocculation index of the slurries tested was less sensitive than direct proportionality to surface area or to the inverse square of particle diameters would require. Application of such a view to degradation effects associated with radiation doses which might be anticipated for realistic reactor breeder blanket slurries suggests that such slurries could be circulated at reasonable velocities and useful concentrations without unreasonable thickening.

Thoria-urania (two-component) and pure thoria (one-component) systems could well differ in the development of crystallinity in the particle by fission recoil mechanisms. If such a difference were realized, different responses of rheological properties to irradiation could be expected. In order to evaluate such possible differences, along with effects of several other parameters, the second in-pile slurry loop experiment was conducted.

# 11. In-Pile Loop Studies of Aqueous Thorium Oxide Slurries

H. C. Savage E. L. Compere J. M. Baker A. J. Shor

## Introduction

Investigation of the effect of reactor radiation on aqueous thoria slurries was continued in a second in-pile pump loop experiment, designated O-1-28S.[1,2] In this loop test a pure thoria dispersed in $D_2O$ was circulated in the loop which was operated in beam hole HN-1 of the Oak Ridge Research Reactor. Loop operation in-pile was from February 12 to May 15, 1962, during which the slurry was circulated for 2306 hr at a temperature of 280°C, accumulating irradiation equivalent to 1616 hr of operation at full reactor power (30 Mw). The slurry concentration of ~900 g of Th per liter at the operating temperature is comparable to that proposed for use as a fluid fertile material in the blanket region of a two-region aqueous thorium breeder reactor.

The primary objective of this loop experiment was to determine combined effects of pumping and reactor irradiation on a pure thorium oxide slurry ($ThO_2$ dispersed in $D_2O$) in which a significant quantity of $Th^{232}$ was converted to $U^{233}$ in a manner simulating that for a thoria slurry circulated in an aqueous thorium breeder reactor. It was planned to operate the loop in-pile for a sufficient length of time to convert 0.1 to 0.2 wt % of the $Th^{232}$ to $U^{233}$. This was estimated to require about seven months of exposure. Failure of one of the electrical wires to the circulating pump caused termination of the test after three months in-pile and precluded reaching this objective.

Pertinent observations and results of the loop operation and slurry behavior of in-pile slurry experiment O-1-28S are discussed below.

## In-Pile Operation

The second in-pile slurry loop experiment, designated O-1-28S, was operated in beam hole HN-1 of the ORR. Pure thoria dispersed in $D_2O$ was to be exposed at a considerably higher average flux than obtainable in the HB-2 hole of the LITR which was used for the previous slurry loop experiment, L-2-27S.[3-5] Substantial exposure of the solids to fission recoils would be realized as a result of the gradual ingrowth and fissioning of $U^{233}$. In addition to being an environment more closely paralleling an actual $ThO_2$ blanket this approach obviated any interaction between the mode of preparation and the fission recoil damage to the slurry solids that might have occurred in experiment L-2-27S, in which a mixed $ThO_2$-$UO_2$ material containing 0.4% enriched uranium was used. It was expected that the run would continue until levels of cumulative fission recoil exposure comparable to run L-2-27S were achieved.

A pure thoria, designated batch DT-46, prepared by oxalate precipitation and subsequently firing at

[1] E. L. Compere, H. C. Savage, J. M. Baker, and A. J. Shor, *Reactor Chem. Div. Ann. Progr. Rept. Jan. 31, 1962*, ORNL-3262, pp 123–25, and Figs. 16.1 and 16.2.

[2] H. C. Savage, E. L. Compere, J. M. Baker, and A. J. Shor, *In-Pile Studies of Aqueous Thoria Slurries as Potential Breeder Reactor Materials. Design and Operation of Loop O-1-28S.* (to be published as an ORNL report).

[3] E. L. Compere, H. C. Savage, A. J. Shor, and J. M. Baker, *Reactor Chem. Div. Ann. Progr. Rept. Jan. 31, 1962*, ORNL-3262, p 114.

[4] H. C. Savage, E. L. Compere, J. M. Baker, V. A. DeCarlo, and A. J. Shor, *In-Pile Loop Irradiation of Aqueous Thoria-Urania Slurry at Elevated Temperatures. Design and Operation of Loop L-2-27S*, ORNL-3222 (Jan. 29, 1962).

[5] H. C. Savage, E. L. Compere, J. M. Baker, V. A. DeCarlo, and A. J. Shor, *Reactor Chem. Div. Ann. Progr. Rept. Jan. 31, 1961*, ORNL-3127, pp 105–10.

1600°C was used in the preparation of the slurry. The thoria was suspended in $D_2O$ to a concentration of 900 g of Th per liter for the start of the in-pile operation. The initial mean particle size was 2.3 $\mu$.

A total volume of 1344 cc of slurry was circulated, of which 815 cc was exposed in the forward or high-flux zone of the loop, which was located closest to the reactor lattice. A maximum thermal neutron flux of about $10^{14}$ $nv$ was available in this zone. An average effective flux of $1.0 \times 10^{13}$ $nv$, over the entire 1344 cc of slurry volume, was obtained (see succeeding section). Flow through the main loop circuit and core was maintained at ~8 fps in conformity with present correlations of minimum dropout velocities.[6]

After installation in beam hole HN-1 of the ORR, slurry was circulated in the loop for 2036 hr, 1616 hr of which was with the reactor at its nominal operating power of 30 Mw. The experiment was terminated because of loss of power to the circulating pump which was caused by short circuiting of electrical leads in the loop–shield-plug connector region. The inaccessibility and high radiation levels in this region precluded repairs. Consequently the loop was removed and the run terminated.

At the termination of the run a flux of $5.8 \times 10^{19}$ $nvt$ (see succeeding section) was achieved. As a result of inbreeding of $U^{233}$, corresponding to a thorium burnup of 0.056 at. %, a fission fragment exposure of $2 \times 10^{16}$ fissions per gram of solids was received.

The pertinent operation conditions, loop parameters, and physical data for the thoria slurry are tabulated in Table 11.1. For the purposes of comparison similar data are also shown for the previous experiment, L-2-27S.[3–5]

It may be noted from the comparative tabulation that the previous experiment, L-2-27S, achieved about three times the fission recoil exposure at about one-third of the flux as a result of the 0.4% $U^{235}$ included in the mixed thoria-urania slurry.

## Slurry Circulation

The slurry was circulated at 280°C for a total of 2360 hr during both out-of-pile and in-pile periods of operation (2036 hr after installation in beam hole HN-1) accumulating 1616 hr of reactor irradiation at its nominal power of 30 Mw.

[6]D. G. Thomas, personal communication.

**Table 11.1. Parameters of In-Pile Slurry Loop Experiments**[a]

| | Experiment Number | |
|---|---|---|
| | L-2-27S | O-1-28S |
| Slurry | | |
| Material | Thoria—0.4% enriched urania, Pd | Pure thoria |
| Particle size, $\mu$ | 1.7 | 2.3 |
| Concentration, g of Th per liter | 980 | 910 |
| Loop | | |
| Slurry volume, ml | 900 | 1344 |
| Core volume, ml | 300 | 815 |
| Core flow, fps | 6 | 8 |
| Operation | | |
| In-pile, hr | 2200 | 2036 |
| Slurry circulation, hr | 3115 | 2360 |
| Average (maximum) flux | $0.22\ (1.0) \times 10^{13}$ | $1.0\ (10) \times 10^{13}$ |
| Fissions per gram of solids | $7 \times 10^{16}$ | $2 \times 10^{16}$ |
| $Pa^{233} + U^{233}$, % Th | 0.015 | 0.06 |

[a]Loop material, type 347 stainless steel; liquid, $D_2O$; atmosphere, $O_2$; temperature, 280°C.

Eighteen slurry samples were removed from the loop during the preirradiation test period; the concentration of slurry as determined from analyses of these samples was in agreement with the inventory values. When the loop was installed in the reactor it contained slurry at a concentration of ~900 g of Th per liter at the operating temperature of 280°C. Seven slurry samples were removed from the loop while in-pile (four after reactor irradiation had begun). Analyses of these samples indicated that all the thoria charged to the loop was suspended and circulating in the main loop stream. Thus no adverse effects on slurry circulation were seen as a result of the combined action of pumping and reactor irradiation. On three occasions the pump was stopped for periods of 4, 18, and 38 hr, and after each such flow interruption the thoria was resuspended without difficulty for continued loop operation.

### Measurements of Recombination of Hydrogen-Oxygen Mixtures in In-Pile Loop

Since the thorium oxide contained no enriched uranium it was anticipated that there would be very little if any radiolytic gas generated until a quantity of $U^{233}$ was produced under reactor irradiation. Therefore a recombination catalyst was not added to the slurry. As expected there was no detectable buildup of radiolytic gas pressure during irradiation.

It was of interest to determine the recombination activity inherent in the loop slurry. Measurements of the recombination rate of added $D_2$ and $O_2$ were made in the loop while operating at 280°C under an excess oxygen atmosphere on two occasions. The first measurement was made before exposure to irradiation. A recombination rate of 0.05 mole of $D_2$ per liter per hour (normalized to 100 psi $D_2$) was obtained. Subsequently the loop was placed in-pile. After 1032 hr of irradiation, it was possible during a reactor shutdown to inject $D_2$ gas into the oxygenated slurry and observe the recombination rate. Three values, ranging between 0.08 and 0.2 mole of $D_2$ per liter per hour (normalized to 100 psi $D_2$), were obtained.

Such rates plus expected recombination by gamma radiation[7] were more than sufficient to account for the maximum estimated $D_2$ production rates.

[7]C. J. Hochanadel, *Proc. Intern. Conf. Peaceful Uses At. Energy, Geneva* **1955**, 739 (1955).

### Corrosion

At the present time only the overall corrosion rate of the loop surfaces exposed to slurry has been determined. Based on the oxygen consumed (by corrosion) the generalized overall loop corrosion rate during in-pile operation was calculated to be 0.6 mil/yr during the 2036 hr of in-pile operation and less than 1 mil/yr during the 324 hr of preirradiation operation. Thus the generalized rate was quite low, and the corrosion rate did not appear to be enhanced by reactor irradiation.

Forty-eight corrosion test specimens of Zircaloy-2, titanium, and type 347 stainless steel were exposed to the circulating slurry at two velocities (11 and 19 fps) and at two neutron flux levels. Examination of these specimens has been postponed indefinitely due to the cutback of the program on studies of aqueous thorium oxide slurries.

### Effects on Slurry Particles

In addition to out-of-pile slurry samples, a total of four irradiated samples were obtained from the loop experiment. Analysis of these samples permitted a detailed account of the in-pile behavior of the slurry. The effects of irradiation and circulation developed progressively as the experiment continued. The mean particle size in the original material was about 2.3 $\mu$. The particles degraded to about 1.5 $\mu$ mean diameter in the fourth in-pile sample, while crystallite size as determined by x-ray line broadening techniques decreased from >2000 to about 1000 A. The resultant increase in surface area from about 1 to 24 $m^2/g$ was larger than expected from the data on crystallite size and mean particle size.

The trends in surface area and particle size are shown in Fig. 11.1. It will be noted that there is little change in particle size distribution in the region of 1.5 $\mu$ and above, but an increase in the amount of material below 1.5 $\mu$ in size. Surface area increased steadily.

Figure 11.2 compares particle size data from this experiment and the previous experiment, L-2-27S, as a function of fission recoil exposure. It appears that particle size degradation was somewhat less severe in the pure thoria experiment, O-1-28S, as shown in Fig. 11.3. After an initial decrease, crystallite size showed little further change with fission recoil exposure. The rate of

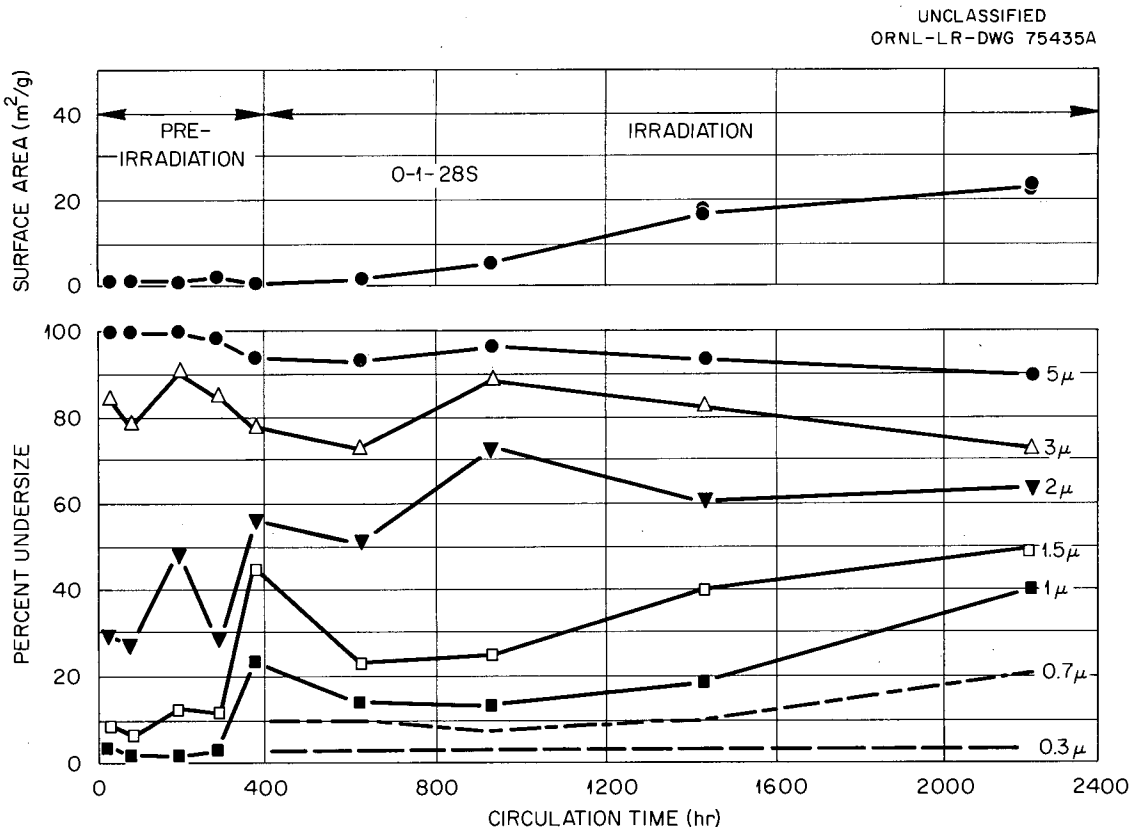


**Fig. 11.1. Effect of Irradiation and Circulation on Slurry Particle Size and Surface Area.**

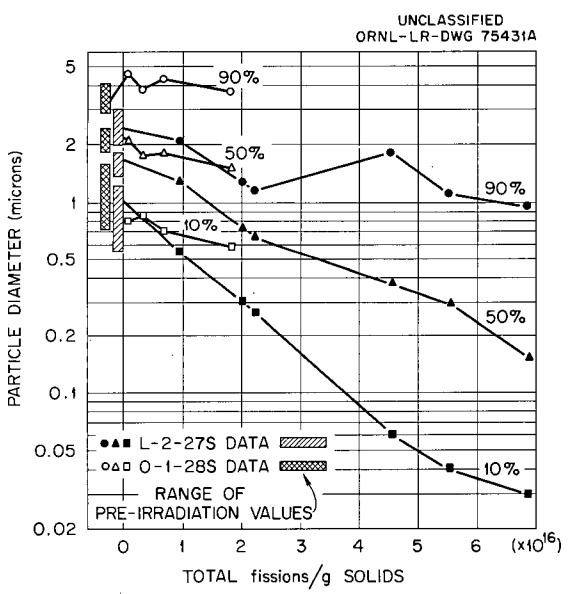


**Fig. 11.2. Particle Diameter at 90, 50, and 10% Undersize vs Total Fissions in In-Pile Slurry Loop Experiments.**

increase of surface area (Fig. 11.4) appears greater in the second (pure-thoria) experiment, indicating that the pattern of degradation in the thoria-urania was different from that of the pure thoria. In addition, while surface areas of irradiated materials in both runs consistently ran above the maximum theoretical value (sphere or cube) for a given mean crystallite size, the discrepancy appeared more prominent in the pure-thoria experiment.

## Determination of Average Slurry Flux and Total Fissions

The determination of the average flux received by the total slurry was based on the protactinium activity in the slurry samples. Reactor shutdowns and changes in power were taken into account. An effective thorium cross section of 9.6 barns was used, as determined by the joint irradiation of thoria and cobalt in the hydraulic rabbit tube facility in the adjacent beam hole HN-3. A 2200-m/sec cobalt activation cross section of 36.7

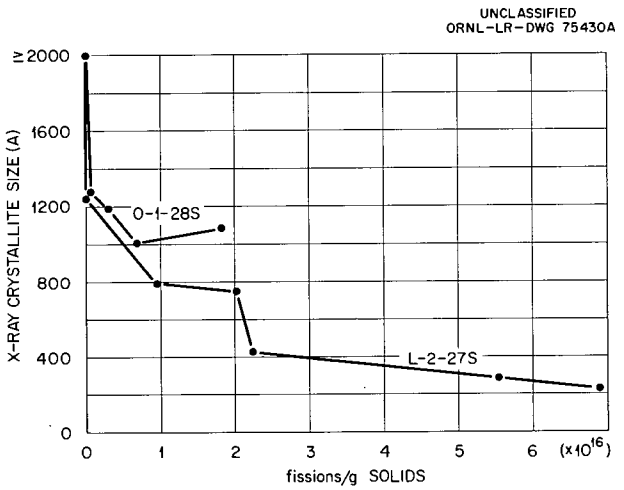


Fig. 11.3. X-Ray Crystallite Size vs Total Fissions.

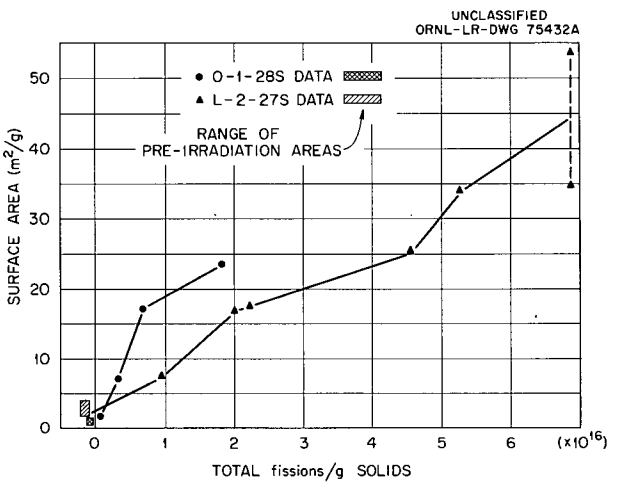


Fig. 11.4. Surface Area vs Total Fissions.

barns was used. Thus the protactinium-determined loop flux values, except for possible flux-hardening effects, were essentially cobalt-based nominal 2200-m/sec values.

Mean total loop fluxes thus obtained by the various samples were as follows:

| In-Pile Hours After Start of Irradiation | Mean Total Loop Flux ($nv$) |
|---|---|
| 226 | $1.02 \times 10^{13}$ |
| 584 | $0.94 \times 10^{13}$ |
| 1064 | $0.92 \times 10^{13}$ |
| 1686 | $1.08 \times 10^{13}$ |

Flux was also determined by the activation of cobalt wire flux monitors attached to the loop core coils. At a mean distance of 2.0 in. from the reactor tank wall, the average flux received by an axial 0.5-in. segment was $2.6 \times 10^{13}$ $nv$. At a mean distance of 5.5 in. the average flux received by an axial 0.5-in. segment was $1.1 \times 10^{13}$ $nv$. The average flux integrated over the loop core was $1.68 \times 10^{13}$ $nv$, which when averaged over the loop slurry volume gives a mean total loop flux of $1.02 \times 10^{13}$ $nv$.

A mean flux of $1.0 \times 10^{13}$ $nv$ for the 1616 effective radiation hours developed in the experiment gives a neutron dose of $5.8 \times 10^{19}$ $nvt$. At a cross section of 9.6 barns, a total thorium conversion of 0.056% is calculated.

The total fissions developed in the thoria solids as a result of the fissioning of inbred $U^{233}$ were estimated by comparison of the determined activity of fission products in the samples with calculated ratios of total fissions to given fission product activity for the respective samples. A computer code, NUCY,[8] was employed to calculate total fissions and fission product activity at an assumed flux of $1 \times 10^{13}$ $nv$. Values in agreement with the NUCY results were obtained by a solution of the equations on an electronic analog computer. The reactor operational schedule was taken into account. Zirconium-95 (63.3-day), cerium-144 (290-day), and cesium-137 (30-year) activities were employed.

[8]D. R. Vondy, *Development of a General Method of Explicit Solution to the Nuclide Chain Equations for Digital Machine Calculations*, ORNL TM-361 (Oct. 17, 1962).

In the case of cesium determinations, a weighted combination of activities in the liquid and solid phases was used. Values of total fissions thus obtained are shown in Table 11.2.

It is estimated by extrapolation of the data from Table 11.2 that at the end of the irradiation (2013 hr in-pile, 1616 hr irradiation) a total of approximately $2 \times 10^{16}$ fissions per gram of solids was developed.

**Table 11.2. Fission Dose in Loop Solids, Based on Radiochemical Data from Successive Slurry Samples**

| In-Pile Hours After Start of Irradiation | Total Fissions per Gram of Solids[a] | | |
|---|---|---|---|
| | $Zr^{95}$ | $Ce^{144}$ | $Cs^{137}$ |
| 226 | $0.06 \times 10^{16}$ | $0.20 \times 10^{16}$ | $3.4 \times 10^{16}$ |
| 584 | $0.33 \times 10^{16}$ | $0.29 \times 10^{16}$ | $0.34 \times 10^{16}$ |
| 1064 | $0.51 \times 10^{16}$ | $0.95 \times 10^{16}$ | $0.59 \times 10^{16}$ |
| 1686 | $1.2 \times 10^{16}$ | $2.0 \times 10^{16}$ | $2.3 \times 10^{16}$ |
| 2013 (shutdown) | | $2 \times 10^{16}$ [b] | |

[a]Based on given fission product nuclide.
[b]Average value by extrapolation.

# 12. Construction and Out-of-Pile Testing of Third In-Pile Slurry Loop Experiment

H. C. Savage E. L. Compere J. M. Baker A. J. Shor

Because of the early termination of loop O-1-28S, a third slurry loop, designated O-1-29S, was constructed. This third loop was modified to increase the radiation dose and minimize the operating time required to convert a significant quantity of the $Th^{232}$ to $U^{233}$. The same core configuration of loop O-1-28S was retained,[1] but more and tighter wound coils were used, which increased the core volume from 800 to 1420 cc. This increased the fraction of slurry in the core (high flux region) to 73%, as compared with 60% in loop O-1-28S. Modifications to the connector section between the loop and shield plug were also made to reduce the possibility of water leakage into this section. Water leakage into this connector (through which all electrical and thermocouple leads pass) caused a short circuit and failure of the electrical lead to the pump in O-1-28S.

Assembly and satisfactory out-of-pile testing (including 100 hr of thorium oxide slurry circulation) of this third loop were completed in December 1962, and installation in beam hole HN-1 of the ORR was scheduled for early January 1963. However, in-pile operation of this loop was canceled when the aqueous thoria slurry program was stopped.

[1] H. C. Savage, E. L. Compere, J. M. Baker, and A. J. Shor, "Second In-Pile Loop Experiment," *Reactor Chem. Div. Ann. Progr. Rept. Jan. 31, 1962*, ORNL-3262, p 123.

# 13. Surface Chemistry of Aqueous Systems

C. H. Secoy

Insoluble metallic oxides, either in bulk form or as surface films on metals, are common materials in a wide variety of applications. They are of special interest in materials development in nuclear science and other high-temperature applications. The surfaces of some oxides have been shown to be never completely free of chemisorbed hydroxyl groups except under the most extreme circumstances. Therefore an intimate knowledge of the interaction of water, gaseous or liquid, with oxides as a class or with particular oxides as individuals should be of value in the development of a variety of materials applications.

Our work so far has been limited to the study of thoria, a material of major current interest. The principal activities have involved continued studies of ion adsorption (especially hydrogen ion) on thoria samples of various degrees of porosity and continued determination of heats of immersion of thoria in water at 25°C, as a function of the temperature history of the material, of outgassing techniques, and of surface area. Progress in these topics is reported in the following sections.

Studies of the electrokinetic transport properties of thoria in aqueous media, including surface conductance, have recently been reactivated after a dormancy of nearly two years. The initial effort has to do with the fabrication, from a zero-porosity thoria pellet, of a capillary with dimensions which are physically measurable as well as optimized for the alternate determination of streaming potential, electroosmotic flow, and cell resistance. Determination of sets of all four measurements at identical environmental conditions should contribute to establishing the validity of assumptions that are required for the interpretation of data obtained from loosely packed powder-plug cells.

Work on the design and construction of the 250°C–high-pressure adiabatic calorimeter has continued, with the major effort located in the Instrumentation and Controls Division. The mechanism for bulb breaking at constant volume has been completely redesigned as a consequence of the discovery that a portion of the heat of wetting of thoria was not released immediately on wetting. Final design decisions have been made for all parts of the calorimeter except the external bath materials and temperature control. Design development work is in progress in this area. All instrumentation except the bath control is available and several of the components are in preliminary operation.

## IONIC ADSORPTION EQUILIBRIA

F. H. Sweeton

Previously reported work[1] showed reproducible adsorption of $HNO_3$ on a particular sample of $ThO_2$ under a given set of conditions. Measurements have now been made of the adsorption of HCl by a different type of $ThO_2$. The significance of the measurements has been improved by a study of the effectiveness of washing prior to adsorption, by a determination of the blank cell adsorption, and by restandardization of the pH and conductance cells with dilute HCl in the concentration range 0.01 to 1.0 m*M*.

### Adsorption by Fused $ThO_2$

**Materials.** – The $ThO_2$ for this test was obtained by grinding and classifying a sample that had

[1] C. H. Secoy, F. H. Sweeton, and H. F. Holmes, *Reactor Chem. Div. Ann. Progr. Rept. Jan. 31, 1962*, ORNL-3262, pp 99–101.

been melted in an electric arc during its manufacture. It is listed as sample B in Table 13.1; sample A, used in the earlier work, is also given for comparison. As before, water used in the adsorbate solutions was redistilled to remove $CO_2$ and $NH_3$. One sample was tested and found to give a pH reading of $\sim$6.7 and a specific conductance of $\sim 0.2 \times 10^{-6}$ ohm$^{-1}$ m$^{-1}$. Commercial standard solutions of NaOH and HCl were used in making up the adsorbate solutions.

**Apparatus.** – The adsorption cell was the same as before[1] except for a slight modification to give more positive protection from atmospheric $CO_2$ when adding $H_2O$ and HCl solutions. The inside surfaces of the cell consisted of Pyrex glass and Teflon. As before it had a Millipore membrane (1000-A pores) for use in filtering.

A paint shaker was again used to put the solid into suspension for equilibrating it with a solution. The shaker was used only for 2 min at a time to avoid degrading the solid particles. A motor drive that rotated the cell in an end-over-end fashion at about 60 rpm was used to maintain the solid in suspension for further equilibration.

A new pH cell was used. Streams of filtrate and of concentrated KCl solution formed a flowing liquid junction in a block of Lucite (methyl methacrylate resin). A glass electrode and a calomel electrode, which were sealed into the block with O-rings, made contact with the two streams. The cell was periodically standardized with commercial buffer solutions at pH's of 2, 4, and 7.

A new electrical conductivity cell was also employed. Like the earlier cell it was constructed of platinum and Pyrex glass, but its cell constant was lower (15 cm$^{-1}$), which gave greater precision at low conductivities. The potential of the pH electrodes was opposed by one from a precision potentiometer, and the difference was detected by a vibrating-reed electrometer (Applied Physics Corp., model 30) which was connected to a recorder. The resistance of the conductance cell was read on a Jones ac bridge.

**Procedure.** – A known amount of $ThO_2$ sample B was put into the adsorption cell at the start of run 6. The $ThO_2$ was washed two times by adding 0.01 *M* NaOH, shaking, and then filtering off the wash solution. Next it was washed similarly with seven batches of the redistilled water. Then the process was repeated adding known amounts of HCl to the water. The pH and conductivity of each filtrate were measured. Occasionally during this part of the experiment, water alone was added in order to approach equilibrium by desorption. In run 7 a similar procedure was followed, starting with the $ThO_2$ left in the cell from the previous run.

**Discussion.** – The adsorptions in runs 6 and 7 were calculated from the amounts of HCl added, the weights of the filtrates, and the measured pH's. These calculated adsorptions are plotted in Fig. 13.1. The average of the similar data for the earlier runs 4 and 5 is included for comparison.

**Table 13.1. Comparison of $ThO_2$ Samples**

| | Sample *A* | Sample *B* |
|---|---|---|
| Source | Decomposition of $Th(C_2O_4)_2$ | Arc-fused $ThO_2$ |
| Specific surface area ($N_2$), m$^2$/g | 6.87 | 1.36 |
| Weight of sample, g | 7.2 | 14.81 |
| Percentage recovered after tests | 93.7 | 99.5 |
| Effective particle diameter by sedimentation, A | 2000–3000 | 7,000–15,000 |
| Effective particle diameter by surface area, A | 900 | 4400 |
| Calculated milliequivalents of surface[a] | 1.05 | 0.429 |

[a]Using $N_2$ surface area by BET method assuming four monovalent sites on an area equal to one face of the $ThO_2$ unit cell; this is equivalent to 2.07 monovalent sites per adsorbed $N_2$ molecule.

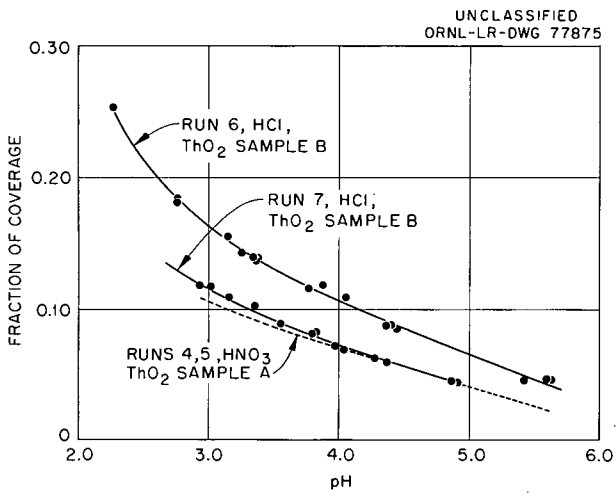


**Fig. 13.1. Acid Adsorption on Thoria.**

Each of the runs is by itself reasonably self-consistent. The spread of the points in either run is not large, even though some of the points were approached from the adsorption side and some from the desorption.

However, the runs differ significantly from each other, the adsorption of run 6 being about 50% greater. A small part of this difference can be explained as due to less effective washing, as will be mentioned later when the use of conductivity to estimate washing efficiency will be discussed, but the reason for the rest of the difference is not understood.

Surprisingly, there is no large difference between these runs, where the $ThO_2$ was presumably free of internal surface, and the earlier runs, where the $ThO_2$ presumably contained appreciable internal surface. It was expected that the internal surface would have a low adsorption capacity, particularly at low ionic concentrations in the solution, and that the observed adsorption when averaged over the whole surface (determined by $N_2$ adsorption) would appear low. A tentative explanation for the observed results is that the internal surface of $ThO_2$ sample A actually was a smaller part of its total surface than had been indicated by comparing the area calculated from $N_2$ adsorption with that calculated from the sedimentation rate.

## Blank Adsorption Run

**Procedure.** – Run 9 was a blank with no $ThO_2$ in the adsorption cell. A Millipore filter with 1000-A pores was present, however, just as in the earlier $ThO_2$ runs. The cell was treated with NaOH three times and washed with water six times. Then it was treated with 0.02 m*M* HCl nine times, with 0.09 m*M* HCl four times, and with 0.9 m*M* HCl three times. As before, the pH and conductance readings of each filtrate were taken.

**Standardization of pH Electrodes.** – The pH readings of the first filtrates (only a little HCl had been added) were high, as though some of the added acid had been adsorbed in the cell. The later readings were used to standardize the pH electrodes in terms of actual HCl concentration and differed by 0.01 to 0.03 pH unit from what was expected on the basis of standard pH buffers. These direct standardizations were used in calculating the adsorption data of runs 6 and 7.

**Constant of Electrolytic Conductance Cell.** – The data of the blank run gave an independent confirmation of the conductivity-cell constant. The new readings agreed, within 2%, with the value determined earlier with 5 m*M* KCl solution.

**Adsorption by Cell and Filter.** – The measured conductivities of the first filtrates after addition of acid to the cell was started during adsorption runs were too large to be explained by the concentration of acid indicated by the pH cell. Presumably this excess conductivity was due to the salt formed by the reaction of the acid with the sodium ion remaining in the system at the end of the washing process. This type of analysis of the blank run indicated that the adsorption cell with its filter membrane neutralized 1.4 $\mu$eq of the added acid; this corresponds to about 0.4% of the total sites expected to be available in the $ThO_2$ sample used in runs 6 and 7. Similar analyses of runs 6 and 7 indicated that, respectively, about 3.5 and 2.0 $\mu$eq of the acid were neutralized by the cell and by the sodium ion remaining on the $ThO_2$. These corrections, if applied to the data of these runs in Fig. 13.1, would lower the respective adsorption curves by 0.010 and 0.005 unit. Thus in these particular tests, the washing, while not complete, did not appear to contribute an unduly large error.

### Fusing of $ThO_2$ in a Plasma Torch

An effort has been made to fuse $ThO_2$ particles in the flame of a plasma torch[2] to produce spheres, which would be ideal for adsorption tests because of their lack of internal surface. The first approach was an attempt to inject $ThO_2$ into the flame as a stream of aqueous slurry, since peptized slurries were not expected to clog small tubes used to carry the slurry to the flame. However, it was found that an injected stream of water broke into droplets too large to be vaporized during residence in the flame. Some exploratory tests were then made using an air suspension of a $ThO_2$ material prepared by the Houdry Process Corp.[3] several years ago by forming gels of $ThO_2$-sol droplets suspended in oil. The spherical particles were easy to handle as an air suspension. The products from these tests are now being studied in an effort to determine the proper operating conditions for melting all the particles without appreciable vaporization.

## THE HEAT OF IMMERSION OF THORIUM OXIDE IN WATER

H. F. Holmes

In the past decade there has been a considerable increase in the number of reported heat-of-immersion measurements. This increase can be attributed to two main factors. The first of these is experimental and can be traced to the development of thermistors and high-gain breaker-type amplifiers. These two developments permit relatively easy construction of the sensitive calorimeters required for these measurements. The second, and most important, factor is the usefulness of heat-of-immersion data. This type of data has been employed in the study of a wide variety of subjects in the general field of surface chemistry. Perhaps the most valuable results are obtained when heat-of-immersion measurements are coupled with adsorption isotherms. In this manner one can obtain the thermodynamic functions for the adsorbed molecules. This fact alone is sufficient reason for heat-of-immersion measurements as a powerful tool in the study of any solid surface.

### Experimental

The calorimeter used for making these measurements is shown in Fig. 13.2. With the exception of the stirrer and sample holder, which are brass, the entire calorimeter was constructed from copper. All metal parts were gold-plated. A reaction was initiated by manually lifting the sample holder assembly. This crushed a sample bulb against the sample breaker. Any one of the five samples could be selected by manual rotation of the sample holder assembly. A cooling coil was used for adjusting the temperature of the calorimeter. O-rings effectively provided airtight seals, as evidenced by no difficulty with evaporation and condensation.

The calorimeter was suspended by nylon rods inside a gold-plated brass submarine jacket. The dead-air gap between the calorimeter and the submarine jacket plus the nylon inserts in the stirrer and sample holder shafts reduced heat exchange to a desirable level. This entire assembly was suspended in a constant-temperature water bath set at 25.0°C.

The electrical circuits used with the calorimeter are shown in Fig. 13.3. Basically, the temperature measuring circuit is a very simple one which utilizes a 100-ohm thermistor as the sensing

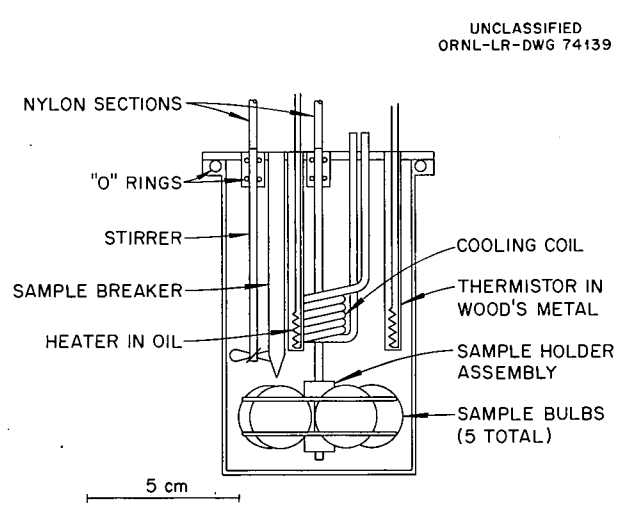


**Fig. 13.2. Calorimeter for Heat-of-Immersion Studies.**

[2]The plasma torch was kindly made available by Ray Wymer of the Chemical Technology Division.

[3]Supplied by John McBride of the Chemical Technology Division.

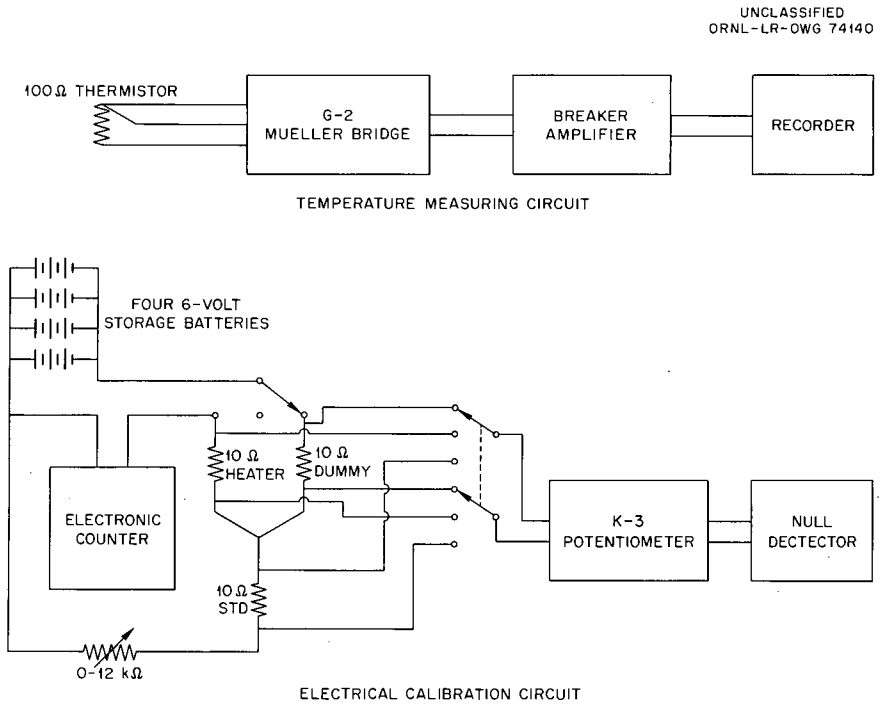


**Fig. 13.3. Instrumentation for Heat-of-Immersion Studies.**

element. The unbalance signal from the Mueller bridge was amplified by a high-gain breaker amplifier and displayed on a strip-chart recorder to give a permanent time-temperature record. In general use, the gain of the amplifier was adjusted so that a 0.001-ohm change in the resistance of the thermistor gave a 20-mv deflection on the recorder. With this gain, full scale on the recorder corresponded to approximately $1.6 \times 10^{-3}$ °C.

The lower part of Fig. 13.3 is a simplified block diagram of the electrical calibration circuit. This is a rather common arrangement in which the heat input of the calorimeter is determined from the voltage drops across the standard resistance and the calibration heater and from the duration of the heating period. The only unique feature of this circuit is the use of an electronic frequency counter, connected directly across the calibration heater and the storage batteries, to time the duration of the heating period. With this arrangement the time-interval measurements were accurate to 0.001 sec. As is usual, the accuracy and sensitivity of the electrical calibration circuit are much better than the corresponding quantities for the temperature measuring circuit.

Some of the characteristics of the loaded calorimeter and its associated instrumentation are: a thermal-leakage constant of approximately $2.5 \times 10^{-3}$ min$^{-1}$, attainment of an isothermal condition within 1 part in $10^4$ two minutes after a heat input, a short-term sensitivity of approximately 0.009 j, which is about 8 $\mu$deg in terms of temperature sensitivity, and, for a reaction period of 1 hr, a useful sensitivity of at least 0.3 j.

The thorium oxide samples used in this work were prepared by thermal decomposition of thorium oxalate which had been precipitated from a nitrate solution with oxalic acid. Four samples were prepared from the same lot of thorium oxalate. The entire lot was first calcined at 650°C for 4 hr. Portions of this were then calcined at 800, 1000, and 1200°C for an additional 4 hr.

The BET nitrogen surface area and the sedimentation particle[4] size are shown in Table 13.2. While calcining at the higher temperatures resulted in a marked decrease in specific surface area, there was very little increase in particle size.

[4]The surface-area and particle-size measurements were performed by the Analytical Chemistry Division.

Table 13.2. Surface Area and Particle Size of $ThO_2$ Samples

| | | | | |
|---|---|---|---|---|
| Calcining temperature, °C | 650 | 800 | 1000 | 1200 |
| Calcining time, hr | 4 | 4 | 4 | 4 |
| Specific surface area, $m^2/g$ | 14.7 | 11.5 | 5.64 | 2.20 |
| Geometric mean Stokes diameter, $\mu$ | 2.63 | 2.67 | 2.72 | 2.97 |
| Geometric standard deviation | 1.37 | 1.37 | 1.38 | 1.39 |

From these data, one can conclude that, in all cases, the majority of the surface is internal. In other words, most of the surface is the result of cracks and crevices in the particles, and the particles themselves are agglomerates of much smaller crystallites.

The samples, contained in thin-walled glass sample bulbs, were outgassed for 24 hr at temperatures ranging from 100 to 500°C and were sealed off under vacuum. With one exception all of the samples were outgassed at a pressure of approximately $1 \times 10^{-5}$ mm Hg. One set of three samples was intentionally outgassed at a pressure of $3.8 \times 10^{-3}$ mm Hg. There was no difference in the results obtained with these samples and the results from the samples outgassed at the lower pressure.

Some of the samples were observed to have a light-gray color after the outgassing treatment. This was more noticeable with the samples of low specific surface area that had been outgassed at the higher temperatures. Within experimental error the sample in which this coloration was observed gave the same results as samples in which the color was absent. Previous reports[5] of discoloring on outgassing other oxides have attributed it either to a loss of lattice oxygen or to the presence of organic impurities. In either case, abnormally high heat-of-immersion results were reported.

Six to eight electrical calibrations and five heat-of-immersion measurements were made for each loading of the calorimeter. The temperature rise for an experiment was obtained by a simple extrapolation of the initial and final drift rates. Electrical calibrations always agreed within about 0.1% and were independent of the rate of heating and the total heat input. It was necessary to apply three corrections to the heat-of-immersion measurements. These were the heat of bulb breaking, the heat produced by the mechanical motion of the sample holder, and the correction for the vaporization of water into the void space in the sample bulb. Reproducibility of the results for a given sample was generally about 2%. Accuracy of the heat measurements was about 1% for all samples.

## Results and Discussion

Although the outgassing technique was not designed to yield accurate weight-loss measurements, a reasonably good estimate of the weight loss could be obtained from the weighings necessary to determine the sample weight. Figure 13.4 shows these weight losses as a function of outgassing temperature. The same general trend was

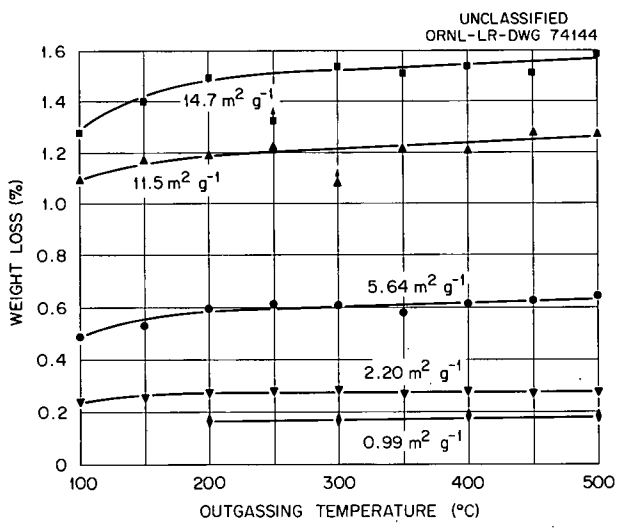


Fig. 13.4. Weight Loss for $ThO_2$ Outgassed for 23 hr at $\approx 1 \times 10^{-5}$ mm Hg.

[5]W. H. Wade and N. Hackerman, *J. Phys. Chem* **65**, 1681 (1961); C. M. Hollabaugh and J. J. Chessick, *J. Phys. Chem.* **65**, 109 (1961).

observed with all of the samples, that is, a relatively large increase in weight loss between 100 and 200°C, followed by a very gradual increase between 200 and 500°C. In all cases the weight loss at 100°C was about 80% of the weight loss at 500°C. Most, if not all, of the adsorbed material was carbon dioxide and water. Both of these substances were clearly visible in the liquid-nitrogen trap on the vacuum system. Additional proof of this can be obtained from the infrared spectra of the surface of thorium oxide samples which have been exposed to the laboratory atmosphere.[6] These spectra have bands which are due to the presence of water and carbon dioxide.

Within experimental error, the weight loss at any given outgassing temperature was directly proportional to the specific surface area. This is good evidence that there has been no change in the relative specific surface areas and that, on a unit area basis, the amount of material adsorbed has been independent of the specific surface area.

The total heats of immersion of the samples are shown in Fig. 13.5 as a function of outgassing temperature. These data are referred to as total heats of immersion because, as discussed later, they can be divided into two distinct parts. It is immediately apparent that there is a marked difference in the behavior of these four samples. At this point it is well to reemphasize the fact that the only difference in these four samples is the original calcining temperature, which resulted in a decreased specific surface area for the higher calcining temperature.

All of the samples showed a general increase in the heat of immersion with increasing outgassing temperature. Values for the 1200°C samples are much smaller than the corresponding values for the other samples and are also much less dependent on outgassing temperature. Since this sample has the lowest specific surface area, one could suppose that the heat-of-immersion values would be a monotonic function of the specific surface areas. That this was not the case can be observed from the behavior of the remaining three samples. The results for the 5.64-$m^2/g$ sample are larger than those for the 14.7-$m^2/g$ sample at lower outgassing temperatures but smaller at higher outgassing temperature. The largest heats of immersion were obtained with the sample which was calcined at 800°C. This was true at all outgassing temperatures except at 500°C, where this sample and the sample calcined at 650°C had approximately equal heats of immersion.

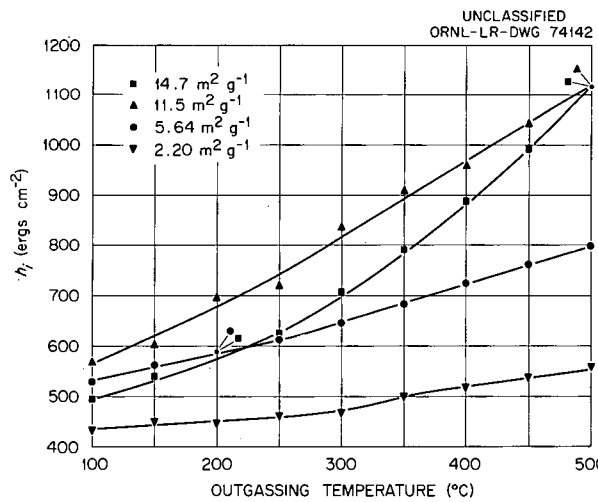


**Fig. 13.5. Total Heat of Immersion of $ThO_2$ in Water at 25°C.**

By making a few assumptions one can estimate the net integral heat of adsorption in the more conventional units of calories per mole of adsorbate. These assumptions are concerned primarily with the heat of immersion of the monolayer-covered solid, the fraction of the surface available to water molecules, and the area occupied by an adsorbed water molecule.

The estimated values of the net integral heat of adsorption of water on thorium oxide, as obtained from this heat-of-immersion data, range from about 7 to 22 kcal/mole, depending on the specific surface area and outgassing temperature. Considering the assumptions involved in these estimates and that this is an average value for the entire first monolayer, this is excellent evidence that chemisorption is occurring. This is what one would expect from a consideration of the observed infrared spectra, since they have bands corresponding to surface hydroxyl groups. From rather limited adsorption data obtained by other workers[7]

[6] L. G. Tensmeyer and M. E. Wadsworth, *Quantitative Determination of Adsorbed Sulfate on Thoria by Means of Infrared Spectroscopy*, Technical Report No. 3, University of Utah, 1959.

[7] A. L. Draper and W. O. Milligan, *Structure and Surface Chemistry of Thorium Oxide*, summary report, The Rice Institute, 1959; A. G. Oblad, S. W. Meller, and G. A. Mills, p 309 in *Proceedings of the Second International Congress of Surface Activity*, vol 2, Academic Press, New York, 1957.

estimates of the heat of adsorption of water on thorium oxide range from about 15 to 45 kcal/mole and are highly dependent on pretreatment, fraction of the surface covered, and temperature.

A comparison of the time-temperature curves for the oxide samples with those for electrical calibration disclosed the fact that in most cases not all the heat was liberated within 2 to 4 min after immersing the sample. The slowly liberated heat was determined from the observed time-temperature curve by calculating what the time-temperature curve would have been if all of the heat had been liberated immediately. The difference between the observed and calculated time-temperature curves at any time was directly related to the heat liberated after that time. It seemed desirable to extrapolate this slow heat back to the time of immersing the sample so that the total heat of immersion could be divided into a slow and an immediate part. From the shape of the observed time-temperature curves it seemed reasonable to assume that the slow heat was an exponential decay process.

Figure 13.6 is a semilog plot of the heat per unit area liberated after any time after immersing the sample. It is evident from the linearity of the plots that, for the purposes of extrapolation, the assumption of an exponential decay process is adequate, although at the present time there is no theoretical reason for assuming such a process. The trend observed in this plot, which happens to be for the 11.5-$m^2/g$ sample, was the general rule. That is, the magnitude of the slow heat increased with increasing outgassing temperature.

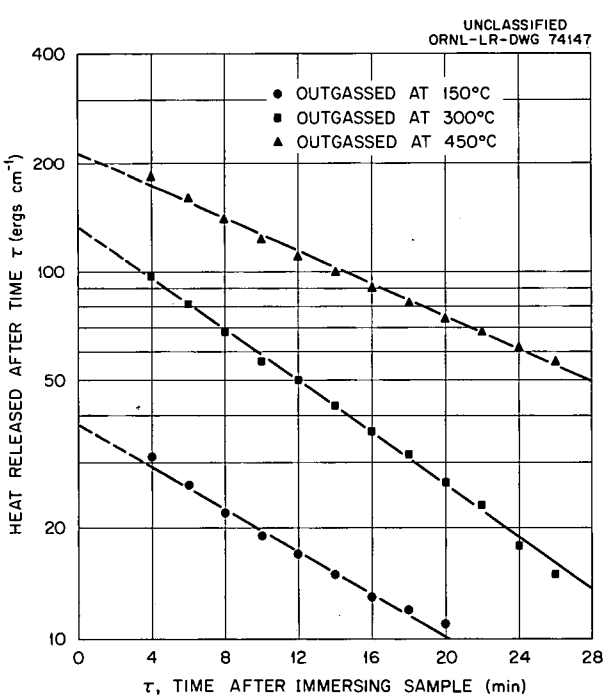


**Fig. 13.6. Heat Released After Time $\tau$.**

For each measurement in which slow heat was observed, it was necessary to construct a plot such as that shown in Fig. 13.6. The linearity of the plots was not limited to the time interval shown in Fig. 13.6, but the time involved was dependent on the particular sample used. In many cases it was necessary to observe the time-temperature curve for as long as 90 min in order to obtain the correct drift rate as inferred from previous experiments in which no heat was being liberated.

In Fig. 13.7 the total slow heat of immersion per unit area is plotted as a function of outgassing temperature. These values were obtained by a linear extrapolation of the semilog plots to the time of immersing the sample. The drastically different behavior of the different samples is quite evident from this plot. Within experimental error no slow heat was ever observed with the 2.2-$m^2/g$ sample. The 5.64-$m^2/g$ sample liberated the smallest quantity of slow heat, and this heat was relatively independent of outgassing temperature when compared with the other two samples. The relative behavior of the 11.5- and 14.7-$m^2/g$ samples was approximately the same as that observed with the total heats of immersion. The relative uncertainty in the slow heat values is much larger than with the total heats of immersion and is estimated to be on the order of 10%.

The half-lives for the decay of the slow heat were in the same order as the magnitudes of the slow heat. These were 5.3, 10.7, and 7.2 min for the 5.64-, 11.5-, and 14.7-$m^2/g$ samples respectively. Within experimental uncertainty the half-life of the slow heat was independent of the outgassing temperature.

Slow heats of immersion have previously[8] been reported for the immersion of alumina and silica in water. For the alumina-water system both the quantity of slow heat and its half-life increased with increasing outgassing temperature. For the

[8]C. A. Guderjahn *et al.*, *J. Phys. Chem.* **63**, 2066 (1959).

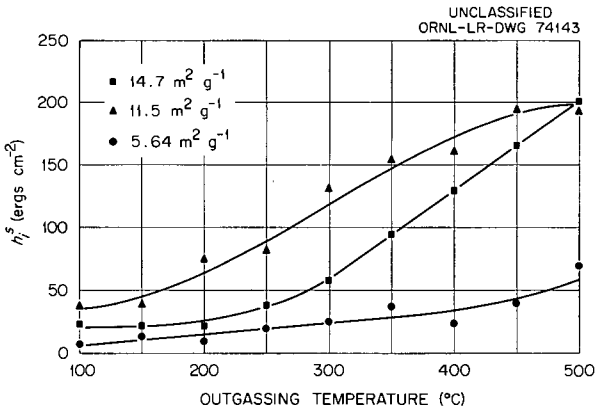


**Fig. 13.7. Slow Heat of Immersion.**

silica-water system only one outgassing temperature was reported.

By subtraction of the slow heat from the corresponding total heat of immersion one can readily obtain the heat per unit area which is released immediately on immersion of the sample. These quantities are shown as a function of outgassing temperature in Fig. 13.8. The immediate heat of immersion for the 2.2-$m^2/g$ sample is, of course, equal to the total heat of immersion and is included for purposes of comparison. With one exception the relative behavior of the different samples with respect to the immediate heats of immersion is the same as that observed with the total and slow heats of immersion. The one exception is that the results for the 11.5- and 14.7-$m^2/g$ samples are more nearly equal than the corresponding values for the slow and total heats of immersion. The fraction of the total heat which is released immediately varies from about 98 to 81% of the total heat of immersion. This fraction is largest for the 5.64-$m^2/g$ sample, smallest for the 11.5-$m^2/g$ sample, and decreases with increasing outgassing temperature.

It is quite evident that these four samples of thorium oxide have remarkably different energetics with respect to the thorium oxide–water interface. Not only is the behavior different but it is also consistently observed with the total, slow, and immediate heats of immersion. It would be valuable to have a model which would elucidate both the mechanism and the energetic behavior observed with this system.

One of the most popular concepts used in recent years to interpret heat-of-immersion data for simple oxides in water has been to postulate the existence of surface hydroxyl groups.[9] This is now taken to be generally true, especially in view of the infrared spectra of such surfaces. The supposition is that these surface hydroxyls may be dehydrated at the higher outgassing temperatures, resulting in sites which may or may not be strained. On exposure to water, the surface oxide groups resulting from dehydration may hydrolyze rapidly, slowly, or not at all, depending on the substrate and the outgassing temperature. Another useful concept has been to postulate the existence of two types of adsorption sites on metal oxides. The concept of two different adsorption sites has, for example, been used to interpret the adsorption of carbon dioxide on thorium oxide.[10]

It is quite conceivable that, by employing the above concepts, one could postulate a model which would account for the behavior of the system under discussion. At the present time, however, the authors do not believe that the experimental data are sufficient to warrant the postulation of such a model. In particular, it is believed that the complete interpretation of this data will require at least two additional types of experimental data. One is the adsorption isotherms for water on these same samples after the samples have been outgassed under the identical conditions used in this work. The other is the determination of the heats of immersion of samples with known amounts of water adsorbed on the surface. Both types of experiments are being initiated.

---

[9] A. C. Zettlemoyer, *Chem. Rev.* **59**, 937 (1959).

[10] C. H. Pitt and M. E. Wadsworth, *Carbon Dioxide Adsorption on Thoria*, Technical Report No. 1, University of Utah, 1958.

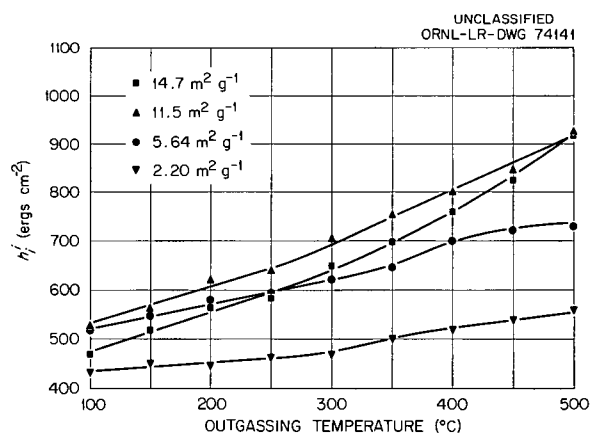


**Fig. 13.8. Immediate Heat of Immersion.**

# 14. Phase-Equilibrium Studies in the System $UO_2$-$ThO_2$-$O_2$

## OPTICAL AND X-RAY ANALYSIS OF AIR-EQUILIBRATED MIXTURES

H. A. Friedman R. E. Thoma

### Equilibration and Examination of Urania-Thoria Mixtures

As a continuation of the investigation[1] of the system $UO_2$-$ThO_2$-$O_2$, mixtures of the hydroxides at 10 mole % intervals were prepared by coprecipitation and were sintered in air at 1500°C to form single-phase solid solutions. The presence of but a single phase was confirmed by metallographic examination. Portions of these solid solutions were exposed to air at temperatures between 640 and 1500°C for periods of time from 10 hr to 22 days. Other portions were reduced by treatment with hydrogen at 800°C for 6 hr and subsequently exposed to air for periods of time as long as 189 days at temperatures from 188 to 640°C. As before, the samples were removed from the furnace periodically and weighed at room temperature to follow the course of the equilibration. After samples had ceased to show weight gains, they were held at temperature for periods of time believed long enough for the completion of the crystallization of any new phases which might form. As will be seen from the discussion, it is doubtful that equilibrium was reached in many cases.

In the previous work the x-ray diffractometer and the polarizing light microscope were used to examine the samples. During the past year the metallograph, electron microscope, and the Debye-Sherrer camera have been used in the examination of specimens. For metallographic examination the sample was mounted in an epoxy resin, ground with a series of progressively finer silicon carbide papers, polished with diamond paste, and then either polished with alundum or "attack-polished" with a mixture of chromic acid solution and alundum. Some of the mounted specimens were etched further with either a water–nitric acid–peroxide solution or hot (105°C) phosphoric acid–hydrofluoric acid solution, depending on the thorium content (solid solutions containing appreciable thoria are not etched by the nitric acid solution).

### Composition-Temperature Relations

The experimental data for the system $UO_2$-$ThO_2$-$O_2$, with the oxygen pressure held constant by the use of air and the thorium-uranium content varied in 10 mole % steps, are displayed in Fig. 14.1. Data from the literature were used in developing the line for the uranium oxides. The boundaries of the single-phase, fluorite, solid-solution region, as revealed by x-ray and metallographic examination, are shown on the figure.

Interpretation of the relations within the single-phase region appears straightforward. The only question appears to arise from the 188°C data. Examination of the surface of these specimens (to which x-ray diffraction is largely limited) revealed that the predominant cubic solid-solution phase of the two which are present was a nonstoichiometric material whose lattice parameters were identical with those expected for specimens having compositions given by smooth extrapolations of the data obtained at higher temperatures. This phase is believed to be a surface coating of the grains with the equilibrium solid material. The interior of the grains, as revealed by metallographic examination and as inferred from the weight gains and results of chemical analysis (techniques which

[1] H. A. Friedman and R. E. Thoma, *Reactor Chem. Div. Ann. Progr. Rept. Jan. 31, 1962*, ORNL-3262, p 161.

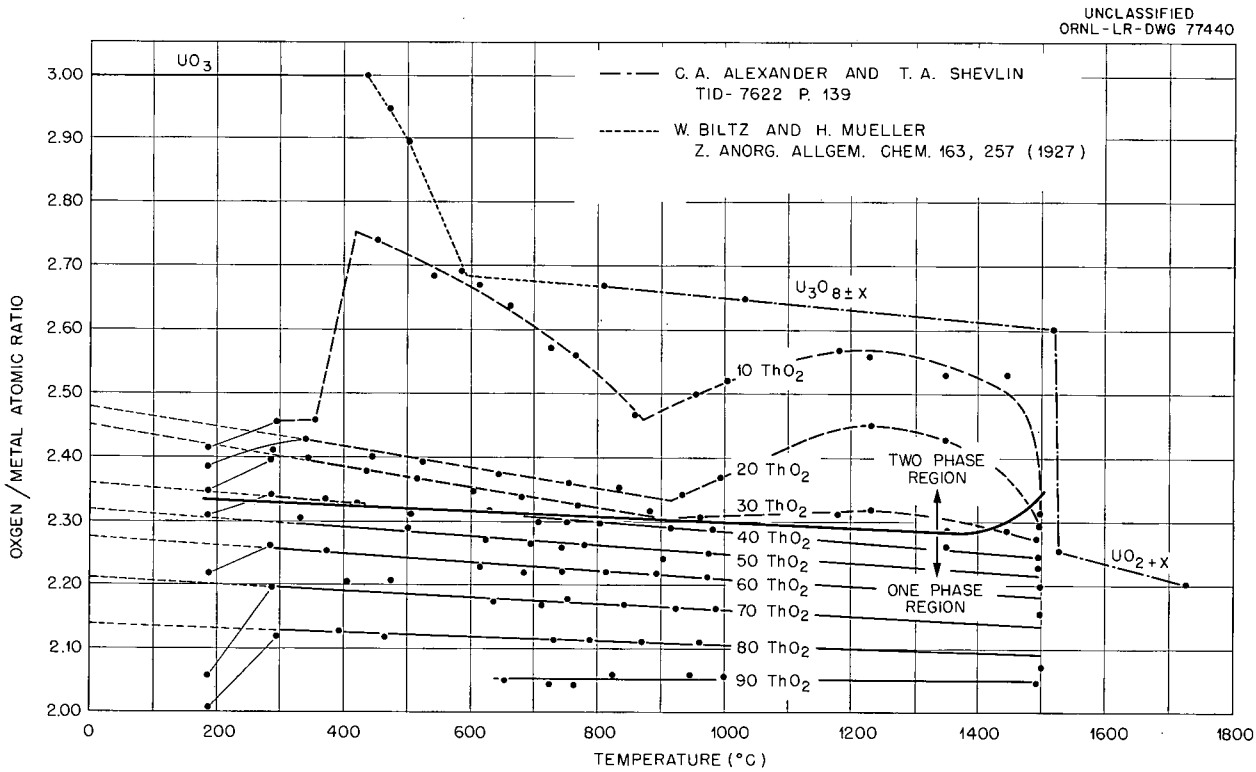


**Fig. 14.1. Composition-Temperature Diagram for the System $UO_2$-$ThO_2$-$O_2$ at 0.21 atm Oxygen.**

indicate the "average" composition of the material), did not show the phase which was seen on the surface by the x-ray diffractometer. Thus, the 188°C specimens most probably did not reach equilibrium compositions except on their surfaces.

Considerable restraint seems advisable in basing any interpretation on the data for compositions above the single-phase line, that is, those generally containing more uranium than thorium. There is serious doubt that all the specimens had reached equilibrium. In particular, specimens which had gained weight to apparent equilibrium at 1180°C failed to lose weight when subsequently exposed at 1000°C for one month. Thus, the apparently *lower* equilibrium oxygen content between 600 and 1200°C may be an indication of failure to achieve equilibrium. The three lowest temperature points for the composition 90% uranium–10% thorium almost surely are not at equilibrium and should ultimately achieve oxygen contents more nearly like those of $UO_3$. The data for temperatures of 1180°C and above appear to be reasonably consistent with equilibrium behavior.

A schematic trilinear plot of isotherms from 400 to 1400°C at 200°C intervals is shown in Fig. 14.2. This diagram is based on the assumption that $ThO_2$ has no solubility in $U_3O_{8\pm y}$ or in $UO_3$. This assumption requires that the tie lines in the two-phase regions terminate at points on the $UO_2$-$UO_3$ side of the diagram consistent with knowledge of the two-component $UO_2$-$UO_3$ system. The transition from $UO_3$ to $U_3O_8$ between 400 and 600°C is complex and not well understood. At least one, and maybe several, three-solid-phase, monovariant areas must exist in this portion of the three-component system diagram. A similar uncertainty exists at temperatures near 1520°C, the $U_3O_{8-y}$-$UO_{2.25}$ transition temperature. The boundary of the solid-solution region may continue without interruption to the uranium side of the diagram, or it may be interrupted by another miscibility gap. However, in the temperature range from 600 to 1400°C, the diagram is believed to be essentially correct.

UNCLASSIFIED
ORNL-LR-DWG 77876

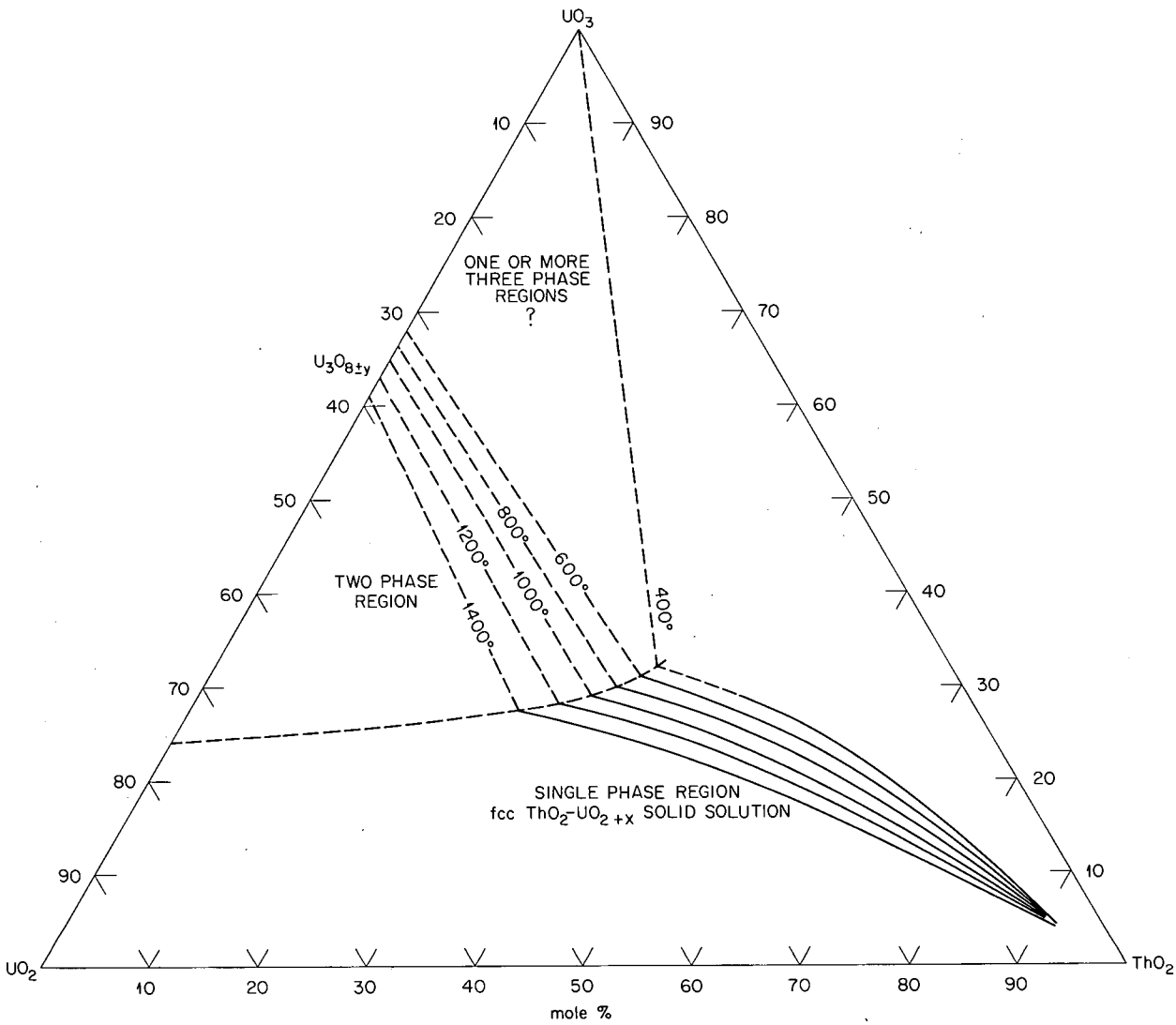


**Fig. 14.2. Isothermal Isobars (Schematic) for the System $UO_2$-$UO_3$-$ThO_2$. $P_{O_2}$ = 0.21 atm.**

## Identification of $U_3O_8$

The use of the Debye-Sherrer camera has permitted the identification of $U_3O_8$ at concentrations well below those which can be revealed by the use of the x-ray diffractometer. The use of the metallograph has permitted the identification of $U_3O_8$ at even lower concentrations, as illustrated by the study of a series of samples which had been equilibrated at 1350°C. The preliminary treatment of these samples did not proceed past the "attack-polish" stage. Figure 14.3 shows the appearance of the specimen containing 90 mole % urania; the metallograph revealed $U_3O_8$ particles, with the cubic solid solution appearing as small white spots on the surface. Metallographic examination of the 80 mole % urania specimen showed more of the cubic solid solution and less of the $U_3O_8$. In both these specimens there was enough $U_3O_8$ to be detectable easily with the x-ray diffractometer. The presence of $U_3O_8$ in the 70 mole % urania specimen was clearly shown by the metallograph, but neither the x-ray diffractometer nor the Debye-Sherrer camera could definitely

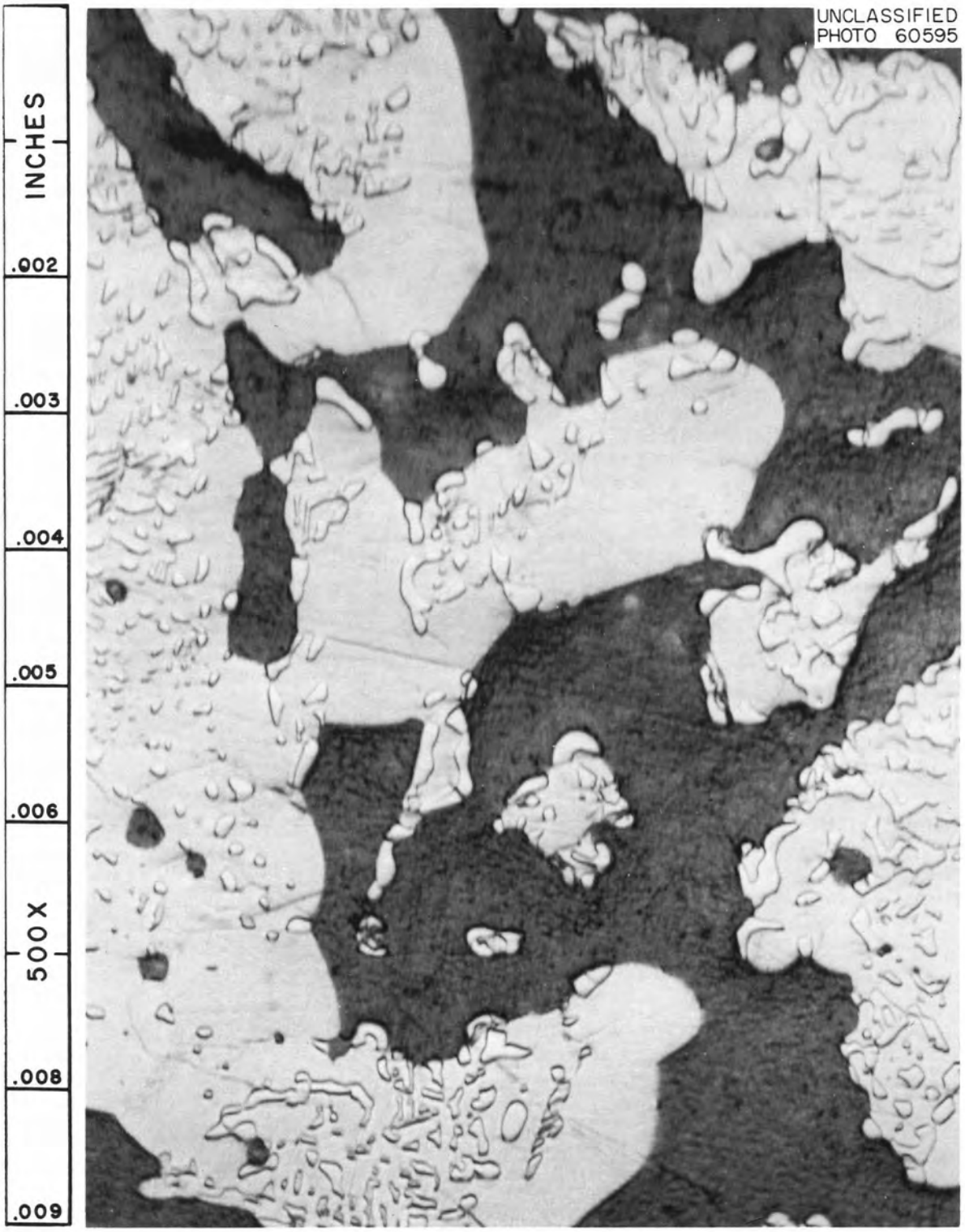


Fig. 14.3. Photomicrograph: 90 mole % Urania Specimen Heated at 1350°C. 500X. Reduced 12%.

detect the $U_3O_8$ in this sample. No evidence of $U_3O_8$ was found by metallographic examination of the 60 mole % urania specimen. Accordingly, the boundary separating heterogeneous from homogeneous material at the 1350°C isotherm was located between the 60 and 70 mole % urania compositions, perhaps nearer to 70 mole %.

### Unidentified Phases

As seen by reference to Fig. 14.1, at temperatures up to 600°C, compositions containing from 60 to 90% uranium should give specimens which are not single-phase solid solutions but show the presence of two or more phases. One of these phases should be a solid solution of the composition and oxygen-to-metal ratio indicated by the boundary line on Fig. 14.1 or Fig. 14.2. The other(s) should most probably be formed from rejected uranium alone, at whatever oxygen-to-uranium ratio is characteristic of uranium oxide at the particular temperature and oxygen pressure of the experiments. Up to a temperature of about 425°C, this phase might well be $UO_3$, and between 425 and 600°C it might be whatever equilibrium solid(s) exists between $UO_3$ and $U_3O_8$. Above 600°C the $U_3O_8$ phase should appear.

In the majority of the specimens containing 60 to 90% uranium that were exposed at temperatures from 188 to 600°C, the presence of "lines" as shown in Fig. 14.4 was observed by the use of the metallograph after the samples had been etched. Electron micrographs[2] of replicas of these specimens revealed the presence of "granules" in the "lines" as shown in Figs. 14.5 and 14.6. It is believed that these lines and granules indicate the presence of a small amount of the expected second phase, as yet unidentified. Only a single cubic phase was identified from x-ray diffraction analysis. The oxygen content of this specimen, containing 90% uranium and exposed at 291°C, as seen from Fig. 14.1, is far below that expected for an equilibrium situation, and it seems reasonable to believe that the second, unidentified phase in the granules is probably a trace of $UO_3$.

Metallographic and electron microscopic examination of the 60% uranium specimen which had been exposed at 421°C revealed similar "granules" in the "lines," but no granules were found in the lines of that specimen which had been exposed at 508°C. It may be significant that the boundary line between single-phase and heterogeneous material appears to cross the 60% uranium line at about 440°C.

[2]Electron microscopy performed by T. E. Willmarth, Analytical Chemistry Division, ORNL.

## OXYGEN DISSOCIATION PRESSURE STUDIES

L. O. Gilpatrick H. H. Stone
C. H. Secoy

### Introduction

An effort has been under way for some time to examine the effect of thorium content on the stability and solid phases present in the system $UO_2$-$ThO_2$-$O_2$.[1] The system $UO_2$-$O_2$ has been investigated by numerous individuals in the past 15 years[3] because of great interest in uranium dioxide as a component in reactor fuel formulations. Among the successful experimental avenues of approach to studying this system has been that of measuring the equilibrium partial pressure of oxygen above the oxide at various temperatures and oxide compositions.[4]

### Preparation of Urania-Thoria Solid Solutions

Our first work was directed to the problem of the preparation of thoria-urania solids suitable for use in the oxygen-solid equilibrium studies. It was thought that a fine state of subdivision and a large surface area would be desirable to promote rapid equilibration between the solid and oxygen. To satisfy these objectives, a method of making solid solutions was developed in which soluble salts of uranium and thorium were first mixed in solution. The uranium in solution was then reduced to U(IV) at the cathode of a mercury cell.

[3]J. Belle, *Uranium Dioxide: Properties and Nuclear Applications*, chap. 6, GPO, Washington, 1961.

[4]W. Biltz and W. Mueller, *Z. Anorg. Allgem. Chem.* **163**, 257 (1927); E. P. Blackburn, *J. Phys. Chem.* **63**, 897 (1959); R. J. Ackerman and R. J. Thorn, "Partial Pressure of Oxygen in Equilibrium with Uranium Oxides," presented at American Chemical Society Meeting in San Francisco, April 1958; L. E. J. Roberts and A. J. Walter, *Equilibrium Pressures and Phase Relations in the Uranium Oxide System*, AERE R-3345 (May 1960); C. A. Alexander and T. S. Shevlin, *The Second Conference on Nuclear Reactor Chem. Gatlinburg, Tenn., Oct. 10–11, 1961*, TID-7622, p 139.

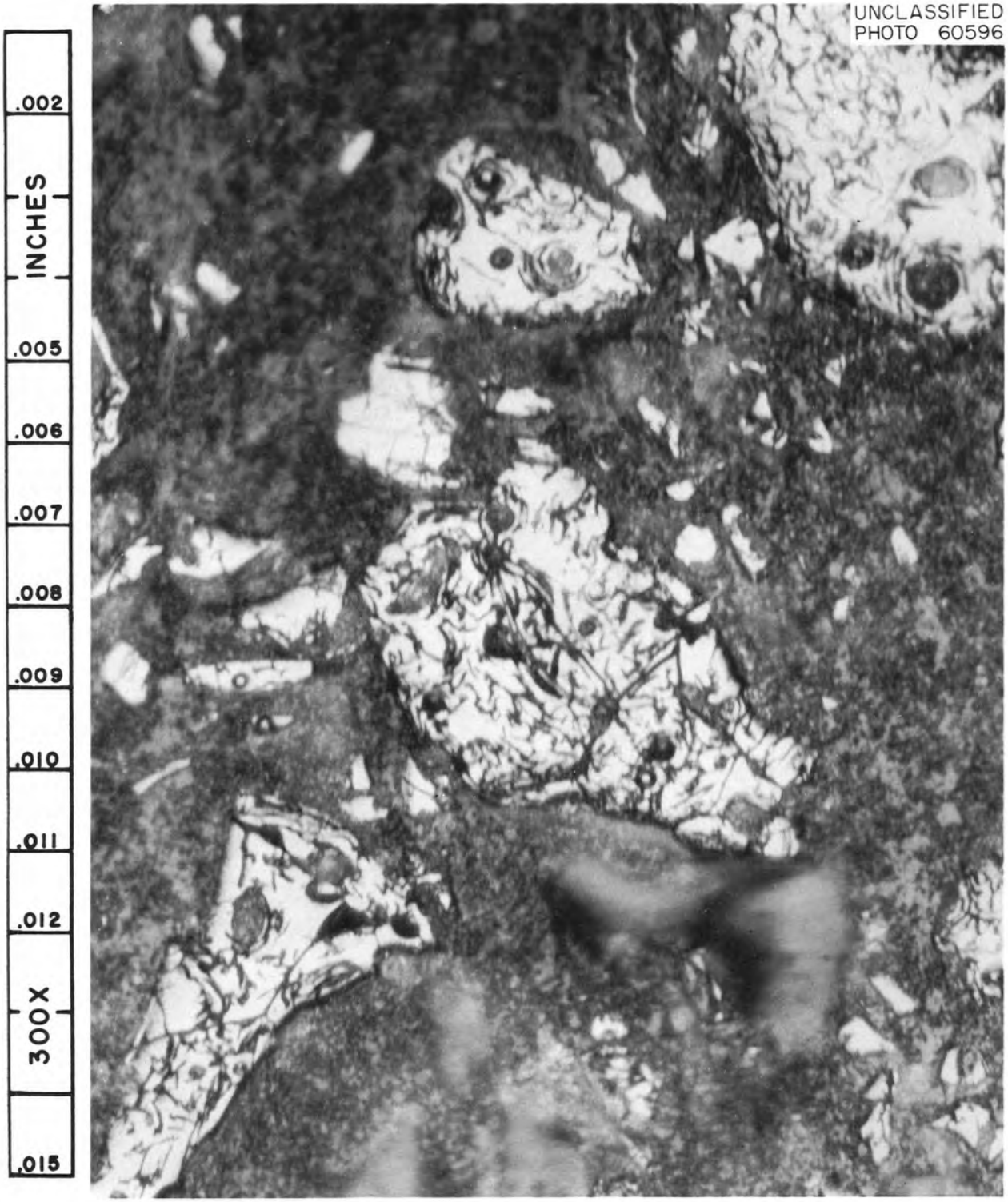


Fig. 14.4. Photomicrograph: 90 mole % Urania Specimen Heated at 291°C. 300X. Reduced 8%.

Fig. 14.5. Photomicrograph: 90 mole % Urania Specimen Heated at 291°C. 8000X. Reduced 7%.

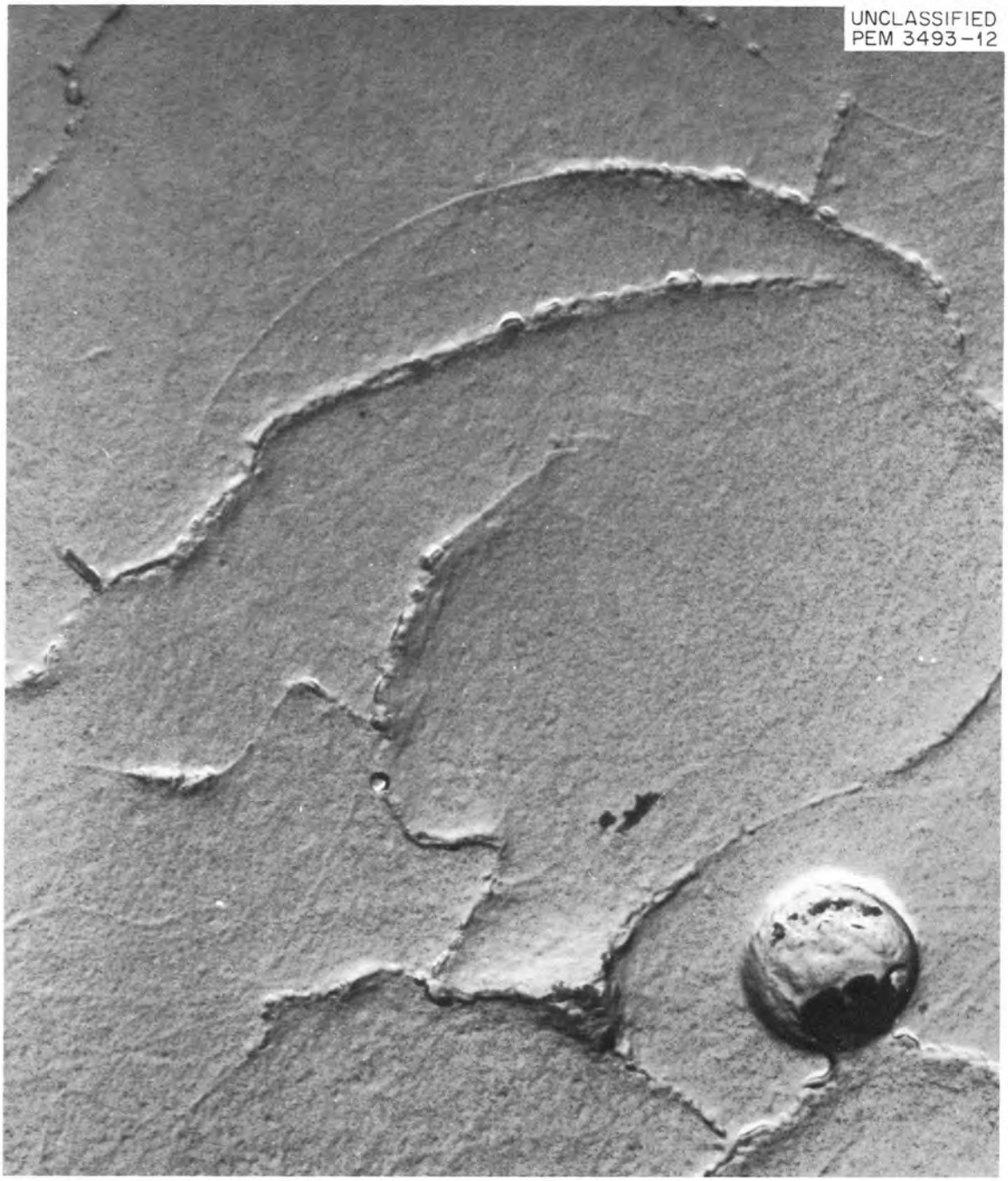


Fig. 14.6. Photomicrograph: 90 mole % Urania Specimen Heated at 291°C. 20,000X. Reduced 14.5%.

(The use of an isolated anode compartment in the cell prevented reoxidation of the solution in the region of the anode.) Hydrated oxalates were quantitatively precipitated from solution as a stable, mixed, crystalline material with both elements in the tetravalent state. Preliminary x-ray studies indicated that the two elements yielded isomorphous oxalate hydrates. It proved possible to produce a solid solution of the oxides by heating the mixed oxalate precipitate in an inert or reducing atmosphere to dehydrate and decompose the oxalate at temperatures lower than those required for oxide preparation by other methods. Material fired at 830°C produced a sharp, cubic x-ray powder pattern with a spacing constant intermediate between those for pure $UO_2$ and $ThO_2$ and a surface area (BET nitrogen adsorption) of 2.5 $m^2/g$. Unfortunately, solid solutions produced by this method were found to contain elemental carbon which, during the course of the oxygen equilibration experiment, could produce carbon monoxide and/or carbon dioxide. In practice, it proved necessary to alternately oxidize and reduce the preparations at a temperature of 1200°C or more to effectively reduce the carbon contamination to the low level needed for the current problem. All the preliminary work reported here was based on solid solutions made by this method which contained uranium and thorium in equal molar amounts.

The alternating oxidation-reduction treatment necessary to remove the carbon reduced markedly the surface area of the material and, consequently, defeated the primary objective in its preparation. Nevertheless, the method remains as an effective way of obtaining solid solutions of higher surface area (containing some carbon) or of low surface area after the oxidation-reduction treatment. Such material, in which the uranium has been held in the tetravalent state during the precipitation step and in which the precipitate has been an isomorphous mixture of the uranium and thorium oxalates, may be of interest for use in other studies of thorium and uranium.

### Dissociation Pressure Measurements

For the purpose of making dissociation pressure measurements, a conventional vacuum system incorporating a mercury diffusion pump and liquid-nitrogen traps was built. The solid solution was contained in a quartz thimble. A platinum wound furnace provided regulated heat. Experimental pressures were measured with a McLeod gage, and provisions were made for frequent sampling of the evolved gases. They were subjected to mass spectrometric analysis.

The first efforts to measure an $O_2$ equilibrium pressure involved material which had not been subjected to the oxidation-reduction treatment. These experiments failed because of the evolution of CO and $CO_2$, which in the static system yielded a continuous rise in system pressure. No evidence of free oxygen could be found.

Subsequent measurements were made on material fired in oxygen (1 atm) at 830°C to reduce the carbon content and to raise the oxygen content to the range most convenient for measurement (i.e., to give the largest pressures of $O_2$). The measured oxygen dissociation pressures for this composition were in fair agreement with those for $U_3O_8$ at similar temperatures with the exception that the addition of 50 mole % $ThO_2$ raised the oxygen partial pressures by about 50% in the temperature interval from 800 to 1000°C.

Immediate experimental difficulties were experienced when attempts were made to measure the partial pressure of oxygen over a solid solution whose oxygen content had been reduced to a level equivalent to $UO_{2.25}$ or lower for the contained uranium. The indicated oxygen pressure was of the order of 10 to 20 $\mu$ in the most favorable cases for temperatures of 1200°C. In all cases large excesses of $CO_2$ accompanied the oxygen. An examination of the thermodynamic equilibrium[5] for the reaction $2CO + O_2 \rightleftharpoons 2CO_2$ shows it to be far to the right ($K \approx 10^{+15}$) at 1200°C. This casts considerable doubt upon the significance of any free oxygen observed in such a system exposed to a temperature above 1000°C, where the combustion of CO is assumed to be rapid.

Several attempts to circumvent these difficulties were made by alternately oxidizing and reducing the material in place with $H_2$ and $O_2$ at 1200°C in an effort to remove spurious carbon from the system. Oxygen was finally added to bring the solid solution to the desired composition. Both oxidation and reduction were observed to proceed rapidly in a matter of 1 or 2 hr. After the initial equilibration period, pressure drifts were observed to be of the order of those due to system outgassing.

---

[5]James P. Coughlin, *U.S. Bureau of Mines Bulletin No. 542*, p 14, 1959.

The oxygen partial pressures observed at temperatures of 900 to 1200° C over a $ThO_2 \cdot UO_{2.13}$ composition were larger than that to be expected[4] from pure $UO_{2.13}$ by about 1 order of magnitude, or, expressed another way, the oxygen partial pressures were equivalent to those of a pure $UO_2$ system at an oxidation state of $UO_{2.18}$. At no time, however, could constant static pressures be achieved owing to the complication of the steady outgassing and formation of $CO_2$.

The quartz thimble for containing the sample in the furnace has been replaced by a Mullite tube, which permits tests to be made at temperatures up to 1500°C. Higher oxygen pressures will be obtainable from such tests, especially with high-oxygen-content solids, and the complications attributable to system outgassing and reactions with traces of carbon will be minimized. Other experimental techniques are being considered for use in the study of solids of low oxygen content. In such cases the solid-phase transition temperatures (the region of main interest) will be lower, and the corresponding dissociation pressures will be very low.

# Part IV

# Support for High-Temperature Solid-Fueled Reactors

# 15. Diffusion Processes

The advancing technology of gas-cooled reactors requires information regarding performance of unclad fuel elements. Unclad systems designed to operate at higher temperatures introduce many new problems inherent in higher-temperature operations such as greater rates of fission-gas release and the enhanced mobility of fuel and of nonvolatile fission products in the fuel elements. Supporting research has been performed in an effort to understand the mechanism of diffusion processes related to the transport of gases and of nonvolatile materials in ceramic matrices. In addition, efforts have been made to apply the basic information obtained toward the optimization of design of unclad reactor fuel elements.

## TRANSPORT OF GASES IN POROUS MEDIA

A. P. Malinauskas E. A. Mason

The simultaneous existence of three driving forces for gas transport in gas-cooled-reactor systems (concentration, pressure, and temperature gradients) has motivated a program of research directed toward the elucidation of gas-transport phenomena in porous media governing coolant contamination as a possible aid in controlling this process. Perhaps the most significant contribution of these investigations thus far has been the development of a model which accurately accounts for the experimental observations.

### Discussion of the "Dusty-Gas" Model

Prior to 1957, the usual manner of describing the migration of a gas through a porous medium was to visualize the septum as a bundle of parallel capillaries.[1] There are two important limitations to this model in the treatment of diffusion of binary gas mixtures. First, its inability to explain the experimentally established fact that, for constant-pressure experiments, the flux ratio of the components is inversely proportional to the square root of their molecular weights and is independent of the total pressure. Second, the model fails to provide the theoretical treatment for transport in the transition from Knudsen diffusion (very low pressures) to ordinary diffusion (pressures of the order of several atmospheres). To fill this void, a model was developed independently by Deriagin and Bakanov[2] and by Evans, Watson, and Mason.[3] This model describes the medium as a localized agglomeration of giant gas (dust) molecules that are rigidly constrained and uniformly distributed in space. The elegance in the development is primarily due to the fact that only the model itself is novel, since the theoretical treatment consists merely in employing the kinetic-theory results formulated earlier by Chapman[4] and by Enskog.[5]

**Diffusion at Uniform Temperature and Pressure.** – At uniform pressures and temperatures,[3] the "dusty-gas" model provided the first satisfactory theoretical derivation of the experimentally discovered fact that the flux ratio for binary mixtures is equal to $(m_2/m_1)^{1/2}$ at all pressures (not just in the Knudsen region). It also provided a rigorous theoretical treatment of the transition region, from

[1] P. C. Carman, *Flow of Gases Through Porous Media*, Academic Press, New York, 1956.

[2] B. F. Deriagin and S. P. Bakanov, *Soviet Phys.–Tech. Phys.* **2**, 1904 (1957).

[3] R. B. Evans III, G. M. Watson, and E. A. Mason, *J. Chem. Phys.* **35**, 2076 (1961).

[4] S. Chapman and T. G. Cowling, *The Mathematical Theory of Non-Uniform Gases*, Cambridge U. P., London, 1960.

[5] D. Enskog, "Kinetische Theorie der Vorgange in Massig Verdunnten Gasen," Inaugural Dissertation, Uppsala (Sweden), 1917.

which was obtained the usual Bosanquet interpolation formula and a differential equation for diffusion which covered the entire pressure range.

**Diffusion in the Presence of Pressure Gradients.** – Extension of the "dusty-gas" model to allow for pressure gradients[6] introduced into the fundamental kinetic theory equations both a pressure diffusion term and an external force term. The latter is needed to keep the porous medium from being pushed along by the pressure gradient. The final diffusion equation has the same form as that in the uniform-pressure case. No additional parameters beyond those necessary to define a diffusing system at uniform pressure are required to compute the diffusion rates when pressure gradients are present. The coefficients of the diffusion equation, however, now depend on position through their dependence on pressure, and the net flux $J$ of all molecules is an undetermined quantity.

A complete solution requires also a forced flow equation, giving $J$ as a function of the pressure gradient. A forced flow equation was derived on the basis of the dusty-gas model, but one parameter had to be made disposable in order to compensate for the fact that the model permits only a diffusive mechanism for flow, never a viscous mechanism.

**Thermal Transpiration.** – The next step was to consider the effects of temperature gradients.[7] For the simplest case of a single gas in a porous medium, the physical phenomenon which occurs is thermal transpiration (also sometimes called thermomolecular pressure difference), in which a temperature gradient causes a pressure gradient to develop. If the pressure gradient is prevented from developing by removing gas from the high-pressure side, then a continuous flow of gas through the porous medium takes place. The effect was discovered in 1879 by Reynolds,[8] who studied it in porous plates. It has usually subsequently been studied in small tubes, since it can be an important source of error in pressure measurements where the manometer is at a different temperature than the rest of the apparatus.

Effects involving temperature gradients in gas *mixtures* in porous media involve multicomponent, thermal diffusion coefficients in the framework of the present model and have not been considered in detail to date because of the mathematical complexity involved. Only two limiting cases are simple when gas mixtures are involved: the case where the mean free path of the gas molecules is large compared to the pore size (Knudsen region), and the case where the mean free path is small compared to the pore size (normal, or hydrodynamic, region). Both cases are understood already, and the model adds nothing new. The interesting case is the transition region between the Knudsen and the normal regions, which has always been difficult to treat theoretically. Here the model is straightforward, but detailed information is lacking at present on the multicomponent thermal diffusion coefficients needed by the model.

The results of the latest extension of the model to nonisothermal systems can be summarized as follows: The model accounts for the phenomenon of thermal transpiration in a consistent way at all pressures from the Knudsen region to the normal region. The kinetic theory transport coefficient which bears the major responsibility for thermal transpiration, according to the model, is the thermal diffusion factor for the gas-dust mixture. The model appears to account for all aspects of the phenomenon which are essentially diffusive in mechanism, but it needs modification at high pressures. Here at least part of the steady-state backflow caused by the pressure gradient is often viscous in nature. This part of the flow needs to be added onto that predicted by the model, which has no provision for describing viscous flows. When the viscous backflow is added, an equation which describes thermal transpiration over the entire pressure range is obtained. This equation discloses two new relations not previously noticed: a relation between the maximum in the thermal transpiration curve and the Knudsen minimum in the permeability curve; and a relation between the height of the thermal transpiration maximum and the translational heat conductivity of the gas. When the model is extended to include capillaries, this latter relation permits the calculation of rotational relaxation times in gases from thermal transpiration measurements. The capillary results also reproduce previous semiempirical and empirical equations known to give good results – the

[6] R. B. Evans III, G. M. Watson, and E. A. Mason, *J. Chem. Phys.* **36**, 1894 (1962).

[7] E. A. Mason, R. B. Evans III, and G. M. Watson, accepted for publication (January 1962) in the *Journal of Chemical Physics*.

[8] O. Reynolds, *Phil. Trans. Roy. Soc.* (London) **170**, pt II, 727 (1879); this remarkable paper also appears as No. 33 in Osborne Reynolds, *Scientific Papers*, vol. I, pp 257–383, Cambridge U. P., New York, 1900.

equations of Weber and of Liang for thermal transpiration and the equation of Knudsen for permeability. The present equations, however, have fewer adjustable parameters than do the previous equations.

## Experimental

A. P. Malinauskas J. Truitt

Detailed reports of the investigations which have been, or presently are being, undertaken will be published in detail elsewhere, and only a brief summary of the experimental work will be presented here.

**Transport Studies with a Uranium-Impregnated Graphite.**[9] – In order to illustrate the validity of the transport equations when fueled graphites are employed, studies of pure-gas flow and binary diffusion were conducted with a graphite specimen that was fabricated in a manner such that the septum matrix was composed of 25.8 wt % of normal uranium in the form of uranium carbide ($UC_x$-graphite). This specimen was similar to some of the fueled graphites used in the ORNL-MTR-48 series of in-pile experiments.[10]

No anomalies were expected for transport through the $UC_x$-graphite medium and, indeed, none were detected. Thus fueled graphites, from the standpoint of septum homogeneity, present no new problems, although alterations in the medium structure will undoubtedly occur over sufficiently large periods of time owing to depletion of the fuel. This particular problem was not investigated.

**Diffusion Under Conditions of Nonuniform Pressure.**[11] – Extensive studies have been made of the diffusion process in the presence of a pressure gradient. Much of the emphasis was placed on the variation of $C_2$, a disposable parameter appearing in the flux equation, with pressure for the gas pair, helium and argon, diffusing through a graphite medium. Unfortunately, the dependence of the viscosity on the concentration of the bulk gas and hence on the distance parameter $z$ along the flow path greatly complicates the flow pattern, so that an unambiguous analysis of the data does not appear possible. However, it appears reasonably well established that $C_2$ varies in a linear manner with the mean pressure $\bar{p}$, which is defined as the arithmetic average of the pressures on the two sides of the septum.

**Multiregion Graphites.** – A series of investigations is presently under way in an effort to test the sensitivity of the "dusty-gas" assumption that the dust particles are uniformly distributed. The septum being employed in these studies consists of a graphite pipe in which the inner and outer surfaces were coated with a less permeable grade of graphite than the inner material. The results obtained thus far, tentative though they may be, nonetheless tend to indicate that the assumption of uniform distribution is valid for a medium fabricated of different grade strata which are in series with respect to the direction of flow.

In this regard a separate set of experiments has likewise been undertaken in an effort to relate the flow properties of each of the strata to those of the medium as a whole.

**The Determination of ($A/L$) for Irregular Shapes.** – If the graphite base stock were strictly uniform, the flow properties of any section cut from it could be related to any other portion of the same stock if the area-to-length ($A/L$) ratios were known. Although this is not normally the case for most commercial graphites, the $A/L$ relation serves nonetheless as a reasonably good approximation. However, it is often convenient to employ graphite bodies of sufficiently complex geometry that a mathematical determination of the $A/L$ ratio is not feasible. For such cases a method utilizing the concept of the specific conductance of ionic solutions has been devised and tested successfully.

**Thermal Transpiration.** – It has already been noted that thermal transpiration experiments appear to be a simple, convenient means of obtaining the translational component of the thermal conductivities of gases. With this primary purpose in mind, an apparatus has been designed to investigate the thermal transpiration phenomenon, and the critical components have already been fabricated.

## Additional Programs

A program of research concerning the diffusion, viscosity, and thermal conductivity phenomena of gases has been initiated. This rather broad program has three aims: (1) to provide data that are

[9] A. P. Malinauskas, to be published.

[10] J. A. Conlin, "ORNL-MTR-48 Experiments," Third Meeting of the Coated Particle Fuels Working Group, Oak Ridge National Laboratory, May 7–8, 1962.

[11] R. B. Evans III, G. M. Watson, and J. Truitt, to be published.

presently unavailable, (2) to study the angular dependence of the potential energy of interaction between molecules, and (3) to investigate the effects of internal degrees of freedom.

The research is planned to proceed in three stages corresponding to each of the three transport properties. Phase I, studies involving the diffusion effect, is already under way with the design and partial construction of a prototype diffusion apparatus which is similar, both in form and principle, to that previously employed by Loschmidt.[12]

### Applications

The studies of gas transport in porous media and the postulation of the "dusty-gas" model have been helpful, not only in the basic study of mechanism of gas transport but also in the prediction of the behavior of volatile fission products in different types of ceramic fuel elements. A series of calculations has been recently initiated concerning the optimization of geometry in various proposed fuel-element configurations. The results of the first of such calculations[13] are summarized below.

**Comparison of Ventilated Fuel-Element Configurations.** – The results of simplified calculations have been obtained, comparing the release of fission gases into the coolant in two ventilated fuel-element configurations that are being considered for use in high-temperature gas-cooled reactors. One configuration was a bare, porous, hollow cylinder with helium flowing through the matrix and sweeping fission gases into the central void space to be exhausted. The other configuration consisted of a cylindrical fueled matrix enclosed by a gas annulus and a porous sleeve with helium flowing through the sleeve to sweep fission gases out of the annulus. The calculations show that, for identical surface temperatures, power output per unit length, and specific helium flushing rates, the sleeved fuel element is approximately 10,000 times more efficient in preventing fission-gas contamination of the coolant than the bare fuel element. A third configuration, a bare fuel element with an unfueled peripheral shell (no gas annulus), appears to be a logical extension of the present comparisons. Similar calculations are scheduled to be made for this case in the near future.

## DIFFUSION OF FUEL IN CERAMIC MATERIALS

R. B. Evans III

This investigation may be classified, at the present time, as a series of experimental studies oriented to supply information applicable to the design and specification of graphite–uranium carbide fuel elements. Four reactor systems are to employ fuel elements of this type, namely: the Dragon Reactor Experiment (Dragon Project) in England,[14] the HTGR Peachbottom Reactor (General Atomic) near Philadelphia,[15] the UHTREX (formerly Turret) Reactor at Los Alamos,[16] and the AVR Pebble Bed Reactor in Germany.[17] In each reactor, helium is to be employed as the coolant, and the fuel elements are to consist of a fueled graphite body and an unfueled sleeve (or shell). Many of the problems associated with the fuel elements are defined by the selection of materials for the fueled body which, in turn, sets the pattern for supporting research efforts. It is of interest, therefore, to review the original and present trends regarding fueled-body materials.

Initially, the fueled body envisioned for all the reactors mentioned above was to be comprised of bare uranium carbide particles uniformly distributed within a porous and permeable graphite matrix. It was not expected that these bodies would retain radioactive contaminants to a satisfactory extent; thus, containment was to be a primary function of the sleeves. Containment was to be accomplished through utilization of low-permeability sleeves accompanied by a back flush of helium, when feasible. Based on the original selection of bare uranium carbide fuel particles, initial research and development efforts centered on the sleeves. The results of these efforts

[12] J. Loschmidt, *Wien. Ber.* **61**, 367; **62**, 468 (1870).

[13] R. B. Evans III and G. M. Watson, *Comparison of Ventilated Fuel Element Configurations*, ORNL TM-474 (February 1963).

[14] G. E. Lockett and R. A. U. Huddle, *Nucl. Power* **5**, 112 (1960).

[15] Staff, *Peachbottom Preliminary Hazards Summary Report*, NP-9115, pt B, vols. I and II (August 1961). This report is available from AEC Division of Technical Information Extension at Oak Ridge, Tenn.

[16] Staff, *Ultra High Temperature Reactor Experiment Hazards Report*, LA-2689 (April 1962). Availability as in ref 15.

[17] O. Machnig *et al.*, *Nucl. Power* **6**, 63 (1961).

(coupled with in-pile test results) indicated that, although back flushing appeared to be promising,[18,19] the expense of permeability reduction treatments for the shells and sleeves might not be justifiable in view of the rather small gains with respect to retention properties.[20] Also, considerable uranium migration occurred within the graphite portions of the fuel elements.[21] (A description of the migration characteristics of uranium from fueled-body material is given in the last portion of this section.)

It is not surprising, then, that emphasis has shifted, within the last year, from the sleeves to the fueled body and, in particular, to the possibility of using coated fuel particles for fueled-body fabrication. The idea here is to stop contaminant migration at its source by coating the fuel with pyrolytic carbon (which is nearly impermeable). Comparisons of the retention properties of bare and coated uranium carbide particles[22] lead to the speculation that the use of fueled bodies with coated particles will place sleeve performance in a secondary role and will greatly reduce fission product release and fuel migration. At present a decision to use coated particles for all reactors mentioned is under strong consideration and, in some instances, has been made. The changes in fuel-element design[23] brought about by the changes in materials selection are illustrated in Figs. 15.1 and 15.2.

The new problems of interest concern the useful lifetime of a coated particle – specifically, whether or not the useful lifetime is interrupted by a coating failure and, if so, the possible causes of failure. This information might enable one to specify a minimum coating thickness for various degrees of burnup. Useful lifetime, failure, and minimum thickness probably depend on coefficients of thermal expansion, coating damage as induced by neutron and fission-fragment exposure, and the fuel content of the coating. Thus, an experimental investigation of uranium migration in graphites should be of interest from an applied point of view.

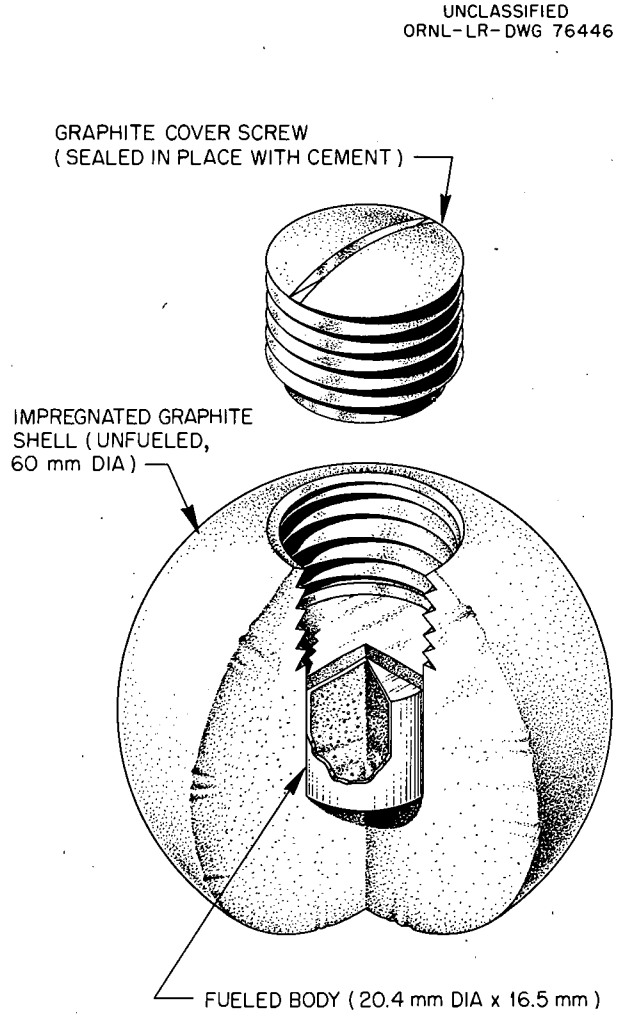


**Fig. 15.1. First Conceptual Fuel-Element Design for the AVR Pebble Bed Reactor. The molar ratio of uranium to carbon in the fueled body is 1:45.**

[18] J. Truitt, *Interdiffusion of Helium and Argon in Speer Moderator No. 1 Graphite (A Terminal Report on Large Pore Graphites – Experimental Phase)*, ORNL-3117 (June 6, 1961). Availability as in ref 15.

[19] L. R. Zumwalt, General Dynamics/General Atomic Division, October 1961, private communication.

[20] Private communication with C. B. Von der Decken of BBC/Krupp, Nov. 2, 1962.

[21] J. G. Morgan and M. F. Osborne, *Irradiation Effects on $UC_2$ Dispersed Graphite – Final Report*, ORNL-3340 (Dec. 23, 1962).

[22] See Fig. 21.5 (in the section, "Continuous Release of Fission Gas During Irradiation of $UC_2$ Coated Particles"). The figure presents plots of $R/B$ vs half-life for bare and coated uranium carbide particles.

[23] The fuel element described in Fig. 15.2 was the result of activities related to PBRE and the earlier Sanderson and Porter studies. Additional details are presented in A. P. Fraas *et al.*, *Preliminary Design of a 10-Mw (t) Pebble Bed Reactor Experiment*, ORNL CF-60-10-63 (rev) (May 8, 1961); Staff, Oak Ridge National Laboratory, *Conceptual Design of the Pebble Bed Reactor Experiment*, ORNL TM-201 (March 1962).

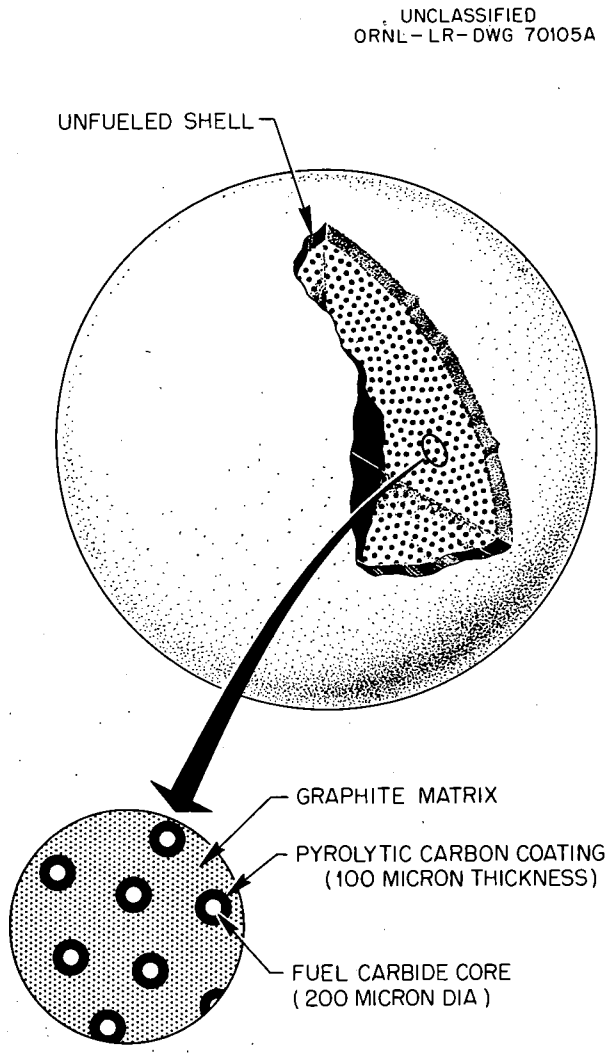


**Fig. 15.2. Alternote Fuel Element for Pebble Bed Reactors.** The primary function of the unfueled shell is to prevent violation of the outermost particles during ball handling.

The objective of the subject studies is to determine the parameters required to estimate the total amount of uranium that will migrate from a uranium carbide source into an initially pure graphite section.

**Basic Considerations.** – There are several possible mechanisms by which fuel materials can diffuse through graphite or carbon matrices at high temperatures. The only acceptable situation for high-temperature gas-cooled reactors is one in which the migration can be contained within the fueled body and is controlled by a very slow process. Therefore, it is always hopefully assumed that the migration will be controlled by a solid-state diffusion mechanism or, at least, by a diffusion process of some kind. With the above considerations in mind, a rather general set of boundary conditions may be selected for the experiments (and perhaps for actual cases). The conditions are that the diffusion occurs as it would in a semi-infinite medium, that source regions are maintained at a constant potential, and that the potentials at external surfaces are zero for very long periods of time.

For the conditions cited, there are three types of migration (diffusion) equations which might be considered. The first one gives the uranium concentration profile, the second gives the instantaneous rate of migration, and the third gives the instantaneous total amount of uranium present in a given increment of graphite. The third equation, which is the working relation for the experiments described here, may be written as

$$M(\Delta x,t')' = A \int_{x_1}^{x_2} C(x,Dt')\,dx\ , \qquad (1)$$

where $M(\Delta x,t')$ is the total amount of uranium present in the graphite volume $A(x_2 - x_1)$ at a fixed time $t'$. The expression $C(x,Dt')$ represents the concentration profile equation in terms of a position $x$ and the product of the diffusion coefficient $D$ and $t$. For ease of discussion Eq. (1) has been written for isothermal and unidirectional migration normal to the area, $A$. During an experiment (and perhaps during a coating lifetime), transient conditions should always prevail. Classical solutions to the equations are common knowledge[24] but the applicability of a selected solution must always be checked to ensure that the solution closely approximates the migration behavior with respect to the experiments and, later, to coatings and/or fuel bodies.

Frequently, the only results required from experiments are a set of diffusion coefficients. This would be the case if one were interested in either impurity-atom diffusion (as represented by the migration of trace amounts of fission products) or self-diffusion. Here one might assume that a tracer-layer technique could be employed. (Utilization of the thin-tracer-layer technique is discussed

[24] A. A. Zhoukhovitsky, *Intern. J. Appl. Radiation Isotopes* **5**, 159 (1959); also C. Leymonie and P. Lacombe, p 175.

in the section "Diffusion in Beryllium Oxide Matrices.") The attractive feature of this method is that one need not determine the exact amount of the minute quantity of impurity introduced on a specimen, since ratios relative to the initial amount (as a function of penetration) lead to a coefficient. But a set of diffusion coefficients is not all that is required to describe migration as it would occur, for example, within a coating on a uranium carbide particle. In this case at least one coating surface always "sees" uranium carbide. This means that a time-constant concentration, $C_0$, will always be maintained at the carbide-coating interface. It is important to note that the term $C_0$ appears in all the diffusion equations mentioned. The utilization of Eq. (1) for coating computation requires a set of $C_0$'s as well as a set of $D$'s, both as a function of temperature. The important point is that two parameters must be determined in the present diffusion experiments.

The relative importance of the $C_0$ term (actually the driving potential for migration) may be established in terms of the conventional diffusion studies. In the latter the state of the diffusing material is known, equilibrium phase relations are applicable (and available), and the potentials are well defined. In the present investigation, however, work has proceeded (perhaps prematurely) without the basic information related to $C_0$. The present investigations are, of necessity, pseudo-phase studies coupled with a determination of diffusion rates. Attempts to measure $C_0$ have complicated the experiments. In fact, a good deal of accuracy regarding the $D$'s has been sacrificed for the sake of determining $C_0$. At present, $C_0$ is envisioned as being a sort of structure-dependent saturation value of uranium in carbons or graphites that are contacted by uranium carbide.

## Uranium Diffusion in Pyrolytic Carbon

C. M. Blood

**Description of Materials.** – The details of manufacturing the pyrolytic carbon under investigation are not available; however, the structure and properties of this material are comparable to those of carbons which have been prepared by the pyrolytic decomposition of methane at 20 mm Hg (total pressure) and 2000°C. The properties of the gross material are nearly the same as those of the grains that constitute its microstructure.[25] These grains are large and conical in shape and are usually described as columnar grains. The planar surface of the gross material corresponding to the planar surface of deposition is parallel to the crystallographic *a* direction of a large majority of the grains; the *c* direction is perpendicular to the deposition surface. The conical vertices of the grains are adjacent to this surface. The material is dense with zero open porosity. In coatings the uranium diffusion would proceed in the *c* direction, starting at the cone vertices. Experimental diffusion specimens are prepared with these orientation considerations in mind, although the massive specimens utilized may have structures unlike those of coatings on fuel particles. The specimens are prepared by placing a strip of uranium metal foil[26] between two pyrolytic carbon coupons. The uranium is converted to one or more of the known carbides by heating in an evacuated furnace. The grain structure is clearly shown in Fig. 15.3, which offers a comparison between pyrolytic carbon and ordinary graphite.

**Current Progress and Results.** – Ten experiments have been initiated to study the pyrolytic carbon–uranium carbide system. A separate diffusion specimen is subjected to an annealing process at high temperatures in each experiment. Complete results are available for five of these specimens. Sectioning operations and uranium analyses are currently under way for the uncompleted specimens. Of the five completed experiments, three were carried out with a very short diffusion-annealing period in order to determine the initial concentration profiles which correspond to zero diffusion time. It was found that the carbon–uranium carbide interface was well defined and that a negligible amount of uranium migration had taken place during specimen fabrication and the brief annealing period. Data obtained from the two remaining completed experiments are shown in Fig. 15.4.

The first and most difficult step in the correlation of data, as they appear in Fig. 15.4, is the estimation of $x = 0$ and $M(0,t')/A$. This expression represents the total amount of uranium beyond $x = 0$ which will have diffused into a unit area of graphite. At present the interface ($x = 0$) can be

[25] P. L. Walker, Jr., *Am. Scientist* **50**, 283 (1962).

[26] C. M. Blood and R. B. Evans III, *Reactor Chem. Div. Ann. Progr. Rept. Jan. 31, 1962*, ORNL-3262, pp 136–42.

**Fig. 15.3. Magnified Cross Section of a Diffusion Specimen Comprised of Pyrolytic Carbon (at Top), Uranium Carbide Layer (Converted Metal Foil), and Ordinary AGOT Graphite.** The cracks induced by thermal stresses during cooling have been propagated along planes perpendicular to the $c$ direction of the pyrolytic carbon.

located only to within one increment or approximately $\pm 15\ \mu$; this level of uncertainty leads to large errors in the $M(0,t')/A$ values. Extrapolations of the data at $x > 0$ form the primary basis for the location of $x = 0$. Once values of the latter are selected and the "background" values (which correspond to the horizontal part of the curves) are subtracted out, the ratios $M(x,t')/M(0,t') = y$ are computed and then plotted vs $x$. These plots reveal that the applicable solution for Eq. (1) may be written in the form:

$$M(x,t') = A \int_x^{\infty} C_0 \operatorname{erfc}\left[(x)/(4Dt')^{1/2}\right] dx \ ;$$

thus, the ratios plotted are given by $(\pi)^{1/2}$ ierfc $[(x)/(4Dt')^{1/2}]$, and $C_0$ may be calculated from the relation $M(0,t')/A = C_0(4Dt'/\pi)^{1/2}$ after $D$ is established. Comparisons of plots of the experimental ratios, $y$, vs $x$ and the generalized function ierfc$(u)$ vs $u$ enable one to estimate average values of $D$. Based on the experimental curves of Fig. 15.4 and the methods outlined, it was found that $D = 6 \times 10^{-11}$ cm$^2$/sec ( in the $c$ direction) and $C_0 = 0.16$ g of uranium per cubic centimeter (at approximately 2000°C. Concentration profiles may be readily computed with the aid of these parameters. Examples are shown in Fig. 15.5. One should note that the area under a curve, measured from any $x$ to $x = \infty$ (plus a "background" correction), is proportional to an ordinate value (at the same $x$) on the corresponding curve in Fig. 15.4.

**Tentative Conclusions.** – The results obtained to date indicate that the present method of specimen fabrication is entirely satisfactory and that the

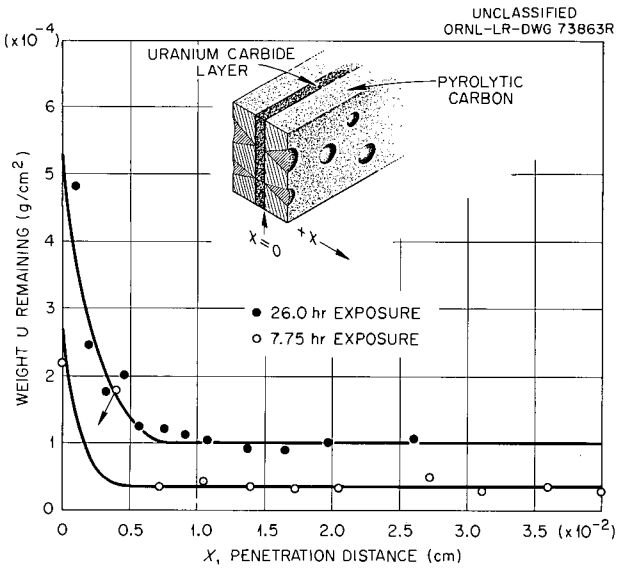


**Fig. 15.4. Plot of Weight of Uranium Remaining Per Unit Area as a Function of Distance from the Interface of Uranium Carbide–Pyrolytic Carbon Diffusion Couples Heated for 7.75 and 26.0 hr, Respectively, at 2000°C in Vacuum.**

classical constant-potential solutions to the diffusion equations describe the experimentally determined migration rates. The low values of the diffusion coefficient indicate that a solid-state mechanism controls uranium migration. Nevertheless, it will be possible to observe measurable amounts of migration, even at lower temperatures, because of the relatively high $C_0$ value of the pyrolytic carbon. This belief is expected to be verified from the next set of experiments, wherein diffusion in the *a* direction will be investigated. The results of pertinent (but dissimilar) studies[27,28] have indicated that the coefficients for nickel in pyrolytic carbon at 947°C are three orders of magnitude greater in the *a* than in the *c* direction. Although the coefficients are very dependent on specimen orientation, it is speculated that $C_0$ should be independent of orientation. A more accurate determination of $C_0$ is expected to be obtained in future experiments.

## Uranium Migration in Porous Graphites

J. Truitt C. M. Blood

**Objectives and Materials.** – When uranium migration studies were initiated in this Laboratory, the possibility of fabricating fueled bodies with uncoated particles dispersed in porous graphites was being given strong consideration; the idea of using coated particles was relatively new and speculative. It is understandable, therefore, that the first experiments performed in this investigation involved porous graphites. In spite of the apparent success of the coating idea, these studies could be of applied significance if it is found that an appreciable number of coatings are violated during fuel-body fabrication or during reactor operation.

The first experiments were performed with AGOT-graphite specimens[26] prepared in the same way as the pyrolytic carbon specimens described in the previous section, namely, by heating uranium-metal foil placed between two graphite coupons. Unfortunately, the $U^0$ and $U^0$-UC liquids persistently

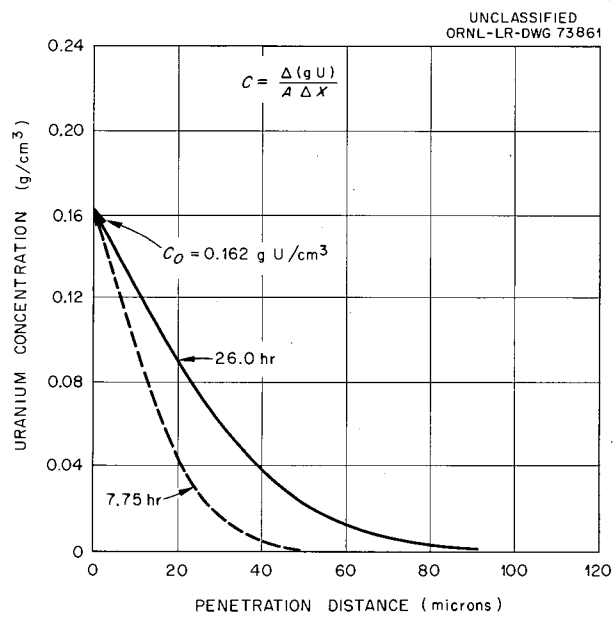


**Fig. 15.5. Calculated Concentration Profiles for Uranium in Pyralytic Carbon After Migration at 2000°C.**

[27] J. R. Wolfe and R. J. Borg, *Self-Diffusion of Nickel and Silver in Pyro-graphite*, UCRL-6828T (Mar. 15, 1962).

[28] R. J. Borg, D. R. McKenzie, and J. R. Wolfe, *The Self-Diffusion of Uranium in Pyrographite*, UCRL-6827T (Mar. 15, 1962). Several coefficients are presented over the temperature range 1480 to 2230°C for uranium diffusion in the *a* direction in this report. A thin-tracer-layer technique was employed; thus $C_0$ values were not reported.

penetrated the pores of the graphite during the time interval in which $U^0$ was undergoing conversion to solid $UC_2$ and $UC\text{-}UC_2$. This precluded the formation of a discrete uranium carbide–graphite interface like the carbide–pyrolytic carbon interface (see Fig. 15.3); accordingly, these experiments were abandoned.

The second set of experiments, with porous graphites, was designed to explore the possibility of fabricating specimens by tightly pressing an initially pure graphite coupon against a second coupon containing a uniform dispersion of uranium carbide (uncoated). The materials utilized were $UC_2$ (25 wt %) impregnated graphite, a furfural-impregnated graphite, and a carbon cement. Note that the materials used were very similar to those envisioned for the fuel element shown in Fig. 15.1. All materials were purchased from vendors who could supply fuel-element components on a commercial basis. The cement was used to attach the $UC_2$-graphite material to one of the coupons. A second graphite coupon was placed along the opposite side of the $UC_2$ source holder and subjected to a diffusion anneal. Other procedures were similar to those employed for pyrolytic carbon experiments.

**Results.** – Data are available for four specimens that were prepared as described above and annealed at 1900°C. A wedge of each graphite coupon (two for each specimen) was removed in a manner such that the machined surface represented an inclined plane which passed through the original carbon-exposed interface at a very small angle. Portions of the coupons, called "*A*" samples, were removed by slicing down in the direction of migration within regions of the wedge.[26] Other portions, called "*B*" samples, were removed by slicing in planes parallel to the original interface. The procedure for preparing the "*A*" samples enables one to detect solid-state migration, which is characterized by steep concentration profiles near the interface (see Fig. 15.5). The procedure for preparing the "*B*" samples is applicable to relatively fast migration situations.

Analysis of the "*A*" samples did not reveal the presence of a steep concentration gradient near the interface. In fact, the total uranium contents of these samples were practically the same in isothermal regions of the coupons. It was felt that the most realistic presentation of these data would be a tabulation of average values of all the uranium analyses that were obtained from a given coupon. All the results for the "*A*" samples are summarized in Table 15.1. These results should be construed as being representative of an average overall concentration of uranium in an unsectioned coupon.

Analysis of nonisothermal sections of the coupons (which are usually discarded) indicates that the extent of migration was smaller at lower temperatures. In addition, it was possible to obtain some approximate concentration profiles based on the "*B*" samples. These results are presented in Fig. 15.6.

**Tentative Conclusions.** – Comparisons of the values for the cemented and noncemented coupons demonstrate that the cement layer at the interface had a negligible effect on the amounts and rates of migration.

Data in Fig. 15.6 show that the effective $C_0$ for these experiments increased as the annealing time increased; furthermore, it appears that the migration was so rapid that a slight accumulation of uranium occurred at the back boundary. The semi-infinite and constant potential boundary conditions applicable to the pyrolytic carbon experiment do not apply in the present case. Note also that the shapes of the curves in Fig. 15.5 which are characteristic of those describing a uniform (Fick law) migration always show the largest concentration gradients near the interface. This is not true for the curves

**Table 15.1. Uranium Migration in a Porous Graphite–$UC_2$ Impregnated Graphite System at an Average Temperature of 1800°C**

| Specimen Number | Diffusion Annealing Period[a] (hr) | Uranium Concentration[b] of Porous Graphite Coupons ($g/cm^3$) | |
|---|---|---|---|
| | | Cemented | Noncemented |
| | | $\times 10^{-4}$ | $\times 10^{-4}$ |
| 1 | 0.083 | 0.02 | 0.04 |
| 2 | 0.083 | 0.21 | 0.08 |
| 3 | 26.5 | 3.8 | 3.3 |
| 4 | 208.3 | 13.6 | 13.4 |

[a]The time required to reach 1800°C was approximately 1 hr in each experiment.

[b]The concentration was based on a graphite density of 1.782 $g/cm^3$ and the total uranium content of the "*A*" samples.

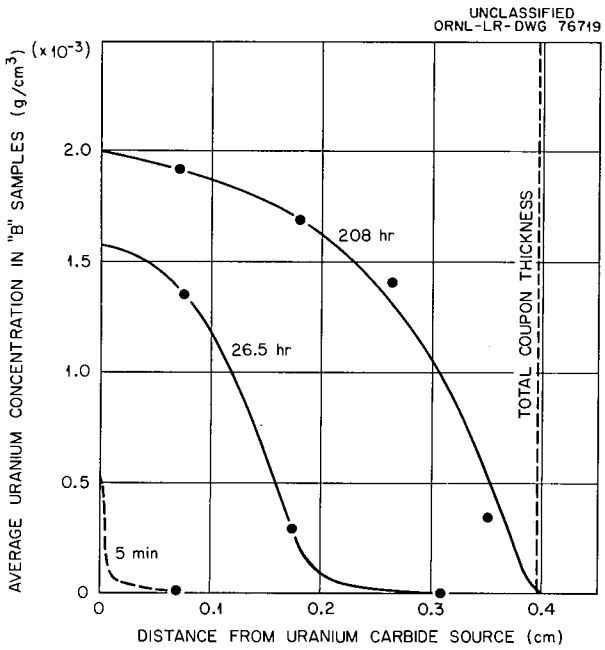


**Fig. 15.6. Concentration Profiles Resulting from the Migration of Uranium into Porous Graphites at 1800°C. The points are based on averages of values for both cemented and noncemented coupons.**

in Fig. 15.6, the shapes of which suggest an additional uranium source within the coupon beyond the interface. The concentrations shown in Fig. 15.6 are very low (and the penetration distances are very high) as compared to solid-state results of Fig. 15.5. It is concluded, therefore, that the uranium migration in the present case is governed by mechanisms and boundary conditions that are entirely different from those discussed in the previous section.

Since the present results cannot be explained on the basis of a solid-state mechanism, it is suspected that the uranium migration is governed by pore-surface effects coupled with an adsorption-desorption phenomenon.

Additional experiments with this system are under way. Nevertheless, the results of these initial experiments suggest that uranium migration from uncoated fuel particles through graphite components might represent a source of considerable contamination of the gas coolant. It should be recognized, however, that temperatures of gas-cooled reactors presently being built or planned are considerably lower than the present experimental temperature, which was selected to reduce the time required for the experiments.

## Diffusion in Beryllium Oxide Matrices

H. J. de Bruin

Preliminary designs[29] for gas-cooled ceramic-fueled and -moderated reactors involve the use of $BeO\text{-}UO_2$ and $BeO\text{-}UO_2\text{-}ThO_2$ in fuel elements, with BeO or BeO and graphite as the moderator. The rates of diffusion of nonvolatile fission products and of fuel through BeO would be useful information for the design of such reactors. Evidence that BeO undergoes structural changes due to nuclear irradiation has been reported,[30] and a difference in the diffusion rates through irradiated and nonirradiated BeO would be expected. Information on the self-diffusion of beryllium through nonirradiated BeO is available;[31] however, similar information on irradiated BeO does not appear in the literature, and the present program is designed to supply data of this type.

Although the diffusion of $UO_2$ in irradiated BeO is probably of greater applied interest than the self-diffusion of Be in BeO, it was deemed advisable to start the program with a study of the self-diffusion phenomenon. The major factor leading to this decision was a desire to develop thin-layer tracer techniques as a complement to the techniques employed in the graphite-carbon experiment.[32] The investigation was begun by testing the apparatus and techniques needed to repeat Austerman's experiments.[31]

**Experimental Procedure.** – Several groups of cylindrical BeO pellets were selected, varying in diameter from 0.25 to 0.8 in. and in density from 80 to 99% of theoretical. The nonirradiated samples were selected on the basis of a microscopic

[29] A. P. Fraas, *Preliminary Designs for Four Integrated Gas-Cooled Ceramic-Fueled and -Moderated Reactor Core and Steam Generator Units*, ORNL-2752, pp 36–47, 60–70 (November 1962).

[30] R. P. Shields, J. E. Lee, Jr., and W. E. Browning, Jr., *Effect of Fast-Neutron Irradiation and High Temperature on Beryllium Oxide*, ORNL-3164 (March 1962).

[31] S. B. Austerman, *Diffusion of Beryllium in Beryllium Oxide*, NAA-SR-3170, pt I (December 1958) and NAA-SR-5893, pt II (May 1961).

[32] C. M. Blood and R. B. Evans III, *Reactor Chem. Div. Ann. Progr. Rept. Jan. 31, 1962*, ORNL-3262, pp 136–42.

investigation of the surface. Irradiated samples for future experiments will be from the same source as those used in radiation damage studies.[30]

The first step in preparing the nonirradiated specimens for diffusion experiments involved annealing them for 2 hr at 2000°C in order to stabilize the BeO microstructure.[31] The diffusion surface at one end of the pellets was ground flat to within 0.5 $\mu$.

An infinitely thin layer of $Be^7$ was placed on the precision-ground surface of a nonporous specimen by covering it with a few milliliters of basic $Be^7Cl_2$ solution. Approximately 5 $\mu$c of $Be^7$ was absorbed during a 24-hr period. The excess liquid was removed, and the pellet was washed, dried, and heated for 2 hr at 500°C in a vacuum. The tenacity of the active layer was tested by forceful cleaning techniques, excluding the use of abrasives; no significant loss of activity was observed. The uniformity of the layer was demonstrated by autoradiography.

The above-mentioned method of depositing $Be^7O$ could not be applied to the more porous specimens (theoretical densities <90%). Such specimens might be placed in contact with other flat surface sources of $Be^7O$ under pressure during diffusion annealing.

The annealing operations were carried out in a vacuum graphite-resistance furnace.[32] A Leeds and Northrup optical pyrometer was used to measure the annealing temperature. The specimen was sectioned after the annealing period by use of the lapping device shown in Fig. 15.7, which is similar to that developed by Austerman.[31] The parallel alignment of the activated surface of a specimen in the device was accomplished to within

Fig. 15.7. Precision Lapping Device.

1 $\mu$. The thickness (5 to 50 $\mu$) of the parallel increments that were removed from the specimen surface was measured to an accuracy of 0.5 $\mu$.

The sectioned specimen was analyzed satisfactorily by measuring the 0.48-Mev gamma emission of $Be^7$. The activity of $Be^7$ remaining in the annealed specimen was measured after the removal of each parallel increment, providing $Be^7$ distribution data. A scintillation detector in association with a single-channel differential analyzer was used for these measurements.

An alternate method of obtaining $Be^7$ distribution data was explored which employs gamma autoradiography. This method involved the application of the wedge technique[32,33] across the diameter of the activated and annealed specimen. The resultant activity gradient across the diameter is related to the sine of the angle ($\sim$1 to 2°) and to the original activity. A lead collimating device was placed between the pellet and the film (Kodak AR-50) in order to provide an intelligible film image. The relative densities of the image obtained were determined with a Joyce microdensitometer.

The results of a preliminary study of this technique indicated that it is difficult to correlate data derived from the gamma-autoradiographic images with those obtained directly by the precision-lapping technique. The gamma radiation background appears to increase with an increase in the fraction remaining obtained from successive collimated film images. If this difficulty can be resolved by further study, this method of obtaining $Be^7$ distribution data would be quite useful.

**Results.** – The diffusion geometry for an infinitely thin layer of $Be^7O$ on the surface of dense, nonporous BeO becomes that of a finite unreplenished plane source with the diffusion path extending into a semi-infinite matrix in the direction normal to the plane surface. The solution to the diffusion equation for these boundary conditions is

$$C(x,t') = \frac{Q}{(\pi D t')^{1/2}} \exp\left(-\frac{x^2}{4Dt'}\right), \qquad (2)$$

where

$C$ = concentration as function of $x$ and $t'$,

$Q$ = total amount of diffusing material placed initially at $x = 0$,

$x$ = depth of penetration normal to the surface in centimeters,

$t'$ = exposure time in seconds for a fixed time interval,

$D$ = diffusion coefficient in square centimeters per second.

The measured amount, $M(x,t')$, in grams per unit area $A$, of $Be^7$ remaining after removal of $\Delta x$ parallel to the activated surface can be defined as

$$M(x_1,t')/A = \int_{x_1}^{\infty} C(x,t')\, dx\,, \qquad (3)$$

where $x_1$ is the depth of sectioning. By substitution of Eq. (2) into Eq. (3) and integrating, the fraction of $Be^7$ remaining becomes

$$\frac{M(x,t')}{AQ} = \frac{2}{(\pi)^{1/2}} \int_{u_1}^{\infty} e^{-u^2}\, du = \operatorname{erfc} u\,, \qquad (4)$$

where $u = x/[2(Dt')^{1/2}]$. Values for the complementary error function (erfc $u$) have been calculated using the penetration data. In the case of the exploratory autoradiographic penetration data, Eq. (2) is used to calculate the value of $D$.

Typical $Be^7$ distribution data for a group of specimens obtained by the sectioning technique are shown in Fig. 15.8. The average $Be^7$ distribution (shown as curve $A$) for BeO specimens from selected groups of pellets indicates that there is very little penetration of the applied tracer into the matrix prior to annealing. Any specimen exhibiting appreciable surface penetration after application of the liquid tracer would disqualify the group it represented for diffusion studies by this method. The corresponding annealing periods and diffusion coefficients are listed in the following table.

| Annealing Temperature (°C) | Annealing Period (sec) | Diffusion Coefficient $D$ ($cm^2$/sec) |
|---|---|---|
| | $\times 10^4$ | $\times 10^{-10}$ |
| 1800 | 8.64 | 6.0 |
| 1650 | 23.4 | 4.0 |
| 1500 | 1.65 | 0.6 |

[33] S. T. Kishkin and S. Z. Bokstein, "Distribution and Diffusion of Components in Metal Alloys Studied by the Autoradiographic Method," *Proc. U.N. Intern. Conf. Peaceful Uses At. Energy, 1st, Geneva, 1955*, p 87, A/Conf. 8/15, United Nations, 1955.

It is evident from the shape of the distribution curves in Fig. 15.8 that the volume diffusion (based on the boundary conditions assumed) only holds for 1 order of magnitude of the fraction remaining. This observation suggests that some other type of diffusion, or some impurity and/or contamination, or change of structure is influencing the $Be^7$ distribution. Further specific conclusions from the results obtained will be dependent on future studies. The next experiments will be on self-diffusion of Be in irradiated BeO and, finally, the diffusion of $UO_2$ in irradiated BeO.

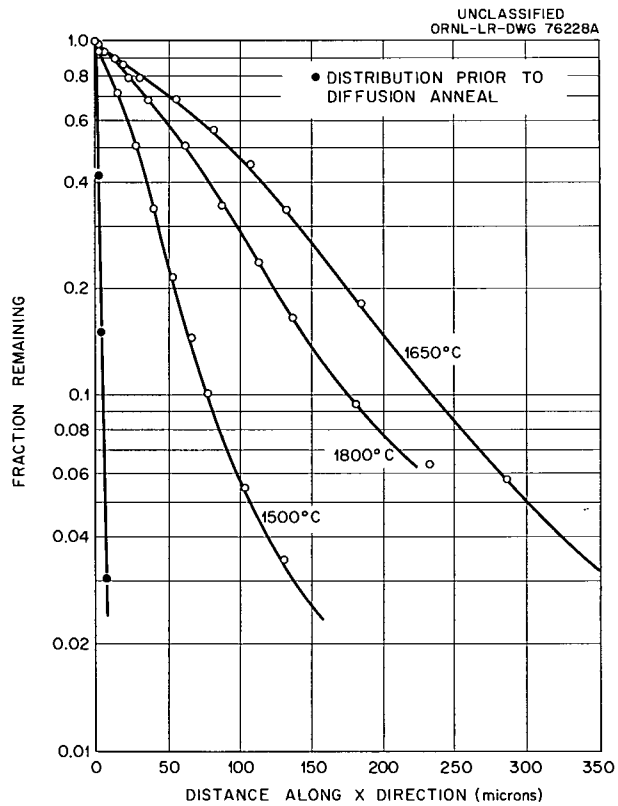


**Fig. 15.8. Beryllium-7 Distribution Data.**

# 16. Reactions of Graphite and Pyrolytic Carbon with Gases

L. G. Overholser

Advanced designs of gas-cooled reactors which utilize cores containing only ceramic materials with high-temperature stability are being considered in order to utilize higher coolant temperatures. Such reactors may be graphite-moderated and utilize fuel elements containing uranium dicarbide cores coated with pyrolytic carbon. Circulation of the helium coolant at temperatures near 1000°C would result in burnout of the carbonaceous materials by contaminants such as $O_2$, $H_2O$, and $CO_2$ that may be present in the coolant. This may lead to deleterious effects on the mechanical properties and result in an increase in the permeability of the carbon coating designed to contain fission products. Rupture of a tube in the steam generator would result in sufficiently high partial pressures of steam in the coolant circuit to give appreciable attack on the pyrolytic-carbon coating which could result in a failure of the coating and a rapid release of part of the contained fission products. Experimental studies have been performed to obtain information relating to the burnout of graphite by low concentrations of $CO_2$ and to establish the incidence of failure of the pyrolytic-carbon coatings when subjected to steam at elevated temperatures.

## REACTION OF GRAPHITE WITH CARBON DIOXIDE

J. P. Blakely N. V. Smith

Experimental studies of the $CO_2$-graphite reaction were initiated using the equipment described previously.[1,2] Helium-$CO_2$ mixtures having a total pressure of 1 atm and low partial pressures of $CO_2$ passed through a quartz reaction chamber containing a suspended graphite specimen and into the sampling manifold. The desired partial pressure of $CO_2$ was obtained by passing helium over a bed of $CaCO_3$ held at a carefully controlled temperature. A liquid-nitrogen-cooled charcoal trap, a heated bed of MnO, and a drying agent were used for purifying the helium. The rate of reaction of the graphite specimen with the He-$CO_2$ mixture was determined from weight changes continuously recorded by a semimicro Ainsworth balance. A Burrell K-7 chromatograph was used to establish the concentration of $CO_2$ and $O_2$ in the entering He-$CO_2$ mixture. Analysis of the effluent gas by this instrument also provided another method of measuring the reaction rate of $CO_2$ with the graphite specimen.

The Burrell K-7 chromatograph utilizes a thermionic type of detector to attain a greater sensitivity than is possible with a thermistor-type detector. The instrument was used with purified helium as carrier gas. A column containing Linde 5A molecular sieve material and a silica-gel column were used to permit analyses for $H_2$, $O_2$, $N_2$, $CH_4$, CO, and $CO_2$. Serious operating difficulties were encountered which prevented full exploitation of the instrument's capabilities. Leaks, irregular flow rates due to clogged orifices, a misaligned filament, and a burned-out filament have been experienced. A grid potential of 21 v is being used instead of 18 v as recommended by

[1] L. G. Overholser and J. P. Blakely, *Reactor Chem. Div. Ann. Progr. Rept. Jan. 31, 1962*, ORNL-3262, pp 144–45.

[2] L. G. Overholser, J. P. Blakely, and N. V. Smith, *GCR Semiann. Progr. Rept. Sept. 30, 1962*, ORNL-3372, pp 279–81.

the vendor in order to obtain the desired sensitivity. The increased grid potential resulted in a high background which was largely eliminated by installation of a line-voltage stabilizer. Poor reproducibility of the instrument's output has required more frequent calibration against gas standards than is considered desirable. Better control of the helium flow by installation of an improved flow regulator and by careful control of the take-off block temperature has resulted in some improvement. It has not been possible to establish whether lack of reproducibility is due to variations in the flow rate or whether it is inherent in the output of the detector. Optimum operating conditions permit the detection of the following concentrations using a 5-$cm^3$ sample: $H_2$ and $N_2$, 2 vpm (volume parts per million); $O_2$, $CH_4$, CO, and $CO_2$, 1 vpm. The concentration limits, however, have been two to three times these values during part of the period of operation.

Studies were made at 875, 925, 975, and 1025°C with a 1-in. sphere (14.4 g) of Speer Moderator-2 graphite. Prior to making the tests, the graphite specimen was heated at these temperatures in pure helium to determine the weight changes due to traces of contaminants in the helium and to outgassing of the graphite. Blank values calculated from the $H_2$ and CO present in the effluent gas agreed satisfactorily with those obtained from weight measurements.

Rates of reaction measured at 875, 925, 975, and 1025°C with a $CO_2$ concentration of 550 vpm are given in Fig. 16.1. These data include rates determined by directly measured weight losses and those calculated from the CO content of the effluent gas. Also included are several directly measured rates obtained at a $CO_2$ concentration of 1100 vpm. The Arrhenius plot of the values obtained by direct weight measurements at a $CO_2$ concentration of 550 vpm corresponds to an activation energy of ~55 kcal/mole. The preliminary values given for the higher $CO_2$ concentration suggest a slightly larger activation energy for these conditions. The apparent order of the reaction with respect to the partial pressure of $CO_2$ appears to be less than unity based solely on rates obtained for 550 and 1100 vpm of $CO_2$. Additional measurements at other $CO_2$ concentrations must be made before the apparent order can be definitely established. Antill and Peakall[3] report an apparent order of unity for $CO_2$ concentrations up to ~500 vpm.

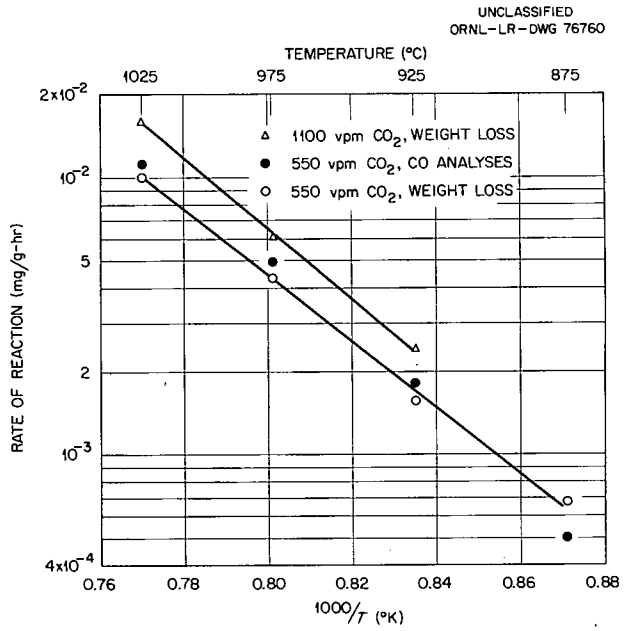


**Fig. 16.1. Arrhenius Plots for $CO_2$-Graphite System at 550 and 1100 vpm of $CO_2$.**

The values given in Fig. 16.1 were obtained at a flow rate of 50 $cm^3$/min. Increasing the flow rate to 200 $cm^3$/min at a $CO_2$ concentration of 550 vpm had no significant effect on the reaction rates at and below 975°C; a small increase was observed at 1025°C. Preliminary observations at a $CO_2$ concentration of 1100 vpm suggest that the increase in reaction rate with flow rate noted at 1025°C may be enhanced by increasing partial pressures of $CO_2$. However, the data are too incomplete to draw any conclusions.

## REACTION OF PYROLYTIC-CARBON-COATED PARTICLES WITH WATER VAPOR

J. P. Blakely N. V. Smith

Studies were undertaken to determine the rate of reaction of pyrolytic-carbon coatings present on various lots of coated uranium particles with water vapor at temperatures around 1000°C, and to establish the incidence of failure of these coatings by leaching the samples with 8 *M* $HNO_3$ following

[3] J. E. Antill and K. A. Peakall, AERE-R-3070 (September 1959).

the steam treatment. A description of the equipment used in these studies and a more complete presentation of the results have been given previously.[4,5]

Steam-helium mixtures having various partial pressures of steam and a total pressure of 1 atm were passed down through a bed of the coated particles at temperatures of 700 to 1100°C. The average reaction rate of the pyrolytic-carbon coating with steam was determined from the loss in weight observed during the indicated time of exposure to steam. The incidence of failure of the pyrolytic-carbon coatings upon exposure to steam was determined from the quantity of uranium leached by an 8 *M* $HNO_3$ treatment for 8 hr at ~90°C, and the total quantity of uranium originally present in the coated particles. Microscopic observations of the particles were made prior to and after the steam and $HNO_3$ treatments. The limited quantities of coated particles available from the various lots examined precluded any extensive study of the important parameters, namely, temperature, time, and partial pressure of steam.

Representative data for three lots of coated particles are given in Table 16.1. The rates of reaction observed at 900 and 1000°C for lots 3M-114 and 3M-117 are in satisfactory agreement, but significantly higher at 1000°C than that found for lot 3M-113. The reaction rates given for lot 3M-114 at 800, 900, and 1000°C are in good agreement with extrapolated data of Pilcher *et al.*[6] for the graphite-steam reaction. The Arrhenius plot of the data obtained for lot 3M-114 at 800, 900, and 1000°C and 355 mm Hg partial pressure of steam corresponds to an activation energy of ~40 kcal/mole. Other data are not sufficiently precise to give a reliable value for the activation energy. Data are presented in Fig. 16.2, which show that the apparent order of the reaction of lot 3M-114 particles with respect to the partial pressure of steam is less than unity at 1000°C. This also is in agreement with the data reported by Pilcher *et al.*[6]

A comparison of the percent of coating removed by the steam treatment with the percent of uranium obtained by the nitric acid leach shows that the various lots of coated particles behave differently. For example, the removal of 25% of the pyrolytic carbon present in lot 3M-113 exposed virtually all the uranium, whereas the coatings on lot 3M-114 particles were protective after a 39% removal of the pyrolytic carbon. The degree of protection afforded by the pyrolytic carbon on lot 3M-117 particles appears to be between that observed for the other two lots.

All three lots of coated particles have a laminar-type coating and a nominal coating thickness of 100 $\mu$. The differences noted must arise from variations in the coating conditions used by the manufacturer. Unfortunately, such information is largely of a proprietary nature. Figures 16.3 and 16.4 provide a clue as to what occurred to the coatings on lot 3M-113 and 3M-114 particles, respectively, when they were exposed to steam at elevated temperatures. The attack in the case of lot 3M-113 particles (Fig. 16.3) is of a localized nature characterized by pits in many of the coatings. This type of attack would result in

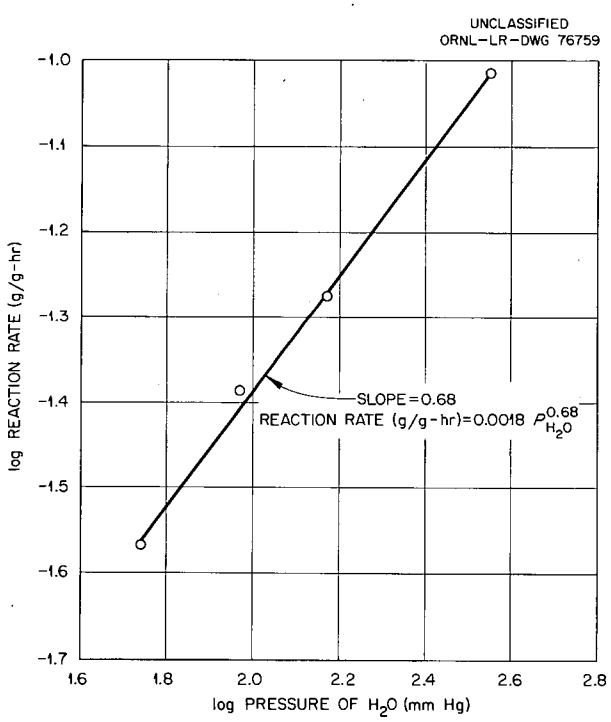


**Fig. 16.2. Apparent Order of Reaction for Lot 3M-114 at 1000°C.**

[4] L. G. Overholser, J. P. Blakely, and N. V. Smith, *GCR Quart. Progr. Rept. Mar. 31, 1962*, ORNL-3302, pp 223–24.

[5] L. G. Overholser, J. P. Blakely, and N. V. Smith, *GCR Semiann. Progr. Rept. Sept. 30, 1962*, ORNL-3372, pp 259–69.

[6] J. M. Pilcher, P. L. Walker, Jr., and C. C. Wright, *Ind. Eng. Chem.* **47**, 1742 (1955).

exposure of the uranium carbide core without extensive removal of the pyrolytic-carbon coating. It will be noted that a number of the particles show signs of only a superficial attack. Figure 16.4 shows that the pyrolytic-carbon coatings on lot 3M-114 underwent a generalized type of attack with little or no pitting in evidence. The coatings on all the particles were damaged with a peeling of the outer portion of the coating very evident. In several cases, the bulk of the coating was removed but no path opened to the core. This generalized attack probably accounts for the protection afforded the cores even after about a 39% removal of the pyrolytic carbon.

The results obtained from the three lots of pyrolytic-carbon-coated particles given in Table 16.1, and two lots examined and reported[4] earlier, show marked differences in behavior which are

**Table 16.1. Reactivity of 3M-113, 3M-114, and 3M-117 Coated Particles with Various Partial Pressures of Steam at 700 to 1100°C**

| Lot Number | Time (hr) | Temperature (°C) | Pressure of $H_2O$ (mm Hg) | Pyrolytic Carbon Reacted (g) | (%) | ($g\ g^{-1}\ hr^{-1}$) | Uranium Removed by $HNO_3$ Leach (%) |
|---|---|---|---|---|---|---|---|
| 3M-113 | 6 | 700 | 355 | 0.002 | 0.2 | 0.0003 | 0.02 |
| | 4 | 800 | 355 | 0.041 | 2.6 | 0.006 | 4 |
| | 7 | 800 | 355 | 0.203 | 11 | 0.016 | 22 |
| | 6 | 1000 | 355 | 0.450 | 25 | 0.042 | 97 |
| 3M-114 | 6 | 800 | 233 | 0.036 | 3.2 | 0.005 | 0.3 |
| | 6 | 800 | 355 | 0.036 | 3.3 | 0.006 | 0.9 |
| | 6 | 900 | 233 | 0.127 | 14 | 0.024 | 0.1 |
| | 6 | 900 | 355 | 0.211 | 18 | 0.030 | 1.4 |
| | 4 | 1000 | 55 | 0.099 | 11 | 0.027 | 0.1 |
| | 4 | 1000 | 92 | 0.149 | 16 | 0.041 | 0.2 |
| | 4 | 1000 | 149 | 0.193 | 21 | 0.053 | 0.1 |
| | 4 | 1000 | 355 | 0.424 | 39 | 0.097 | 1.3 |
| 3M-117 | 4 | 800 | 355 | 0.069 | 6.4 | 0.016 | 0.4 |
| | 4 | 800 | 635 | 0.163 | 16 | 0.040 | 1.3 |
| | 1 | 900 | 355 | 0.030 | 2.8 | 0.028 | 3.0 |
| | 2 | 900 | 355 | 0.075 | 6.9 | 0.035 | 6.2 |
| | 4 | 900 | 355 | 0.142 | 13 | 0.034 | 5.9 |
| | 1 | 900 | 635 | 0.052 | 6.2 | 0.062 | 4.1 |
| 3M-117 | 2 | 900 | 635 | 0.172 | 17 | 0.083 | 4.1 |
| | 1 | 1000 | 355 | 0.084 | 6.4 | 0.064 | 4.4 |
| | 2 | 1000 | 355 | 0.133 | 13 | 0.063 | 3.4 |
| | 4 | 1000 | 355 | 0.417 | 40 | 0.10 | 6.8 |
| | 1 | 1000 | 635 | 0.114 | 12 | 0.12 | 4.1 |
| | 1 | 1100 | 635 | 0.421 | 46 | 0.46 | 40 |

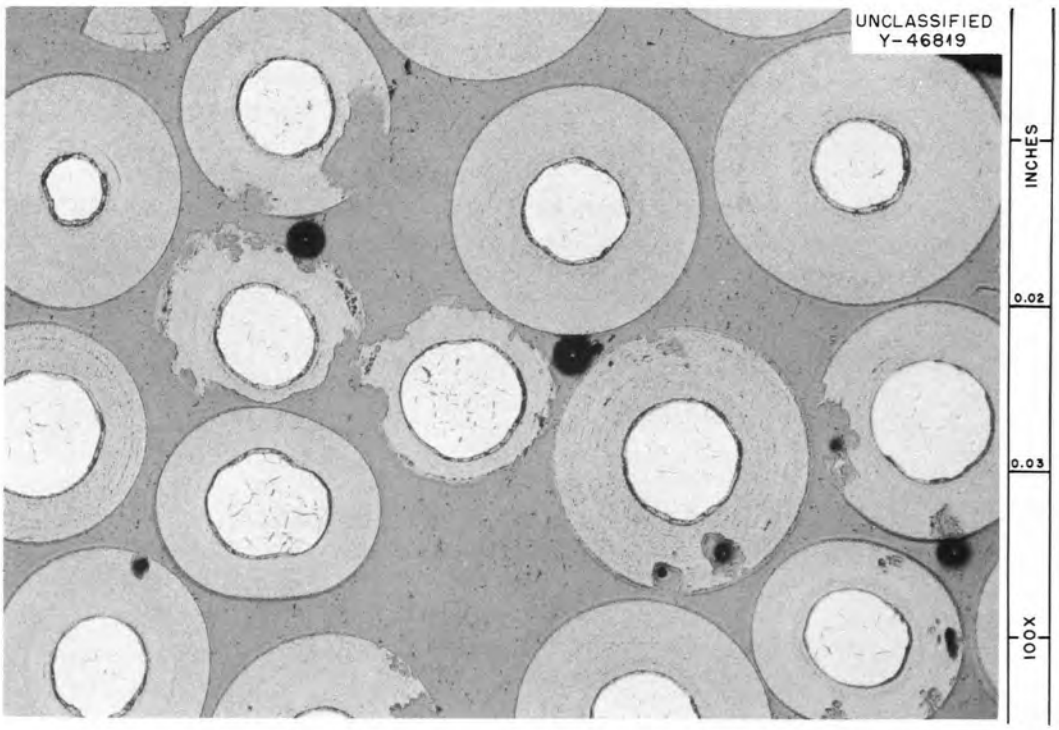


Fig. 16.3. Photomicrograph of 3M-113 Particles Following 7-hr Exposure to Steam. Reduced 15%.

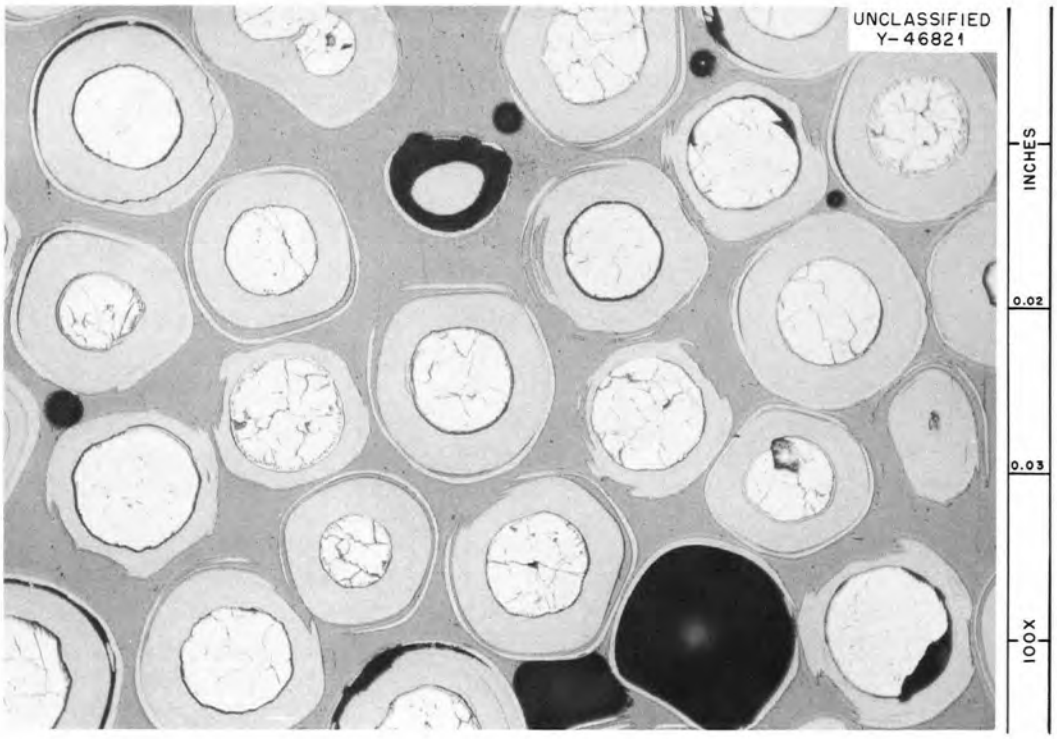


Fig. 16.4. Photomicrograph of 3M-114 Particles Following 4-hr Exposure to Steam. Reduced 15%.

probably associated with different modes of attack by steam at elevated temperatures. Differences in reaction rates and degree of protection have been observed for the various lots of particles under comparable conditions of exposure. There is no clear-cut relationship between the amounts of pyrolytic carbon removed from the coatings and the incidence of failure as determined by the nitric acid leach. It appears unlikely that the coatings would afford protection at 1100°C for any reasonable period of time at a steam pressure of 1 atm. Prolonged exposure at temperatures of 800°C and below appears to be permissible for at least some of the lots of coated particles examined. Experimental evaluation of a particular lot of particles would be necessary before its compatibility with steam at 900 to 1000°C could be predicted with any degree of certainty.

# 17. Measurement of Temperature in Reactor Environments

It is necessary that the techniques of temperature measurement keep pace with technological developments in other fields during the design and construction of advanced concepts of nuclear energy devices. Research leading to such devices and subsequent applications rely upon the accurate measurement of temperature. The required sensors must be capable of sustained operation at elevated temperatures in radiation environments and exposed to diverse atmospheric conditions.

The study has been devoted primarily to thermocouples, since they appeared to be satisfactory for many of the applications. However, detailed studies of the reliability of proposed thermocouples in the expected environments were necessary. The uses of bare-wire and metallic sheathed thermocouples in pure helium atmospheres and in atmospheres exposed to graphite, carbon monoxide, and hydrogen have been studied extensively. An experiment was designed to show the effects of nuclear radiation on thermocouple emf output. Such experiments will be of great value in determining the reliability and life expectancy of thermocouples used in nuclear power reactors.

## STABILITY OF CHROMEL-P/ALUMEL THERMOCOUPLES SHEATHED IN STAINLESS STEEL

W. T. Rainey, Jr. R. L. Bennett
H. L. Hemphill

Chromel-P/Alumel thermocouples sheathed in stainless steel have shown[1] a drift in emf output when exposed at elevated temperatures to gases desorbed from graphite (predominantly hydrogen and carbon monoxide). Further tests showed that similar thermocouples developed emf errors when exposed to a 7-psig hydrogen atmosphere at 870°C, but remained reasonably constant in 7-psig carbon monoxide and 150-psig hydrogen. Representative thermocouples were examined for homogeneity upon termination of the tests. Emf profile data were obtained for the individual wires in grounded-junction thermocouples by spot-welding a homogeneous platinum wire to the stainless steel sheath at the hot junction. Each thermocouple was then inserted into an isothermal tube furnace to a depth greater than its test exposure depth. After temperature equilibrium, it was withdrawn stepwise. The emf data recorded at each position of platinum vs Chromel, Alumel, and sheath was converted to an error emf by subtraction of the theoretical value. Emf error profiles for these couples are shown in Fig. 17.1.

Insulated (ungrounded-junction) couples were used in the 150-psig hydrogen test, so it was not possible to measure profiles for the individual legs. The values plotted are errors measured for Chomel vs Alumel. Since the couple showed an essentially flat emf error profile, it was assumed that the individual legs were still homogeneous and had not been chemically damaged by the exposure.

The emf error profiles of wires exposed in 7-psig hydrogen were typical of those observed previously after exposure to selectively oxidizing atmospheres. Only the Chromel wire showed evidence of inhomogeneity, and this appeared in the region 9 to 12 in. from the hot junction. Inhomogeneities in this region were responsible for emf drifts during the tests, since they were in the steepest thermal-gradient section of the test furnace.

The profiles of those thermocouples exposed to 7-psig carbon monoxide showed that appreciable composition changes occurred in both wires. This

[1] W. T. Rainey, Jr., and R. L. Bennett, *Reactor Chem. Div. Ann. Progr. Rept. Jan. 31, 1962*, ORNL-3262, p 152.

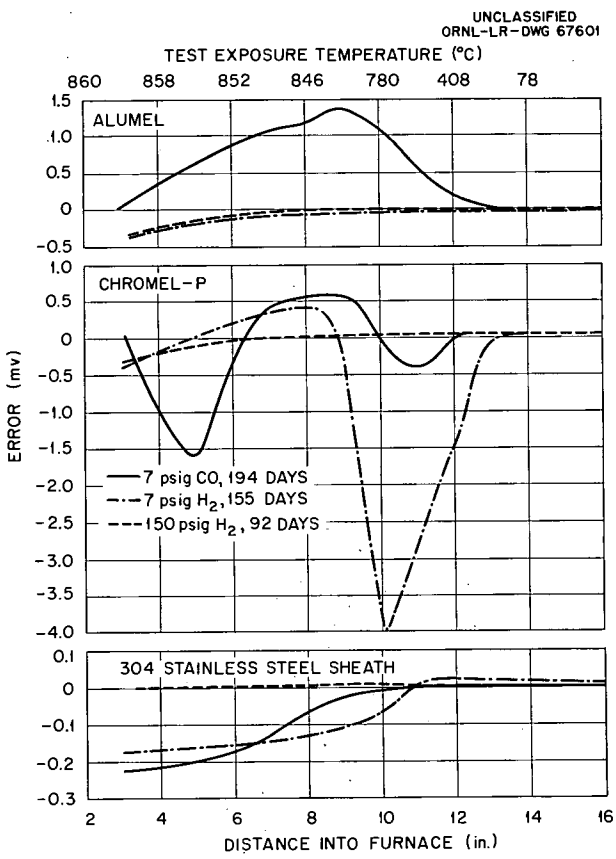


**Fig. 17.1. Thermal-Gradient EMF Profiles of Test Thermocouples.**

attack did not result in large emf errors during the test, since the major changes occurred in reasonably isothermal regions. The slight positive emf drift which was measured was the result, primarily, of a combination of the positive error in the Alumel and the negative error in the Chromel in the region 10 to 12 in. from the junction. This small peak in the Chromel wire corresponded to that observed frequently in selectively oxidizing atmospheres. Figure 17.2 shows a cross section of this thermocouple at 9 in. from the hot junction. The Alumel wire (on the left) showed rather severe attack which was responsible for the emf error profile. Other sections showed the attack to be most severe in the 7-to-9-in. section and to decrease in other sections. The Chromel wire was only slightly attacked, and the sheath showed no evidence of carburization.

The larger peak in the Chromel profile is explained by Fig. 17.3. The Chromel wire was severely attacked in this region, and, as in other nearby sections, the attacking agent appeared to be concentrated on the side toward the sheath. The attack on the Alumel in this section was less than in the 9-in. section, as also indicated by the profile, and it seemed to be mainly distributed over the surface rather than concentrated in one direction. This was usually the case with Alumel. This micrograph shows heavy carburization of the sheath, as was the case in all sections from the high-temperature portion of the furnace. Further metallurgical study will be required for identification of the precipitated phases in these wires.

The discovery of the severe attack on both the Chromel-P and Alumel, which was not revealed by the drift data, prompted a new set of tests under conditions more closely simulating those of the EGCR and PBRE. The thermocouples were exposed at 700°C to an outgassed graphite block in a flowing helium atmosphere containing 350 ppm CO. These thermocouples, which have now been exposed for eight months, developed a positive error of 10 to 15°C during the first month and have remained relatively constant since that time. One of the thermocouples was withdrawn after six months and its thermal-gradient emf profile was determined. Both wires had developed inhomogeneities in the sharp gradient region. The Alumel showed a positive emf error, and the Chromel-P had a negative error. The relative positions in the gradient and the magnitude of the errors were such that the resultant thermocouple error was positive.

Thermocouples which were exposed to a graphite–purified helium system at 700°C showed an average drift of only −4°C after 161 days of exposure. However, profile measurements showed that a nonhomogeneous region had developed in the region exposed in the temperature range of 470 to 670°C.

Tests are being performed to compare emf drifts in samples from different manufacturers. Since exposure to 7-psig hydrogen at 870°C produced rapid emf drifts, these conditions were selected for the tests. The variation in drift results was considerable. For example, drifts after 60 days ranged from essentially 0 to −1.05 mv (−21°C) for two different lots of stock from the same vendor. As was reported previously,[1] drift data cannot be easily correlated with differences in thermocouple stock or slight differences in handling of materials during fabrication of the hot junctions.

It was concluded that exposure of stainless-steel-sheathed Chromel-P/Alumel thermocouples to

graphite-contaminated atmospheres may lead to eventual failure of the thermocouple. The expected service life and reliability of the thermocouple are, naturally, functions of the exposure conditions. The thermocouples appeared reliable for at least six months at temperatures of about 700°C, even though the wires were attacked slightly. Attack of the thermocouples was more rapid at 870°C, even though the emf output was often unaffected during the test. Those thermocouples exposed to gases desorbed from graphite (especially hydrogen) showed rapid emf drifts, and this phenomenon seemed to be closely related in some unexplained way to the manufacturing techniques used by the supplier.

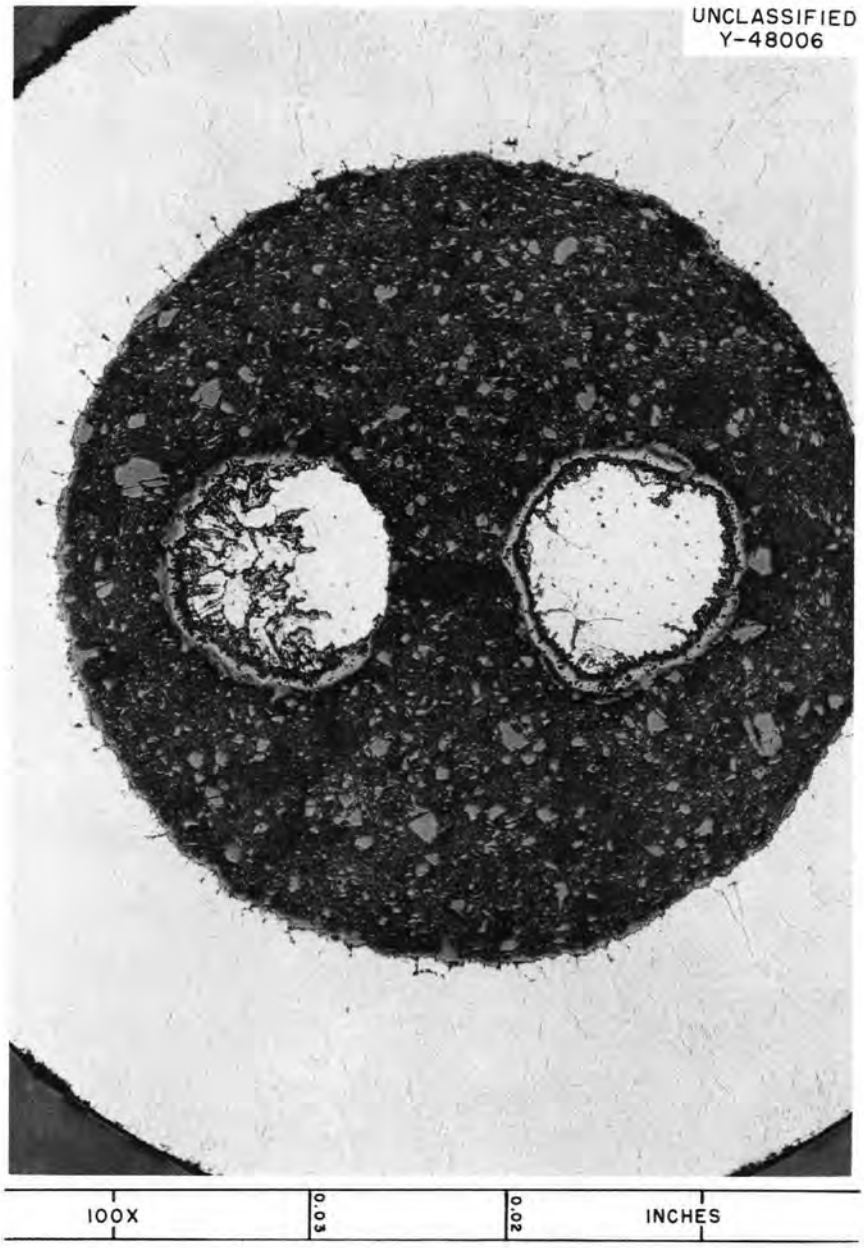


Fig. 17.2. Cross Section at 9 in. from Hot Junction of Stainless-Steel-Sheathed Chromel/Alumel Couple After Exposure to Carbon Monoxide.

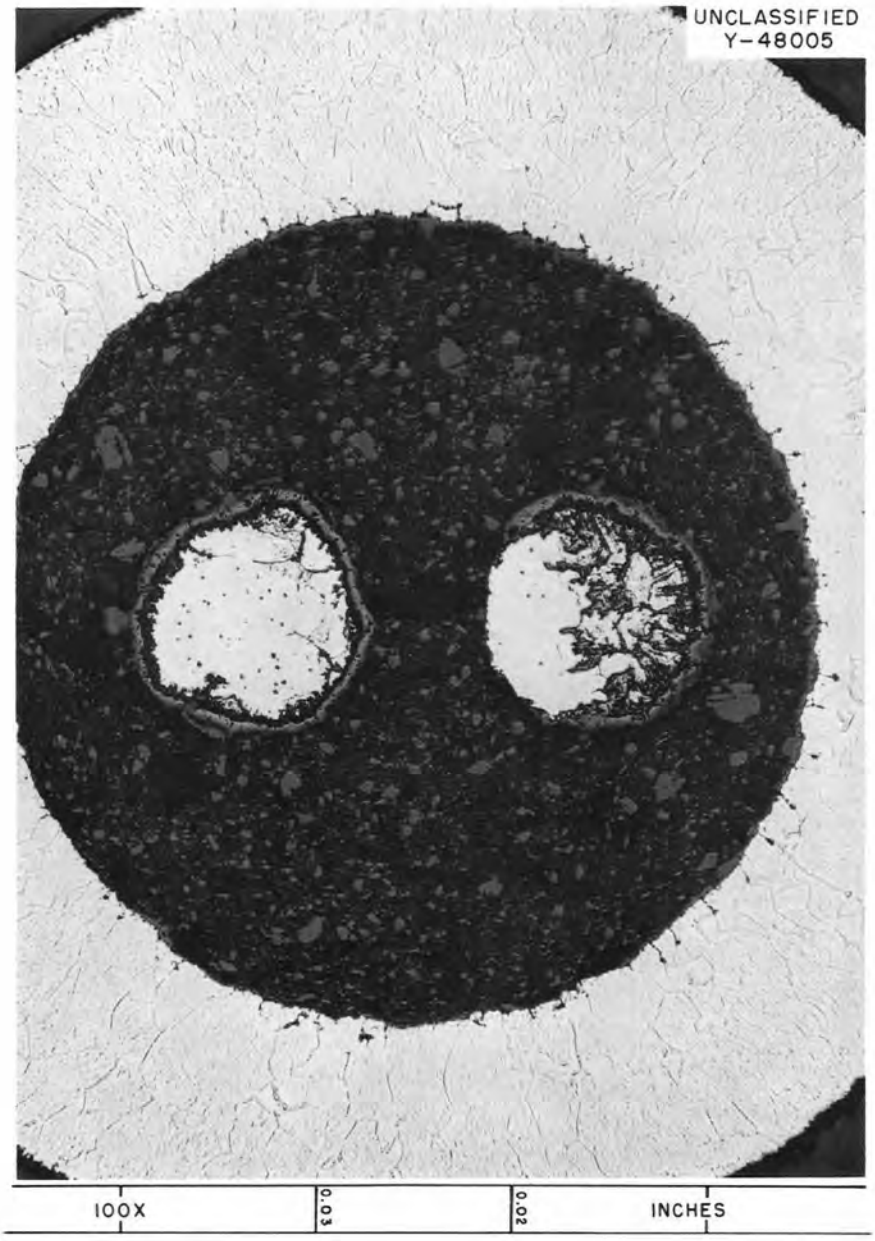


Fig. 17.3. Cross Section at 4.75 in. from Hot Junction of Stainless-Steel-Sheathed Chromel/Alumel Couples After Exposure to Carbon Monoxide.

## THERMOCOUPLE STABILITY UNDER PBRE CONDITIONS

R. L. Bennett H. L. Hemphill

Test wires were exposed for 54 days at 760°C (1400°F) and 982°C (1800°F) in stainless steel containers to a flowing helium atmosphere (1 atm, 5 $cm^3$/min) containing 500 ppm $H_2$ and 500 ppm CO in the presence of (but not in contact with) either AGOT graphite or Si-SiC-coated AGOT graphite. The following wires were included in each test:

| | |
|---|---|
| Chromel-P | Platinum |
| Special Chromel-P | Pt–0.1% Mo |
| Chromel-A | Pt–5.0% Mo |
| Chromel-AA | Pt–10% Rh |

| | |
|---|---|
| Geminol-P | Pt–20% Rh |
| Alumel | Pt–30% Rh |
| Special Alumel | Pt–40% Rh |
| Geminol-N | Platinel 1503 |
| Nickel | |
| Tungsten | Platinel 1786 |
| Rhenium | Monel |
| W–26% Re | Stainless Steel, type 347 |
| Molybdenum | Inconel |
| Mo–50% Re | Niobium |
| Ni–18% Mo | Tantalum |

After removal from the containers, the wires were compared thermoelectrically at 420°C with as-received wires.

After exposure at 760°C, the following wires were in error less than 0.5% at 420°C: Chromel-P, Special Chromel-P, Special Alumel, Geminol-P, molybdenum, Ni–18% Mo, Pt–5.0% Mo, Geminol-N, and tungsten. The Pt-Rh alloys were in error 0.5 to 1.0% and were the only wires to develop greater errors in the presence of silicon.

After exposure at 982°C, only the Ni–18% Mo and tungsten wires were in error less than 0.5% at 420°C. The physical condition of all wires was poor, and more wires were lost due to both mechanical failure and chemical decomposition than at 760°C.

Similar tests are under way with most of the wires listed above, isolated from each other to prevent cross contamination. The present tests do not include exposure to Si-SiC-coated AGOT graphite, since such exposure did not appear detrimental to most wires. Samples removed after 22 days of exposure to both temperatures were in good physical condition. Thermoelectric and metallographic comparisons will be carried out on these and other wires to be removed periodically from the test furnace.

It has been concluded that the presence of Si-SiC coating on AGOT graphite was not detrimental to bare-wire thermocouple stability, except for the platinum alloys. Most of the damage to the wires was the result of exposure to carbon or carbon monoxide. Selected wires may have a reasonable life expectancy in such atmospheres at 760°C, even when unprotected, and it is possible that properly sheathed base-metal thermocouples would be satisfactory for indefinite periods of time. It seems unlikely that bare wires will give satisfactory service at temperatures in the 1000°C range. Even though the materials tested for use as sheaths did not hold up well in these tests, they might be adequate to protect the wires for sufficient time under expected service conditions to warrant periodic replacement.

## REFRACTORY METAL THERMOCOUPLES

R. L. Bennett H. L. Hemphill

Tungsten vs tungsten–26% rhenium thermocouples have been tested for stability in pure and in slightly contaminated helium atmospheres. Pure helium and helium-CO tests (1 atm, 10 $cm^3$/min) were carried out in a graphite-helix furnace with the test thermocouples and the black body mounted vertically in the heating element. The hot junction, which was positioned at the high-temperature point of the heater, was formed by wedging the wires into the tungsten black body. The test temperature was maintained constant within ±5°C by manual control of the input power, and it was monitored by use of an optical pyrometer.

Bare tungsten vs tungsten–26% rhenium thermocouples were found to be stable thermoelectrically at 1750°C in pure helium. The emf's of alloy wires from two vendors coupled against a common tungsten wire were constant within ±10°C for an exposure of 950 hr. Negative drifts were observed in early tests but these were believed to be due to trace contaminants.

Tests of tungsten, tungsten–5% rhenium, tungsten–26% rhenium, rhenium, and iridium–60% rodium were made in a helium atmosphere containing 100 ppm of CO at 1750°C. Large drifts in the emf of the W/W–26% Re couple were observed. A change of about +3.0 mv (180°C) in 90 hr was typical for thermocouples made of 0.020-in.-diam wire. As expected, smaller wire (0.010 in.) changed more rapidly, about +7.0 mv (400°C) in 24 hr. It was found that the emf outputs of rhenium and iridium–60% rhodium were not appreciably changed by exposure under these conditions. After 50 to 75 hr exposure of 0.010-in. wires, the following couple drifts were noted: W vs Re, –2.4 mv; W–5% Re vs W, –6.0 mv; W vs W–26% Re, +3.5 mv; W–5% Re vs W–26% Re, –2.5 mv. At this temperature, the polarity of the individual wires is W–5% Re < W < Re < W–26% Re in order of increasing negativity. If the rhenium were unchanged, the individual wire drifts would be: W, –2.4 mv; W–5% Re, –8.5 mv, W–26% Re, –5.9 mv. Drift rates with 25 ppm CO in the helium atmosphere were approximately the

same as with 100 ppm. The rates were generally rather rapid for the first 100 hr of exposure and then leveled off to slower drifts.

Exposures to the He–100 ppm CO at lower temperatures showed similar results at reduced rates. At 1370°C the following couple drifts occurred after 216 hr of exposure: W vs Re, –0.43 mv; W–5% Re vs W, –0.83 mv; W vs W–26% Re, +1.40 mv; W–5% Re vs W–26% Re, –1.26 mv. This corresponded to the following individual wire drifts: W, –0.43 mv; W–5% Re, –1.26; W–26% Re, –1.83. The positive drift of the W–5% Re vs W–26% Re couple and negative drift of the W–5% Re vs W couple appeared to contradict the results at 1750°C. However, the sign of the couple drift is only an indication of the relative rates of drift of individual wires and may be reversed by changes in conditions, even though the same chemical reactions occur.

Tungsten and tungsten–5% rhenium wires were thermoelectrically stable at temperatures below about 1150°C in the same atmosphere. Tungsten–26% rhenium was not tested.

Tungsten vs tungsten–26% rhenium couples have also been studied in flowing helium atmospheres containing low oxygen concentrations. The couples were tested in alumina protection tubes at 1200°C. Emf measurements of couples exposed to a helium atmosphere containing 100 ppm $O_2$ became very erratic within 2 hr and, in some cases, developed reversed polarity. Such results are believed to be due to spurious emf's developed between metals and oxides. Exposure of these couples to He–10 ppm $O_2$ at 1200°C resulted in an immediate drift. The emf error after 2 hr of exposure was +0.68 mv (34°C). Thermal-gradient profile measurements showed that the nonhomogeneity causing the error was in the region of the wire exposed at 950 to 1150°C. Since the atmosphere flowed along the wires inside the protection tube, reaction would be expected to occur first in the gradient region. The fact that no reaction was detected in the hotter, isothermal (1200°C) region of the tube probably indicated removal of oxygen from the helium before it reached this region. In all cases, the couples failed within 18 hr due to oxidation and eventual loss of electrical continuity.

The results of tests to date indicate that tungsten, rhenium, and tungsten-rhenium alloys are thermoelectrically stable in completely inert atmospheres at 1750°C and lower temperatures. However, both metals and their alloys are easily oxidized at elevated temperatures and are not recommended for use when traces of air or moisture could be present. Pure rhenium appears to be the most stable metal tested in atmospheres containing traces of CO at temperatures above about 1150°C; neither tungsten nor the tungsten-rhenium alloys are recommended under these conditions. The alloy wires appeared to be much more stable in emf output in the presence of CO at 1150°C than at higher temperatures.

## THERMOCOUPLE TRANSMUTATION STUDIES

W. T. Rainey, Jr. R. L. Bennett

Design of an experiment for irradiation and thermoelectric calibration of a set of thermocouple wires was completed by personnel of the Reactor Division in cooperation with members of the Reactor Chemistry Division. A mockup of the assembly was constructed and is presently undergoing out-of-pile thermal cycling tests.

The apparatus was designed for use in the F-9 facility of the ORR during periods between fuel-meltdown experiments. Since the primary purpose of the experiment is to measure thermocouple emf changes due to transmutation, attempts were made to ensure uniform irradiation of the sections of the wires under test and to permit accurate control and measurement of temperatures during recalibrations.

The irradiation section of the assembly contains the test wires (about 20 individual wires) mounted on a retractable tantalum tube with a common hot junction at the lower end. In the extended position, the wires are located in a resistance-heated molybdenum furnace designed to reach a temperature of at least 1500°C. The location of the thermal gradient between furnace and ambient temperature is determined by insulating wafers in the upper section. In the retracted position, the wires are enclosed in an aluminum sleeve having good thermal contact with the coolant water in order to dissipate gamma heating. It is estimated that wire temperatures will be about 200°C during irradiation. The cold junctions between thermocouple and copper wires are located in a unit maintained at pool temperature with arrangements for measurement of cold junction temperature with standard thermo-

couples. Copper instrument wires and heater power leads are brought out through watertight seals.

Radiation monitors or standard thermocouples can be inserted in the central tube adjacent to the test wires during irradiation or recalibration.

Irradiation of the wires will be carried out with the thermocouple wires in the retracted position. The assembly will be removed periodically from the reactor and hung on the side of the pool for recalibration. The wires will be extended into the furnace unit, and a standard thermocouple will be inserted into the center tube. Measurements of emf will be made while the furnace temperature is increasing and during cooling to note whether annealing effects are measurable.

The furnace unit has operated successfully to date in a mockup immersed in water for thermal cycling tests (maximum 800°C).

# 18. Alternate Coolants for Gas-Cooled Reactors

The possibility of lowering cooling costs in advanced gas-cooled reactors by the use of more efficient coolants is an attractive one. A hypothetical ideal coolant should, under reactor operating conditions, be radiolytically and thermally stable, be inert to the materials it contacts, have good heat transfer properties, and be abundant and cheap. Obviously, many compromises are made in the selection of a coolant. As a preliminary aid in the search for alternate coolants, some considerations were given to the thermal and radiation stability of possible coolants and to the heat transfer properties of dissociating gaseous mixtures.

## THERMAL AND RADIATION STABILITY OF PROPOSED NUCLEAR REACTOR GAS COOLANTS

W. T. Rainey, Jr. R. L. Bennett
G. W. Keilholtz

A literature survey has been made to collect information relative to the thermal and radiolytic stability of materials suggested as possible coolants because of satisfactory physical properties. The following compounds have been suggested for consideration: $B_2H_6$, $BF_3$, $CF_4$, $MoF_5$, $MoF_6$, $NbF_5$, $NF_3$, $SF_6$, $SiF_4$, and $SiH_4$. Detailed information on the reactivity of these compounds has been reported previously.[1] Information indicating compatibility with expected contaminants in gas-coolant systems has also been collected. Only $SiF_4$, $SF_6$, and $CF_4$ are suggested as possibly satisfactory coolants on the basis of the collected information and thermodynamic calculations.

The equilibrium constants for decomposition of the molecules into elements are given in Table 18.1. These constants were calculated[2] from the standard free energies of formation at the stated temperatures. No consideration was given to any other possible decomposition reactions or to

[1] W. T. Rainey, Jr., and R. L. Bennett, *Thermal and Radiation Stability of Suggested Alternative Gas Coolants*, ORNL CF-62-11-9 (Nov. 5, 1962).

[2] *JANAF Thermochemical Data*, Dow Chemical Co., Midland, Mich., 1961.

**Table 18.1. Equilibrium Constants for the Decomposition of Molecules into Elements**

| Molecule | Log $K_p$ [a] | | |
|---|---|---|---|
| | 800°K(981°F) | 1200°K(1700°F) | 1600°K(2420°F) |
| $BF_3$ | −62.47 | −46.01 | −33.64 |
| $B_2H_6$ | +13.20 | +11.86 | +11.59 |
| $CF_4$ | −111.27 | −51.64 | −31.78 |
| $NF_3$ | −8.94 | −0.81 | +1.86 |
| $SiF_4$ | −196.31 | −94.37 | −60.39 |
| $SiH_4$ | +8.28 | +6.58 | +6.11 |
| $SF_6$ | −139.38 | −60.57 | −33.05 |

[a] $K_p$ = (elements)/(molecule).

possible reactions between reactants and construction materials.

These data reflect the thermodynamic stability of each compound and could be used to calculate compositions of the gases at equilibrium, subject to the above-mentioned limitations. However, kinetic data, which would be of more practical value, are limited. Even thermal decomposition kinetic data would be of questionable value in estimating the stability of compounds in radiation environments.

The low thermal stability of $B_2H_6$, $SiH_4$, and $NF_3$ would prevent the use of these gases. They would be rather reactive also toward oxidizing contaminants which would be present in a practical reactor gas system.

Boron compounds could not be used without removal of the high cross section $B^{10}$ isomer. Pile irradiation of $BF_3$ has shown it to be easily decomposed. A thermal neutron dose of $10^{20}$ *nvt* resulted in about 25% decomposition.[3] The chemical reactivity of molybdenum and niobium fluorides seems sufficient of eliminate them from consideration.

The carbon, silicon, and sulfur fluorides appear to be the most promising compounds for use as coolants. Radiolytic decomposition of $CF_4$ in BEPO (the British experimental pile) resulted in a $G(F_2)$ of 0.28 molecule of fluorine formed per 100 ev of energy absorbed.[4] It is plausible to expect liberation of $F_2$ from $SiF_4$ and $SF_6$ during irradiation. However, these three compounds are extremely stable thermally and should be chemically inert under reactor conditions.

An experimental investigation of radiation damage to $CF_4$, $SiF_4$, and $SF_6$ has been started. Cobalt-60 irradiation will be used to measure decomposition rates of these three compounds at ambient temperature. Qualitative and quantitative analyses of reaction products will be made by use of a mass spectrometer, with initial emphasis on measurement of fluorine formation. The gamma dosimetry for gases enclosed in metal capsules is difficult to calculate accurately. Therefore, chemical dosimetry using gases of known *G* value, such as nitrous oxide, acetylene, or methane, will be necessary for satisfactory estimation of absorbed energy doses. It will also be necessary to determine reaction rates in the presence of construction materials, carbon, and trace impurities such as water, hydrogen, and carbon oxides.

[3]W. K. McCarty, *Experimental Determination of the Radiation Decomposition of Boron-10 Enriched Trifluoride and the Resultant Corrosion of the Containing Materials*, NAA-SR-1999 (Oct. 15, 1957).

[4]P. C. Davidge, *The Decomposition of Ammonia and Carbon Tetrafluoride by Pile Irradiation*, AERE-C/R-1569 (Dec. 21, 1955).

## HEAT TRANSFER PROPERTIES OF DISSOCIATING GASEOUS MIXTURES[5]

C. S. Shoup, Jr.

A dissociating gas may in principle be more effective as a heat transfer medium and thermodynamic working fluid than a nondissociating gas as a consequence of the contribution of its heat of dissociation to the thermal conductivity and specific heat of the gaseous mixture. For this reason, the effects of various parameters on the transport and thermal properties of dissociating gaseous mixtures were studied within the range of 500 to 2000°C.

In order to take advantage of the increase in thermal conductivity and specific heat due to the dissociation, the heat of dissociation must be relatively large, the molecular weight and molecular volume of the gas must be relatively small, and both associated and dissociated molecules must be present in appreciable amounts within the temperature range of interest. Very few dissociating gases meet all of these requirements.

In order to illustrate the effects of dissociation on the heat transfer properties of gaseous mixtures, estimates were made for the thermal conductivity, specific heat, viscosity, and specific volume of helium–aluminum chloride and helium-fluorine mixtures as a function of temperature at various pressures and compositions. Most of the calculations were based on equations previously derived,[6–8] and neglect any effects due to thermal diffusion or pressure gradients. Thermodynamic functions were taken from the JANAF tables.[2] The maxima in the thermal conductivity and specific heat curves, which are due to the heat of

[5]For a more detailed discussion, see ORNL TM-440 (December 1962).

[6]J. N. Butler and R. S. Brokaw, *J. Chem. Phys.* **26**, 1636 (1957).

[7]R. S. Brokaw, *J. Chem. Phys.* **32**, 1005 (1960).

[8]J. O. Hirschfelder, C. F. Curtiss, and R. B. Bird, *Molecular Theory of Gases and Liquids*, p 528, Wiley, N.Y., 1954.

dissociation, can be varied over a wide range of temperatures by controlling the pressure and helium concentration.

Gaseous aluminum chloride has been shown to offer some slight advantages over helium as a heat transfer agent under certain conditions, despite its high molecular weight.[9] These advantages are primarily due to its relatively low viscosity and a greater than linear increase in specific volume with temperature due to the increased degree of dissociation of the dimer at high temperatures. However, the effective thermal conductivity of dissociating aluminum chloride vapor is an order of magnitude less than that of helium, and the effective specific heat is also considerably less than that of pure helium (see Fig. 18.1).

Although present technology is not sufficiently advanced to make the use of fluorine practical in a closed cycle at high temperatures, fluorine serves as an excellent example of the effects of

[9]M. Blander *et al.*, *Aluminum Chloride as a Thermodynamic Working Fluid and Heat Transfer Medium*, ORNL-2677 (1959).

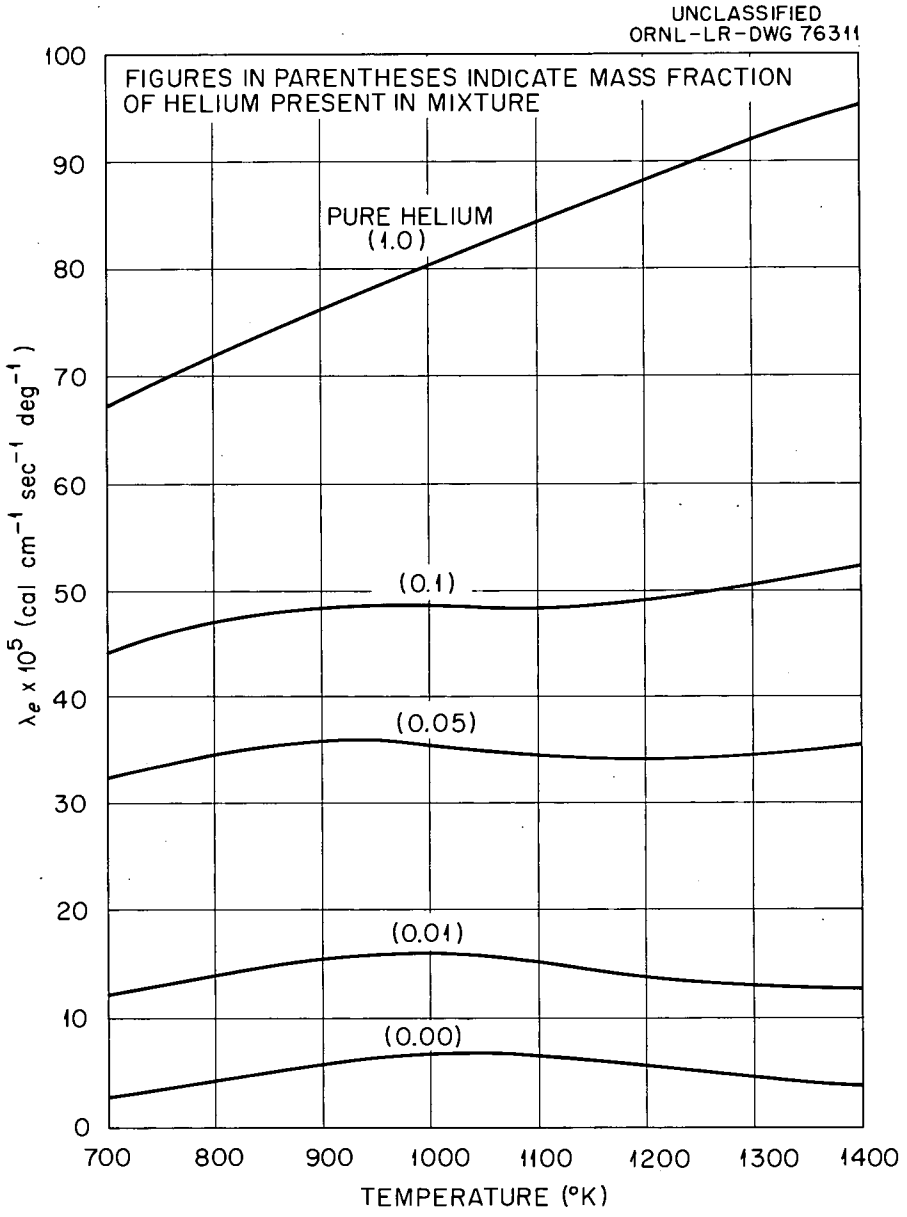


Fig. 18.1. Thermal Conductivity of $Al_2Cl_6 \rightleftharpoons 2AlCl_3$ at 10 atm Pressure.

dissociation on the thermal properties of a dissociating gas due to its high heat of dissociation and low molecular weight. A mixture of helium and fluorine has a thermal conductivity and specific heat which can be as much as a factor of 2 greater than the corresponding values for pure helium, depending on the pressure and composition of the mixture. On the other hand, the viscosity of a helium-fluorine mixture is approximately 10% greater than that of pure helium and is only slightly dependent on composition (see Figs. 18.2, 18.3, and 18.4).

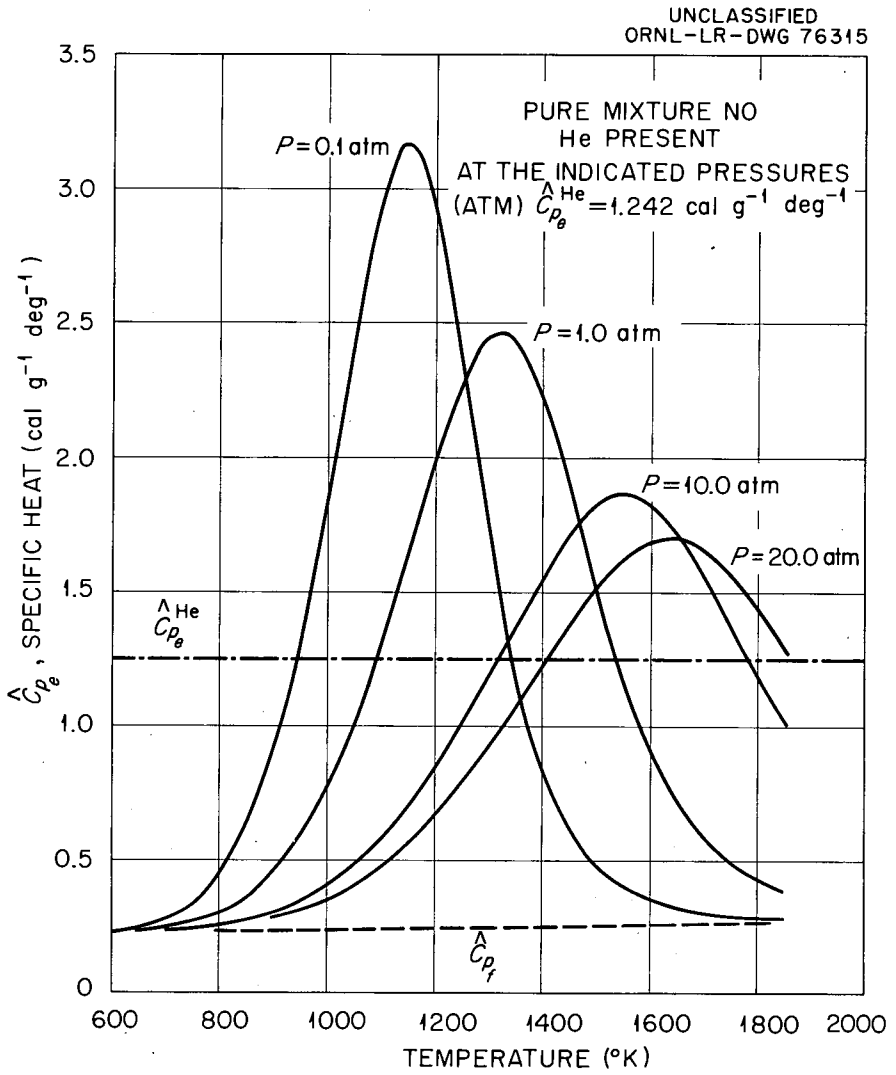


Fig. 18.2. Specific Heat, $\hat{C}_{p_e}$, of $F_2 \rightleftharpoons 2F$.

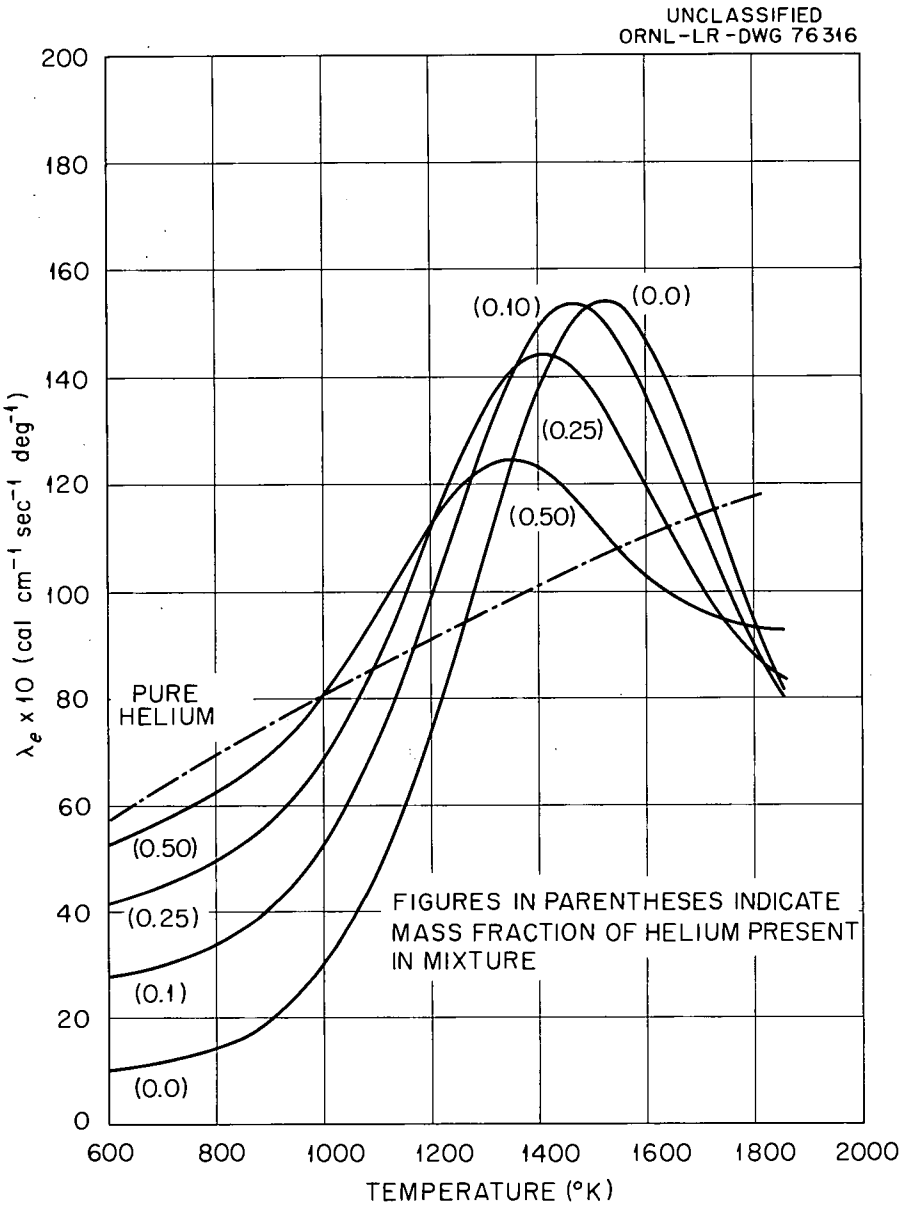


**Fig. 18.3. Thermal Conductivity of $F_2 \rightleftharpoons 2F$ at 10 atm Pressure.**

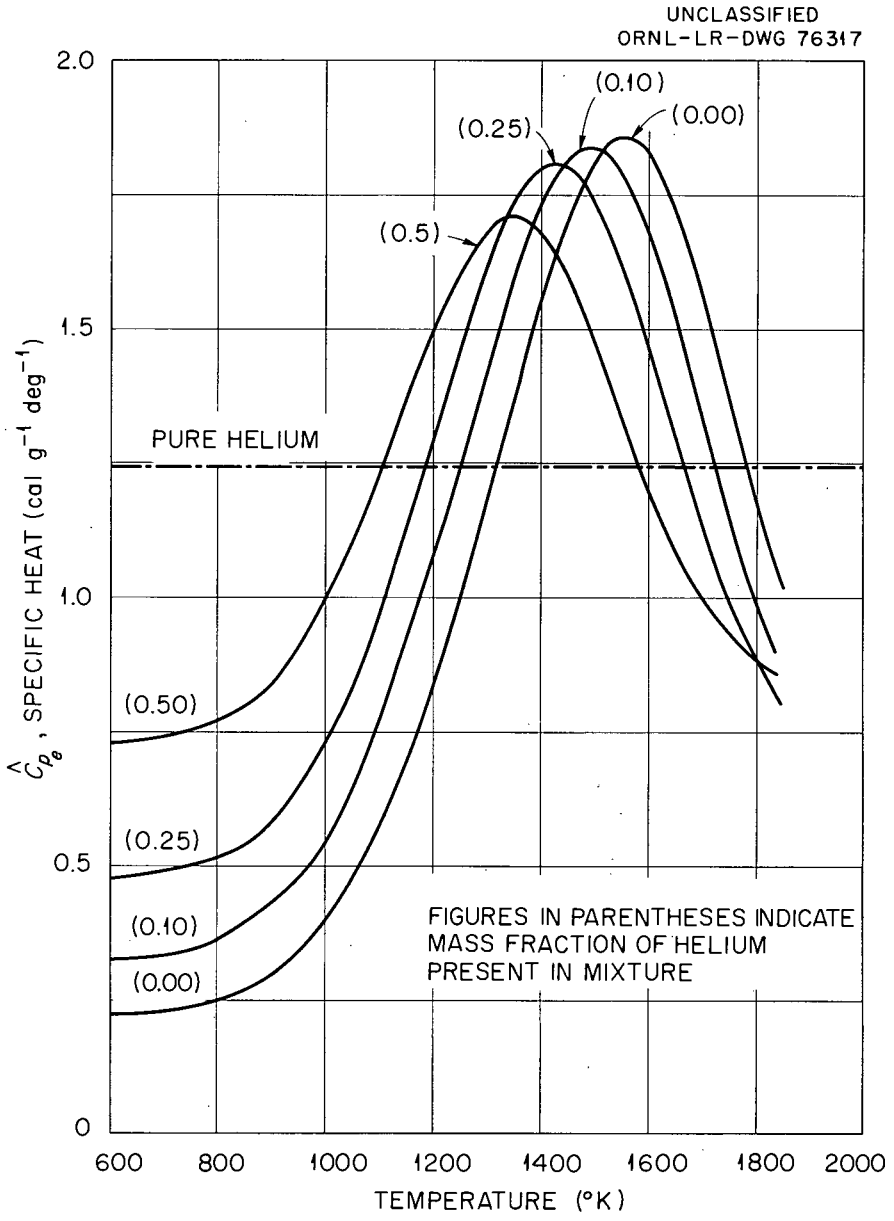


**Fig. 18.4. Specific Heat of $F_2 \rightleftharpoons 2F$ at 10 atm Pressure.**

# 19. Effect of Irradiation on Beryllium Oxide

G. W. Keilholtz J. E. Lee, Jr. R. E. Moore

The BeO irradiation program at ORNL has been directed toward determination of the effects of high fast-neutron flux at elevated temperatures on commercial grade oxide without additives. The results of five experiments in this series have been reported previously.[1-4] In those experiments, sintered compacts receiving a neutron dose of $1.5 \times 10^{21}$ (>1 Mev) at 110°C disintegrated to powder, and those receiving $2.6 \times 10^{21}$ *nvt* at 800 to 950°C fractured. Some specimens irradiated at intermediate temperatures and neutron doses survived intact. Irradiation in the $10^{21}$ *nvt* range produced increases in linear dimensions, anisotropic lattice expansion, and lattice defects. These effects, as well as gross damage effects, generally increased with increasing neutron dose and decreased with increasing temperature.

Postirradiation examination of specimens from two additional experiments (41-6 and 41-7) containing a total of 54 specimens is virtually complete.[5] Two additional experiments (41-8 and 41-9) containing a total of 340 specimens are undergoing irradiation at present.

[1] G. W. Keilholtz *et al.*, *Reactor Chem. Div. Ann. Progr. Rept. Jan. 31, 1962*, ORNL-3262, pp 157–60.

[2] R. P. Shields, J. E. Lee, Jr., and W. E. Browning, Jr., *Effects of Fast Neutron Irradiation and High Temperatures on Beryllium Oxide*, ORNL-3164 (Mar. 16, 1962).

[3] R. P. Shields, J. E. Lee, Jr., and W. E. Browning, Jr., *Trans. Am. Nucl. Soc.* 4(2), 338 (1961).

[4] G. W. Keilholtz *et al.*, "Radiation Damage in BeO," in *Proceedings of the Symposium on Radiation Damage in Solids and Reactor Materials, Venice, May 7–11, 1962*, to be published by IAEA, Vienna.

[5] G. W. Keilholtz, J. E. Lee, Jr., and R. E. Moore, "Behavior of BeO Under Irradiation," *GCR Semiann. Progr. Rept. Sept. 30, 1962*, ORNL-3372.

## OBSERVATIONS FROM EXPERIMENT 41-6

The six specimens irradiated in assembly 41-6 were cylinders of larger size (1.18 in. in diam by 3 in. in length) than any others in this series. They were prepared[6] from Brush Beryllium's UOX grade BeO by cold pressing and sintering at 1450°C for 1.5 hr. As a consequence of the short and low-temperature sintering procedure the material was extremely fine grained ($3 \pm 1$ $\mu$ diam), and was appreciably less dense (2.52 g/cm$^3$) than other materials used in this series. Three of the six samples were exposed in capsules of stainless steel while the other three were exposed directly to the coolant gas.

Table 19.1 shows the dosage and exposure temperature obtained during the irradiation, and indicates that five of the six specimens were fractured during this test. Fracturing of specimens 2 through 6 was predominantly circumferential (see Fig. 19.1) indicating that thermal stress may have initiated the fractures. There was no significant difference in gross damage effects between the encapsulated specimens (2, 4, 6) and specimens 3 and 5, which were unclad. The survival of specimen 1, which was also unclad, may be attributed to its substantially lower neutron dose. It was observed while the samples were being broken and ground for postirradiation examinations that specimens 2 through 6 had less resistance to crushing than control specimens. Specimen 1 seemed to have retained most of its structural strength.

No significant changes in the dimensions of the specimens as a result of irradiation could be

[6] These materials were prepared by R. L. Hamner of the ORNL Metals and Ceramics Division.

**Table 19.1. Irradiation Conditions and Gross Damage Observed in Experiment 41-6**

| Specimen Number | Neutron Flux, *nv* | Neutron Dose, *nvt* | Temperature (°C) | Observation |
|---|---|---|---|---|
| | $\times 10^{14}$ | $\times 10^{21}$ | | |
| 1 | 1.0 | 0.2 | 530 | Sound specimen |
| 2 | 2.4 | 0.5 | 730 | Fractured |
| 3 | 2.9 | 0.6 | 925 | Fractured |
| 4 | 3.4 | 0.7 | 900 | Chipped |
| 5 | 4.8 | 1.0 | 840 | Severely fractured |
| 6 | 4.4 | 0.9 | 925 | Severely fractured |

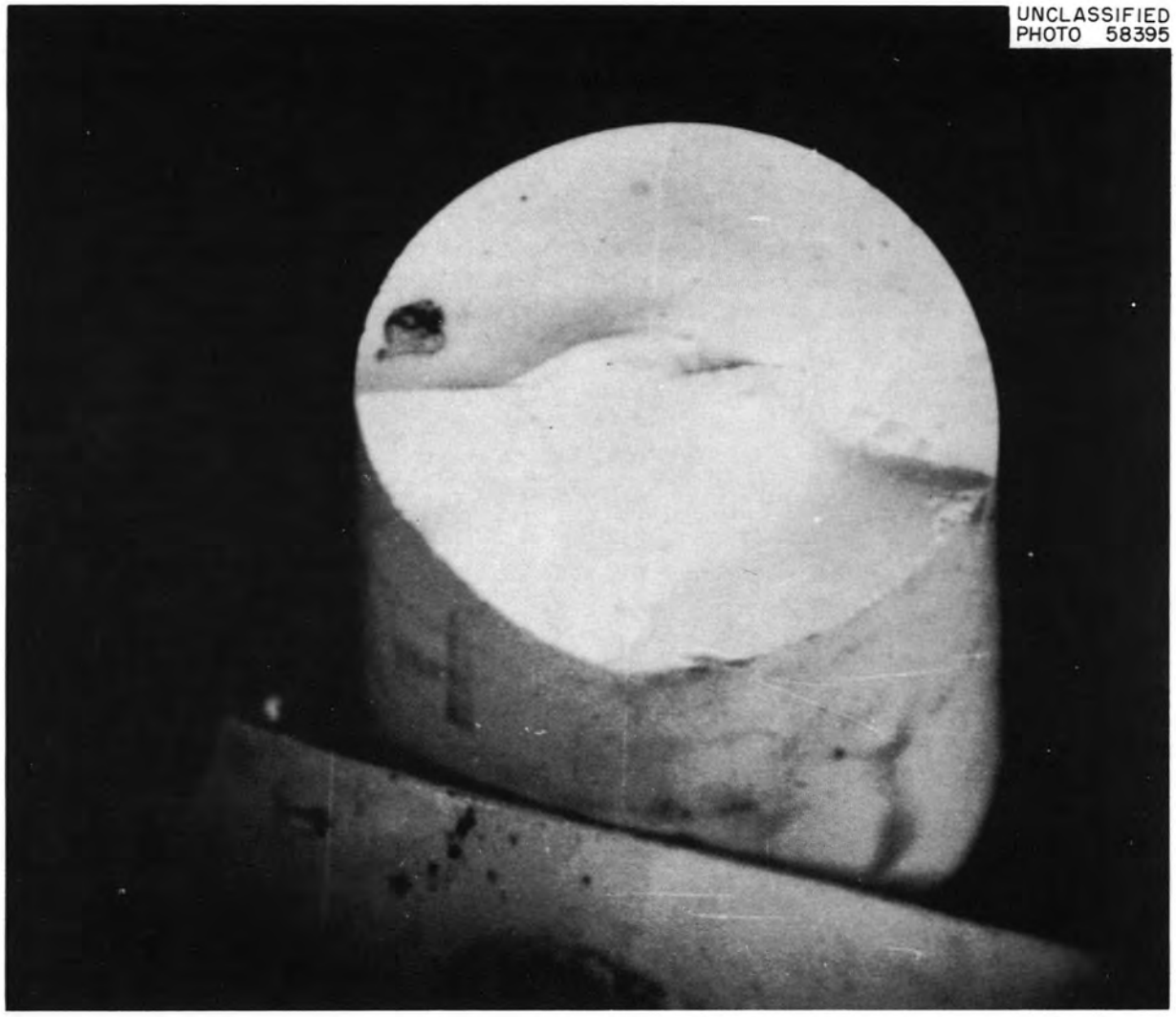


Fig. 19.1. Circumferential Fracture of BeO Specimen 5, ORNL Experiment 41-6.

detected. Grain boundary separation could not be seen in photomicrographs of irradiated samples, but the grain size may have been too small to permit separation to be detected. However, pullout of grains during polishing indicated some grain boundary weakness.

Examination of finely ground samples by x-ray diffraction showed values of the fractional elongation of the $c$ axis ($\Delta c/c_0$) from 0.00046 to 0.00125 for these specimens. The largest increase occurred with specimen 1; since this specimen received the lowest neutron dose, the large increase must be due to lack of annealing at its low exposure temperature. Conversely, x-ray line broadening was considerable in specimens 2–6 but appreciably less for specimen 1.

Tritium was lost almost completely from these specimens as expected from previous data for specimens irradiated at elevated temperature. The helium retained by these specimens was shown to be approximately proportional to the fast-neutron dosage but was less by about 60% than values predicted from previous tests in this series. It may be that the fine grain size and the lower density of BeO in this experiment are responsible for the ease of release.

## OBSERVATIONS FROM EXPERIMENT 41-7

Assembly 41-7, which contained a total of 48 cylindrical specimens each 0.800 in. in diam by 0.5 in. in length, was constructed with specially designed cooling passages[1] to permit at least a partial separation of the effects of neutron flux and specimen temperature. The assembly consisted of 8 capsules of stainless steel each of which contained 6 specimens of BeO. The top specimen in each capsule was hot-pressed material with a density of 2.8 g/cm$^3$ fabricated by machining from larger blocks. All other specimens were prepared by cold pressing and sintering.[6] Sintering at 1750°C for 1 hr yielded densities of 2.9 g/cm$^3$ and grain sizes of 29 ± 2 $\mu$ for the specimens.

### Visual Observation of Specimens

Table 19.2 summarizes the irradiation conditions and the condition of specimens at time of first observation. In general, the gross damage seems less than that in 41-6 (above) for which the neutron flux and dosages were considerably smaller; this suggests, again, that thermal stress was important in the large specimens of 41-6. The most damage observed in 41-7 was in specimens from capsule 1 which was irradiated at the lowest temperature.

Nearly all the fractures observed in 41-7 were radial; Fig. 19.2 shows a typical fractured specimen. Some of these fractures (see Fig. 19.3) were probably initiated by the cutting wheel during removal of the capsule during the hot cell disassembly operation.

Specimens from capsules 1 to 6 were easily ground to powder while those from 7 and 8 powdered with considerably more difficulty.

### Crushing Strength

The specimens lost approximately 60% of their crushing strength, but no quantitative correlation of crushing strength with temperature and fast neutron dose is possible. Test specimens which had no visible fractures after irradiation disintegrated directly to powder during the crushing tests; unirradiated control specimens cracked before powdering. This suggests the presence of microcracks between the grains of the irradiated material. It is apparent that samples irradiated at temperatures as high as 1100°C do not retain their crushing strength.

### Thermal Conductivity

Measurement of temperature drop from center to edge of specimens during irradiation shows a decrease in thermal conductivity during the exposure. Figure 19.4 shows a plot of the fractional loss against neutron dose for capsules 3 and 5. The thermal conductivity decreased at a greater rate in the higher flux region (capsule 5) but appeared to level at about 40 to 45% of the original value as the neutron dose approached $4 \times 10^{21}$ *nvt*. The fact that these capsules were exposed at very nearly the same temperature suggests that the difference in their behavior should be ascribed to difference in dosage rate. The slopes of the curves in the lower dose range ($<10^{21}$ *nvt*) are uncertain, however, because of the widely scattered $\Delta T$ values. Any conclusions regarding the effect of dose rate must, accordingly,

**Table 19.2. Irradiation Conditions and Gross Damage Observed in Experiment 41-7**

| Capsule Number | Specimen[a] | Neutron Flux, *nv* | Neutron Dose, *nvt* | Temperature (°C) | Observation |
|---|---|---|---|---|---|
| | | $\times 10^{14}$ | $\times 10^{21}$ | | |
| 1 | 1, 4, 6 | 1.6 | 1.20 | 583 | Fractured |
| | 5 | | | | Fractured, some powder present |
| | 2, 3 | | | | Sound |
| 2 | 1–6 | 2.6 | 1.95 | 906 | Sound |
| 3 | 1–5 | 3.5 | 2.65 | 915 | Sound |
| | 6 | | | | Fractured |
| 4 | 1, 4 | 4.3 | 3.28 | 969 | Fractured |
| | 2, 3, 5 | | | | Sound |
| | 6 | | | | Possible fracture |
| 5 | 1–3 | 4.8 | 3.65 | 926 | Possible fracture |
| | 4–6 | | | | Sound |
| 6 | 1–6 | 4.7 | 3.63 | 825 | Sound |
| 7 | 2–6 | 4.0 | 3.05 | 935 | Sound |
| | 1 | | | | Fractured |
| 8 | 1–4, 6 | 2.9 | 2.25 | 1100 | Sound |
| | 5 | | | | Possible fracture |

[a]Specimens are numbered 1–6 from the top to the bottom of each capsule. Specimen 1 of each capsule was hot pressed; specimens 2–6 were cold pressed and sintered. The observation of "possible fracture" means that the fracture, if present, was too small to be visually certain of its existence. Those specimens observed as sound may have contained internal fractures which were not visible.

await additional data. There can, however, be little doubt of the effect of neutron dosage on thermal conductivity.

### Dimensional Changes

The results of dimensional measurements on specimens from 41-7 are summarized in Table 19.3. A preferred diametric growth is shown in the values of the gross anisotropic ratio. The volume increase–integrated neutron flux curves for the two types of BeO (Fig. 19.5) are similar in shape, but the hot-pressed material underwent a greater expansion. Larger volume increases of hot-pressed beryllium oxide, as compared with cold-pressed and sintered material, have also been reported by other investigators.[7,8]

### Metallographic Examinations

**Photomicrographs.** – Grain boundary separation as a result of irradiation is clearly shown by a comparison of irradiated and control material in the

[7]B. S. Hickman, *The Effect of Neutron Irradiation on Beryllium Oxide*, AAEC-E-99 (October 1962).

[8]B. S. Hickman and R. J. Hemphill, *Dimensional Changes in Irradiated BeO*, AAEC, MP-TN-2 (May 22, 1962).

Fig. 19.2. Typical Fractured Pellet, ORNL Experiment 41-7, Specimen 7-4-4.

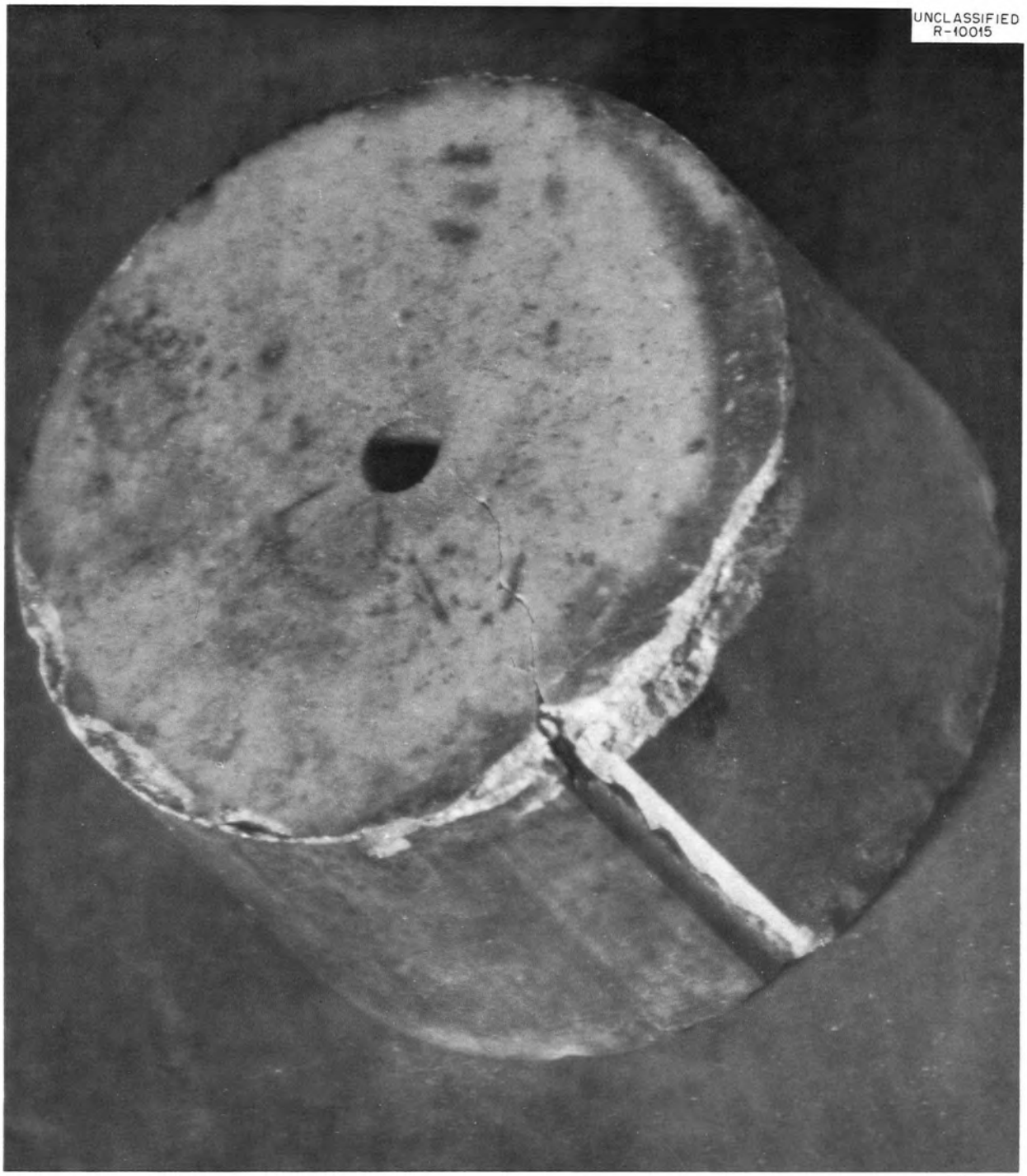


Fig. 19.3. Fracture Starting at Mark Made by Cutting Wheel, ORNL Experiment 41-7, Specimen 7-1-6.

**Table 19.3. Summary of Dimensional Changes of BeO Specimens in Experiment 41-7**

| Capsule Number and BeO Type | Integrated Flux, *nvt* | Temperature (°C) | Diameter Increase (%) | Length Increase (%) | Anisotropic Ratio (diam increase/length increase) | Volume Increase (%) |
|---|---|---|---|---|---|---|
| | $\times 10^{21}$ | | | | | |
| 1 CP[a] | 1.20 | 583 | 1.00 | 1.00 | 1.00 | 3.00 |
| 2 HP | 1.95 | 906 | 0.68 | 0.80 | 0.85 | 2.16 |
| CP | | | 0.53 | 0.17 | 3.12 | 2.23 |
| 3 CP | 2.65 | 915 | 0.61 | 0.34 | 1.79 | 1.56 |
| 4 HP | 3.28 | 969 | 0.95 | 0.64 | 1.49 | 2.54 |
| CP | | | 0.51 | 0.25 | 2.04 | 1.27 |
| 5 HP | 3.65 | 926 | 1.15 | 1.08 | 1.07 | 3.38 |
| CP | | | 0.90 | 0.51 | 1.77 | 2.31 |
| 6 HP | 3.63 | 825 | 1.44 | 1.49 | 0.97 | 4.37 |
| CP | | | 1.62 | 0.98 | 1.66 | 4.22 |
| 7 HP | 3.05 | 935 | 0.79 | 0.88 | 0.90 | 2.46 |
| CP | | | 0.57 | 0.20 | 2.86 | 1.34 |
| 8 HP | 2.25 | 1100 | 0.64 | 0.20 | 3.20 | 1.48 |
| CP | | | 0.39 | 0.08 | 4.87 | 0.86 |

[a]HP = hot pressed; CP = cold pressed and sintered.

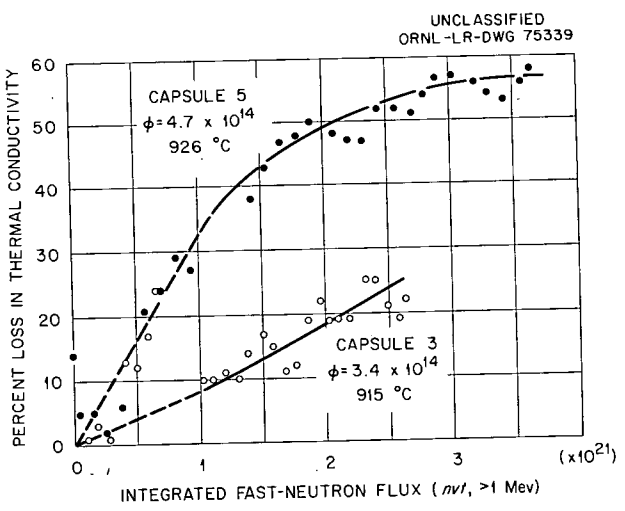


**Fig. 19.4. Percent Loss in Thermal Conductivity of BeO vs Integrated Fast-Neutron Flux in Experiment 41-7.**

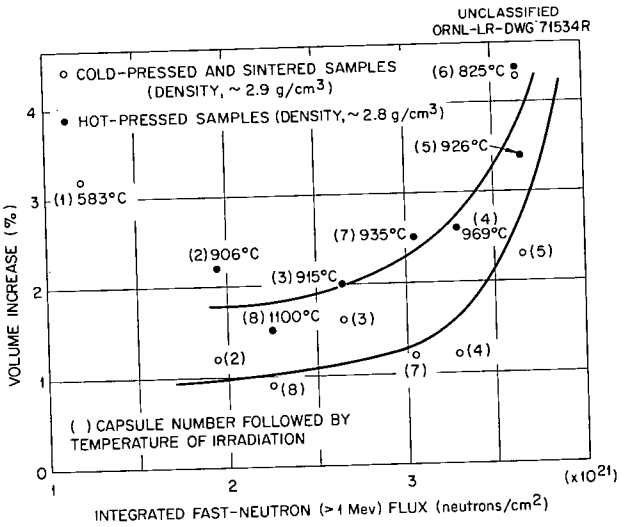


**Fig. 19.5. Percent Volume Increase of BeO Specimens vs Integrated Fast-Neutron Flux in Experiment 41-7.**

as-polished condition. Grain boundaries are not clearly outlined in photomicrographs of the hot-pressed control material at 100X. Material from the same source irradiated to $3.65 \times 10^{21}$ *nvt* at 926°C in capsule 5 is shown in Fig. 19.6. The fact that the grain boundaries are clearly outlined without etching indicates grain separation. Similarly, grain boundaries are not clearly visible in the cold-pressed and sintered control material but a considerable amount of separation can be seen (Fig. 19.7) in the cold-pressed BeO which received $3.65 \times 10^{21}$ *nvt* at 926°C. Some transgranular fractures can be seen in this sample at higher magnifications. Considerably less grain boundary separation was observed in specimens irradiated to lower neutron doses at higher temperatures. On the other hand, cold-pressed BeO in capsule 1 which received an even lower neutron dose ($1.2 \times 10^{21}$ *nvt*), but at a much lower temperature (583°C), exhibits a high degree of grain separation.

Photomicrographic evidence of grain boundary separation of BeO irradiated to very low doses ($<5.4 \times 10^{20}$ *nvt*) at 100°C or lower temperatures has previously been presented by other investigators in the field.[9,10] No evidence of grain growth has been observed in any specimens from 41-7.

**X-Ray Diffraction Studies.** – The x-ray diffraction results for finely ground specimens of experiment 41-7 have only recently been received and are now

[9] J. Elston, "Radiation Damage in Solids," in *Proceedings of the Symposium on Radiation Damage in Solids and Reactor Materials, Venice, May 7–11, 1962*, to be published by IAEA, Vienna.

[10] *High Temperature Materials Program Progress Report, No. 12, Part A*, GEMP-12A (June 15, 1962).

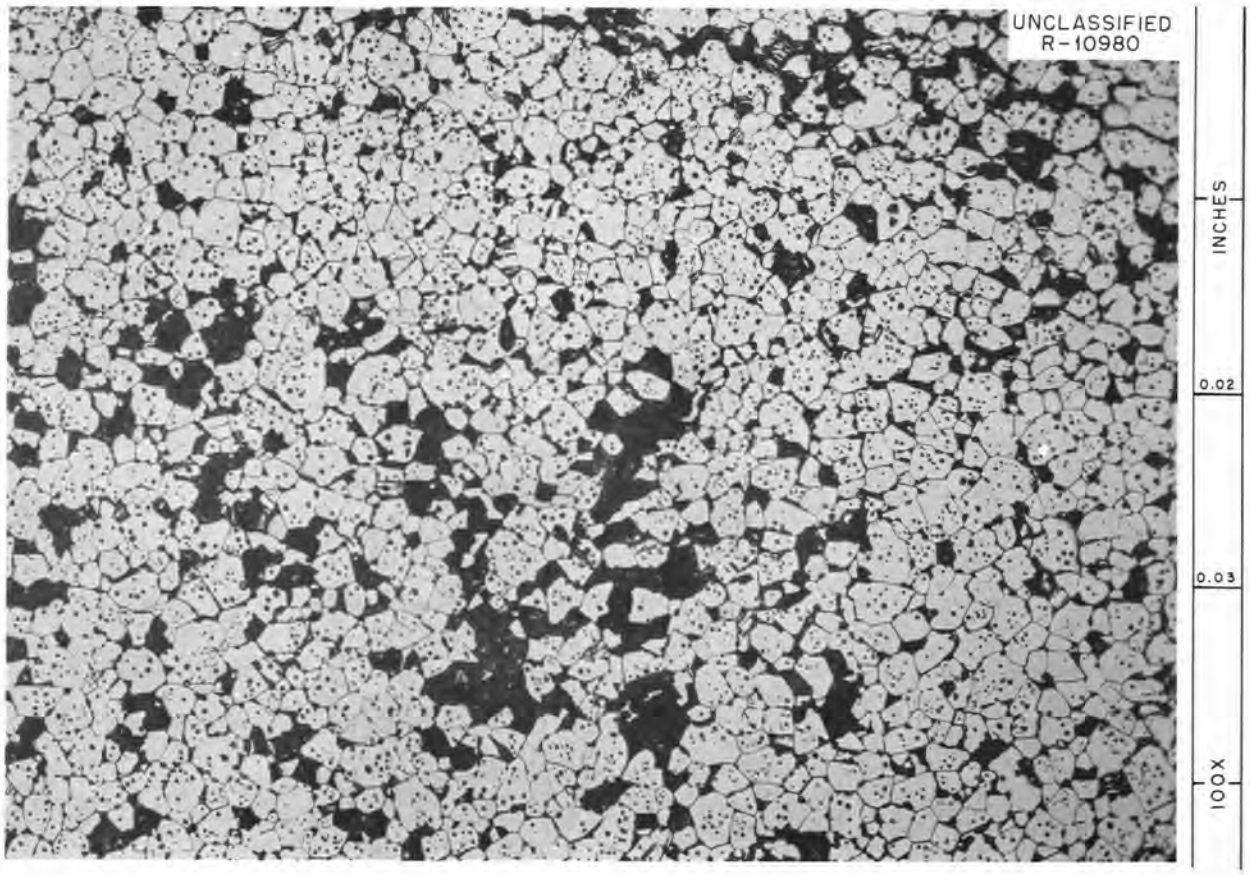


Fig. 19.6. Photomicrograph of Irradiated Hot-Pressed BeO Specimen 7-5-1 Exposed to $3.65 \times 10^{21}$ *nvt* (> 1 Mev) at 926°C in Experiment 41-7 (As Polished, 100X).

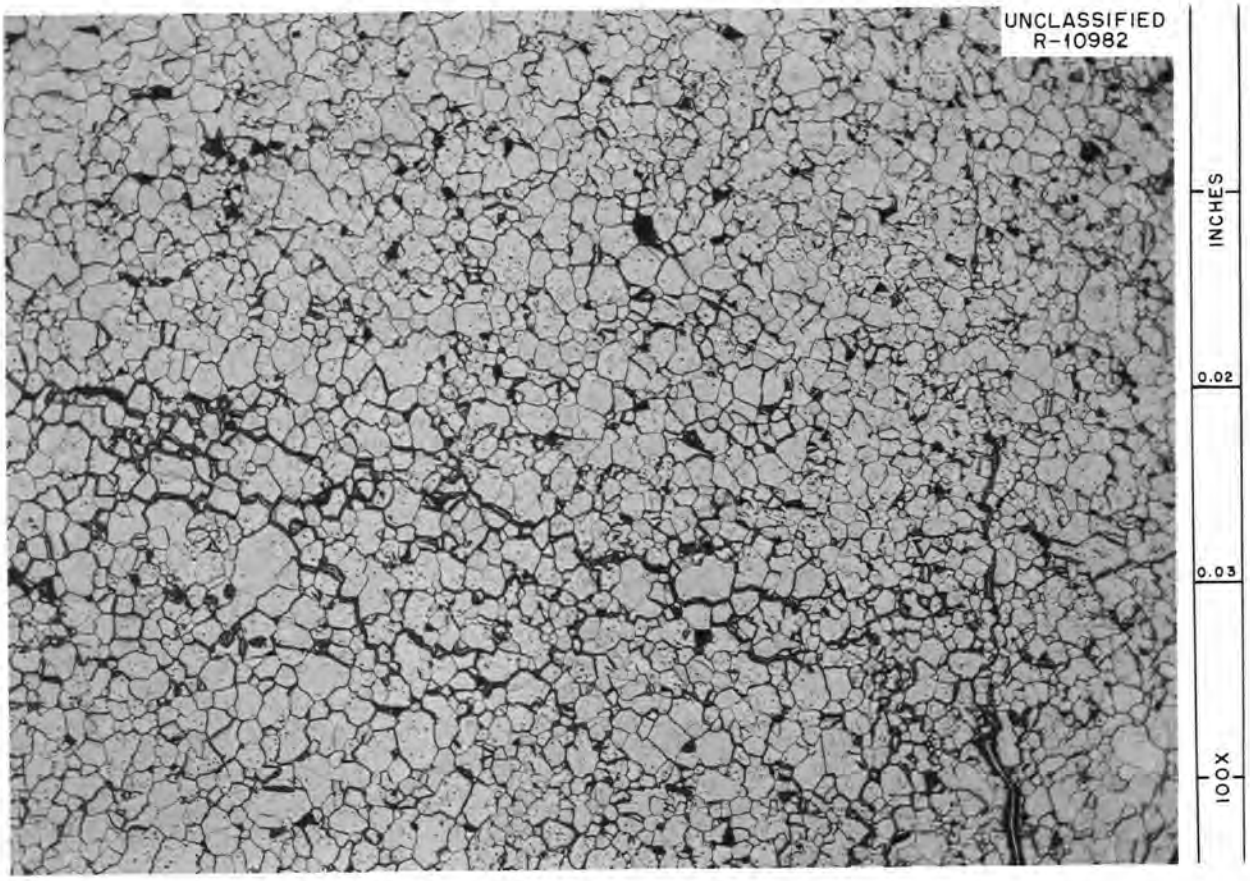


Fig. 19.7. Photomicrograph of Irradiated Cold-Pressed and Sintered BeO Specimen 7-5-2 Exposed to $3.65 \times 10^{21}$ *nvt* (> 1 Mev) at 926°C in Experiment 41-7 (As Polished, 100X).

being evaluated. It appears, however, that the values of $\Delta c/c_0$, as expected in view of the high irradiation temperatures, are quite low (<0.0017), but they are approximately proportional to the integrated neutron flux. The anisotropic lattice expansion ratios $(\Delta c/c_0)/(\Delta a/a_0)$ average about 8.

**Gas Analysis.** – In previous experiments,[2] the helium generated in irradiated BeO was found to be largely retained. Incomplete results of gas analyses of samples irradiated in experiment 41-7 indicate that as much as 50% of the generated helium escaped during exposure to higher neutron doses ($>3 \times 10^{21}$ *nvt*). This may be rationalized by assuming that grain boundary separation occurring at high neutron doses permits some of the helium to diffuse out of the compacts. Tritium was found to be lost nearly completely, as was the case in previous experiments at high temperatures.

## Discussion

Grain boundary separation can account for a large part of the observed changes in physical properties of BeO compacts exposed to high fast-neutron doses. These changes include fracturing and powdering, reductions in crushing strength, volume increases, and decreases in thermal conductivity.

The results of experiments 41-6 and 41-7 confirm earlier conclusions[1-4] that damage tends to increase with increasing neutron dose and decrease with increasing temperature; an in-pile annealing effect is indicated. Therefore, at operating temperatures at which annealing occurs, damage effects are expected to be a function of the neutron flux.

Fracturing of specimens in experiment 41-6 was more severe than in experiment 41-7, which received a much higher neutron dose, while by other criteria, such as dimensional increase and grain boundary separation, the damage to the material of experiment 41-6 was much less severe. This fact, when coupled with the observation of circumferential fracturing, leads to the conclusion that thermal stress played a major role in failure of specimens in 41-6 where the lower density (and consequently lower thermal conductivity), as well as the larger size of the specimens, contributed to greater thermal stress than in other experiments in this series.

The amount of preferred orientation, if any, in the polycrystalline compacts of experiment 41-7 is probably too small to account for the anisotropic volume increases recorded in Table 19.3. The gross fractures observed in this experiment were generally radial, and if the microfractures (grain boundary separation) are also oriented preferentially in this same direction, the preferred growth of the diameters is understandable. It should be noted in Table 19.3 that there is an indication of an inverse relationship between the gross anisotropic ratio and the volume increase. That is, as the separation of grains increases, the probability of a preferred direction of microfractures becomes less.

Volume increase in an irradiated compact may be resolved into three components and represented by the approximate equation

$$\frac{\Delta V_T}{V_0} = \frac{\Delta V_l}{V_0} + \frac{\Delta V_d}{V_0} + \frac{\Delta V_g}{V_0},$$

where

$\Delta V_T$ = total volume increase,

$\Delta V_l$ = volume increase calculated from lattice parameters,

$\Delta V_d$ = volume increase caused by lattice defect agglomeration,

$\Delta V_g$ = volume increase caused by grain boundary separation,

$V_0$ = unirradiated volume.

The lattice parameter expansion, $\Delta V_l/V_0$, is much less at high temperatures (250–1100°C) than at very low temperatures,[2] but the effect of temperature on $\Delta V_d/V_0$ has not yet been determined. X-ray diffraction results show that the defect volume increase, $\Delta V_d/V_0$, like $\Delta V_l/V_0$, is anisotropic, producing an additional preferred growth in the direction of the *c* axes of individual crystals. Values of $\Delta V_d/V_0$ can be obtained from measurements of the densities and lattice parameters of single crystals included in experiments now in progress. It should be possible then to calculate from the equation the values of $\Delta V_g/V_0$ for corresponding sintered compacts.

The two principal mechanisms of grain boundary separation in pure BeO which have been proposed are: (1) anisotropic expansion of crystals resulting in stresses at the grain boundaries which ultimately overcome the intergranular bonding forces, and (2) breaking apart of grain boundaries by gas pressure of helium which diffuses to the grain boundaries after its production by neutron reactions within the crystals. It seems certain that the first mechanism applies at low neutron doses and low temperatures because under these conditions grain boundary separation occurs with a very small helium production.[9] Whether this mechanism is also dominant at high temperatures and high neutron dose is still questionable.

Reactor operational variables and fabrication variables all have a bearing on irradiation damage effects. Grain boundary strength, which depends on sintering temperature and time, purity, and other factors, is undoubtedly significant. Irradiation studies under carefully controlled conditions are required to determine the relative importance of the many variables. To this end, experiments[11] are now in progress in which the variables of grain size, density, specimen size, neutron flux, neutron dose, and temperature are separated. More than 300 cold-pressed cylindrical compacts made from the same starting material and sintered at the same temperature, as well as single crystal specimens, are included in experiments 41-8 and 41-9.

---

[11] D. A. Gardiner, *The Experimental Design for BeO Irradiation Experiments ORNL-41-8 and ORNL-41-9*, ORNL-3310 (July 2, 1962).

# Part V
# Irradiation Behavior of High-Temperature Reactor Materials

## INTRODUCTION TO PART V

The group responsible for the studies reported in Part V and for a portion of the efforts described in Chapter 30 was transferred to the Reactor Chemistry Division from the Solid State Division on July 1, 1962. The status of these studies as of August 1962 was, accordingly, described in the annual report* of the latter division. The description below attempts, therefore, to emphasize more recent findings in a presentation as brief as is consistent with providing an overall statement of the program.

---

*O. Sisman *et al.*, *Solid State Div. Ann. Progr. Rept. Aug. 31, 1962*, ORNL-3364, chaps. 20–23.

# 20. Postirradiation Examination of Fuel Materials

O. Sisman J. G. Morgan

## FUEL MATERIALS WITH METAL CLADDINGS

### Postirradiation Examination of $UO_2$ Fuel Capsules – EGCR Program

D. F. Toner
E. L. Long, Jr.[1]
H. E. Robertson
A. L. Johnson
C. D. Baumann
J. G. Morgan
M. F. Osborne
J. W. Gooch

**ORR Capsules (Group IV).** – Several divisions at ORNL participate in the program of irradiation testing of fuel elements for the Gas-Cooled Reactor effort. In general, the test elements are fabricated by Metals and Ceramics Division personnel and are irradiated by personnel from the Reactor Division. Postirradiation examination of the test assemblies is the responsibility of the Reactor Chemistry Division. In direct support of some phase of the ORNL-EGCR program, the examination of a total of 21 separate fuel elements consisting of $UO_2$ clad in 304 or 347 stainless steel is briefly described below.

Six stainless-steel-clad $UO_2$ fuel elements were irradiated in the ORR poolside facility[2] at temperatures of 1300 to 1600°F to burnups of 1000 to 3000 Mwd per metric ton of uranium. Two of these capsules,[3] intended to serve as proof tests for EGCR instrumented fuel assemblies, contained pellets of $UO_2$ and were fitted with six clad thermocouples and one central thermocouple. Three of the remaining capsules were fabricated by swaging at 800°C; the other was fabricated by hand-tamping $UO_2$ powder (to final density 59% of theoretical) into a ½-in. type 304 stainless steel tube.

Examination of the two instrumented assemblies revealed that failure had occurred during irradiation. Separation of the braze material (GE-81) from the thermocouple sheath and cracking of the braze material itself were evident. In addition, depression of the cladding at the pellet-to-pellet interfaces was observed. The severe deformation resulted in intergranular voids in the cladding. Metallographic examination revealed the voids to have the same shape and size in longitudinal and transverse planes of the cladding, which suggests that shear stresses rather than hoop stresses may be responsible. Sigma phase was found in some areas of the cladding of both fuel elements. Since the sigma phase occurred only in a small, spherical precipitate, it was concluded that sigma phase does not cause the deleterious effect on the cladding during irradiation.

None of the swaged or tamped fuel elements[4] failed during operation with cladding temperatures of 1300°F to burnups of 2500 Mwd per metric ton of uranium with linear heat ratings[5] of 8000 and 15,000 Btu $hr^{-1}$ $ft^{-1}$. Swaged elements operated at 15,000 Btu $hr^{-1}$ $ft^{-1}$ showed sintering or even melting (see Fig. 20.1) of the $UO_2$ at the center of the element; no evidence of sintering was observed in $UO_2$ near the cladding. No sintering of $UO_2$ was observed in the swaged or tamped elements at the lower heat rating. As expected,[6]

[1]Metals and Ceramics Division.

[2]Irradiation experiments performed by the Reactor Division.

[3]D. F. Toner *et al.*, *Gas-Cooled Reactor Program Quart. Progr. Rept. Mar. 31, 1962*, ORNL-3302, pp 67–76.

[4]D. F. Toner *et al.*, *Gas-Cooled Reactor Program Quart. Progr. Rept. Mar. 31, 1962*, ORNL-3302, pp 76–83, and J. G. Morgan *et al.*, *Gas-Cooled Reactor Program Semiann. Progr. Rept. Sept. 30, 1962*, ORNL-3372.

[5]W. C. Thurber, "Compact Powder Fuel Irradiation Studies at Oak Ridge National Laboratory," presented at *the Symposium on the Powder Packed $UO_2$ Fuel Element*, Windsor, Connecticut, Nov. 30–Dec. 1, 1961.

[6]C. R. Kennedy and J. T. Venard, *Collapse of Tubes by External Pressure*, ORNL TM-166 (Apr. 17, 1962).

the cladding collapsed on the tamped element. Both fabrication methods seem satisfactory for irradiation as described above.

Sigma phase was found in some areas of the cladding on all specimens. This phase occurred only as small spherical particles and does not appear to affect the cladding integrity.

**Fig. 20.1. Cross Section of Capsule 06-4, Showing a Central Void in the $UO_2$.**

**ORR Capsules (Group V).** – Two EGCR prototype fuel elements, consisting of $UO_2$ pellets from production runs in stainless steel claddings at Westinghouse were irradiated to 1600 to 1700 Mwd per metric ton of uranium in the ORR poolside facility. These experiments, for which cladding temperatures averaged about 1400°F, were intended to test the $UO_2$ pellets and to test pressure transducers for monitoring of fission-gas buildup.[7]

Both transducers failed, one before and one during in-pile operation. Preliminary examination of these capsules showed failure of the transducer tubing in several places. Cesium-137 activity was found in the NaK coolant, a pinhole was found in the stainless steel cladding, and NaK coolant was found inside the element. Metallographic examination of the cladding of the capsule which failed during in-pile operation showed many intergranular voids in the region of the leak, shown in Fig. 20.2. The voids were confined to a small ridge in the cladding that had suffered a strain of 4 to 5%. Severe cracking of the $UO_2$ was noted in both tests.

**Loop 1 Capsules.** – Elements of type 304 stainless steel, 19 in. long and 0.75 in. in diameter, containing hollow $UO_2$ fuel pellets were irradiated in GCR-ORR Loop No. 1 for periods of 7 to 14 weeks at cladding temperatures between 1300 and 1500°F.[8] The irradiation conditions are shown in Table 20.1.

Postirradiation examination[9] has shown that, under the EGCR design operating conditions, the $^3/_4$-in. hollow-pellet stainless-steel-clad fuel elements are satisfactory. In addition, it has been demonstrated that the cored pellets do not disintegrate even though cracked during irradiation, that the fuel elements maintain dimensional stability, and that no reactions between $UO_2$ and the stainless cladding occur during irradiation.

The lead tube, which is immediately above the fuel element, and the shroud, which surrounds the fuel element, in experiment No. 5 were rusty and very brittle. Subsequent metallographic examination of these accessory parts of the experiment showed an intergranular fracture which penetrated the wall of both parts. A typical microstructure is shown in Fig. 20.3. At higher magnification a corrosion product, probably an oxide, was revealed in the grain boundaries. Analysis of the rust showed that Fe, Cr, and Ni were the principal constituents and that smaller quantities of Bi, Zn, Au, Ag, Mn, Mo, Cu, and Si were present. Structurally, the rust was the gamma $Fe_2O_3 \cdot H_2O$. Similarly, rust was observed on the insert of element 7A and on the shroud of element 7C.

[7] F. R. McQuilkin *et al.*, *Gas-Cooled Reactor Program Quart. Progr. Rept. Mar. 31, 1962*, ORNL-3302, p 59.

[8] J. K. Franzreb, *Gas-Cooled Reactor Program Quart. Progr. Rept. Mar. 31, 1962*, ORNL-3302, p 66; D. F. Toner *et al.*, *Gas-Cooled Reactor Program Quart. Progr. Rept. Mar. 31, 1962*, ORNL-3302, p 67; J. G. Morgan *et al.*, *Gas-Cooled Reactor Program Semiann. Progr. Rept. Sept. 30, 1962*, ORNL-3372.

[9] D. F. Toner *et al.*, *Gas-Cooled Reactor Program Quart. Progr. Rept. Mar. 31, 1962*, ORNL-3302, pp 83–96.

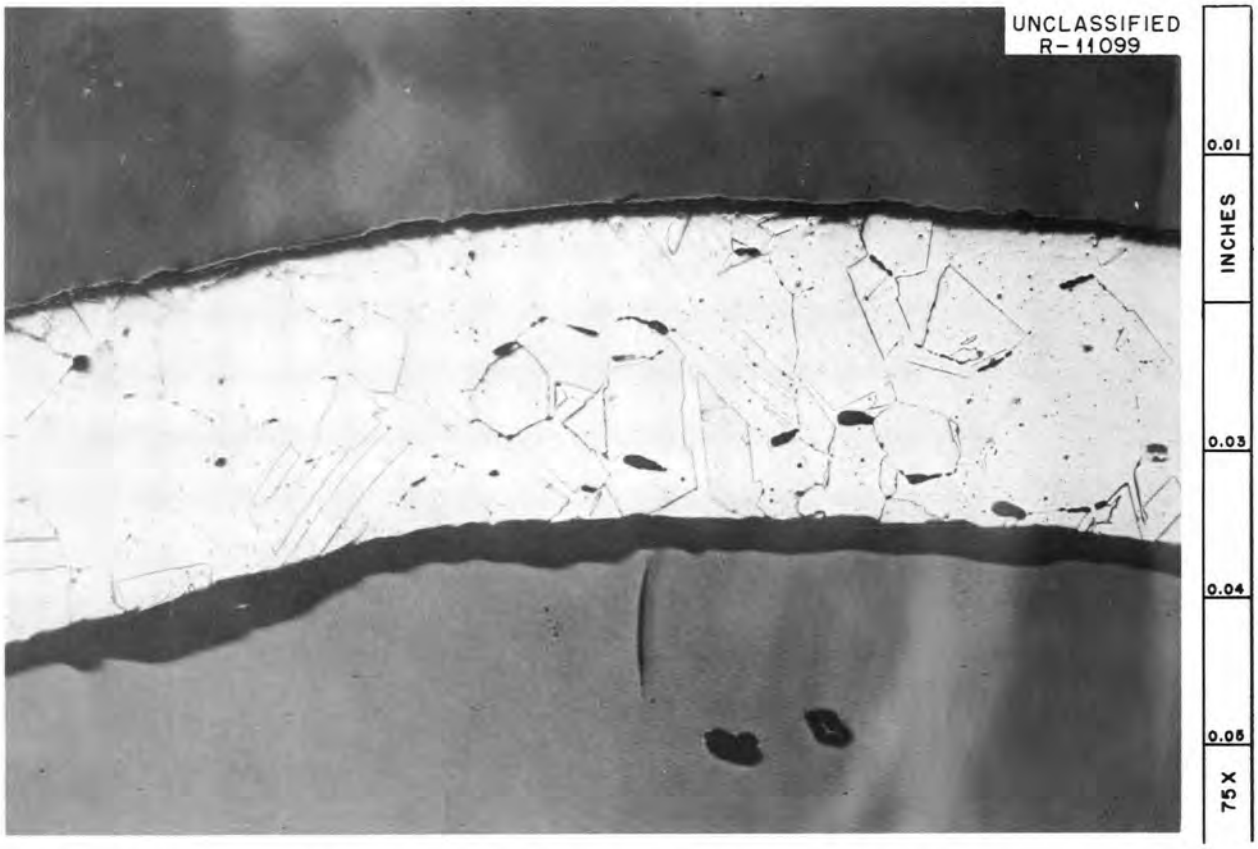


**Fig. 20.2. Transverse Section Through the Cladding of ORR Capsule 02-5 Near a Leak.** Note intergranular voids. Etchant: glyceregia.

**Table 20.1. Irradiation Conditions for Loop 1 Capsules**

| Element No. | Approximate Flux[a] | Time of Irradiation (weeks) | Linear Heat Rating (Btu $hr^{-1}$ $ft^{-1}$) | Environment |
|---|---|---|---|---|
| | $\times 10^{13}$ | | | |
| 5 | 2.3 | 7 | 24,000–28,000 | Flowing He at 300 psi |
| 6 | 2.3 | 7 | 24,000–28,000 | Flowing He at 300 psi |
| 7A | 2.3 | 7 | 24,000–28,000 | Flowing He at 300 psi |
| 7B | 2.3 | 7 | 24,000–28,000 | Flowing He at 300 psi |
| 7C | 2.3 | 14 | 24,000–28,000 | Flowing He at 300 psi |
| 8[b] | 2.3 | 7 | 46,000 | Flowing He at 300 psi |
| 9[b] | 2.3 | 7 | 33,000–43,000 | Flowing He at 300 psi |

[a]Since each capsule has at least 4 different $U^{235}$ enrichments, the exact burnup depends on the position of the pellet. Burnups range from 200 to 1100 Mwd per metric ton of uranium.

[b]Experiments 8 and 9 were designed for linear heat ratings of 50,000 Btu $hr^{-1}$ $ft^{-1}$, the others for 35,000 Btu $hr^{-1}$ $ft^{-1}$. Experiment 8 had a 0.006-in. Inconel wire brazed to the outside cladding at a pitch of 0.090 in.

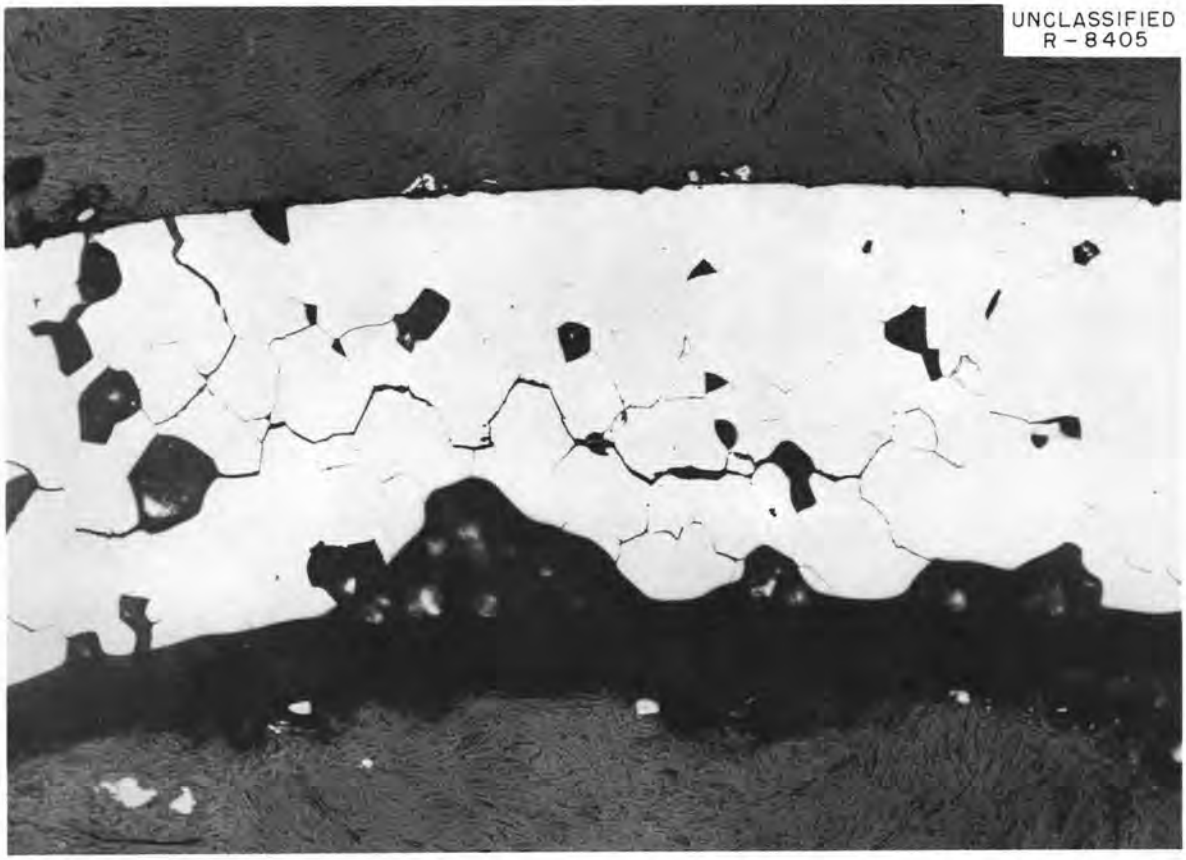


**Fig. 20.3. Transverse Sample Taken from Near One of the Breaks in the Type 304 Stainless Steel Lead Tube from Element 5.** Friability of the tubing was demonstrated when whole grains loosened during mounting and fell out during polishing. As polished. 100X.

Studies of the temperatures and of the helium purities under which these experiments were operated indicated that the stainless steel which was attacked was at temperatures between 1000 1200°F and that up to 800 ppm of hydrogen and 500 ppm of $H_2O$ were present in the helium coolant stream. After the fuel elements had been removed from the reactor, they were encapsulated in a loading tube under 20 psig of nitrogen and stored in the ORR pool. On at least two occasions water was observed in the loading tube when the fuel element was brought into the hot cell.

For the next two experiments (elements 8 and 9), the gas in the loading tube was changed from nitrogen to helium. No rusting or corrosive attack was observed on any part of these two experiments.

It is suggested that during reactor operation a slight sensitization of the stainless steel occurred in the temperature range from 1000 to 1200°F. Subsequently, when the fuel element was put into the loading tube, water leaked in through the valve and came in contact with the fuel element. Gamma activity from the fuel element could cause dissociation of nitrogen and water to form nitric acid, which could then attack the sensitized areas of the shroud, lead tube, and fuel element that were in the temperature range indicated above. Stobbs and Swallow[10] observed that a pressurized-water loop with an air-cooled annulus surrounding it was attacked by concentrated nitric acid in the Materials Testing Reactor.

[10] J. J. Stobbs and A. J. Swallow, *Met. Rev.* **7**(25), 95 (1962).

**ETR Prototype Capsules.** – The examination of three ETR-irradiated capsules[11] was completed; examination of a fourth capsule is in progress. Fabrication and irradiation data are summarized in Table 20.2. The results of one experiment (E-12) were similar to those reported previously for ORR-irradiated capsules.[12] There were no large changes in the appearance or structure of this capsule. However, two of the other three capsules had suffered gross fractures in the stainless steel cladding (see Fig. 20.4). Dimensional measurements showed diameter increases up to about 0.060 in., about 8% (capsule E-4). When the capsules were disassembled, longitudinal voids were found in the centers of the originally solid fuel columns, and extensive columnar grain growth around these voids was apparent. These phenomena are typical of sintered $UO_2$ which has been heated to high temperatures in a steep thermal gradient.[13,14]

Only preliminary information is available for capsule E-6. Neither visual examination nor leak testing indicated a cladding failure. Dimensional measurements indicated an unusual degree of distortion of the capsule, which had become elliptical in section along most of the length. There was a slight general swelling with a maximum eccentricity of 0.058 in., as compared with 0.002 in. before irradiation.

Metallographic examination of fuel and cladding samples from the capsules that failed has been completed. There was no evidence that any portion of the $UO_2$ had been molten during irradiation. Since the region of columnar grain growth extended from the central void to about 0.15 in. from the outside surface of the fuel pellet, it is obvious that the maximum design temperature of 3700°F was exceeded in both capsules. The $UO_2$ structures indicated that the maximum central temperature was ~5000°F. In addition, the results of burnup analysis (Table 20.2) indicated that both capsules had been overpowered as much as 50%. There was a slight reduction in the thickness of the cladding at the fractures. As shown in Fig. 20.5, a heavy precipitate was found along the inner surface and the intergranular fractures. This precipitate, which extended from the inner surface of the cladding to about mid-wall throughout the capsule, appeared to consist of nitrides. The probable source of this nitrogen was an abundance of $UN_2$ in the outer regions of the $UO_2$ fuel pellets.

It is concluded that the primary causes of cladding failure in capsules E-1A and E-4 were (1) formation of nitrides in the inner surface region of the cladding and (2) overheating of the $UO_2$ fuel. The nitrides tended to weaken and embrittle the cladding, making it more susceptible to fracture when subjected to the unusual stress from the overheated fuel.

[11]The capsules were fabricated by the Metals and Ceramics Division. The experiments were assembled and operated by the Reactor Division.

[12]J. G. Morgan *et al.*, *Solid State Div. Ann. Progr. Rept. Aug. 31, 1961*, ORNL-3213, pp 105–106.

[13]V. B. Lawson and J. R. MacEwan, *Thermal Simulation Experiments with a $UO_2$ Fuel Rod Assembly*, CRFD-915 (March 1960).

[14]J. L. Bates, *Nucleonics* **19**, 6 (June 1961).

**Table 20.2. Data Summary for ETR-Irradiated Prototype Capsules**

| Capsule No. | Type of Fuel Pellet | $U^{235}$ Enrichment (%) | Design Heat Flux (Btu $hr^{-1}$ $ft^{-2}$) | Average Cladding Temperature (°F) | Uranium Burnup[a] (Mwd per metric ton) |
|---|---|---|---|---|---|
| E-1A | Solid | 0.71 | 159,000 | 1290 | 5050 |
| E-4 | Solid | 0.71 | 159,000 | 1320 | 8300 |
| E-12 | Hollow BeO bushing | 1.0 | 153,000 | 1500 | 1140 |
| E-6 | Hollow | 1.0 | 200,000 | 1300 | 8600[b] |

[a]Based on $Ce^{144}$/U ratio.

[b]Estimated.

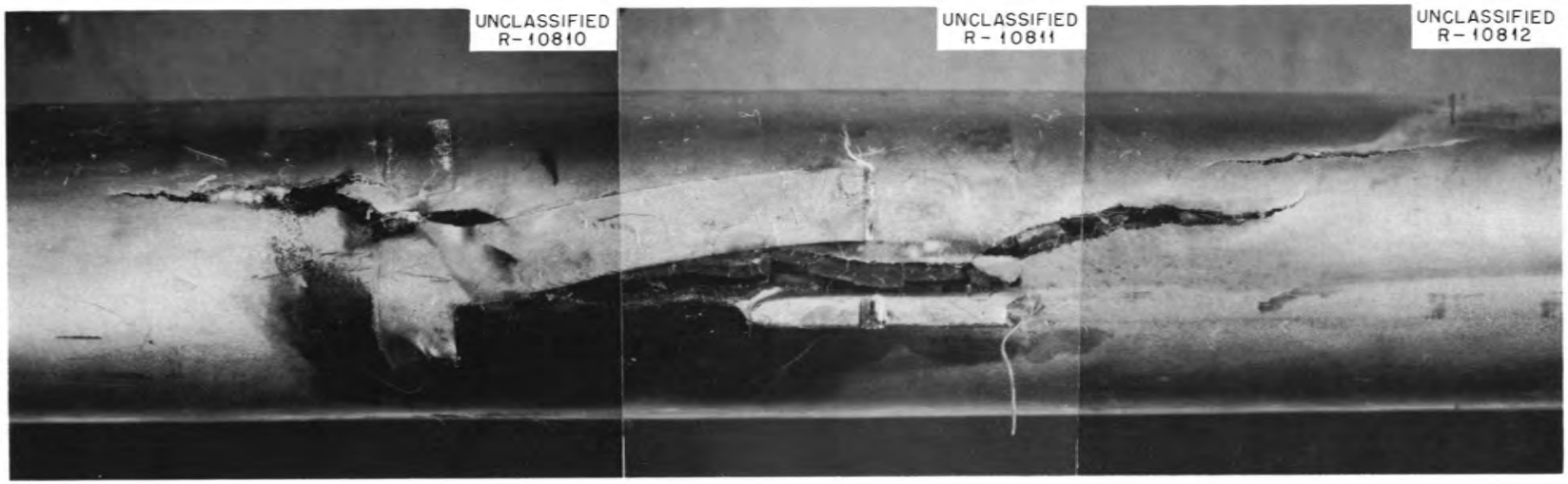


Fig. 20.4. Closeup View of Cladding Fracture, Capsule E-4. Note that pieces of sheathed thermocouple and foil thermocouple strap adhered to cladding. 2.5X. Reduced 10%.

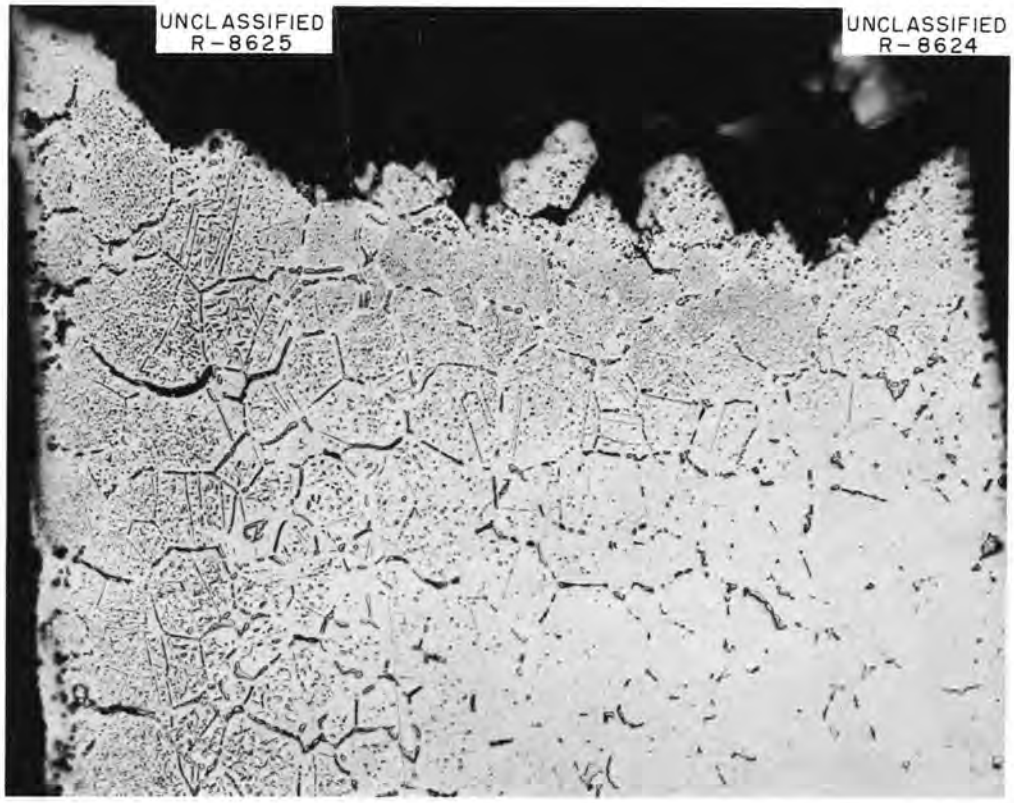


Fig. 20.5. Fracture in Cladding of Capsule E-1A. Note heavy precipitate along inner surface and fracture region. Etched. 250X.

Table 20.3. Irradiation Conditions for French Fuel Elements

| Identification | Flux ($nv$) | Time at Full Power (days) | Burnup (Mwd per metric ton of uranium) | Cladding Temperature (°F) | Wall Thickness (in.) | Pressure (psi) |
|---|---|---|---|---|---|---|
| | $\times 10^{13}$ | | | | | |
| 04-5 (CEA-4) | 5.0 | 125.3 | 7470 | 1140 av<br>1370 max | 0.0126–0.0134 | 850 |
| 05-5 (CEA-1) | 5.0 | 125.3 | 7610 | 1154 av<br>1270 max | 0.0118–0.0126 | 850 |

**Irradiation of Capsules from France.** – Two thin-walled type 347 stainless-steel-clad $UO_2$ fuel elements fabricated by the French Commissariat a l'Energie Atomique were irradiated in the ORR poolside facility. The capsules were ~6 in. long by 0.46 in. in diameter and contained solid $UO_2$ pellets ~0.4 in. long by 0.43 in. in diameter. The irradiation conditions are shown in Table 20.3. Thermal cycles between 50 and 60°F occurred during irradiation because of an unstable heat-transfer condition in the NaK coolant.

The postirradiation examination of these capsules revealed that an even burnup had been obtained. No separations between pellets were noted, and

dimensional stability during irradiation was excellent. No changes in length or diameter were noted except for 0.002-in. collapse of the cladding. Two pinhole leaks were found in the cladding of one capsule by noting a stream of bubbles when tested under vacuum in oil; the second capsule did not leak. Pellets in both fuel elements were badly cracked.

The metallographic results from the two capsules can be summarized as follows. There was no evidence of cladding deformation at any of the pellet-to-pellet interfaces in the specimens examined. Nothing in the areas observed, including the end-cap welds, suggested potential failure. The grain size of the cladding was extremely fine (ASTM No. 10–11). An intermittent reaction product that appeared to be an oxide was seen in the inner surface regions of the cladding to a maximum depth of 1 mil. A few pieces of $UO_2$ had adhered to the cladding, which indicated intimate contact during irradiation. Even though there were many fractures in the fuel pellets, no small pieces of $UO_2$ were found that had been dislodged or shifted at the pellet-cladding interfaces. A typical area from a longitudinal section is shown in Fig. 20.6. No reason for the observed failure of one of the claddings can be offered.

### Maritime Reactor Fuel – Postirradiation Examination

M. F. Osborne J. G. Morgan

Four additional Maritime Reactor fuel bundles, similar to those reported previously,[15] have been examined. Each of these fuel-rod bundles had been irradiated in the pressurized-water loop facility in the ORR.[16] Each bundle consisted of three fuel rods 18 in. long and 0.5 in. in diameter, shown in Fig. 20.7. Each rod was made of type

[15] J. G. Morgan *et al.*, *Solid State Div. Ann. Progr. Rept. Aug. 31, 1961*, ORNL-3213, pp 112–13.

[16] *Maritime Reactor Program Ann. Progr. Rept. Nov. 30, 1961*, ORNL-3238, p 41.

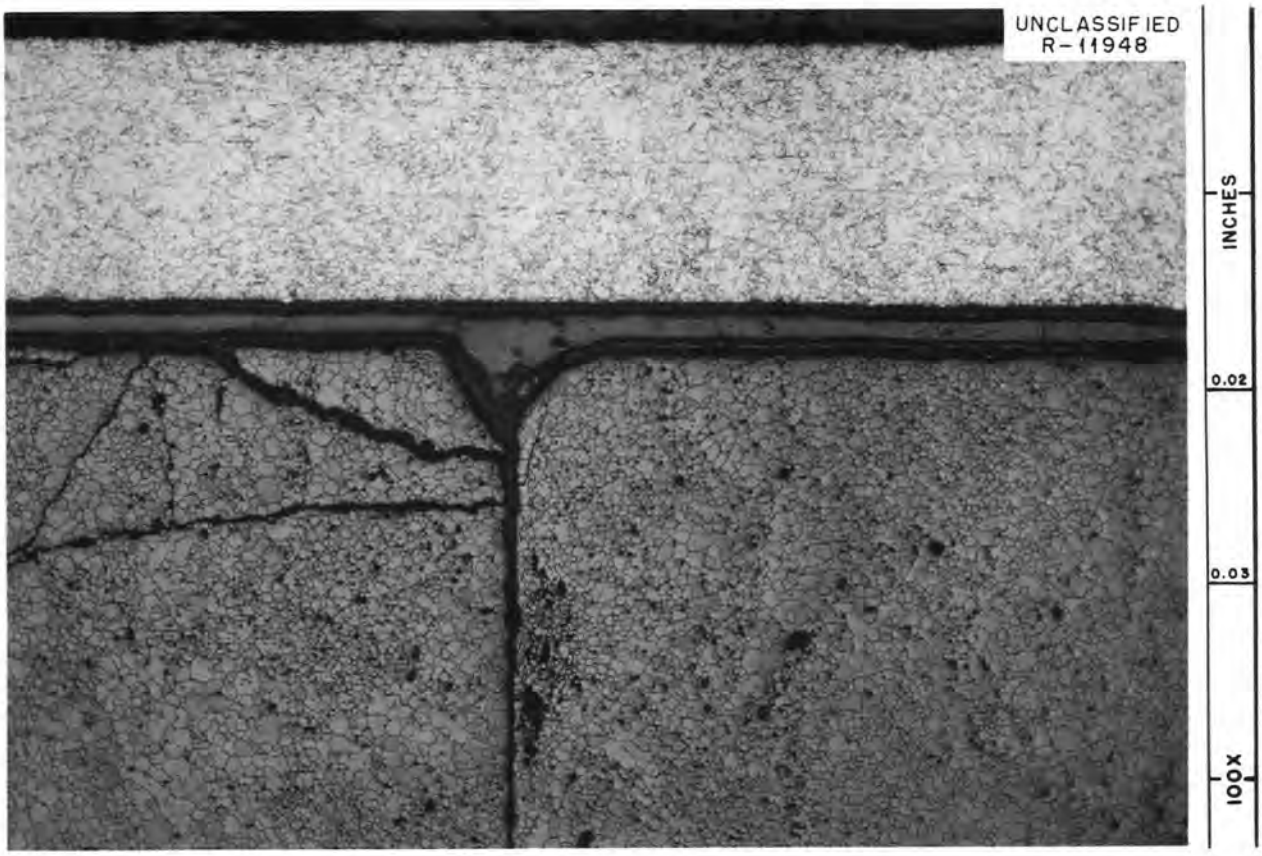


Fig. 20.6. Typical Area from a Longitudinal Section of French Capsule 05-5. Etched. 100X.

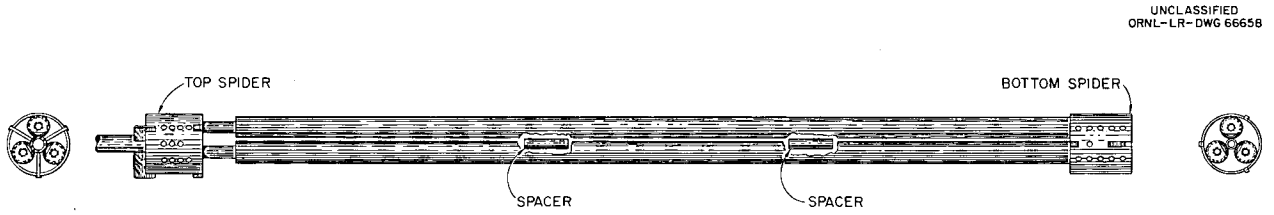


**Fig. 20.7. Schematic of Experimental Fuel-Rod Bundle, Maritime Reactor Program.**

304-L stainless steel tubing containing fused and ground $UO_2$.

The fuel rods were fabricated by two processes: (1) 0.75-in.-OD tubing containing $UO_2$ powder was swaged to the finished diameter, and (2) 0.5-in.-OD tubes were loaded with $UO_2$ by vibratory compaction. Uranium dioxide densities of about 90% of theoretical were attained by both methods.[17] Fuel enrichment ranged from 0.80 to 2.83% $U^{235}$.

The rods were cooled by high-purity water at 1750 psi and 500°F, flowing at about 10 fps. The experiments were irradiated to burnups of 4600 Mwd per metric ton of uranium, with center fuel temperatures estimated to be as high as 5000°F and a maximum heat flux of 400,000 Btu $hr^{-1}$ $ft^{-2}$.[18]

Except for the accumulation of a dark oxide film, there was no change in the exterior appearance of the irradiated rods. Radiochemical analysis of this film showed that the principal components were stainless steel corrosion products: Cr, Fe, Mn, and Co. No significant rod bowing was found. Diameter measurements indicated that one fuel rod was 0.007 to 0.01 in. smaller after irradiation; the diameter change of another rod varied from +0.011 to −0.005 in. Diameter changes for the other ten rods were within experimental uncertainty.

Samples of the gas from each rod were analyzed for both stable and radioactive components. The fractions of the $Kr^{85}$ released from the fuel, based on measured burnup, are shown in Table 20.4. As expected, the fission-gas release increased with increasing irradiation temperature and burnup, reaching a maximum of 23%. Gamma scans of the fuel rods were similar to that reported previously;[15] no unusual distributions of radioactivity were found. The ratios of peak to average radioactivity varied from 1.14 to 1.23, indicating relatively uniform burnup along the length of the rod.

The fuel rods were sectioned transversely and longitudinally for examination of the fuel. Transverse cracks in the fuel are correlated with irregularities in the gamma scan. One fuel rod (denoted 601) contained a void about 6 in. long and about 0.04 in. in the maximum diameter in the center of the fuel column. This type of central void, with the accompanying growth of columnar grains around it, is formed in $UO_2$ when steep thermal gradients exist at temperatures greater than 3000°F.[13,14] Partial sintering of the $UO_2$ was observed in several other fuel rods which experienced temperatures greater than 3000°F.

To evaluate the breeding efficiency of this fuel, some samples were analyzed by mass spectrometry for the plutonium content. These results, shown in Table 20.4, agreed fairly well with values calculated from the neutron flux.

The examination of two more fuel bundles, experiments 5 and 7, has been started. These experiments were similar to No. 4 and No. 6, respectively, and were irradiated to a somewhat higher burnup. Visual examination disclosed no unusual features or evidence of damage. The typical dark oxide film, present in various amounts, was generally heavier near the ends of the rods.

## Fast-Breeder Reactor Fuel[19] – Postirradiation Examination

M. F. Osborne J. G. Morgan

Tests[20] of fuel material for use in core B of the sodium-cooled Enrico Fermi reactor are continuing. Test specimens consist of two fuel plates, each

[17] J. T. Lamartine, *Preirradiation Data: Maritime ORR Loop Expts. 4, 5, and 6*, ORNL CF-62-3-88 (Mar. 28, 1962).

[18] V. O. Haynes, *ORR Pressurized-Water Loop Experiments: General Description and Operation Information for Expts. 4, 5, and 6*, ORNL CF-61-2-92.

[19] J. I. Federer, T. S. Lundy, and M. C. Ziemke, *Fast Breeder Reactor Assistance Program – Phase I – Irradiation of $UO_2$–Stainless Steel Fuel Specimens*, ORNL CF-60-1-14 (Jan. 7, 1960).

[20] The experiments have been fabricated and irradiated by the Metals and Ceramics Division and the Reactor Division respectively.

Table 20.4. Data Summary for Maritime Reactor Fuel Examinations

| Experiment No. | Rod No. | Fabrication Method | Maximum Heat Flux[a] (Btu $hr^{-1}$ $ft^{-2}$) | Maximum Fuel Temperature[a] (°F) | Maximum Burnup[b] (Mwd per metric ton of uranium) | $Kr^{85}$ Release[c] (%) | Plutonium Concentration (mg of Pu per g of U) |
|---|---|---|---|---|---|---|---|
| 3 | 3A1 | Cold swaged | 100,000 | 2200 | 2480 | 3.7 | |
| | 3B1 | Cold swaged | 100,000 | 2700 | 3030 | 3.4 | |
| | 3C1 | Cold swaged | 100,000 | 2700 | 3320 | 7.6 | 1.74 |
| | 3N1 | Cold swaged | 100,000 | 2200 | 2950 | 3.3 | |
| | 3O1 | Hot swaged | 120,000 | 2200 | 2900 | 3.1 | |
| | 3P1 | Hot swaged | 120,000 | 2700 | 3820 | 3.2 | 3.52 |
| 4 | 4N1 | Cold swaged | 200,000 | 3800 | 3120 | 4.1 | 1.65 |
| | 4O1 | Vibratory compacted | 275,000 | 2900 | 2870 | 2.2 | |
| | 4P1 | Vibratory compacted | 275,000 | 2900 | 2440 | 2.9 | 1.87 |
| 6 | 6N1 | Vibratory compacted | 400,000 | 4500 | 3750 | 4.7 | 1.34 |
| | 6O1 | Vibratory compacted | 400,000 | 4500 | 4660 | 23.4 | |
| | 6P1 | Vibratory compacted | 400,000 | 5000 | 4150 | 10.5 | 1.58 |

[a]Calculated.
[b]Based on $Ce^{144}$/U ratio.
[c]Based on average burnup.

2.0 × 0.5 × 0.116 in., with a fueled core of 33.2% by weight of fully enriched $UO_2$ dispersed in 347 stainless steel clad with 0.007-in. thickness of this steel. The fuel plates are immersed in sodium; temperatures are monitored by sheathed thermocouples pressed against each side of the plates. A maximum cladding temperature of 1200°F was predicted.

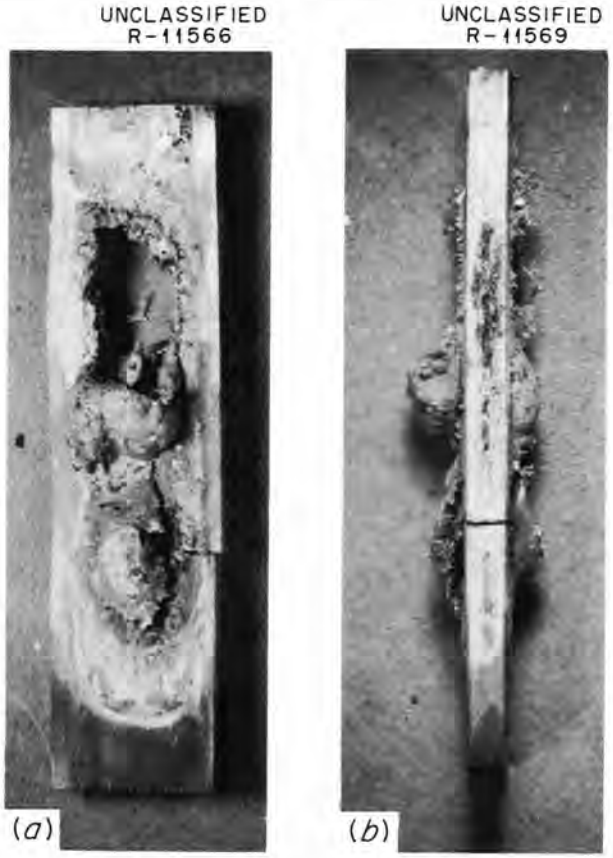


**Fig. 20.8. Top Fuel Plate from MTR-46-2, Showing Severe Damage Apparently Due to Overheating.**

The first experiment (MTR-46-4) showed relatively little damage on irradiation to about 6% burnup of the uranium.[21] However, very drastic effects (see Table 20.5) were observed in the two subsequent experiments carried to substantially higher burnups. Examination of experiment MTR-46-2 revealed that the central portion of the top fuel plate (No. 6) had melted (Fig. 20.8), and that part of it had fallen to the bottom of the container; the bottom fuel plate (No. 5) was visibly swollen. Radiochemical analysis of the sodium coolant showed that a large fraction of the $Cs^{137}$ produced had escaped from the fuel. Burnup analysis of a section of the bottom fuel plate by mass spectrometric techniques indicated that 25.9% of the uranium atoms had fissioned. Metallographic examination of the fuel plates is incomplete.

The appearance of the fuel plates from experiment MTR-46-5 was similar to that of the bottom plate in MTR-46-2; both plates were badly swollen, but there were no obvious cladding failures. However, there was a significant amount of $Cs^{137}$ present in the sodium coolant, which indicates some failure of the cladding. No breaks were found by dye penetrant testing.

[21] J. G. Morgan and M. F. Osborne, *Solid State Div. Ann. Progr. Rept. Aug. 31, 1961*, ORNL-3213, pp 113–14.

**Table 20.5. Results of Examination of Fermi Fuel Plates**

| Experiment No. | Plate No. | Maximum Increase in Thickness (in.) | Maximum Increase in Thickness (%) | Burnup (at. % uranium) | Density Decrease (%) |
|---|---|---|---|---|---|
| MTR-46-4 | 1 | 0.0010 | 0.9 | 5.63[a] | 0.6 |
| | 10 | 0.0007 | 0.6 | 6.07[a] | 0.4 |
| MTR-46-2 | 5 | 0.0489 | 44. | 25.9[b] | 12.6 |
| | 6[c] | | | | |
| MTR-46-5 | 8 | 0.0322 | 27. | | 8.34 |
| | 9 | 0.0376 | 31. | | 6.16 |

[a]Based on $Ce^{144}/U$ ratio.
[b]Based on $U^{235}/U^{236}$ ratio.
[c]No measurements due to melting of fuel.

### Fuel Cycle Program[22] – Postirradiation Examination of Fuel

M. F. Osborne J. G. Morgan

The ORNL Fuel Cycle Program[23] attempts to demonstrate suitable techniques for remote reprocessing and refabrication of reactor fuel containing $U^{233}$. The process currently under study uses the sol-gel process[23] to prepare $UO_2$-$ThO_2$ powders for production of fuel rods by vibratory compaction techniques. The 15 fuel rods prepared and irradiated for examination to date have consisted of type 304 stainless steel filled (to 83 to 86% of theoretical density) with an oxide mixture containing 4.5% by weight of fully enriched $U^{235}O_2$ in $ThO_2$. Fuel material from three sol-gel process runs has been used; control material obtained as fused and ground oxide from Spencer Chemical Company has been used in three rods, and standard pelletized fuel has been used in one. Irradiations were performed at linear heat ratings from 20,000 to 50,000 Btu $hr^{-1}$ $ft^{-1}$ to burnups from 3500 to 33,000 Mwd per metric ton of metal.

Postirradiation examination of the 15 rods has included determination of dimensional changes, radioactivity scans, and determination of released fission gas. Final determination of fuel burnup and metallographic examination of cladding and fuel have been completed for only three of the rods.

No significant changes were observed in the dimensions of any rod. Bowing of the specimens was similar to that before irradiation; changes in rod diameter did not exceed 0.003 in. and were generally increases.

Fission-gas release, measured by comparison of collected $Kr^{85}$ with $Kr^{85}$ expected from fuel burnup measurements (or estimates), was less than 5% for all, and less than 2% for most of the rods. Final values await measurement of burnup actually achieved. It should be noted that the helium cover gas in the sealed rods is quite impure; large quantities of air, $CO_2$, Ar, and $H_2$ were observed by mass spectrometry.

The three rods for which metallographic examination is complete show no evidence of control void formation or grain growth within the oxide and no significant changes in microstructure of the cladding material. There are no indications of reaction at the fuel-cladding interface in any rod examined.

[22]Administered by the Metals and Ceramics Division.

[23]S. A. Rabin, *Status of the Fuel Cycle Irradiation Program at ORNL*, ORNL CF-62-7-55 (July 1962).

## SYSTEMS WITHOUT METAL CLADDING

### Postirradiation Examination of Coated Particles

J. G. Morgan D. F. Toner
M. F. Osborne E. L. Long, Jr.[24]

Air-cooled core facilities in the LITR are in use for irradiation of particles of uranium carbide coated with pyrolytic carbon. A total of four capsules, prepared by personnel from the Metals and Ceramics Division and irradiated under supervision of personnel from the Reactor Division, have been examined.

Each capsule consisted of two separate sections, denoted "*a*" (top) and "*b*" (bottom) as shown in Fig. 20.9. The fuel particles were contained in tantalum cans which were sealed inside and insulated from Inconel outer containers; the containers were filled with purified helium. All capsules contained coated particles with 200- to 250-$\mu$-diam cores of uranium dicarbide coated with 100- to 125-$\mu$-thick coatings of pyrolytic graphite.

Table 20.6 shows the materials used and the irradiation conditions for these four tests along with the extent of coating failure as indicated by the fraction of uranium leached from the irradiated specimens with nitric acid.

The top sections of capsules 1 and 2 were found to have leaked, since no fission gas was found after irradiation. Capsule 1a showed no evidence of oxidation of the tantalum can and, presumably, leaked only at low temperature after exposure. Capsule 2a showed marked oxidation of the tantalum; leakage of air during the high-temperature irradiation may be responsible for the behavior of the thermocouple (see Table 20.6) and for the poor performance of the coated particles. No evidence of leakage was obtained for other capsules in this series.

Examination of the particles after irradiation revealed behavior consistent with that established by acid leaching. No marked changes in gross appearance of the irradiated particles were observed; those exposed in capsule 2a were duller in

[24]Metals and Ceramics Division.

appearance, probably because of some oxidation during exposure. Some particles with cracked coatings were observed in all capsules.

Metallographic examination showed that some reaction between the fuel core and the particle coating had occurred in all cases. The fuel cores in all particles had changed in appearance, and the microstructure was not as well defined after irradiation. Under the oxidizing conditions of capsule 2a, all particles with cracked coatings showed badly damaged cores.

The particles with duplex coatings (laminar coating inside and columnar coating outside) suffered less damage than either singly coated type. Some reaction appeared at the core-coating interface, but "spearhead" features penetrated only the laminar coating (see Fig. 20.10); the columnar coating was relatively unaffected.

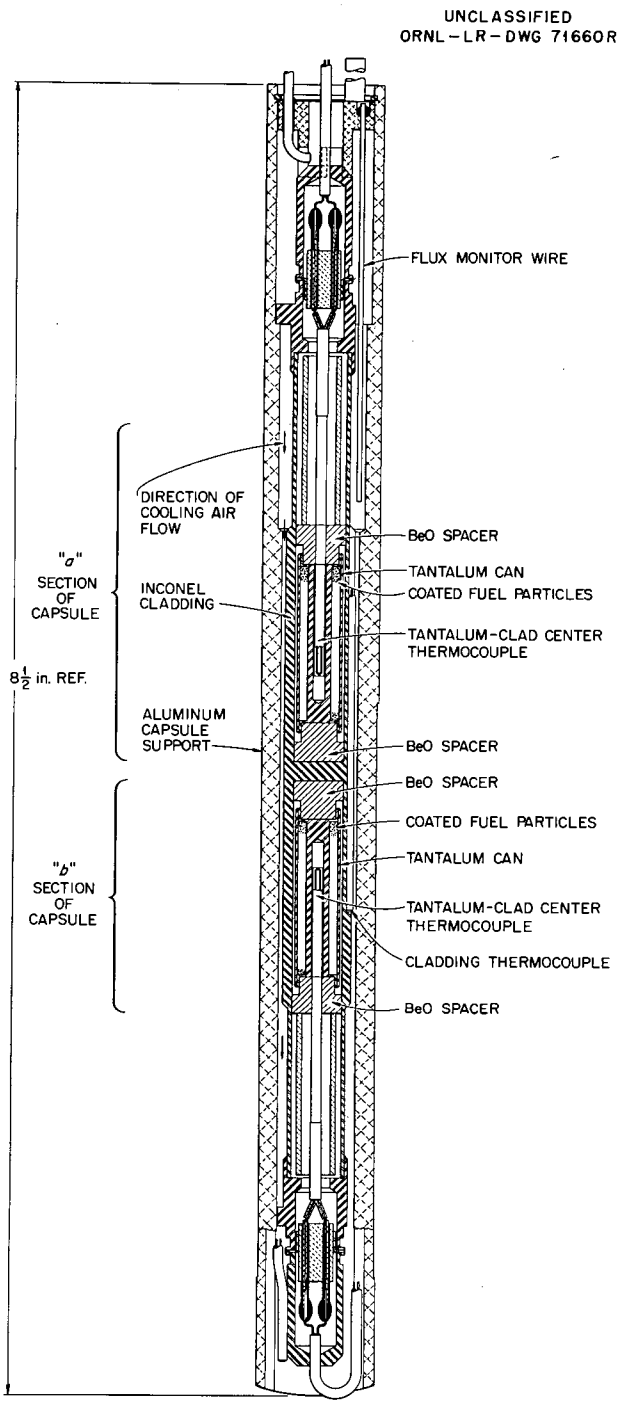


**Fig. 20.9. Diagram of Coated-Particle Irradiation Capsule.**

## Postirradiation Examination of Graphite-Matrix Fuel

J. G. Morgan D. F. Toner
M. F. Osborne H. E. Robertson
E. L. Long, Jr.[24]

Several additional experiments in the series[25,26] to examine the behavior of various fueled-graphite elements under irradiation have been completed. In these experiments specimens obtained or fabricated by personnel from the Metals and Ceramics Division have been irradiated by Reactor Division personnel in facilities in the MTR or ORR. In all experiments the specimens were exposed in cans of relatively impermeable graphite and were continuously swept with a slow flow of helium so that fission-gas release data could be obtained.

Table 20.7 shows the type of specimen used and summarizes the irradiation conditions employed for irradiations in the MTR. The fuel pellets from these three experiments are shown in Fig. 20.11. Specimens from experiments –4 and –5 showed small decreases in length and diameter; the pellet from experiment –6 showed no measurable dimensional changes.

Metallographic examination showed several changes due to irradiation. The uncoated particles in experiment –4 showed little change in appearance at 0.9% burnup and 2500°F but became porous and amorphous and had partially migrated into the graphite at 3.5% burnup at 2800°F. All the coated

[25] *Solid State Div. Ann. Progr. Rept. Aug. 31, 1960*, ORNL-3017, pp 113–14.

[26] *Solid State Div. Ann. Progr. Rept. Aug. 31, 1961*, ORNL-3213, pp 110–11.

$UC_2$ particles from experiment –5 had broken coatings regardless of position in the pellet; the fuel core material had lost its well-defined microstructure. Most particles in the specimen from experiment –6 (see Fig. 20.12) showed beginning of wedge-shaped fractures at core-coating interfaces; about 10% of the coatings had failed at 5.4% burnup of the uranium. Gaps were present at most of the coating-matrix interfaces. The carbide fuel contained a light-colored second phase which was more oxidation resistant than the original material.

Analysis of the fuel matrices and the graphite cans showed that significant migration of the uranium and of fission products had occurred. In experiment –5, for example, the uranium concentration of inner portions of the graphite can was 4% of the value for the fuel; the corresponding

**Table 20.6. Irradiation Conditions and Examination Data for Coated Particles**

| Coating Type | Capsule No. | Control Temperature (°F) | Uranium Burnup (at. %) | Uranium Removed by Leaching (%) |
|---|---|---|---|---|
| Columnar[a] | 1a | 1950 | 4.7 | 22.0 |
| | 1b | 2100 | 4.7 | 2.0 |
| Laminar[b] | 2a | 2400[c] | 7.0[d] | 10 |
| | 2b | 2500[d] | 7.0[d] | 0.62 |
| Duplex[e] | 3a | 1850 | 5.2 | <0.5 |
| | 3b | 1950 | 5.0 | |
| Columnar[f] | 4a | 2300 | 6.1 | 52 |
| | 4b | 2400 | 5.5 | 45 |

[a]Batch HTM-1, High Temperature Materials, Inc.
[b]Batch 3M-SP-2, Minnesota Mining and Manufacturing Co.
[c]Thermocouple indicated rise to 3200°F and then failed.
[d]Estimated.
[e]Batch NCC-BE, National Carbon Co.
[f]Batch HTM-2, High Temperature Materials, Inc.

**Table 20.7. Conditions for Irradiations in the MTR-48 Series**

| Experiment No. | Type of Fuel Particle in Graphite Matrix | Fuel Loading (g of $U^{235}$ per $cm^3$) | Maximum Fuel Temperature (°F) | Burnup (at. % $U^{235}$) |
|---|---|---|---|---|
| –4 | Uncoated $UC_2$ | 0.169 to 0.517 | 2500 to 2800 | 3.5 to 0.9 |
| –5 | Pyrolytic-carbon-coated $UC_2$ | 0.0841 | 2600 | 17 |
| –6 | Pyrolytic-carbon-coated $(U, Th)C_2$ | 0.088[a] | 2000 | 5.38[a] |

[a]Total fuel loading was 0.282 g/$cm^3$ (U + Th), and total fuel burnup was 1.56 at. % (U + Th).

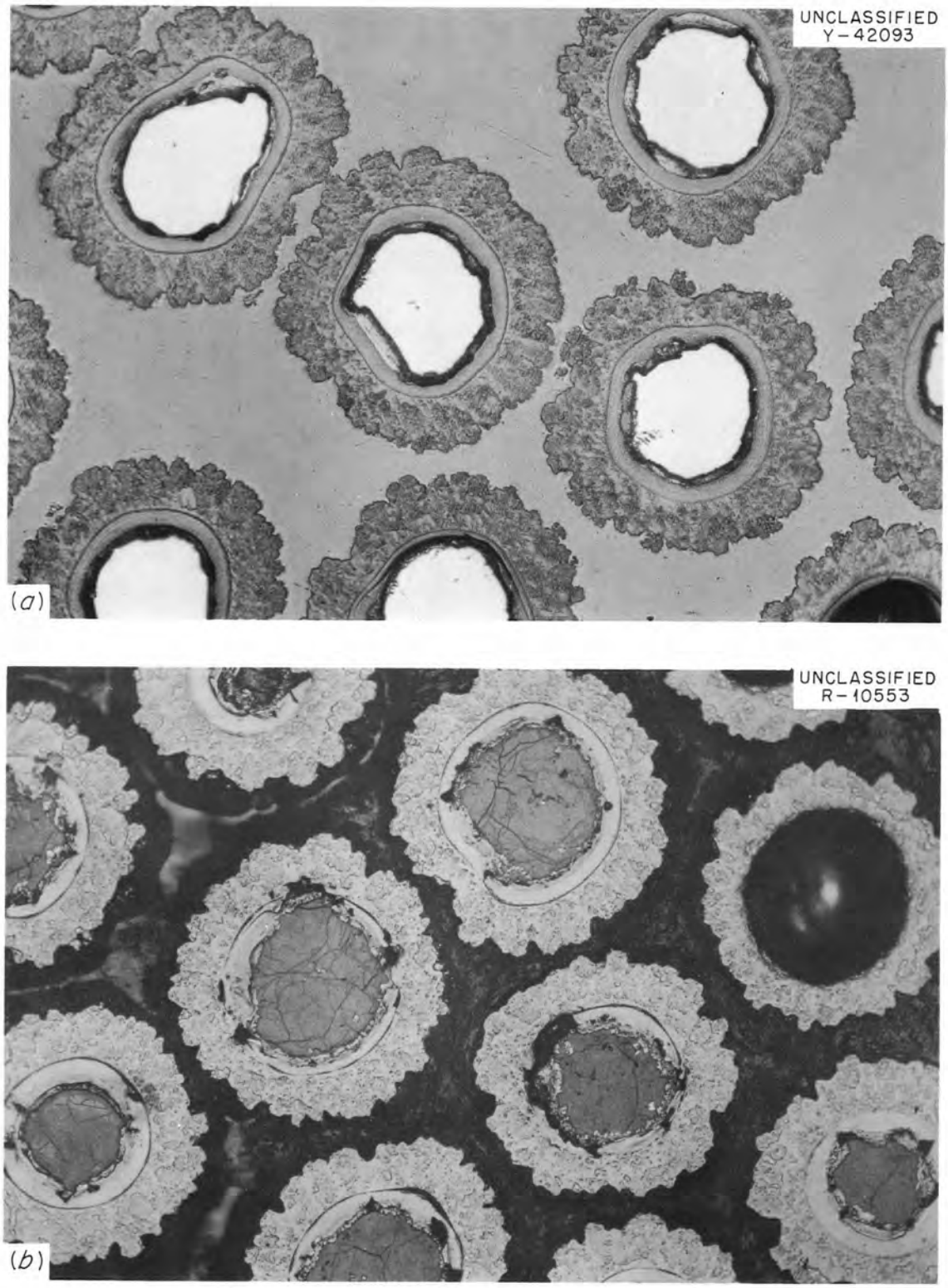


Fig. 20.10. Pyrolytic-Carbon-Coated Uranium Carbide Particles with Duplex Coatings. (Batch NCC-BE). (*a*) Unirradiated particles. As polished. 100X. (*b*) Irradiated particles from LCP-3a. Etched. 100X. Note: (1) that only a few of the "spearhead" fractures extend beyond the interior coating, and (2) that there is a lack of grain contrast in the fuel cores.

UNCLASSIFIED
R-6483

(a) MTR-48-4

UNCLASSIFIED
R-8970

(b) MTR-48-5

UNCLASSIFIED
R-10498

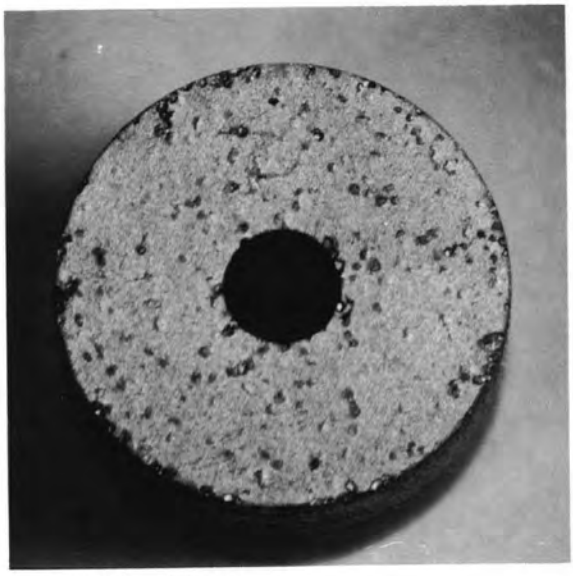

(c) MTR-48-6

Fig. 20.11. Appearance of Irradiated Fuel Pellets from MTR-48 Experiments.

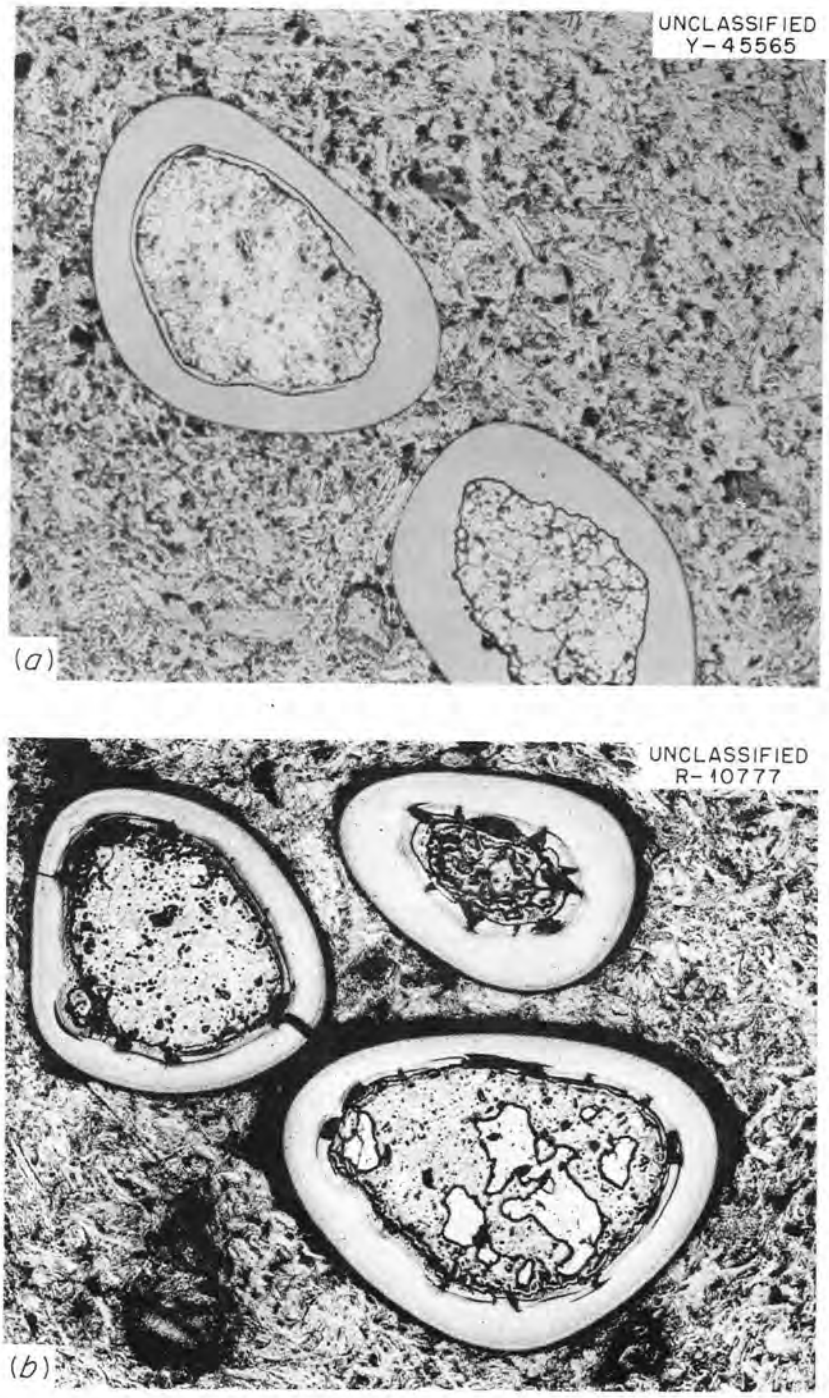


Fig. 20.12. Typical Areas from Pyrolytic-Carbon-Coated $(U,Th)C_2$ Particles Dispersed in Graphite from MTR-48-6. (*a*) Unirradiated control. (*b*) Irradiated. Air-etched. 100X.

figure for outer portions of the can was 0.4%. About 30% of the $Cs^{137}$ formed in this experiment was found in the graphite can.

The ORR poolside facility has been used to irradiate three assemblies, each containing 12 fuel bushings (0.6 in. in diameter) inside a pyrolytic graphite sleeve. Materials and irradiation conditions are summarized in Table 20.8. All assemblies were irradiated at about the same power density (120 w/cm$^3$), and each assembly received several thermal cycles which coincided with the reactor cycles.

Fission-gas release data shown in Table 20.8 are the values at the end of the irradiation period; data for the entire cycle were reported previously.[27]

Postirradiation examination of these experiments is incomplete, but the observations to date show considerable differences in behavior among the three assemblies. All 12 bushings in experiment 01-5 were cracked, and all showed swelling of about 1%, as measured by decrease in inside diameter of the bushings. Experiment 08-5 showed similar behavior although only 4 of the 12 specimens were cracked. Examination of the most severely damaged specimen from this assembly (see Fig. 20.13) shows that several cracks in particle coatings coincide with cracks in the graphite matrix. No cracked bushings occurred in experiment 08A-5, and dimensional measurements revealed small volume decreases on irradiation. Differences among these specimens may have resulted from thermal stresses induced during irradiation because of uneven fuel distribution; it is more likely, however, that the sound specimens have superior mechanical and thermal properties.

[27] *GCR Semiann. Progr. Rept. Sept. 30, 1962*, ORNL-3372 (in process).

**Fig. 20.13. Cracked Bushing from Capsule 08-5.**

**Table 20.8. Conditions for Irradiations in the ORR Series**

| Experiment | Coated Particle Batch No. | Nature of Particle Coating and Thickness | Central Fuel Temperature | Estimated Burnup (at. % uranium) | $Kr^{88}$ (2.8 hr) $R/B$ Ratio[a] |
|---|---|---|---|---|---|
| 01-5 | 3M-101-61 | Laminar – 85 $\mu$ | 1200–2400°F[b] | 9.0 | $\sim 1 \times 10^{-2}$ |
| 08-5 | 3M-101-61 | Laminar – 85 $\mu$ | 1600–1700°F[c] | 5 | $1.0 \times 10^{-3}$ |
| 08A-5 | NCC-G | Duplex – 82 $\mu$ | 1600–1750°F[d] | 9.0 | $\sim 3 \times 10^{-4}$ |

[a] Release rate/birth rate ratio.
[b] Received one thermal cycle to 3200°F.
[c] Received one thermal cycle to 2400°F.
[d] No thermal cycles to higher than indicated temperature.

# 21. Fission-Gas Release

R. M. Carroll J. G. Morgan O. Sisman

## CONTINUOUS RELEASE OF FISSION GAS DURING IRRADIATION OF $UO_2$

R. M. Carroll P. E. Reagan
T. W. Fulton

It has been shown[1] that release of the fission gases krypton and xenon from fissioning $UO_2$ proceeds at low temperatures by a temperature-independent process, generally presumed to be by direct recoil. At elevated temperatures this process is augmented by a temperature-dependent process usually presumed to include diffusion of the fission products. The temperature-dependent process becomes noticeable at about 525°C for polycrystalline sintered specimens of $UO_2$ and shows an activation energy of 30 to 40 kcal/mole. Rate of release of the fission gases generally increases with increasing irradiation for such specimens; these increases may be due to specimen damage with consequent increase in real surface area.

An in-pile facility is in operation for the study of factors controlling the fission-gas release from $UO_2$ during irradiation.[2] The fuel specimens, typically in the form of two thin plates, are assembled in parallel with thermocouples sandwiched between them and pressed against the outer surfaces (Fig. 21.1). The depressed flux (inside the capsule) is measured by determining the activation of the argon used as the sweep gas. This method gives the thermal flux to within 10% at the moment the fission gas is released.[3]

This facility has been used to examine specimens of fused-crystal, single-crystal, and sintered polycrystalline $UO_2$. The fused-crystal specimens were obtained by slicing a lump of fused $UO_2$ which consisted of grains so large that the plate thickness was less than the average grain diameter; the high-quality single-crystal $UO_2$ was obtained from Hanford.

The fused-crystal specimens contained high concentrations of voids and impurities; microstructure determinations before and after irradiation revealed that the voids migrated during irradiation to combine and align along metallographic planes in spite of the fact that the specimens never attained temperature above 1000°C.

The thermocouples attached to the specimens have also served as probes to measure electrical conductivity of the $UO_2$ during irradiation.[4] Table 21.1 shows the resistivity and activation energy for specimens of the various types. Electrical resistivity of the single-crystal material dropped by 200-fold as soon as irradiation began; this immediate decrease was due to ionizing radiation since resistivity increased when the specimen was withdrawn from the flux. The change in resistivity became irreversible, however, after about 24 hr of irradiation. Activation energy dropped from 11.3 ev to 1.6 ev during the first few hours of irradiation and then stabilized at 0.4 ev for subsequent treatment. Irradiation apparently decreases resistivity by providing carriers and decreases the activation energy through induced disorder in the $UO_2$ lattice; the effect is much more pronounced in highly ordered structures such as the single-crystal specimen.

---

[1] R. M. Carroll, "Continuous Release of Fission Gas from $UO_2$ During Irradiation," *Symposium on Radiation Effects in Refractory Fuel Compounds*, ASTM Special Technical Publication No. 306.

[2] R. M. Carroll and C. D. Baumann, *Experiment on Continuous Release of Fission Gas During Irradiation*, ORNL-3050 (Feb. 9, 1961).

[3] R. M. Carroll, *Nucleonics* **20**(2) (1962).

[4] M. D. Karkhanavala and R. M. Carroll, *In-Pile Measurement of the Electrical Resistivity and Thermoelectric Power of Sintered $UO_2$*, ORNL-3093 (April 1961).

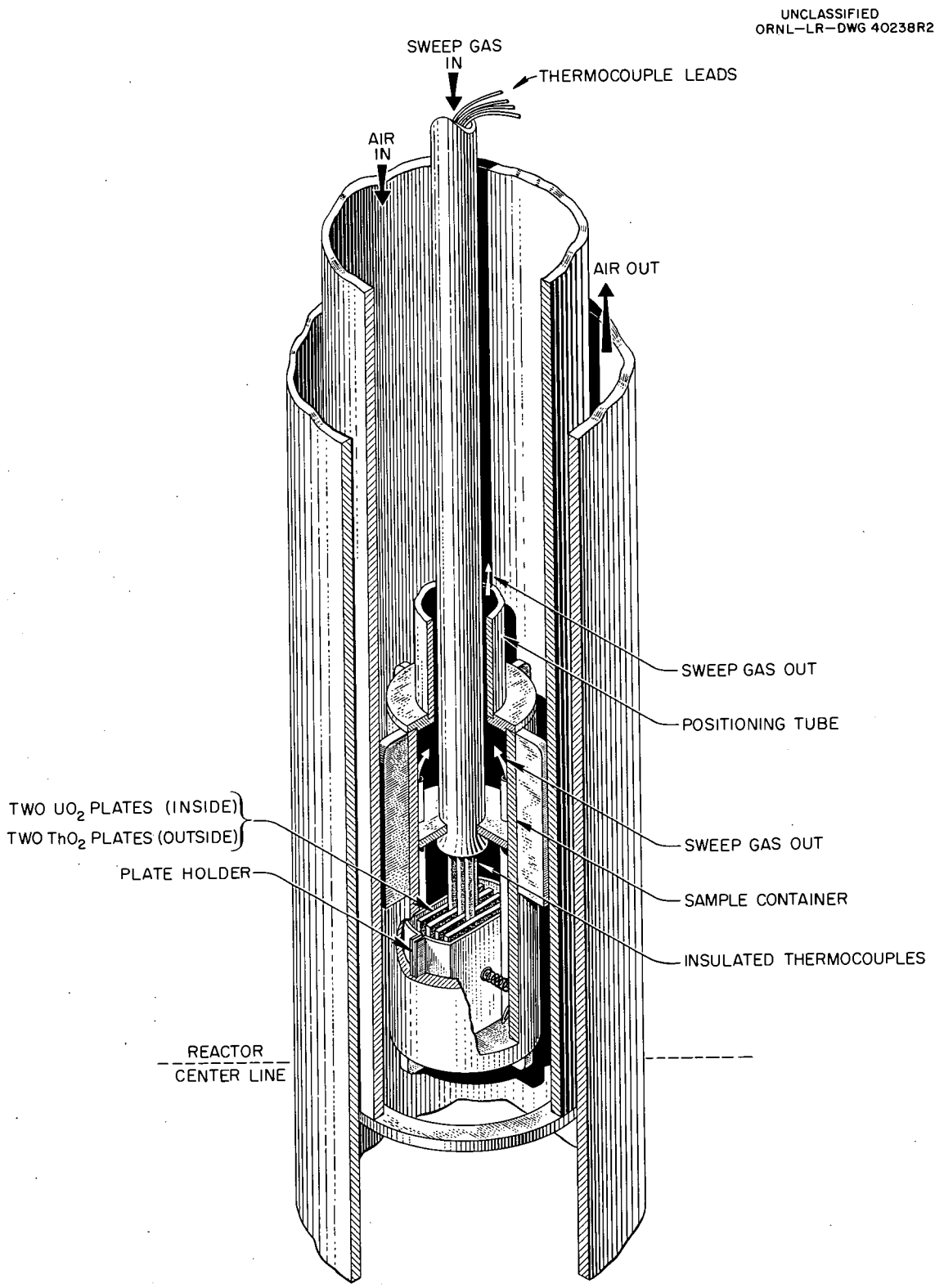


**Fig. 21.1. Thin-Plate $UO_2$ Specimen Positioned in Facility Tube.**

**Table 21.1. Comparison of Resistivity and Activation-Energy Values for Various $UO_2$ Specimens**

| Specimen | Resistivity at 700°C (ohm-cm) | | Activation Energy (ev) | |
|---|---|---|---|---|
| | Before Irradiation | After Irradiation to $10^{18}$ *nvt* | Before Irradiation | After Irradiation |
| Sintered, fine grain | 2.0 | 0.8 | 0.65 | 0.50 |
| Fused crystal, very large grain | 1.7 | | 0.52 | |
| Single crystal | ~500 | 2.5 | 11.3 | 0.4 |

The fused-crystal specimens showed, after several weeks of irradiation, a perceptible increase in steady-state release rate of fission products; postirradiation examination showed that the specimens had broken, apparently along the grain boundaries, and the increased rate may have been due to increased surface area. The single-crystal material, however, showed a release rate which decreased in 30 days to 65% and in 90 days to 25% of the value established during the first week; the rate appears to have leveled after 90 days ($8.2 \times 10^{19}$ *nvt*). (This reduced rate is not due to uranium burnup, which totaled only 8% and which was more than compensated by produced plutonium.) It may be that fission fragment damage creates defacts in the single-crystal lattice and that these defects retard movement of fission fragments through the lattice.

Iodine release measurements show that about 45 to 48% of the 133 and 75 to 78% of the 135 isobar escaping from the specimen escapes as iodine or a precursor of iodine. This fraction seems to be independent of the type of specimen or conditions of irradiation.

Temperature dependence of the gas release shows the activation energy to be 30 to 40 kcal per mole for the sintered specimens and the fused-crystal material but 46 to 50 kcal per mole from the single-crystal specimens. The temperature-dependent process for release sets in at about 630°C with single-crystal material; this is about 100°C higher than for the polycrystalline materials.

Thin-plate specimens of sintered $UO_2$, containing excess oxygen, released bursts of fission gas when the specimens were heated or cooled.[1] When the fused-crystal specimens were studied in thermal cycles, fission gas bursts on heating were always produced, but no bursts were found on cooling.

A difference in enrichment of the specimens has required a tenfold higher neutron flux for the fused-crystal specimen than for the sintered specimen to produce nearly equal fission rates. Contrary to expectations, the $Xe^{133}/Xe^{135}$ ratios in the released gas are the same for both specimens; this surprising result suggests that movement of the iodine precursor is the important portion of the release mechanism.

If the low-temperature (temperature independent) escape process were by fission recoil and the high-temperature process were by diffusion, then, as a consequence both of decay half-times and of differences in neutron cross section in the various chains, the isotopic proportions in the released gas should change with irradiation temperature. However, there is no significant effect of temperature on the isotopic ratio of the released gas; moreover, the isotopic ratio is not that anticipated from direct recoil. No firm explanation can, at present, be given as to why the temperature dependence indicates two mechanisms while the gas composition data indicates only one. The following points may be considered:

Escape of fission gases by direct recoil is a minor part of the overall process. However, fission fragments near the surface can free atoms of fission gas that would otherwise be trapped. The gas so liberated would have the isotopic composition of trapped (and aged) gas.

Inclusions, fission products, and small voids are very mobile in the $UO_2$ lattice. Larger discontinuities such as grain boundaries, large pores, or perhaps even the specimen surface act as

traps both for mobile fission products and for smaller inclusions and voids. Fission fragment tracks act as discontinuities, trap mobile fission fragments, and reduce the gas release rate. Discontinuities caused by fission fragment tracks slowly anneal so an equilibrium concentration of them is achieved; this equilibrium concentration is a function of temperature.

Under these conditions with the fission fragments very mobile and their escape rate determined only by concentration of traps, the escape rate, and activation energy for escape, would be the same for all gases; this is in accord with the observations. Such a situation would also permit the observed phenomena that all isotopes attain equilibrium in the released gas much sooner than can be explained by diffusion theory.

The bursts of fission gas that occur when $UO_2$ is heated cannot be explained by diffusion theory (which assumes a smooth concentration gradient of fission gas within the $UO_2$). Assuming the surface of the specimen acts as a discontinuity, much like a grain boundary, then a concentration of fission gas would accumulate just at the surface. An increase of temperature would reduce the concentration equilibrium of traps and cause the release of gas from these traps.

The only justification for the above theory is that it conforms to the phenomena that have been observed. There is little doubt, however, that conventional diffusion theory is inadequate to explain the escape of fission gas from $UO_2$.

## CONTINUOUS RELEASE OF FISSION GAS DURING IRRADIATION OF $UC_2$ COATED PARTICLES

P. E. Reagan R. M. Carroll
T. W. Fulton

Uranium carbide particles coated with pyrolytic carbon to retain fission fragments are under study for use in graphite matrices as fuels for high-temperature gas-cooled reactors. Experiments to study fission-gas release from such particles have been operated at lattice positions B9 and C1 of the Oak Ridge Research Reactor.

The fuel particles are arrayed in a monolayer between concentric cylinders of graphite (Fig. 21.2) to permit control and measurement of temperature. Both ends of the inner cylinder are vented to allow fission gases to escape into the sweep gas (helium or argon) which passes to a station where samples are drawn for analysis by gamma ray spectrometry. The fuel particle holder is sealed into an air-cooled capsule which is inserted vertically into the ORR lattice. Figure 21.3 shows the flow diagram for this assembly. Neutron flux and temperature of the specimens can be varied independently over wide limits by changing position within the lattice, cooling air velocity, and helium or argon purge gas.

This assembly is in use to study fission-gas release rates (expressed as $R/B$, the ratio of release rate to birth rate) from uncoated uranium carbide and from particles with three types of pyrolytic coatings. Information concerning the particles tested is shown in Table 21.2, while photomicrographs of the unirradiated materials are shown as Fig. 21.4.

These materials have been given long-term irradiations at neutron fluxes ranging from 2.5 to $5.5 \times 10^{13}$ neutrons $cm^{-2}$ $sec^{-1}$ and burnups from 4.3% for the bare uranium carbide particles to 30%

UNCLASSIFIED
ORNL-LR-DWG 57280R2

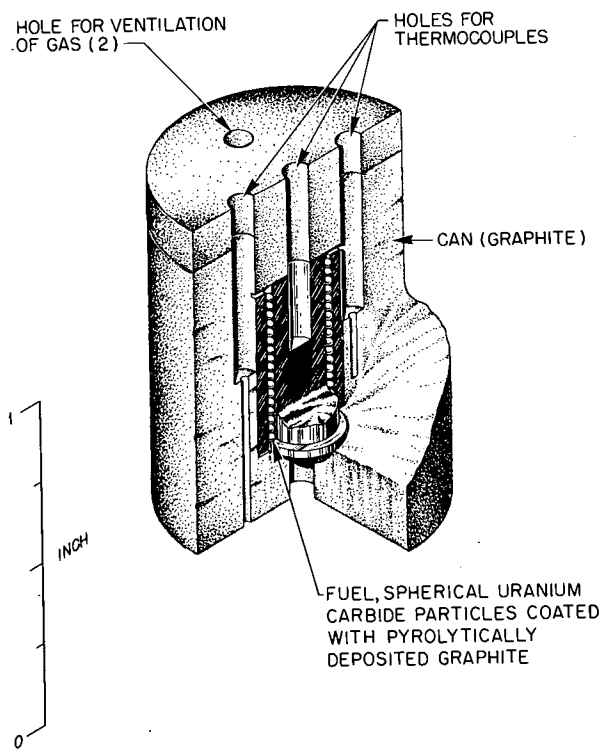


**Fig. 21.2. Coated-Particle Capsule for ORR Facility.**

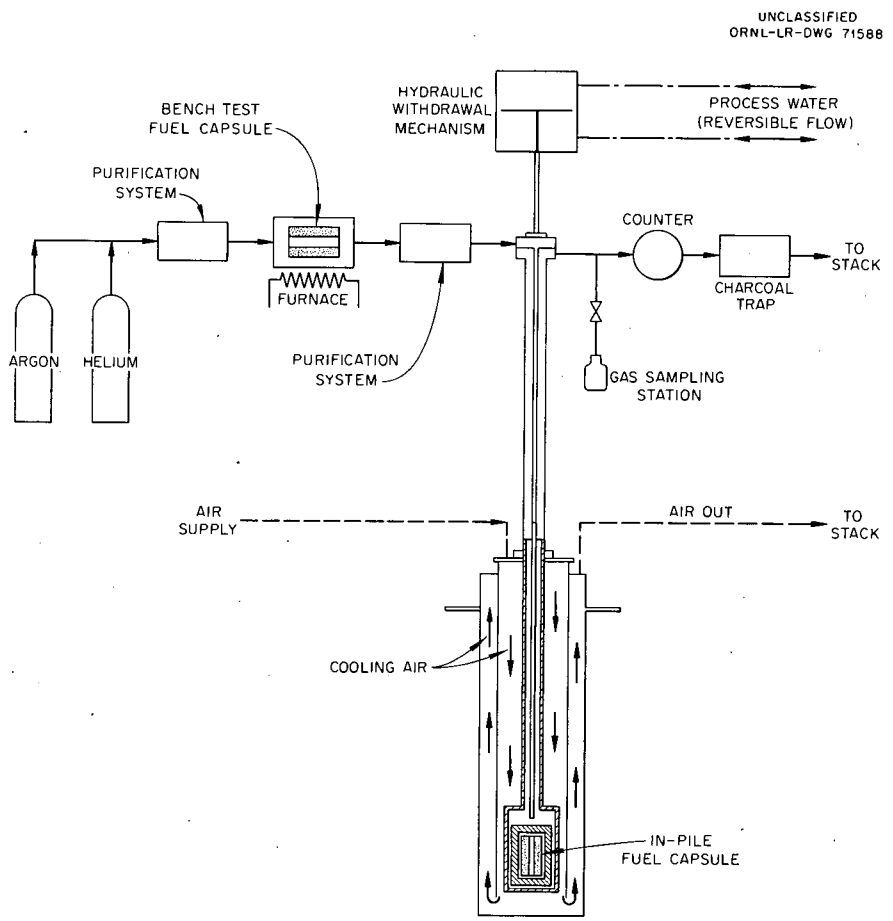


**Fig. 21.3. Flow Diagram of In-Pile Test Facility.**

**Table 21.2. Coated-Particle Capsule Data**

| Capsule No. | Coating Type | Manufacturer and Batch | Particle Size ($\mu$) Average Overall Diam. | Particle Size ($\mu$) Coating Thickness | $U^{235}$ (g) |
|---|---|---|---|---|---|
| C1-7 | Laminar | 3M Company 3M-SP-2 | 414 | 82 | 0.087 |
| B9-7 | Columnar | HTM, Inc. HTM-1 | 364 | 82 | 0.063 |
| B9-8 | Duplex | National Carbon NCC-AD | 460 | 80 | 0.086 |
| B9-9 | Duplex | National Carbon NCC-AD | 460 | 80 | 0.085 |
| C1-8 | Bare | 3M Company 3M-101-U | 228 | No coating | 0.0045 |

UNCLASSIFIED
R-9092

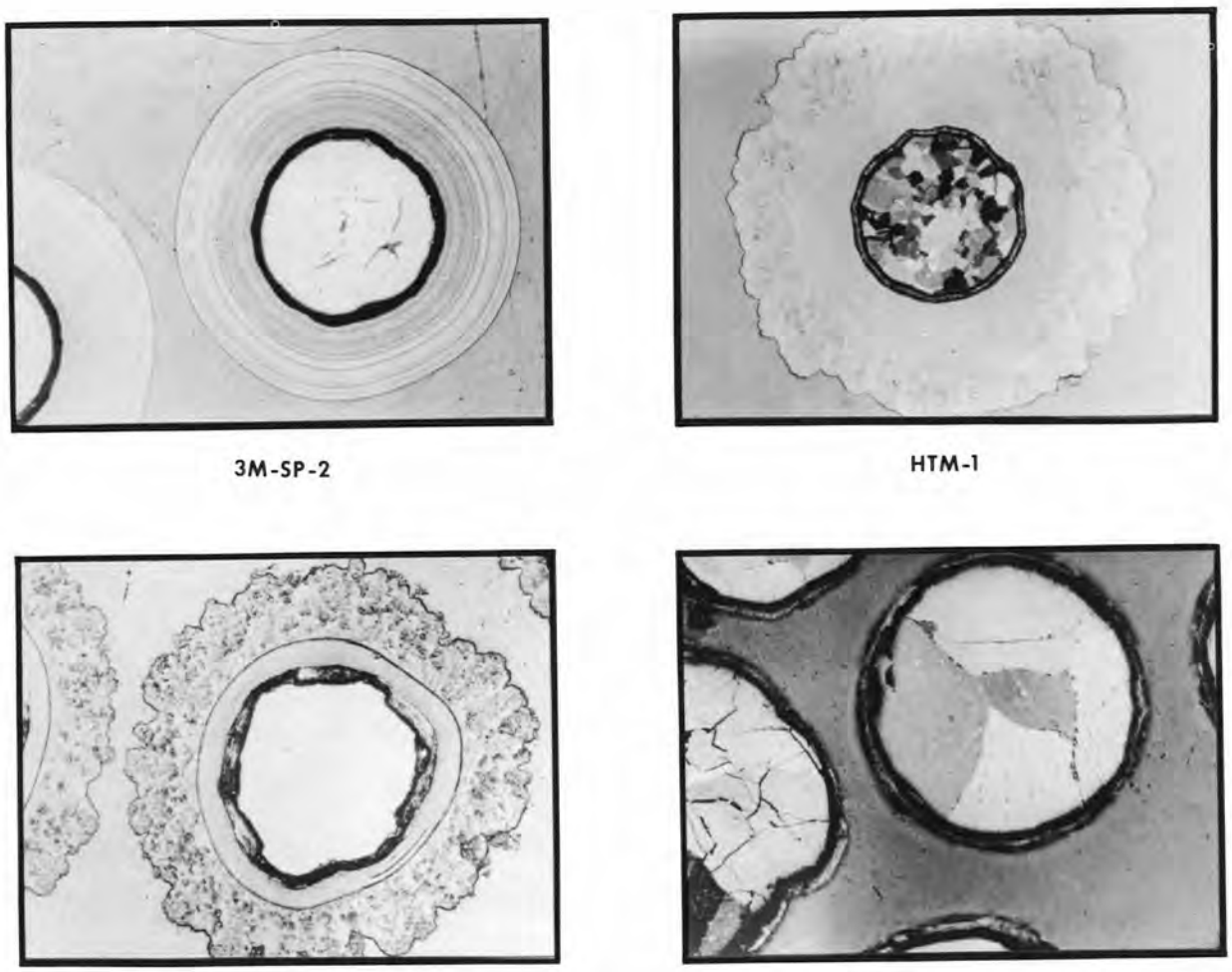


Fig. 21.4. Pyrolytic-Carbon-Coated Uranium Carbide Particles.

for one batch of the duplex-coated specimens. Irradiation temperatures have been varied systematically for all batches of specimens, the extremes being 1350 to 1815°F except for one batch (capsule B9-9) which was irradiated to 9% burnup at 800°F and to an additional 3% at 1200°F to test the effect of irradiation at low temperatures. Typical data are shown in Fig. 21.5 where the steady-state release rate for the gaseous isotopes from all types of particles at 1500°F are plotted against half-life of the isotopes involved.

The use of pyrolytic carbon coatings on uranium carbide particles is a promising method of reducing fission-gas release. The duplex-type coating in this set of experiments retained fission gas better than either of the other two types of coatings by a factor of 10 at 1500°F. This is true up to about 10% burnup.

It appears that small spontaneous activity bursts are caused by rupture of the coating of single particles. These bursts contain about $1.2 \times 10^{-5}$ curie of gas; whereas, after 30 days of irradiation

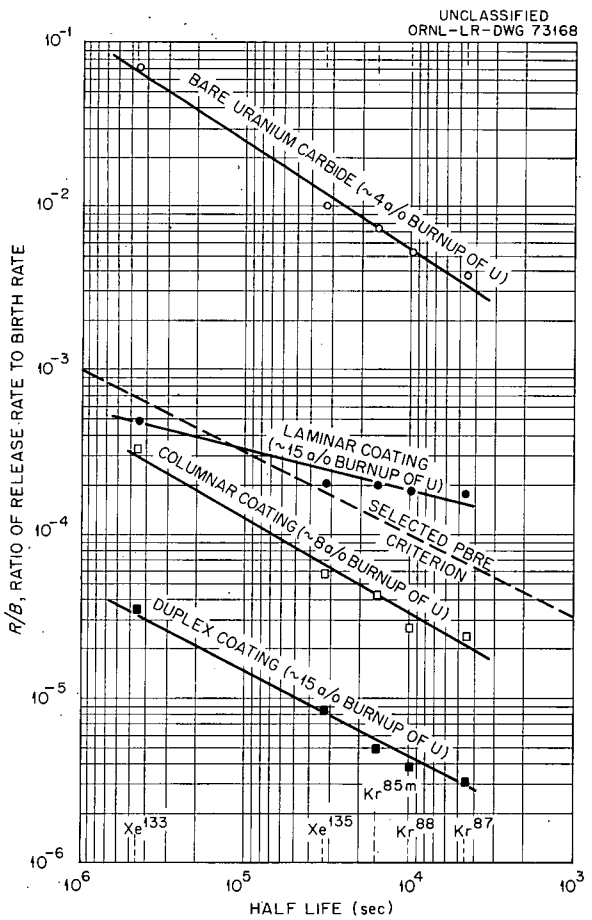


**Fig. 21.5. Relationship Between $R/B$ and Half-Life for Release of Inert Gases from Pyrolytic-Carbon-Coated Uranium Carbide Particles at 1500°F and High Burnup.**

time, one coated particle contains about $1.1 \times 10^{-4}$ curie of gas. Irradiation of bare particles demonstrated that most of the generated gas is contained in the uranium carbide. If a particle should suddenly release one-tenth of its radioactive gas, this could cause the observed burst.

The ratios of the fractional release rates $R/B$ from bare particles to the rates from the several coated particles are shown in Table 21.3. These factors for each coating are in close agreement for each isotope involved except for the laminar coatings of 3M-SP-2. Lack of agreement in this case may be due to the fact that the "bare" uranium carbide particles have a thin, spongy coating of graphite which probably acts as a barrier for recoil particles. When the laminar layer breaks it probably removes this barrier along with the laminar shell.

Except for the laminar-coated particles, all specimens released fission gas in almost the same proportions. These proportions would change if different coatings required different times for the gas to pass through them. This indicates that the major escape of fission gas is through breaks in the coatings rather than by diffusion through intact coatings. The laminar-coated particles probably failed by complete separation of the coating from the uranium carbide, including the removal of the spongy graphite layer. This would allow a higher proportion of direct-recoil escape from the laminar-coated particle and therefore change the isotopic composition of the released gas. Early particle rupture is likely caused by differential thermal expansion.

**Table 21.3. Pyrolytic Carbon Coating Efficiency Factor at 1500°F**

| Capsule No. and Coating | Ratio of $R/B^{(a)}$ for Bare Particles to $R/B$ for Coated Particles | | | | |
|---|---|---|---|---|---|
| | $Xe^{133}$ | $Xe^{135}$ | $Kr^{85m}$ | $Kr^{88}$ | $Kr^{87}$ |
| 3M-SP-2, laminar coating | 140 | 50 | 37 | 28 | 20 |
| HTM-1, columnar coating | 200 | 160 | 200 | 250 | 250 |
| NCC-AD, duplex coating | 2000 | 1100 | 1500 | 1250 | 1300 |

[a] Release rate/birth rate.

## FISSION-GAS RELEASE FROM HIGH-BURNUP FUEL

M. T. Morgan

R. M. Martin[5] D. C. Evans[5]

A postirradiation annealing experiment has been designed to study the effects of high burnup on fission-gas release from $UO_2$ and other reactor fuel materials. It offers the opportunity to study fission-gas release from prototype fuel elements, and from a wide variety of advanced fuel materials.

The flow diagram for the experiment is shown in Fig. 21.6. A molybdenum susceptor containing the fuel sample is heated by high-frequency induction

[5]Co-op student from the University of Tennessee, Knoxville.

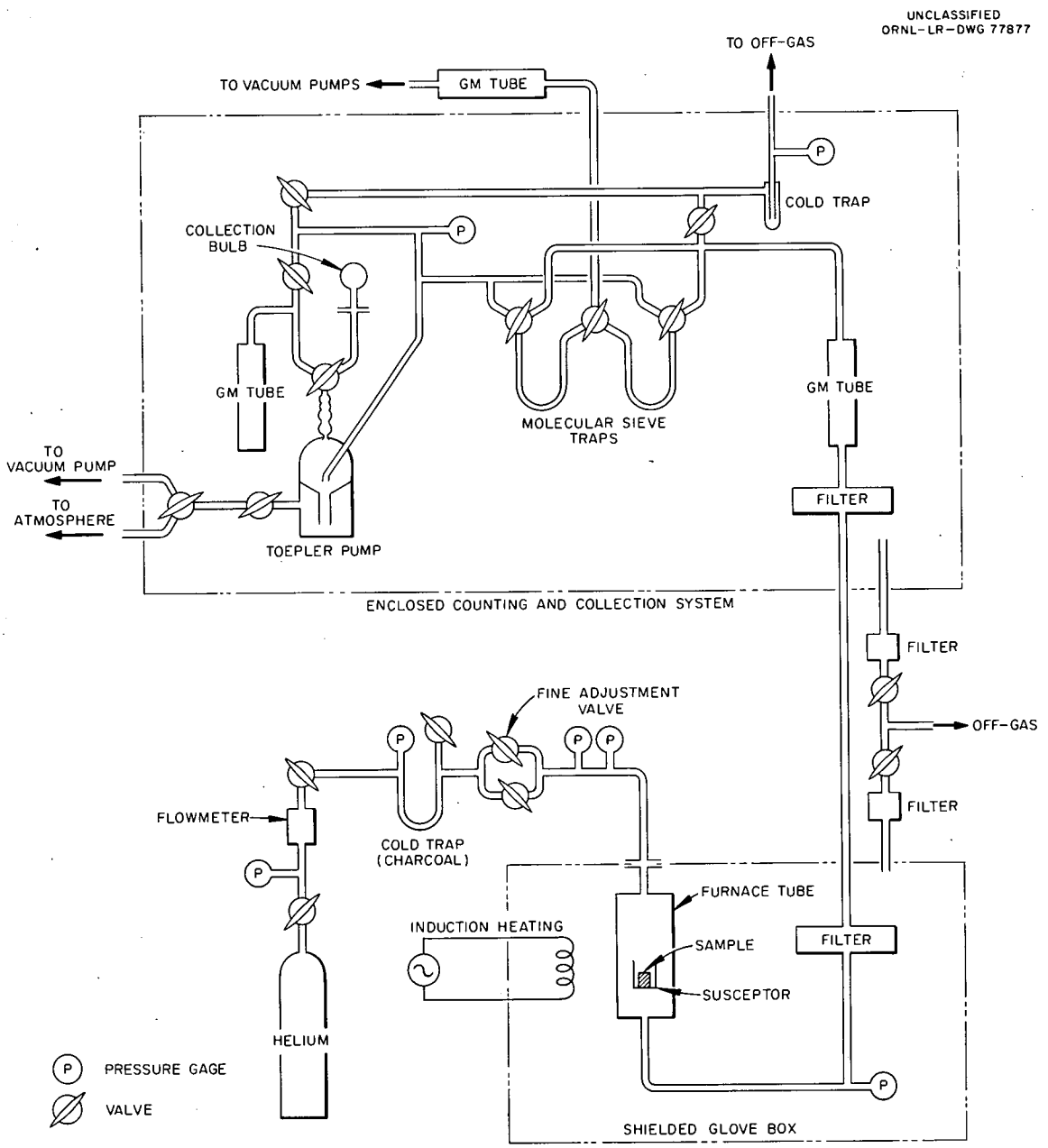


Fig. 21.6. High Temperature–High Burnup Fuel Gas Diffusion Apparatus.

current supplied by a 10-kw-output electron high-frequency generator. Purified helium sweep gas, passing over the sample, carries the released $Kr^{85}$ through the filter to remove radioactive dust and into the enclosed vacuum, counting, and collection systems. The $Kr^{85}$ is continuously monitored as it flows through the Geiger counter cell and is collected in molecular sieve traps at −196°C. The helium carrier gas passes through the traps and is exhausted. Two traps are used alternately and switched at intervals so that one trap is collecting while the other is being exhausted. The trap being exhausted is heated and the $Kr^{85}$ is pumped into a totalizing counting system by means of a Toepler pump. This gas is later transferred into collection bulbs for further analysis.

The furnace tube and filter are housed in a glove box shielded with 4 in. of lead and fitted with modified Castle manipulators. The vacuum, counting, and collection systems are contained in a separate closed hood. The counting cells consist of coaxial tubes enclosing thin-walled Geiger tubes. The system was designed to analyze the released gases for $Kr^{85}$ since this gas has a 10-yr half-life and other radioactive gases would have decayed in most of the samples to be used.

The first studies were made on high-density $UO_2$ samples from LITR experiment L-22a. This material was irradiated to a burnup of 12,000 Mwd per metric ton of uranium at approximately 730°C. A rapid increase in the rate of $Kr^{85}$ release as a function of time was observed in the range of 1500 to 1600°C. This process produced an unusual curve in the plot of the fractional release, $F$, vs the square root of time, $t$ (see Fig. 21.7). The linear portion of the graph during the first $4\frac{1}{2}$ hr indicates an apparent steady-state condition from which erroneous assumptions might have been drawn if the experiment had been terminated at this point.

Further evidence of unusual behavior at 1500°C is shown in Fig. 21.8. Here "bursts" of $Kr^{85}$ are indicated by the monitor on the flowing gas during steady operation at 1500°C. This phenomenon was observed on two samples at 1500°C. The largest burst was 175,000 counts/min, which is equivalent to $1 \times 10^{-4}$ of the total $Kr^{85}$ contained in the sample. This effect may be too small to be noticed if it exists below 1500°C and may be submerged in the higher steady-state release above 1500°C. A possible explanation for these phenomena at 1500°C is grain growth or chemical change. The "bursts" during steady-state operation may be due to voids containing fission gas being swept to the surface or to surface-connected channels. Metallographic examinations of these samples are planned, and should show any grain growth and void migration.

The value of the diffusion parameter $D' = D/a^2$ (calculated by the equation $F = 6\sqrt{D't/\pi}$, where $D$ = diffusion coefficient, $a$ = equivalent sphere radius, $F$ = fraction of total gas released, and $t$ = time of heating) for a sample annealed at 1400°C was $1 \times 10^{-15}$ $sec^{-1}$. Values of $D'$ for higher temperatures are not given since the phenomena observed show that gas release at these temperatures is due partly to mechanisms other than diffusion.

Work will continue on $UO_2$ samples from capsule L-22a as soon as metallographic examinations have been completed on some of the annealed

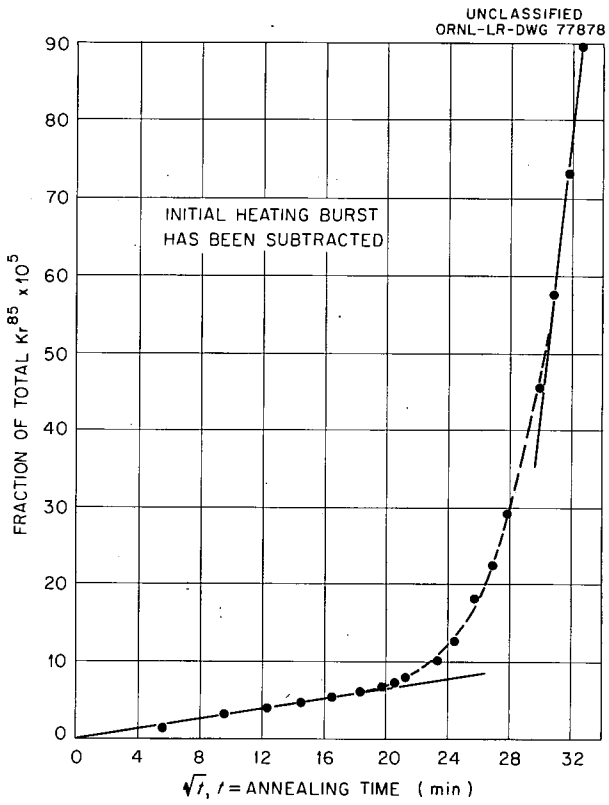


**Fig. 21.7. Krypton-85 Released from $UO_2$ Sample L-22a at 1500°C.**

samples. In the meantime a sample of pyrolytic-graphite-coated $UC_2$ particles from ORR experiment B9-8 will be studied. These particles have a burnup of 30% of the $U^{235}$.

Since other experiments[6] indicate that $1 \times 10^{21}$ fissions per cc is the starting point of serious damage in $UO_2$ with respect to burnup, an attempt is being made to obtain single crystals of enriched $UO_2$ to be irradiated to burnups in excess of $1 \times 10^{21}$ fissions per cc as a part of this series of studies.

[6] J. Belle (ed.), *Uranium Dioxide Properties and Nuclear Applications*, USAEC, 1961, pp 559 and 569.

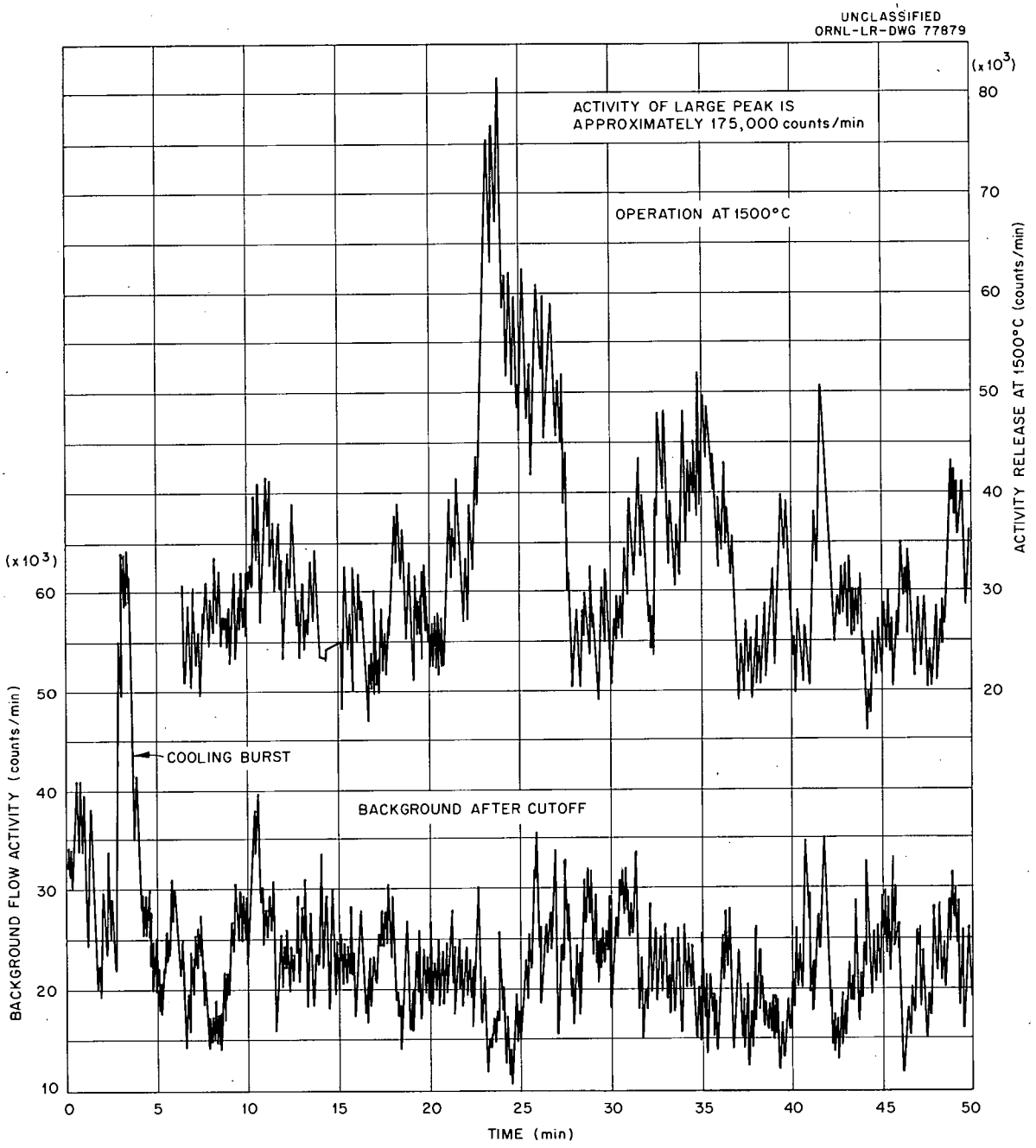


**Fig. 21.8. Comparison of Background and Activity During Steady-State Operation at 1500°C to Show "Burst" Type Fission-Gas Release.**

# 22. Radiation Stability of Ceramics

C. D. Bopp O. Sisman R. L. Towns

## APPARATUS FOR THERMAL ANALYSIS

An apparatus, based on modifications of an assembly described by Allison,[1] has been constructed for thermal analysis of small samples (0.01 to 10 g) of materials with poor thermal conductivity. This apparatus, shown in Fig. 22.1, is calibrated[2] by techniques which use Peltier power generated by passage of current through a thermocouple junction attached to the sample crucible.

The assembly and the calibration technique have been tested by measurement of the heats of fusion on 50- to 100-mg samples of Sn, AgCl, and NaCl; agreement within ±5% (the reproducibility of repeated trials with this apparatus) with published heats of fusion was obtained for these substances, which melt below 900°C. Techniques for study of heats of transition at higher temperatures and for determination of specific heat of samples have been established. This apparatus is presently employed in study of radiation-induced changes in several ceramic materials.

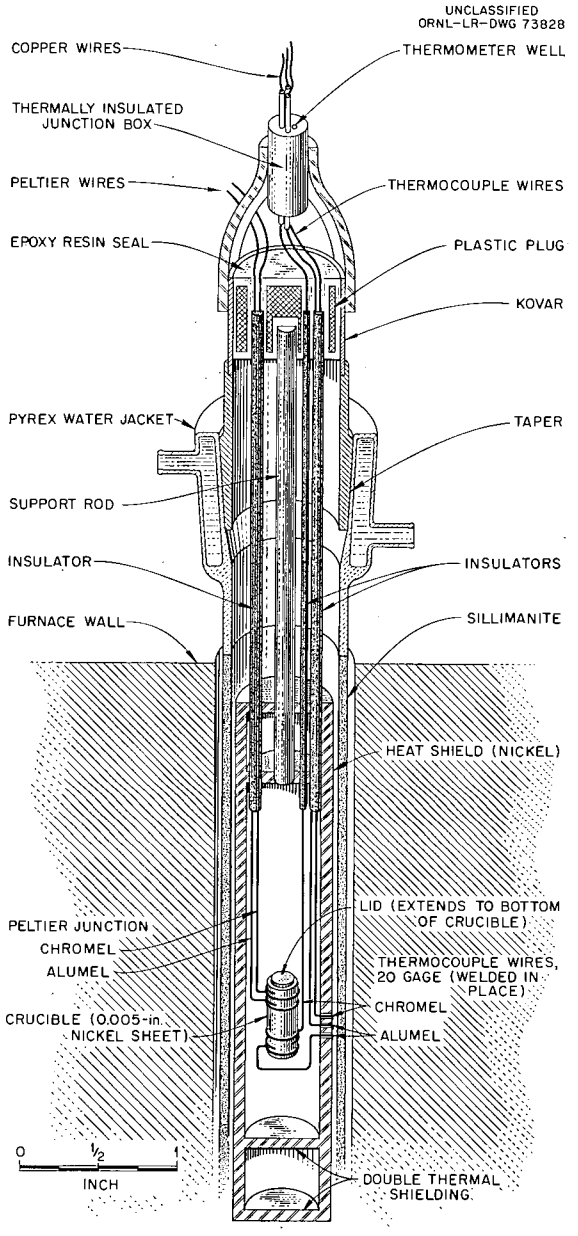


Fig. 22.1. Thermal-Analysis Apparatus.

## RADIATION STABILITY OF A ZIRCON CERAMIC

Thermal analysis and x-ray diffraction[3] techniques have been employed in a further study of an irradiation-induced change in a zircon ceramic for which change in density, thermal conductivity, and Young's modulus have previously been reported.[4] Radiation causes this material to resemble

[1] E. B. Allison and (Mrs.) J. Taylor, *Trans. Brit. Ceram. Soc.* **54**, 677 (1955).

[2] W. Steiner and O. Krisement, *Arch. Eisenhuettenw.* **32**, 701 (1961).

[3] Debye-Scherrer method by M. C. Wittels and F. A. Sherrill.

[4] O. Sisman, C. D. Bopp, and R. L. Towns, *Solid State Div. Ann. Progr. Rept. Aug. 31, 1957*, ORNL-2413, p 80.

metamict zircon[5-8] in that heating to successively higher temperatures produces partial annealing, decomposition, and reformation of the zircon; some of these changes may be missing in specific specimens.

Four samples of the zircon, irradiated at less than 100°C as shown in Table 22.1, have been examined; after exposure all samples except the first were completely amorphous on examination by x-ray diffraction techniques. The change in the hydrostatically measured density is used to rank the exposures listed since this property is easy to measure and the accuracy is probably better than that for the flux estimates. The two highest exposures for which the density change was saturated are designated by listing the density change followed by "a" or "b." It cannot be stated with certainty whether the damage is primarily by fission fragment recoils from trace contamination of fissionable elements (uranium 0.022%; thorium 0.035%)[9] or from fast neutron scattering.

As shown in Table 22.2, three exothermic peaks were found in the apparent specific heat of the irradiated material; none of these appeared on reheating the specimens. Combination of these data with that from x-ray examination of the heated specimens indicates the low-temperature phenomenon to be due to partial annealing (which was missing from the most highly irradiated specimen), the 880°C peak to be due to decomposition to zirconia, and the 1090°C peak (which appeared in only one specimen examined) to be due to reformation of zircon from zirconia and silica.

[5]M. V. Akhmanova and L. L. Leonova, *Geokhimiya* **1961**, 401.

[6]H. D. Holland and D. Gottfried, *Acta Cryst.* **8**, 291 (1955).

[7]M. V. Stackelberg and K. Chudoba, *Z. Krist.* **97**, 252 (1937).

[8]J. Orcel, *Compt. Rend.* **236**, 1052 (1953).

[9]Uranium by delayed-neutron activation analysis, F. F. Dyer; thorium by activation analysis, W. T. Mullins.

**Table 22.1. Irradiation of Zircon**

| Density Decrease (%) | Reactor Type | Integrated Neutron Flux (neutrons/cm$^2$) | |
|---|---|---|---|
| | | Thermal | Epithermal |
| | | $\times 10^{20}$ | $\times 10^{20}$ |
| 6.7 | Light water | 5 | 0.5 |
| 7.8 | Graphite | 1.3 | 1.0 |
| 10a[a] | Graphite | 2.0 | 1.6 |
| 10b[a] | Light water | 30 | 3 |

[a]Density decrease saturated in these samples.

**Table 22.2. Thermal Analysis of Irradiated Zircon**

| Threshold Temperature of Peak (°C) | Irradiation-Induced Density Decrease (%) | Energy Under Peak (calories/g) |
|---|---|---|
| 200 ± 30 | 6.7 | 0.5 ± 0.3 |
| | 10a | 0.03 |
| (Low-temperature peak not detected) | 10b | |
| 880 ± 10 | 6.7 | 15 |
| | 7.8 | 15 |
| | 10a | 16 |
| | 10b | 16 |
| 1090 | 6.7 | 25 ± 10 |
| (High-temperature peak not detected below 1200°C) | 7.8 | |
| (High-temperature peak not detected below 1200°C) | 10a | |

# Part VI
# Nuclear Safety Program

## INTRODUCTION TO PART VI

The recent announcement of the proposed construction of a large nuclear power reactor near the heart of New York City indicates that the problem of assuring the safe containment and disposal of accident-released fission products will be accented in the next few years. Studies of the type reported here are designed to provide an adequate scientific basis for predicting the extent of the hazards of released fission products and to aid the formulation of methods of dealing with these hazards. Attention has continued to be focused on $UO_2$ fuel materials because of their current importance. Efforts are being devoted to making the simulated-reactor-accident experiments more realistic and, consequently, more pertinent to reactor hazards evaluations.

# 23. Release of Fission Products on Out-of-Pile Melting of Reactor Fuels

G. W. Parker G. E. Creek
W. J. Martin R. A. Lorenz

Studies of fission-product release from irradiated $UO_2$ are being performed under out-of-pile conditions to permit maximum freedom in the designing and conducting of experiments. Emphasis is currently being placed on development of methods and equipment for melting large quantities of irradiated $UO_2$ under conditions that are more realistic than those employed in earlier $UO_2$-melting experiments.

## FISSION-PRODUCT RELEASE FROM $UO_2$ MELTED BY THE TUNGSTEN-CRUCIBLE METHOD

A brief description of the tungsten-crucible method of melting $UO_2$ was given in a previous progress report.[1] One of the principal advantages of this method is that it can be scaled up to any desired batch size (it was more convenient to melt about 30 g of $UO_2$ under the prevailing experimental conditions). Other advantages include the ability of tungsten to contain molten $UO_2$, which permits an extended molten period without loss of material except by volatilization, and the adaptability of the tungsten-crucible method to the use of thermocouples for temperature measurements. The fact that it is limited to an inert-gas atmosphere is not regarded as a serious disadvantage, since it has already been shown that the effect of atmosphere on release is minor at the melting temperature of $UO_2$.

The program included experiments in which tracer-irradiated $UO_2$ pellets were melted and held molten for a longer period than in previous work. This was done as part of a series of experiments to investigate the effect of duration of the molten period on fission-product release. The rf furnace and fission-product fractionation assembly are shown in Fig. 23.1. A thin-walled tungsten crucible inside a small thorium oxide crucible, which served as a heat reflector, was used as the heater and container. Helium gas, purified by passing over hot zirconium, flowed upward through the furnace at a rate of 700 cc/min, measured at room temperature. The appearance of a typical melt is shown in Fig. 23.2. Released solids that plated out in the furnace tube, deposited on the wall of a miniature expansion chamber, or collected on a Millipore filter were dissolved separately and the solutions analyzed. Charcoal traps were also employed, to collect iodine and the rare gases. The tungsten crucible was placed in a nitric acid solution to dissolve the $UO_2$ for chemical recovery of the fission products remaining in the melt. Release values were calculated from a complete material balance.

### Release as a Function of Length of Time in the Molten State

One question which has provoked much speculation concerns the possible variation of fission-product release with the length of time irradiated fuel is kept above the melting temperature. Little freedom in extending this period was possible before the tungsten-crucible melting method was developed. Relatively little can be said about the results of the first experiments, shown in

[1] G. W. Parker *et al.*, *Nuclear Safety Semiann. Progr. Rept. June 30, 1962*, ORNL-3319, pp 11–29.

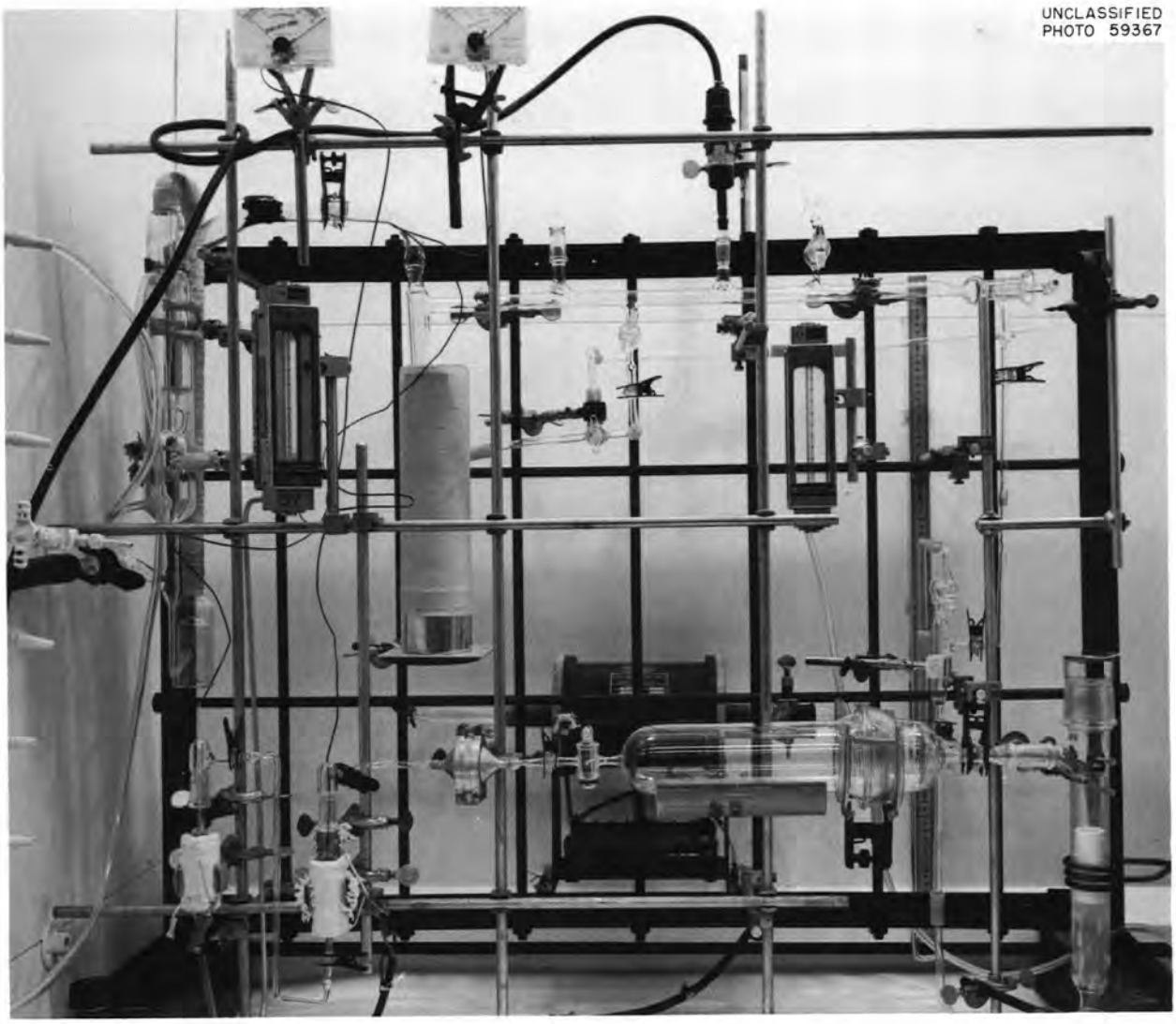


Fig. 23.1. The rf Furnace and Fission-Product Fractionation Assembly.

Table 23.1, which are quite tentative, but it appears that scaleup has served to reduce some of the release values, expecially those for tellurium and cesium. Some of the data in Table 23.1 seem to indicate an increased release with increased molten time, but insufficient data are available at present to be conclusive on this point. The materials deposited in different parts of the apparatus were analyzed separately and the results summarized in Table 23.2. It will be of interest to conduct melting experiments with similar amounts of highly irradiated $UO_2$ when suitable hot-cell facilities become available.

## Size of Uranium Oxide Particles Plated Out from Molten $UO_2$

A size analysis was performed on the material which appears to be released rather promptly as a vapor when $UO_2$ is melted. In practice it is useful to watch for the oxide smoke to rise above the sample as an indication that melting has actually occurred. Much of the vaporized oxide plated out in the furnace tube just above the crucible. A fraction of the vapor was carried into the expansion chamber, where most of it deposited on the bottom.

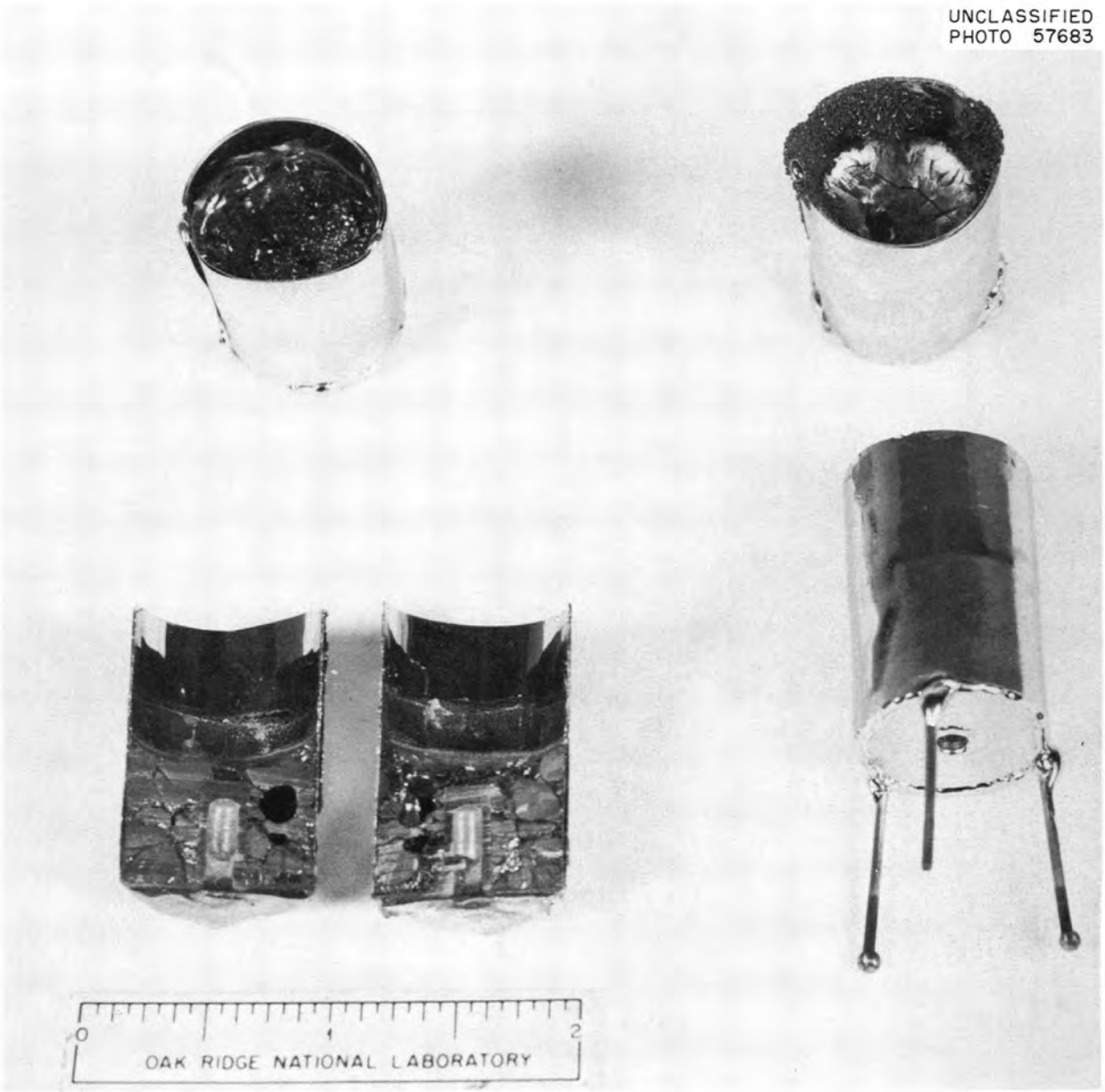


Fig. 23.2. Tungsten Crucibles and $UO_2$ After Melting.

A filter was inserted beyond this chamber to stop all remaining solids. Examination of samples from different areas showed a mixture of sizes in the furnace tube, a slightly larger particle size in the fore part of the chamber than in the rear, and a still smaller size on the filter. A photograph of particles collected on the filter is shown in Fig. 23.3. The median 50% size varied from 0.03 to 1.0 $\mu$ for all samples. A count analysis is given in Fig. 23.4.

**Table 23.1. Fission-Product Release from $UO_2$ Melted in Helium by the Tungsten-Crucible Method**

Sample: 29 g of tracer-irradiated PWR $UO_2$
Atmosphere: Purified helium flowing at a rate of 700 cc/min

| Run No. | Time (min) | | Percent $UO_2$ Vaporized | Gross Gamma Release (%) | Percent Release | | | | | | | |
|---|---|---|---|---|---|---|---|---|---|---|---|---|
| | Preheat | Molten | | | Rare Gases | I | Te | Cs | Ru | Sr | Ba | Ce |
| 10-24-62 | 4.75 | 1.0 | 0.097 | 22.6 | 92.9 | 76.9 | 89.9 | 62.5 | 0.45 | 0.33 | 4.8 | 0.05 |
| 10-31-62 | 5.0 | 1.5 | 0.157 | 15.1[a] | 98.0 | 98.3 | 97.6 | 66.0 | 0.05 | 0.47 | 2.6 | 0.07 |
| 11-7-62 | 4.75 | 2.0 | 0.156 | 25.6 | 99.3 | 98.8 | 99.1 | 59.6 | 0.32 | 0.41 | 3.0 | 0.17 |
| 11-12-62 | 4.5 | 2.5 | 0.246 | 12.6[a] | 99.0 | 95.0 | 98.9 | 72.0 | 0.33 | 0.53 | 2.4 | 0.13 |
| 11-15-62[b] | 4.5 | 1.5 | | 13.7[a] | 98.7 | 88.4 | 91.8 | 80.2 | 0.20 | 0.26 | 2.6 | 0.40 |
| 11-19-62[b] | 4.5 | 2.5 | | 12.6[a] | 99.3 | 92.9 | 96.2 | 89.4 | 0.70 | 0.50 | 3.6 | 0.10 |

[a]Decayed 4 to 7 days longer than previous sample.
[b]Slightly higher-density $UO_2$.

**Table 23.2. Distribution of Fission Products Released from $UO_2$ Melted in Helium by the Tungsten-Crucible Method**

Run 10/24 preheated 4.75 min, molten 1.0 min
Run 10/31 preheated 5.0 min, molten 1.5 min
Run 11/7 preheated 4.75 min, molten 2.0 min

| Location of Activity | Percent in Each Location | | | | | | | | | | | | | | |
|---|---|---|---|---|---|---|---|---|---|---|---|---|---|---|---|
| | Total Gamma | | | Iodine | | | Tellurium | | | Cesium | | | Strontium | | |
| | Expt 10/24 | Expt 10/31[a] | Expt 11/7 | Expt 10/24 | Expt 10/31 | Expt 11/7 | Expt 10/24 | Expt 10/31 | Expt 11/7 | Expt 10/24 | Expt 10/31 | Expt 11/7 | Expt 10/24 | Expt 10/31 | Expt 11/7 |
| Furnace | 17.8 | 11.6 | 14.0 | 45.3 | 64.1 | 20.1 | 62.9 | 68.5 | 66.3 | 51.6 | 43.6 | 23.7 | 0.2 | 0.4 | 0.3 |
| Expansion chamber | 0.8 | 1.1 | 1.8 | 2.8 | 13.5 | 2.7 | 4.7 | 3.0 | 8.0 | 4.5 | 15.8 | 4.7 | 0.1 | 0.04 | 0.04 |
| Filter | 2.8 | 2.3 | 9.0 | 8.0 | 18.1 | 40.5 | 13.4 | 11.3 | 25.2 | 6.4 | 6.8 | 31.2 | 0.02 | 0.04 | 0.08 |
| Charcoal | 1.2 | 0.1 | 0.8 | 42.0 | 2.8 | 35.5 | | | | | | | | | |
| Total | 22.6 | 15.1 | 25.6 | 98.1 | 98.5 | 98.8 | 81.0 | 82.8 | 99.5? | 62.5 | 66.2 | 59.6 | 0.32 | 0.48 | 0.42 |

[a]Decayed 1 week longer than other samples.

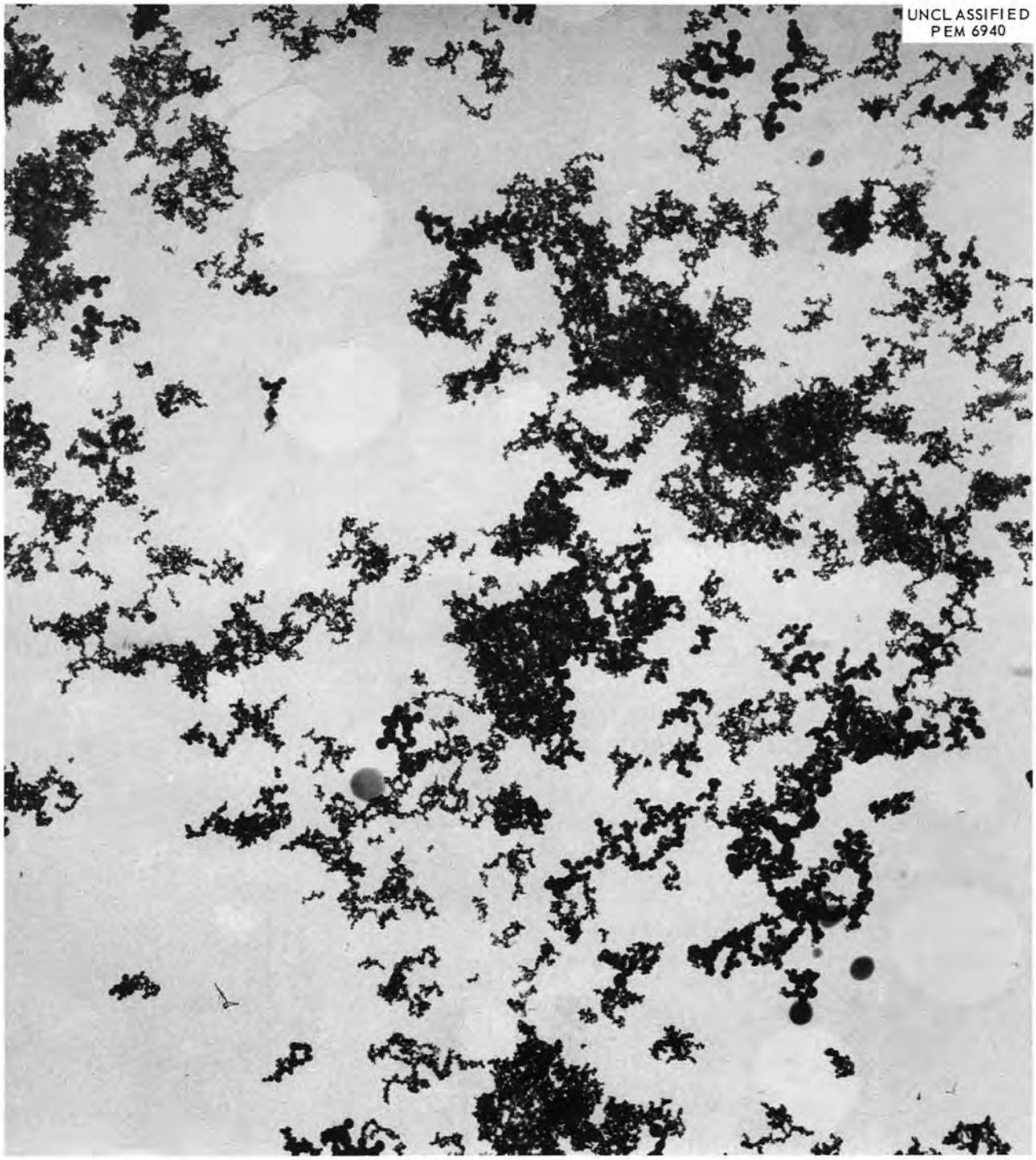


Fig. 23.3. $UO_2$ Particles Collected on the Millipore Filter Paper. 26,000X.

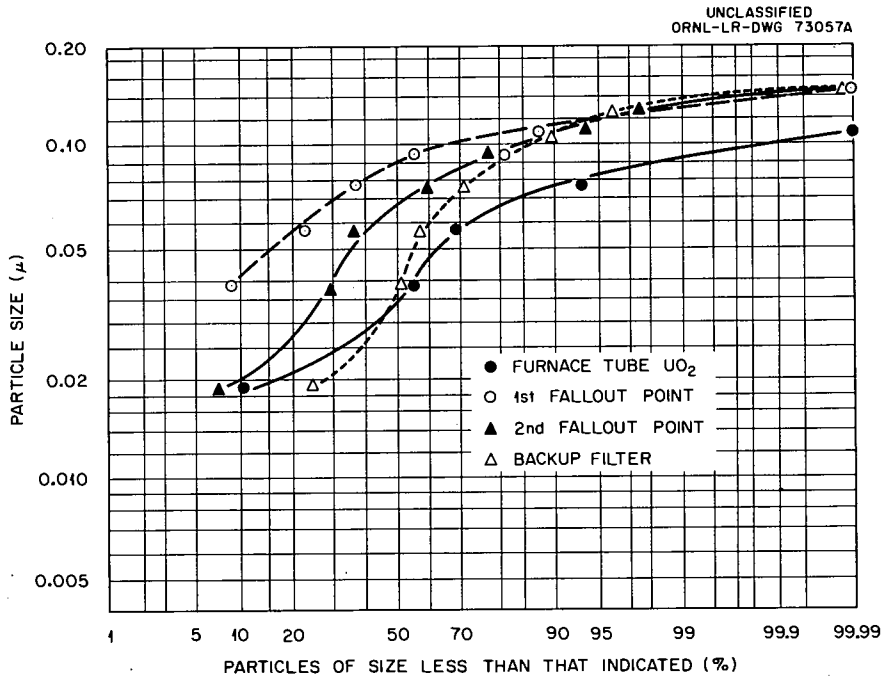


Fig. 23.4. Particle-Size Evaluation of Oxides from $UO_2$ Samples Melted in Helium by the Tungsten-Crucible Method.

## FISSION-PRODUCT RELEASE FROM $UO_2$ MELTED BY A CENTERED TUNGSTEN RESISTOR

Nuclear melting has been more directly simulated by use of the technique of center heating, with a tungsten resistor (Fig. 23.5) surrounded by cored $UO_2$ pellets, than was possible with previously available techniques. Experiments in which unirradiated $UO_2$ was melted in a helium atmosphere were reported in a previous progress report.[1] Fission-product release was investigated by melting 39-g samples of tracer-irradiated $UO_2$ in the experimental assembly shown in Fig. 23.6.

### Comparison with Previous Melting Experiments

In Table 23.3 are summarized the results obtained on melting three unclad specimens, one specimen clad with stainless steel, and two clad with Zircaloy. In comparing these results with those from the micro-sample (~30 mg) experiments,

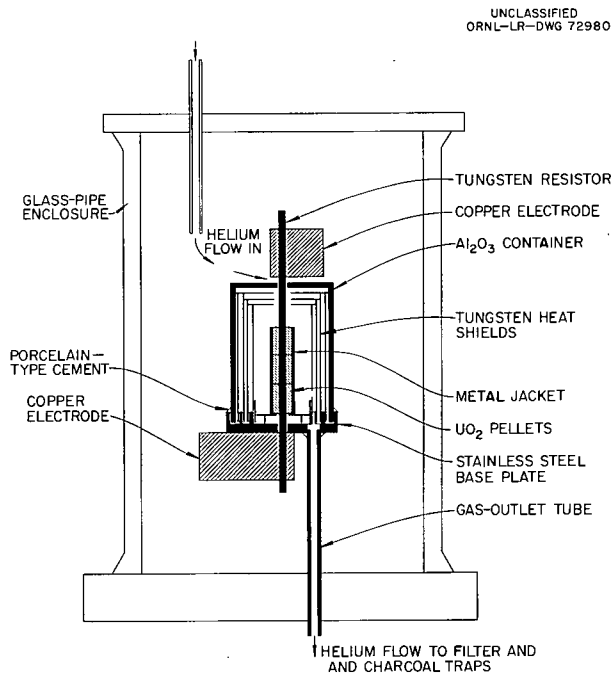


Fig. 23.5. Single-Element Tungsten-Resistor Furnace.

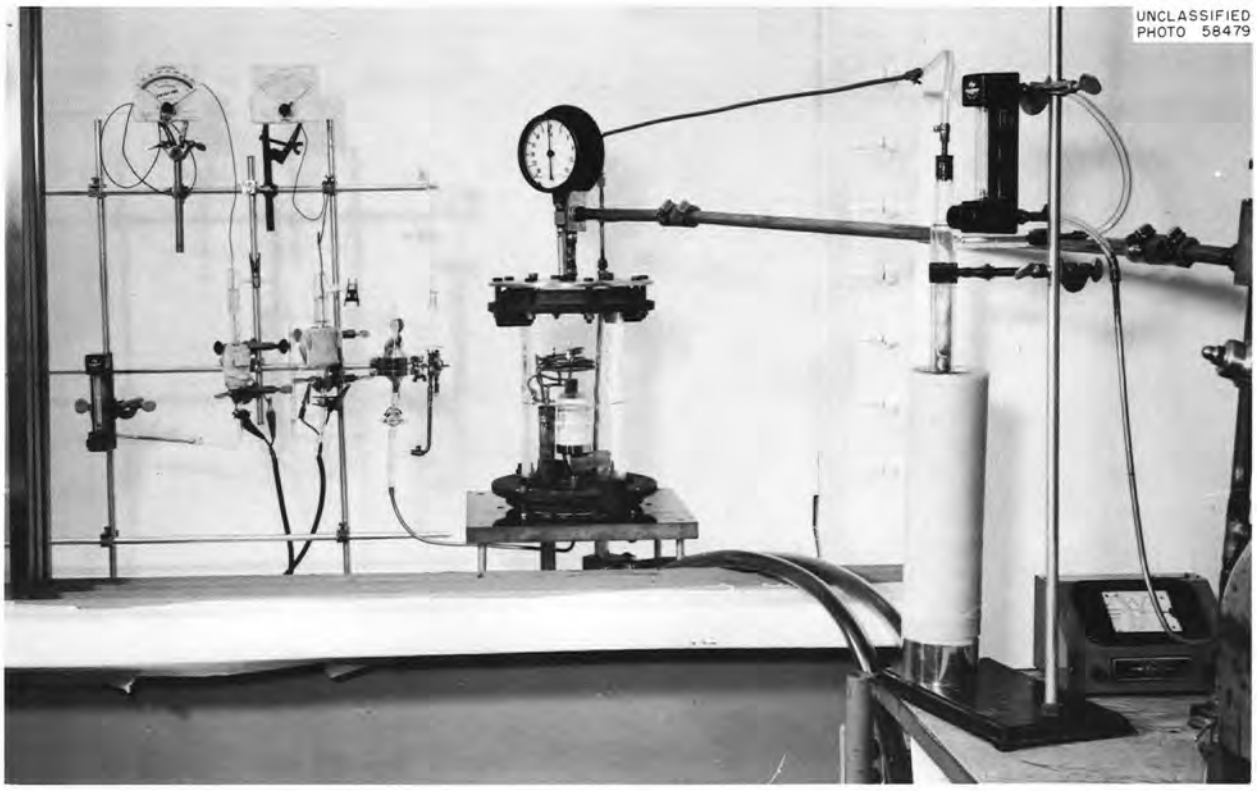


**Fig. 23.6. Furnace Assembly and Fission-Product-Release Train for Tungsten-Resistor Melting Method.**

**Table 23.3. Fission-Product Release from $UO_2$ Melted in Single-Element Tungsten-Resistor Furnace**

Sample: 39 g of $UO_2$ (PWR type) irradiated at tracer level
Atmosphere: Pure helium flowing at a rate of 400 cc/min

| Element | Heat Duration (min) | Vaporized (%) | Gross Gamma Release (%) | Percentage of Individual Fission Products Released | | | | | | | |
|---|---|---|---|---|---|---|---|---|---|---|---|
| | | | | Xe-Kr | I | Te | Cs | Ru | Sr | Ba | Ce-RE[a] |
| $UO_2$ (bare) | 5.0 | 0.8 | 7.1 | 63 | 47 | 56 | 44 | 1.6 | 1.6 | 5.3 | <0.6 |
| $UO_2$ (bare) | 4.0 | 0.2 | 5.7 | 50 | 30 | 42 | 41 | 0.4 | 0.9 | 2.9 | <0.5 |
| $UO_2$ (bare) | 4.4 | 0.3 | 6.9 | 41 | 25 | 29 | >40 | 0.03 | 1.2 | 4.3 | 0.5 |
| $UO_2$ (SS clad) | 4.7 | 0.2 | 5.0 | 56 | 52 | 73? | 46 | 0.5 | 1.0 | 3.4 | 0.1 |
| $UO_2$ (Zr clad) | 7.0 | 0.1 | 2.6 | 52 | 24 | 1.9 | 27 | 0.08 | 11.6 | 7.7 | 0.5 |
| $UO_2$ (Zr clad) | 6.7 | 0.04 | 5.2 | 41 | 50 | 0.6 | 32 | 0.2 | 9.9 | 7.5 | 0.5 |
| $UO_2$ + BeO[b] | 1.5 | 20 | 30 | 100 | 90 | 92 | 91 | 61 | 2.1 | 4.6 | 2.2 |

[a]Rare earths.

[b]Previous results of melting micro-size sample of highly irradiated $UO_2$ in impure helium by use of the carbon-arc image method.

it is apparent that two differences in experimental conditions must be taken into consideration. These are: (1) oxygen present in the impure helium employed in the former work apparently caused a high ruthenium release by oxidizing Ru to $RuO_4$, and (2) incomplete melting of the center-heated specimens resulted in incomplete rare-gas release. It is, in fact, probable that the percent of gas release is actually a measure of the percent of the sample melted.

## Effect of Cladding Material on Fission-Product Release

The presence of cladding material during melting experiments was not expected to have any effect on fission-product release. Melting $UO_2$ in contact with stainless steel resulted in a heterogeneous segregated residue (Fig. 23.7), while Zircaloy apparently wet the molten $UO_2$ and formed a solid solution (Fig. 23.8). It is not especially sur-

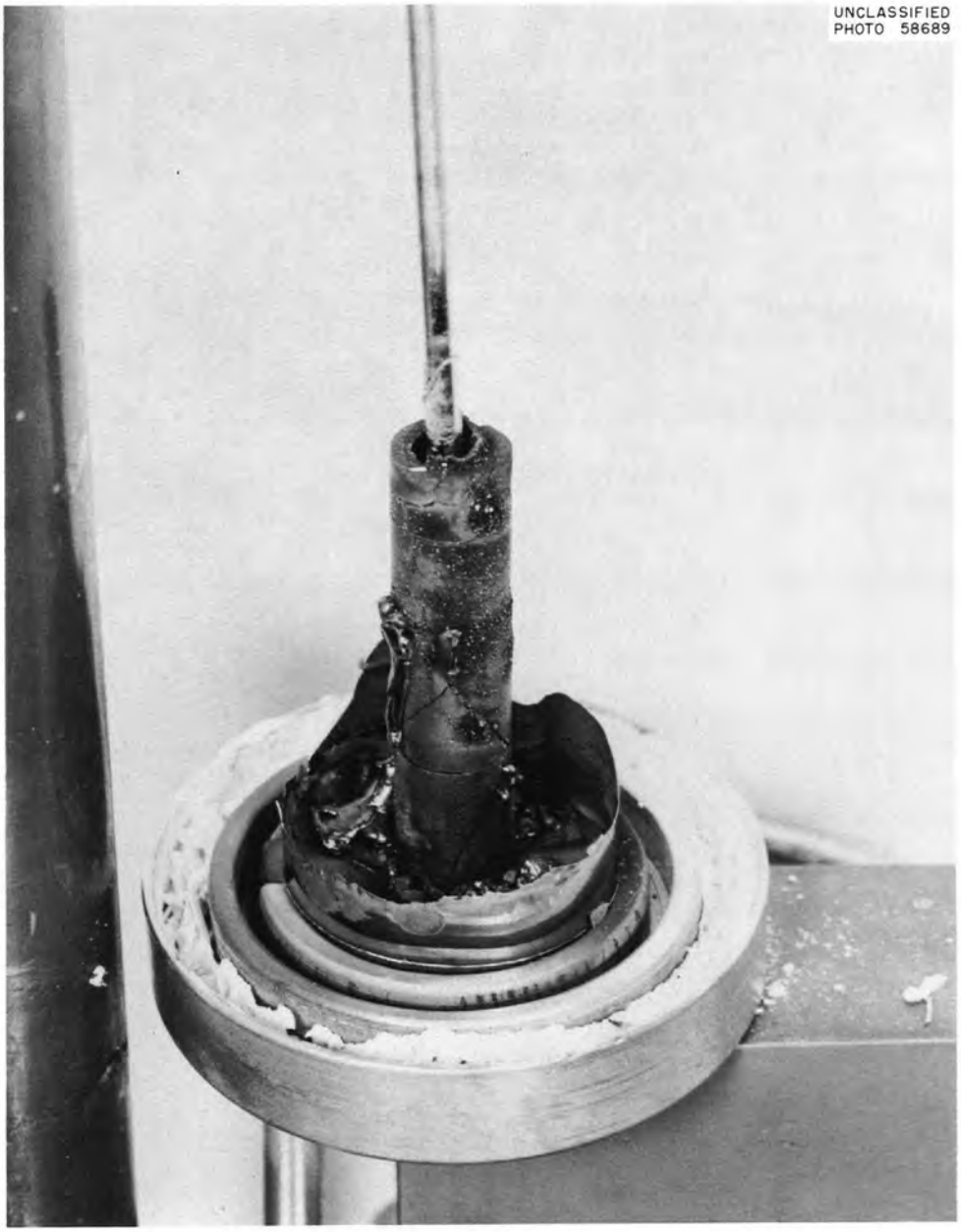


Fig. 23.7. Appearance of Stainless-Steel-Clad Pin After Melting.

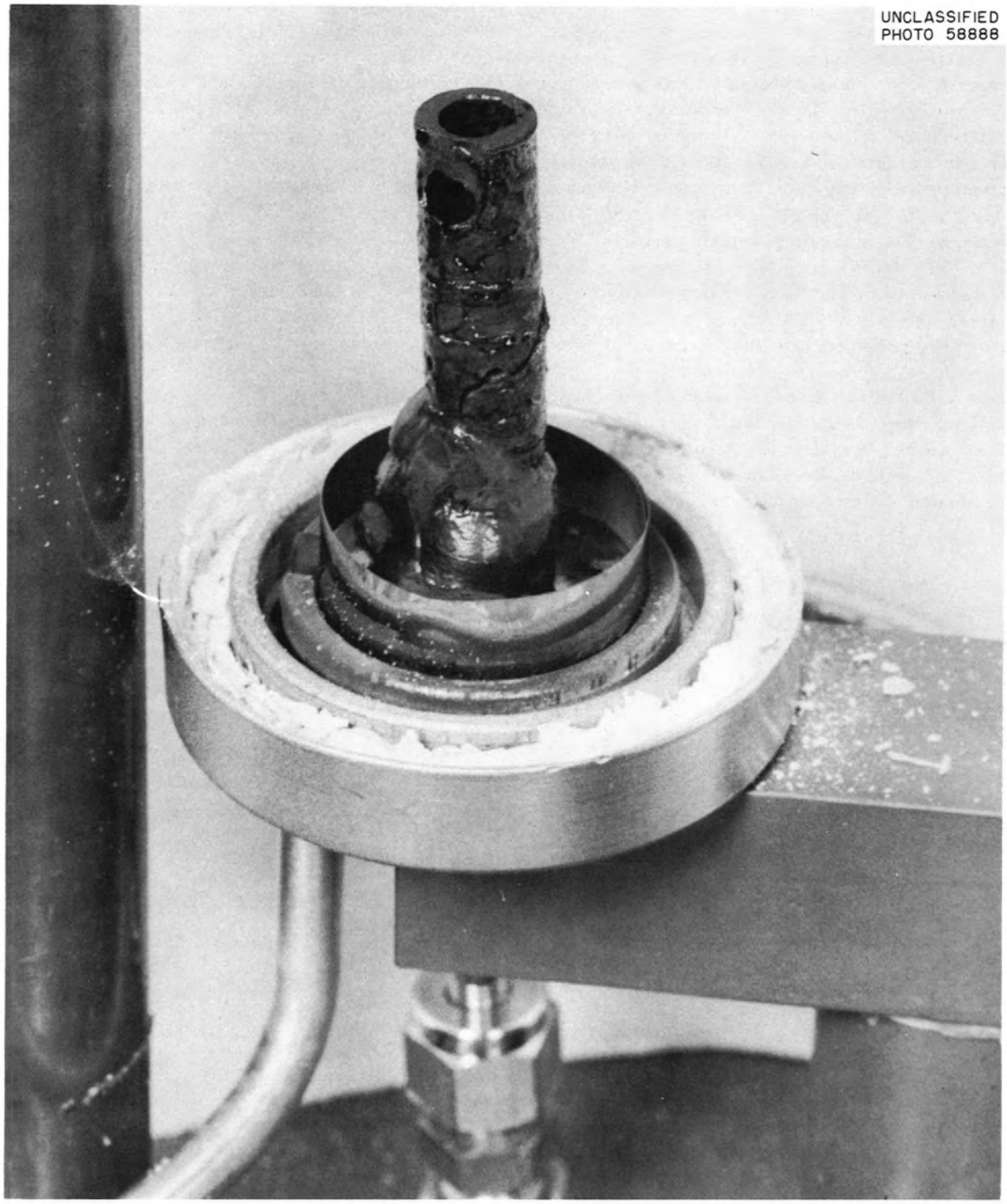


Fig. 23.8. Appearance of Zirconium-Clad Pin After Melting.

prising that some effect of this wetting action of Zircaloy was noted in the release data. A remarkable reduction of the release of tellurium, by a factor of almost 100, was observed. A slight reduction in cesium and iodine release also seems to be indicated by the data obtained. This advantage is offset by a seriously increased release of strontium, from 1% to 10%. Barium release also increased from 3% to 7%. This effect is probably related to oxygen depletion of the system by hot zirconium, but it requires further attention. Very little $UO_2$ appeared to have vaporized and deposited on nearby surfaces, and only trace amounts reached the filter. With these exceptions, and that of the ruthenium behavior attributed to impure helium, the micro-size samples appear to have given valid release data, as compared with values obtained with 39-g samples. Enough uranium oxide reached the filter in some experiments to permit a particle-size analysis. The sizes and distribution observed are consistent with those previously observed in similar experiments. A particle distribution analysis (Fig. 23.9) illustrates the range of particle sizes encountered in these experiments.

Data showing the location of various deposited fission products are given in Table 23.4.

## Scaleup of the Tungsten-Resistor Melting Method to a Multiple-Pin Assembly

One of the most important simulation concepts yet to be demonstrated on a scale intermediate between that of present laboratory experiments and full reactor size is the plate-out effect of fission products from a completely melted fuel pin surrounded by partially melted pins. The tungsten-resistor melting method offers a practical approach to this demonstration, and it has been scaled up in design to a seven-cluster assembly. It is conceived as being fitted with six unirradiated pins

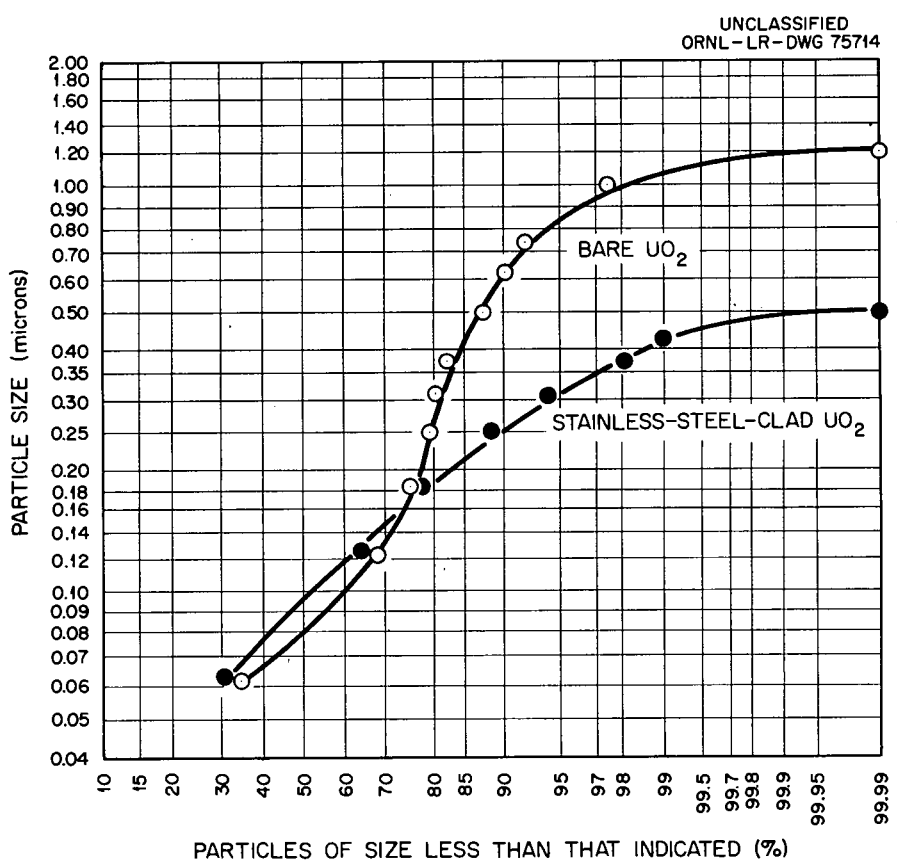


Fig. 23.9. Particle-Size Analysis of $UO_2$ Vaporized from Stainless-Steel-Clad and Bare $UO_2$ Fuel Pins.

Table 23.4. Distribution of Released Fission Products from $UO_2$ Melted in Helium by Centered-Resistor Method

| Location of Activity | Percent in Each Location[a] | | | | | | | | | | | | | | | | | |
|---|---|---|---|---|---|---|---|---|---|---|---|---|---|---|---|---|---|---|
| | $UO_2$ | | | Iodine | | | Tellurium | | | Cesium | | | Strontium | | | Barium | | |
| | Bare[b] | SS Clad | Zr Clad[c] | Bare[b] | SS Clad | Zr Clad | Bare[b] | SS Clad | Zr Clad | Bare[c] | SS Clad | Zr Clad | Bare[b] | SS Clad | Zr Clad | Bare[b] | SS Clad | Zr Clad |
| Furnace hot zone | 0.81 | 0.36 | 0.18 | 0.5 | 1.3 | 0.7 | 5.0 | 25.0 | 0.2 | 41.3 | 12.6 | 17.4 | 2.5 | 1.8 | 22.6 | 9.1 | 5.75 | 16.6 |
| Base and gas tube | 0.005 | 0.01 | 0.004 | 44.2 | 50.5 | 58.0 | 68.3 | ~65 | 2.1 | 13.5 | 45.0 | 23.6 | <0.05 | 0.02 | 0.02 | <0.03 | 0.036 | 0.1 |
| Filters | 0.0008 | 0.01 | 0 | 23.8 | 41.5 | 19.3 | 17.0 | 10 | 0.2 | 21.5 | 25.2 | 10.7 | 0.003 | 0.016 | <0.02 | 0.008 | 0.004 | 0.01 |
| Charcoal | | | | 2.2 | 0.4 | 0.9 | | | | | | | | | | | | |
| Total | 0.81 | 0.38 | 0.18 | 70.7 | 93.7 | 78.9 | 90.3 | ~100 | 2.5 | 76.3 | 82.8 | 51.7 | 2.6 | 1.83 | 22.6 | 9.1 | 5.79 | 16.71 |

[a] All release data normalized to 100% melting (100% gas release).
[b] Average of 3 runs.
[c] Average of 2 runs.

on the outer circle, with only the center pin having a fission-product inventory. Examination of the outer pins after melting will show where the fission products deposit after release from the adjacent hot fuel. A 25-kw saturable reactor has been obtained for use as the power supply, and a demonstration test will be conducted in the near future.

## HOT-CELL CONSTRUCTION FOR MELTING MTR-IRRADIATED CAPSULES

Approximately 60 stainless-steel- and zirconium-clad capsules containing up to 80 g of $UO_2$ are being irradiated in the MTR to provide samples for an extensive hot-cell enlarged-scale melting program. Irradiation of the capsules began on August 6, 1962. Design work has been completed for most of the complex in-cell melting, handling, and chemical processing equipment. Much of the equipment has been constructed; however, some items are still in the development stage. Three separate cells will be required to accomplish the multiple operations necessary for the program. A schematic plan of equipment layout is given in Fig. 23.10.

A 5-Mc induction generator will be used for melting irradiated-fuel specimens in a hot cell. This permits heating to be accomplished by direct coupling with the oxide fuel itself, following decladding by induction coupling to the stainless steel or zirconium cladding material.

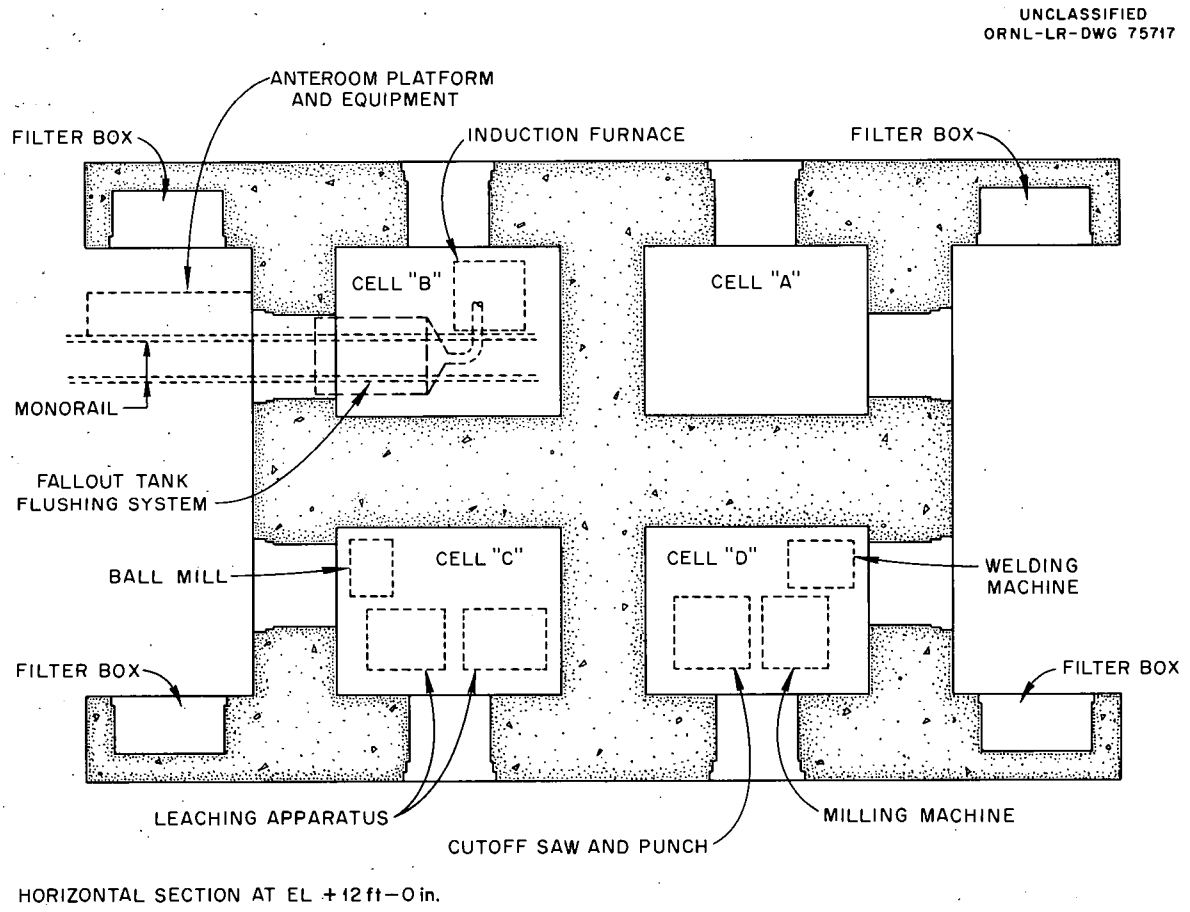


**Fig. 23.10. Hot-Cell Plan for Remote Handling and Melting of Clad $UO_2$ Fuel Capsules.**

# 24. Release of Fission Products on In-Pile Melting of Reactor Fuels Under Transient Reactor Conditions

G. W. Parker R. A. Lorenz

Preparations are being made for experiments on the release of fission products from $UO_2$ melted under transient reactor conditions in the TREAT, and an initial program proposal was reviewed with TREAT management for the purpose of exchanging ideas before making a final design of the experimental assembly. In general, the proposal appeared to satisfy the TREAT management requirements.

The fuel piece and the experimental assembly, revised as a result of the above-mentioned discussions, have the appearance shown in Fig. 24.1. It was suggested that a pressure gage and valve be added, as shown, and that an overall assembly with graphite reflectors should be constructed using a nominal 4-in. stainless steel sheath tube for insertion in the lattice.

## HAZARDS ANALYSIS

Apparatus leak rates and the thermal conduction of the meltdown-furnace assembly were studied in preparation for a hazards analysis, because of their importance to the safety of the experiments. Temperature profiles produced by heating the $UO_2$ capsule to 1300°C are shown in Fig. 24.2. Ten minutes was required to heat the capsule to this temperature, at which time the external-wall temperature of the autoclave was about 100°C. After heating 1 hr, with an internal pressure of 30 psia argon and a capsule temperature of 1300°C, the external-wall temperature of the autoclave reached 300°C. This indicates that there is a wide margin of safety in strength of the autoclave in case a high internal pressure should be encountered.

Leak testing was performed by cold hydrostatic pressure to 15,000 psi and by thermal cycling with 1000 psi helium internal pressure. Leakage was below the limit of helium detection ($1 \times 10^{-9}$ cc/sec) with no thermal cycling and with the standard 25-mil stainless steel gasket. A slight leak of $1 \times 10^{-8}$ cc/sec resulted on cycling from room temperature to 250°C. Gold plating the gaskets appeared to reduce leakage on thermal cycling. For safety considerations, it is significant that the expected maximum pressure of argon is about one-twentieth of that of the helium used in these tests and that leakage of a significant amount of fission gas could occur only if the maximum observed leak rate was exceeded by a factor of more than 100. Thus a safety factor of $10^3$ was demonstrated by these tests.

## GAS TRANSFER

The evacuated autoclave in the assembly is designed to serve as a sampling device which will be opened by an explosive valve following the transient. In order to ensure that the filters will not be damaged by the pressure surge, it is proposed that a length of capillary tubing or other device be used to restrict the flow. The rate of pressure drop was measured with a coiled 4-ft section of 20-mil-ID capillary tubing which will permit a safe transfer rate of ~1200 cc/min. An initial pressure of 60 psig completed the transfer in about 1 min.

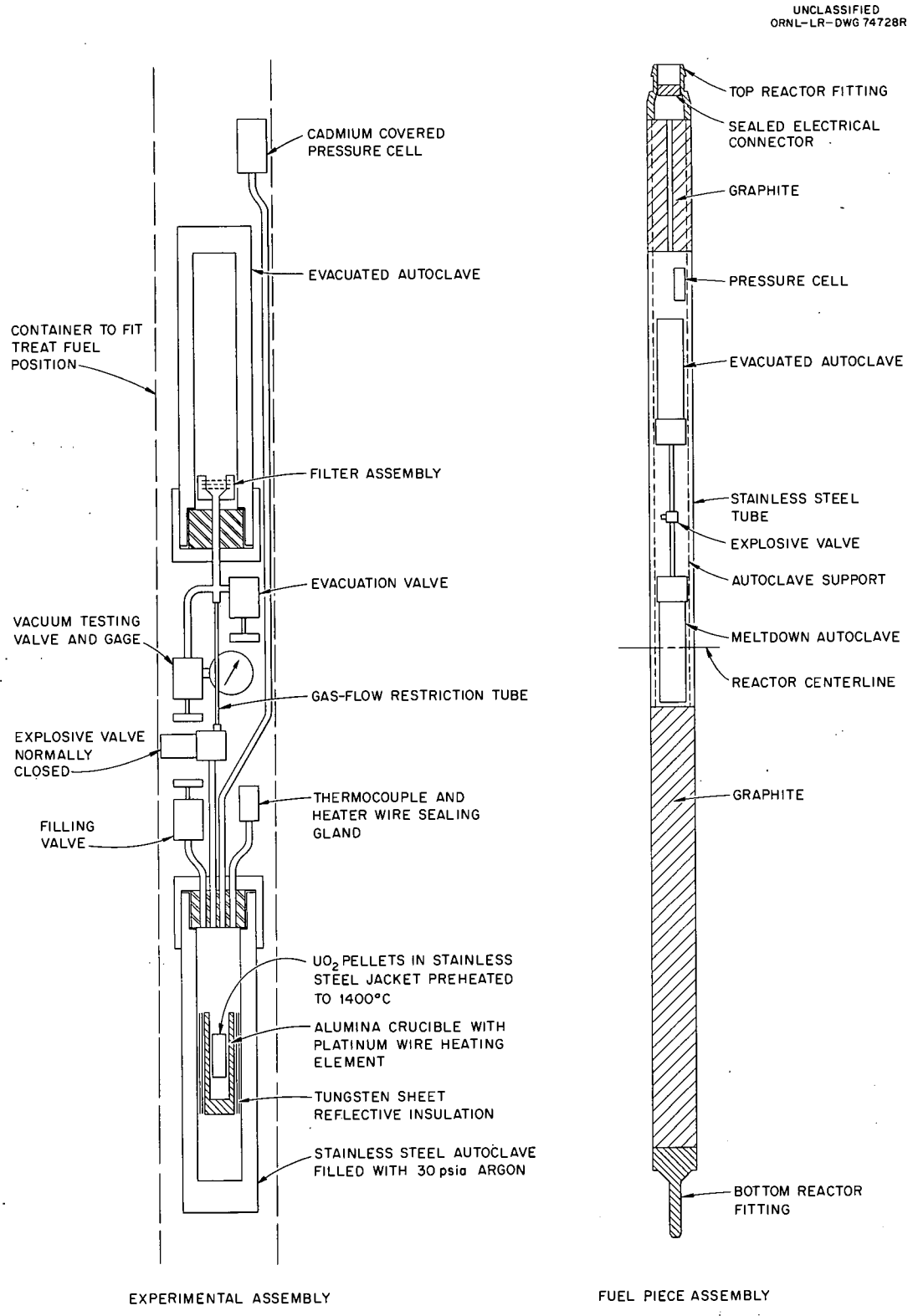


**Fig. 24.1. Experiment Assembly and Fuel Piece for Fission-Product Release from $UO_2$ by Fast Transient Melting.**

## MELTING SCHEDULE

A minimum amount of examination equipment (no hot cell facilities) will be required in order to conduct the initial series of tracer-level melting experiments. It is probable that this type of experiment can be conducted promptly, and materials are presently being obtained for this series, which is expected to begin during the early part of 1963. Hot cell facilities are being designed and constructed for handling the preirradiated fuel specimens that will be used in later experiments. Designs for a dismantling assembly and a shipping cask to be used in connection with high-activity-level melting experiments are under study.

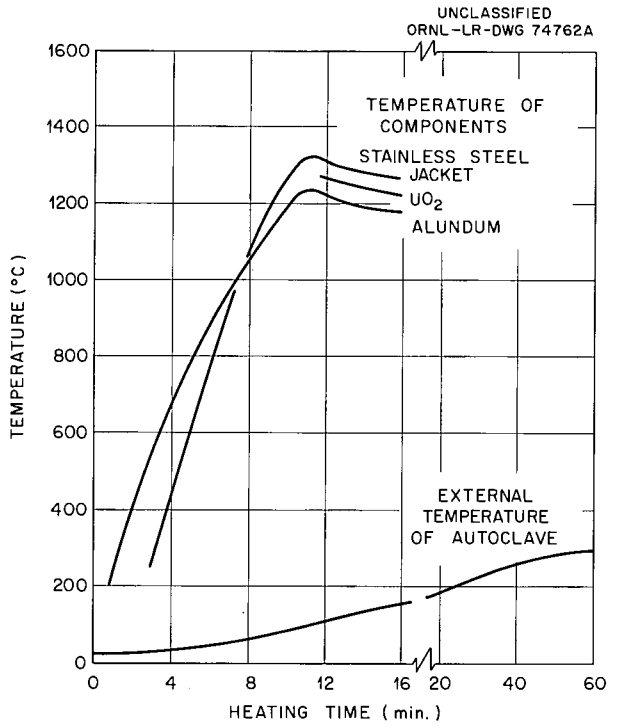


**Fig. 24.2. Temperature Histogram in Components of TREAT Autoclave Assembly with a 1300°C Furnace Temperature.**

# 25. Release of Fission Products on the In-Pile Melting or Burning of Reactor Fuels

W. E. Browning, Jr. B. F. Roberts
C. E. Miller, Jr. R. P. Shields
W. H. Montgomery

In-pile experiments of the type previously described[1] are being continued to study the release of fission products during simulated reactor accidents. Ten experiments were performed, and the results lead to valuable generalizations regarding the release of fission products when fuel elements are destroyed in a reactor environment.

Two types of experiments were conducted in the Oak Ridge Research Reactor to simulate reactor accidents in which fuel elements were destroyed by melting or burning. One type consisted of melting or vaporizing a miniature stainless-steel-clad $UO_2$ fuel element in a helium atmosphere. In the other type, a miniature fuel element composed of spheroidal particles of uranium carbide coated with pyrolytic carbon and embedded in a graphite matrix was burned in air. In each case, fission and gamma heat raised the temperature of the fuel element high enough to cause destruction.

## RELEASE OF FISSION PRODUCTS BY IN-PILE MELTING OF $UO_2$

The apparatus employed and the results of visual examination of the first two $UO_2$-melting experiments were described in a previous report.[1] In experiments of this type, miniature fuel elements are supported by a $ThO_2$ holder in a helium-filled $ThO_2$ cylinder. Thermal insulation surrounding the chamber consists of porous zirconium oxide, which is contained in two concentric vessels of stainless steel. The outer wall of the furnace assembly is cooled by reactor cooling water. A slow stream of helium is passed over the specimen during melting and is swept through filters and adsorbers to determine the amounts and forms of fission products released. Nine melting experiments have been performed to date.

Experiments 3 through 9 were a continuation of the series designed to determine the reproducibility of the $UO_2$ melting experiments and to identify uncontrolled variables which affect fission product release. Each contained $UO_2$ fuel with the same enrichment (6.5%), and, in general, the conditions were maintained constant. Variation of fission power in the experimental reactor lattice position during the period covered by these experiments caused a considerable spread in the maximum temperatures. Experiments 3, 4, 5, and 9 of this series were the hottest, and the fuel temperatures were in a relatively narrow range. The $UO_2$ in each of these experiments was completely melted, and spatters of $UO_2$ were found on the inside surface of the thoria cylinder. Figure 25.1 shows the fuel residues and the thoria parts of experiment 4. This condition is typical of this group of experiments.

Somewhat lower temperatures were achieved in experiments 6, 7, and 8. Examination of these experiments in the hot cells showed that the fuel in experiment 6 was 88% melted and in experiment 8 it was 79% melted, whereas the fuel in experiment 7 did not melt, but formed a central void similar to that produced in experiment 1. The fuel residues in both experiments 6 and 8 were similar to those in experiments 3, 4, 5, and 9 (solid masses with apparent spattering of fuel on the side of the $ThO_2$ cylinder). Figure 25.2 shows the appearance of

[1] W. E. Browning, Jr., *et al.*, *Reactor Chem. Div. Ann. Progr. Rept. Jan. 31, 1961*, ORNL-3127, pp 149–52; *Jan. 31, 1962*, ORNL-3262, pp 172–76.

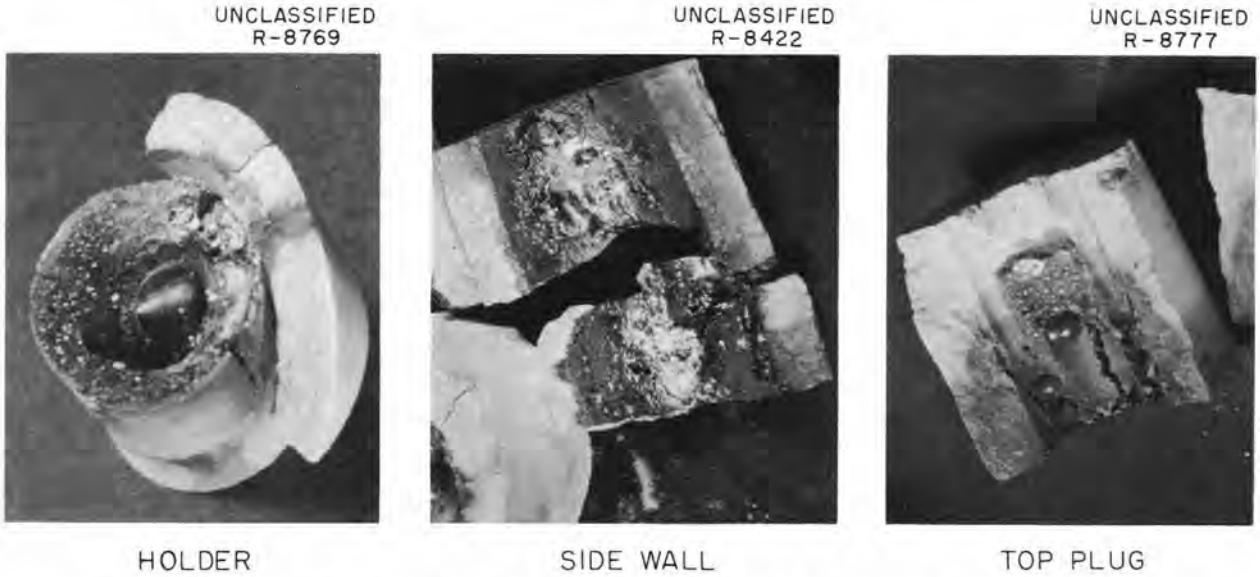


Fig. 25.1. $UO_2$ Residue and Thoria Parts from $UO_2$-Melting Experiment 4 (Typical of Experiments 3, 4, 5, and 9).

Table 25.1. Material Released from the Fuel in $UO_2$ Melting Experiments (%)[a]

| Experiment | $Sr^{89}$ | $Zr^{95}$ | $Ru^{106}$ | $I^{131}$ | $Te^{132}$ | $Cs^{137}$ | $Ba^{140}$ | $Ce^{144}$ | $UO_2$ |
|---|---|---|---|---|---|---|---|---|---|
| 2 | 99.8 | 87.3 | 88.0 | | | | 99.7 | 93.0 | 50.0 |
| 3 | 93.0 | 86.9 | 51.2 | | | | 96.1 | 85.2 | 42.7 |
| 4 | 76.6 | 55.5 | 82.8 | 99.6 | | | 94.1 | 58.9 | 44.5 |
| 5 | 57.3 | 42.9 | 90.8 | 99.4 | 98.4 | 97.2 | 55.4 | 44.6 | 34.5 |
| 6 | 54.6 | 60.1 | 59.8 | 99.0 | 91.4 | 98.6 | 51.7 | 48.7 | 46.8 |
| 7 | 5.21 | 0.908 | 10.9 | 96.0 | | 96.5 | 14.0 | 2.50 | 0.710 |
| 8 | 43.7 | 58.1 | 57.4 | 98.7 | 97.6 | 98.0 | 70.0 | 43.4 | 36.0 |

[a]Sample length, 1 in.; diameter, 0.210 in.; sample molten 5 min except in experiment 2 where it was molten for 10 min; helium flow, 400 cc/min.

the fuel and fuel holder from experiment 8. The fuel residue from experiment 7 (Fig. 25.3) was crystalline in nature, exhibiting the same pyramid-shaped crystal structure previously observed in experiment 1.

Radiochemical analyses were performed for experiments 2 to 8. Two release values were determined for each fission product in these experiments. Each value is based on the total amount of that fission product found throughout the experimental assembly. The first is release from the fuel and is given in Table 25.1. The data in Table 25.1, except that for experiment 7, show, in general, that nearly all the iodine, tellurium, and cesium and more than one-half the strontium, zirconium, ruthenium, barium, and cerium were released from the fuel. From one-third to one-half the $UO_2$ was released from the fuel, and the fission products contained in this fraction of the $UO_2$ were considered to be released. Fission product release was generally greater in experiment 2, which apparently reached a higher maximum temperature and which was irradiated unclad.

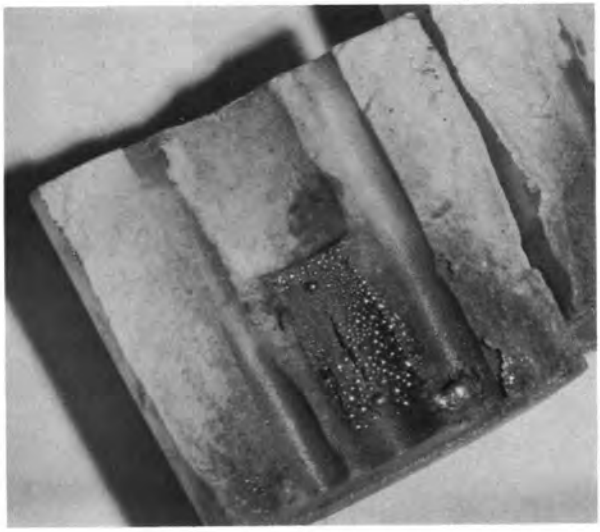


TOP PLUG

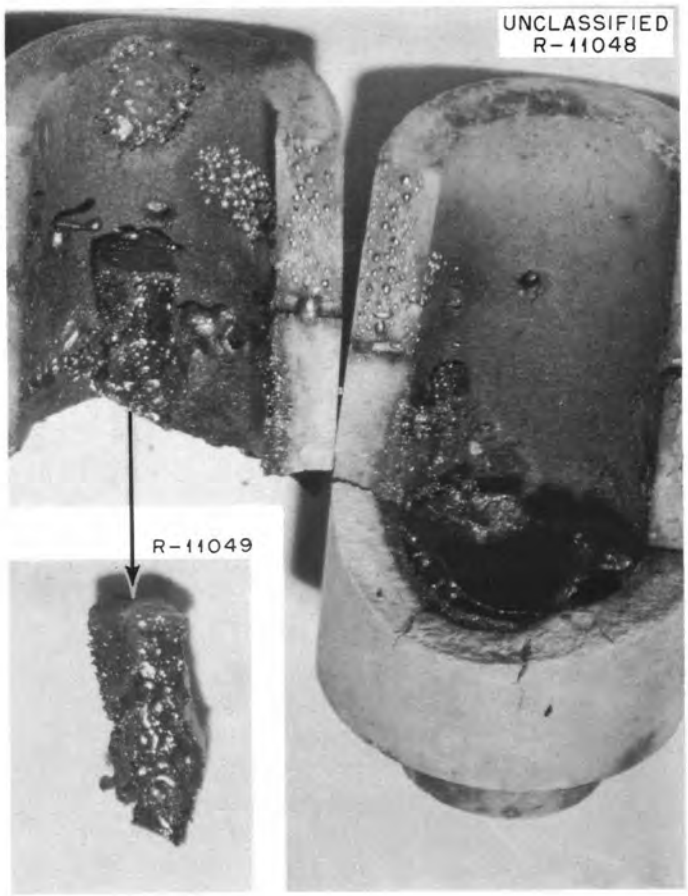


UNMELTED $UO_2$

$ThO_2$ SIDE WALL

Fig. 25.2. $UO_2$ Residues and Thoria Parts from Experiment 8 (Typical of Experiment 6).

The second release value is that from the high-temperature zone of the furnace. This zone consists of the volume enclosed by and including the $ZrO_2$. The temperature of this zone during the period in which the $UO_2$ is molten is 1000°C or higher. These values are given in Table 25.2. In experiment 2, strontium and barium were swept out of the furnace in the form of gaseous krypton and xenon by the helium during irradiation of the unclad fuel. Barium-140, for example, was found in the charcoal trap where it would be expected if it had been carried as $Xe^{140}$. Comparing the release of fission products from the high-temperature zone (Table 25.2) with that released from the fuel (Table

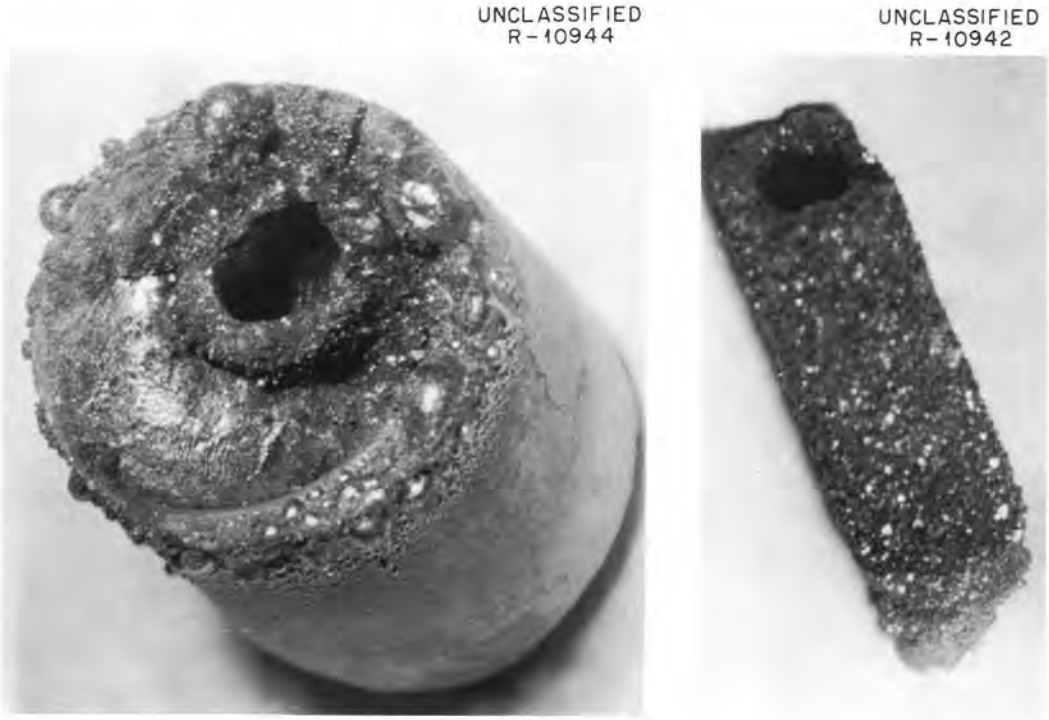


Fig. 25.3. $UO_2$ Residue from Experiment 7.

Table 25.2. Material Released from High-Temperature Zone[a] of the Furnace in $UO_2$ Melting Experiments (%)[b]

| Experiment | $Sr^{89}$ | $Zr^{95}$ | $Ru^{106}$ | $I^{131}$ | $Te^{132}$ | $Cs^{137}$ | $Ba^{140}$ | $Ce^{144}$ | $UO_2$ |
|---|---|---|---|---|---|---|---|---|---|
| 2 | 20.1 | 0.115 | 2.84 | | | | 14.5 | 0.508 | 4.08 |
| 3 | 1.24 | 0.110 | 0.614 | | | | 0.732 | 1.78 | 0.0520 |
| 4 | 2.90 | 0.0465 | 6.60 | 94.5 | | | 0.941 | 0.651 | 0.0773 |
| 5 | 1.44 | 0.0200 | 5.22 | 87.0 | 79.2 | 79.0 | 2.30 | 0.328 | 0.233 |
| 6 | 0.911 | 0.0896 | 1.32 | 94.3 | 48.8 | 81.9 | 0.547 | 0.0675 | 0.291 |
| 7 | 0.866 | 0.0370 | 2.15 | 49.7 | 11.5 | 74.1 | 0.576 | 0.322 | 0.00894 |
| 8 | 1.28 | 0.0508 | 1.73 | 95.4 | 81.4 | 87.5 | 0.824 | 0.244 | 0.0197 |

[a]High-temperature zone includes fuel material and thermal insulation, with a minimum temperature of 1000°C.
[b]Experimental conditions the same as those listed in Table 25.1.

25.1), there is a slight decrease in the release of iodine, tellurium, and cesium, and a considerable decrease in the release of strontium, zirconium, ruthenium, barium, cerium, and uranium. Release of these latter fission products and uranium from the high-temperature zone is generally less than 3%. This decrease in release values from the high-temperature zone as compared with that from the fuel under the existing experimental conditions is considered to be significant, since, during an actual reactor accident, temperatures corresponding to those of the high-temperature zone of these experiments would probably occur only in the immediate vicinity of the fuel.

## RELEASE OF FISSION PRODUCTS BY IN-PILE BURNING OF $UC_2$-GRAPHITE FUEL

One experiment was conducted in which part of a miniature fuel element consisting of pyrolytic-carbon-coated uranium carbide in a graphite matrix was burned at temperatures up to approximately 1400°C in the same in-pile apparatus used for melting $UO_2$. In this experiment, fission and gamma heat in the irradiation position produced a sufficiently high temperature for the fuel to burn when air was substituted for helium. The sample was allowed to burn for 15 min during which time approximately 59% (determined by weight) of the specimen was consumed. Metallographic sections of the coated uranium carbide particles which were subjected to various degrees of oxidation are shown in Fig. 25.4. These particles, which had fallen away from the burning fuel element, were recovered from the region around the holder.

Radiochemical analyses of materials from the burning experiment showed that only 38% of the uranium was liberated during the burning although 59% of the fuel element was consumed, confirming a recognized inhomogeneity of the fuel material with respect to distribution of $UO_2$. Table 25.3 shows the release data from this experiment. In interpreting the relatively low release from the fuel, it must be remembered that a large fraction of some of the fission products were probably retained inside those particles having an undamaged pyrolytic-carbon coating, especially those in the unburned portion. The release of strontium, zirconium, barium, cerium, and uranium from the high-temperature zone of the furnace was very low, but large fractions of ruthenium, iodine, tellurium, and cesium were released. The inclusion of ruthenium in the latter group was probably due to the formation of volatile ruthenium oxide.

## DETERMINATION OF PARTICLE SIZE AND FISSION PRODUCT DISTRIBUTION BY DIFFUSION COEFFICIENT MEASUREMENT

Data have been presented on the amounts of fission products released during a simulated loss-of-coolant accident. An additional objective of this program is to study the behavior of the fission products that are released. The 40-in.-long stainless steel exit tube which carries gas and gas-borne activity from the furnace to the filters is being used as a diffusion channel to determine the diffusion coefficient of each fission product. This method of analysis, which interprets the observed distribution of the various fission products along the wall of the tube, has been described previously by Browning and Ackley.[2] The results of this type of analysis, as applied to the $UO_2$ experiments,

[2] W. E. Browning, Jr., and R. D. Ackley, *Reactor Chem. Div. Ann. Progr. Rept. Jan. 31, 1962*, ORNL-3262, pp 180–83; p 244, this report.

**Table 25.3. Material Released in First In-Pile Fuel Burning Experiment (%)[a]**

| | $Sr^{89}$ | $Zr^{95}$ | $Ru^{106}$ | $I^{131}$ | $Te^{132}$ | $Cs^{137}$ | $Ba^{140}$ | $Ce^{144}$ | U |
|---|---|---|---|---|---|---|---|---|---|
| Release from fuel | 13.8 | 3.74 | 48.2 | 28.8 | 42.7 | 51.3 | 14.3 | 9.05 | 2.12 |
| Release from high-temperature zone[b] of furnace | 1.20 | 0.463 | 40.7 | 26.8 | 35.1 | 36.9 | 0.499 | 6.24 | 0.369 |

[a] Sample length, 0.5 in.; diameter 0.6 in. with 0.25-in.-diam axial hole; sample burning time, 15 min; air flow, 400 cc/min.

[b] High-temperature zone includes fuel material and thermal insulation; minimum temperature, 400°C.

UNCLASSIFIED
PHOTO 58984

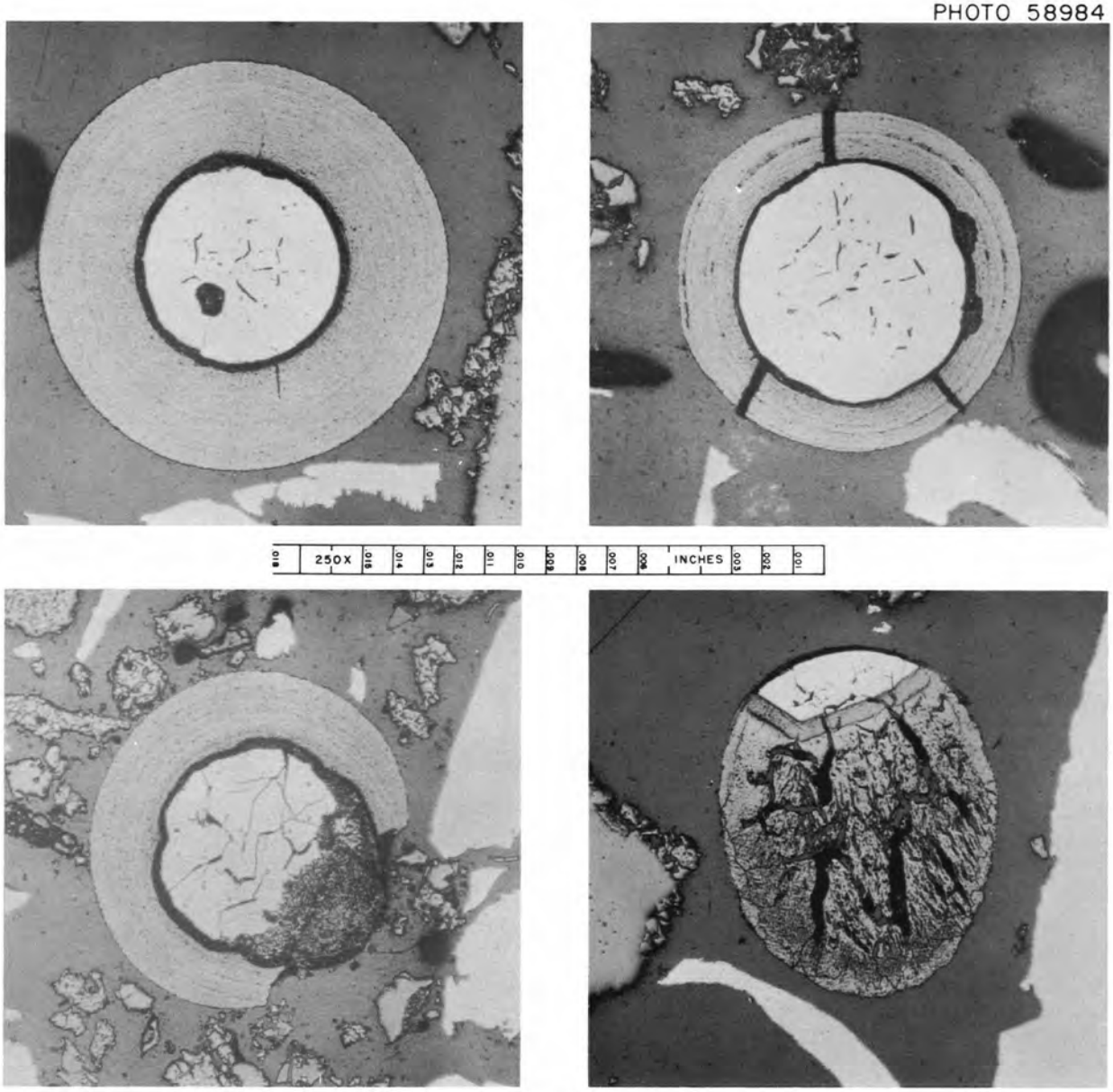


Fig. 25.4. Pyrolytic-Carbon-Coated Uranium Carbide Particles Showing Various Stages of Oxidation. Reduced 8%.

given in Table 25.4, show that the particles apparently fall in two size groups in the millimicron range. One group is centered around an apparent size of 22 A. An average of 39% of the iodine carried out of the reactor furnace by the exit gas was carried by these particles; values in individual experiments ranged from 8 to 75%. Iodine having a diffusion coefficient corresponding to that of the vapor form was apparently not present in the exit gas. Some of the cesium, strontium, tellurium, and barium were also found to be associated with the 22-A group of particles. The other group of particles was somewhat larger in diameter, 30 A, having a diffusion coefficient approximately one-half that of the smaller particles. Zirconium and uranium were associated with this group of particles, and in one experiment, ruthenium and cerium also appeared to be present. However, ruthenium and cerium did not usually appear among these fine particles but were carried on larger particles. For each isotope, the remainder of the activity which was released from the furnace, exclusive of that tabulated, evidently was in the form of larger particles. Data from downstream parts of the exit gas system are presently being analyzed to determine particle sizes.

**Table 25.4. Average Percent of Each Isotope Carried by Very Fine Particles in Exit Gas**

| Isotope | Percent Carried |
|---|---|
| **Effective Particle Diameter of Group, 22 A** | |
| $I^{131}$ | 39 |
| $Sr^{89}$ | 5 |
| $Te^{132}$ | 3 |
| $Cs^{137}$ | 15 |
| $Ba^{140}$ | 13 |
| **Effective Particle Diameter of Group, 30 A** | |
| $Zr^{95}$ | 3 |
| $Ru^{106}$ | 10 |
| $Ce^{144}$ | 13 |
| $UO_2$ | 9 |

## FRACTIONATION STUDIES

The distribution of fission products and uranium among the various regions in each experiment is being analyzed and interpreted in terms of the fractionation processes which govern the behavior of these materials. Fractionation refers to any alterations of the radionuclide composition occurring during the experiment which result in a sample composition different from that predicted for normal fission yields. Similar fractionation studies have been carried out by Freiling in the study of debris from nuclear detonations.[3] Fractionation occurs because of differences in characteristics of the fission products leading to differences in release or deposition mechanisms. A study of fractionation, then, should lead to a better understanding of both the mechanisms and the characteristics. As an example of the type of analysis which is being used in the fractionation studies, the ratio of $Ba^{140}/Zr^{95}$ vs $Sr^{89}/Zr^{95}$ is plotted in Fig. 25.5, based on data from experiment 7. The equation of the line determined empirically is shown. In this

[3]E. C. Freiling, *Science* **13**, 1991–98 (1961).

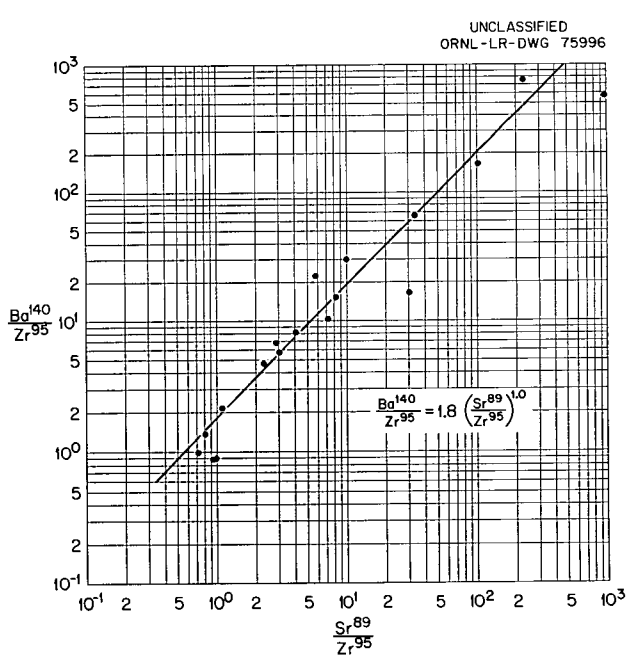


Fig. 25.5. Fractionation of $Ba^{140}$ vs $Sr^{89}$.

plot, the abscissa may be regarded as a measure of the intensity of the volatilization conditions to which each sample, represented by a point, was exposed. Since $Sr^{89}$ is more volatile than $Zr^{95}$, points to the right represent volatilized materials and points to the left represent residues from which volatile materials were lost. The ordinate is a measure of the degree to which $Ba^{140}$ volatilized for each volatilization condition on the abscissa. This plot indicated that $Ba^{140}$ and $Sr^{89}$ behave similarly and that both are more volatile than $Zr^{95}$, which was the reference material. In a similar plot for ruthenium from experiment 7, the slope was greater than 1, indicating that the ruthenium was more volatile than the strontium. In experiment 8, the slope for ruthenium was 1, indicating that the volatility of the two was the same. The difference in the slope probably represents a difference in the release mechanism since the fuel in experiment 7 did not melt while that in experiment 8 did. One conclusion resulting from the fractionation studies is that, in several of these experiments, ruthenium followed the stainless steel cladding as the cladding melted into a puddle and subsequently vaporized to other areas of the assembly. The mechanism of this behavior is not yet known. However, it is anticipated that this type of study will lead to the formulation of models which explain the observed distributions and which may provide a basis for prediction of the behavior of accident-released fission products under various conditions, especially the behavior leading to escape from a controlled system. A knowledge of fractionation mechanisms will aid in the recognition of the relative importance of the various factors which define a reactor accident.

## SUMMARY

In both the melting and burning in-pile experiments, although large fractions of the fission products were released from the fuel, they were almost entirely retained inside the high-temperature zone of the furnace with the exception of iodine, cesium, and tellurium; when oxygen was present, ruthenium was also released. The noble gases appeared to be released completely. These results suggest that, for the conditions tested, effective retention of many fission products may be expected by high-temperature surfaces near the hot zone in reactor accidents.

Fractionation studies which are now under way are expected to provide a basis for prediction of the behavior of accident-released fission products under various conditions. Particle-size studies indicate that significant fractions of the fission products released from the high-temperature zone were carried by particles as small as 20 to 30 A in diameter. This work is being continued with emphasis being placed on the effects of the conditions of reactor accidents on the amounts and forms of released fission products.

# 26. Characterization and Control of Accident-Released Fission Products

The behavior of released fission products dispersed in gases depends markedly on their physical and chemical form; consequently, the prediction of their transport in gases or the selection and design of systems for their removal from gases require information as to the distribution of radioactivity among the vapors and the different particle sizes which occur. Two methods of determining the distribution of radioactive materials carried in gases were investigated.

## DIFFUSIONAL CHARACTERIZATION OF MILLIMICRON-SIZE RADIOACTIVE AEROSOLS AND THEIR REMOVAL FROM REACTOR GASES

W. E. Browning, Jr. R. D. Ackley

An important mechanism in aerosol transport and deposition is that of diffusion, and since the diameter of a particle is related to its diffusion coefficient, it is possible to measure the size of particles and to identify molecular vapors by means of their diffusion coefficients. A method of determining diffusion coefficients of fine particles and of radioactive vapors such as iodine by measuring the distribution of radioactivity on the walls of cylindrical and rectangular channels previously exposed to gas carrying radioactive materials and flowing under laminar conditions was described earlier.[1] The equation for cylindrical geometry was not presented earlier, and since cylindrical tubes are currently being employed exclusively in this work, Eq. (1), corresponding to deposition of a given species in a cylindrical diffusion channel, obtained from the equation of Gormley and Kennedy,[2] is presented:

$$n_s = \frac{N_0 D}{Q} \left(9.4106\, e^{-11.489\, DZ/Q} + 6.8309\, e^{-70.06\, DZ/Q} + 5.8198\, e^{-179.07\, DZ/Q}\right) . \quad (1)$$

In Eq. (1), $n_s$ = number of particles deposited per unit length, $N_0$ = number entering the channel, $D$ = their diffusion coefficient, $Q$ = volumetric flow rate of carrier gas, and $Z$ = distance from channel entrance. For the case of a multiplicity of species, the deposition would be given by a summation of expressions of the form of Eq. (1). The diffusion-channel method was tested using radioiodine vapor, $I^{131}$-labeled 0.004-$\mu$ aluminum oxide particles, and $I^{131}$-labeled 0.25-$\mu$ tobacco-smoke particles; the particle sizes and/or diffusion coefficients of these three materials were obtainable by independent means. In all three cases, good agreement between theory and experiment was observed, indicating that this method is applicable over the range of interest. More recently, an additional determination of the size of the aluminum oxide particles was made by means of electron microscopy. The observed diameters were in the range 0.003 to 0.008 $\mu$ with a modal value of 0.0043, which is in excellent agreement with the earlier determinations.

This method of measuring gas-borne radioactive materials has been applied to the problem of removing millimicron-diameter radioactive particles from air streams. Such particles may be too small

[1] W. E. Browning, Jr., R. D. Ackley, and R. E. Adams, *Reactor Chem. Div. Ann. Progr. Rept. Jan. 31, 1962*, ORNL-3262, pp 179–83.

[2] P. G. Gormley and M. Kennedy, *Proc. Roy. Irish Acad.* **A52**, 163–69 (1949).

in mass for efficient filtration by inertial impaction, but sufficiently large that diffusion is too slow for efficient deposition.

### Behavior of Millimicron-Size Particles in Conventional Gas-Cleaning Systems

Aluminum oxide particles with a nominal diameter of 0.004 $\mu$ labeled with $I^{131}$ were employed for studies of the removal of small particles by various gas-cleaning systems. The particles were generated in air passing through an aluminum-wire spark gap, and this air stream was mixed with another carrying radioiodine vapor. After the mixture aged, excess $I_2$ vapor was stripped out and the radioactive-particle-laden air stream was made to flow through the filter medium being tested, usually at a face velocity of 5 fpm. In some instances, a third air stream was introduced after the aging chamber to give the desired total flow. On either side of the filter medium, side streams under laminar-flow conditions were drawn through the diffusion channels, which were silver-plated copper tubes 2 ft in length with an ID of 0.8 cm. The tests were made at room temperature and at atmospheric pressure. Figure 26.1 illustrates the experimental arrangements employed. Changes were observed in particle-size distribution due to a deliberate variation in aging times.

Two tests were performed with high-efficiency, low-pressure-drop filter media. The results of one test are shown in Fig. 26.2. This medium does not appear to be effective for removal of radioactivity in the form of iodine vapor or particles ranging up to 0.004 $\mu$, since it exhibited efficiencies ranging from about 10 to 75%.

The results of a test with a 0.75-in.-deep bed of $-6$ $+16$ mesh activated carbon are given in Fig. 26.3. The results from two tests may be summarized by stating that, while iodine vapor removal was essentially complete, the removal efficiency for the 0.003- to 0.006-$\mu$ particles produced in these tests was observed to be only 75 to 90%, the higher efficiency being associated with the finer particles.

UNCLASSIFIED
ORNL-LR-DWG 68735R

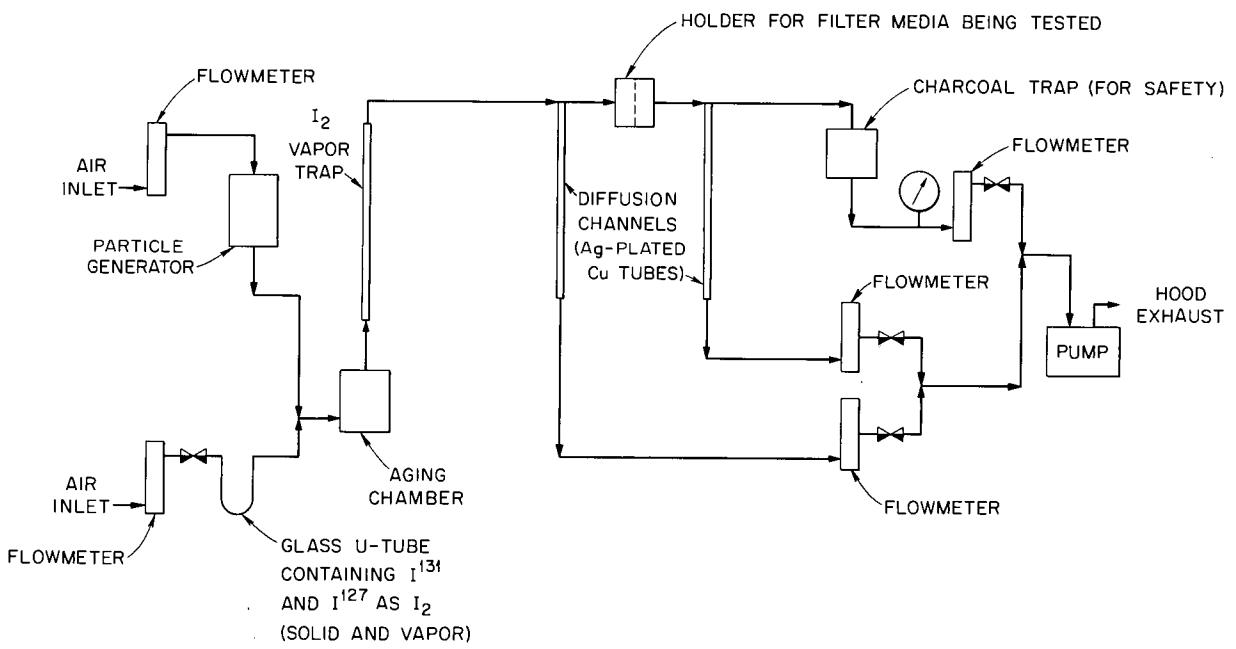


**Fig. 26.1. Particle Diffusion Apparatus for Investigating the Efficiency of Filters for Removal of Very Fine Particles.**

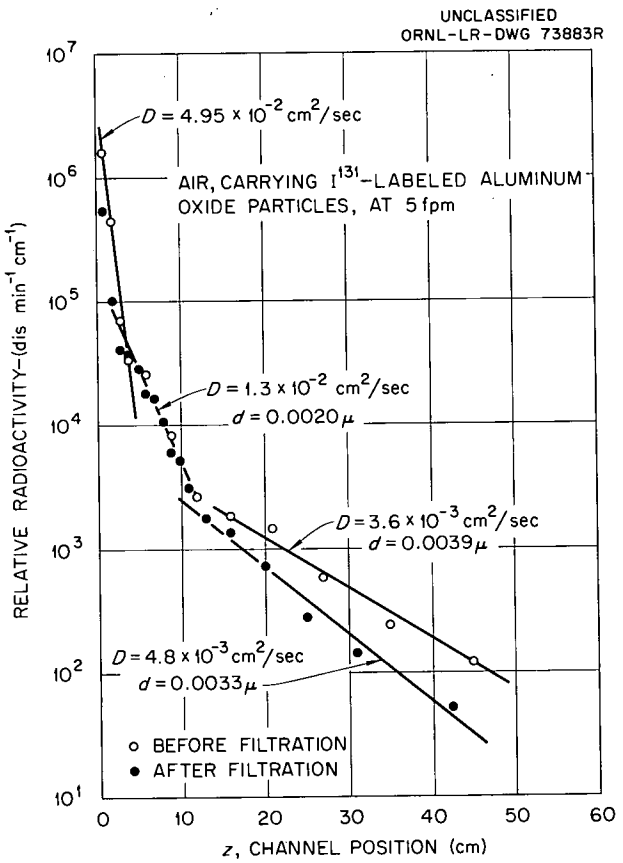


**Fig. 26.2. Removal of Very Fine Particles from Air by a High-Efficiency Filter.**

The fact that radioactive particles with diameters of ~0.003 μ are apparently produced on melting irradiated nuclear fuel is reported elsewhere in this document.[3] This observation, together with the results obtained for charcoal adsorbers and high-efficiency filters, suggests that development of less-conventional gas-cleaning methods or improvement of existing methods may be required to assure the safety of reactor containment systems. Accordingly, the work to be described next was undertaken.

## Removal of Millimicron Particles by Less-Conventional Methods

The objective of one removal method was to cause the radioactive particles to increase in size by serving as condensation nuclei for steam so that they could be removed by a high-efficiency filter. Figure 26.4 shows the apparatus employed. Cool air carrying particles was mixed with air saturated with water vapor at approximately 95°C, resulting in fog formation. A condenser was used to remove excess water vapor in order to prevent interference with the use of the exit diffusion tube. The results of this study are summarized in Fig. 26.5, where the left side of the figure shows data obtained in a control experiment. Comparison of the data for filtration with and without fog formation indicates removal efficiencies of 99% vs 85% for 0.002-μ particles and 85% vs 35% for 0.007-μ particles. These results are encouraging, but the improvement in removal efficiencies is not enough to provide the basis for a final design. Optimization of this method might provide a partial answer to the problem of small-particle containment; however, it appeared desirable to explore some other possible methods.

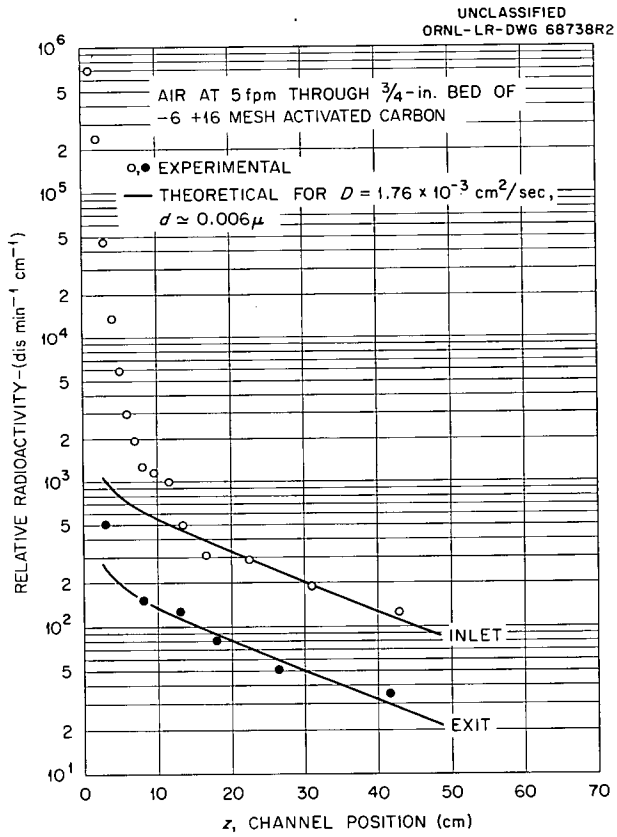


**Fig. 26.3. Removal of Very Fine Particles and $I^{131}$ Vapor from Air by an Activated Carbon Bed.**

[3] W. E. Browning, Jr., *et al.*, "Release of Fission Products on the In-Pile Melting or Burning of Reactor Fuels," p 236, this document.

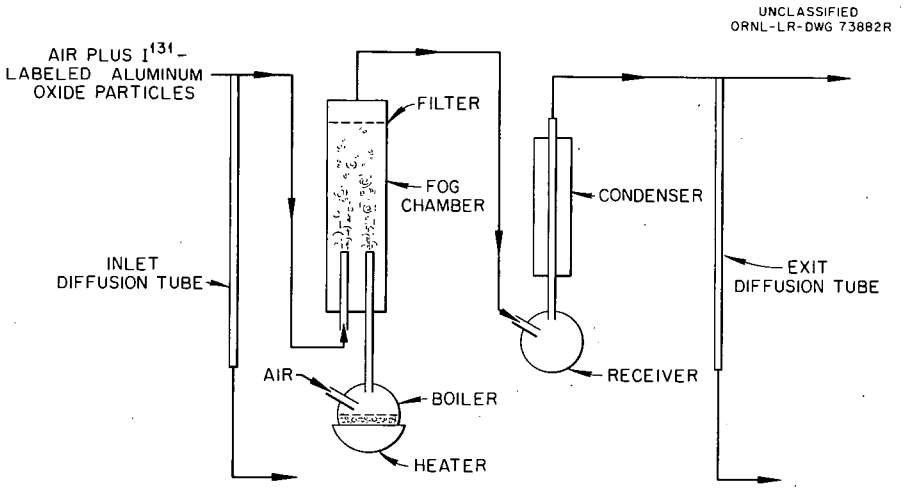


**Fig. 26.4. Diffusion Apparatus Used for Investigating the Effect of Fog Formation on the Filtration of Very Fine Particles.**

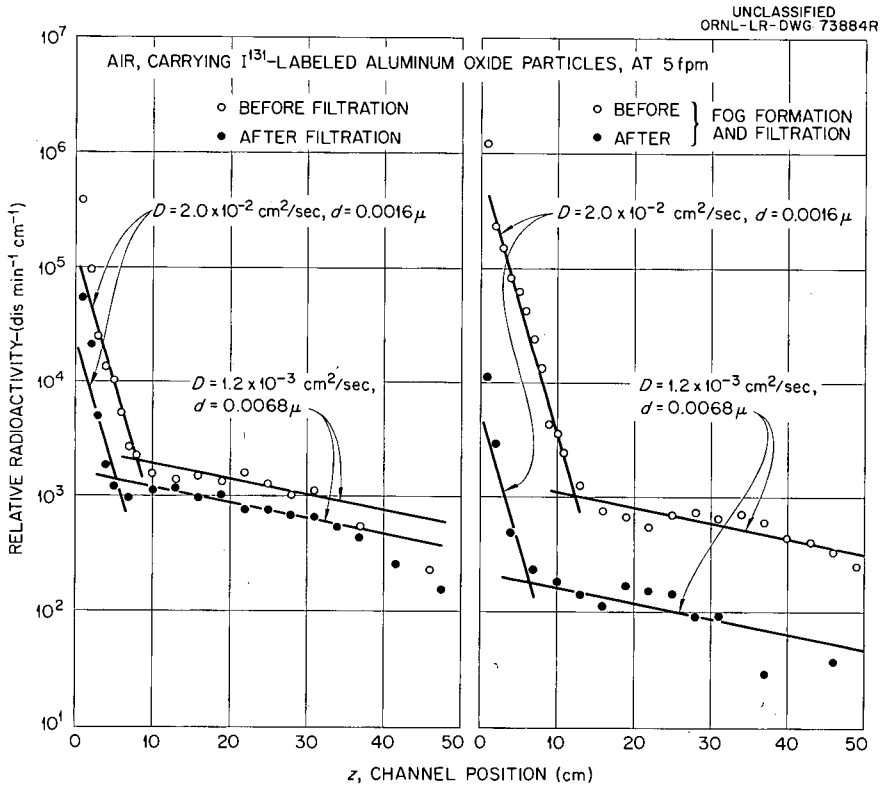


**Fig. 26.5. Effect of Fog Formation on the Filtration of Very Fine Particles.**

If air carrying millimicron-size particles is used to generate foam or small bubbles, the particles may diffuse to the air-liquid interface and be retained. The use of foam for removal of iodine and particles with diameters $\geqq 0.074\ \mu$ from air has been reported by Silverman and co-workers.[4] Figure 26.6 shows the apparatus used to investigate the removal efficiency of foam when air carrying radioactive aluminum oxide particles was the dispersed or internal phase. The dispersion medium or external phase was an aqueous solution of organic liquids formulated to produce a given height of foam under the operating conditions. In an actual application, the air in a reactor vessel might be recirculated through a pool of water containing a suitable foaming agent. Three tests were performed: one with a 1-ft foam column, one with a 3.5-ft foam column, and one with a 5-in. column of pure water as a control. The control test showed negligible removal of the nominally 0.007-$\mu$ component but about 95% removal of a composite component believed to include a mixture of iodine vapor and particles with diameters less than 0.002 $\mu$. The results obtained with a 3.5-ft column are shown in Fig. 26.7, which indicates a removal efficiency of about 85% for the 0.007-$\mu$ particles. Rather surprisingly, the results for the 1-ft foam column were not appreciably different from those obtained with the 3.5-ft column. This phenomenon may receive further study, and other methods of removing very fine particles from gases, will be tested.

[4]L. Silverman, M. Corn, and F. Stein, *Proceedings of the Seventh AEC Air Cleaning Conference, October 10–12, 1961*, TID-7627, pp 390–405.

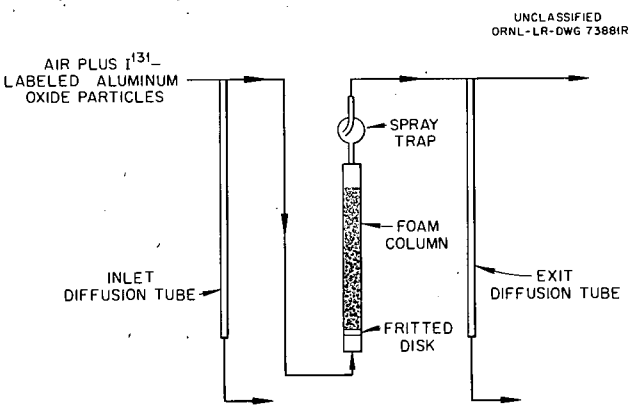


**Fig. 26.6. Diffusion Apparatus for Investigating Efficiency of Foam for Removal of Very Fine Particles from Air Streams.**

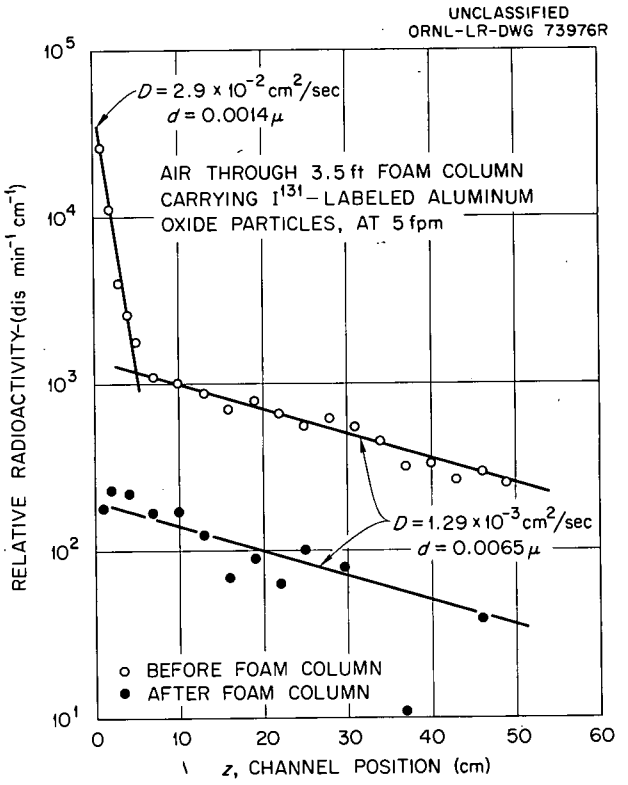


**Fig. 26.7. Removal of Ultrafine Particles from an Air Stream by a Foam Column.**

The data summarized in Table 26.1 show that millimicron-size particles are capable of carrying radioactive materials through conventional gas-cleaning devices. Some progress has been made in developing more efficient methods of removing such materials from gases, and these studies are being continued.

## MEASUREMENT OF RADIOACTIVE AEROSOLS BY USE OF FIBROUS FILTERS

W. E. Browning, Jr. M. D. Silverman

The transport of an aerosol through an array of fibers brings into play the processes of inertial impaction, interception, and diffusion. Since all these processes have important effects on the behavior of radioactive materials in gases, it

**Table 26.1. Observed Efficiencies of Various Methods of Removing Ultrafine Particles or Radioiodine Vapor from Air**

| Method | Identity or Nominal Size of Component | Removal Efficiency (%) |
|---|---|---|
| High-efficiency filter | $I_2$ and/or <0.002 $\mu$ | 75 |
| | 0.002 $\mu$ | <10 |
| | 0.004 $\mu$ | ~50 |
| Activated-carbon bed | $I_2$ | >99 |
| | 0.005 $\mu$ | 75–90 |
| Fog chamber and filter: | | |
| Without fog formation | 0.002 $\mu$ | 85 |
| | 0.007 $\mu$ | 35 |
| With fog formation | 0.002 $\mu$ | 99 |
| | 0.007 $\mu$ | 85 |
| Foam column: | | |
| 5-in. water column (no foam) | $I_2$ and/or <0.002 $\mu$ | 95 |
| | 0.007 $\mu$ | ~10 |
| 1-ft foam column | $I_2$ and/or <0.002 $\mu$ | 98 |
| | 0.007 $\mu$ | 85 |
| 3.5-ft foam column | $I_2$ and/or <0.002 $\mu$ | 99 |
| | 0.007 $\mu$ | 85 |

would be useful to be able to measure radioactive aerosols by observing their distribution in fibrous beds. A method is being developed to measure aerosols by determining their distribution as a function of depth in fibrous filters under carefully controlled conditions. It is anticipated that this work will also extend the theory of the performance of fibrous filters to conditions for which little information is now available.

The measurement of the distribution of aerosol materials with depth in ordinary paper filters is made difficult by the thinness and the complexity of the medium. Sisefsky[5] described a method of determining particle penetration depths. He passed an aerosol containing radioactive solid particles about 2 $\mu$ in diameter through a thin glass-fiber filter and obtained a rough indication of the relative sizes and amounts present by peeling off successive layers of the filter with the use of pressure-sensitive tape. Interpretation of these data is impeded by poor depth resolution and by the large range of fiber diameters employed.

Theoretical calculations performed to determine the effects of various conditions on the interaction of aerosols with fibers showed that fiber diameter has a very strong effect. The wide variation in fiber diameter employed in commercial fibrous filters would necessitate the use of approximations and averages in handling the data obtained from filtration experiments involving these media. This difficulty was overcome by obtaining a commercial synthetic fiber, Dacron polyester staple, of unusually uniform size (99% was 11.3 ± 0.8 $\mu$). The fiber was carded into a web and rolled to give a product which had the appearance and feel of filter paper. A number of $1\frac{1}{2}$-in.-diam disks of this material were placed between metal washers and enclosed in a Teflon holder to give a compact filtering device, which permitted separation of the fiber bed into discrete layers for radioassay after exposure to the aerosol-carrying gas stream.

A radioactive aerosol containing $Zn^{65}$ was produced by passing an air stream through a chamber in which a spark generated by a Tesla coil crossed a $\frac{1}{16}$-in. gap between two pieces of irradiated zinc foil. A schematic diagram of the apparatus is shown in Fig. 26.8. An electron micrograph of samples of this aerosol collected on a membrane filter showed that the particles had diameters in the range 40 to 300 A.

Data obtained in the first series of experiments are presented in Fig. 26.9. Although preliminary in nature, the results indicate that the technique used was satisfactory and that it should provide useful information on particle size and on filtration mechanisms. The slope of the distribution curve on a semilog plot equals the coefficient of interaction between aerosol and fibers, composed of terms corresponding to each of the interaction processes, which is characteristic of the aerosol species. Data are shown for four different gas

[5] J. Sisefsky, *Nature* **182**, 1437 (1958).

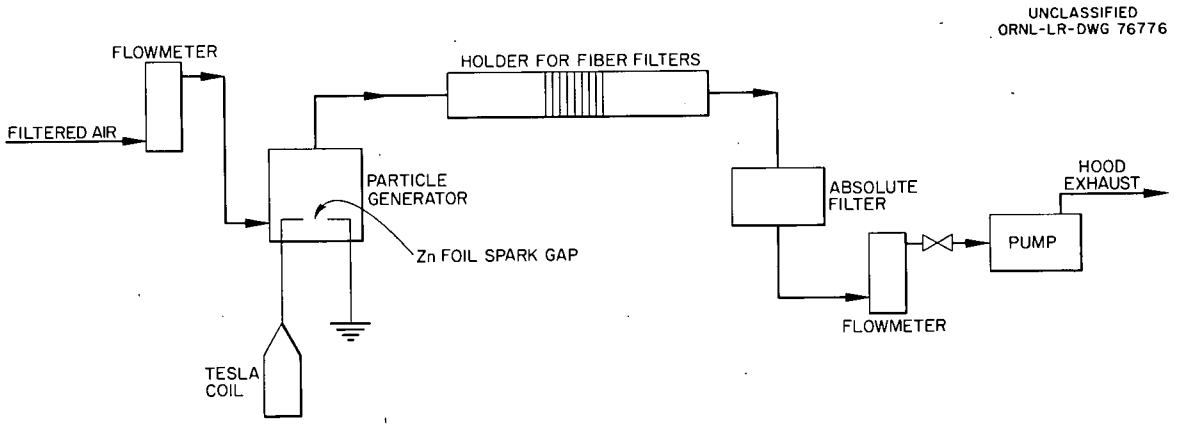


**Fig. 26.8. Apparatus for Measuring Aerosols by Use of Fibrous Filters.**

velocities. It is evident that at 0.4 to 1.7 fpm the relative concentration of activity in the filters was reduced by a factor of $10^4$ or 99.99%, whereas at 2.8 to 40 fpm, the reduction was not as great, that is, $10^3$ or 99.9% over a filter depth which contains $10^5$ cm of fiber length per $cm^2$ of filter area. At this time it is uncertain whether the tails of the curves are meaningful, since the lowest counting rates were near background. Future experiments will be performed with more highly irradiated specimens which should provide higher counting rates and, it is hoped, more data in this area.

All the flow rates are within the viscous- or laminar-flow region. At the lowest linear velocity (~0.4 fpm), where diffusion would be the controlling factor, the collection efficiency increased with decreasing velocity as expected. At the higher flow rates, where the primary mechanism of filtration of particles of this size is interception, the efficiency appeared to be independent of velocity, in agreement with theory. This investigation is being continued to provide a more specific identification of the mechanisms which produce the distribution patterns observed. Interpretation of distributions in terms of aerosol characteristics will then be possible.

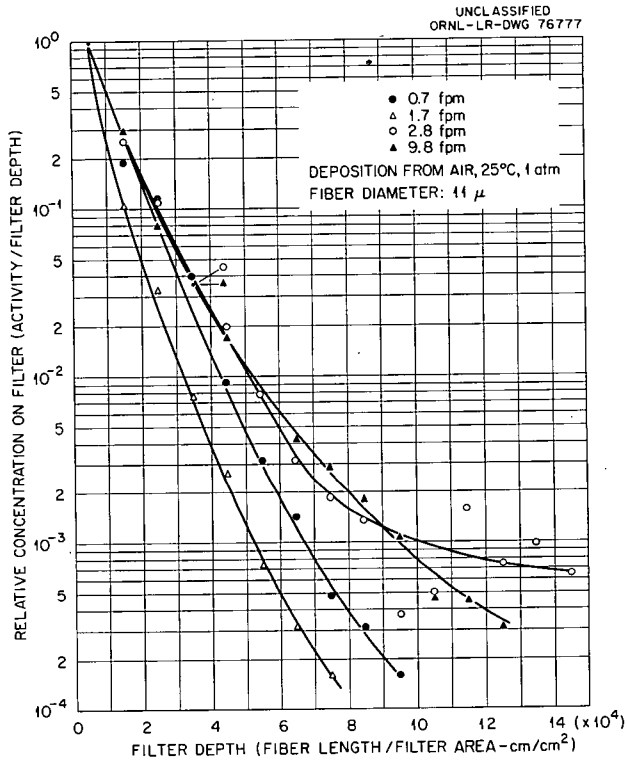


**Fig. 26.9. Distribution of $Zn^{65}$ Aerosol Through Dacron-Fiber Filters.**

# 27. Fission Product Transport Evaluations

C. J. Barton M. E. Davis G. W. Parker

## PARTICLE-SIZE STUDIES

Little progress was made in the study of particles produced in simulated reactor accident experiments, due to lack of funds for the necessary hot-cell installations. Construction of the previously described[1] box having Lucite walls and an aluminum frame was completed, and it will be installed in a hot cell for preliminary tests with unirradiated $UO_2$, and possibly with slightly irradiated $UO_2$, when installation of the RF power equipment for melting samples, described elsewhere in the document, is completed. This should be accomplished in the near future.

## IDENTIFICATION OF CHEMICAL SPECIES

Apparatus designed to permit determination of the heat of vaporization of radioactive species by a counting technique and the results of two exploratory experiments with radioiodine in this apparatus were described[1] earlier. This apparatus was modified by elimination of the sidearm through which a steel rod was inserted to break the thin window of the iodine capsule. The modified version, made of quartz, had a quartz plunger containing an iron core to break the window. With helium flowing through the apparatus at a constant rate and at a constant temperature, the rate of increase of the radioiodine-vapor content of a small charcoal trap near the top of the furnace tube was followed by means of a crystal detector connected to counting equipment which permitted both manual counts and continuous recording. The helium temperature was measured by an iron-constantan thermocouple junction just below the ampoule.

Because of difficulties experienced in the effort to obtain equilibrium-rate data with this arrangement, the rate of transfer of iodine was reduced to a more manageable value by changing the sample ampoule from the thin-window type to one having a 1-mm-ID capillary tube 4 cm long, through which the iodine had to diffuse before it reached the carrier gas stream. The break seal on the side of the capillary was broken after insertion of the ampoule in the apparatus by removing the charcoal trap at the exit end of the furnace tube and inserting a long glass rod. The data obtained could be correlated by an Arrhenius-type plot, yielding heats of vaporization ranging from about 13.0 to 15.0 kcal/mole. The average of six values obtained was 14.2 kcal, which agrees reasonably well with the published value[2] of 14.9 kcal for solid iodine. It seems probable that this technique could be refined to diminish the scatter of data, but other factors, including the difficulty involved in extrapolating to the carrier-free situation and in applying the technique to release experiments, encouraged the investigation of an alternate technique suggested by R. F. Newton. He postulated that the heat of vaporization might be determined by measuring, over a range of temperatures, the relative concentration of radioactive species in the vapor phase in an evacuated bulb which is in equilibrium with a solid or liquid phase in another bulb to which it is connected by means of a capillary. The vapor-phase bulb is maintained at a higher temperature than the sample bulb in order to prevent deposition of solid or liquid material on the wall. The experimental arrangement is shown in Fig. 27.1.

[1] C. J. Barton and G. W. Parker, *Nucl. Safety Progr. Rept., Aug. 17, 1962*, ORNL-3319, p 39.

[2] F. R. Bichowsky and F. D. Rossini, *The Thermochemistry of Chemical Substances*, Reinhold Publishing Co., New York, 1936.

Experiments to test this concept have been conducted with Pyrex bulbs 1 cm in diameter connected by a capillary tube 10 cm in length having an inside diameter of about 1 mm. The experiments performed to date have been with bulbs containing 0.20, 0.25, 0.40, and 4.1 mg of iodine carrier, along with about 0.1 mc of $I^{131}$. Typical data obtained are displayed in Fig. 27.2. The upper bulb, which was viewed by the crystal detector, was maintained at a fixed temperature in most of the experiments, but it was found that the slope of the curve obtained with a fixed temperature differential varied only slightly from that obtained with the fixed top-bulb temperature. The data in Fig. 27.2 show that the surface effect noted in the iodine transport experiments is evidenced in the behavior of iodine at lower temperatures in the sealed Pyrex tubes and that the temperature at which deviation from the linear relation occurred cannot be readily correlated with the amount of iodine present. Further tests will be required in order to determine whether the value for the heat of vaporization of solid iodine observed with the 0.4-mg sample (14.4 kcal) is reproducible and can be obtained with other amounts of iodine. The reason for the large variation in heat of vaporization values obtained to date is not clear, but it was recently observed that some sample ampoules contained a small amount of water or stopcock grease which may help to account for the anomalous behavior. It may be significant that the 0.4-mg $I_2$ sample, which gave the best value for the heat of vaporization of iodine, showed no visual evidence of contamination.

Since this technique could be more easily and safely applied to the study of released fission products than the transport method, further study is planned in an effort to find conditions which will yield usable data.

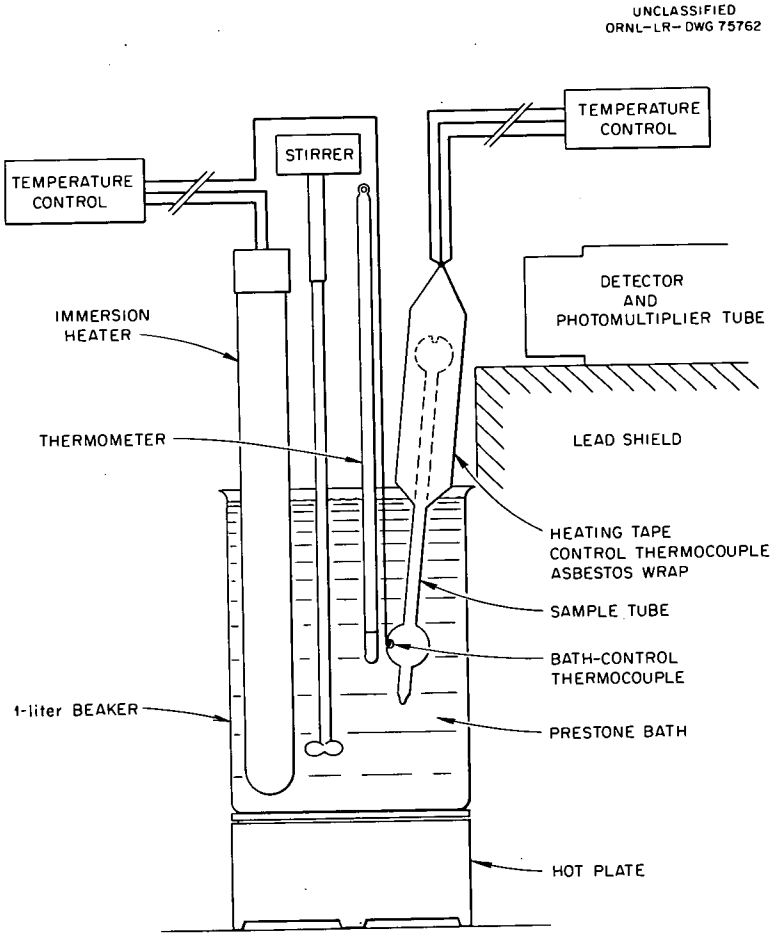


**Fig. 27.1. Sealed-Tube Iodine Equilibration Apparatus.**

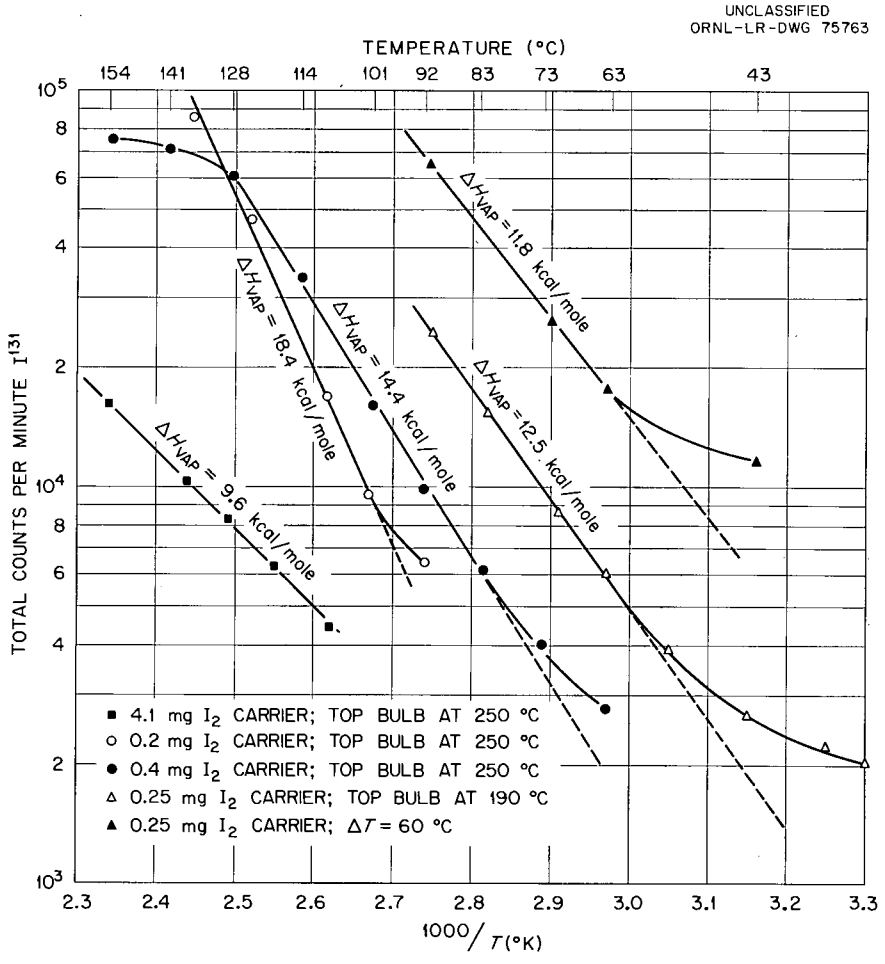


**Fig. 27.2. Iodine Equilibration Data from Sealed-Tube Experiments.**

# Part VII

# Support for Other ORNL Programs

# 28. Molten Fluoride Mixtures as Possible Fuel Reprocessing Solvents

R. E. Thoma
H. A. Friedman
G. M. Hebert
R. L. Boles[1]
B. J. Sturm
E. H. Guinn

A study of $AlF_3$ phase behavior in molten fluoride systems was initiated as a part of an effort to adapt the Fluoride Volatility Process to the recovery of uranium from aluminum-based fuels. In this process both aluminum and uranium are converted into fluorides by the action of HF. Desirable characteristics of a fluoride solvent for these fluorides include:

1. low cost of the solvent components,
2. liquidus temperatures below 600°C for mixtures containing 0 to 30 mole % concentrations of $AlF_3$,
3. low viscosity,
4. a sufficient concentration of nonassociated fluoride ions in the molten state to permit a rapid rate of fuel element dissolution, and
5. low vapor pressure at temperatures of 600°C.

Mixtures of the component pair $LiF\text{-}BeF_2$ are obtainable which appear to meet most of the required characteristics. The eutectic mixtures in this binary system melt at 355°C.[2] A preliminary study of the ternary system $LiF\text{-}BeF_2\text{-}AlF_3$ indicated that the capacity of this solvent for $AlF_3$ at 600°C was ~31 wt % $AlF_3$.

Within the ternary system $LiF\text{-}BeF_2\text{-}AlF_3$, aluminum crystallizes only as the intermediate compound $3LiF \cdot AlF_3$ and as the component $AlF_3$. A preliminary phase diagram of the system is shown in Fig. 28.1. The phase diagram is comprised of the two subsystems $LiF\text{-}3LiF \cdot AlF_3\text{-}BeF_2$ and $3LiF \cdot AlF_3\text{-}BeF_2\text{-}AlF_3$. The compound $3LiF \cdot AlF_3$ forms a quasibinary system with $BeF_2$, with a temperature maximum of 337°C at 60 mole % $BeF_2$ (Fig. 28.2). Liquidus temperatures along the composition section $2LiF \cdot BeF_2\text{-}AlF_3$ appear to fall below 600°C for all concentrations of $AlF_3$ lower than ~25 wt %.

Laboratory studies by the ORNL Chemical Technology Division, in which tests of the dissolution rates of aluminum by HF in the solvent mixture $LiF\text{-}BeF_2$ were conducted, indicated that the rates were markedly reduced as the $AlF_3$ concentration increased. It is believed that a large fraction of the fluoride in molten mixtures having compositions near those of the solvent mixture $LiF\text{-}BeF_2$ (67-33 mole %) is present as complex ions such as $BeF_3^-$ and $BeF_4^{2-}$. Measurements of such properties as vapor pressure and electrical conductivity in cryolite-like melts indicate that $AlF_3$ tends to complex fluoride ions as $AlF_6^{3-}$. Thus, as the aluminum fluoride dissolves in molten mixtures of fluorides, additional species compete for nonassociated fluoride ions. Shaffer and Watson[3] showed that the Henry's law constants for the solubility of HF in molten fluoride mixtures were distinctly composition dependent. As aluminum ions reduce the free-fluoride ion concentration, HF is expected to become less soluble, and, accordingly, in poorly stirred dissolution

[1]Summer employee, 1962.

[2]C. J. Barton, L. M. Bratcher, and W. R. Grimes, *Phase Diagrams of Nuclear Reactor Materials*, ORNL-2548 (Nov. 6, 1959), pp 14, 33, 56.

[3]*Reactor Chem. Div. Ann. Progr. Rept. Jan. 31, 1960*, ORNL-2931, p 31.

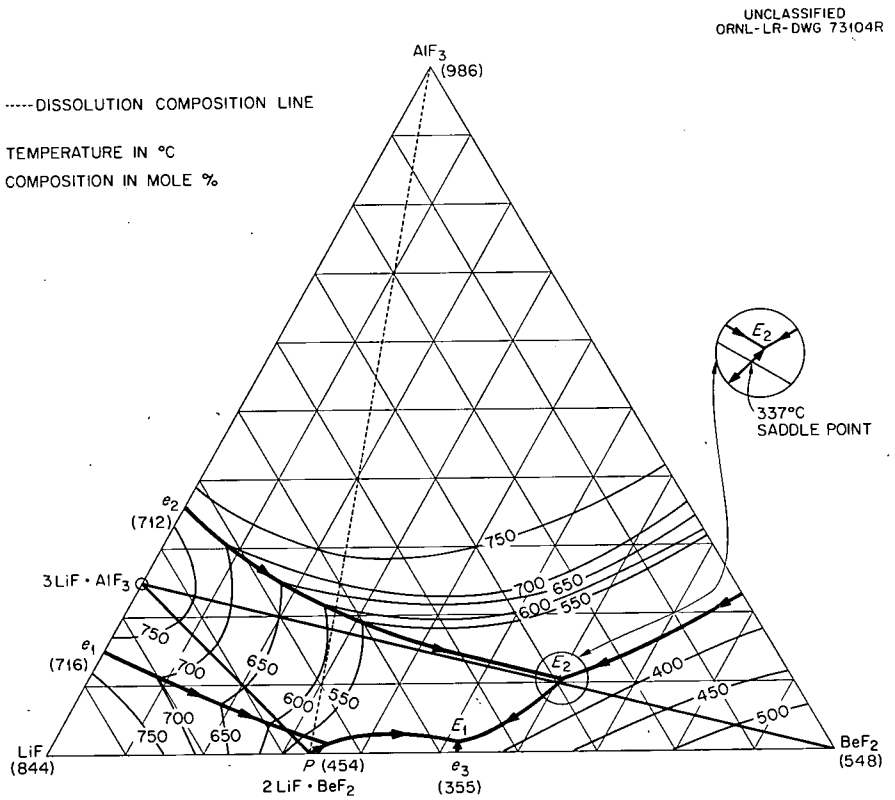


**Fig. 28.1. The System $LiF\text{-}BeF_2\text{-}AlF_3$.**

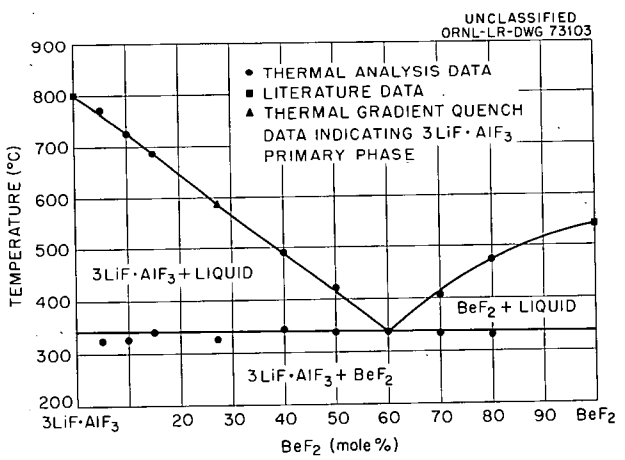


**Fig. 28.2. The Quasibinary System $3LiF\cdot AlF_3\text{-}BeF_2$.**

tests, the $H^+$ would be less available to the surface. On the basis of these concepts, additional investigations of other fluoride systems are planned.

In conjunction with this investigation, two types of new equipment have been utilized, differential-thermal-analysis apparatus and visual-polythermal-analysis apparatus. Using the latter apparatus, observations are made of the freezing-melting reactions taking place in the molten mixtures protected from contamination by an inert gas blanket. Cooling-curve data are obtained concurrently. Equipment for conducting differential thermal analysis of $AlF_3$-based fluoride mixtures was designed, constructed, and calibrated. Determinations were made of solid-state and liquid-solid phase transitions at temperatures as high as 1000°C. Provision was made to stir the molten mixtures. Calibration of the apparatus against a known solid-state transition in $SiO_2$ showed that the transition could be detected with an accuracy of ±1°C. With this apparatus, a solid-state transition in $AlF_3$ was detected at 448°C (reported as 454°C by O'Brien and Kelley[4]), and the technique was judged to be appropriate for use with the aluminum-based systems of interest.

---

[4]C. J. O'Brien and K. K. Kelley, *J. Am. Chem. Soc.* **79**, 5616 (1957).

# 29. Radioiodine-Adsorption Systems for the NS "Savannah"

W. E. Browning, Jr. R. E. Adams W. M. Johnson

The NS "Savannah" presents a rather unique nuclear hazards problem because of its mobility and its international aspects. Two compartment ventilation systems are provided in order to assure positive control of radioactive iodine vapor and particulate matter which may be released from the reactor by accident and leak into the reactor compartment. The normal ventilation system has a 4000-cfm capacity with provisions for processing the gases through three cleaning stages: roughing and high-efficiency filters for control of particulate material and silver-plated copper-mesh units for iodine control. An auxiliary or emergency system of 200-cfm capacity is provided with five stages of gas cleaning. The ventilation gases are passed through (1) a prefilter, (2) a high-efficiency filter, (3) a silver-plated copper-mesh bed, (4) an activated-charcoal unit, and (5) a second silver-plated copper-mesh bed. This system serves as a backup to the normal system and does not operate continuously.

While the information available at the time of design of this system was sufficient to demonstrate the feasibility of using activated charcoal for the removal of iodine vapor from moist air at elevated temperatures, it was not sufficient to ensure that the full-scale units as designed for the NS "Savannah" would provide the required iodine-removal efficiency under conditions that could occur following a reactor emergency involving fission-product release. Accordingly, an experimental program was undertaken to determine the iodine efficiency that may be expected of the activated-charcoal unit installed aboard the NS "Savannah" and to evaluate other iodine problems revealed by the primary study. Initial results have been reported.[1]

## LABORATORY IODINE STUDIES

The laboratory studies are divided into two parts. Small-scale tests are being conducted on 10-g samples of activated charcoal to determine the iodine-adsorption efficiency under stated operating conditions. This phase of the study is intended to provide quantitative or semiquantitative information as to the behavior of various types of charcoal at design and off-design conditions. To date, 60 tests have been completed on four types of charcoal (including Pittsburgh BPL, which is used in the full-scale units) under various temperature and humidity conditions. The activated-charcoal samples tested have exhibited both normal and abnormal penetration of iodine. Variations in the environmental conditions of the laboratory, conditions of operation of the experiments, materials used in construction of the experimental apparatus, and the iodine vapor sources may, either singly or in combination, be responsible for this behavior. These possible causes of this rather unpredictable penetration of iodine are under experimental study.

The second part of the laboratory study involves the testing of iodine-adsorption units, 11 × 11 in. by 1.125 in. thick, produced by Flanders Filters, Inc. These units, containing Pittsburgh BPL charcoal, were manufactured using the same materials and techniques as those used in producing the full-scale iodine unit installed aboard ship. The experimental apparatus for these tests is illustrated in Figs. 29.1 and 29.2. The system is

[1] W. E. Browning, Jr., R. D. Ackley, and R. E. Adams, *Reactor Chem. Div. Ann. Progr. Rept. Jan. 31, 1962*, ORNL-3262, pp 177–79.

constructed of 4-in.-diam glass pipe with metal pieces making the transition to the 11 × 11 in. filter unit. The system is heated, externally, by flexible heating tapes to prevent premature condensation of steam on the walls of the system. This heated zone terminates at point *B*, Fig. 29.1. Beyond this point, efforts are made to condense the steam for recovery of iodine. A typical test involves the following operations. Iodine vapor ($I^{127}$ containing radioactive $I^{131}$) is introduced continuously into the air-steam mixture passing into the system. Iodine vapor escaping from the iodine-adsorption unit under test is collected downstream by the condensate, which is drained periodically from the system, on small rings comprising the steam-condenser column packing or in the two room-temperature charcoal adsorbers. During operation, a small portion of the steam–air–iodine vapor mixture is passed through samplers, located upstream and downstream from the test unit. After completion of the test, the system is cooled, completely drained, and disassembled. The iodine-adsorption efficiency of the unit under test is then determined by radiochemical assay of the system from point *A* to point *C* (Fig. 29.1) as indicated. By comparing the amount of iodine residing in the test unit with the total amount found in the test unit, in all downstream components, and in condensates, an iodine-adsorption efficiency is obtained. In addition, an iodine-adsorption

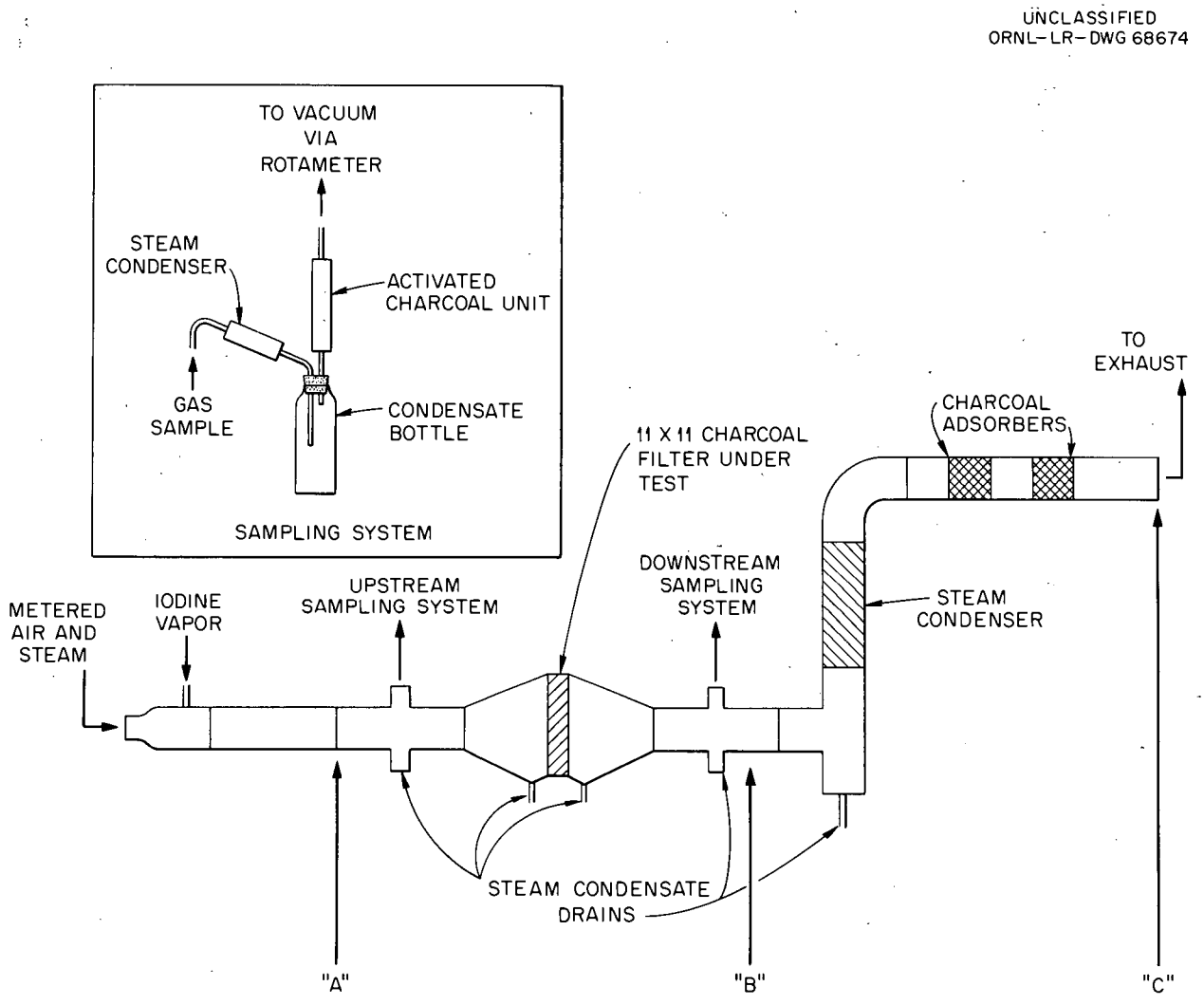


**Fig. 29.1. Iodine-Adsorption Testing System for 11 × 11 in. Charcoal Units – NS "Savannah" Project.**

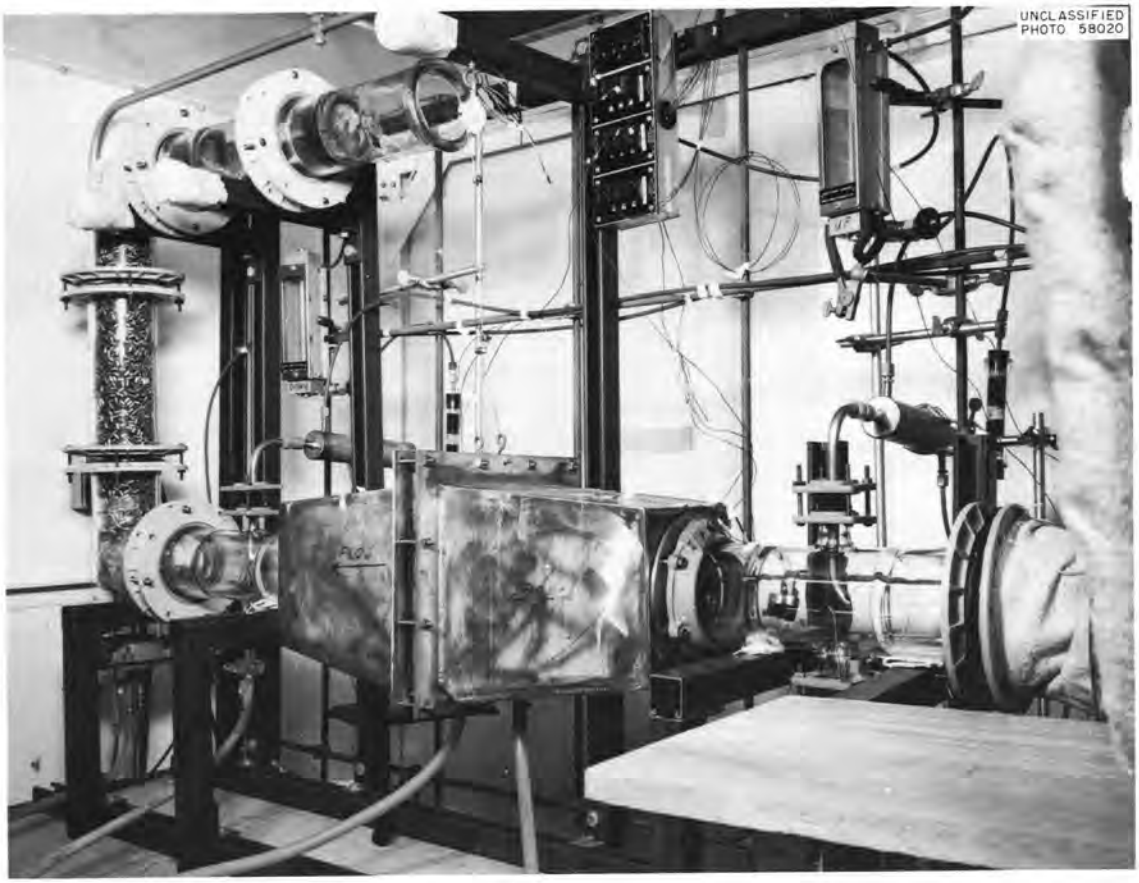


Fig. 29.2. Iodine-Adsorption Testing System Before Installation of Heaters and Insulation.

efficiency is calculated from the data obtained by the two analytical samplers. Allowances for the observed deposition of iodine on the walls of the system are made in calculating this efficiency. Details and results of 14 tests on the 11 × 11 in. iodine filter units are contained in Table 29.1. These tests, conducted with continuous iodine injection at 96 to 100°C and with 80 to 90% saturated steam in air, have shown the efficiency of the charcoal unit alone to be (99.86 ± 0.07)% at the 95% confidence level. Eleven of the tests were of 12 hr duration while three were continued for 24 hr. No significant duration effect was noted.

## RADIOIODINE TESTS ON BOARD NS "SAVANNAH"

In-place tests were conducted on the NS "Savannah" reactor-compartment emergency ventilation system to determine whether the installation of the adsorber unit would permit the efficiency of the adsorbent medium itself to be achieved. The charcoal adsorbers were installed in the emergency ventilation system on December 15, 1961, and were operated only intermittently for testing and system adjustment up to May 27, 1962, the time of the first in-place tests. Prior to installation they were subjected to two Freon penetration tests at the Edgewood Army Chemical Center and a stable-iodine penetration test at Armour Research Foundation. In the latter test, 200 g of iodine was adsorbed.

Elemental iodine labeled with $I^{131}$ tracer was injected into the duct leading from the reactor compartment to the filter-adsorber assembly for the in-place tests. Samples of air before and after this assembly were passed through charcoal traps which were then radioassayed. The iodine was injected over a 15-min period and the test was continued for 2 hr at the ambient temperature of the

**Table 29.1. Iodine-Removal Efficiency Tests on 11 × 11 in. Charcoal Adsorbers**

| Run Number | Temperature (°C) | Face Velocity (fpm) | Steam Saturation (%) | Iodine-Removal Efficiency (%) | |
|---|---|---|---|---|---|
| | | | | Inventory | Sampling |
| 1 | 96 | 4.6 | 91.3 | 99.84 | 99.93 |
| 2 | 100 | 4.3 | 80.7 | 99.63 | 98.95 |
| 3 | 26 | 4.8 | | 99.98 | 99.86 |
| 4 | 99 | 4.5 | 83.8 | 99.95 | 98.57 |
| 5 | 100 | 4.4 | 82.1 | 99.73 | |
| 6 | 98 | 4.8 | 88.9 | 99.67 | 99.50 |
| 7 | 99 | 4.5 | 85.2 | 99.95 | 99.12 |
| 8 | 99 | 4.8 | 86.3 | 99.95 | 97.38 |
| 9 | 98 | 4.8 | 89.0 | 99.86 | 98.04 |
| 10 | 99 | 4.7 | 86.1 | 99.90 | 97.84 |
| 11[a] | 100 | 4.7 | 83.4 | 99.90 | 99.43 |
| 12 | 98 | 5.0 | 89.6 | 99.83 | 99.38 |
| 13[a] | 98 | 4.9 | 88.6 | 99.95 | 99.56 |
| 14[a] | 98 | 4.9 | 89.3 | 99.72 | 95.00 |
| | | | | Mean 99.86 ± 0.07 | 98.66 ± 0.82 |

[a]Twenty-four-hour test; all other tests 12 hr.

reactor compartment. Earlier laboratory tests showed that, at room temperature in air, no movement of iodine in the charcoal trap is observed after the initial injection. No radioiodine was found downstream from the adsorber within the limits of detection. Two tests were conducted using different amounts of tracer, and the limits of sensitivities were such that 1/1400 and 1/15,000, respectively, of the iodine collected upstream could have been detected in the downstream collector. This corresponds to efficiencies of >99.93 and >99.99%. These tests indicate that the charcoal adsorber assembly, as installed, is capable of achieving the iodine-removal efficiency observed in laboratory tests.

A similar in-place efficiency test was conducted on the main reactor-compartment ventilation system. The silver-plated copper-mesh iodine adsorber was installed on December 14, 1961, and it was operated almost continuously up to the time of the in-place test. In this test two downstream iodine collectors were used, one immediately following the air-cleaning assembly, and the other on the deck of the ship at the base of the stack. Approximately the same amounts of iodine were found in the two downstream collectors. Comparison of this amount with that found in the upstream collector yielded an efficiency of 95%. This result is consistent with laboratory tests on silver-plated mesh in air at room temperature.

The second series of in-place tests was conducted on August 15–16, 1962. Test procedures and equipment used were identical to those in the initial tests and the iodine efficiency of the emergency ventilation system was determined to be 99.7%. The distribution of iodine radioactivity on the components of the downstream sampler suggested strongly that the iodine was predominantly associated with particulate matter. The distribution of activity in the upstream sampler was indicative of iodine in the vapor state. This behavior is contrary to that observed during the

initial in-place tests of May 1962. Strict comparison of these efficiency values may be subject to question since modifications were accomplished on the emergency system shortly before the test.

In a similar manner, an efficiency test was conducted on the main reactor-compartment ventilation system in the manner described above. The efficiency was found to be between 90 and 95%, based on the $I^{131}$ radioactivity found in the two downstream samplers. This is consistent with the 95% efficiency determined in the initial in-place test and results obtained in laboratory tests on silver-plated mesh in air at room temperature.

The emergency ventilation system was tested again in September and November 1962; efficiencies comparable to those of the initial series of tests were obtained. Overall behavior of these tests was identical to that of the initial series at Yorktown, Virginia, during May 1962. These tests are summarized in Table 29.2.

## DEVELOPMENT OF IN-PLACE TEST USING STABLE IODINE

A method of determining the efficiency of an iodine-removal system, in-place, using normal iodine is of considerable interest for application to the ventilation systems on the NS "Savannah." Normal iodine is preferable to $I^{131}$ tracer for in-place tests because of the elimination of risk of contaminating the ship. Tests using $I^{131}$ have had to be performed while the ship was in a relatively unpopulated harbor or at sea, and these tests have often interfered with the operating schedule of the ship. While the ship is in any harbor or while it is carrying passengers, tests using normal iodine could be performed without risk to the population.

Two series of in-place efficiency tests using normal iodine were carried out on September 11, 1962. Approximately 1.5 g of elemental iodine

**Table 29.2. In-Place $I^{131}$ Tests – NS "Savannah"**

| Ventilation System | Flow Rate (cfm) | $I^{131}$ Injected (mc) | $I^{127}$ Injected (mg) | Decontamination Efficiency (%) |
|---|---|---|---|---|
| **Initial Tests – May 1962 – Yorktown, Va.** | | | | |
| Emergency | 200[a] | 5 | 1–2 | >99.93 |
| Emergency | 200[a] | 15 | 1–2 | >99.99 |
| Main | 4000 | 5 | 10 | 95 |
| **Second Series – August 1962 – Yorktown, Va.** | | | | |
| Emergency | 200[a] | 15 | 2 | 99.7 |
| Main | 4000 | 5 | 10 | 90–95 |
| **Third Series – September 1962 – Norfolk, Va.** | | | | |
| Emergency | 200[a] | 15 | 2 | >99.99 |
| Emergency | 200[a] | 15 | 2 | 99.99 |
| **Fourth Series – November 1962 – Seattle, Wash.** | | | | |
| Emergency | 200[a] | 7 | 3 | 99.97 |
| Emergency | 200[a] | 7 | 3 | >99.97 |
| Main | 4000 | 2.5 | 10 | 98.6 |

[a]System under emergency mode of operation with maximum off-gas dilution; all tests of 2-hr duration.

vapor was injected into the intake duct leading from the compartment into the five-stage filter unit of the emergency ventilation system. Samples of the air stream before and after the filter unit were taken during the 2-hr test. Similar samples were taken for a 2-hr period prior to injection of the iodine vapor. The samplers from these tests were returned to Oak Ridge and analyzed for iodine content by activation analysis. Each of the samplers from the background test contained approximately 0.5 $\mu g$ of iodine. This amount agrees with the amount of iodine found in samples of the charcoal which was not exposed to the air in the ship. Iodine-removal efficiencies greater than 99.99% were obtained in these two tests. These results compare favorably with efficiencies of 99.99 and 99.99+% obtained using $I^{131}$ on the night of September 12–13, 1962 (Table 29.2).

The second series of tests at Seattle, Washington, on November 8–9, 1962, included the main reactor-compartment ventilation system. The amount of iodine present in the background samples, while larger than desired, has not interfered greatly with the sensitivity of the test procedure. Assuming that the iodine found in the downstream samplers resulted primarily from actual iodine penetration, then iodine efficiencies greater than 99.9% were measured for the emergency system. For test of the main ventilation system, a second downstream sampler was installed on deck at the base of the off-gas stack. Efficiencies determined by the three samplers compare favorably with an efficiency of 98.5% determined by $I^{131}$ tests. A summary of these tests appears in Table 29.3.

To date, the correspondence between the $I^{127}$ and the $I^{131}$ tests has been acceptable. However, additional experience should be obtained before placing full reliance on this testing method. Further development of certain phases of the testing procedure and slight modifications of the sampling equipment also appear desirable.

## DEVELOPMENT OF ENVIRONMENTAL MONITORING CARTRIDGE

Environmental monitoring for the presence of radioiodine in the various compartments of the ship is accomplished by passing a measured

**Table 29.3. In-Place $I^{127}$ Tests[a] – NS "Savannah"**

| Ventilation System | Amount $I_2$ Injected (mg) | Amount $I_2$ Collected ($\mu g$) | | | Efficiency (%) | |
|---|---|---|---|---|---|---|
| | | Up | Down | Stack | Up/Down | Up/Stack |
| **Initial Tests – September 1962 – Norfolk, Va.** | | | | | | |
| Emergency | 0 | 0.6 | 0.5 | | | |
| Emergency | 1600 | 15,500 | 0.5 | | >99.99 | |
| Emergency | 1200 | 10,700 | 0.9 | | >99.99 | |
| **Second Series – November 1962 – Seattle, Wash.** | | | | | | |
| Emergency | 0 | 1.22 | 3.71 | | | |
| Emergency | 1440 | 6,330 | 0.25 | | >99.99 | |
| Emergency | 1590 | 7,700 | 3.73 | | >99.95 | |
| Main | 0 | 4.10 | 0.90 | 4.79 | | |
| Main | 1490 | 683 | 10.1 | 6.16 | 98.5 | 99.1 |
| Main | 1320 | 636 | 18.3 | 5.94 | 97.1 | 99.1 |

[a]Emergency system, 200 cfm; main system, 4000 cfm; test duration, 2 hr.

volume of air through an activated-charcoal cartridge and determining the iodine radioactivity in the cartridge by use of one of several types of radiation detection instruments. High-volume air flow and small sample size are necessary operational features; therefore, high linear gas velocities exist in the charcoal mass. Twelve experimental tests have been completed under conditions of low mass concentration of iodine in the air and high linear gas velocity. With linear gas velocities of 295 fpm and iodine concentrations of the order of 1 $\mu g/m^3$, efficiencies consistently greater than 90% were obtained for Pittsburgh PCB charcoal, −6 +16 mesh, in depths of 1.75 in. for a 45-min test period. The average efficiency under these conditions was 97.4%. Efficiencies in this range of values are considered adequate for environmental monitoring purposes.

# 30. Effects of Radiation and Heat on Organic Materials

The acid concentration produced by irradiation of solutions of $C_2H_2Cl_4$ in $C_8F_{16}$ and in $C_{10}H_{22}$ has been measured to determine the suitability of these systems as dosimeters. The $C_8F_{16}$ solutions, to which 0.3 wt % $C_{10}H_{22}$ had been added to provide an adequate source of hydrogen, showed inconsistent acid yields unless water in excess of saturation concentration (0.2 wt %) was present. The $C_{10}H_{22}$ solution showed a dependence on both the temperature and the dose rate during irradiation.

Studies designed to obtain a better understanding of the mechanisms of the pyrolytic and the radiolytic decomposition of organic coolants used in reactors were performed. Pure biphenyl was pyrolyzed at 425°C under conditions that permitted less than 1% decomposition to occur. The decomposition products were separated in a vacuum system into three fractions having different boiling ranges which were analyzed by use of gas chromatography. A silica gel column in series with a molecular sieve (Linde 5A) column showed the presence of hydrogen, methane, ethane, propylene, ethylene, and propane in the gaseous products, with hydrogen being the major component. Benzene was identified as the lone intermediate-boiling component, using a column of 30 wt % Apiezon L on Chromosorb P. Terphenyl and quaterphenyl isomers comprised the high-boiling or polymeric fraction. They were identified by means of an inorganic-salt column, 20 wt % LiCl on Chromosorb P. The data indicate that the pyrolytic decomposition of biphenyl proceeds essentially by symmetrical splitting of the biphenyl molecule to form phenyl radicals which either (1) add hydrogen to form benzene or (2) react with other biphenyl molecules to produce terphenyls, quaterphenyls, and hydrogen.

The investigation of differences in the effects of gamma radiation and mixed reactor radiation on polystyrene was extended by employing infrared and gas-chromatographic analyses. Infrared spectrum measurements showed more rapid growth of certain bands in reactor-irradiated specimens than in specimens exposed to gamma radiation alone. The volatile products of gamma irradiation of polystyrene were indicated by gas chromatography to be benzene and hydrogen. The hydrogen yield, $G(H_2)$, was measured to be ~0.015 molecule per 100 ev. The evolution of benzene from irradiated polystyrene was found to be incomplete after 5 to 7 hr at 100°C.

A technique was developed for preparation of infrared specimens of polybutadiene by x-ray curing of films cast from $CS_2$ solution on mercury or on glass. The infrared absorption of the peaks characteristic of *cis* and *trans* olefin groups in polybutadiene and simple hydrocarbons was measured as a function of concentration of olefin.

A versatile gamma source comprising a $Co^{60}$ assembly in a 7 × 10 ft shielded compartment has been designed for the irradiation of plastics and rubbers during mechanical testing.

## RADIATION DOSIMETRY

C. D. Bopp
W. K. Kirkland
O. Sisman
W. W. Parkinson

The use of mixtures of a hydrocarbon with halogenated compounds to measure radiation dose by means of the hydrogen ion production was described earlier.[1] By selection of mixtures having the minimum and the maximum hydrogen content, it should be possible to prepare dosimeters sensitive only to gamma radiation in the first case and

[1]C. D. Bopp *et al.*, *Solid State Div. Ann. Progr. Rept. Aug. 31, 1961*, ORNL-3213, p 101.

sensitive to both gamma and fast neutrons in the second case.

A solution of low hydrogen content consisting of 0.3 wt % $C_{10}H_{22}$ and 0.3 wt % $C_2H_2Cl_4$ in $C_8F_{16}$ would receive no more than 5% of its total dose from interaction with neutrons when exposed to the flux of most reactors. This mixture gave hydrogen ion yields of poor reproducibility in a series of irradiations in a gamma source. The variation in yields apparently resulted from variations in moisture condensed in the solution by the chilling process employed during evacuation and sealing of the containers. Efforts to reduce water contamination did not improve the reproducibility of yields. On the other hand, the introduction of water slightly in excess of the saturation value resulted in consistent yields. Since the solubility of water in the mixture is low, the added water does not increase the interaction with fast neutrons appreciably. The acid produced in wet dosimeter mixtures with about 0.002 g of water per gram of solution is plotted in Fig. 30.1.

Solutions of 0.3 wt % $C_2H_2Cl_4$ in $C_{10}H_{22}$ were prepared for use as a dosimeter solution sensitive to both fast neutrons and gamma radiation. Specimens were irradiated in gamma sources at two intensities and temperatures to measure the dependence on dose rate and on temperature. The hydrogen ion (acid) yields are shown in Fig. 30.2. The high yields at 80°C indicate that, in the reaction mechanisms of acid production, there is at least one rate-controlling process which is temperature dependent, perhaps a diffusion process or an atomic abstraction step. The lower yield at high intensity suggests that, in the overall reaction, there is a step which destroys an active species without producing hydrogen ions, and which is bimolecular and hence intensity dependent. The data in Fig. 30.2 also show that acid production is not linear with dose beyond yields of 0.02 meq/g.

These intensity- and temperature-dependent steps are probably inherent in the acid-production reactions in a hydrocarbon solvent. The possibility of altering the acid-production reactions was investigated by adding water and ethanol to the dosimeter solution. Sufficient ethanol was added to make up 21.1 wt % of the solution to permit dissolving 0.21 wt % of water. The resulting dosimeter solution (78.4 wt % $C_{10}H_{22}$, 21.1 wt % $C_2H_5OH$, 0.24 wt % $C_2H_2Cl_4$, and 0.21 wt % $H_2O$) has been irradiated at three temperatures, and the acid production is plotted in Fig. 30.3. The results demonstrate that the addition of ethanol and water does not eliminate the dependence on temperature, nor does it improve the linearity of acid production with dose.

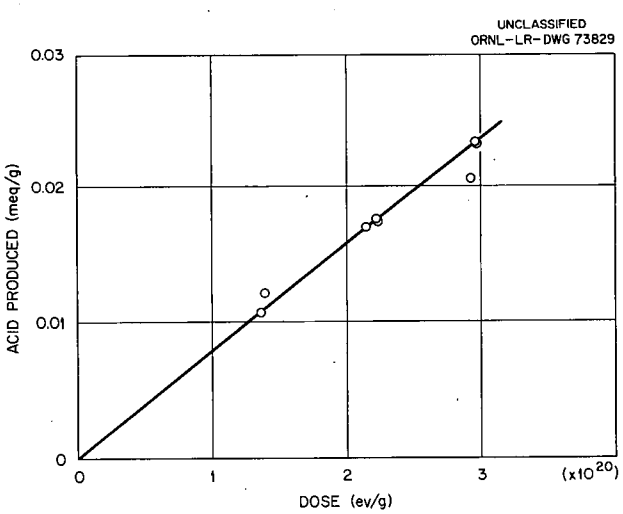


Fig. 30.1. Acid Production in Wet $C_8F_{16}$-$C_{10}H_{22}$-$C_2H_2Cl_4$.

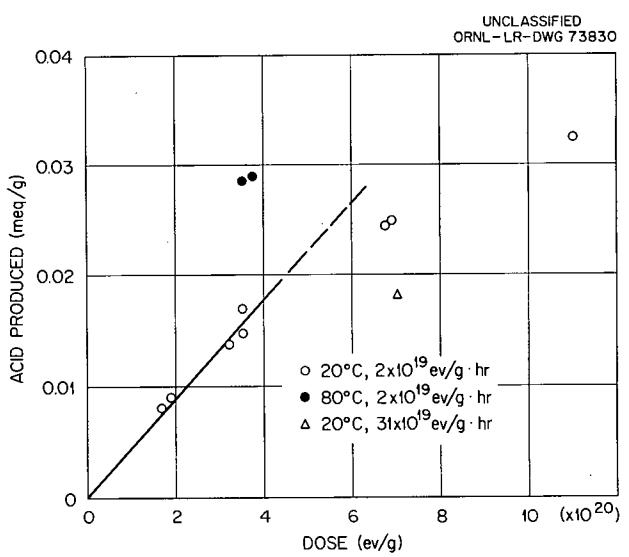


Fig. 30.2. Acid Production in $C_{10}H_{22}$-$C_2H_2Cl_4$.

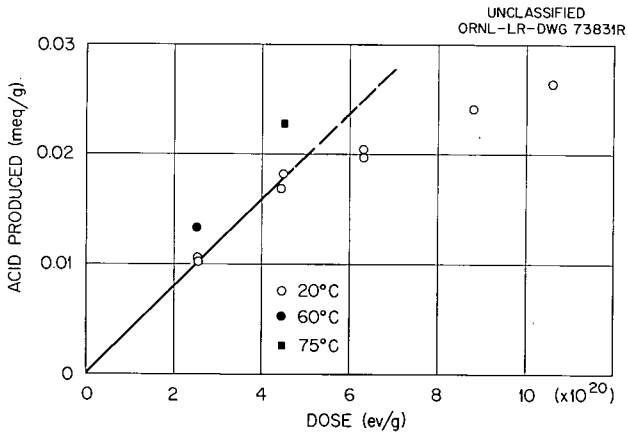


Fig. 30.3. Acid Production in $C_{10}H_{22}$-$C_2O_5OH$-$C_2H_2Cl_4$-$H_2O$.

## EFFECTS OF RADIATION ON POLYMERS

W. W. Parkinson W. K. Kirkland
R. M. Keyser O. Sisman

### Differences in the Effects of Gamma and Reactor Radiation on Polystyrene

Previous measurements[2] demonstrated that, for equal energy deposition, the mixed gamma radiation and neutrons of the ORNL Graphite Reactor produced 2.4 times as many cross links in polystyrene as gamma radiation alone. Other workers have found that energetic particles and gamma radiation produce about the same effects in simple aliphatic hydrocarbons.[3,4] Recently developed evidence indicates that in aromatic liquids, product yields differ for heavy particles (e.g., neutrons and alphas) and gamma radiation.[5,6] Therefore, it is desirable to investigate the differences in molecular structure and in the volatile radiolysis products from polystyrene resulting from irradiation in a gamma source and in a reactor. Radiation-induced changes in the molecular structure of polystyrene are indicated by comparison of infrared spectra obtained before and after irradiation. The volatile radiolysis products are being analyzed by gas-chromatographic methods.

### Infrared Analysis

Polystyrene films of about 0.001-, 0.002-, and 0.004-in. thickness have been irradiated up to doses of $2.5 \times 10^{23}$ ev/g in a water-cooled $Co^{60}$ gamma source and in the ORNL Graphite Reactor. Measurements of infrared spectra show that there is a loss of phenyl groups, indicated by the reduction in the C-H stretching bands of the aromatic ring at 3088 and 3065 $cm^{-1}$, and by the reduction in aromatic C-H bending modes at 1030 and 905 $cm^{-1}$. The reduction in these bands after $2.5 \times 10^{23}$ ev/g amounts to about 10% of the original optical density, but it is not large enough to show, conclusively, differences between reactor irradiation and gamma irradiation.

New bands appear at 865, 820, and 675 $cm^{-1}$, and these peaks show a greater increase for reactor irradiation than for gamma irradiation. The 865 and 820 bands have not been identified with a definite molecular species, but the 675 band corresponds very closely to the 671-$cm^{-1}$ band for out-of-plane C-H bending in benzene.[7] This band also has about the same frequency as a similar bending mode (680 to 740 $cm^{-1}$) in *cis* olefin groups. The narrow width of the band, however, resembles more closely the sharp benzene band than the broad band of the olefin group.

The reduction in phenyl groups could result from rupture of the aromatic ring to form olefinic side chains. Reduction of phenyl groups could also result from breakage of the bond between the main chain and the benzene ring, followed by evolution of benzene. The latter possibility is suggested by the reduction in the 675-$cm^{-1}$ band observed in irradiated specimens after they had stood in air for several weeks. Further investigation will be carried out by measurement of the 675- and 1030-$cm^{-1}$ bands after heating irradiated specimens under vacuum. The 1030-$cm^{-1}$ band is attributed to a C-H bending mode of the aromatic ring of both benzene and polystyrene.

[2] W. W. Parkinson *et al.*, *Solid State Div. Ann. Progr. Rept. Aug. 31, 1961*, ORNL-3213, p 92.

[3] H. A. Dewhurst and R. H. Schuler, *J. Am. Chem. Soc.* **81**, 3210 (1959).

[4] A. E. DeVries and A. O. Allen, *J. Phys. Chem.* **63**, 879 (1959).

[5] W. G. Burns, W. Wild, and T. F. Williams, *Proc. U.N. Intern. Conf. Peaceful Uses At. Energy, 2nd, Geneva, 1958* **29**, 266 (1958).

[6] T. Gaumann and R. H. Schuler, *J. Phys. Chem.* **65**, 703 (1961).

[7] N. Herzfeld *et al.*, *J. Chem. Soc.* **1946**, 272.

A marked difference between gamma- and reactor-irradiated samples is the rate of oxidation upon exposure of the samples to air after irradiation. The growth of infrared bands at 3400 and 1710 $cm^{-1}$, characteristic of the $-OH$ and $>CO$ groups, respectively, is an indication of oxidation rate. These bands are negligible in samples which have received $2.5 \times 10^{23}$ ev of gamma radiation per gram. In contrast, samples receiving equivalent doses of mixed reactor radiation show adsorptivities in these bands of 3 to 4 per cm of thickness after 45 days in air.

## Gas-Chromatographic Analysis

Samples of polystyrene were irradiated for doses up to $1.8 \times 10^{23}$ ev/g in a water-cooled $Co^{60}$ source having a dose rate of $3 \times 10^{20}$ ev $g^{-1}$ $hr^{-1}$. The retention characteristics of the gas-chromatographic columns made it necessary to separate the volatile products into condensable and noncondensable fractions before analysis. This was accomplished by transferring the products through a detachable U-shaped trap immersed in liquid nitrogen and into a Toepler pump. After irradiation all samples were annealed for 4 hr at a temperature of 100°C or higher before being opened and were maintained at elevated temperatures during transfer of radiolysis products to reduce the solubility of gaseous products in the polystyrene.

The noncondensable fraction was collected in the Toepler pump, where its volume was measured. Gas-chromatographic analysis, using a Perkin-Elmer model 154 vapor fractometer with a thermal-conductivity detector and a silica gel column, revealed that the noncondensable fraction consisted of hydrogen with trace amounts of methane too small to measure. The Toepler pump therefore afforded a convenient means of measuring the amount of radiation-produced hydrogen in each sample. Hydrogen yields as a function of radiation dose are presented in Fig. 30.4. If a linear dependence of hydrogen yield on radiation dose is assumed, then the *G* value for hydrogen production (molecules of $H_2$ produced per 100 ev of energy absorbed) is 0.016 over the dose range investigated.

The condensable fraction was introduced into the chromatograph and was found to consist of benzene along with very small amounts of higher-boiling compounds. The identification was carried

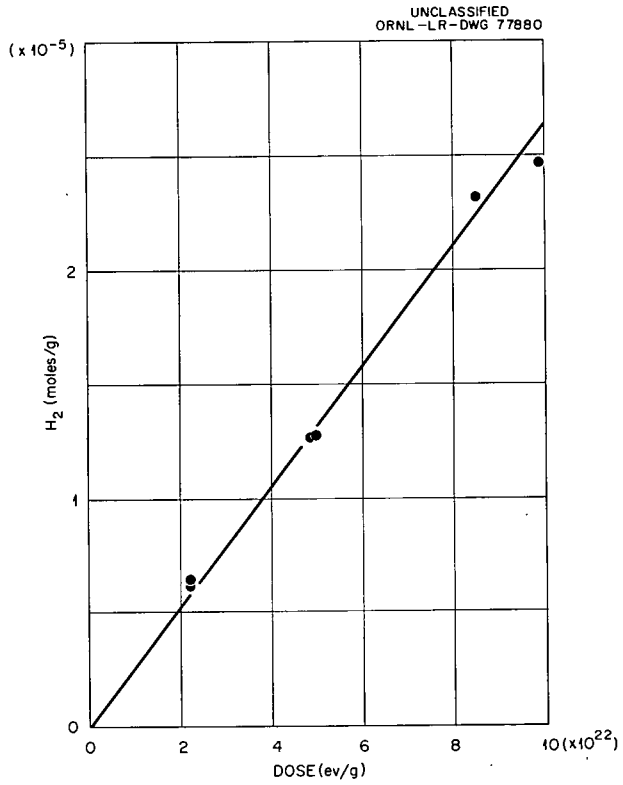


**Fig. 30.4. Radiation Yield of Hydrogen from Polystyrene.**

out by comparing the retention times of benzene with those of the unknown peak in two separate analyses: one on a column of didecyl phthalate on Celite and the other on a column of triphenyl phosphate on Celite. Furthermore, infrared spectra of the effluent from the chromatograph were identical with that of pure benzene. Calibration of the chromatograph in terms of the peak height resulting from a known quantity of benzene allowed a quantitative determination of the benzene. The system shown in Fig. 30.5 was assembled for introducing small, known amounts of benzene vapor into the chromatograph for calibration. The apparatus consists of a reservoir of benzene maintained at a temperature of 20.00 ± 0.05°C, a gas buret, a mercury manometer, and a detachable U-shaped trap. Benzene vapors were allowed to expand into a known volume in the gas buret, the vapor pressure was measured, and the vapor was condensed into the trap with liquid nitrogen. The ideal gas law was found to be sufficiently accurate for calculating amounts of benzene introduced into the chromatograph. The trap was then removed from the system and attached to the chromatograph,

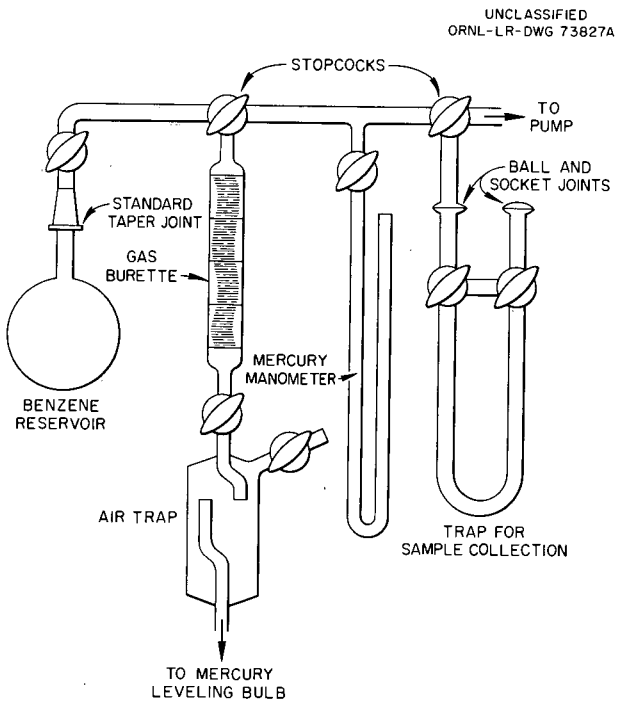


**Fig. 30.5. Apparatus for Transferring Known Amounts of Benzene Vapor.**

and the contents were flushed into the column with the carrier gas.

A water-soluble grease was used as a stopcock lubricant, since most hydrocarbon-base greases exhibited considerable absorption of benzene vapors. With the use of this grease and the system described, it was possible to introduce known amounts of benzene into the chromatograph with a reproducibility within 2% or better in the range of 1 to 15 micromoles.

Although benzene is a common impurity in polystyrene, the measured benzene yields were shown to be an actual radiation product from two observations: (1) the benzene evolved increased with dose and (2) no detectable amounts of benzene were obtained when unirradiated polystyrene was heated in exactly the same fashion as irradiated specimens. The possibility that benzene arises from the action of radiation on impurities in the polystyrene cannot be entirely discounted, but the high yields at the higher doses in comparison with the expected level of impurities make this process unlikely.

A preliminary tabulation of benzene yields was presented in an earlier report,[8] based on evaluation of product during postirradiation heating at 100°C. Subsequent measurements of yields evolved by heating to 180°C have shown that a major portion of the benzene was not evolved from the sample (pellets about 2 × 2 × 4 mm) during heating at 100°C for 5 to 7 hr. The hydrogen yields were not affected by the differences in postirradiation sample-collection temperatures.

The greater yields of benzene at the higher sample-collection temperatures could arise from either slow, temperature-dependent diffusion of benzene from the interior of the pellets or from increased thermal decomposition of free radicals. However, the latter process seems rather unlikely in view of the fact that Florin *et al.*[9] found that the intensity of the electron-spin-resonance spectra of trapped free radicals decreased 30% after only 15 min at 75 to 80°C. These possibilities were investigated by comparing the rate of benzene evolution from pellets with that from finely powdered (40-mesh) specimens at a sample-collection temperature of 180°C. The rate of benzene evolution from the powder was significantly higher. Furthermore, as mentioned earlier, in infrared films of irradiated polystyrene the 675-$cm^{-1}$ band tentatively assigned to benzene decreased over a period of weeks at room temperature in air. Thus, it appears likely that the slow evolution of benzene is a diffusion-controlled process and is not dependent on thermal decomposition of radiation-produced free radicals.

## INFRARED STUDIES OF ELASTOMERS

Radiation-induced changes in the internal molecular configuration of plastics and elastomers influence the gross mechanical properties of these materials, although not as directly as do radiation-induced cross-linking and scission. These changes in molecular configuration can be observed by infrared absorption spectra. Measurements of the infrared spectra of natural and synthetic rubbers before and after irradiation have shown that radiation produces significant changes in the various

[8] W. W. Parkinson *et al.*, *Solid State Div. Ann. Progr. Rept. Aug. 31, 1962*, ORNL-3364, p 193.

[9] R. E. Florin, L. A. Wall, and D. W. Brown, *Trans. Faraday Soc.* **56**, 1304 (1960).

isomeric configurations and in the total concentration of the olefin group, $>C=C<$. Earlier reports[10] described a scheme for quantitative analysis of the olefin isomers by the determination of a relation between the absorption coefficient of the band characteristic of each isomer and its concentration.

Earlier work on polybutadiene, which contains olefin groups in at least three of the possible configurations of these groups, has been resumed. The preparation of polybutadiene samples has been improved by cross-linking (curing) the films by irradiation with low doses of 50-kev-peak x rays in a vacuum. Films having a thickness suitable for the specific absorption band under study can be obtained for x-ray curing by casting from a $CS_2$ solution on a mercury or glass surface.

Polybutadienes having various contents of the different olefin configurations show an absorption peak which appears in the frequency range 680 to 730 $cm^{-1}$. This peak is tentatively assigned to the *cis* olefin group, since simple olefinic hydrocarbons in the *cis* configuration show a characteristic peak varying through this frequency range.[11]

To investigate the connection between this peak and the unsaturated group, a high-*cis* polybutadiene and one having both *cis* and side-chain olefin groups were brominated by exposure to bromine vapor. In the high-*cis* polymer, the decrease in the optical density of the peak at 730 $cm^{-1}$ was roughly proportional to the increase in weight as the bromine was added to the unsaturated groups. In the latter polymer, in which the characteristic peak occurs at 680 $cm^{-1}$ with a small shoulder at 720, the peak height also decreased as weight increased. The decrease in these peaks as the olefin groups are destroyed by bromination indicates that the peak appearing in the 680- to 730-$cm^{-1}$ range does, indeed, arise from the *cis* olefin group. (The other configurations of the group give rise to peaks at frequencies above 800 $cm^{-1}$.) The variation in the frequency at which the peak appears can be explained as being caused by differences in the neighboring groups adjacent to the *cis* group.[11]

To establish the equations between absorption coefficient and concentration of the various olefin groups, spectral measurements have been made on several known hydrocarbon liquids in different concentrations in $CS_2$ solution. For the *cis* olefin group, the peak at 720 $cm^{-1}$ has been measured in *cis*-2-hexane, *cis*-3-hexane, and *cis*-2-pentene. For the *trans* olefin configuration, *trans*-2-hexane, *trans*-3-hexane, and *trans*-3-pentene were used in measurements of the peak at 965 $cm^{-1}$. The peak at 910 $cm^{-1}$ arising from terminal olefin groups ($-HC=CH_2$) is being measured in 1-octane and 3-methyl-1-pentene. The use of hexenes and pentenes instead of the octenes used in previous determinations of the absorption coefficients[10] permits extending olefin concentration to a range more closely approaching that encountered in polybutadiene and natural rubber.

## A VERSATILE GAMMA IRRADIATION FACILITY

In order to irradiate specimens of plastics and rubbers while mechanical properties are being measured over a broad range of temperatures, a source is required which has an intensity of at least $10^6$ r/hr, uniform over a region about 2 in. in diameter and 2 in. high, and with maximum accessibility above and around the intense-radiation region. To meet these requirements, a facility comprising a cobalt source in a shielded compartment 7 × 10 ft and 7 ft high has been designed. The shielded compartment is designed with concrete walls adequate for 20,000 curies of cobalt.

The source itself is composed of cobalt pellets enclosed in tubes to form cylindrical source assemblies. These assemblies are arranged vertically around a circle $2\frac{7}{16}$ in. in diameter to give a cylindrical source array. The source array is mounted on a screw jack by which the source can be retracted into a hole in the floor of the shielded compartment. A lead shielding plug is moved horizontally to close the storage hole when the source is lowered, thus permitting the arranging of specimens and apparatus in the compartment for irradiation.

## PYROLYSIS AND RADIOLYSIS OF BIPHENYL

W. T. Rainey, Jr. L. B. Yeatts, Jr.

In the development of organic-moderated and -cooled reactors, an extensive research effort at other laboratories was devoted to the selection of

[10] W. W. Parkinson *et al.*, *Solid State Div. Ann. Progr. Rept. Aug. 31, 1961*, ORNL-3213 p 93.

[11] L. J. Bellamy, *The Infrared Spectra of Complex Molecules*, 2d ed., p 48, Methuen, London, 1958.

satisfactory organic compounds for practical reactor operation. This "screening" effort included exposure of prospective moderator-coolants to relatively high temperatures and radiation, simultaneously. Fairly detailed data for this combined effect were obtained by in-pile experiments on mixtures of the terphenyl isomers and of these isomers plus biphenyl. These mixtures yielded numerous decomposition products when exposed to heat and radiation over an extended period of time.

It is not possible at this time to write detailed kinetic equations or mechanisms for the decomposition reactions. It is believed that the complexity of the chemical kinetic problem can be reduced markedly by (1) investigating the decomposition of each pure component of the mixture individually, (2) studying the effects of heat and radiation separately, and (3) permitting only low percentage conversion to occur, in order to aid in the identification of precursors and initial products. Therefore, research on the pyrolytic decomposition of pure biphenyl was made the initial effort at ORNL. Less than 1% decomposition of the biphenyl is permitted to occur during the pyrolysis.

Recrystallized biphenyl was weighed (3 g) into pyrolysis bulbs constructed from 1-in. Pyrex pipe in order to withstand the pressure of about 400 psi. The samples were sublimed twice under vacuum to ensure the complete removal of air and water vapor. The bulbs were sealed off, placed in stainless steel bombs, and loaded into a furnace regulated at 425°C. Under these experimental conditions, the biphenyl was in the gas phase during pyrolysis. The bombs were removed and quenched in water after the desired heating period to preclude further decomposition.

The pyrolytic products were separated into three fractions in a vacuum system. An automatic Toepler pump was used to collect the gases and low-boiling products for chromatographic analysis. This was done during two different volatilizations and condensations of the undecomposed biphenyl to prevent the loss of products by entrapment in the solid phase. The intermediate-boiling fraction was frozen in a trap and then dissolved in acetone containing *o*-xylene, which served as an internal standard. The high-boiling fraction remained behind in the pyrolysis tube and was dissolved in benzene prior to a separate analysis.

A schematic diagram of the apparatus used for the analysis of the permanent gases and low-boiling products is shown in Fig. 30.6. The tank helium flowed through the reference side of the thermistor detector blocks in series before it reached the gas sampling section. The sample was swept into the first column, the 11 ft × $^3/_{16}$ in. OD column of silica gel with 3 wt % squalane, where the permanent gases passed unresolved (unseparated) onto the 10 ft × $^3/_{16}$ in. OD molecular sieve 5A column. The low-molecular-weight hydrocarbons, resolved (separated) on the silica gel column, passed through the thermistor detection cell No. 1 and on to the molecular sieve column, where they were adsorbed irreversibly (this requires that this

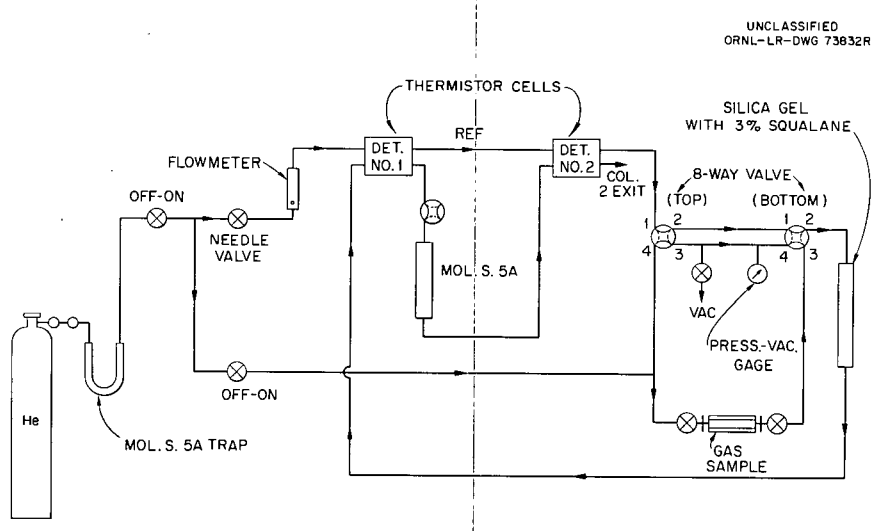


**Fig. 30.6. Schematic Diagram of Gas Chromatograph for Analysis of Low Boilers.**

column be replaced periodically). The molecular sieve 5A resolved the permanent gases and methane, which were detected by cell No. 2.

Figure 30.7 shows typical chromatograms obtained from the analysis of pyrolytic gases and low-boiling products. The unresolved mixture of permanent gases and methane was eluted from the silica gel column first, followed by the low-molecular-weight hydrocarbons in the order listed. The retention times in minutes are shown in parentheses. Carbon dioxide was also identified by this column. Peak 9 has been attributed to the presence of propylene since the time this figure was drawn. The unresolved mixture from this column was resolved on the molecular sieve 5A column into hydrogen, oxygen, nitrogen, methane, carbon monoxide, and, lastly, an unidentified peak at 26.5 min. The presence of carbon monoxide and carbon dioxide suggested the presence of oxygen from air, water vapor, or both during the pyrolysis of biphenyl. However, when the pyrolysis was performed in bulbs which had been treated overnight in a vacuum furnace at a temperature higher than that used for the pyrolysis and then cooled in a helium atmosphere, appreciable quantities of carbon monoxide were still present in the pyrolytic-gas samples. It is suggested that the glass serves as a source of an oxygen-containing compound which reacts with the organic materials at these temperatures. The presence of oxygen and nitrogen in the sample indicates some leakage in the vacuum system during sample fractionation and collection. However, their presence is detrimental only insofar as they may obscure, or prevent complete resolution of, other peaks.

Both the acetone solution of the intermediate boilers and the benzene solution of the high boilers were analyzed chromatographically on an F and M model 500 temperature-programmed unit. This unit employs detector cells with hot-wire

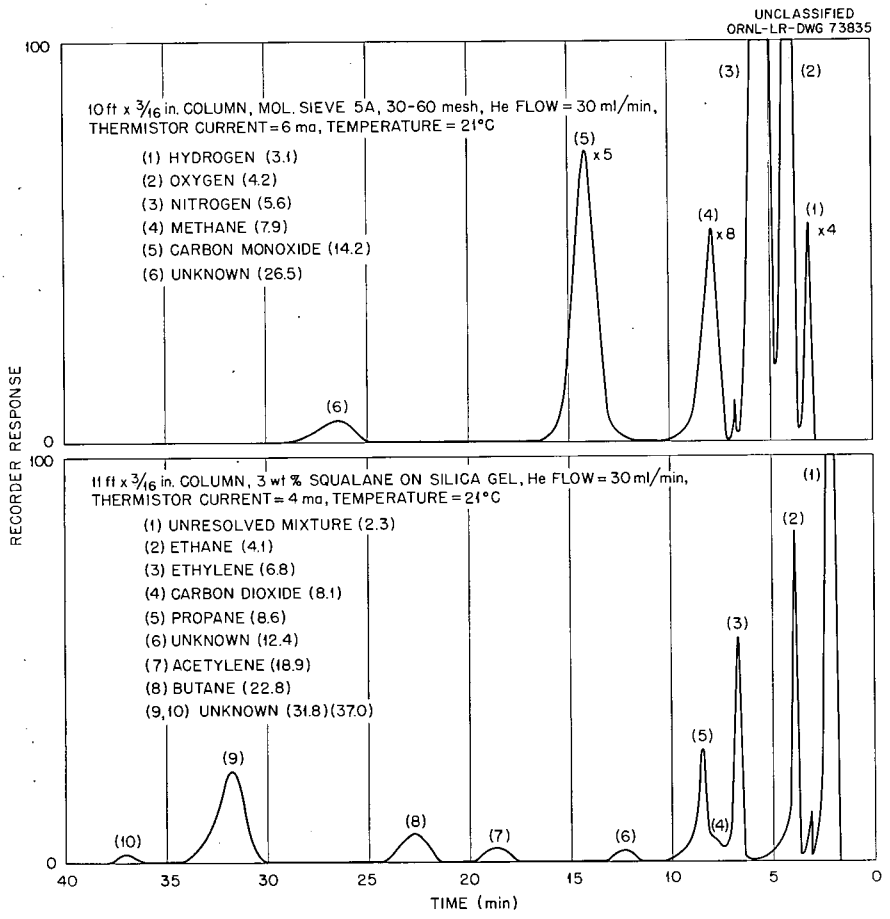


**Fig. 30.7. Chromatograms of Gaseous Products from the Pyrolysis of Biphenyl.**

filaments, which were used with a bridge current of 100 ma. The carrier gas flowed through the system at the rate of 30 ml/min. The solution of intermediate boilers was analyzed on a 6 ft × $\frac{1}{4}$ in. OD column of 30 wt % Apiezon L plus 2 wt % Carbowax 20M on Chromosorb P, with temperature programming at 11°C/min from 125 to 250°C. The only detectable material present was benzene.

A chromatogram of the high-boiling fraction is shown in Fig. 30.8. The presence of eight pyrolytic products is indicated. It cannot be stated unequivocally that peak 7 is not due to *m*-quaterphenyl rather than 1,3,5-triphenylbenzene, since it was impossible to resolve these two compounds with the LiCl column. It is suspected, from their retention times, that the unidentified peaks indicate the presence of additional quaterphenyl isomers. The inability to procure these isomers prevents definite identification at this time.

The amounts of the principal products formed during the pyrolysis of pure biphenyl at 425°C are presented in Table 30.1. Among the gases, the comparatively high yield of hydrogen is striking. It can be seen that benzene is the most abundant of all the initial pyrolytic products. The yield listed for the unknown materials was calculated on the basis that they are quaterphenyl isomers, all of which vary little in thermal conductivity. Nevertheless, the molar yield of terphenyls constitutes somewhat more than 55% of the high-boiling products.

Relatively poor sensitivity in the detection of hydrogen, with helium used as carrier gas, was observed during the acquisition of these results. Replacing helium with argon has resulted in an increase in hydrogen sensitivity by a factor of approximately 50. Therefore, future gas samples will be split into two equal portions. One will be used for hydrogen analysis with argon as the carrier gas and the other for the remaining gas analyses with helium as carrier.

Whereas the analytical precision for most of the pyrolytic products is better than ±2%, the reproducibility of the pyrolysis experiments is such that the following variation of results was found: ±4.2% for hydrogen, ±10% for methane, ±5.4% for ethane, ±12.5% for propane, and ±4.2% for benzene.

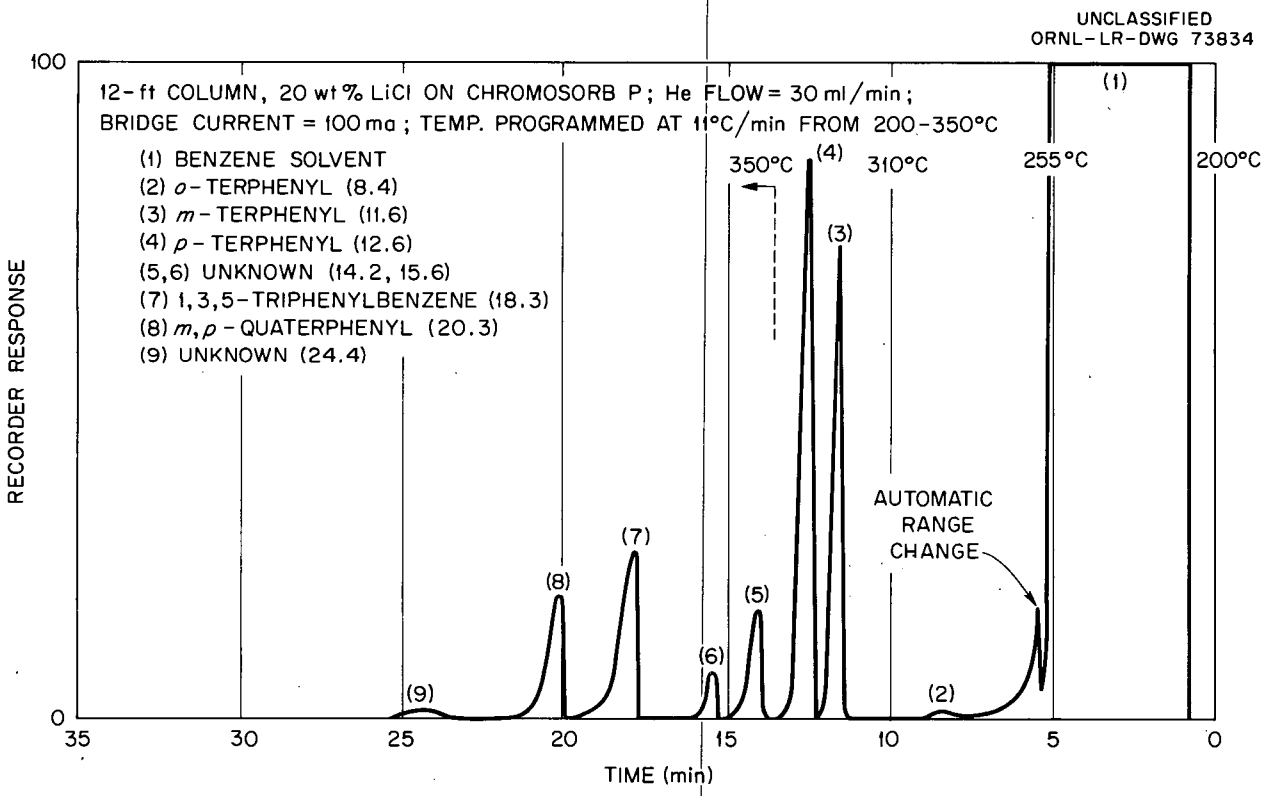


Fig. 30.8. Chromatogram of the High-Boiling Fraction of Biphenyl.

**Table 30.1. Yields of Initial Primary Products from the Pyrolysis of Biphenyl at 425°C**

Sample: 3 g of biphenyl (= 0.0195 moles)

| Compound | Yield | | |
|---|---|---|---|
| | μl | mg | Moles per mole of Biphenyl |
| Gas[a] | | | $\times 10^{-4}$ |
| Hydrogen | 90 | | 2.1 |
| Methane | 11 | | 0.25 |
| Ethane | 5 | | 0.1 |
| Propylene | ~4 | | ~0.1 |
| Ethylene | ~4 | | ~0.1 |
| Propane | ~2 | | ~0.05 |
| Intermediate Boilers[b] | | | |
| Benzene | | 6.1 | 40 |
| High Boilers[b] | | | |
| *o*-Terphenyl | | Trace (<0.15) | |
| *m*-Terphenyl | | 2.9 | 6.5 |
| *p*-Terphenyl | | 3.5 | 8.1 |
| Unknown | | (1.8) | (3.0) |
| 1,3,5-Triphenylbenzene | | 2.5 | 4.2 |
| *m,p*-Quaterphenyl | | 2.4 | 4.0 |

[a] Biphenyl heated 12 hr.
[b] Biphenyl heated 16 hr.

A comparison of the principal initial products found on pyrolyzing biphenyl and those found on irradiating[12] samples of this material is of interest. With less than 1% conversion occurring, hydrogen is by far the major gaseous product in both cases. However, radiolysis produces only unsaturated hydrocarbons as the remaining gases, while pyrolysis yields both saturated and unsaturated hydrocarbons, with the saturated compounds being more abundant. Benzene is the sole intermediate-boiling product of pyrolysis, but it represents only a small portion of this fraction produced radiolytically. In the latter case, hydrogenated biphenyls predominate, with some unsaturated compounds again being present. Pyrolysis yields both terphenyls and quaterphenyls in the residue (high-boilers) fraction, whereas terphenyls are not among the initial major products from the radiolysis of biphenyl. On the other hand, hydrogenated quaterphenyls have not been identified among the pyrolytic products, yet they constitute the major portion of the high-boiling fraction resulting from radiolysis.

With the quantitative data now available, an insight has been gained into the general mechanisms for product formation during the pyrolysis of pure biphenyl at 425°C. The two main degradation paths appear to be the symmetrical splitting of the biphenyl molecule to form phenyl radicals which either (1) hydrogenate to produce benzene or (2) react with biphenyl to produce terphenyls, quaterphenyls, and hydrogen. The presence of aliphatic hydrocarbon bases in low yield further indicates degradation of the benzene ring to a minor degree.

[12] R. O. Bolt *et al.*, *Progress Report for Jan. 1–Mar. 31, 1962*, California Research–AEC Report No. 16.

# 31. Chemical Support for Saline Water Program

## DETERMINATION OF THE SOLUBILITY OF $CaSO_4$ IN $H_2SO_4$-$H_2O$ SOLUTIONS AT HIGH TEMPERATURE

W. L. Marshall E. V. Jones[1]

A major obstacle to the development of economic, high-temperature distillation units for the desalination of water is the formation of scale on heat-exchanger surfaces. From seawater these scales consist chiefly of calcium sulfate, calcium carbonate, and magnesium hydroxide. Systematic determinations at high temperature of the solubility of these and other constituents of saline waters may contribute greatly toward reducing the problems of scale formation. The solubility of metal sulfates in water, in acid solution, and in NaCl solution will provide information from which dissociation constants, solubility products, and Debye-Hückel parameters may be derived. This information will contribute to our understanding of the general behavior of electrolyte solutions at high temperature and pressure. A research program on the solubility of scale constituents has recently been established by means of laboratory studies which make use of pure materials under carefully controlled conditions. Such studies are needed if a fundamental basis is to be provided for ultimate large-scale tests by others on naturally occurring saline waters.

### The Solubility of $CaSO_4$ in $H_2SO_4$-$H_2O$ Solutions, 125 to 350°C

Using the direct sampling technique and methods discussed elsewhere,[2] determinations were made of the solubility of $CaSO_4$ in $H_2SO_4$-$H_2O$ solutions at temperatures from 125 to 350°C. Powdered, reagent-grade $CaSO_4 \cdot 2H_2O$ was used in the experiments. This solid, in contact with aqueous solutions, was shaken in high-pressure vessels at each temperature for lengths of time varying from 1.5 hr to 2 days. Concentrations of $H_2SO_4$ were varied from 0 to 1.0 *m*. Samples of the solution phases were withdrawn and analyzed for calcium by flame photometry,[3] and for $H_2SO_4$ by direct acid-base titration after removal of calcium with a cation exchange resin.

In a special run at 225°C an effort was made to establish the effect of time on the attainment of equilibrium. In this run, samples of liquid phases were drawn for analysis both after 1 hr and after 16 hr. The results showed no detectable change in solubility after the longer length of time. Since in all experiments samples were drawn for analyses after times of 1 hr or longer at each temperature, it is believed that all results, with the exception of some of the runs at 125°C, represent equilibrium conditions. Solubility equilibrium in many runs was approached from both higher and lower temperatures with essentially identical results.

Inspection of x-ray diffraction patterns of most of the solid phases removed from the pressure vessels after runs at temperatures above 175°C showed the solids to be anhydrous $CaSO_4$ (anhydrite) but also showed $CaSO_4 \cdot 2H_2O$. Microscopic examination of the solids obtained after the 1-hr run at 125°C showed the monoclinic structure which is characteristic of $CaSO_4 \cdot 2H_2O$. In water the transition from the solid $CaSO_4 \cdot 2H_2O$ to $\beta$-$CaSO_4$ was reported by very early investigators[4]

[1]Consultant.

[2]W. L. Marshall and J. S. Gill, *J. Inorg. Nucl. Chem.* **22,** 115 (1961).

[3]These analyses were performed by T. C. Rains *et al.*, Analytical Chemistry Division.

[4]J. H. van't Hoff *et al.*, *Z. Physik. Chem. (Leipsig)* **45,** 257 (1903).

to occur in the vicinity of 65°C. Later investigators have reported that the transition occurs at 41 ± 1°C. The saturating solid at 125°C after the short length of time is probably either the metastable $CaSO_4 \cdot 2H_2O$ (gypsum) or the metastable $CaSO_4 \cdot \frac{1}{2}H_2O$ (hemihydrate), since (1) the solubility data appear to show a discontinuity which is not in thermodynamic conformity with an extrapolation of the solubility data from higher temperatures, and (2) previously reported temperatures of the transition $CaSO_4 \cdot 2H_2O$ to $CaSO_4$ are inconsistent; many others have had much difficulty with the occurrence of metastability. Additional runs at 125°C for times longer than 1 hr for solutions containing excess $H_2SO_4$ gave considerably lower solubilities, which were consistent with the data obtained at higher temperatures. Nevertheless, the solubilities of $CaSO_4$ in $H_2O$ at 125, 150, and 175°C corresponded to compiled solubilities of $CaSO_4 \cdot \frac{1}{2}H_2O$ (hemihydrate).[5]

The true nature of the solid phases, even at temperatures above 175°C, has not been resolved completely. Since the solubilities in $H_2SO_4$-$H_2O$ solutions at 125, 150, and 175°C extrapolate to the solubility of $CaSO_4 \cdot \frac{1}{2}H_2O$ in pure $H_2O$, obtained in this investigation and by others,[5] and are also self-consistent with those solubilities at higher temperature, it may even appear that $CaSO_4 \cdot \frac{1}{2}H_2O$ is the stable solid at the higher temperatures. Nevertheless, by x-ray diffraction examination of the solids which were removed from the pressure vessels after the runs and examined at 25°C, $\beta$-$CaSO_4$ was found to be present. By means of preliminary extrapolations of the data plotted as the logarithm of the solubility against a function of the ionic strength, only the solubilities at 325 and 350°C extrapolated into the values of Booth and Bidwell[6] for the solubility in $H_2O$ of anhydrous $CaSO_4$.

The experimental data are shown in Fig. 31.1. Since at constant molality of $H_2SO_4$ there was only a small change in solubility between 125 and 350°C, the data at each temperature were displaced uniformly from those at other temperatures in order to avoid confusion of points. In Fig. 31.2 solubilities at several constant molalities of $H_2SO_4$, obtained from the separate curves of Fig. 31.1, are plotted vs temperature to show the self-consistency of the data.

Although the solubilities of anhydrous $CaSO_4$ in $H_2SO_4$-$H_2O$ are considerably lower than those of

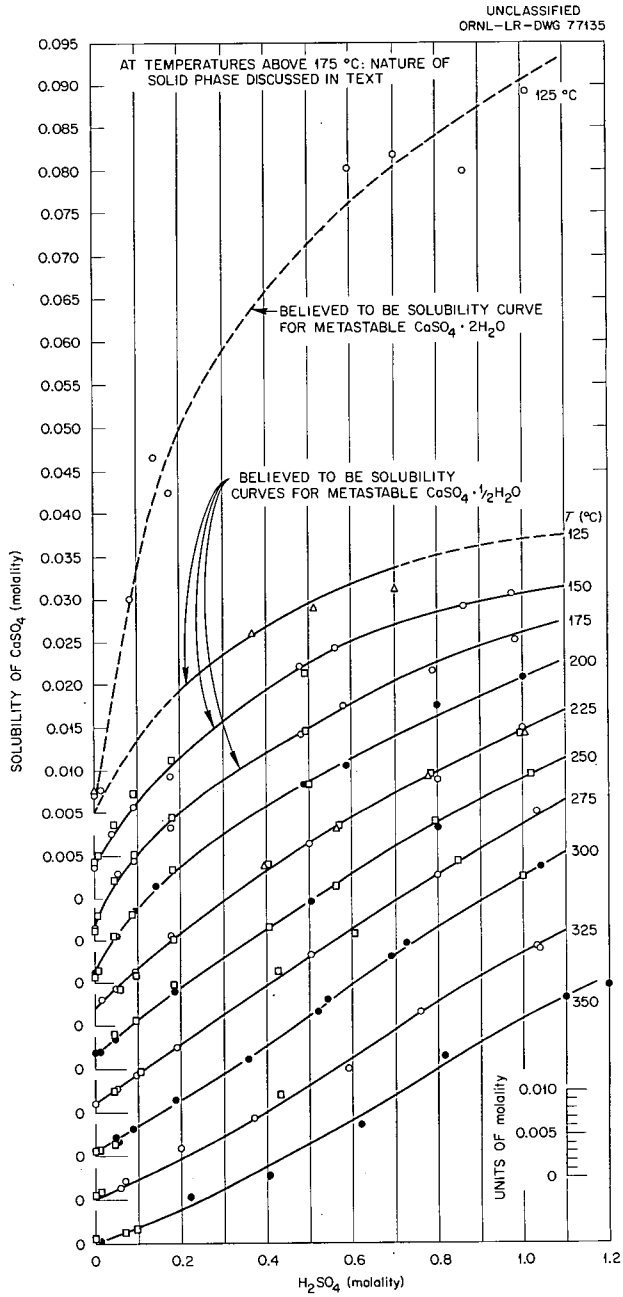


**Fig. 31.1. The Solubility of $CaSO_4$ in $H_2SO_4$-$H_2O$ Solution, 150 to 350°C.**

[5]E. Posnjak, *Am. J. Sci.* **35A,** 247 (1938). Includes Posnjak's own data and evaluation of some previous results.

[6]H. S. Booth and R. W. Bidwell, *J. Am. Chem. Soc.* **72,** 2567 (1950).

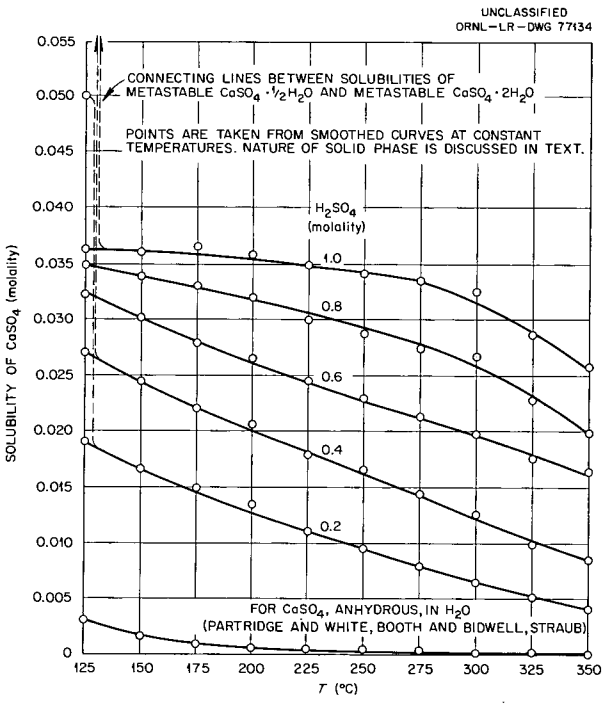


**Fig. 31.2. The Solubility of $CaSO_4$ in Various $H_2SO_4$-$H_2O$ Solutions as a Function of Temperature.**

$NiSO_4 \cdot H_2O$,[7] the general relationships are the same. At constant temperature the solubilities increase as the concentrations of $H_2SO_4$ increase, but, as the temperature increases the solubilities decrease. The metastabilities of $CaSO_4 \cdot 2H_2O$ and $CaSO_4 \cdot \frac{1}{2}H_2O$, with the subsequent transitions to the anhydrous salt at high temperature, both in $H_2O$ and in $H_2SO_4$ solution, are similar to the metastability of the $NiSO_4$ hydrates and may be significantly related to scale formation on heat-exchanger surfaces at temperatures somewhat above 100°C.

## CORROSION OF ALUMINUM ALLOYS IN SALT SOLUTIONS

E. G. Bohlmann

A study of the corrosion of aluminum alloys in salt solutions is under way. The program was stimulated by favorable data on aluminum corrosion in high-purity water and indications[8] that corrosion resistance was not affected by the presence of dissolved chlorides. The successful operation of the aluminum seawater-distillation unit developed at Fort Belvoir also showed promise for aluminum alloy applications in seawater service.[9]

Studies are being carried out in two 100-gpm dynamic loops constructed of titanium alloys. The loops can be operated at temperatures to 300°C, at pressures to 200 psi, and with flow rates in the range 0 to ~100 fps over corrosion specimens. They are equipped for sampling, atmosphere control, and continuous replenishment as required.

Several preliminary loop runs with synthetic seawater at ~100°C have been completed. The data obtained are consistent with expectations based on previous experience. Thus, there was a rapid initial attack with the formation of protective oxide, which substantially reduced continuing corrosion; weight losses after 700 hr were in about the same range (<1 mil) as those after 200 hr. The presence of alloying elements such as copper and nickel promoted drastic pitting attack. A somewhat surprising result, however, was the lack of dependence of the corrosion on fluid flow at bulk velocities of up to 75 fps, in the absence of impingement.

Because of the confirmation of the potential usefulness of aluminum alloys in seawater at elevated temperatures, the future program envisions evaluation, in simple sodium chloride solutions, of the effects of such variables as pH, salt concentration, temperature, and various seawater constituents such as oxygen, carbon dioxide, and copper ion. The equipment makes it possible to carry out the studies with a variety of alloys under various flow conditions and velocities.

---

[7] W. L. Marshall, J. S. Gill, and Ruth Slusher, "Aqueous Systems at High Temperature. VI. Investigations on the System $NiO$-$SO_3$-$H_2O$ and Its $D_2O$ Analogue from $10^{-4}$ to 2 *m* $SO_3$, 150 to 400°C," *J. Inorg. Nucl. Chem.* **24**, 889 (1962).

[8] V. H. Troutener and R. L. Dillon, *Corrosion* **15**, 9t–16t (1959).

[9] R. J. Gainey, *Use of Aluminum for Sea Water Distillation Equipment*, U.S. Army Engineers Research and Development Laboratories, Fort Belvoir, Va., Report 1705-TR (Jan. 9, 1962).

# 32. Corrosion Studies for Chemical Reprocessing Plants

J. C. Griess
J. L. English P. D. Neumann
L. L. Fairchild L. Rice[1]
D. N. Hess

## CORROSION STUDIES FOR THE TRANSURANIUM PROCESSING FACILITY

Corrosion tests have been continued to evaluate the behavior of materials potentially useful in the fabrication of process equipment for the transuranium processing facility. Most of the process solutions will contain high concentrations of chloride ions, and the alpha radiation from the transuranium elements will produce radiolysis products of an oxidizing nature. Most of the tests have been conducted both in the presence and absence of oxidizing agents. A major portion of the results has been reported elsewhere in detail,[2-4] and only a summary of these results will be given here. The data concerning the corrosion of Zircaloy-2 have not been reported previously and are presented in greater detail.

Although Hastelloy C corroded at very high rates in high-temperature hydrochloric acid solutions, it was hoped that the alloy might be useful in certain low-temperature applications. However, subsequent tests in the temperature range 35 to 43°C showed it to be unacceptable in hydrochloric acid solutions containing oxidants. One difficulty encountered with welded specimens of the alloy was its susceptibility to preferential attack in heat-affected zones adjacent to welds. Penetration up to 35 mils as a result of this type of attack was not uncommon in hydrochloric acid solutions even at temperatures as low as 35°C during 1000-hr exposures. Although a post-weld heat treatment at 1232°C effectively eliminated sensitivity of the alloy to this form of attack, the general attack rate was still to high to be acceptable. In other tests to examine the effect of oxidant species on corrosion of Hastelloy C by 6 *M* HCl at 35°C, it was found that, in the absence of an added oxidant, extremely good resistance was obtained (8 mils/yr). When the test solution was oxygenated or when hydrogen peroxide was added continuously, the rates increased to 62 and 48 mpy respectively. The addition of iron to an oxygenated 6 *M* HCl solution at 43°C caused a further marked acceleration in the attack rate of Hastelloy C. With no excess iron present, a rate of 120 mpy was observed during a 400-hr test period. The addition of 200 ppm ferric ion to the solution increased the rate to 275 mpy during the same time.

Studies were conducted also to determine the susceptibility of tantalum to hydrogen pickup in a number of TRU-related environments since the metal will be used in the fabrication of some of the process equipment in the separations facility. Extremely good corrosion resistance was generally observed and no hydrogen pickup was experienced, with two exceptions. Tantalum-plated stainless steel in 6 *M* HCl at 105°C showed appreciable hydrogen pickup when the base metal dissolved through defects in the plate. In several tests the

[1]Present address: Creole Petroleum Co., Maracaibo, Venezuela.

[2]D. E. Ferguson, *Transuranium Quart. Progr. Rept. Feb. 28, 1962*, ORNL-3290, pp 76–78 (June 6, 1962).

[3]D. E. Ferguson, *Transuranium Quart. Progr. Rept. Aug. 31, 1962*, ORNL-3375 (to be published).

[4]D. E. Ferguson, *Transuranium Quart. Progr. Rept. Nov. 30, 1962*, ORNL-3408 (to be published).

remaining tantalum plate contained between 2000 and 3100 ppm hydrogen. Less severe hydrogen uptake was encountered in tantalum sheet contacted by dissolving aluminum in a similar environment. After 7 hr contact time, hydrogen concentrations of 55 to 65 ppm were detected in metal which contained between 1 and 2 ppm of hydrogen initially. Further tests are necessary to demonstrate the adequacy of tantalum cladding for the dissolver where aluminum-clad target rods will be dissolved in contact with tantalum. In similar tests niobium was subject to hydrogen pickup and severe embrittlement in practically all chloride-bearing environments tested, even when not in electrical contact with dissolving metals.

Zircaloy-2 is an attractive alloy for use in the transuranium processing facility because of its excellent resistance to all concentrations of hydrochloric or nitric acids at temperatures up to boiling. However, in mixed solutions of the two acids at high concentrations, corrosion was almost catastrophic. An investigation was undertaken to determine the effect of low concentrations of nitric acid in 3- and 6-*M* HCl solutions at 43°C and at the boiling point on the corrosion of Zircaloy-2. The nitric acid concentrations examined were 0.1 and 0.5 *M*.

Duplicate weld specimens of the alloy were exposed in both solution and vapor phases. Test solutions were oxygen aerated and were replaced at 100-hr intervals. Average corrosion rates are given in Table 32.1. At 43°C the presence of nitric acid in either the 3- or 6-*M* HCl solutions resulted in no significant attack on the Zircaloy-2. The highest rate, 12 mpy, occurred in the 6 *M* HCl–0.1 *M* $HNO_3$ environment. At the boiling point in 3 *M* HCl, the attack was appreciable on solution-exposed specimens in the presence of 0.5 *M* $HNO_3$, whereas the attack was minor in the 0.1 *M* $HNO_3$ solution. A reversal of this behavior was obtained in 6 *M* HCl at boiling. At the lower nitric acid concentration, the observed rate was 65 times greater than was the rate obtained in the presence of 0.5 *M* $HNO_3$, 130 vs 2 mpy respectively. None of the specimens used in the entire investigation were subject to selective attack in heat-affected zones adjacent to welds.

A number of plastics exhibited promising corrosion behavior after 1000-hr exposures at 80°C in organic processing solutions that will be used in the transuranium separation facility. The plastics include Homalite CR-39 (allyl diglycol carbonate), Homalite CR-100 (polyester), Polypenco K-51 (polycarbonate), Hysol (epoxy), Shell 1516 (polypropylene), Kynar (vinylidene fluoride), Plaskon (urea formaldehyde), Melmac 1077 (melamine formaldehyde), Nylon (polyamide), Penton-9215 (chlorinated polyether), and Teflon (polytetrafluoroethylene). The organic test solutions consisted of (1) 1 *M* mono-2-ethylhexylphenylphosphonic acid in diethylbenzene; (2) 30% Alamine 336 chloride in diethylbenzene; and, in a number of cases (3) 30% di-2-ethylhexylphosphoric acid in normal decane. Although a number of the plastic specimens underwent staining and general discoloration, the observed weight and dimensional changes were of minor consequence.

Hycar OR (synthetic nitrile rubber) behaved very poorly in the above solutions. Specimens were tacky, badly swollen, and blistered after 100 hr.

**Table 32.1. Corrosion of Welded Zircaloy-2 by Oxygenated Mixed Hydrochloric-Nitric Acid Solution**

Test time: 500 hr

| Medium | Temp (°C) | Penetration Rate (mils/yr) | |
|---|---|---|---|
| | | Solution | Vapor |
| 3 *M* HCl | 43 | <1 | <1 |
| 3 *M* HCl–0.1 *M* $HNO_3$ | 43 | <1 | <1 |
| 3 *M* HCl–0.5 *M* $HNO_3$ | 43 | 8 | 2 |
| 6 *M* HCl | 43 | <1 | <1 |
| 6 *M* HCl–0.1 *M* $HNO_3$ | 43 | 12 | 2 |
| 6 *M* HCl–0.5 *M* $HNO_3$[a] | 43 | 1 | 2 |
| 3 *M* HCl | ~110 | <1 | <1 |
| 3 *M* HCl–0.1 *M* $HNO_3$ | ~110 | 1 | 6 |
| 3 *M* HCl–0.5 *M* $HNO_3$ | ~110 | 66 | 5 |
| 6 *M* HCl | ~110 | <1 | <1 |
| 6 *M* HCl–0.1 *M* $HNO_3$ | ~110 | 130 | 5 |
| 6 *M* HCl–0.5 *M* $HNO_3$ | ~110 | 2 | 5 |

[a]Penetration rates are for 100 hr rather than 500 hr.

## CORROSION TESTING PROGRAM IN SUPPORT OF POWER-REACTOR FUEL-ELEMENT REPROCESSING

This corrosion testing program assists the Chemical Technology Division in the development of power-reactor fuel reprocessing and the storage and disposal of the associated waste products. Each new dissolution and separation process proposed must be evaluated in terms of the corrosion problems resulting from the process. Candidate materials for construction of containers, piping, reaction vessels, and other process equipment are screened under simulated process conditions. Those with potentially useful corrosion resistance are subjected to longer-term tests, depending on their required service life. Because of the wide scope of the chemical processing development, a large variety of materials are tested under many different conditions.

In the chemical processing area, tests have been mainly concerned with the selection of materials for various phases of the Chloride Volatility Process and for reprocessing of graphite-bearing fuels, both by high-temperature oxidation and subsequent acid dissolution and by direct acid treatment of the fuels. The latter process involves the use of hydrofluoric acid in combination with nitric acid, both with and without additional oxidizing agents.

Waste storage tests have been carried out to choose suitable materials for temporary storage of liquid waste and for concentration of wastes by evaporation. Tests were also made to determine the corrosive effects of calcining the residues, either alone or with the addition of glass-producing substances, on the container materials. A few tests are also in progress related to the storage of these wastes in salt mines.

The results of this testing program are an integral part of the process development program and as such are included in reports issued by the Chemical Technology Division.[5]

[5] R. E. Blanco, *Chemical Development Section B Quart. Progr. Rept.*, ORNL-TM-377 (January–July 1962); ORNL-TM-403 (July–September 1962); and an ORNL-TM (October–December 1962) to be published.

# 33. Chemical Support for Thermonuclear Program

J. D. Redman R. A. Strehlow

## VACUUM STUDIES

Chemical support of the Sherwood Project[1] has continued with principal attention being devoted to vacuum technique improvements. The utilization of composite pumping systems, in which vapor-deposited titanium is supplemented by diffusion pumps, allows very low pressures to be maintained with a large gas throughput. The Reactor Chemistry Division now has responsibility for the development of titanium and other metal film pumping. This work in its present stage of development is substantially reported elsewhere.[2] Vacuum system design for specialized component studies for the period represented in the present report included the building of a bakeable metal gasket test facility and a mechanical pump oil use test.

## IONIZATION GAGE STUDIES

Additional data from studies of Bayard-Alpert-type ionization gages have confirmed the notion that a nude ionization gage (i.e., one with a metal screen in place of the usual glass envelope) at its base pressure is able to indicate the presence of a class of gaseous molecules which yield no positive ion current in a glass-enveloped gage. With the use of the calibration curves for nude vs enveloped gages as an index of this type of response, it has been observed that, in an oil-pumped system, the characteristic kind of curvature shown in Fig. 33.1 did not occur when the calibrations were performed in a system pumped by a mercury diffusion pump. However, when an oil atmosphere was simulated by the rather simple expedient of operating the mercury-pumped system with a number of ordinary neoprene O-rings present in the chamber, the results shown in Fig. 33.2 were obtained. It seems reasonable that a pumping action of this type gage for high-molecular-weight (organic) species may be such that the fraction of molecules yielding ion current is substantially lower for the enveloped gage than the corresponding fraction for the nude gage (due to geometrical as well as electrical factors). The enveloped gage reads low when used in the presence of significant amounts of oil or other organic materials. The principal limitations

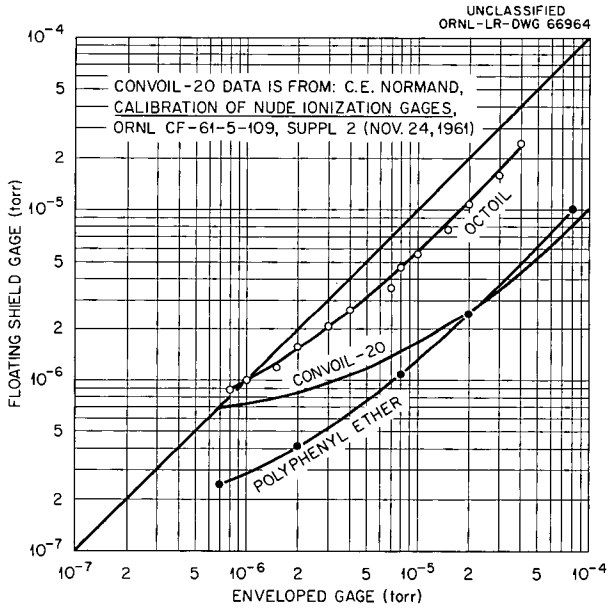


**Fig. 33.1. Relative Pressure Readings from Enveloped and Floating-Screen Gages in Systems Pumped 30 Days with Various Diffusion-Pump Oils. Convoil-20 data were taken from** *Thermonuclear Div. Progr. Rept. Oct. 31, 1961,* **ORNL-3239, pp 85–95.**

[1] *Reactor Chem. Div. Ann. Progr. Rept. Jan. 31, 1962,* ORNL-3262, p 199.

[2] *Thermonuclear Div. Semiann. Progr. Rept. Oct. 31, 1962,* ORNL-3392, pp 86–88.

of enveloped gages in the pressure range of $10^{-8}$ to $10^{-6}$ torr appear to be only where this type of environment exists.

An enveloped gage was modified by moving the tubulation so that an appreciably larger fraction of entering molecules would enter the region inside the grid structure on their first transit through the ionizing region. This modified gage was tested and compared with a conventional enveloped gage on an unbaffled, highly contaminated vacuum system. Curvature similar to that observed in the nude vs enveloped gage calibrations (Figs. 33.1 and 33.2) was observed.

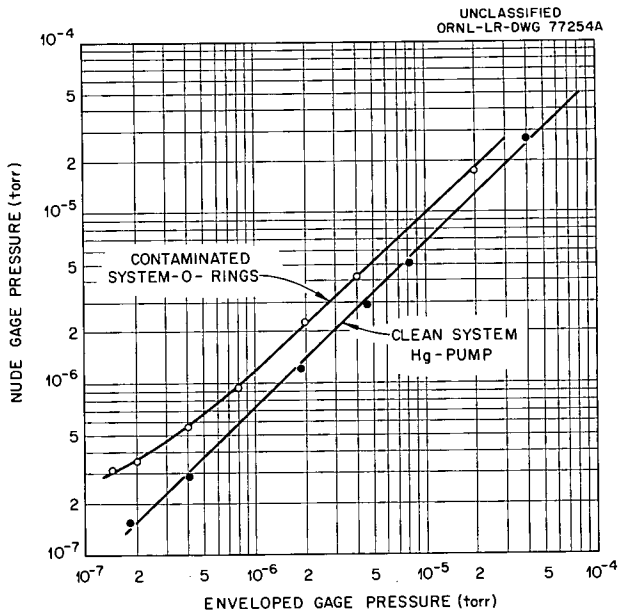


**Fig. 33.2. The Effect of System Cleanliness on Ionization Gage Characteristics.**

# 34. Research and Development on Pure Materials

## PREPARATION OF SINGLE-CRYSTAL LiF

C. F. Weaver R. G. Ross
R. E. Thoma

The demand for single crystals of lithium fluoride with selected isotopic ratios of lithium increased during the past year. Accordingly, the principal efforts of the pure-materials program have been to produce research specimens and to improve the procedures described previously.[1] A detailed report of this work is in preparation.[2]

### Crystals Produced

Four crystals weighing approximately 300 g each have been produced and are shown in chronological sequence in Figs. 34.1 to 34.4. The crystal shown in Fig. 34.3 contains 98.06% $Li^7$. The remaining three contain 99.99% $Li^7$. A series of six crystals containing approximately 96, 90, 80, 70, 50, and 1% $Li^7$ will be produced during the next several months. These isotopic compositions were selected to provide maximum discrimination in studies of thermal conductivity.

### Preparation of Charge

Pure lithium fluoride was prepared as indicated earlier.[1] Typical analyses of this precipitated and dried charge material are shown in Tables 34.1 and 34.2. The concentrations of other elements, if present, were below the limits of detection by the methods used. This material was then melted and dehydrated with HF in a grade-A nickel container. The charges for the first and second crystals were melted in a pure helium atmosphere and dehydrated at 900°C with a mixture of HF and $H_2$. Under these conditions the moisture present in the dried charge caused a small amount of container corrosion, adding the constituents of the alloy[3] (nickel, copper, iron, manganese, silicon, carbon, and sulfur) to the melt. With the addition of the HF + $H_2$ mixture, most of these impurities were reduced and precipitated as fine specks which settled out of the melt. An additional portion of these impurities was segregated during the freezing process, forming a brownish central core of the ingot. The portion which was colorless and free of specks was separated by a handpicking operation in a vacuum dry box. The yield of usable material produced by this method was approximately 65%. The charges for the third and fourth crystals were melted in a hydrogen atmosphere, which reduced considerably the degree of corrosion by inhibiting such reactions as HF + Ni → $NiF_2$ + $H_2$ (which occur even before the addition of HF for dehydration purposes because some of the moisture present in the lithium fluoride reacts as follows: $H_2O$ + LiF → LiOH + HF). The presence of HF at temperatures below the maximum temperature (~ 900°C) of the process is undesirable since the magnitudes of the free energy changes favoring the corrosion reactions increase with a decreasing temperature.[4] The yield of usable lithium fluoride was increased to about 90%. Both methods produced material of about the same

[1] C. F. Weaver, B. J. Sturm, and R. E. Thoma, *Reactor Chem. Div. Ann. Progr. Rept. Jan. 31, 1962*, ORNL-3262, pp 187–90.

[2] C. F. Weaver *et al.*, *The Production of LiF Single Crystals with Selected Isotopic Ratios of Lithium*, to be published as ORNL-3341.

[3] Taylor Lymann (ed.), *Metals Handbook*, p 1047, American Society for Metals, Cleveland, 1948.

[4] Alvin Glassner, Figs. 2*a*–2*g* of *The Thermochemical Properties of the Oxides, Fluorides, and Chlorides to 2500°K*, ANL-5750.

Fig. 34.1. Lithium Fluoride Bicrystal Which Weighed 300 g (Showing Minor Bubble Formation).

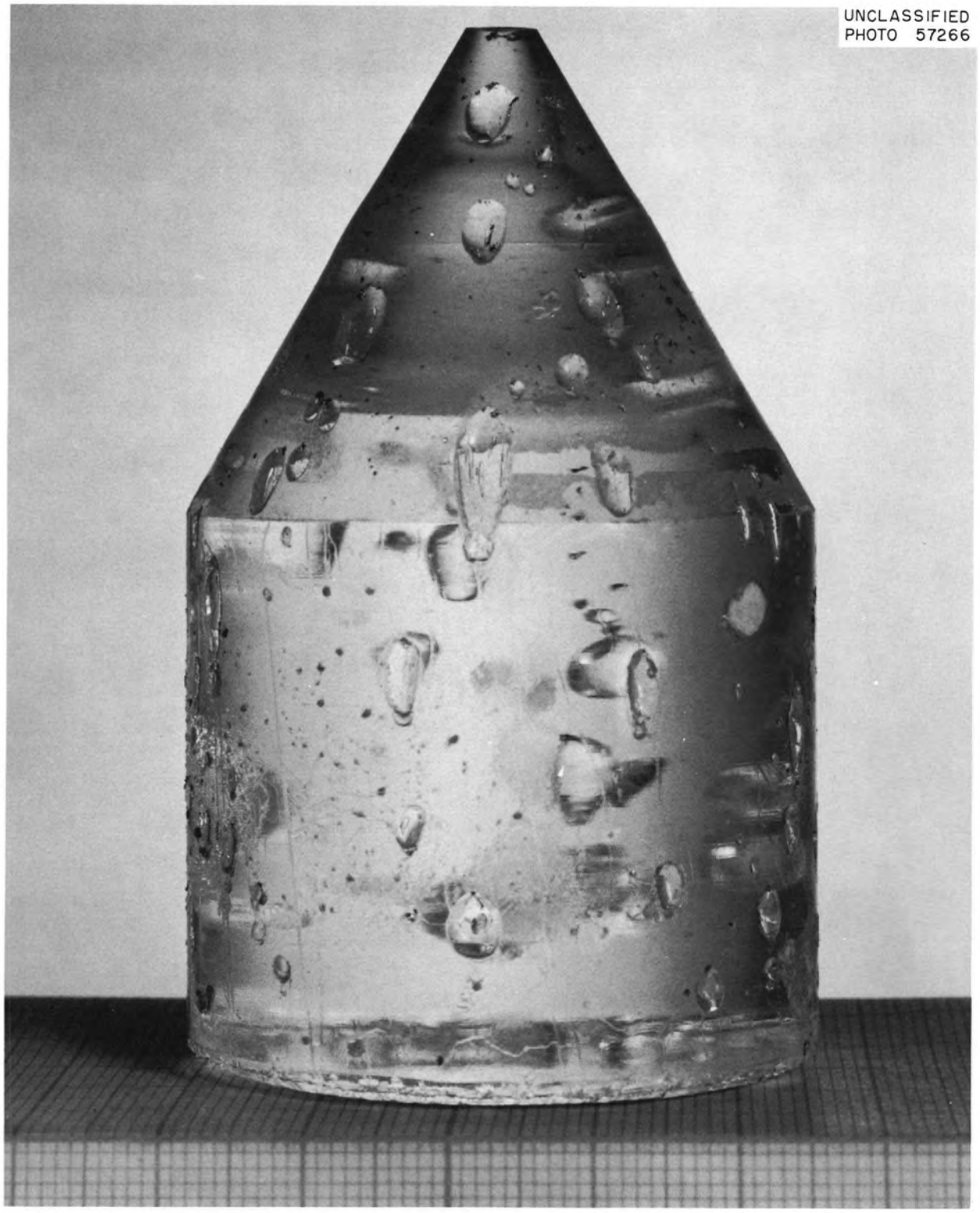


Fig. 34.2. Lithium Fluoride Single Crystal Which Weighed 260 g (Showing Extensive Bubble Formation).

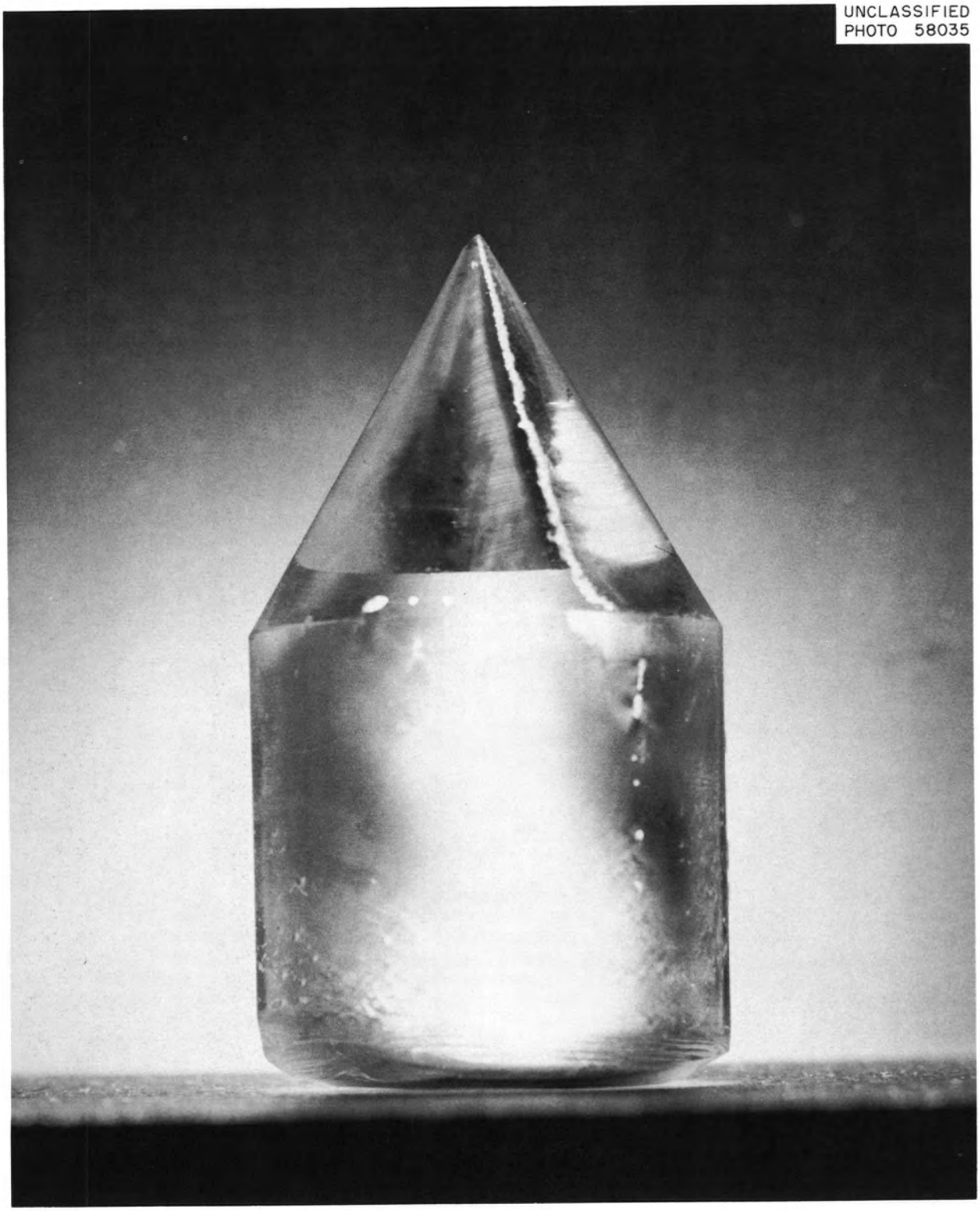


Fig. 34.3. Lithium Fluoride Single Crystal Which Weighed 278 g.

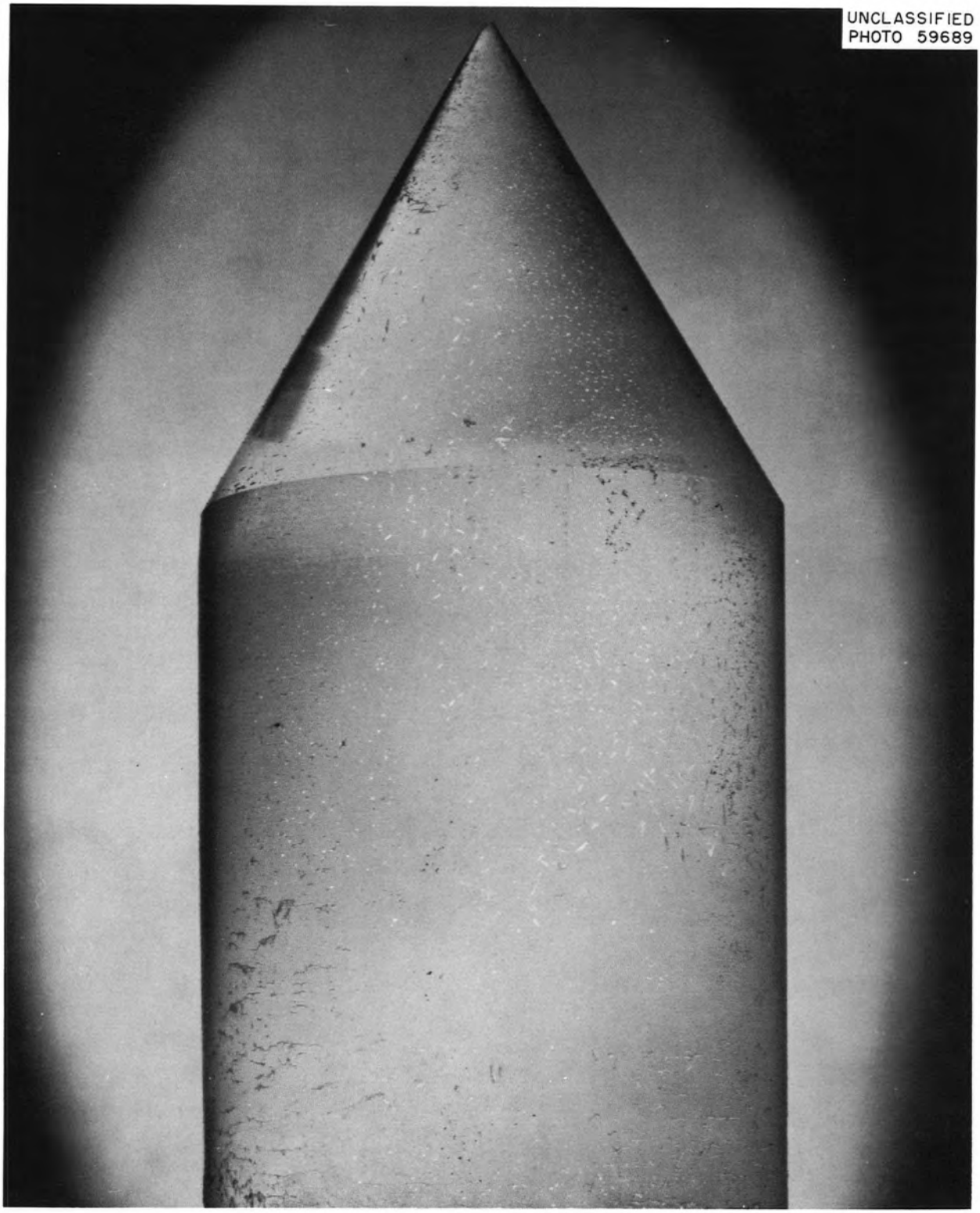


Fig. 34.4. Lithium Fluoride Single Crystal Which Weighed 349 g.

**Table 34.1. Spectroscopic Analysis[a] of LiF**

| Material | Element (ppm) | | | | | | | | | | | | |
|---|---|---|---|---|---|---|---|---|---|---|---|---|---|
| | Ag | Al | B | Ca | Cu | Fe | Hg | K | Mg | Mn | Na | Si | Ti |
| Heat-lamp-dried LiF | | | | | <5 | | 100 | | | | 5 | <100 | |
| HF-dehydrated LiF | | 20 | | 100 | | | | | 10 | 10 | <50 | | |
| First crystal top | | <100 | | 20–50 | | | | | 50 | 70 | 100 | <100 | <100 |
| First crystal top, middle | | <100 | | 20–50 | | | | | 100 | | 50 | 100 | <100 |
| First crystal bottom, middle | | <100 | | 20–50 | | | | | 50 | | 100 | | |
| First crystal bottom | | | | 20–50 | | | | | 100 | | 50 | | |
| Second[b] crystal top | | <10–300 | nd[c]–500 | 30 | | | | 20 | 20–50 | <100–300 | 30 | nd–200 | |
| Second crystal bottom | | nd–<100 | | <10–20 | | | | 20 | | | 10 | nd–300[d] | 100 |
| Third crystal top | | <20 | | | | | | | <10 | 20 | <50 | | <20 |
| Third crystal bottom | <1 | | | | | <1 | | | <10 | 2 | 5 | | |

[a]Analyses performed by J. A. Norris' group.
[b]Eleven analyses were performed on each portion of the second crystal; the ranges of the results are shown in this table.
[c]Not detected.
[d]Of the eleven analyses, eight did not show silicon, one gave <100 ppm, one 100 ppm, and one 300 ppm.

Table 34.2. Activation Analysis[a] of LiF

| Material | Element (ppm) | | | |
|---|---|---|---|---|
| | Cu | Hg | Mg | Mn |
| Heat-lamp-dried LiF | 2.7 | 73.1 | | 0.1 |
| First crystal middle[b] | | | 3–7[b] | 6–8[b] |
| Second crystal bottom | | | | 1.5 |
| Third crystal bottom | | | | 1.4 |

[a]Analyses performed by E. I. Wyatt's group except where stated otherwise.
[b]Analyses performed at Cornell University, R. L. Sproull, personal communication.

purity. A typical analysis is given in Table 34.1. The advantages of melting in hydrogen were a smaller loss of expensive material and a considerable reduction in the time consumed in hand-picking. The HF-dehydrated LiF was converted to a single crystal with >99% yield. At present the yield of single-crystal LiF is approximately 85% of that theoretically available from the $LiOH{\cdot}H_2O$ starting material.

### Crystal Growth from the Melt

Visual monitoring of growth of the lithium fluoride crystals from the melt has been achieved by the addition of a quartz window to the capsule header as shown in Figs. 34.5 and 34.6. It was reported previously[5] that an attempt to grow an LiF crystal under pressures of $10^{-3}$ to $10^{-4}$ mm Hg, as recommended in literature,[6,7] failed because the charge evaporated completely from the capsule. In a second attempt, the charge was outgassed at room temperature at $10^{-4}$ mm of pressure, but during all heating operations a pressure of 1000 mm was maintained. The bicrystal shown in Fig. 34.1 was produced. At this stage the window was added. It was found that the lithium fluoride could be melted under $10^{-3}$ to $10^{-4}$ mm pressure with less than 1% of the charge lost by evaporation if a pressure of approximately 1000 mm He was applied within an hour after melting. The crystals shown in Figs. 34.2 to 34.4 were produced under these conditions. The top 3 mm of the bicrystal in Fig. 34.1 was cloudy, but no portions of the last three crystals exhibited this defect. Several times, as noted through the quartz window, the formation of a polycrystalline ingot was observed. Whenever this occurred the ingot was immediately remelted. A considerable amount of time was saved because it was not necessary to open a capsule or cool the furnace to determine that an interface existed.

It was also found that melting the original charge, under helium atmosphere, or remelting, under helium, an ingot which contained an interface resulted in bubble formation at the melt-nickel interface. A few such bubbles may be seen in Fig. 34.1 and many in Fig. 34.2. The crystals shown in Figs. 34.3 and 34.4 were produced with vacuum melting only. Figure 34.7 illustrates what may be seen through the window. This is a view of the second crystal (Fig. 34.2) showing the included bubbles. The crystal was entirely grown but not annealed at this stage and was at a temperature of about 830°C. The analyses of the first three crystals produced may be seen in Tables 34.1 and 34.2. In no cases have these materials shown infrared absorption due to hydroxyl ion inclusion; the absence of hydroxyl ions is evidence that the dehydration step was successful. The absence of strain has also been shown by observing the annealed crystals with polarized light.

[5]C. F. Weaver, B. J. Sturm, and R. E. Thoma, *Reactor Chem. Div. Ann. Progr. Rept. Jan. 31, 1962*, ORNL-3262, pp 187–90.

[6]D. C. Stockbarger, *Discussions Faraday Soc.* **5**, 299–306 (1949).

[7]M. A. Vasilyeva, "Growing Lithium and Sodium Fluoride Single Crystals of High Transparency in the Ultraviolet and Infrared," pp 191–96 in *Growth of Crystals*, (ed. by A. V. Shubnikov and N. N. Sheftol), vol 1, translated from Russian, Consultants Bureau, New York, 1959.

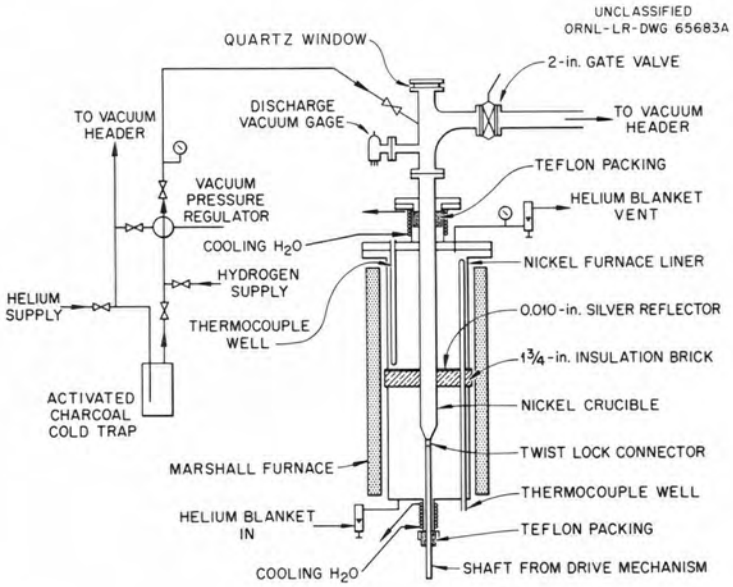


Fig. 34.5. LiF Crystal Growing Apparatus.

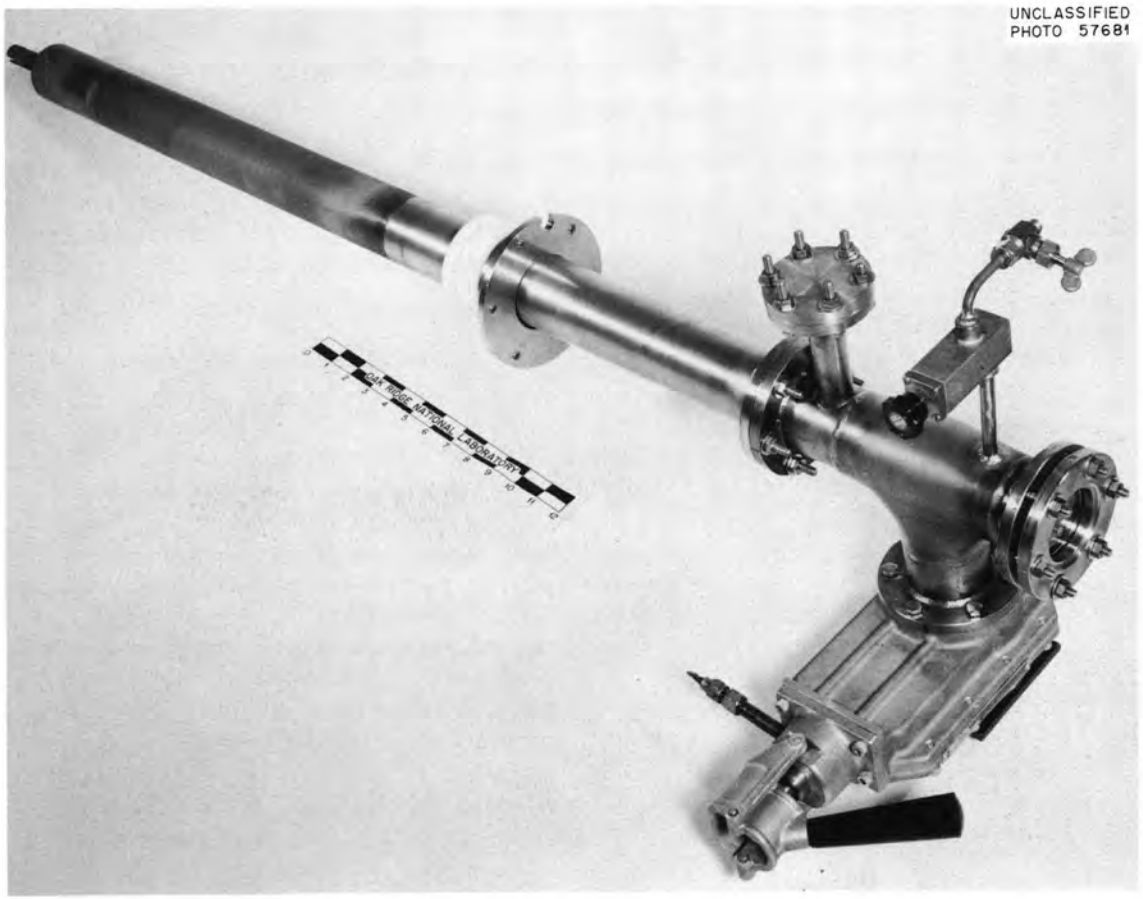


Fig. 34.6. LiF Growth Capsule with Window-Containing Header Attached.

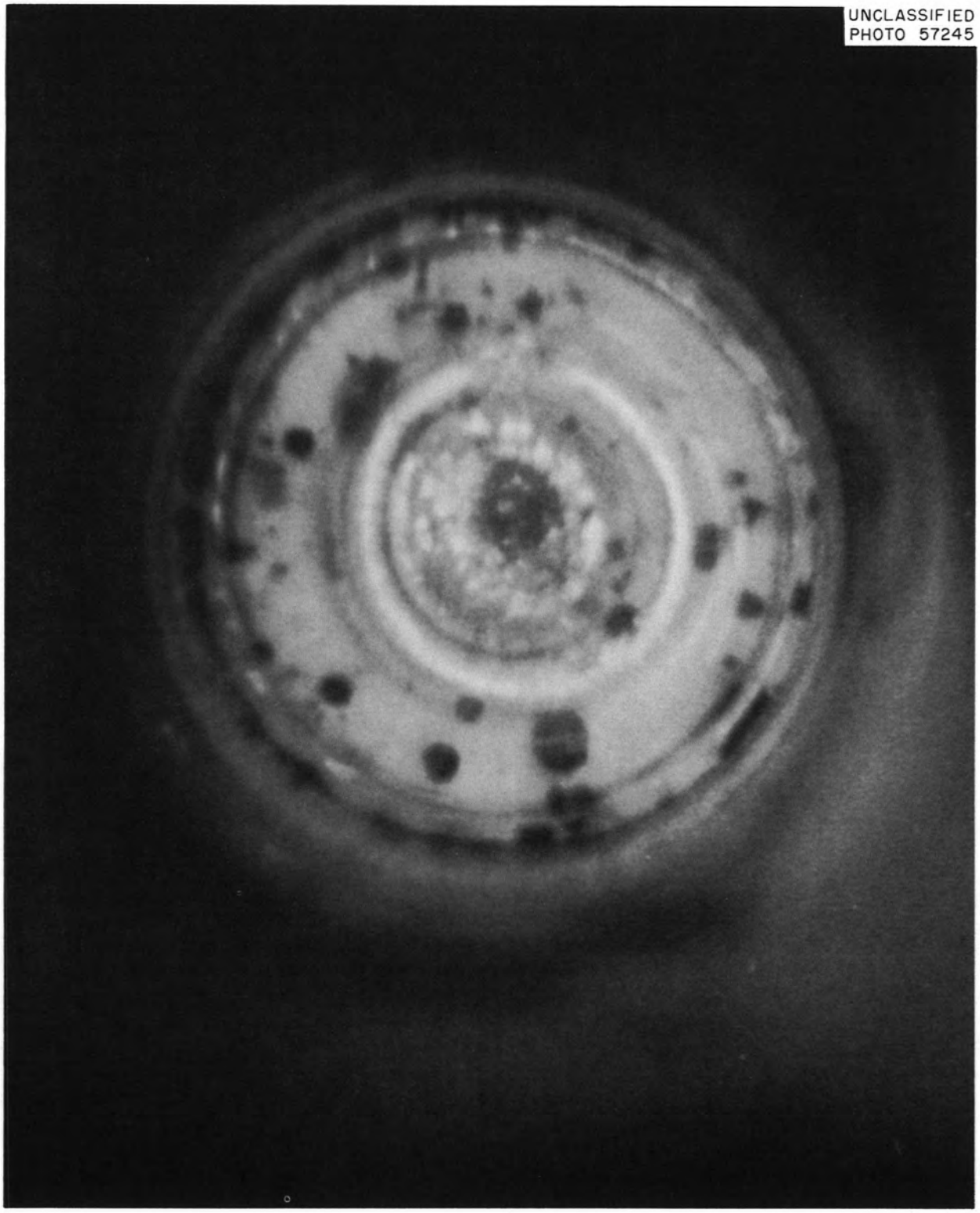


Fig. 34.7. Crystal at 830°C Viewed Through Quartz Window.

### Discussion

The low-temperature thermal conductivity of these crystals is under study at the Materials Science Center at Cornell University. The high-temperature thermal conductivity is being studied at Oak Ridge National Laboratory. The bottom portions of these crystals are being used to produce improved standards for spectroscopic analysis of LiF. From Table 34.1 it can be seen that the concentrations of impurities decrease from the first to the third crystals. The first two crystals are now being reanalyzed, with the use of new standards, to determine whether the trend in Table 34.1 reflects improved purity in the crystals or improved analyses. In this respect, the calcium analysis is of interest. The first and second crystals showed up to 50 ppm calcium, but spectroscopic analysis at Cornell detected no calcium in the first crystal.[8] The earlier reports of calcium impurity at ORNL are now believed to have resulted from analytical problems,[9] which have been eliminated with the new standards. Spectroscopic analysis of the third crystal does not show calcium.

## PREPARATION OF SINGLE-CRYSTAL MgO

C. F. Weaver B. J. Sturm
R. E. Thoma

The search for appropriate solvents and thermal conditions for the growth of MgO from solution has continued. It has been demonstrated that all the alkali fluorides form simple eutectic systems with MgO and have extensive primary phase regions of MgO. However, the temperature coefficients of MgO solubility are too low in the temperature ranges ($\lesssim 1200°C$) examined to allow useful growth by slowly cooling a melt.

A loop of circulating molten-salt solvent offered promise and was tested as a means for growing crystals of MgO. Circulation of molten salt in the loop of metal tubing was obtained by heating one leg to cause thermal convection. Pieces of commercial MgO were supplied to the hot leg. Being slightly more soluble at the higher temperatures, MgO should dissolve in the circulating liquid and deposit in the cooler leg in the form of single crystals. Such a loop is shown in Fig. 34.8. By the use of an LiF-NaF eutectic (mp, 652°C)[10,11] circulating under a hydrogen atmosphere at a rate of approximately 200 g/min[12] in a nickel loop with hot and cold legs about 880 and 750°C respectively, MgO crystals as large as $6 \times 3 \times 2.5$ mm (shown in Fig. 34.9) were obtained in 3.75 days. It was not necessary to provide seed crystals; spontaneous seeding occurred on the surface of the nickel in the cold leg. Longer runs were not possible in nickel loops as stress cracks developed. Substitution of Inconel permitted much longer loop operation, but spontaneous seeding no longer seemed to occur. The transition metal content of the crystals grown in the loop was about the same as that of the starting material; however, this contamination could probably be lowered by the addition of a suitable reducing agent to the melt.

Recently, experiments have been made to grow crystals in the MgO primary phase fields of the systems $B_2O_3$-MgO and $CaF_2$-MgO with temperature cycles ranging from 1500°C down. Similar work is now planned from 2200°C down to explore the possibility of utilizing the high solubilities and temperature coefficients of solubility which are reported[10,13] to be available in this temperature range.

---

[8] R. L. Sproull, Cornell University, personal communication.

[9] J. A. Norris, ORNL, personal communication.

[10] E. M. Levin, H. F. McMurdie, and F. P. Hall, *Phase Diagrams for Ceramists*, American Ceramic Society, Columbus, Ohio, 1956.

[11] R. E. Thoma, *Phase Diagrams of Nuclear Reactor Materials*, ORNL-2548 (Nov. 6, 1959).

[12] G. H. Llewellyn, *Mass Flow Rate as a Function of Temperature Gradients in a Thermal Circulation Loop*, ORNL CF-62-11-65 (Nov. 27, 1962).

[13] E. M. Levin and H. F. McMurdie, *Phase Diagrams for Ceramists — Part II*, American Ceramic Society, Columbus, Ohio, 1959.

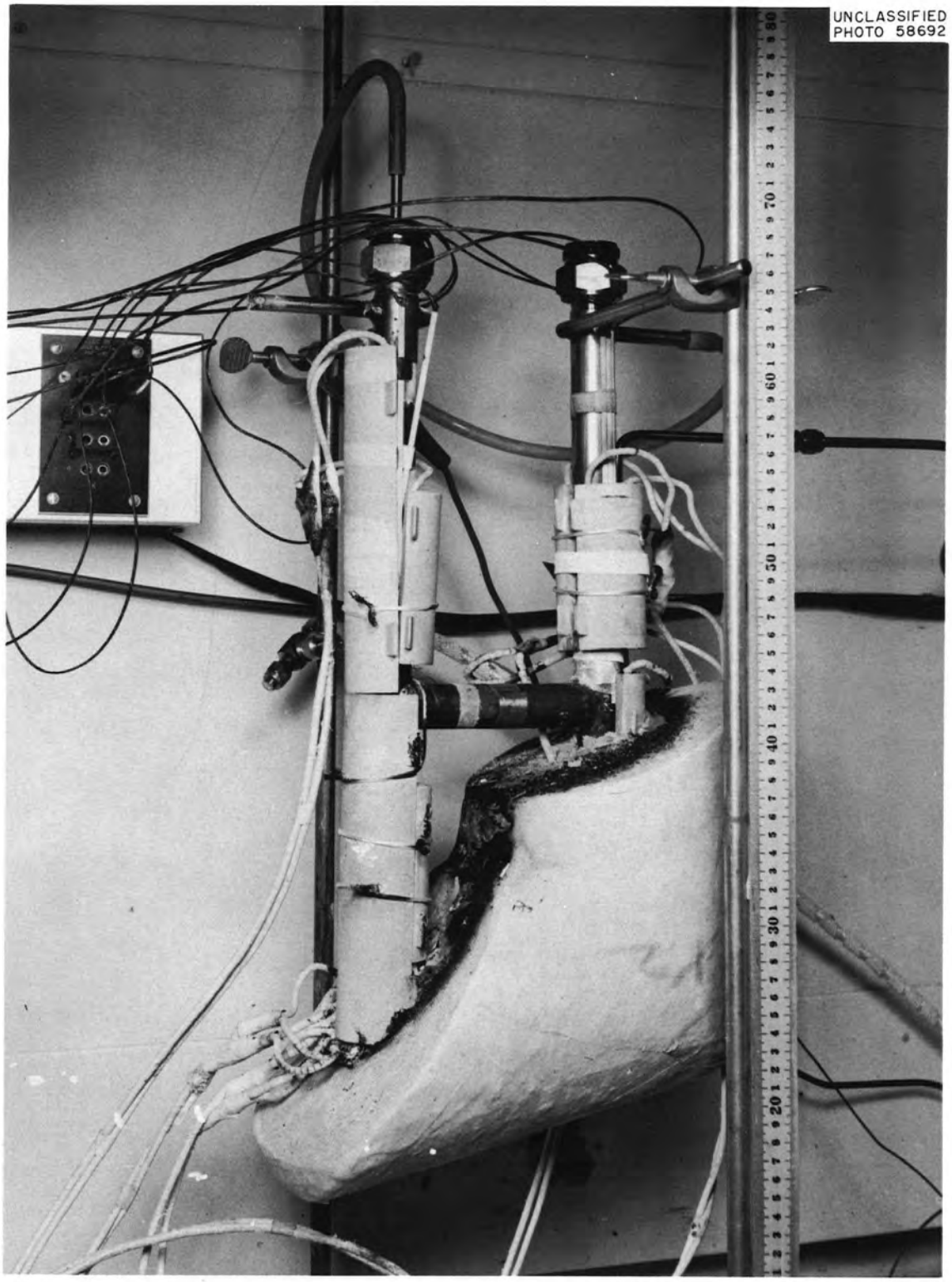


Fig. 34.8. Loop Used to Grow Crystals Shown in Fig. 34.7.

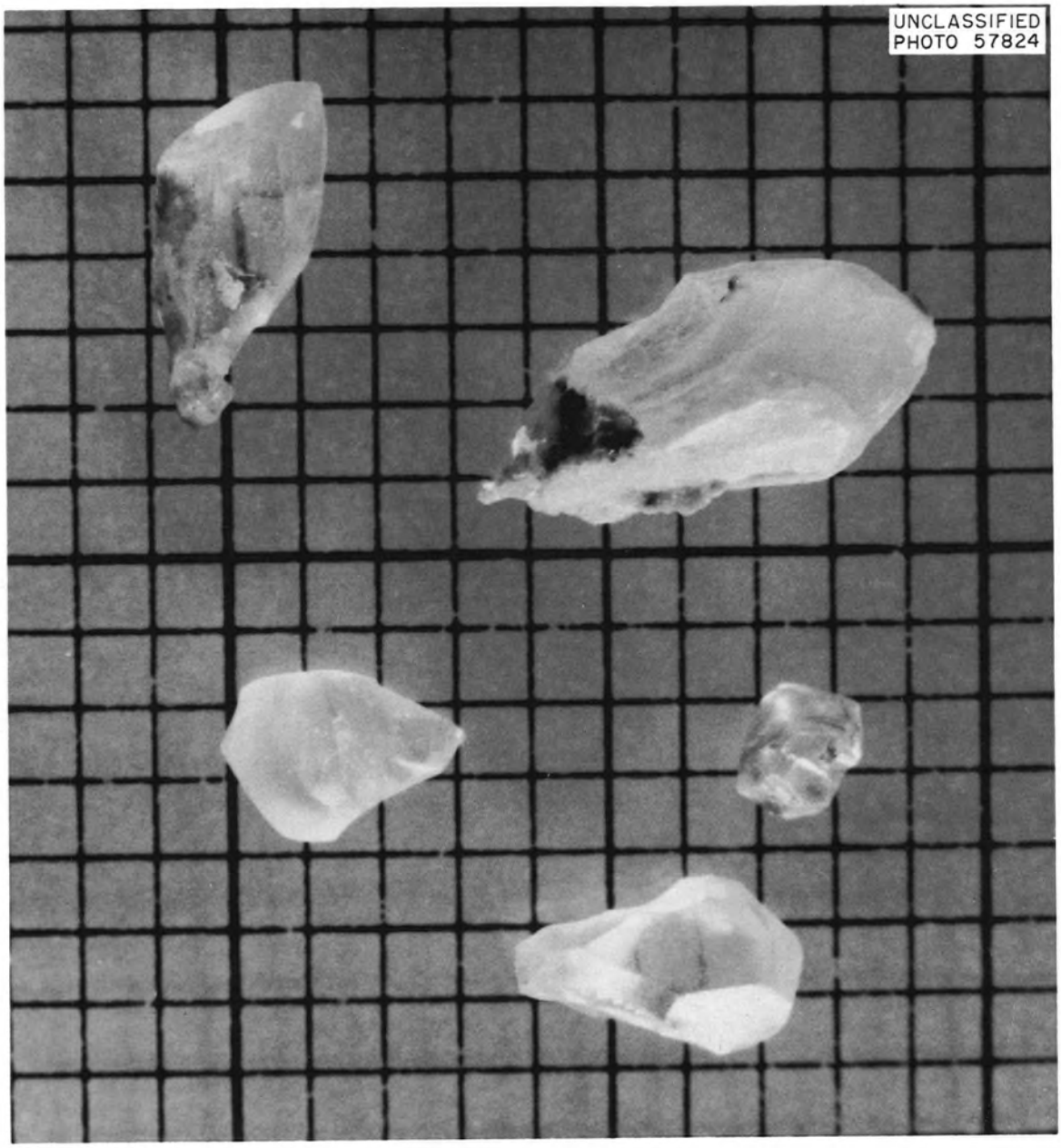


Fig. 34.9. MgO Crystals Grown in NaF-LiF Eutectic Mixture in a Nickel Loop (1-mm Grid).

# PURIFICATION OF BERYLLIUM BY ACETYLACETONE-EDTA SOLVENT EXTRACTION[14]

C. E. L. Bamberger[15] C. F. Baes, Jr.
H. F. McDuffie

The development and application of a solvent extraction process for the preparation of high-purity BeO have been described previously.[16,17] Ethylenediaminetetraacetic acid (EDTA-$H_4Y$) is used as a masking or sequestering agent to retain metallic impurities in an aqueous phase from which the beryllium is extracted into an organic phase ($CCl_4$) as a complex with acetylacetone (HX). Subsequent back-extraction of the beryllium into nitric acid, followed by precipitation of beryllium hydroxide, filtering, drying, and calcination to 1000°C, has given products of high purity (e.g., <10 ppm each of Ca, Al, and Si; <5 ppm each of Fe, Mg, and Cu; all other metallic impurities below the level of detection, <5 to 10 ppm in most cases).

During the past year the fundamental chemistry of this process has been more fully investigated as a means of extending its applicability to the treatment of a variety of starting materials and to the production of a variety of products. In addition, steps have been taken to improve product recoveries.

## Chemistry of Extraction

A quantitative examination of the following pertinent equilibria was carried out:

$$Be^{2+}(aq) + HX(aq) \rightleftharpoons BeX^{+}(aq) + H^{+}(aq) \ , \qquad Q_1 \ , \qquad (1)$$

$$Be^{2+}(aq) + 2HX(aq) \rightleftharpoons BeX_2(aq) + 2H^{+}(aq) \ , \qquad Q_2 \ , \qquad (2)$$

$$BeX_2(aq) \rightleftharpoons BeX_2(org) \ , \qquad Q_{DB} \ , \qquad (3)$$

$$HX(aq) \rightleftharpoons HX(org) \ , \qquad Q_{DX} \ , \qquad (4)$$

$$BeX_2(s) \rightleftharpoons BeX_2(aq) \ . \qquad (5)$$

The equilibrium quotients $Q_1$ and $Q_2$ were determined as a function of ionic strength by aqueous phase potentiometric measurements of hydrogen ion concentration. The results (Fig. 34.10) indicate that $Q_2$ is more highly dependent on ionic strength than is $Q_1$, though both reactions involve a $\Delta z^2$ of −2. There are no values of $Q_1$ and $Q_2$ reported in the literature at the same temperature (25°C) and at known ionic strength with which the present results may be compared.

$Q_{DB}$ is virtually equal to the overall beryllium extraction coefficient $D$, $D \equiv [\Sigma\ Be](org)/[\Sigma\ Be](aq)$ at aqueous pH values above 5.5. It was determined as a function of ionic strength in two phase equilibrations with the aid of $Be^7$ tracer and the previously described[16] spectrophotometric method of analysis. The results (Fig. 34.11) show a surprisingly large increase of $Q_{DB}$ with ionic strength. The effect was largest with NaCl as the aqueous salting agent, though even the disodium salt of EDTA produced a similar effect. That this is a salting-out effect was confirmed by the corresponding opposite variation in the solubility of solid $BeX_2$ in the aqueous phase (also shown in Fig. 34.11). It is perhaps also reflected in the higher ionic strength dependence of $Q_2$ compared with $Q_1$, implying as it does the lesser tendency of aqueous $BeX_2$ to form as the ionic strength is increased. This salting-out effect is much larger than that usually encountered and should be investigated further. If it is assumed for the present that it may be attributed entirely to $BeX_2(aq)$ hydration, and thus is related to changes in the aqueous water activity, then calculation shows

[14] Based largely on work included in a paper by R. E. Moore, J. H. Shaffer, C. F. Baes, Jr., H. F. McDuffie, and C. E. L. Bamberger, presented at the Solvent Extraction Chemistry Symposium, Gatlinburg, Tenn., Oct. 23–26, 1961; submitted for publication in *Nuclear Science and Engineering*.

[15] CNEA, Argentina, International Atomic Energy Agency Fellow at Oak Ridge National Laboratory.

[16] *Reactor Chem. Div. Ann. Progr. Rept. Jan. 31, 1962*, ORNL-3262, p 153.

[17] R. E. Moore, J. H. Shaffer, and H. F. McDuffie, *The Preparation of High-Purity Beryllium Oxide Through the Acetylacetone-EDTA Solvent Extraction Process*, ORNL-3323 (Sept. 13, 1962).

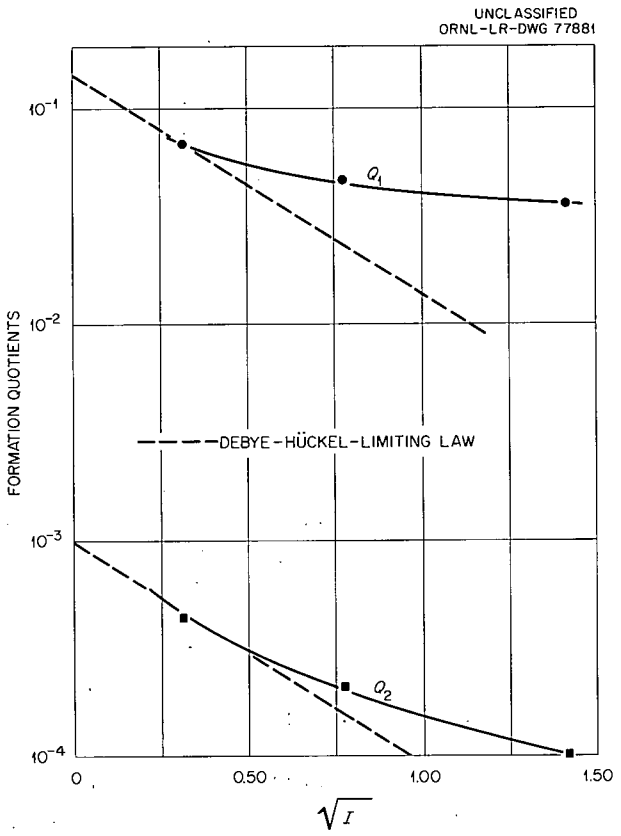


**Fig. 34.10. Effect of Ionic Strength on $Q_1$ and $Q_2$.**

that approximately 18 hydrate water molecules must be assumed to be associated with aqueous $BeX_2$ to explain the magnitude of the effect.

The distribution coefficient $Q_{DX}$ of acetylacetone between carbon tetrachloride and various aqueous solutions has also been examined as an important parameter in the process.

The constants $Q_1$, $Q_2$, $Q_{DB}$, and $Q_{DX}$ are related to $D$, the overall beryllium extraction coefficient, by the expressions

$$D = \frac{Q_{DB}}{\dfrac{[H^+]^2(aq)}{Q_2[HX]^2(aq)} + \dfrac{Q_1[H^+](aq)}{Q_2[HX](aq)} + 1},$$

$$Q_{DX} = \frac{[HX](org)}{[HX](aq)}.$$

Using the measured values of these constants, values of $D$ were calculated by these relations for a series of beryllium extraction measurements. These are compared with observed values in Fig. 34.12. The agreement between predicted and observed behavior is considered adequate in view of the uncertainties involved in the evaluation of the variables $[H^+](aq)$ and $[HX](aq)$. Thus it appears that the chemistry of the process is described in its essentials by reactions (1) to (4) and that these will be adequate for predicting important process parameters in future applications. Beryllium hydrolysis, known to be important in noncomplexing aqueous media at pH values above 3, has not appeared to be significant in the investigations thus far. This presumably results from the complexing effect of HX, which is usually present in such aqueous solutions during the extraction steps.

The rates of the various reactions have been examined briefly. Reactions (1) and (2) presumably involve the dehydration of the very strongly hydrated beryllium ion, and yet both seem quite rapid, equilibration usually being attained in a matter of minutes. Reaction (3) is similarly fast with sufficient agitation.

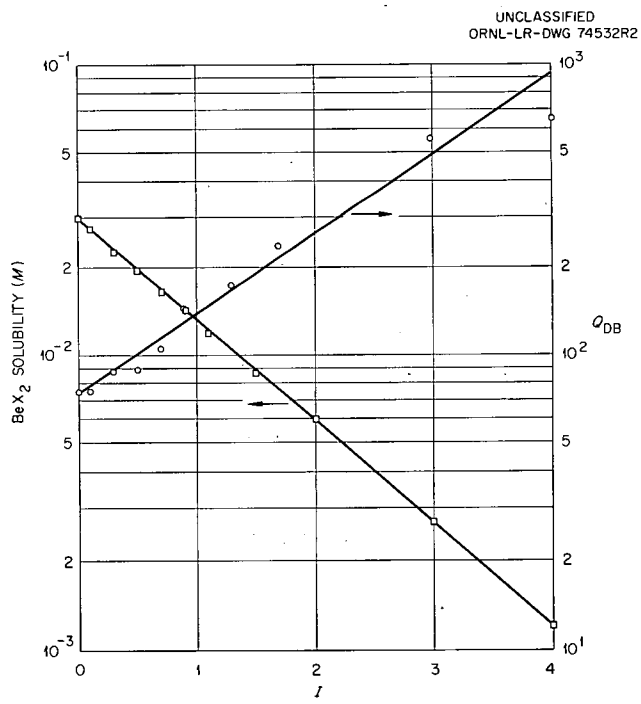


**Fig. 34.11. Effect of Ionic Strength on $BeX_2$ Solubility and on $Q_{DB}$.**

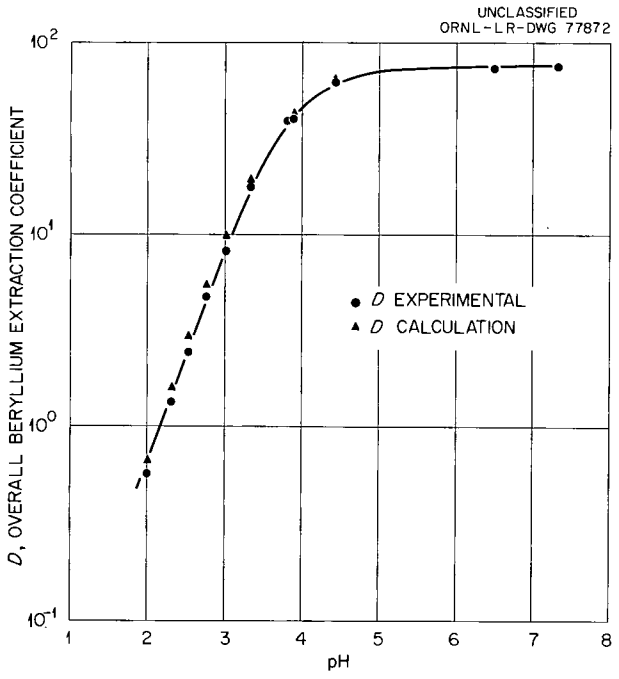


**Fig. 34.12. Comparison of Calculated and Observed Values of *D* as a Function of pH.**

The extraction behavior of $Mg^{2+}$ was examined further since the appreciable extraction reported previously[18] seemed inconsistent with available literature values for the corresponding formation quotients. New measurements based on spectrographic and flame photometric analysis failed to confirm the extraction of magnesium, and it is now believed that the earlier results, based on colorimetric analysis, were in error and that magnesium is not extracted.

## Increased Processing Efficiency

Thus far in the application of this process, the primary objective has been to attain the highest possible purity with the simplest processing procedures. As a consequence, low product recoveries (typically 25%) were accepted. Some of these losses may be attributed to insufficient agitation of the liquid phases in the large plastic containers used, to the poor filterability of the precipitated $Be(OH)_2$, and to ignition losses resulting from the presence of acetylacetone in the precipitate. The major losses probably occurred after the back-extraction. An appreciable amount of acetylacetone enters the aqueous phase during this step because its distribution coefficient $Q_{DX}$ is low ($\sim 3$). (Multiple scrubbing with $CCl_4$ would be necessary to remove it.) In some preparations, the acid strip solution was half neutralized with ammonia before $CCl_4$ scrubbing. This removed the HX, but at the expense of a corresponding amount of beryllium loss to the scrub solution.

During the past year, these various difficulties have been examined in order to improve the yield of the process. Losses in various processing steps have been measured using $Be^7$ tracer and the spectrophotometric method described previously[19] for analysis. The results (Table 34.3) show that in no step is the loss great. Use of a large excess of solid EDTA as the sequestering agent, however, appears to cause an unnecessary loss which may be avoided by limiting the amount of EDTA added.

The efficiency of scrubbing the acid solution to remove HX may be improved by replacing $CCl_4$ with chloroform as the scrubbing agent, the HX distribution coefficients to this solvent being $\sim 25$.

An improved technique for the precipitation of $Be(OH)_2$ (ref 20) which results in a granular solid of good filterability has been employed in current processing. It consists of precipitation at a controlled rate with gaseous ammonia at 75°C. Losses in this processing step thus can be reduced.

Finally, the effects of these process modifications are being tested in all-plastic stirred vessels suitable for the handling of 100-g batches of BeO. This equipment, in which the hot precipitation step has already been tested successfully, permits much better agitation during processing, thus materially reducing the time required and the losses of product. It is anticipated that yields of approximately 90% will be demonstrated with the modified process in this all-plastic equipment.

[18] R. E. Moore, J. H. Shaffer, and H. F. McDuffie, *The Preparation of High-Purity Beryllium Oxide Through the Acetylacetone-EDTA Solvent Extraction Process*, ORNL-3323 (Sept. 13, 1962).

[19] *Reactor Chem. Div. Ann. Progr. Rept. Jan. 31, 1962*, ORNL-3262, p 153.

[20] A. Suner, C. Bamberger, and F. Laguna, *Precipitation of Beryllium Hydroxide with Inert Gas–Ammonia Mixtures*, paper presented at The Third Conference on Nuclear Reactor Chemistry, Gatlinburg, Tenn., Oct. 9–11, 1962; proceedings to be published, TID-7641.

**Table 34.3. Losses in Various Beryllium Purification Steps (for Phase Ratios of 1)**

| Step | Beryllium Lost (%) |
|---|---|
| 1. First water scrub on $BeX_2$-$CCl_4$ solution (after 20 min) | 1.8 |
| First water scrub (after 20 hr) | 1.9 |
| 2. Second water scrub | 1.5 |
| 3. First scrub with saturated solution of EDTA | 1.5 |
| 4. Second EDTA scrub (solid EDTA plus water) | 3.6 |
| 5. Water scrub | 1.3 |
| 6. $HNO_3$ stripping (after 20 min) | 0.9 |
| $HNO_3$ stripping (after 60 min) | 0.9 |
| $HNO_3$ stripping (after 180 min) | 0.9 |
| 7. First $CCl_4$ scrub of strip solution | 0.12 |
| 8. Second $CCl_4$ scrub of strip solution | 0.018 |
| 9. Third $CCl_4$ scrub of strip solution | 0.012 |

# Publications

| AUTHOR(S) | TITLE | PUBLICATION |
|---|---|---|
| Adams, R. E. | Seventh AEC Air Cleaning Conference | *Nucl. Safety* **3**(3), 41 (1962) |
| Adams, R. E., and W. E. Browning, Jr. | Removal of Radioiodine Vapor from Gases at Elevated Temperatures | *Trans. Am. Nucl. Soc.* **5**(1), 47 (1962) |
| | The Removal of Iodine from Gas Streams | TID-7627, p 242 (1962) |
| Alvarez-Funes, A., J. Braunstein, and M. Blander | Thermodynamic Association Constants of Silver Ions with Bromide or Iodide Ions in Molten Potassium Nitrate and Their Comparison with the Quasi-Lattice Theory | *J. Am. Chem. Soc.* **84**, 1539 (1962) |
| Baes, C. F. | An Isopiestic Investigation of Di(2-ethylhexyl)-Phosphoric Acid (DPA) and Tri-*n*-octylphosphine Oxide (TPO) in *n*-Octane | *J. Phys. Chem.* **66**, 1629, (1962) |
| | The Extraction of Metallic Species by Dialkyphosphoric Acids | *J. Inorg. Nucl. Chem.* **24**, 707 (1962) |
| Baes, C. F., and N. J. Meyer | Acidity Measurements at Elevated Temperatures: I. Uranium(VI) Hydrolysis at 25° and 94°C | *Inorg. Chem.* **1**, 780 (1962) |
| Barton, C. J. | Environmental Contamination Around Nuclear Facilities | *Nucl. Safety* **4**(2) (1962) |
| Barton, C. J., G. M. Hebert, and W. L. Marshall | Aqueous Systems at High Temperature. II. Liquid-Liquid Immiscibility in the System $UO_3$-$SO_3$-$N_2O_5$-$H_2O$ above 300°C | *J. Inorg. Nucl. Chem.* **21**, 141 (1961) |
| Barton, C. J., and R. A. Strehlow | Blankets for Thermonuclear Reactors | ORNL-3258 (June 27, 1962) |
| Bauman, H. F., J. R. Buchanan, J. R. Engel, P. N. Haubenreich, and D. M. Richardson | Summary of HRT Runs 22, 23, and 24 | ORNL TM-106 (Mar. 6, 1962) |
| Bennett, R. L., W. T. Rainey, Jr., and W. M. McClain | Drift Studies on Chromel-P/Alumel Thermocouples in Helium Atmospheres | *Temperature, Its Measurement and Control in Science and Industry*, ed. by A. I. Dahl, vol 3, pt 2, pp 289–94, Reinhold, New York, 1962 |

| AUTHOR(S) | TITLE | PUBLICATION |
|---|---|---|
| Blander, M. | Excess Free Energies and Heats of Mixing in Certain Molten Salt Mixtures | *J. Chem. Phys.* **37**, 172 (1962) |
| | Thermodynamic Properties of Molten Salt Solutions | ORNL-3293 (Oct. 12, 1962) |
| | Van der Waals Energy Changes in the Mixing of Molten Salts | *J. Chem. Phys.* **36**, 1092 (1962) |
| Blankenship, F. F., and W. R. Grimes | Recent Developments in the Chemistry of the Molten Salt Reactor Experiment | TID-7622 (July 1962) |
| Boles, R. L., and R. E. Thoma | Volatility Process Phase Studies — A Survey of Molten Fluoride Solvent Mixtures Suitable for Dissolution of $AlF_3$ | ORNL TM-400 (Oct. 22, 1962) |
| Bopp, C. D., W. W. Parkinson, and O. Sisman | Plastics | *Radiation Effects on Organic Materials*, ed. by R. O. Bolt and J. G. Carroll, Academic Press, New York, 1962 |
| Bopp, C. D., and R. L. Towns | Calorimetric Measurement of Nuclear Heating in a Reactor | *Nucl. Sci. Eng.* **13**, 245 (1962) |
| Braunstein, J., M. Blander, and R. M. Lindgren | The Evaluation of Thermodynamic Association Constants in Solutions with an Application to Molten Salt Solutions | *J. Am. Chem. Soc.* **84**, 1529 (1962) |
| Braunstein, J., and R. M. Lindgren | The Association of Cadmium Ion with Bromide and Iodide Ions in Molten Equimolar $NaNO_3$-$KNO_3$ | *J. Am. Chem. Soc.* **84**, 1534 (1962) |
| Browning, W. E., Jr. | Methods of Measuring Temperature in Nuclear Reactors | *Progr. Nucl. Energy, Ser. IV* **5**, 1 (1963) |
| | Removal of Radioiodine from Gases | *Nucl. Safety* **4**(2), 18 (1962) |
| Browning, W. E., Jr., and R. D. Ackley | Characterization of Gas-Borne Radioactive Materials by a Diffusion Cell Technique | *Trans. Am. Nucl. Soc.* **5**(1), 47–50 (1962) |
| Browning, W. E., Jr., and H. L. Hemphill | Thermocouples for Measurement of the Surface Temperature of Nuclear Fuel Elements | *Temperature, Its Measurement and Control in Science and Industry*, ed. by A. I. Dahl, vol 3, pt 2, pp 723–33, Reinhold, New York, 1962 |
| Browning, W. E., Jr., and C. E. Miller, Jr. | Calculated Radiation Induced Changes in Thermocouple Compositions | *Temperature, Its Measurement and Control in Science and Industry*, ed. by A. I. Dahl, vol 3, pt 2, pp 271–76, Reinhold, New York, 1962 |
| Burns, J. H. | The Crystal Structure of Lithium Fluoroantimonate(V) | *Acta Cryst.* **15**, 1098 (1962) |
| | Unit Cell and Space Group of $LiBrO_3$ | *Acta Cryst.* **15**, 89 (1962) |
| Cannon, M. C., W. R. Grimes, W. T. Ward, and G. M. Watson | Adsorption of Xenon and Argon on Graphite | *Nucl. Sci. Eng.* **12**, 4–9 (1962) |

| AUTHOR(S) | TITLE | PUBLICATION |
|---|---|---|
| Cantor, S., and T. S. Carlton | Freezing Point Depressions in Sodium Fluoride. II. Effect of Tetravalent Fluorides | *J. Phys. Chem.* **66**, 2711 (1962) |
| Carroll, R. M. | Argon Activation Measures Irradiation Flux Continuously | *Nucleonics* **20**, 42 (1962) |
| | Fission Product Release from $UO_2$ | *Nucl. Safety* **4**(1), 35 (1962) |
| Clark, W. E., L. Rice, D. N. Hess, E. S. Snavely, and B. L. Johnson | Supplemental Studies of the Corrosion of Materials of Construction for the Darex Process | ORNL TM-417 (Nov. 19, 1962) |
| Compere, E. L., A. J. Shor, L. F. Woo, and H. C. Savage | Irradiation Effects on Thoria-Urania Slurries | TID-7622 (July 1962) |
| DeVan, J. H., and R. B. Evans III | Corrosion Behavior of Reactor Materials in Fluoride Salt Mixtures | ORNL TM-328 (Sept. 19, 1962) |
| Engel, J. R., H. F. Bauman, J. R. Buchanan, P. N. Haubenreich, H. B. Piper, and D. M. Richardson | Summary of HRT Run 25 | ORNL TM-173 (July 25, 1962) |
| Evans, R. B., III, G. M. Watson, and E. A. Mason | Gaseous Diffusion in Porous Media. II. Effects of Pressure Gradients | *J. Chem. Phys.* **36**, 1894 (1962) |
| Evans, R. B., III, G. M. Watson, and J. Truitt | Interdiffusion of Gases in a Low Permeability Graphite at Uniform Pressure | *J. Appl. Phys.* **33**(9) 2682 (1962) |
| Franck, E. U., J. E. Savolainen, and W. L. Marshall | Electrical Conductance Cell Assembly for Use with Aqueous Solutions up to 800°C and 4000 Bars | *Rev. Sci. Instr.* **33**(1), 115 (1962) |
| Friedman, H. A., G. M. Hebert, and R. E. Thoma | Thermal Analysis and Gradient Quenching Apparatus and Techniques for the Investigation of Fused Salt Phase Equilibria | ORNL-3373 (Dec. 18, 1962) |
| Grimes, W. R., J. H. Shaffer, R. A. Strehlow, W. T. Ward, and G. M. Watson | Radioisotopes as Tracers for Reactions in Molten Fluoride Media | *Radioiostopes in the Physical Sciences and Industry, Proc. Conf. Copenhagen,* Sept. 16–18, 1960, vol 3, pp 575–90, IAEA, Vienna, 1962 |
| Grimes, W. R., G. M. Watson, J. H. DeVan, and R. B. Evans III | Radiotracer Techniques in the Study of Corrosion by Molten Fluorides | *Radioisotopes in the Physical Sciences and Industry, Proc. Conf. Copenhagen,* Sept. 16–18, 1960, vol 3, pp 559–74, IAEA, Vienna, 1962 |
| Jenks, G. H., and J. E. Baker | Determination of the Effect of High Excess $H_2SO_4$ Concentrations on the Radiation Induced Corrosion of Zirconium and Titanium Alloys in 0.17 *m* $UO_2SO_4$ | ORNL-2943 (Apr. 16, 1962) |
| | In-Pile Loop Investigations of Corrosion of Zircaloy-2 and Other Possible Reactor Materials in 0.04 *m* $UO_2SO_4$ at 280°C | ORNL-2962 (Apr. 23, 1962) |

| AUTHOR(S) | TITLE | PUBLICATION |
|---|---|---|
| Jones, E. V., and W. L. Marshall | Aqueous Systems at High Temperature. IV. Compositions of Heavy- and Light-Liquid Phases in the Systems $UO_3$-$SO_3$-$H_2O$ and $UO_3$-$SO_3$-$D_2O$, 280–350°C | *J. Inorg. Nucl. Chem.* **23**, 287 (1961) |
| | Aqueous Systems at High Temperature. V. Distribution of CuO and NiO Components in the Two-Liquid-Phase Region of the System $UO_3$-$SO_3$-$H_2O$ and Its $D_2O$ Analog, 300–350° | *J. Inorg. Nucl. Chem.* **23**, 295 (1961) |
| Keilholtz, G. W., J. E. Lee, R. P. Shields, and W. E. Browning, Jr. | Radiation Damage in BeO | *Symposium on Radiation Damage in Solids and Reactor Materials, Venice, Italy, 1962*, vol II, IAEA, 1962 |
| Kelly, M. J., W. W. Johnston, and C. D. Baumann | The Effects of Nuclear Radiation on Thermocouples | *Temperature, Its Measurement and Control in Science and Industry*, ed. by A. I. Dahl, vol 3, pt 2, pp 265–69, Reinhold, New York, 1962 |
| Manning, D. L., R. C. Bansal, J. Braunstein, and M. Blander | Association Constants in the System Silver Nitrate–Sodium Bromide–Sodium Nitrate and Their Comparison with the Quasi-Lattice Theory | *J. Am. Chem. Soc.* **84**, 2028 (1962) |
| Manning, D. L., J. Braunstein, and M. Blander | Association Constants of $Ag^+$ and $Cl^-$ in Molten $KNO_3$ | *J. Phys. Chem.* **66**, 2069 (1962) |
| Marshall, W. L., and J. S. Gill | Aqueous Systems at High Temperature. III. Investigations on the System $UO_3$-CuO-NiO-$SO_3$-$H_2O$ at 300°C | *J. Inorg. Nucl. Chem.* **25**, 115 (1961) |
| Marshall, W. L., E. V. Jones, G. M. Hebert, and F. Smith | Aqueous Systems at High Temperature. VII. Liquid-Liquid Immiscibility and Critical Phenomena in the Systems $UO_3$-$SO_3$-$H_2O$, $UO_3$-$SO_3$-$D_2O$, CuO-$SO_3$-$D_2O$, 270–430°C | *J. Inorg. Nucl. Chem.* **24**, 995 (1962) |
| Miller, C. E., R. P. Shields, B. F. Roberts, and W. E. Browning, Jr. | Release of Fission Products by the In-Pile Melting of Uranium Dioxide Fuel | *Trans. Am. Nucl. Soc.* **5**(1), 43 (1962) |
| Moore, R. E., J. H. Shaffer, and H. F. McDuffie | Preparation of High-Purity Beryllium Oxide | TID-7622 (July 1962) |
| | The Preparation of High-Purity Beryllium Oxide Through the Acetylacetone-EDTA Solvent Extraction Process | ORNL-3323 (Sepc. 13, 1962) |
| Morgan, J. G., and M. F. Osborne | Irradiation Effects on $UC_2$ Dispersed in Graphite – Final Report | ORNL-3340 (Dec. 26, 1962) |
| | Radiation Effects on Fueled BeO | ORNL TM-311 (Oct. 4, 1962) |
| Morgan, J. G., M. F. Osborne, and O. Sisman | Irradiation Effects in the EGCR Fuel | *Nucl. Sci. Eng.* **14**, 69 (1962) |

| AUTHOR(S) | TITLE | PUBLICATION |
|---|---|---|
| Osborne, M. F., A. E. Goldman, E. L. Long, Jr., F. R. McQuilkin, and J. G. Morgan | Beryllium Sheathed $UO_2$ Fuel Element Irradiation Tests | *Trans. Am. Nucl. Soc.* **5**, 43 (1962) |
| Overholser, L. G. | Hydrogen Hazards in Graphite Reactors | *Nucl. Safety* **4**(1), 72 (1962) |
| Overholser, L. G., and J. P. Blakely | Evolution of Gas from Graphite | TID-7622 (July 1962) |
| | The Degassing Behavior of Commercial Graphites | *Proc. Conf. Carbon, 5th*, vol 1, pp 194–204, Pergamon, 1962 |
| Parker, G. W. | Review of IAEA Meeting on Reactor Siting | *Nucl. Safety* **3**(4), 12 (1962) |
| Parker, G. W., G. E. Creek, and W. J. Martin | Fission Product Release from $UO_2$ | *Proceedings of Panel on Safe Siting of Nuclear Reactors*, IAEA, Oct. 31–Nov. 3, 1961, PL-42/VR/1-V1 (Mar. 9, 1962) |
| | Fuel Element Decomposition Products | *Proceedings of 7th AEC-Brookhaven Air Cleaning Conference*, TID-7627, pp 261–83 (March 1962) |
| | Release of Fission Products from Reactor Grade $UO_2$ by Diffusion, Oxidation, and Melting | TID-7622 (July 1962) |
| Redman, J. D., and R. A. Strehlow | Calibration of Ionization Gauges Operated Without a Glass Envelope | ORNL TM-115 (Feb. 15, 1962) |
| Robbins, G. D., and J. H. Burns | X-Ray Diffraction Study of $Cs_3ZrF_7$ | ORNL TM-310 (Aug. 7, 1962) |
| Savage, H. C., E. L. Compere, J. M. Baker, V. A. DeCarlo, and A. J. Shor | In-Pile Loop Irradiation of Aqueous Thoria-Urania Slurry at Elevated Temperature. Design and In-Pile Operation of Loop L-2-27S | ORNL-3222 (Jan. 29, 1962) |
| Shaffer, J. H., W. R. Grimes, and G. M. Watson | Boron Trifluoride as a Soluble Poison in Molten Salt Reactor Fuels | *Nucl. Sci. Eng.* **12**, 337 (1962) |
| Shields, R. P., J. E. Lee, and W. E. Browning, Jr. | Effects of Fast-Neutron Irradiation and High Temperature on Beryllium Oxide | ORNL-3164 (Mar. 19, 1962) |
| Shields, R. P., C. E. Miller, Jr., R. A. Lorenz, and W. E. Browning, Jr. | Release of Fission Products on the In-Pile Melting of Reactor Fuels | TID-7622 (July 1962) |
| Shoup, C. S., Jr. | Transport Properties of Dissociating Gaseous Mixtures | ORNL TM-440 (Dec. 18, 1962) |
| Sisman, O., W. W. Parkinson, and C. D. Bopp | Polymers | *Radiation Effects on Organic Materials*, Academic Press, New York, 1962 |
| Soldano, B. A., and C. S. Patterson | Osmotic Behavior of Aqueous Salt Solutions at Elevated Temperatures. Part II | *J. Chem. Soc.* **175**, 937 (1962) |

| AUTHOR(S) | TITLE | PUBLICATION |
|---|---|---|
| Strehlow, R. A. | Vapor Pressure Measurement Methods for Diffusion Pump and Mechanical Pump Oils | ORNL TM-205 (Apr. 20, 1962) |
| Sturm, B. J. | Phase Equilibria in the System Chromium(II) Fluoride—Chromium(III) Fluoride | *Inorg. Chem.* **1**, 665 (1962) |
| Thoma, R. E. | Cation Size Effects on Complex Fluoride Compound Formation | *Inorg. Chem.* **1**, 220 (1962) |
| Thoma, R. E., H. Insley, H. A. Friedman, and C. F. Weaver | Phase Equilibria in the System $NaF-ThF_4-UF_4$ | *J. Am. Ceram. Soc.* **46**, 37 (1963) |
| Truitt, J., N. V. Smith, G. M. Watson, R. B. Evans III, and E. A. Mason | Transport of Noble Gases in Graphites | ORNL TM-135 (Feb. 7, 1962) |
| Watson, G. M., R. B. Evans III, W. R. Grimes, and N. V. Smith | Solubility of Noble Gases in Molten Fluorides. III. In Lithium-Beryllium Fluoride | *J. Chem. Eng. Data* **7**, 285 (1962) |
| Watson, G. M., R. B. Evans III, and J. Truitt | A Diffusion Model for the Transport of Gases in Porous Media | TID-7622 (July 1962) |
| Weaver, C. F., and R. E. Thoma | Production of Single Crystals of Lithium Fluoride with Selected Isotopic Ratios of Lithium | *Branched Chain* **18**(2), 12–13 (1962) [published by the East Tennessee Section of the American Chemical Society] |

# Papers Presented at Scientific and Technical Meetings

| AUTHOR(S) | TITLE | PLACE PRESENTED |
|---|---|---|
| Adams,* R. E., and W. E. Browning, Jr. | Removal of Radioiodine Vapor from Gases at Elevated Temperatures | American Nuclear Society, Boston, June 18–21, 1962 |
| Baes, C. F., Jr. | The Determination of Acidity at Elevated Temperatures | American Chemical Society, Washington, D.C., Mar. 20–29, 1962 |
| | Physicochemical Aspects of Selected Solvent Extraction Systems | ORINS Lecture at Louisiana State University, Apr. 11, 1962 |
| | Problems of the Precise Measurement of Acidity at Room Temperature and at Elevated Temperatures | ORINS Lecture at Loyola University, Apr. 9, 1962 |
| | | ORINS Lecture at Tulane University, Apr. 10, 1962 |
| | | ORINS Lecture at the University of Texas, Apr. 12, 1962 |
| | | ORINS Lecture at the University of Arkansas, Apr. 13, 1962 |
| | The Synergistic Effect in Organophosphate Extraction Systems | Solvent Extraction Chemistry Symposium, Gatlinburg, Tenn. Oct. 23–26, 1962 |
| Baes,* C. F., Jr., and T. H. Handley | PWR Chemistry: Studies of the ORR In-Pile Loop | Conference on Nuclear Reactor Chemistry, 3d, Gatlinburg, Tenn., Oct. 9–11, 1962 |
| Blood, C. M., F. F. Blankenship, W. R. Grimes,* and G. M. Watson | Activities of Some Transition Metal Fluorides in Molten Fluoride Mixtures | Seventh International Conference on Coordination Chemistry, Stockholm, June 25–29, 1962 |
| Bohlmann, E. G., E. L. Compere,* S. A. Reed, and D. M. Richardson | Compatibility Studies with Liquid Coolants | Coated Particle Fuels Working Group, 3d Meeting, May 7–8, 1962, ORNL |
| Braunstein, J. | Solvent Effect on the Association of Cadmium Ion with Bromide Ion in Molten Alkali Nitrates | American Chemical Society, Washington, D.C., Mar. 20–29, 1962 |

*Speaker.

| AUTHOR(S) | TITLE | PLACE PRESENTED |
|---|---|---|
| Browning,* W. E., Jr., and R. D. Ackley | Characterization of Gas-Borne Radioactive Materials by a Diffusion Cell Technique | American Nuclear Society, Boston, June 18–21, 1962 |
| | Characterization of Millimicron Radioactive Aerosols and Their Removal from Gases | Conference on Nuclear Reactor Chemistry, 3d, Gatlinburg, Tenn., Oct. 9–11, 1962 |
| Burns, J. H. | The Crystal Structure of $LiCsF_2$ | American Crystallographic Association, Philadelphia, June 18–22, 1962 |
| | The Crystal Structures of Two New Alkali Fluorides: $LiBrF_2$ and $LiCsF_2$ | American Chemical Society Regional Meeting, Gatlinburg, Tenn., November 1962 |
| Carroll, R. M. | Fission Gas Release Studies | General Electric Company, Pleasanton, Calif., May 1, 1962 |
| | | Karlsruhe, Germany |
| | Fission Gas Release in $UO_2$ During Irradiation | Graduate Engineering Education Program sponsored by General Electric Company, Richland, Wash., August 1962 |
| | Fundamental Behavior of Ceramic Fuels | US/UK Exchange under terms of Libby-Cockcroft Agreement, Harwell, England, Sept. 24–28, 1962 |
| | | US/Euratom Exchange, Brussels, Oct. 1–5, 1962 |
| Carroll, R. M., and P. E. Reagan* | Fission Gas Release from Pyrolytic-Carbon-Coated Fuel Particles During Irradiation | American Ceramics Society Regional Meeting, Seattle, Wash., Oct. 16–19, 1962 |
| Compere, E. L., S. A. Reed, D. M. Richardson, and L. F. Woo (presented by G. M. Watson) | Compatibility Studies with Liquid Coolants | Ceramic-Coated Particles and Graphite-Matrix Fuels Meeting, Battelle Memorial Institute, Nov. 5–6, 1962 |
| Compere,* E. L., H. C. Savage, A. J. Shor, and E. G. Bohlmann | In-Pile Testing of Circulating Thoria Suspensions | Thorium Fuel Cycle Symposium, Gatlinburg, Tenn., Dec. 5–7, 1962 |
| Evans, R. B., III | Diffusion of Fuel and Nonvolatile Fission Products in Fueled-Graphite Systems | Coated Particle Fuels Working Group, 3d Meeting, ORNL, May 7–8, 1962 |
| Evans,* R. B., III, E. A. Mason, and J. Truitt | Diffusion of Gases in Graphite Pores | Carbon Mass Transfer Problems Meeting at AEE, Winfrith, England, Mar. 28–30, 1962 |

*Speaker.

| AUTHOR(S) | TITLE | PLACE PRESENTED |
|---|---|---|
| Friedman, H. A. | Analytical Techniques Used in Evaluating High-Temperature Phase Equilibria: Application to the $UO_2$-$ThO_2$-$O_2$ System | Analytical Chemistry in Nuclear Reactor Technology, 6th Conference, Gatlinburg, Tenn., Oct. 9–11, 1962 |
| | Techniques Used in Evaluating High-Temperature Phase Equilibria: Application to the $UO_2$-$ThO_2$-$O_2$ System | Tennessee Academy of Science Annual Meeting, Nov. 23–24, 1962 |
| Griess,* J. C., H. C. Savage, J. G. Rainwater, J. L. English, and T. H. Mauney | The Corrosion of Aluminum Alloys Under Simulated ATR and HFIR Conditions | Research Reactor Fuel Element Conference, Gatlinburg, Tenn., Sept. 17–19, 1962 |
| Grimes, W. R. | Materials Problems in Molten Salt Reactors | American Nuclear Society Topical Meeting, San Diego, Apr. 12–13, 1962 |
| Holmes,* H. F., and C. H. Secoy | The Heat of Immersion of Thorium Oxide in Water | American Chemical Society Regional Meeting, Gatlinburg, Tenn., Nov. 1–3, 1962 |
| Jenks,* G. H., and R. J. Davis | Effect of Reactor Radiations on Zircaloy-2 Corrosion in High-Temperature Aqueous Environments | Conference on Nuclear Reactor Chemistry, Gatlinburg, Tenn., Oct. 9–11, 1962 |
| Keilholtz,* G. W., J. E. Lee, Jr., and R. E. Moore | Behavior of BeO Under Irradiation | Second AEC BeO Coordination Meeting, Atomics International, Los Angeles, Aug. 23–24, 1962 |
| Keilholtz,* G. W., J. E. Lee, Jr., R. P. Shields, and W. E. Browning, Jr. | Radiation Damage in BeO | Symposium on Radiation Damage in Solids and Reactor Materials, Venice, Italy, IAEA, May 7–11, 1962 |
| Kirslis, S. S. | Corrosion and $CF_4$ Generation in the MSRE Environment | Conference on Nuclear Reactor Chemistry, Gatlinburg, Tenn., Oct. 9–11, 1962 |
| Miller,* C. E., Jr., R. P. Shields, B. F. Roberts, and W. E. Browning, Jr. | Release of Fission Products by the In-Pile Melting of Uranium Dioxide Fuel | American Nuclear Society, Boston, June 17–21, 1962 |
| Moore, R. E., J. H. Shaffer, C. F. Baes, H. F. McDuffie,* and C. E. L. Bamberger | Purification of Beryllium by Acetylacetone-EDTA Solvent Extraction | Solvent Extraction Chemistry Symposium, Gatlinburg, Tenn., Oct. 23–26, 1962 |
| Overholser, L. G. | Compatibility of Pyrolytic-Carbon-Coated Carbide Fuel Materials with Water Vapor | Coated Particle Fuels Working Group, 3d Meeting, ORNL, May 7–8, 1962 |
| Overholser,* L. G., and J. P. Blakely | Outgassing Characteristics of Various Graphites | US-UK Gas-Coolant Compatibility Meeting, Harwell, England, Apr. 2–4, 1962 |

*Speaker.

| AUTHOR(S) | TITLE | PLACE PRESENTED |
|---|---|---|
| Overholser, L. G., N. V. Smith, and J. P. Blakely, (presented by G. M. Watson) | Compatibility of Pyrolytic-Carbon-Coated Uranium Carbide Particles with Water Vapor | Ceramic-Coated Particles and Graphite-Matrix Fuels Meeting, Battelle Memorial Institute, Nov. 5–6, 1962 |
| Parker,* G. W., G. E. Creek, and W. J. Martin | Parametric Studies of Fission Product Release from $UO_2$ Fuels | Nuclear Reactor Chemistry Conference, Gatlinburg, Tenn., Oct. 9–11, 1962 |
| Parkinson, W. W. | The Effects of Radiation on Organic High Polymers | ORINS Lecture at Texas Woman's University, Apr. 8, 1962 |
| | | Agricultural and Mechanical College of Texas, May 7, 1962 |
| Quist, A. S., H. R. Jolley, E. U. Franck, J. E. Savolainen, and W. L. Marshall* | Electrical Conductance Measurements in Aqueous Systems from 25 to 800°C and at Pressures up to 4000 Bars | American Chemical Society, Washington, D.C., Mar. 21–29, 1962 |
| Rainey,* W. T., Jr., and R. L. Bennett | Stability of Base Metal Thermocouples During Exposure to Various Atmospheres | Instrument Society of America, 17th Annual Conference, Oct. 15–18, 1962 |
| Rainey, W. T., Jr., and L. B. Yeatts, Jr.* | Studies on Pyrolysis Products of Pure Biphenyl | Nuclear Reactor Chemistry Conference, Gatlinburg, Tenn., Oct. 9–11, 1962 |
| Reagan, P. E. | Fission Gas Release from Coated Particles Irradiated in ORR Facilities B9 and C1 | Coated Particle Fuels Working Group, 3d Meeting, ORNL May 7–8, 1962 |
| | | American Ceramics Society Regional Meeting, Seattle, Wash., Oct. 16–19, 1962 |
| Reed,* S. A., W. J. Leonard, and E. L. Compere | Hydriding of Zirconium Alloys in Circulating High-Temperature Aqueous $ThO_2$ and Thorium-Uranium Oxide Slurries | Nuclear Reactor Chemistry Conference, Gatlinburg, Tenn., Oct. 9–11, 1962 |
| Rice,* L., D. N. Hess, and E. S. Snavely | Corrosion of Ni-o-nel During Exposure to Sulfex and Related Process Solutions | AEC Corrosion Symposium, Brookhaven National Laboratory, May 23–25, 1962 |
| Roberts,* B. F., C. E. Miller, Jr., R. P. Shields, and W. E. Browning, Jr. | Release of Fission Products by the In-Pile Destruction of Fuel | Nuclear Reactor Chemistry Conference, Gatlinburg, Tenn., Oct. 9–11, 1962 |
| Shoup,* C. S., Jr., and W. H. Fletcher | Molecular Force Fields for Methyl Isocyanide | American Chemical Society Regional Meeting, Gatlinburg, Tenn., Nov. 1–3, 1962 |

*Speaker.

| AUTHOR(S) | TITLE | PLACE PRESENTED |
|---|---|---|
| Sisman, O. | Irradiation Effects in Plastics | Graduate Engineering Education Program sponsored by General Electric Company, Richland, Wash., August 1962 |
| Thoma, R. E. | Fluoride Solvent Systems for Volatility Processing – Status Report | Volatility Processing Symposium, ORNL, Nov. 14, 1962 |
| Thoma,* R. E., C. F. Weaver, G. M. Hebert, and J. H. Burns | Crystallographic and Phase Studies in the System $NaF-YF_3$ | American Chemical Society Regional Meeting, Gatlinburg, Tenn., November 1962 |
| Thoma,* R. E., C. F. Weaver, H. Insley, and G. M. Hebert | Phase Studies of the MSRE Fuel System | Nuclear Reactor Chemistry Conference, Gatlinburg, Tenn., Oct. 9–11, 1962 |
| Toner, D. F. | LITR Static Capsule Tests for Coated $UC_2$ Particles | Coated Particle Fuels Working Group, 3d Meeting, ORNL, May 7–8, 1962 |
| | Postirradiation Examination of MTR-48 Fuel Bodies | Coated Particle Fuels Working Group, 3d Meeting, ORNL, May 7–8, 1962 |
| Truitt,* J., R. B. Evans III, and A. S. Meyers, Jr. | Counter-Flow of Gases in Porous Media | American Ceramic Society Meeting, New York, Apr. 29–May 3, 1962 |
| Truitt,* J., and N. V. Smith | Permeability Studies of Helium-Graphite Systems for the Experimental Gas-Cooled Reactor | American Ceramic Society Meeting, Bedford Springs, Pa., Oct. 4–6, 1962 |
| Watson,* G. M., C. M. Blood, and R. B. Evans III | Solid State Diffusion of Uranium Through Graphites | Ceramic-Coated Particles and Graphite-Matrix Fuels Meeting, Battelle Memorial Institute, Nov. 5–6, 1962 |

*Speaker.

**ORNL-3417**
**UC-4 – Chemistry**
**TID-4500 (19th ed., Rev.)**

*INTERNAL DISTRIBUTION*

1. C. E. Larson
2. Biology Library
3. Reactor Division Library
4–6. Central Research Library
7–8. ORNL – Y-12 Technical Library, Document Reference Section
9–43. Laboratory Records Department
44. Laboratory Records, ORNL R.C.
45. A. M. Weinberg
46. J. A. Swartout
47–66. G. E. Boyd
67. F. R. Bruce
68. W. H. Jordan
69. H. G. MacPherson
70. A. H. Snell
71. A. L. Boch
72. R. B. Briggs
73. J. A. Lane
74. W. D. Manly
75. H. C. McCurdy
76. D. S. Billington
77. F. L. Culler
78. J. H. Frye, Jr.
79. M. T. Kelley
80. E. H. Taylor
81. S. E. Beall
82. M. A. Bredig
83. L. T. Corbin
84. J. E. Cunningham
85. J. H. Crawford
86. A. P. Fraas
87. E. M. King
88. R. N. Lyon
89. A. J. Miller
90. J. C. White
91. M. J. Skinner
92. W. R. Grimes
93. E. G. Bohlmann
94. H. F. McDuffie
95. G. M. Watson
96. F. F. Blankenship
97. C. H. Secoy
98. C. F. Baes
99. C. J. Barton
100. W. E. Browning
101. S. Cantor
102. R. M. Carroll
103. E. L. Compere
104. R. B. Evans III
105. J. C. Griess
106. G. H. Jenks
107. G. W. Keilholtz
108. W. L. Marshall
109. J. G. Morgan
110. L. G. Overholser
111. G. W. Parker
112. W. W. Parkinson
113. W. T. Rainey
114. H. C. Savage
115. J. H. Shaffer
116. O. Sisman
117. R. A. Strehlow
118. R. E. Thoma
119. D. F. Toner
120–139. G. C. Warlick
140. E. V. Jones (Consultant)
141. Farrington Daniels (Consultant)
142. F. T. Miles (Consultant)
143. F. T. Gucker (Consultant)
144. Leo Brewer (Consultant)
145. H. Insley (Consultant)
146. J. E. Ricci (Consultant)
147. D. G. Hill (Consultant)
148. G. W. Morey (Consultant)
149. Henry Eyring (Consultant)
150. M. G. Fontana (Consultant)
151. R. M. Fuoss (Consultant)
152. Norman Hackerman (Consultant)
153. H. S. Harned (Consultant)
154. E. A. Mason (Consultant)
155. T. N. McVay (Consultant)
156. George Scatchard (Consultant)
157. T. F. Young (Consultant)
158. J. W. Cobble (Consultant)
159. P. H. Emmett (Consultant)
160. R. F. Newton (Consultant)
161. Rafael Perez-Belles (Consultant)

## *EXTERNAL DISTRIBUTION*

162. R. W. McNamee, Union Carbide Corp., New York
163. Research and Development Division, AEC, Washington
164. Research and Development Division, AEC, ORO
165. Reactor Development Division, AEC, Washington
166. Reactor Development Division, AEC, ORO
167. Union Carbide and Carbon Chemicals Company (South Charleston)

168–751. Given distribution as shown in TID-4500 (19th ed., Rev.) under Chemistry category (75 copies – OTS)